Iridium(I) Complexes for the Functionalisation of Carbon-Hydrogen Bonds

Renan Zorzatto

PhD Thesis

2018

Author Declaration

This thesis is the result of the author's original research. It has been composed by the author and has not been previously submitted for examination which has led to the award of a degree.

The copyright of this thesis belongs to the author under the terms of the United Kingdom Copyright Acts as qualified by University of Strathclyde Regulation 3.50. Due acknowledgement must always be made of the use of any material contained in, or derived from, this thesis.

Signed:

Date:

"The important thing is to never stop questioning.

Curiosity has its own reason for existing."

Albert Einstein

Abstract

The development of catalytic systems for the functionalisation of carbon-hydrogen bonds has been an intensive area of research for the last 5 decades. In this context, transition metal complexes play a crucial role in reaction discovery, mechanistic evaluation and synthetic applications. In the Kerr group, this technology has been explored in the context of hydrogen isotope exchange, resulting in the development of highly active iridium(I) complexes bearing phosphines and NHC ligands.

Despite their broad functional group compatibility, existing methods for isotope exchange are ineffective in the labelling of sterically encumbered directing groups. Hence, in the first chapter we investigate the synthesis of three new iridium(I) complexes bearing chelating phosphine-functionalised NHC ligands, and their application in the isotope exchange of sterically hindered carbamates. Our initial studies revealed high catalytic efficiency and tolerance for steric encumbrance, prompting us to perform a combined theoretical and experimental investigation of the reaction mechanism.

Therefore, by conducting DFT calculations and kinetic experiments, we were able to identify a rich dynamic behaviour in solution and ultimately propose a reaction mechanism. Additionally, our interest in the activation of carbon-hydrogen bonds resulted in the exploration of a theoretical model for the prediction of enthalpies of activation, resulting in the identification of relevant electronic and steric descriptors.

From the knowledge gathered in our initial studies, the second chapter describes the application of our novel iridium catalysts in the functionalisation of carbon-hydrogen bonds in the context of hydroarylation of olefins. Thus, we identified carboxylic acids as suitable directing groups for this transformation and employed Design of Experiments to optimise the reaction conditions. Synthetic studies were focused on the preparation of 14 substrates, enabling quick assessment of the capabilities and limitations of this reaction. These investigations resulted in a synthetic method suitable for the synthesis of bi- and tricycles featuring tertiary and quaternary benzylic stereocentres in a racemic fashion.

Finally, we investigated the mechanism of this process by DFT calculations, which led us to identify a plausible reaction pathway which should guide future kinetic evaluations.

Acknowledgements

CONTENTS

Abbreviations

ºC	Degrees Celsius
Ac	Acetyl
Ad	Adamantyl
ADMET	Absorption, Distribution, Metabolism, Excretion and Toxicity
AIBN	2,2'-Azobis(2-methylpropionitrile)
Ar	Aryl
Atm	Atmospheres
BAr_F	Tetrakis[3,5-bis(trimethyl)phenyl]borate
Bn	Benzyl
CMD	Concerted Metalation Deprotonation
COD	1,5-Cyclooctadiene
Cy	Cyclohexyl
DFT	Density Functional Theory
DMSO	Dimethyl sulfoxide
eq.	Equivalents
Et	Ethyl
FG	Functional Group
g	Grames
G	Gibbs Free Energy
H	Enthalpy
h	Hours
HIE	Hydrogen Isotope Exchange
Hz	Hertz
J	Coupling Constant
K	Kelvin
K_{calc}^{298}	Calculated Equilibrium Constant at 298 K
kcal	Kilocalories
L	Ligand
Me	Methyl
Mes	2,4,6-trimethyl-1-phenyl
mL	Millilitres

mmi	Membered Metallocyclic Intermediate
mmol	Millimoles
Mol	Moles
MS	Molecular Sieves
NHC	*N*-Heterocyclic Carbene
NHC-P	Phosphine Functionalised *N*-Heterocyclic Carbene
NMR	Nuclear Magnetic Resonance
	s – singlet
	d – doublet
	t – triplet
	q – quartet
	m – multiplet
	app. – apparent
	br – broad
OA	Oxidative Addition
PES	Potential Energy Surface
Ph	Phenyl
ppm	Parts Per Million
Pr	Propyl
Py	Pyridine
rt	Room temperature
RE	Reductive Elimination
SCF	Self-Consistent Field
S_N2	Second-Order Nucleophilic Substitution
^{t}Bu	1,1-dimethyl-1-ethyl
TEP	Tolman Electronic Parameter
Tert	Tertiary
THF	Tetrahydrofuran
Tol	Tolyl
wt.	Weight
θ	Tolman's Cone Angle
Mmol	Micromoles

CHAPTER 1

Hydrogen Isotope Exchange of Carbamates

1. Introduction

1.1 Transition Metals and Catalysis

Since the discovery of coordination compounds by Werner in 1893,[1] and subsequent contributions to the field of homogeneous organometallic complexes by Vaska *et al.* in the 1960s,[2-4] research interest in the chemistry of transition metals and synthetic applications of their organometallic compounds has grown at an increasing rate. In this regard, Figure 1.1 presents the gross number of publications exploring transition metals, highlighting important points in the timeline of this field of research. A second trend line concerning the use and application of iridium and its compounds is also presented for comparison.
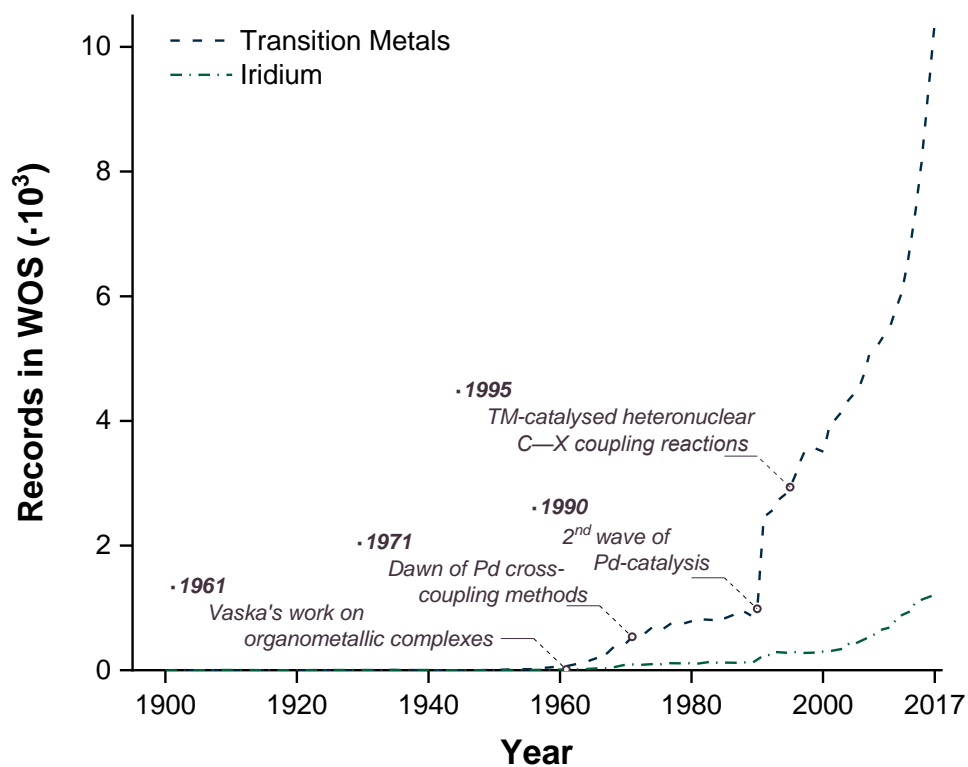

Figure 1.1: Timeline of transition metals in chemistry.[†]

[†]Data retrieved from the Web of Science[6] – WOS – on 07/2018 based on research topics indicated in the legend. Timestamps based on references 2-5.

Owing to their ability to act as both Lewis acids and -bases, in conjunction with a tendency to engage in direct interactions with unsaturated carbon-bonds, transition metals are of particular interest to synthetic organic chemistry.[7-8] An important characteristic of late transition metals, especially for the subgroup of platinum metals (Ru, Rh, Pd, Os, Ir and Pt),[9] is the existence of partially occupied d-orbitals at these metal centres. This fundamental property enables transition metals to act as acceptors of electron density from organic fragments, such as donor atoms present in functional groups and π systems of C—C multiple bonds, consequently enabling their behaviour as Lewis acids.[8,10]

Additionally, a second important property of transition metals is directly related to their more diffuse d-orbitals, an especially prominent feature in second- and third row transition elements.[8] Their capacity to distribute electron density through large volumes confers the ability to participate in covalent interactions with substrates, which ultimately leads to the formation of bonds to the metal centre and enables access to reactive intermediates that might facilitate chemical transformations, or even alter their outcome.[10]

Therefore, it is the synergy of these electronic features which enable transition metals to associate organic molecules in interactions with high covalent character, thus resulting in strong binding to ligands.[8,10] Consequently, the design and modification of these ancillary ligands can be employed as effective methods to confer a set of desired steric and electronic properties to the metal centre, which in turn could facilitate a given transformation.[8] Finally, the existence of distinct stable coordination geometries in transition metal complexes, for which an ample range of oxidation states is available; and their ability to reversibly react with organic molecules, make these entities especially suited to engage in organic processes, and ultimately control their outcome.[7-8,10]

Further research efforts aimed at understanding and exploiting the properties of organotransition metal complexes in organic synthesis helped to establish a solid theoretical foundation in which modern catalytic protocols could be developed. Of note are studies performed by Hartwig *et al.* on the evaluation of palladium-catalysed carbon-heteroatom bond formation;[11] Suzuki,[12] Negishi,[13] Sonogashira,[14] Stille,[15] and co-workers on the establishment of a refined understanding of transition metal

catalysed C—C cross-coupling reactions; Bergman *et al.* on the direct functionalisation of C—H bonds;[16] Crabtree and co-workers on the stereochemical assignment of complexes in solution;[17] among others. Table 1.1 summarises the four most recurrent elemental processes in organometallic chemistry, which have been extensively explored in organic chemistry, being ubiquitous in reaction mechanisms of processes catalysed by transition metals.[8,10]

Table 1.1

Elemental Process	Qualitative Trends
Oxidative Addition	Favourable for **electron rich** metal centres Preferred in less hindered centres Necessitates a vacant coordination site Rate is affected by dissociative/associative processes happening before/during the reaction
Reductive Elimination	Favourable for **electron poor** metal centres Aided by increased steric hindrance on the metal Creates a vacant coordination site Rate is affected by the dissociation of product
Migratory Insertion	Insertion: requires *cis-* geometry of reacting ligands De-insertion: requires vacant site *cis-* to reacting moiety Electrophile and nucleophile migrations are possible and happen through concerted processes
Ligand Displacement	Proceed through associative or dissociative pathways Electron poor, steric accessible, electronic unsaturated metals favour association Electron rich, steric hindered, electronic saturated metals favour dissociation

1.2 Iridium in Organic Chemistry

Sharing the properties common to late transition metals of the third series (*vide supra*), iridium finds wide applicability in organic processes.[8,18] Initially neglected as a suitable element for catalysis, mainly due to higher activity and availability of other platinum metals, iridium has the ability to form remarkably stable organometallic complexes, with most of its early usages restricted to the characterisation of intermediates in catalytic processes mediated by its lighter analogue, rhodium.[19]

Pioneering studies by Crabtree and co-workers[20] in the field of hydrogenation of olefins led to the discovery of a remarkably active catalyst — [Ir(COD)(PCy$_3$)py]PF$_6$

— which was able to effectively reduce tri-and tetra- substituted alkenes, which had proven to be unreactive towards the well-known Wilkinson's catalyst, [Rh(PPh$_3$)$_3$Cl],[21] thus highlighting the capacity iridium complexes possess to engage in rather demanding transformations.[19] Scheme 1.1 presents the rates of hydrogenation of cyclohexene, in mol of substrate reduced (mol of catalyst)$^{-1}$ h^{-1}, with the different catalysts tested in these seminal studies.[20-21]
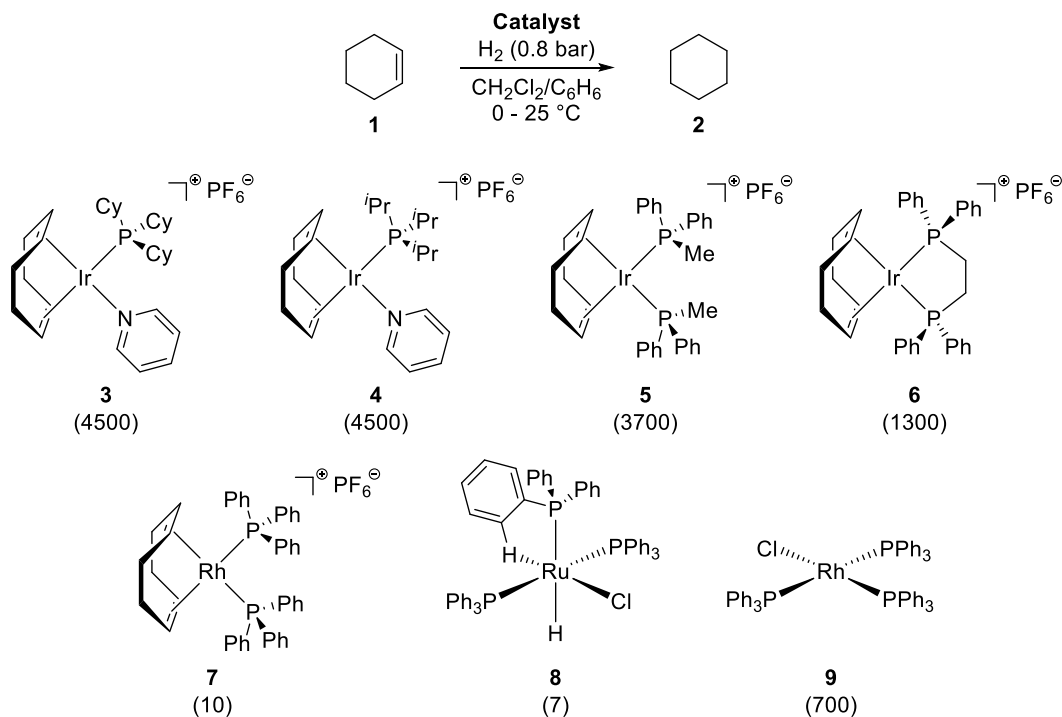
Scheme 1.1: Rates of hydrogenation of cyclohexene by selected catalysts.[20-21]

Remarkably, around a six-fold increase in reaction rate was observed when Crabtree's catalyst **3** was employed, compared to the then widely adopted Wilkinson's catalyst **9**. Furthermore, subsequent applications in the chemoselective hydrogenation of hindered enones,[22] and in the selective reduction of alkenes directed by β-hydroxy groups[23-24] contributed to establishing **3** as a standard homogeneous catalyst for the hydrogenation of olefins.[19]

A second important contribution which furthered the application of iridium in catalysis is related to studies by Bergman and co-workers, who demonstrated that iridium(III) complexes were able to engage in direct activation of the C—H bonds of simple hydrocarbons such as benzene, cyclohexane and neopentane.[25] Scheme 1.2

illustrates the systems employed to activate C_{sp^2}—H and C_{sp^3}—H bonds of rather chemically inert molecules.
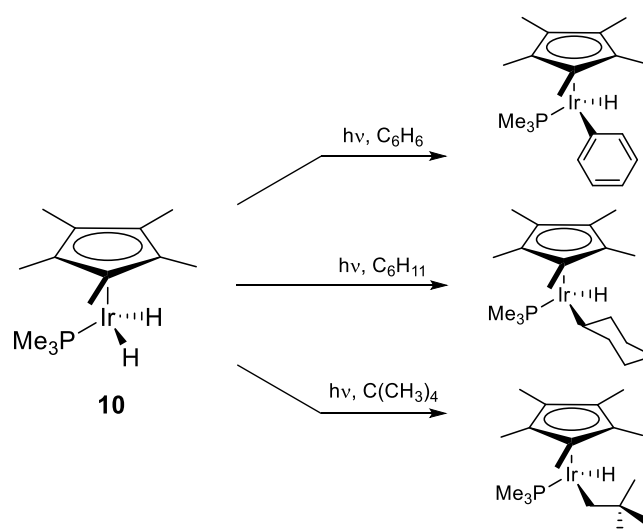
Scheme 1.2: Early examples of direct C—H activation.[25]

These initial studies were crucial to establish iridium as a competent metal for catalysis and, since then, many applications have been devised. Of note are the works of the research groups of Crabtree in chemoselective hydrogenation methods and transfer hydrogenation, as well as mechanistic evaluations of these systems;[17,20-24,26-32] Bergman[25,33-37] and Goldman[38-43] in studies on the C—H activation of a broad range of molecules; Pfaltz in the synthesis of chiral ligands for asymmetric catalysis;[44-52] Krische in the development of enantioselective C—C bond formation which relies on synergistic allylic alkylation and hydrogen auto-transfer;[53-63] and Kerr in the development of selective hydrogen isotope exchange of C—H bonds in aromatic molecules and conjugated alkenes;[64-79] among others. Scheme 1.3 depicts representative examples of systems and applications highlighted by these groups.

Crabtree 2009

R^1	R^2	%Conv.
Ph	Ph	98
Ph	PhCH$_2$	86
Ph	PhCH$_2$CH$_2$	55
n-Pr	Ph	43
n-Pr	PhCH$_2$	56

Pfaltz 2000s

R^3	Yield (%)	A:B	%ee
C$_6$H$_5$	99	95:5	91 (*R*)
4-MeOC$_6$H$_4$	98	99:1	95 (*R*)
CH$_2$CH$_2$C$_6$H$_5$	93	62:38	78 (*R*)

R^4	R^5	R^6	R^7	Conv. (%)	%ee
H	Me	H	Ph	>99	93 (*S*)
H	H	Me	CH$_2$OH	86	93 (*R*)
OMe	Me	Me	H	>99	92 (*R*)
OMe	Me	H	Me	>99	97 (*R*)

Krische 2015

R^8	Yield (%)	dr	%ee
C$_6$H$_5$	96	5:1	97
4-BrC$_6$H$_4$	90	4:1	96
2-Furyl	73	10:1	97
2-(6-methylpyridyl)	78	5:1	97
Cyclopropyl	64	4:1	95

Kerr 2014

R^9	%D	A:B	R^9	%D	A:B
H	78	99:1	Br	87	98:2
CF$_3$	89	98:2	Me	70	99:1
Ph	82	98:2	MeO	81	99:1
Cl	90	97:3			
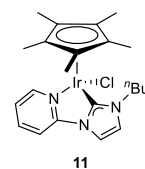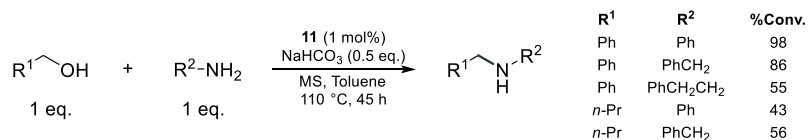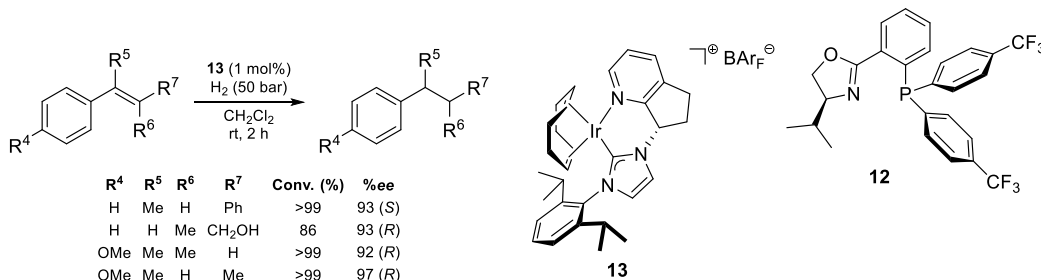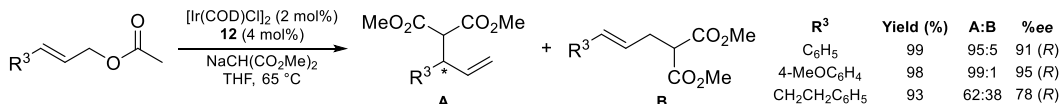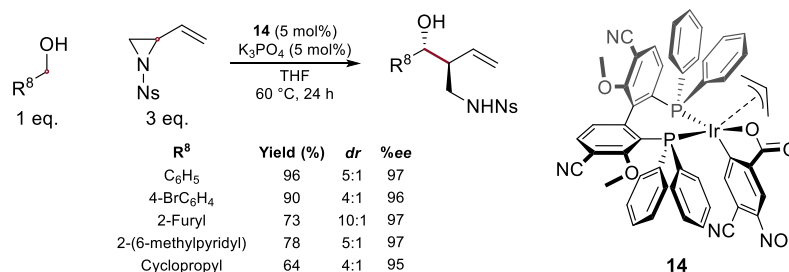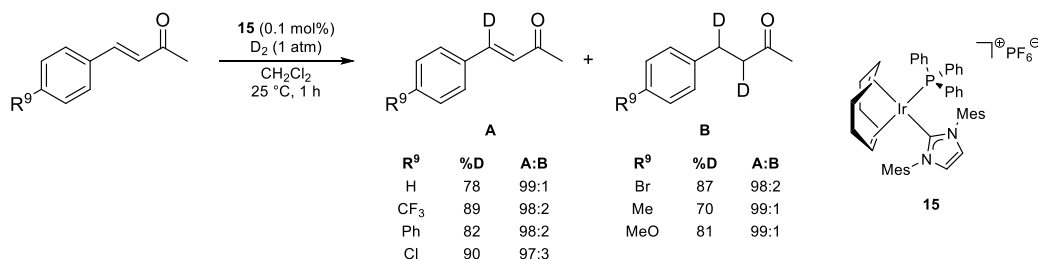
Scheme 1.3: Selected examples of iridium catalysts in organic synthesis.

1.2.1 Activation of C—H bonds

Initially regarded as an exotic process mostly confined to academia, the activation of C—H bonds has experienced a remarkable evolution in the last few decades. Owing to their intrinsically low polarity and high bond dissociation energy, direct homolytic cleavage of most C—H bonds typically found in organic compounds requires an energy input of 70 – 110 kcal mol^{-1} to be realised.[80] In this regard, the use of transition metal complexes to assist C—H bond breaking events, with concurrent

development of a more sophisticated mechanistic picture to account for often quizzical experimental observations,[81] has been a topic of pronounced interest in organometallic chemistry since the early 1980s. Perhaps most relevant to this field is the seminal work of Bergmann and co-workers (*vide supra*), which resulted in an improved understanding of transition metal-mediated C—H activation, fostering a more comprehensive theoretical framework which furthered the development of catalytic systems.[82]

Mechanistically, these transition metal-mediated processes can proceed through four broadly accepted pathways:

i.   Oxidative addition: low-valent late transition metal centres featuring strongly σ-donating ligands typically engage in direct oxidative addition of C—H bonds, resulting in alkyl- or aryl-hydrido species which can be further functionalised;[25-43,82]

ii. Concerted metalation-deprotonation (CMD): commonly observed in organometallic complexes of group 8 – 10 metals which possess a coordinated carboxylate ligand, activation through CMD occurs through a concerted 6-memebered metallacylic transition state that results in the simultaneous transfer of a proton from an agostic[83] C—H bond to the coordinated carboxylate, with concurrent formation of a new M—C bond.[84] A second closely related mechanistic pathway has also been identified whenever high valent metal centres are implicated.[83] More specifically, stepwise C—H activation events that proceed through electrophilic metalation to afford a Wheland intermediate, which subsequently engages in a base-assisted deprotonation to reinstate aromaticity, also result in the formation of an arylmetal species with the overall loss of one proton;[83]

iii. σ-Bond metathesis: a process that results in a concerted exchange of a σ-bonded ligand and an agostic C—H bond, producing a new pair of σ-, and agostically bound moieties at the metal centre. This elemental process has been observed in both early and late transition metal centres, respectively requiring the presence strong σ-donors and alkyl-, or often hydride, ligands;[81,85,86,87]

iv. Hydrogen atom transfer (HAT): often exploited in an indirect process involving transition metals, it is typically characterised by a single electron transfer at a site vicinal to a C—H bond, resulting in weakening of the strong covalent interaction between these two centres. Subsequent proton loss then generates a carbon centred radical and a new σ-bond between the abstractor and the extruded hydrogen atom.[80] This process is often mediated by photocatalysts in presence of specific radical quenchers able to capture the newly generated carbon centred radicals to deliver synthetically useful compounds.[88,89]

A depiction of these process with representative examples[89,90] is presented in Schemes 1.4 and 1.5.
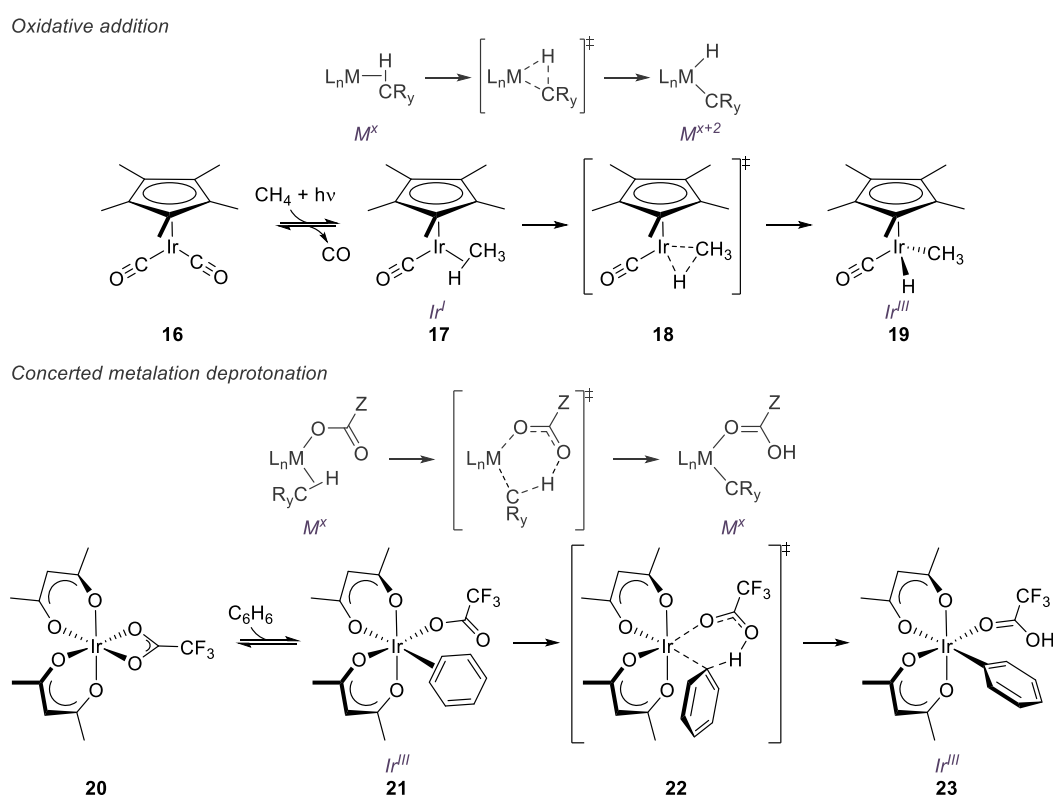
Scheme 1.4: Generic depiction[†] and representative examples for oxidative addition and CMD processes.[90,91]

[†]Subscript y represents the number of substituents ($1 \leq y \leq 3$); x denotes oxidation state; $Z = CR_3$, OR.
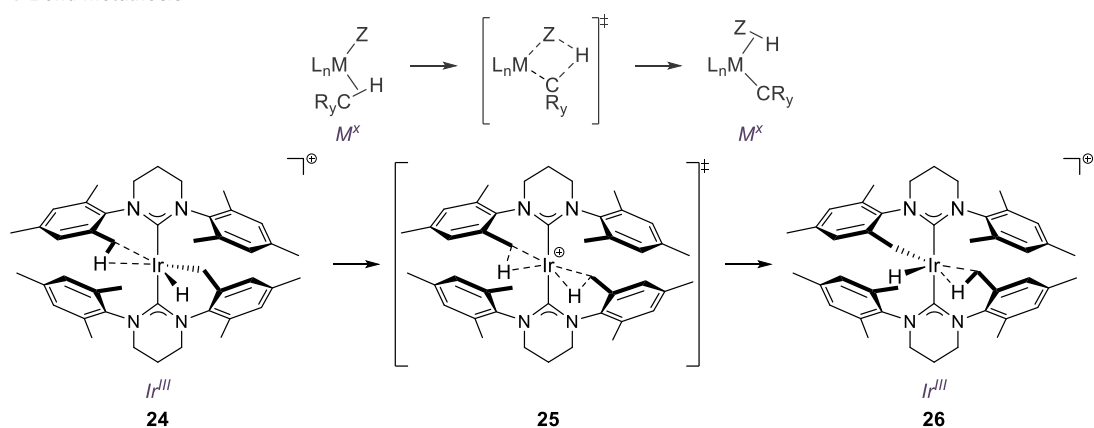
σ-*Bond metathesis*

Hydrogen atom transfer
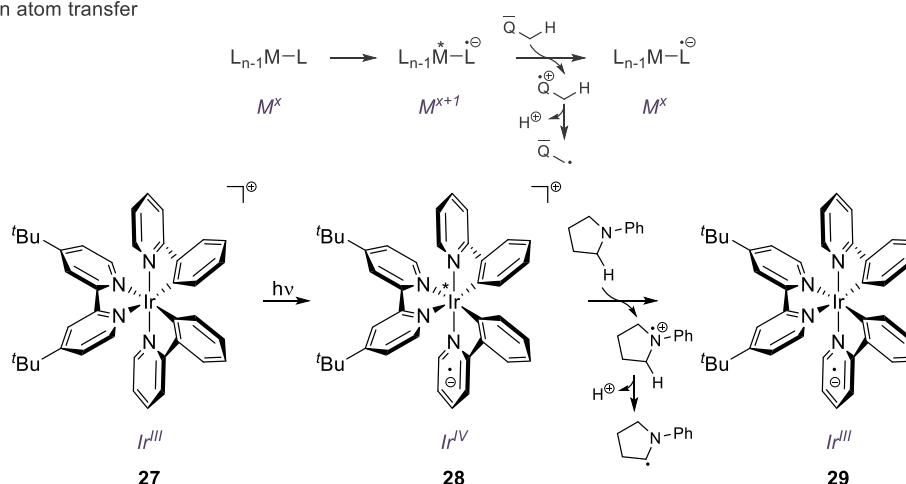
Scheme 1.5: Generic depiction[†] and representative examples for σ-bond metathesis and hydrogen atom transfer processes.[89-92]

[†]Subscript y represents the number of substituents (1 ≤ y ≤ 3); x denotes oxidation state; Q denotes an electron-rich group which stabilises radical cation intermediates.

As illustrated previously, one of the most remarkable features of iridium complexes and their platinum metals counterparts is the capacity to cleave otherwise stable C— H bonds.[8,19] Moreover, as illustrated by the examples in Schemes 1.4 and 1.5, organometallic complexes of iridium are especially attractive for their ability to activate C—H bonds through most of the available mechanistic pathways. In this regard, it is also clear, from both the aforementioned instances and extensive literature on these subjects (*vide infra*), that judicious choice of ancillary ligands is required to modulate the metal centre and promote the desired reaction outcome.

A second important aspect, ubiquitous in activation processes that generate metal hydrides, is the existence of a σ-complex between the C—H bond to be activated and the metal centre which precludes the activation event. This interaction is described as agostic,[83] and is often taken to be analogous to those arising from π-donors which follow the Dewar-Chatt-Duncanson model.[94,95] Thus, the agostically ligated C—H bond engages in an interaction in which its $\sigma_{C—H}$ orbital donates electron density to empty orbitals at the metal centre, whilst concurrent back-donation from filled d-orbitals in the metal partially replenishes electron density into the $\sigma^*_{C—H}$ orbital.[8] The overall effect is a weakening of the C—H bond and consequent propensity to engage in activation events featuring lower energy barriers than those stipulated by bond dissociation energy thresholds. For instance, intermediates **17**, **24** and **25** in Schemes 1.4 and 1.5 exhibit explicit agostic interactions, while access to transition state **22** from intermediate **21** occurs *via* a ring slipping process which establishes an equilibrium between the $(\pi_{C=C})$-η^2-C_6H_6 and the agostically bonded $(\sigma_{C—H})$-η^2-C_6H_6 modes of coordination to iridium, the latter being capable of engaging in an activation event through **22**.[84] A pictorial representation of this important interaction is illustrated in Scheme 1.6.
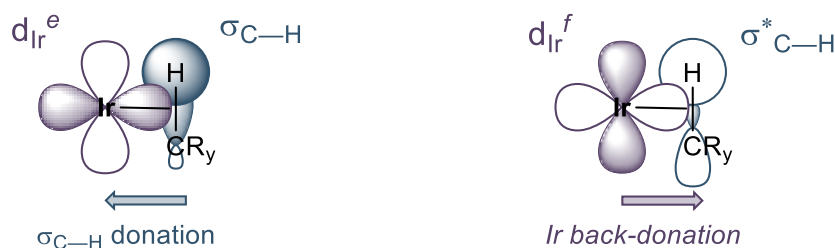
Scheme 1.6: Simplified description of agostic interaction.[†]

[†]Subscript y represents the number of substituents (1 ≤ y ≤ 3); superscripts *e* and *f* denote empty and filled orbitals, respectively.

Finally, a drawback of the mechanistic promiscuity displayed by iridium complexes, especially in situations when more than one pathway can be accessed *via* interactions with different ligands in their coordination sphere, is related to the contrived nature of studies aiming to probe the mechanism of C—H activation. For instance, while σ-bond metathesis is often observed when organometallic complexes of iridium contain anionic ligands in their coordination sphere, *e.g.*, alkyl-, alkenyl-, aryl-, halides and

hydrides; for some iridium complexes, an oxidative addition pathway competes with, or entirely overrides, the metathetic process.[96] An analogous scenario is observed when low valent complexes undergo C—H activation in the presence of carboxylates. In these latter cases, ambiguity among oxidative addition, σ-bond metathesis and CMD pathways also exists.[97] Unsurprisingly, sophisticated mechanistic studies are often required in order to differentiate between these activation modes.

An interesting example is provided in Scheme 1.7.[96] In this case, reaction of the neutral iridium trihydride [(PPh$_3$)$_2$IrH$_3$] **30** with imidazolium salt **31** afforded two different products which underwent C—H activation through distinct mechanisms. Thus, coordination of the C—H bond at C2 of the imidazolium ring affords complex **32a**, which engages in an activation event *via* a σ-bond metathesis delivering [(η^2-H$_2$)H$_2$Ir(PPh$_3$)$_2$] **34a**. Upon loss of H$_2$, this generates a stable and isolable product **35a** featuring a normal NHC unit. Alternatively, coordination at C4 of the imidazolium ring delivers the agostically bound complex **32b** which, in turn, effects C—H activation through an oxidative addition pathway to produce the Ir(V) intermediate **34b**. This complex then loses H$_2$ *via* reductive elimination of two of its hydrides and affords product **35b**, which features a tightly bonded abnormal NHC.[96]
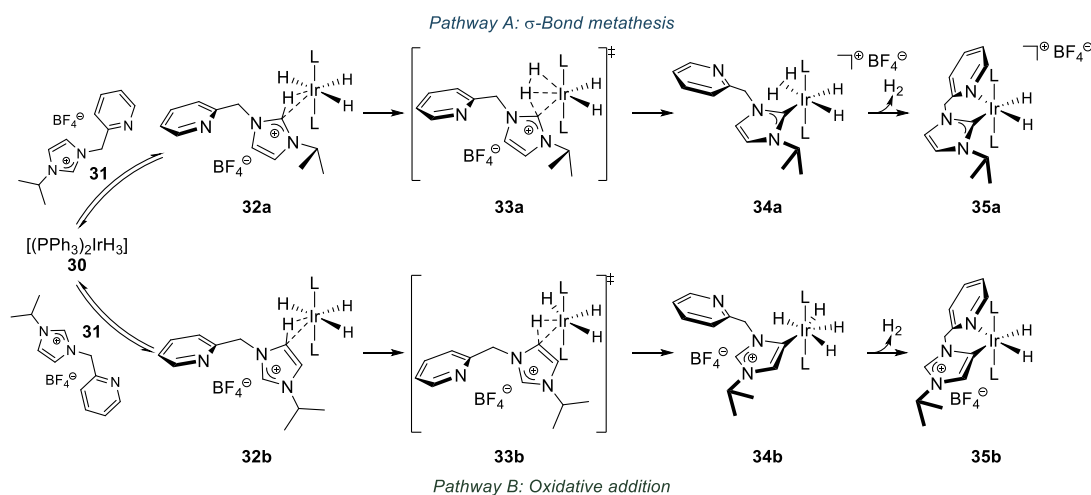
Scheme 1.7: Divergent pathways in C—H activation involving iridium hydrides.[†][97]

[†]L = PPh$_3$.

1.2.2 Hydrogen Isotope Exchange

Isotopically enriched organic molecules find applications in a broad range of industrial and research settings.[78,79] For instance, labelled molecules are ubiquitous in biochemical studies aiming to probe the absorption, distribution, metabolism and excretion (ADME) of drug candidates and pharmaceuticals,[78-99] where they play a central role in determining important physicochemical properties and reduce attrition at earlier stages of the drug development process.[99] In addition, the prevalence of deuterated molecules amongst stable isotopically labelled internal standards for LC-MS applications,[78,79,100] in conjunction with the ample use of tritium-enriched isotopologues derived from molecular probes and pharmaceuticals as radioactive tracers in biological applications,[78-99] furthers the need for reliable and practical synthetic methods to access isotopically enriched entities.

In this regard, the search for suitable chemical methods targeting the installation of isotopes of hydrogen in a cost- and time efficient manner has driven the development of several synthetic protocols. Of particular relevance are methods which focus on the direct replacement of hydrogen by its heavier isotopes ^{2}H and ^{3}H, thus effecting hydrogen isotope exchange – HIE.

This transformation can be accomplished in several ways, the most prevalent and contemporarily used ones being: acid/base catalysed exchange and heterogeneous- and homogeneous transition metal catalysts.[79] The former is usually employed when the target molecule contains aromatic rings attached to an electron-rich group able to stabilise Wheland intermediates or, alternatively, when a hydrogen is rendered acidic due to close proximity to strong electron-withdrawing functionalities, *e.g.*, keto-, carboxy-, nitro-, cyano-, (hetero)aromatics and highly electronegative atoms.[79,101] Methods which rely on the use of transition metal catalysts, on the other hand, present broader functional group compatibility and, particularly for homogeneous systems, can effect isotope exchange with high degrees of chemo- and regioselectivity.[79,102,103] Schemes 1.8 and 1.9 illustrate these categories, illustrated by some relevant examples.
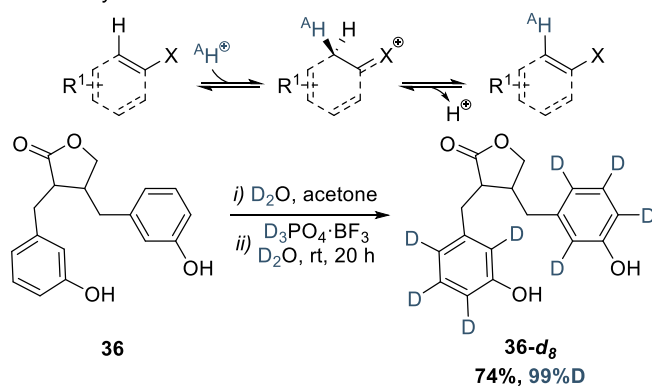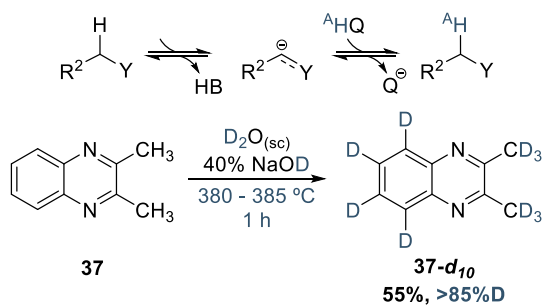
Scheme 1.8: Acid[104] and base[105] catalysed HIE.[†]

[†]X denotes an EDG; Y indicates an EWG; Q represents a conjugate base; [A]H is a higher isotope of [1]H.
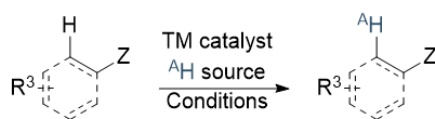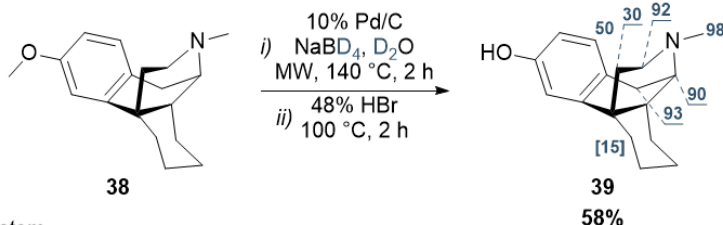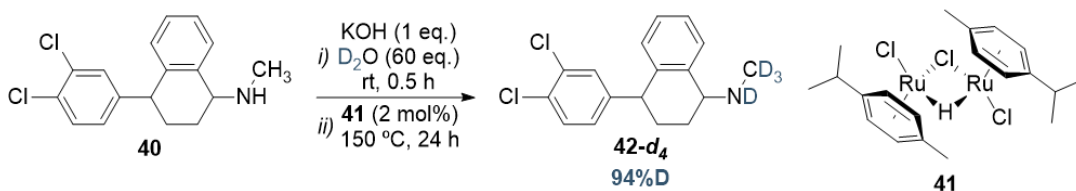
Scheme 1.9: Transition metal-catalysed[106,107] HIE.[†]

[†]Z denotes an arbitrary functionality; [A]H is a higher isotope of ^{1}H; for **39**, numbers indicate D incorporation; values in brackets represent incorporation at indistinguishable alicyclic positions.

As exemplified in Scheme 1.8, acid and base mediated HIE protocols suffer from poor selectivity, affording products in which exchange takes place at multiple sites. For instance, d_8-enterolactone **36-d_8** was obtained in 99% isotopic purity after treatment with the mixed Brønsted/Lewis acid $D_3PO_4 \cdot BF_3$,[104] whilst d_{10}-(2,3-dimethyl)quinoxaline **37-d_{10}** was isolated with 85% deuterium incorporation after reaction in the presence of 40% NaOD in supercritical D_2O at 380 – 385 °C.[105] Despite the high levels of incorporation attained, typical reaction conditions require strong acids or bases to promote isotope exchange and employ harsh reaction conditions that can lead to extensive decomposition.[79]

In this regard, molecules bearing sensitive functionalities, as well as compounds containing stereocentres prone to epimerisation under acidic or basic conditions, are typically unsuitable for these protocols.[79,102] In the latter case, however, loss of stereochemical integrity can be circumvented using chiral auxiliaries or, conversely, by enantioselective transformations in which a suitable precursor to the compound of interest is converted to the desired labelled product.[79]

Despite their drawbacks, it must be emphasised that applications which require a high degree of isotope incorporation without desire for high site selectivity, *e.g.*, in the synthesis of standards for mass spectrometry and perdeuterated molecules; acid and base catalysed HIE, and unselective heterogeneous metal catalysts become valid methods.[79,102]

In the realm of transition metal catalysed methods, a compromise between selectivity and degree of incorporation is often encountered, as exemplified in Scheme 1.9. Thus, by employing heterogeneous catalysis with 10% Pd/C and $NaBD_4$ in D_2O as the deuterium source, dextromethorphan **38** was unselectively deuterated, affording, after removal of the *O*-methyl group with 48% HBr, dextrorphan **39** with an average deuterium incorporation of 40% over all of the 20 exchangeable positions.[106] On the other hand, by employing the homogeneous ruthenium catalyst **41**, Chatterjee *et al.* were able to obtain d_4-sertraline **40-d_4** with excellent selectivity and levels of incorporation.[107] This example is also mechanistically interesting, for the introduction of the isotopic label was attributed to a process involving sequential N—H activation *via* direct oxidative addition followed by a β-hydride elimination

and migratory insertion of a deuteride into the imine transiently formed during the reaction, which places the label at the observed position.[107]

These examples help illustrate the main features practitioners must consider when selecting a method for hydrogen isotope exchange, namely:

i.   Final application: defines the extent of incorporation desired and whether site specificity is required. As previously mentioned, analytical standards for MS often sacrifice selectivity in favour of high degree of isotope incorporation, thus benefiting from catalytic systems employing acids, bases and heterogeneous metal catalysts;

ii. Molecular complexity: fully functionalised molecules bearing well-defined stereocentres are commonly found among pharmaceutical compounds and drug candidates. Therefore, methods that place a strong focus on functional group compatibility and mild reaction conditions are preferred. Additionally, and especially in pharmaceutical applications, high site selectivity is also required, and, perhaps unsurprisingly, homogeneous transition metal catalysts largely dominate this field;

iii. Radioactivity: whenever the use of tritium is required, radioactive waste generation and its management after reaction completion are typically regarded as the most important factors. Therefore, more selective methods that install the radioactive isotope in a controlled fashion whilst minimising hazardous waste production are preferred. Owing to these features, homogeneous catalysts are routinely employed in tritiation processes.

Given the prevalence of isotopically enriched molecules in the ADME process, their extensive usage in mechanistic studies of organic, organometallic and enzymatic reactions, and the recent search for deuterated drug molecules which feature lower metabolic decomposition rates, thus leading to less potential side effects; the development of homogeneous catalysts for HIE remains the main focus of research in this field.

Historically, one of the first examples of a homogeneous hydrogen isotope exchange reaction was reported by Hodges and Garnett, who used Na_2PtCl_4 as a catalyst and deuterium oxide as the isotopic source.[108] In the two decades that followed this

pioneering disclosure, homogeneous HIE systems have been developed employing rhodium, ruthenium and platinum catalysts.[79]

Notwithstanding their catalytic activity, these initial systems possessed low selectivity and were mostly unable to differentiate between C—H bonds in aromatic rings and in alkyl groups, and therefore more successfully applied in the HIE of only simple substrates such as hydrocarbons, primary aliphatic alcohols and molecules containing poorly coordinating functional groups, such as carboxylic acids and nitro-aromatics.[108,109] It was only in 1995, almost 30 years after Hodges and Garnett's work, that the first highly selective system was developed by Hesk and Evans, employing Crabtree's catalyst **3** to deliver deuterium exchange in acetanilides with remarkable selectivity for the positions *ortho-* to the functional group.[109] Scheme 1.10 presents selected examples of these initial systems.[108-111]
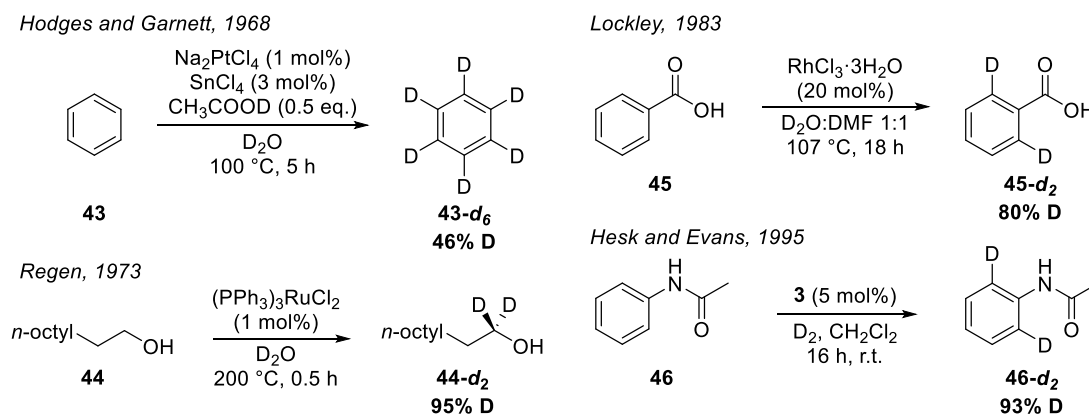
Scheme 1.10: Catalytic HIE employing complexes of Pt, Ru, Rh and Ir.[108-111]

Even though Hesk and Evans's system provided improvements in activity and *ortho-*selectivity for various substrates,[109] catalyst **3** presents a rather limited functional group tolerance, being often inactive in HIE reactions of molecules containing carboxylic acids, phenols, amines and nitriles;[109] it often generates large amounts of undesired radioactive side products when employed in conjunction with tritium gas; and displays appreciable solubility only in dichloromethane, which limits its applicability.[65]

Moreover, under an atmosphere of hydrogen or its isotopes, **3** and its analogues have a high tendency to form bridged complexes devoid of catalytic activity, thus leading

to deactivation.[16] Scheme 1.11 depicts the formation of such clusters starting from the pyridine-phosphine system **3**[112] and the bis-phosphine complex [Ir(COD)(PPh$_3$)$_2$] **48**.[21,26] Therefore, the requirement of stoichiometric or even super-stoichiometric amounts of **3** in HIE reactions is necessary to compensate for its rather facile deactivation.[67]
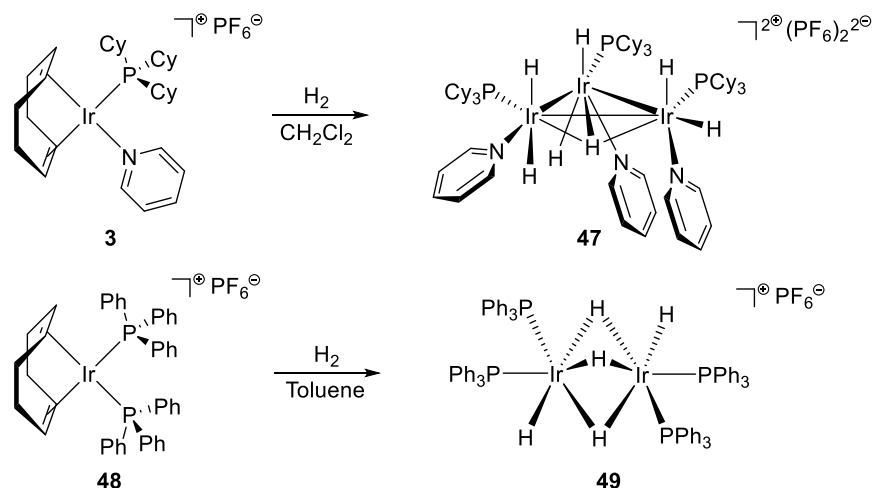
Scheme 1.11: Formation of inactive iridium hydride clusters.[21,26,112]

Different approaches to overcome these setbacks have been examined, but none proved more selective and efficient than the application of complexes of iridium(I) bearing phosphines and carbenes as ligands. Initial investigations by Nolan[113] and Buriak[114-115] demonstrated that iridium(I) carbene complexes, containing either pyridine or a phosphine in the ligand sphere, effectively catalysed the hydrogenation of olefins at catalyst loadings as low as 0.01 mol%. Notably, systems developed by Buriak reduced targeted olefins using an atmospheric pressure of hydrogen gas, once again pointing to the high reactivity profile of these Ir(I) NHC/phosphine species.[115] Early research in the Kerr group led to the development of iridium complexes bearing bulky *N*-heterocyclic carbenes and sterically demanding phosphines, which proved to be highly active in hydrogenations and HIE reactions,[64,66] Scheme 1.12.
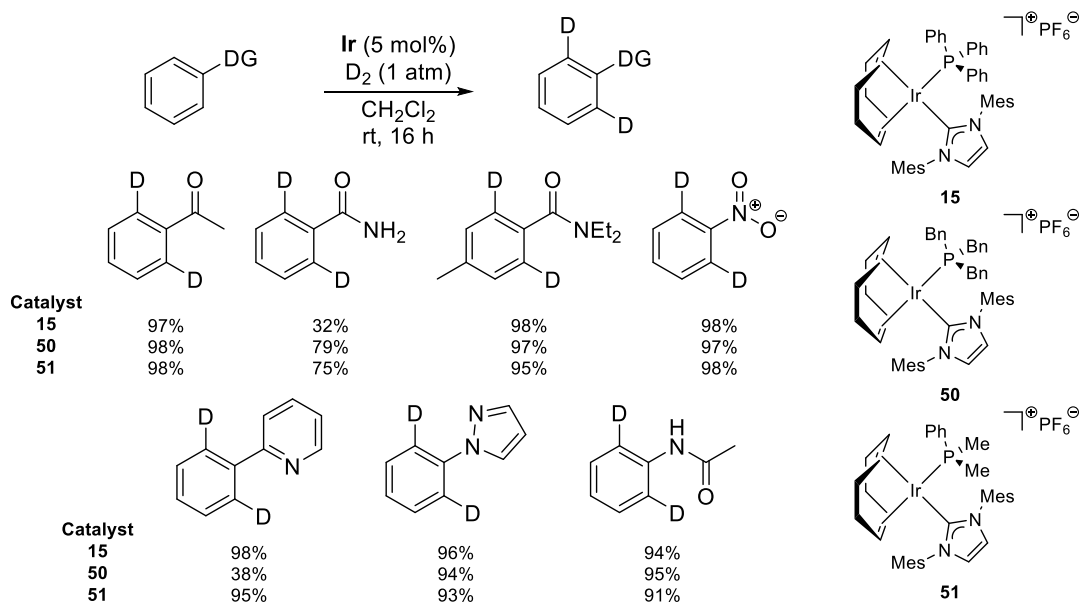
Scheme 1.12: First developments of HIE by Kerr *et al.*[64]

These initial studies prompted further investigations of complexes bearing different *N*-heterocyclic carbene and phosphine ligands, with concomitant exploration of alternative substrate motifs in the HIE process. Hence, the labelling of α,β-unsaturated systems,[69] and selective *ortho-* deuteration of pharmaceutically relevant heterocycles, including a range of *N*-heterocyclic motifs, were subsequently disclosed.[72,76] Selected examples of these developments are illustrated in Scheme 1.13.

The remarkable selectivity and activity of catalysts **15**, **50** and **51**, paired with their ability to promote HIE in fully functionalised organic molecules and biologically active compounds, as depicted in Scheme 1.14, soon attracted the attention of the pharmaceutical industry, establishing Kerr's catalysts as new, commercially available[116] standards for selective isotope exchange.

15 (0.1 - 5.0 mol%)
D_2 (1 atm)
CH_2Cl_2
25 °C, 1 h

α,β-unsaturated systems

44   84   93   84

Heterocyclic DGs

93   89   86   82
93   89   86   82

Heterocycles

93   7   97   82
       97   97 30

30
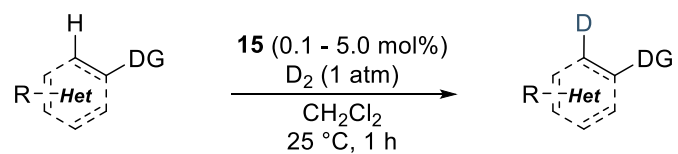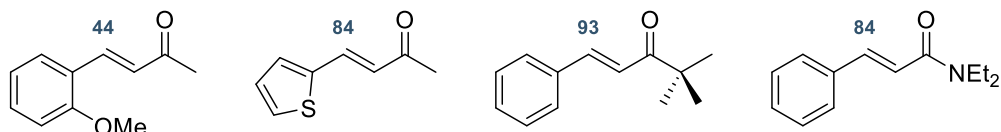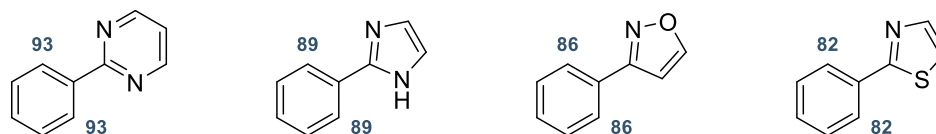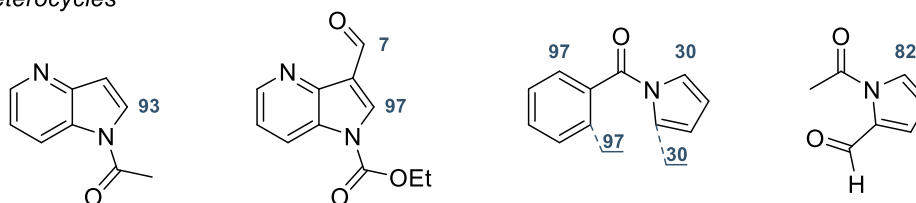
Scheme 1.13: Selected examples of advances in directed HIE. [†][69,72,76]

[†]Colour-coded positions indicate the deuterium incorporation determined by ^{1}H NMR spectroscopy.
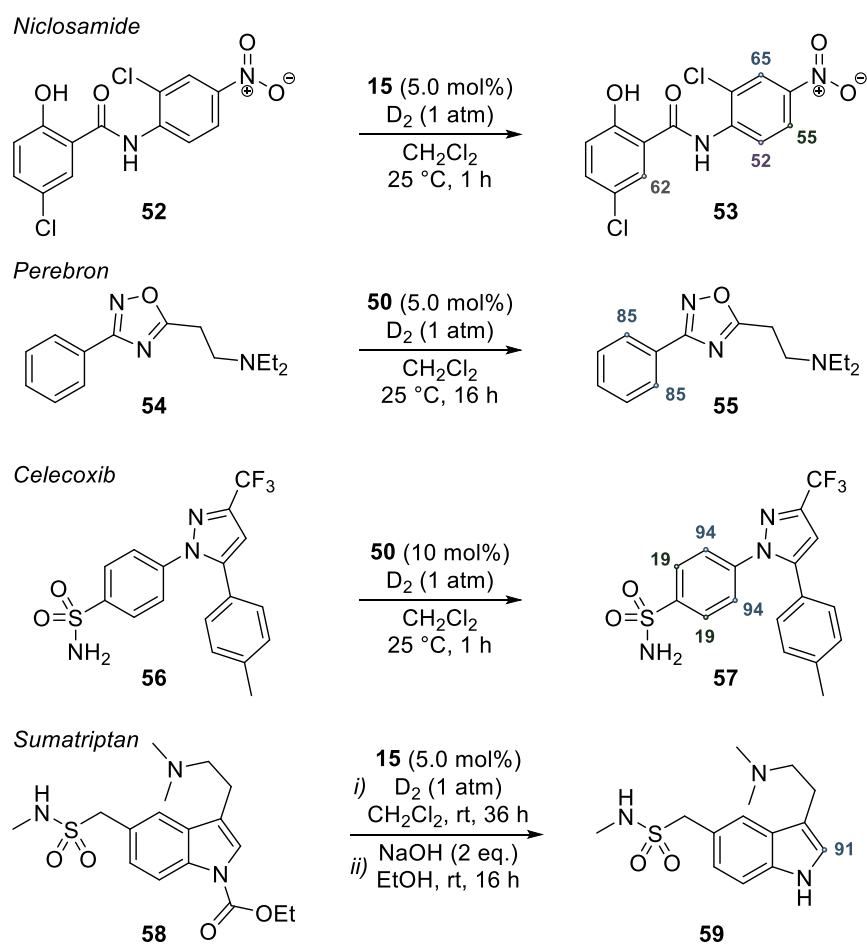
Scheme 1.14: Selected examples[70,76] of drug molecules labelled by Kerr's catalyst.[†]

[†]Colour-coded positions indicate the deuterium incorporation determined by ^{1}H NMR spectroscopy.

Even though commonplace in HIE protocols employing Crabtree's catalyst, several drug candidates and molecules with potential biological activity display a poor solubility profile in chlorinated solvents,[65] making CH_2Cl_2 unsuitable for the labelling process. This issue is especially relevant due to the extensive usage of HIE as an integral part of the ADME toolkit to assess drug candidates, which allows researchers to follow the fate of biologically active molecules, thus constituting an essential part of the drug development cycle.[78-99] Therefore, as a part of the overall activity evaluation of these catalytic systems, studies were conducted in which alternative solvents were pursued.

Therefore, after careful evaluation of different counter anions and solvent effects in the HIE process,[68] a novel catalyst was devised in which the rather small PF_6 counter anion was replaced by a more lipophilic counterpart BAr_F. Figure 2 summarises the

notable improvement in activity at low catalyst loadings when employing the new complex synthesised in the deuteration of acetophenone in a variety of solvents with markedly different partition properties.
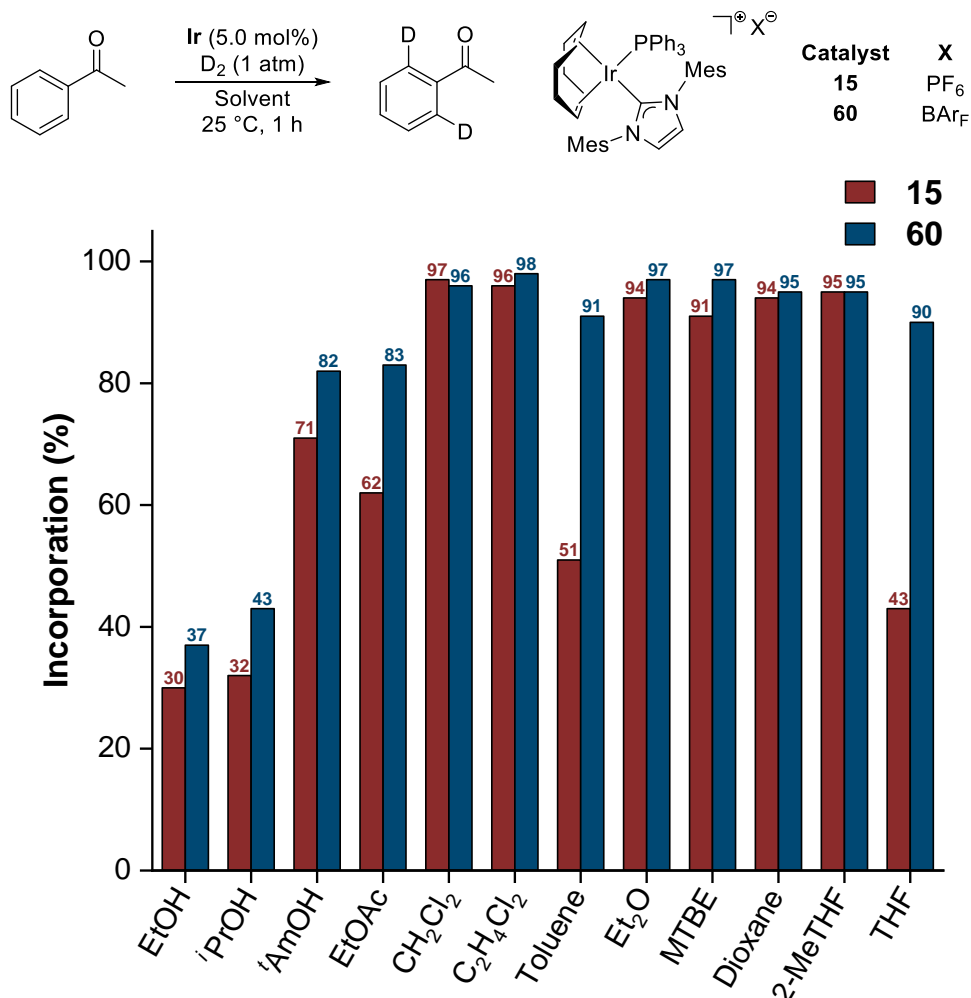
Figure 2: Activity in the HIE of acetophenone with catalysts **15** and **60**.[†68]

[†]Incorporation determined by ^{1}H NMR.

From these studies, it was possible to attribute the higher activity of **60** to two important factors: *i)* an increase in the overall size of the anion leads to a more spatially distributed charge, thus decreasing the interionic interaction[117] with the iridium cation; and *ii)* the presence of aryl units on the counter anion of **60** confers lipophilicity to the overall structure,[118] leading to solubilisation in solvents possessing low dielectric constants.

Therefore, a combination of conclusions drawn from investigations into the solvent scope of **60**, the synthesis of novel heteroleptic iridium(I) catalysts bearing different

NHC and phosphine combinations, and the development of sophisticated mechanistic knowledge at both experimental and theoretical levels (*vide infra*), enabled access to HIE processes with unprecedented motifs of pharmaceutical relevance. Of note, are the inclusion of challenging tetrazoles[75] and primary sulfonamides[74] as suitable directing groups, and the selective labelling of aldehydes at the formyl position.[77] Scheme 1.15 provides relevant examples of these second major developments within the Kerr group.

Even though many of the major developments in the realm of directed HIE were accomplished by investigations of Kerr and co-workers, some notable contemporaneous developments in the field warrants further discussion.

More specifically, research developed by Atzrodt, Derdau *et al.* led to the discovery of novel catalysts for efficient labelling of secondary and tertiary sulfonamides, and sulfonylureas.[119] During their investigation, they evaluated a commercially available catalyst **63**, previously developed by Burgess *et al.* for enantioselective hydrogenation of aryl alkenes,[120] and compared its activity to catalyst **60** across a total of 35 examples.[119] Notably, complex **60** displayed comparable or superior performance to **63** for most of the substrates tested, only being surpassed by the latter in the labelling of tertiary sulfonamides. Unfortunately, no attempt to investigate possible departures from the mechanism established by Kerr *et al.*[74] was performed, despite the authors' unsubstantiated allusion to a similar mechanistic rationale for HIE reactions with **63**.[119]

Then, in collaboration with Tamm *et al.*, a new iridium(I) catalyst **64** bearing an electron-rich *P*,*N*-bidentate ligand was developed,[121] displaying remarkable activity across a vast range of directing groups. Particularly interesting is the capacity to introduce hydrogen isotopes *ortho-* to poorly coordinating directing groups such as *O*-*tert*-butyl-*N*-aryl carbamates,[121] phenyl methyl ethers,[121] and phosphonamides.[122] Despite remarkable activity under typically mild reaction conditions, once again the authors did not investigate any mechanistic aspects involved in these processes. In a final contribution, the application of catalyst **60** in the HIE of aliphatic amides was disclosed.[123] Selected examples of this developments are illustrated in Scheme 1.16.

Tetrazoles
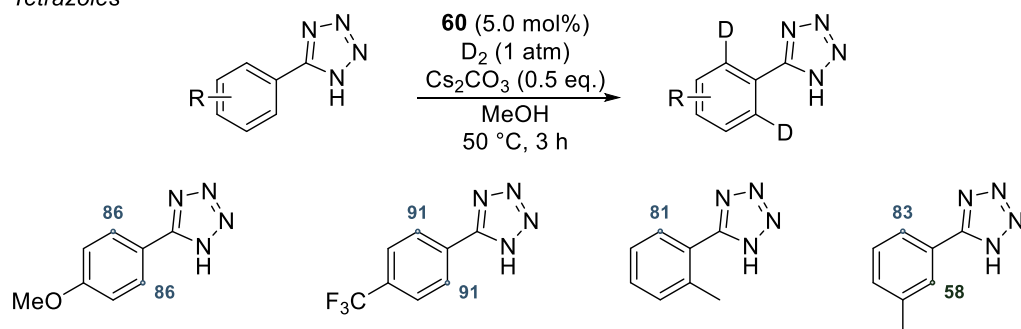
Sulfonamides
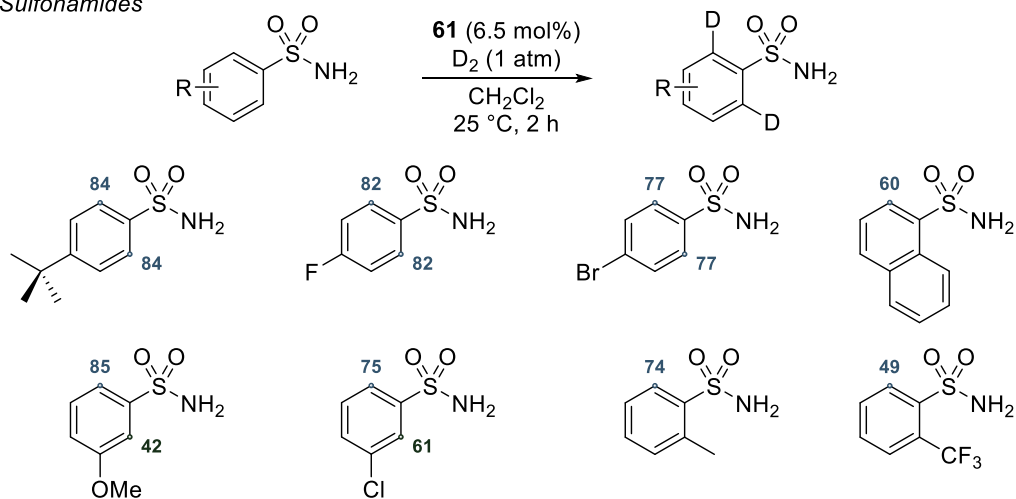
Aldehydes
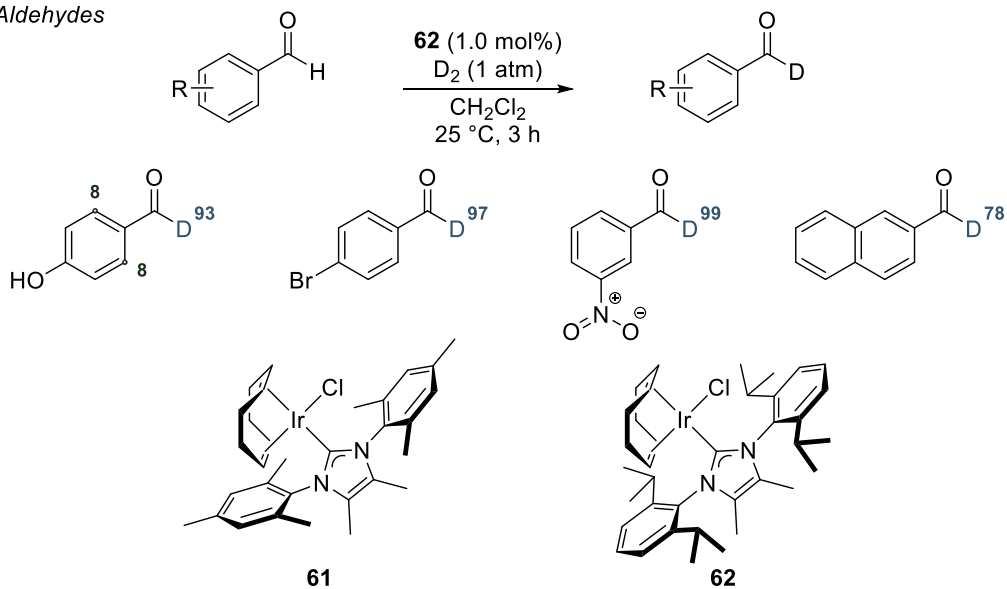
Scheme 1.15: Selected examples of novel iridium catalysts in HIE of challenging directing functionalities.[†75-77]

[†]Colour-coded positions indicate the deuterium incorporation determined by ^{1}H NMR spectroscopy.
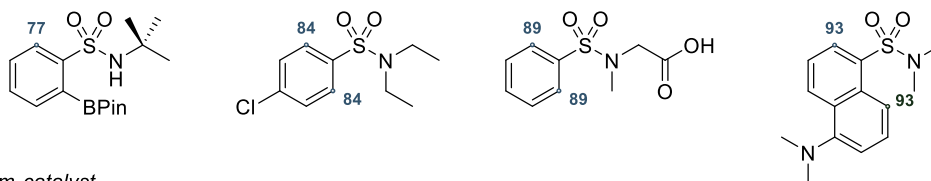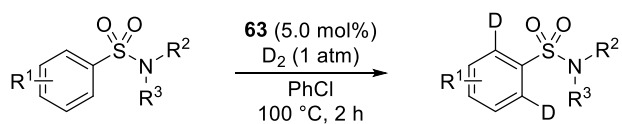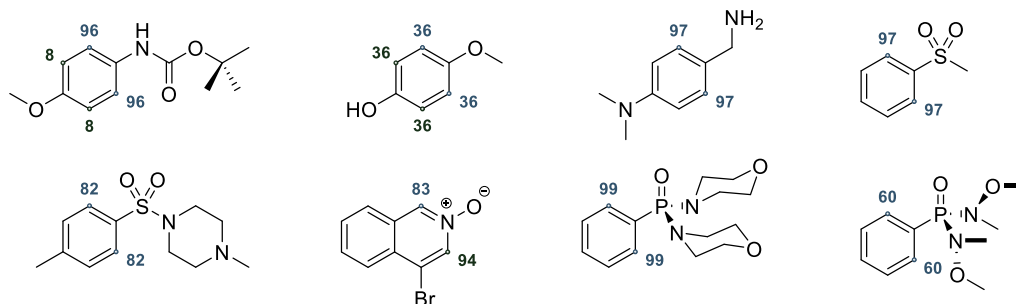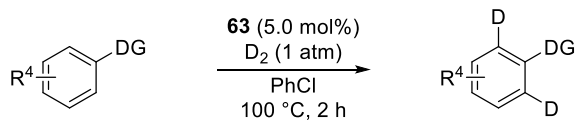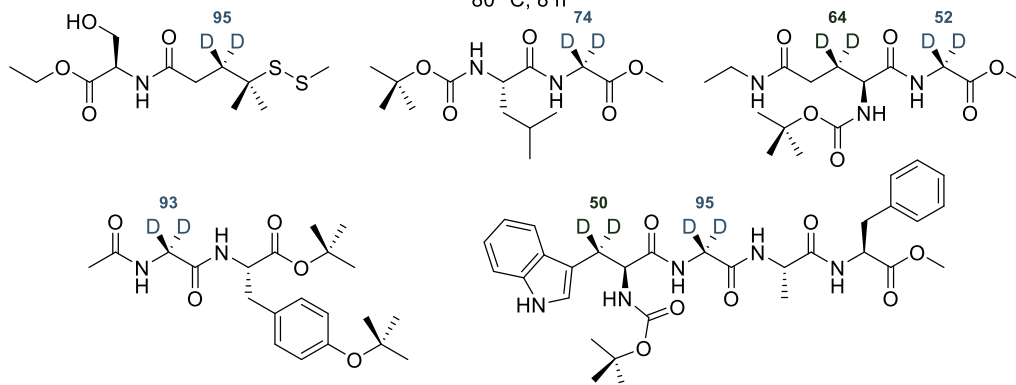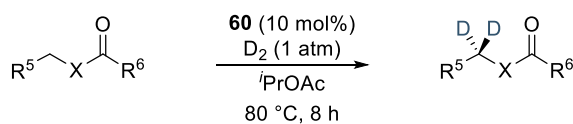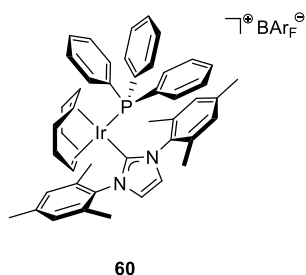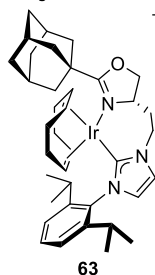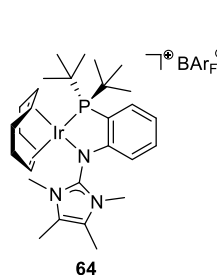
Scheme 1.16: Recent developments in HIE.[†][121-123]

[†]Colour-coded positions indicate the deuterium incorporation determined by ^{1}H NMR spectroscopy;

Finally, a set of contemporaneous noteworthy developments introduced by the research groups of Chirik, and MacMillan in collaboration with Hesk, contributed to diversify the nature of efficient transition metal catalysts for hydrogen isotope exchange,[124-126] as illustrated in Scheme 1.17.

Chirik *et al.* devised two novel iron and cobalt catalysts and assessed their activity in the undirected HIE of various aromatic substrates. In their first contribution, an iron(0) complex bearing an electron-rich *C,N,C*-tridentate ligand displayed remarkable activity on both deuteration and tritiation of simple aromatic molecules and drug motifs.[124] While the mechanism of this process remains unclear, catalyst **65** was highly selective towards C—H activation at C_{sp^2} centres, with orthogonal selectivity to that displayed by classical Ir catalysts, *i.e.*, no clear preference for introduction of isotopes *ortho-* to directing groups was observed.[124]

Furthermore, a second class of cobalt(II) catalysts bearing α-diimine ligands was also synthesised and explored in the HIE of simple aromatics.[125] Interestingly, cobalt complex **66** displayed high selectivity for isotope exchange at C_{sp^3} centres, which occur in a stereoretentive fashion, and differs from the innate preference of **65**.[124,125]

On the other hand, MacMillan *et al.* harnessed the unique capability of photocatalysts to generate radical intermediates to perform deuteration and tritiation of fully functionalised drug molecules, providing access to gram scale deuterated drug isotopologues, and their tritiated counterparts with high specific activity.[126] In their seminal work, the authors alternate between a standard iridium(III) photocatalyst **67** and an organic photocatalyst **68** as radical generators, and employ thiol **69** as additive to enable mild deuteration and tritiation protocols with D_2O and T_2O, respectively.[126] This process operates through a photo redox cycle which is akin to those well-established in the literature,[89] and delivers high levels of deuterium incorporation with appreciable preference for Csp^3 centres α- to amines. Remarkably, complex drug motifs such as (–)-Levofloxacin **79** and Azithromycin **80** were suitable substrates for HIE, which was accomplished with full retention of the stereochemistry at non-labelled positions.[126] Scheme 1.17 presents this last set of developments.
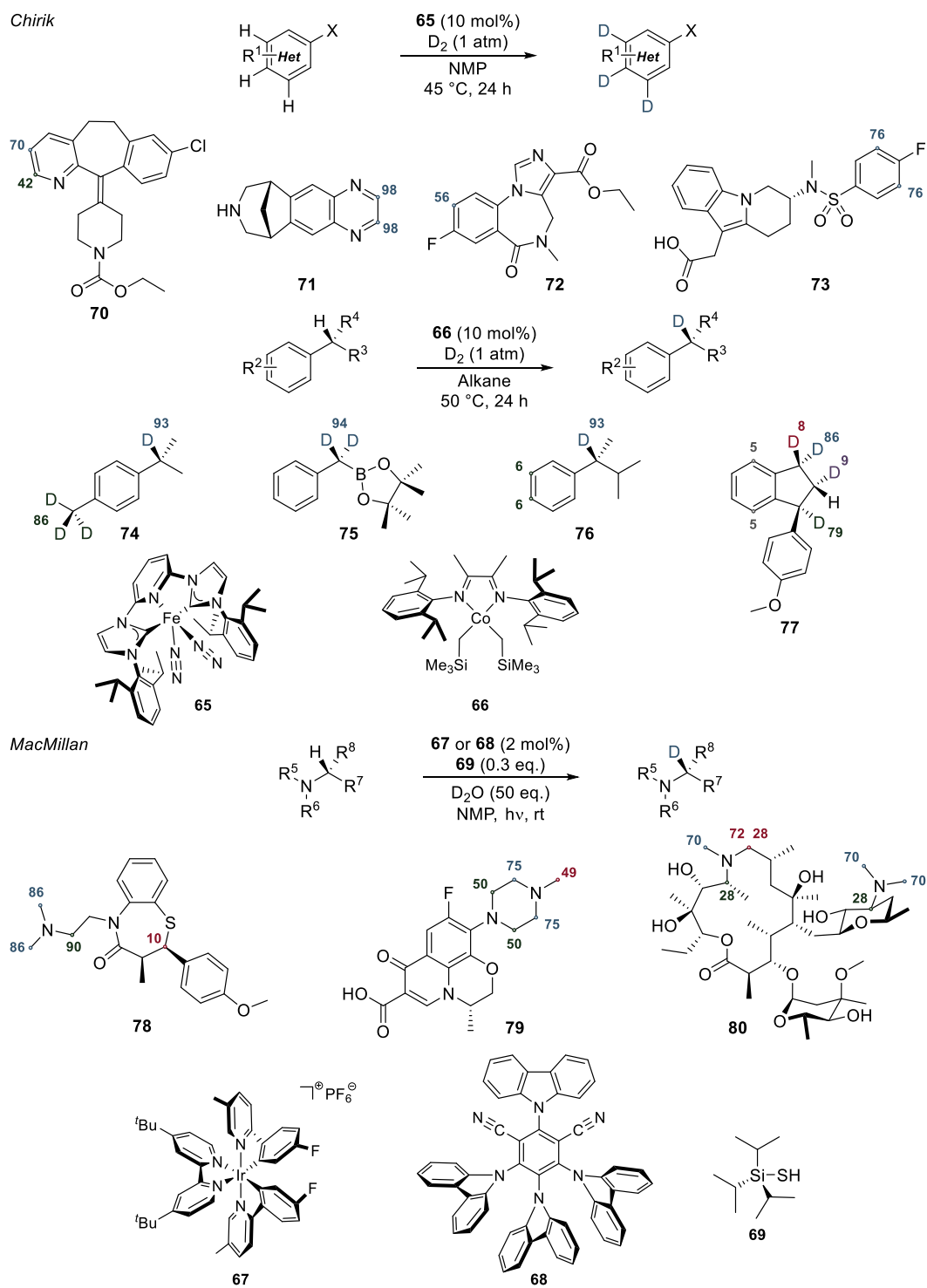
Scheme 1.17: Novel systems for HIE.[†][124-126]

[†]Colour-coded sites represent deuterium incorporation as an average for all exchangeable positions; for **80**, two diastereotopic protons were labelled to different extents.

During the course of the various investigations concerning directed HIE documented herein, some interesting trends could be determined:

i.   The use of coordinating solvents, such as methanol and tetrahydrofuran; or the presence of coordinating functionalities on the substrate, such as nitriles, alcohols, amines and pyridines; is detrimental to the process. Presumably, strong coordination to iridium precludes the de-coordination necessary to restart the catalytic cycle (*vide infra*);

ii.   In the presence of different directing groups, labelling can be observed in distinct sites with levels of incorporation depending on both the ability of the metal to interact with the directing functionalities, and on the thermodynamic stability of potential metallocycles generated during the process (*vide infra*);

iii.   Sterically demanding directing groups, such as sulfones and sulfonamides required higher catalyst loadings to promote deuterium incorporation, which is substantially inferior when compared to other directing functionalities. This recurrent issue can only be circumvented by accumulation of detailed mechanistic information and catalyst redesign.

1.3.2.1 Reaction Mechanism

A mechanism for the HIE reaction was initially postulated by Heys and co-workers in 1996,[127] based on spectroscopic[127] and crystallographic[128] data. Further contributions from Kerr and co-workers[70] with kinetic isotope effect (KIE) measurements and DFT studies corroborated those earlier findings, setting the mechanism depicted in Scheme 1.18 as a reference for typical directed HIE reactions. In this example, acetophenone **81** and catalyst **60** are employed to illustrate the fundamental steps involved in the conversion towards **81-*d*$_2$**.
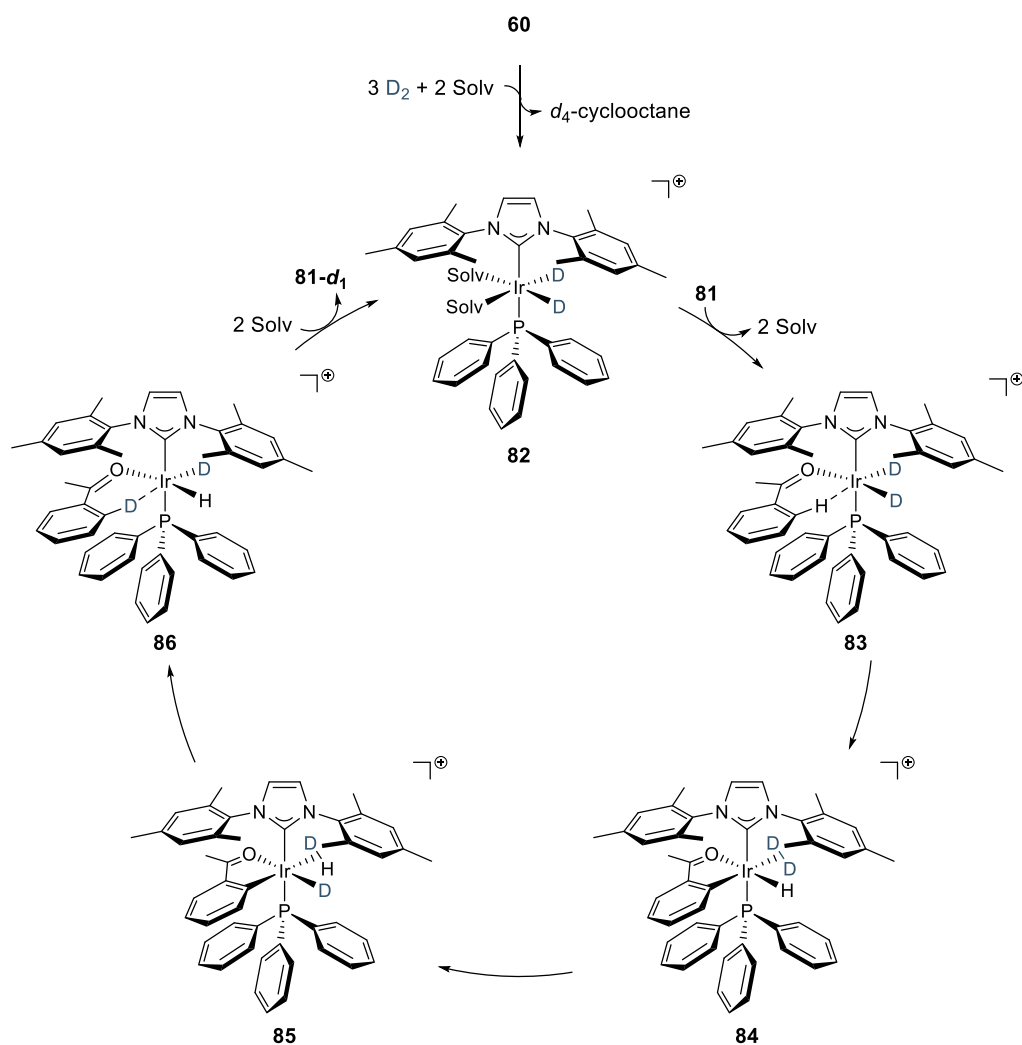
Scheme 1.18: Mechanism of the HIE reaction with substrate **81**.[70]

Thus, a rapid reduction of the coordinated cyclooctadiene[128] by exposure of precursor complex **60** to molecular deuterium leads to the formation of the iridium(III) deuteride **82**, which is the active species in the catalytic cycle.[127] Coordination of substrate **81** with concomitant dissociation of two solvent molecules leads to intermediate **83**, which is capable of undergoing activation of the agostically coordinated C—H bond to deliver the 5-membered metallocyclic intermediate **84**. Being a heptacoordinated species, complex **84** is expected to be highly fluxional.[129] Therefore, a fast and reversible exchange between the coordinated molecular deuterium and the metal hydride takes place to deliver **85**, which contains a deuteride *cis-* to the aryl portion of **81**. Subsequent C—D bond formation delivers intermediate

86 and produces the labelled compound **81-d_1**, whose de-coordination restores the catalytically active species **82**.[127]

Additionally, combined theoretical and experimental studies established two key features in the mechanism depicted in Scheme 1.18.[70] Firstly, engagement of the substrate *via* an agostic interaction with the C—H bond to be activated is necessary prior to the activation event. Secondly, despite the inherent promiscuity of iridium(III) hydrides to cleave C—H bonds through different processes (*cf.* Section 1.2.1), KIE data stipulated that a σ-bond metathesis[87] was operative for reactions with **60** and its congeners.[70] Thus, the entire process occurs at the same oxidation level, *i.e.*, intermediates **82 – 86** contain an Ir[III] centre, despite transition states which connect the pairs **83 – 84**, and **85 – 86** depicting an unmistakable Ir[V] character.[70]

Despite the apparent simplicity of the mechanism illustrated in Scheme 1.18, caution is advised whenever attempting to extend those conclusions to other systems. For instance, further investigations by Kerr *et al.* regarding the HIE of primary sulfonamides[74] and formyl- selective labelling of aldehydes[77] unveiled important factors that were not apparent from earlier studies.

More specifically, a delicate balance of stabilisation through different binding modes and activation energies of their respective C—H bond breaking events was postulated to account for the observed selectivity when employing catalyst **61** in the HIE of substrates bearing multiple directing groups.[74] In their study, a remarkable switch in preference for labelling sites was demonstrated in deuterations with complexes **15** and **61**. While the more sterically encumbered species **15** promoted effective isotope exchange directed through the pyrazole unit of the COX-2 inhibitor Celecoxib **87**,[130] with minimal level of incorporation *ortho-* to the sulfonamide moiety, catalyst **61** depicted reversed selectivity, providing excellent incorporation directed by the SO_2NH_2 group, with limited deuteration *via* interaction with the pyrazole unit.[74] This distinct selectivity arises from the difference in aggregated values for binding and C—H activation of **87** in reactions with **15** and **61**. Scheme 1.19 illustrates these findings.

Catalyst	Incorporation (%D)	
	D^1	D^2
15	16	95
61	97	11

$\Delta\Delta G_{Bind}{}^{88} = +13.1$
$\Delta\Delta G_{TS}{}^{88} = +0.6$

$\Delta\Delta G_{Bind}{}^{89} = +3.7$
$\Delta\Delta G_{TS}{}^{89} = +0.7$
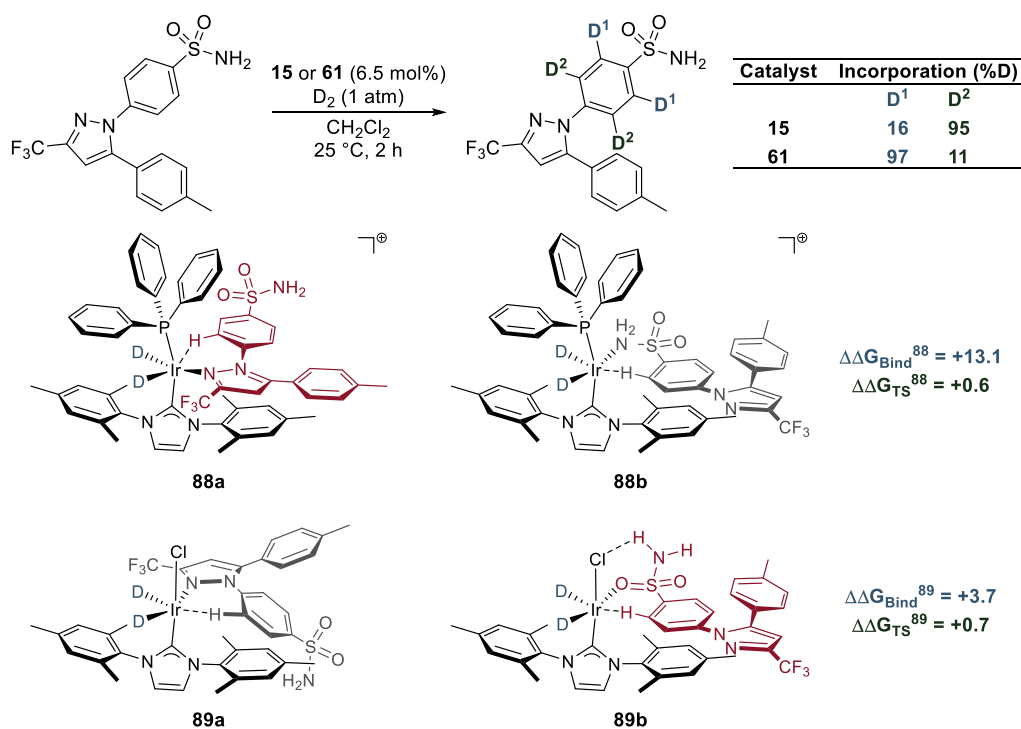
Scheme 1.19: Coordination modes and calculated energetic data for the HIE of **87**.[†74]

[†]Energies are given in kcal mol^{-1}; $\Delta\Delta G_{Bind}{}^Q = \Delta G_{Bind}{}^{Qb} - \Delta G_{Bing}{}^{Qa}$; preferred conformers shown in red.

Similarly, the selective introduction of deuterium at the formyl- position of aromatic aldehydes was found to proceed through an Ir^{III} → Ir^V → Ir^{III} cycle as opposed to the previously discussed σ-bond metathesis pathway.[77] DFT calculations employing benzaldehyde **90** as substrate and **62** as catalyst indicated this process is initiated by a (*C*, *H*)-κ^2-coordination of the formyl- hydrogen in **90**, delivering intermediate **91**. Subsequent C—H activation *via* oxidative addition produces Ir^V complex **92**, which undergoes facile H—D reductive elimination affording **93**. At this stage, free rotation of the η^2-(HD) ligand followed by its oxidative addition delivers a second Ir^V intermediate **94**, which possess a deuteride *cis-* to the formyl- group. A final C—D reductive elimination installs the label, forming complex **95**, and the catalytic cycle restarts with substrate displacement, consequently liberating **90-*d₁*.**[77] This unprecedented mechanism is illustrated in Scheme 1.20.
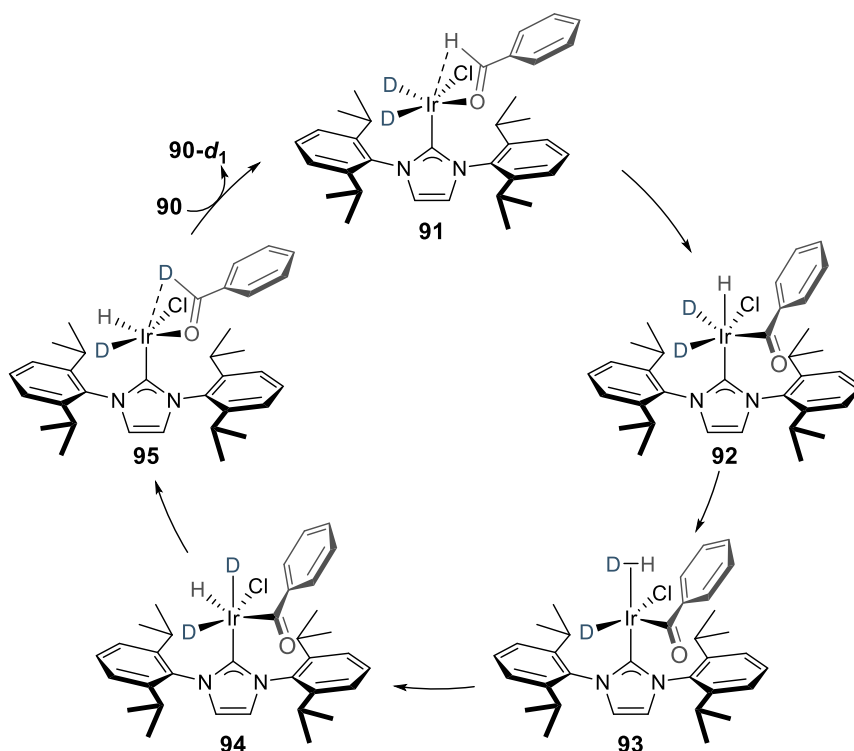
Scheme 1.20: Proposed mechanism for formyl- selective labelling of **90**.[77]

These examples illustrate the importance of conducting detailed mechanistic studies when assessing HIE reactions catalysed by Ir complexes. Additionally, since the original mechanistic proposal,[127] it was evident that the higher thermodynamic stability of a 5-membered metallacycle over a 6-membered one dictated the outcome of the HIE process. Thus, in the absence of severe steric hindrance in the coordinated substrate, a 5-membered metallocyclic intermediate (5-mmi) is preferred over a 6-mmi, therefore leading to higher deuterium incorporations *via* the former.[128] Scheme 1.21 illustrates this concept and present examples where this thermodynamic effect is observed.
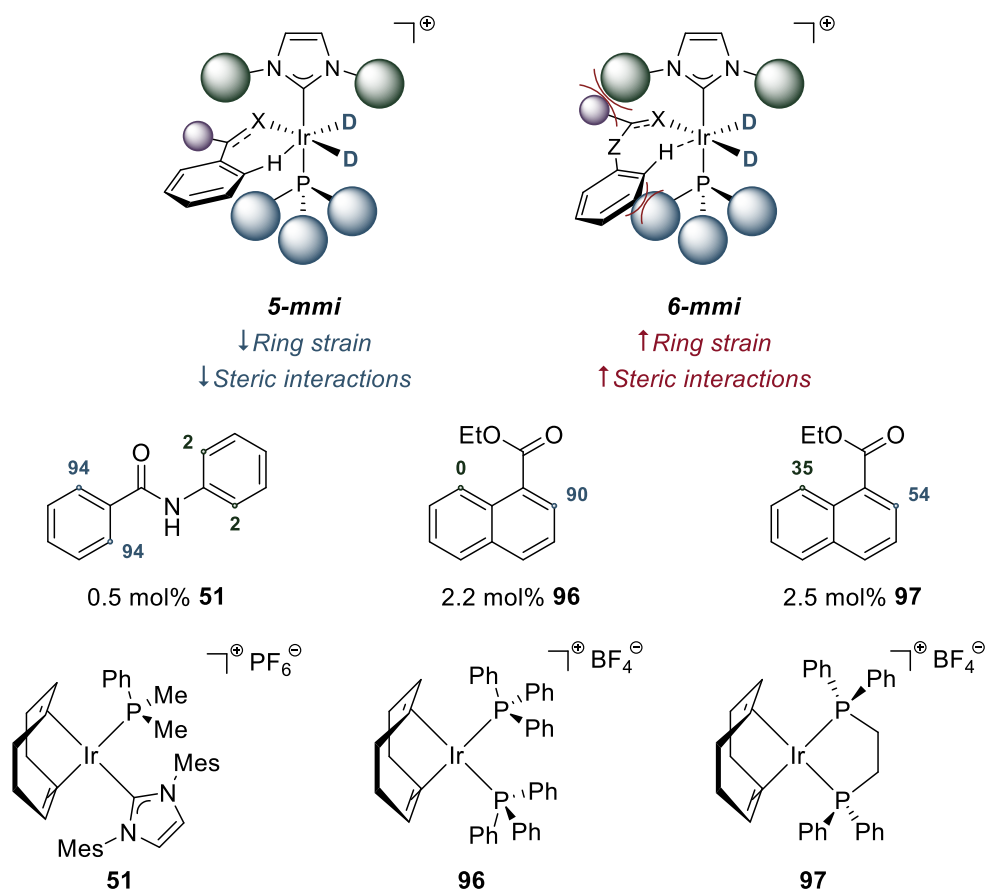
Scheme 1.21: Nature of metallocyclic intermediates and associated HIE results.[70,127,128]

Notably, catalysts **96** and **97** display remarkably different activity in the deuteration of ethyl 1-naphthoate. Whilst complex **96** is ineffective in labelling the substrate through a 6-mmi, **97** is able to perform this hydrogen isotope exchange.[127] In his seminal study, Heys demonstrated changes in selectivity when moving from mono- to bidentate phosphine ligands in a range of simple molecules. In addition, the activity of iridium complexes bearing chelating ligands was consistently smaller than their monodentate analogues. Table 1.2 summarises important observations for pre-catalysts **96** and **97**.[127]

Table 1.2: Catalytic activity of **96** and **97** in the HIE of several substrates.

98 99 100

101 102 103
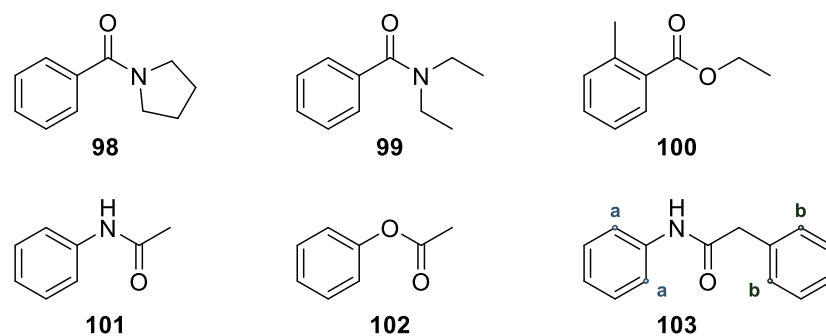
Entry	Substrate	Catalyst	Loading (mol%)	%D	ξ (mol$_D$ mol$_{cat}^{-1}$)†
1	98	96	1.9	55	58.4
		97	2.2	72	65.5
2	99	96	1.9	3	3.2
		97	2.2	67	60.4
3	100	96	1.6	67	41.9
		97	1.9	14	7.4
4	101	96	1.5	11	14.7
		97	1.7	77	90.6
5	102	96	35	< 1	< 0.1
		97	38	69	3.6
6	103	96	4.6	2.4[a] < 0.1[b]	2.1 —
		97	5.4	40[a] 44[b]	29.4 32.7

†ξ – incorporation activity over selected site. Calculated as mol D (loading)$^{-1}$.

A brief analysis of ξ values calculated from reported data[127] demonstrates a stark difference in the activities of **96** and **97**. Thus, substrates possessing steric encumbrance in the vicinity of the coordinating atom (entries 1 and 2) are more effectively labelled by catalyst **97**, whereas **96** is more efficient towards the ester **100**, where the steric hindrance at the phenyl ring bears little influence in the deuteration process (entry 3). Additionally, in all cases where a 6-mmi is implicated (entries 4 – 6), catalyst **97** is more active than **96**. These observations can be rationalised in terms of repulsive steric interactions which are ubiquitous in transition metal catalysed processes,[8] influencing the thermodynamic stability of differently sized metallacycles. Scheme 1.22 illustrates this concept with **99** and **101** as representative examples.
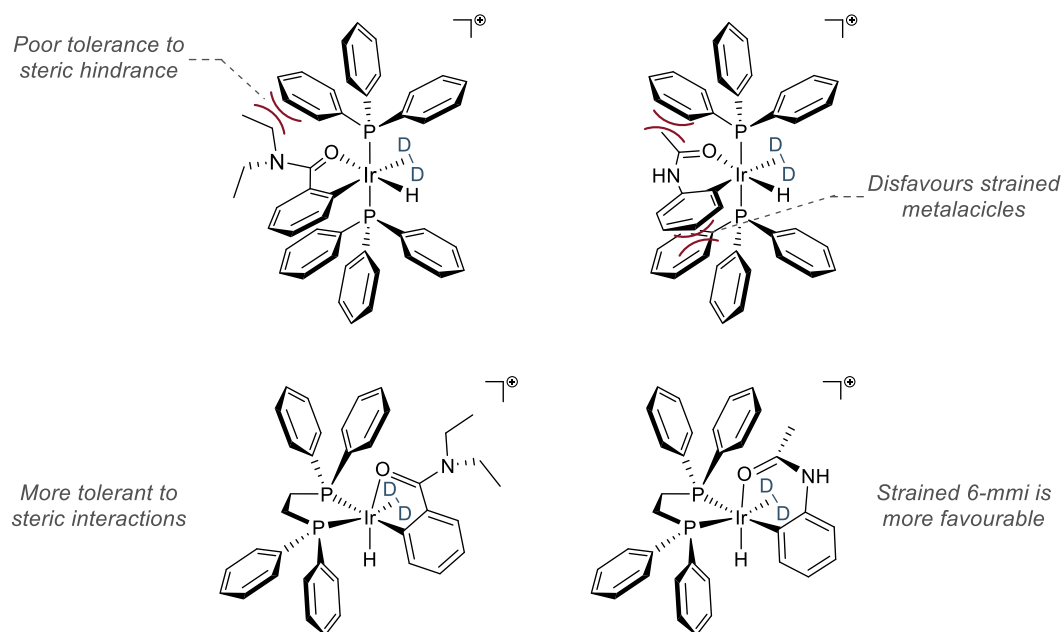
Scheme 1.22: Steric factors in metallacycle intermediates

Finally, it is worth noting that, apart from the detailed mechanistic studies devised to evaluate several HIE processes reported by Kerr *et al.*,[71,74,77] there is a lack of similarly meticulous investigations probing chelating ligands, with most authors assuming a direct correspondence to the well-established pathways discussed herein.

1.3 *N*-Heterocyclic Carbenes and Phosphines as Ligands

One of the most important advances in ligand synthesis during the last two decades was the isolation of a stable *N*-heterocyclic carbene (NHC) by Arduengo and co-workers in 1991.[131] Since then, many variations on this versatile ligand have been reported. Scheme 1.23 presents a small collection of these coordinating groups, featuring the diversity of structural motifs possible to attach to the heteroatoms within the 1,3-diazacyclopentane core.[131-133]
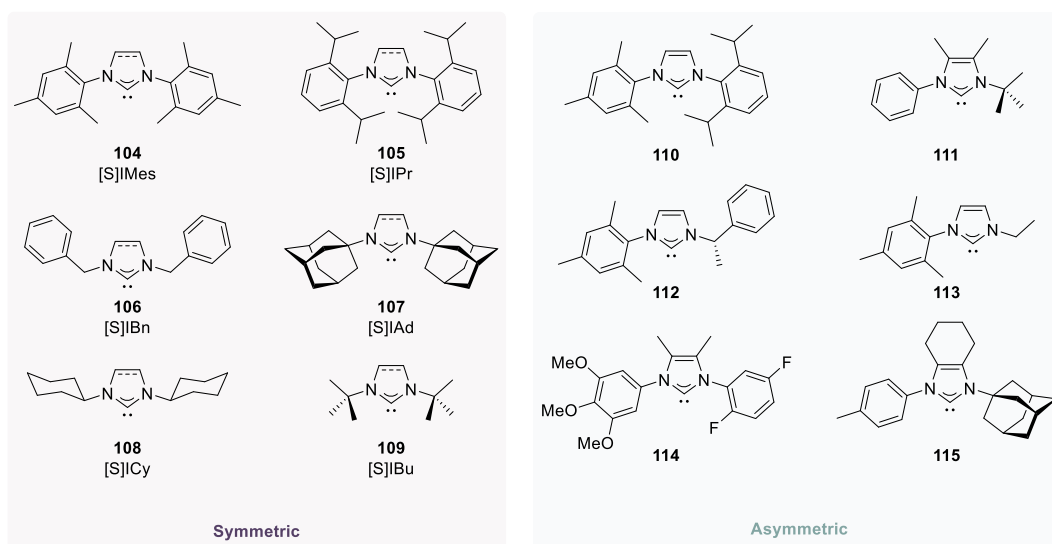
Scheme 1.23: Selected examples of NHC ligands.[131-133]

Evidently, the potential to access structures bearing diverse substituents makes NHCs very attractive from an organometallic chemistry point of view, for steric parameters can be finely tuned to impart the desired effect on a given metal centre. Notwithstanding these observations, NHCs also possess unique electronic properties due to the existence of a semi-filled orbital of π-symmetry on the carbenic carbon, whose occupancy depends on the extent of donation from the nitrogen atoms on the heterocyclic backbone.[134] Scheme 1.24 illustrates the electronic interactions present in a typical NHC, and expected interactions upon coordination to a metal centre.[134,135]
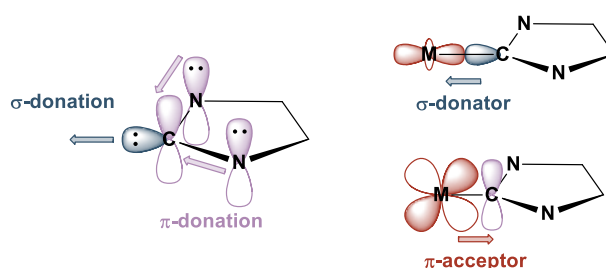
Scheme 1.24: Simplified representation of electronic effects of NHC ligands.[134,135]

Hence, *N*-heterocyclic carbenes act as strong σ-donors through the lone pair at the carbenic carbon (assuming a singlet as the electronic ground state).[134] Moreover, the semi-filled π orbital at the carbon centre can accept electron density from the metal, thus acting as a π-acceptor, as implied by the Dewar-Chatt-Duncanson model.[94,95]

Furthermore, the exact nature of the NHC-metal bond intrinsically depends on both fragments, *i.e.* the carbene and the metal to which it is coordinated.[136,137]

Another important factor that contributes to the success of NHCs in catalysis is the existence of several different routes to their parent azolium salts, which are deprotonated to generate the free carbene.[138]

On the other hand, phosphines are historically prominent in organometallic complexes, remaining one of the most versatile classes of ligand.[8,10] Their synthesis can be readily accomplished from reactions between phosphorus trichloride and an appropriate main group organometallic reagent. Moreover, since phosphorus can be bonded to three different substituents and possesses an inversion barrier much higher than that of amines, phosphines can be chiral at the phosphorus atom. In addition to these features, structural motifs can be envisaged in which two or more coordinating atoms are tethered together, thus acting as chelating ligands to metals.[8,10] Scheme 1.25 presents some examples of these extremely versatile ligands.[10,139-141]
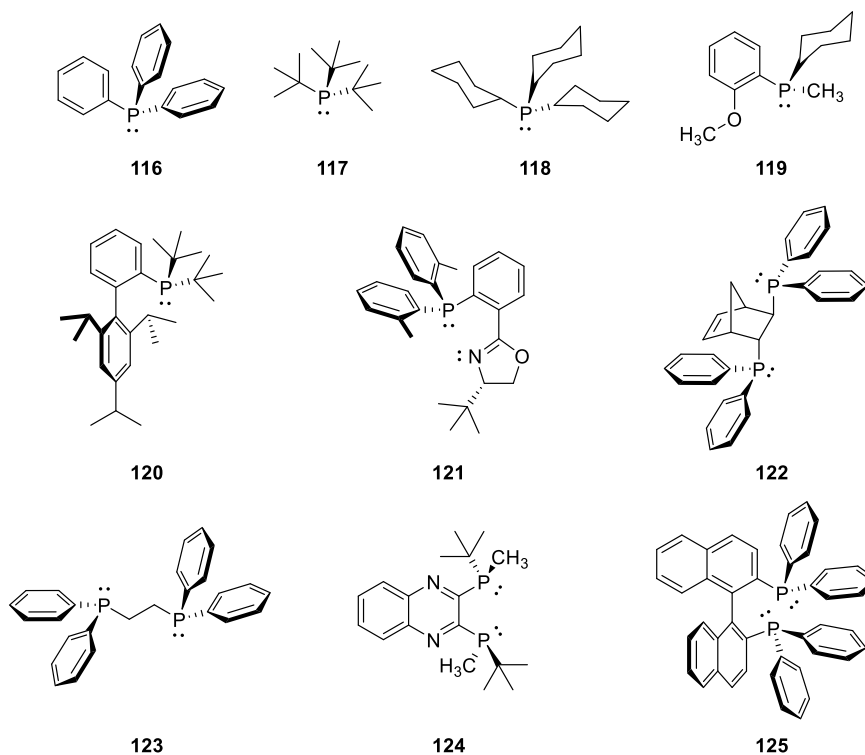
Scheme 1.25: Examples of well-established phosphine ligands.[10,139-141]

As previously described for NHCs, phosphines are also able to act as σ-donors and π-acceptors. Additionally, being a third-row element, phosphorus gives rise to soft

coordinating ligands whose electron-donating abilities and steric factors can be practically varied at will.[141] Scheme 1.26 elucidates these features.
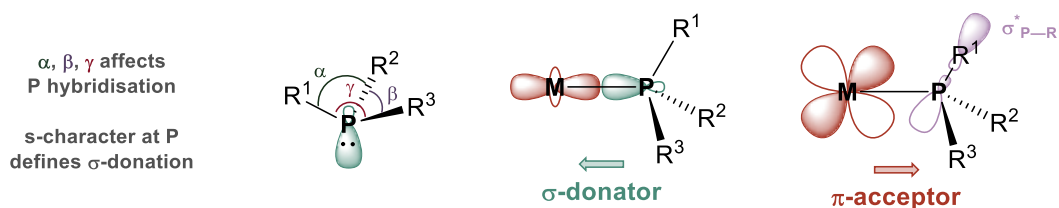
Scheme 1.26: Depiction of electronic effects associated with phoshpines.[142]

Notably, and differing from NHCs, which present a rigid N—C—N coordinating moiety, phosphines are subject to variation of their electronic parameters due to geometrical distortion caused by their substituents,[142] thus introducing another possibility for controlling their electronic properties.

1.3.1 Steric Parameters

Initially intended as substitutes for commonly-used phosphines,[138] for which evaluation of steric parameters is well-established (*vide infra*), analysis of the steric hindrance imposed by NHCs is more demanding. Scheme 1.27 illustrates geometrical features of both ligands and demonstrates the notable difference of these coordinating moieties.
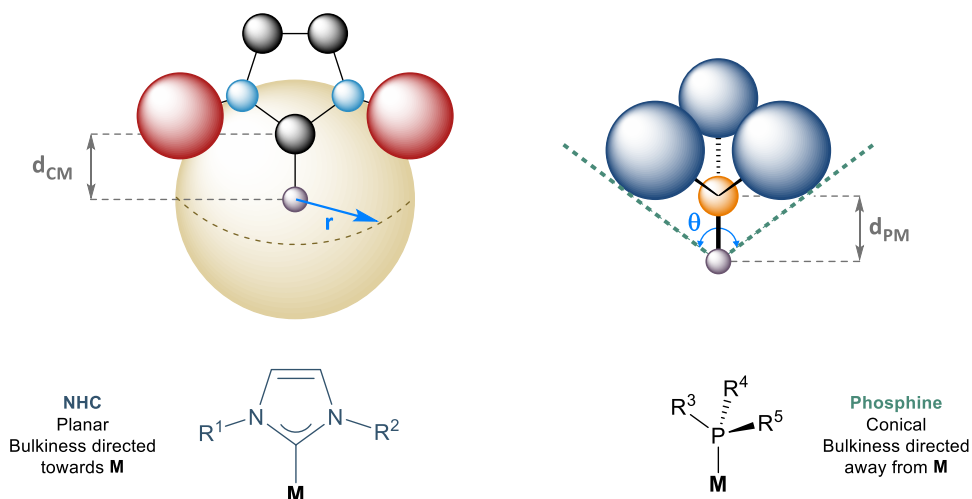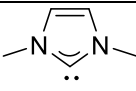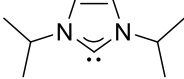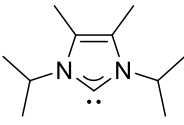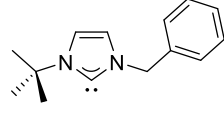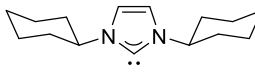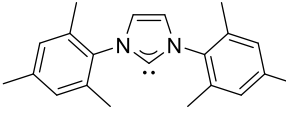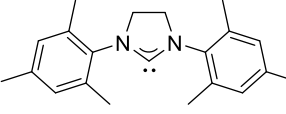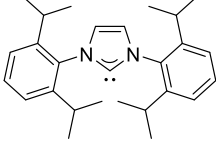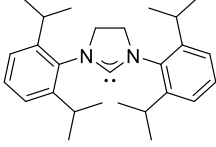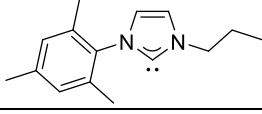
Scheme 1.27: Steric parameters inherent to NHC (*left*) and phosphine (*right*) ligands.[†]

[†]d_{XY} – distance between atomic centres X and Y; r – radius of hypothetical sphere; θ – cone angle.

Therefore, given their planar shape, imidazolium ligands cannot be directly compared to phosphines. Recognising this difficulty, Cavallo *et al.* developed a method to calculate steric parameters of *N*-heterocyclic carbenes.[143] Thus, by comparing the volume occupied by atoms in the NHC contained in the first coordination sphere of a putative metal centre with the total spherical volume (r in Scheme 1.27), it is possible to define the Percent Buried Volume ($\%V_{Bur}$).[143] This parameter directly reflects the steric encumbrance imparted by the coordinated carbene. Subsequently, Clavier and Nolan employed the $\%V_{Bur}$ method to evaluate steric parameters of various NHCs and phosphines when coordinated to transition metals, with special focus placed on organometallic complexes of Au(I).[144] In this seminal work, the authors evaluate around 700 crystal structures of complexes bearing NHCs and phosphines with the $\%V_{Bur}$ model and determine a reasonable correlation between values calculated for phosphines and the well-established Tolman cone angle (*vide infra*).[144,145] Additionally, changes of $\%V_{Bur}$ and the coordinating geometry of the parent complex are well evidenced, revealing the flexible nature of *N*-heterocyclic carbenes. Table 1.3 presents selected examples of $\%V_{Bur}$ in complexes of the type **L**AuCl.[144]

Table 1.3: Steric parameters of selected NHC ligands.[144]

Entry	Ligand	$\%V_{Bur}$ (d = 2.00 Å)	$\%V_{Bur}$ (d = 2.28 Å)
1		26.3	22.7
2		27.4	23.5
3		38.4	33.9
4		33.0	28.8
5		27.4	23.5
6		36.5	31.2
7		36.9	31.7
8		44.5	39.0
9		47.0	41.5
10		33.3	28.6

Some interesting trends can be observed from the data summarised in Table 1.3:

i. Increase in the steric hindrance on alkyl *N*-substituents expectedly leads to higher $\%V_{Bur}$ values, as suggested in entries 1, 2 and 5;

ii. Entries 2 and 3 demonstrate that addition of methyl substituents on the imidazole backbone can promote a significant increase in steric hindrance;

iii. The reduction of the heterocyclic double bond does not result in changes in %V$_{Bur}$ for [S]IMes (entries 6-7), however, a significant difference is observed for [S]IPr (entries 8-9);

iv. Steric factors in asymmetric imidazoles are dominated by the bulkiest *N*-substituent, as evidenced in entries 4 and 10;

Phosphines, on the other hand, possess a characteristic conical shape which lends itself to well-defined steric parameters, historically described by the model developed by Tolman.[145] In his evaluation of steric hindrance, Tolman constructed three-dimensional physical representations of phosphorus compounds in order to measure structural features of a wide variety of ligands, and correlate such data with kinetic and thermodynamic parameters. After comprehensive evaluation, Tolman found the internal angle of an imaginary cone that touches the outermost van der Waals *radii* of the substituents on phosphorus to be the most representative steric factor.[138]

Given the simplicity of his model and its surprising predictive capacity, the so-called Tolman cone angle, θ, is a reference in steric evaluations of phosphine containing organometallic complexes. Table 1.4 summarises values for representative phosphorus ligands along with corresponding percent buried volume.[138,144]

Table 1.4: Cone angle and buried volumes for selected phosphines.[138,144,145]

Entry	Ligand	θ (°)	%V_{Bur}
1		87	—
2		121	47.0 (23.5)[a]
3		125	51.4 (25.7)[a]
4		127	52.2 (26.1)[a]
5		128	36.5[b]
6		145	34.8[b]
7		157	—
8		170	38.8[b]
9		184	43.9[b]
10		194	44.8[b]

[a] %V_{Bur} in (**L—L**)PdCl$_2$ complexes, half-volume value in parenthesis; [b] %V_{Bur} in **L**AuCl complexes.

Some interesting features arise from inspection of Table 1.4. Firstly, the steric hindrance of chelating phosphines (entries 2 – 4) increases with extension of the tether length. Owing to Tolman's method,[145] only the half buried volume of the entire ligand, in parenthesis, is directly comparable to θ.[144] Secondly, despite the series being reasonably consistent in terms of steric factors, with both θ and %V_{Bur} increasing with more sterically encumbered substituents on the phosphorus centre,

triphenylphosphite, entry 5, represents a clear outlier. This value is a consequence of Tolman's method, which is believed to underestimate cone angles for more flexible groups attached to phosphorus.[144] Finally, the applicability of the buried volume model to phosphines represents a milestone in evaluation of steric parameters, for it allows for a more localised and precise steric assessment and also provides figures which are directly comparable to those obtained for NHCs.[144]

Notwithstanding its potential to evaluate steric factors, this method relies on static molecular geometries and is affected by the limitation therein introduced, namely: it is unable to account for subtle changes in the coordination sphere, for instance, those introduced by the existence of rotamers. Solution behaviour is, therefore, neglected, and different geometries around the coordination sphere might lead to the assignment of practically indistinguishable steric parameters for electronically distinct species.

1.3.2 Electronic Parameters

As depicted in Scheme 1.28, the electronic interactions between *N*-heterocyclic carbenes and transition metals are of a complex nature. Additionally, as demonstrated by Tantarelli and Zuccacia *et al.*,[136,137] interactions with NHCs and metals of the third transition series are even more complicated due to substantial overlap between the valence orbitals of the metal and those from the NHC. For instance, Zuccacia *et al.* demonstrated that an NHC coordinated to a neutral Au(I) complex acts as a good σ-donor with a capacity to accept back-donation through orbitals of π symmetry; whereas the same ligand attached to a cationic AuCO fragment acts exclusively as a σ-donor.[137] These observations point to the electronic versatility of NHCs, and restate the necessity of taking into account all ligands in the coordination sphere prior to describing electronic parameters in any given transition metal complex.

Thus, when attempting to quantify electronic parameters of NHCs, the most commonly employed method relies on the stretching frequency (υ_{CO}) of the CO ligands in organometallic complexes of the type $(NHC)\mathbf{M}(CO)_n$. The so-called Tolman Electronic Parameter (TEP)[145] constitutes a relative scale in which the υ_{CO} of a ligand $\mathbf{L}$ in the complex $\mathbf{L}Ni(CO)_3$ is taken as a direct measurement of the ability
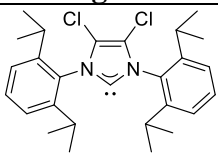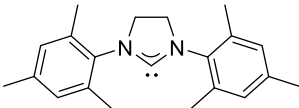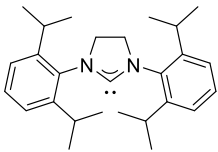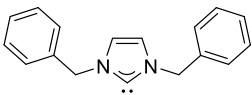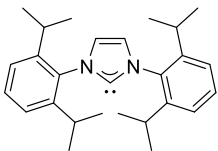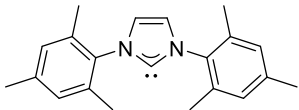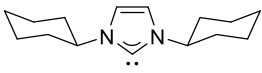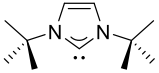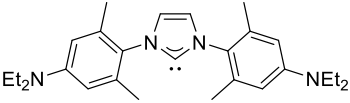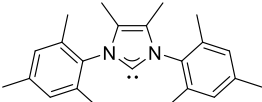
of **L** to donate electrons to the metal centre. Such a phenomenon is straightforwardly interpreted in terms of the Dewar-Chatt-Duncanson model: as the electron donating ability of **L** increases, the metal becomes more electron rich, thus enhancing the π back donation M $\rightarrow$ CO, responsible for populating the π^*_{CO} orbital. This back donation then leads to a weakening of the C$\equiv$O bond, which is readily detected by a corresponding decrease in υ_{CO}. Owing to the extreme toxicity of Ni(CO)$_4$, precursor in the synthesis of **L**Ni(CO)$_3$ complexes, Nolan *et al*. developed an alternative system for the evaluation of TEP values in which complexes of the type **L**Ir(CO)$_2$Cl replace the correspondent nickel analogues.[146]

Scheme 1.28 illustrates a generic example of donation and back-donation in metal carbonyl complexes, and Table 1.5 presents some relevant NHC examples in order of increasing electron donation.[146,147,149]
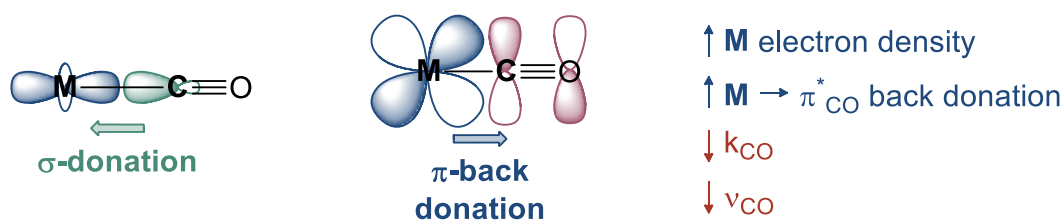
Scheme 1.28: Prototypical example of the Dewar-Chatt-Duncanson model.[94,95]

Table 1.5: Stretching frequencies and TEP values for selected NHC motifs.[146-149]

Entry	Ligand	$\upsilon_{CO}{}^{Ni}$ (cm^{-1})[a]	$\upsilon_{CO}{}^{Ir}$ (cm^{-1})[b]	TEP (cm^{-1})
1	(structure with Cl, Cl substituents)	—	2028.3	2055.1
2	(structure)	2051.5	2024.6	2050.8
3	(structure)	2052.2	2024.6	2050.8
4	(structure)	—	2024	2050.3
5	(structure)	2051.5	2023.9	2050.2
6	(structure)	2050.7	2023.1	2049.6
7	(structure)	2049.6	2023	2049.5
8	(structure)	—	2022.3	2048.9
9	(structure with Et$_2$N, NEt$_2$ substituents)	—	2021	2047.8
10	(structure)	—	2019.8	2046.7

[a] υ_{CO} of A$_1$ symmetry in **L**Ni(CO)$_3$; [b] average of observed υ_{CO} values in **L**Ir(CO)$_2$Cl.

As demonstrated in Table 1.5, the electron donating ability of NHCs is quite invariant, with TEP values spanning a range of only 8.4 cm^{-1} across a series which displays substantially distinct structural motifs. Interestingly, the ubiquitous ligands SIMes and SIPr (entries 2-3) are essentially indistinguishable in electronic terms, whereas their unsaturated counterparts (entries 5-6) are also very similar. Moreover,

it is noted that the electron-donating ability of NHCs is significantly affected when substitution on the backbone is introduced. For instance, addition of two electron-withdrawing chlorines on IPr (entries 1 and 5) promotes significant reduction in the donating ability of this NHC, whereas attachment of electron-donating methyl substituents on IMes (entries 6 and 10) has a pronounced and opposite effect.

Finally, it is interesting to note that NHCs are generally more electron donating than the most σ-donating phosphines, *e.g.*, P^{t}Bu$_3$ possesses a TEP of 2056.1 cm^{-1},[145] which is higher than the figure for even the most electron-poor NHC on Table 1.5, demonstrating the electron rich nature of the NHC—M interaction.

Substantially more studied than NHCs, the electronic properties of phosphorus ligands were also a focus of Tolman's research, which defined and determined the TEP model (*vide supra*) to describe electronic effects on phosphorus ligands.[138] Table 1.6 summarises TEP values for representative ligands.

Table 1.6: TEP values for selected phosphines.[145]

Entry	Ligand	TEP (cm^{-1})
1	P(O^{i}Pr)$_3$	2075.9
2	PHPh$_2$	2073.3
3	PPh$_3$	2068.9
4	PMePh$_2$	2067.0
5	P(o-Tol)$_3$	2066.6
6	P(CH$_2$Ph)$_3$	2066.4
7	PMe$_2$Ph	2065.3
8	PMe$_3$	2064.1
9	PEt$_3$	2061.7
10	PCy$_3$	2056.4
11	P(^{t}Bu)$_3$	2056.1

As expected in terms of inductive effects of organic substituents,[150] the TEP value decreases with increasing electron density over the phosphorus atom. Additionally, simple evaluation of the Walsh diagram for the deformation of a planar structure of D$_{3h}$ symmetry to a pyramid of C$_{3v}$ symmetry[142] allows one to predict an increase in electron donating ability for phosphines featuring larger cone angles. This ultimately results in the inseparable nature of steric and electronic parameters in phosphorus ligands, which is a well-recognised issue in catalysis.[151]

Moreover, it is important to note that, despite efforts in quantification and establishment of predictive models that account for steric and electronic parameters in metal complexes, the evaluation of chelating ligands has been mainly overlooked, presumably due to their intricate behaviour in organometallic complexes. A notable exception can be found in a second generation of algorithms devised to evaluate buried volume. More specifically, Cavallo *et al.* improved the method for analysing steric parameters in ligands and generalised their original findings to encompass a large variety of spatial environments around transition metals, including chelating ligands and enzymatic pockets.[152] This advance in parametrisation represents a major development in the field, for it allows for direct comparison of strikingly different binding motifs under a unique theoretical framework.[152]

1.4 Phosphine-Functionalised *N*-Heterocyclic Carbenes

Owing to their relatively short history in catalysis, the development of functionalised *N*-heterocyclic carbenes still lags well behind the existing chemistry of phosphorus ligands.[141] Notably, the usually harsh conditions employed to construct C—P bonds through S_N2 substitutions on halophosphines, which generally requires the use of Grignard or organolithium reagents as carbon nucleophiles,[141] is incompatible with the acidic nature of azolium salts.[153] On the other hand, the inherent basicity of dialkyl phosphides[154] imposes a second challenge to routes targeting the coupling between an NHC and a phosphine.

Thus, perhaps unsurprisingly, the development of NHC-*P* ligands is still in its early stages. Scheme 1.29 summarises the main classes of these cheating ligands reported to date, providing relevant examples.[153-159]
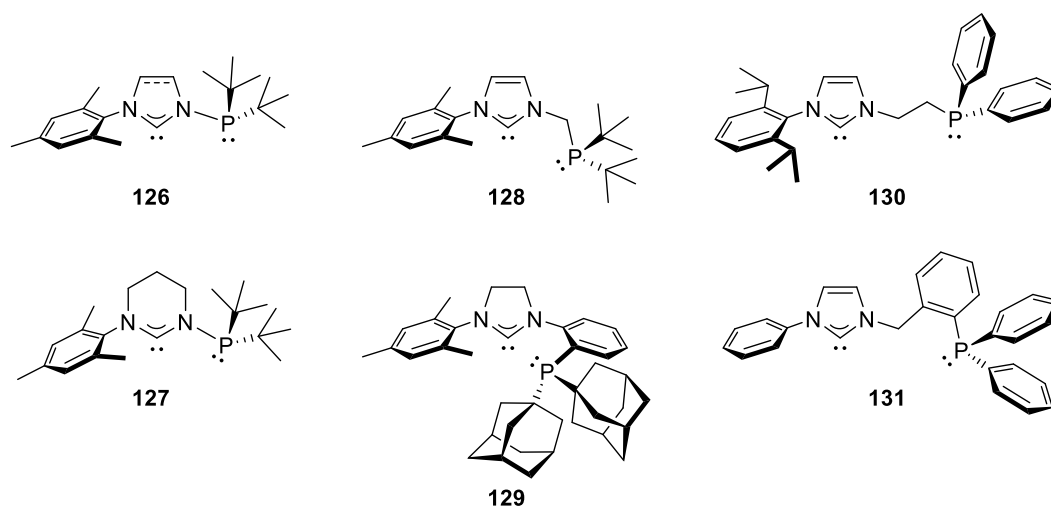
Scheme 1.29: Examples of reported NHC-*P* ligands.[153-159]

In the context of Ir(I) complexes for HIE, some important features of these ligands are described below, which are also illustrated in Scheme 1.30:

i.   Combination of both NHC and phosphine in the same motif leads to an ancillary ligand which displays both strong σ-donation and good π-acceptor abilities;

ii.   Being tethered, the ligand will occupy coordinating sites *cis*- to each other in an octahedral geometry, thus altering both the steric interactions and the electronic properties of the metal centre;[8,142]

iii.   Oxidative addition of a symmetric substrate into a square-planar complex will produce a mixture of isomeric structures, whose stability and reactivity are strictly dependent on the nature of the incoming substrate and the *C*- and *P*-substituents on the ligand.[8]
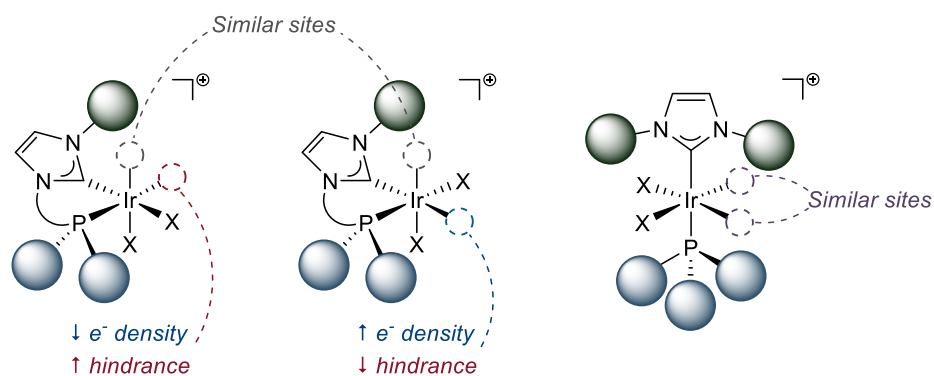
Scheme 1.30: Electronic and steric differences among ligand classes.[†]

Of special interest is the system reported by Labande, Poli and co-workers,[157] which are structurally related to ligands of type **130**. Containing a flexible ethylene bridge, this specific class of ligands is expected to display unique properties when compared to the other systems from Scheme 1.29. Since their unconstrained tether allows for easier geometric rearrangement around a metal centre, ligands akin to **130** would be expected to aid transformations in which high steric encumbrance is involved in the coordination sphere during catalysis. Exploring these premises, initial studies in the Kerr group has focused on the synthesis of iridium complexes bearing ligands of this kind, and their application in HIE processes involving sterically demanding substrates, as summarised in Scheme 1.31.[160]
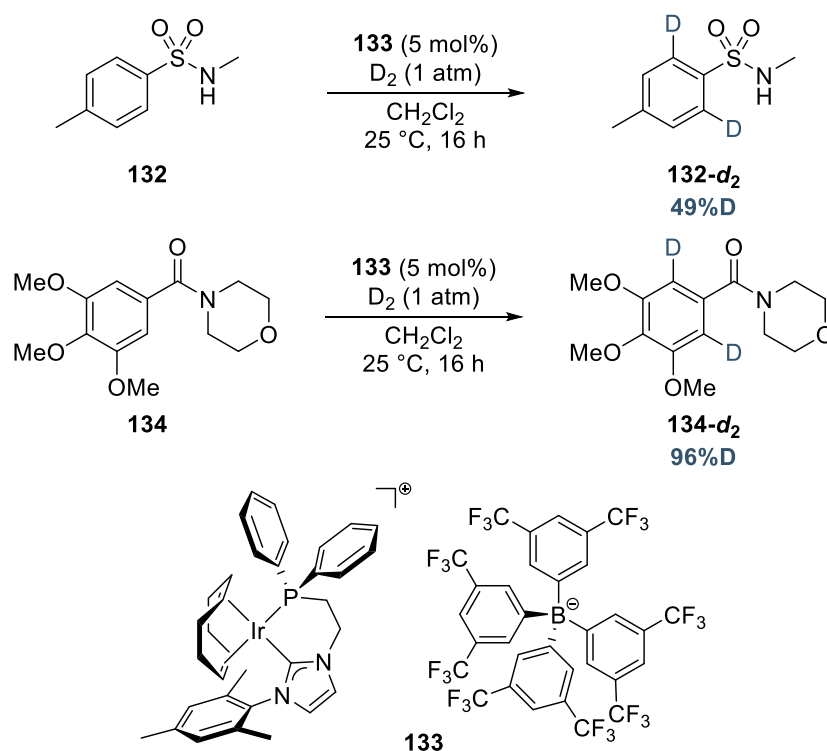
Scheme 1.31: Demonstration of catalytic activity for HIE with complex **133**.[160]

Notably, the sterically hindered labelling sites in trimetazone **134**, which also possess four competing coordinating oxygen atoms in its structure, were effectively accessed by catalyst **133**. In addition, the sulfonamide was able to act as a directing group for

this iridium complex, demonstrating its applicability on more challenging tetrahedral systems.

Interestingly, previous theoretical investigations within the Kerr group unveiled an elegant and comprehensive model which addresses the application of iridium complexes to HIE reactions (*vide infra*).[160] Then, by combining the determination of geometrical features and energetic data of iridium(III) dihydride complexes, and their respective adducts with organic substrates suitable for the isotope exchange process, a model was devised to probe the reaction profile of such catalysts and their probability of succeeding in HIE.[160]

An extensive *in silico* evaluation of more than 70 systems by DFT, and their detailed examination employing the buried volume model to assess steric hindrance on iridium complexes featuring methyl phenylsulfone as a molecular probe was then performed. Subsequent correlation of these parameters with the amount of energy released upon coordination of the substrate to the corresponding iridium(III) fragment — the binding energy[148] — led to a set of chelating systems with a favourable energetic profile, which could be employed in HIE of these poorly active substrates.[160] Scheme 1.32 illustrates the best NHC-P ligands uncovered by this theoretical design.

135a
ΔE_{bind} = -29.5

135b
ΔE_{bind} = -27.5

135c
ΔE_{bind} = -24.9

135d
ΔE_{bind} = -27.8

135e
ΔE_{bind} = -31.6

135f
ΔE_{bind} = -27.4

135g
ΔE_{bind} = -27.4

135h
ΔE_{bind} = -27.8
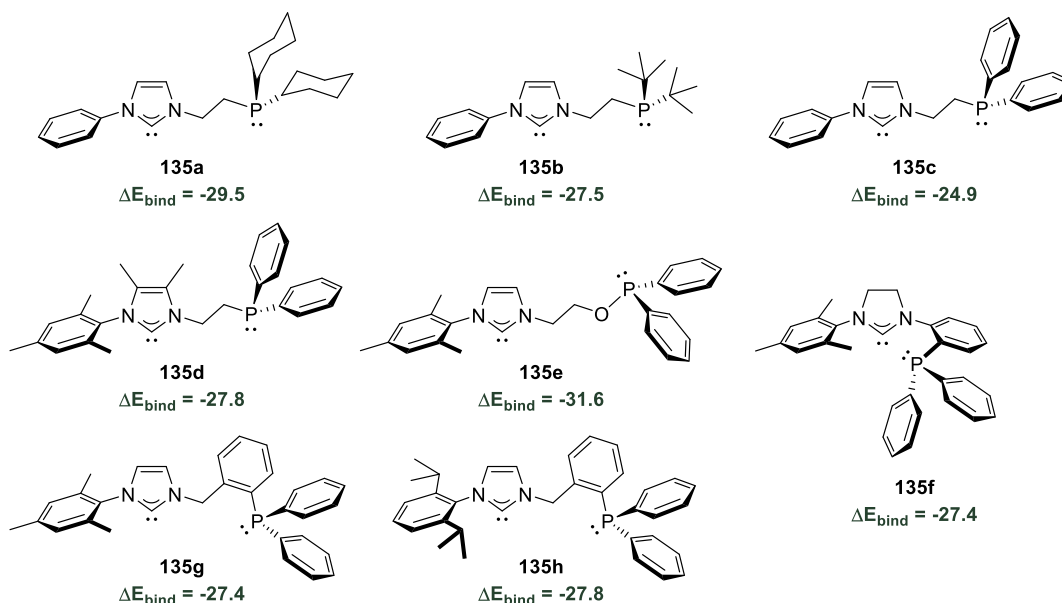
Scheme 1.32: Structure of predicted ligands with favourable binding energies.[†][160]

[†]Binding energies given in kcal mol^{-1}; binding to catalyst **60** yields ΔE_{bind} = -15.3 kcal mol^{-1}.

Detailed theoretical examination of these thermodynamic parameters in conjunction with experimental validation led to a remarkable fundamental relationship, *i.e.*, more negative, thus favourable, binding energies were qualitatively associated with higher catalyst turnover for the HIE of substrates bearing hindered directing groups.[160] Although experimental data from isotope exchange reactions with iridium complexes bearing chelating phosphines offer additional logical support to this hypothesis (*cf.* Table 1.2), the theoretical framework built to describe intricate steric and electronic factors involved in the C—H activation event is unique, for it enables direct comparison between mono- and polydentate ligands employing a single set of descriptors.[160]

Interestingly, apart from ligands **135f**-**h**, closely related to those reported by Stradiotto,[159] and Andersson *et al.*[155] all other chelating structures in Scheme 1.32 bear flexible tethers, highlighting the importance of a geometrically unconstrained chelate in the coordination sphere during the HIE process.

Beyond applications in isotope exchange, the few existing contributions dealing with NHC-*P* ligands have focused on their use in hydrogenation of olefins[161,162] and construction of C—X bonds (X = C, N).[155-159,163] Given the intrinsic properties of this versatile ligand scaffold, a more detailed exploration at both theoretical and experimental levels is highly desirable.

2. Proposed Work

Our previous developments in directed HIE resulted in highly selective and efficient protocols applicable to a wide range of sterically accessible functionalities. These reactions typically proceed *via* 5-membered metallocyclic intermediates featuring low ring strain, thus requiring diminished steric encumbrance at the vicinity of the directing group. In an effort to expand the applicability of our protocols to include poorly ligating, hindered functionalities, we envisioned a series of novel chelating NHC-P scaffolds able to free steric congestion around the metal centre, enabling access to a wider variety of functional groups. Accordingly, our first effort will focus in the development of a modular, robust and scalable protocol to access this underrepresented class of ligands and explore their coordination to iridium.
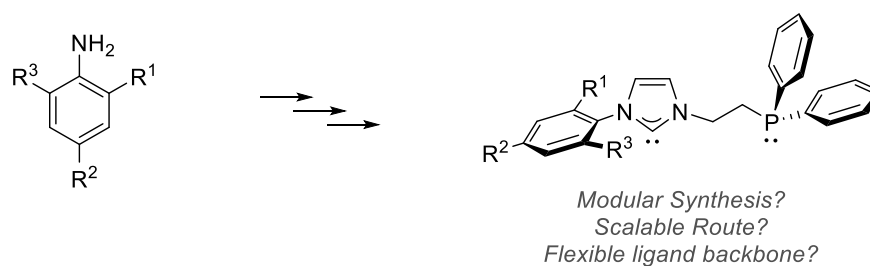
Scheme 1.33: Targeted ligand scaffold and key issues.

Once accessed, these novel ligands will be coordinated to iridium to generate suitable pre-catalysts for applications in C—H functionalisation in the context of HIE. Subsequently, we aim to better understand the solution properties of these organometallic complexes. To that effect, the behaviour of stabilised iridium hydrides of type $[(NHC-P)IrH_2L_2]^+$ will be evaluated by ^1H NMR spectroscopy and compared to existing data on heteroleptic monodentate complexes of type $[(NHC)(PR_3)IrH_2L_2]^+$. The information gathered in these studies will provide valuable insights into reactivity of this novel iridium complexes and reveal possible departures from their monodentate analogues.

We will then proceed to evaluate our new complexes in the HIE of substrates bearing sterically hindered directing groups. Our aim is to verify whether the synergy between a more accessible metal centre and our assumptions regarding the stabilisation of 6-membered metallocyclic intermediates will deliver improved reactivity at the vicinity of challenging directing functionalities.
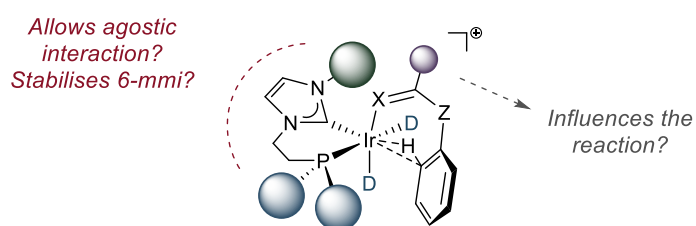
Scheme 1.34: Key questions regarding catalytic activity.

During our investigations, we will focus our efforts on the exploration of carbamates, a ubiquitous functionality that remains largely underexplored in the context of directed HIE. Once we identify suitable reaction conditions, we will explore the

applicability of novel iridium complexes in the labelling of various carbamates with aromatic substituents featuring diverse steric and electronic properties.

Our third line of enquiry will concern the development of mechanistic understanding of the process. Although the reactivity of iridium complexes of type [(NHC)(PR₃)Ir(COD)]X is well-understood, no clear mechanistic picture for complexes bearing a chelating ligand is available. Therefore, we will employ a combined theoretical and experimental approach aiming to deliver a thorough understanding of the reaction mechanism. Accordingly, we will utilise DFT calculations to model the reaction pathway and derive calculated kinetic parameters that can be confirmed through experimentation.
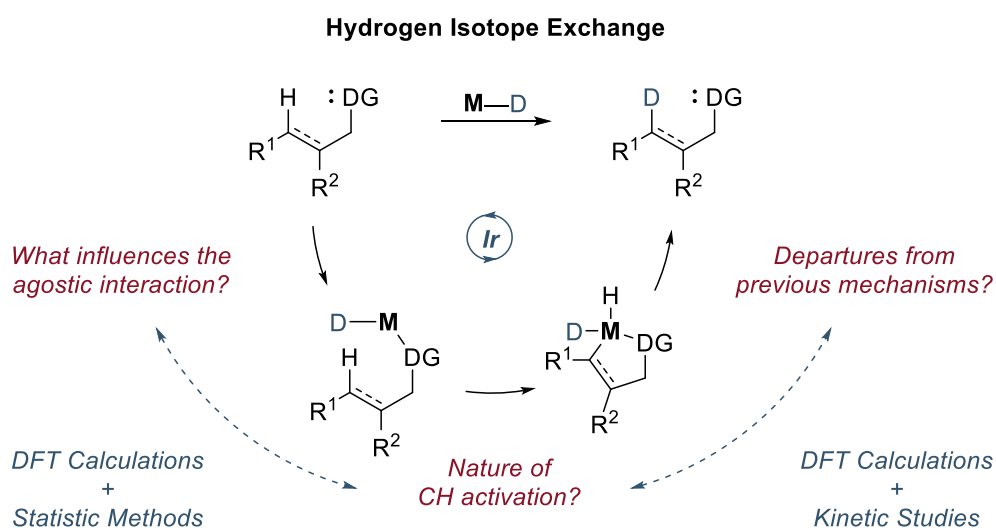
Scheme 1.35: Strategy towards rationale mechanistic proposal.

Finally, with the information gathered from these studies, we wish to identify the fundamental parameters involved in the C—H activation event, a crucial step implicated in all functionalisation protocols. Thus, we will further scrutinise the nature of transition state structures obtained by DFT calculations and endeavour to decompose the activation energy for this process into simpler descriptors bearing intuitive physicochemical meaning.

3. Results and Discussion

3.1 Synthesis of Phosphine Functionalised NHCs

The modulation of electronic and steric properties of ligands used in metal-catalysed processes is of fundamental importance for controlling reaction outcome and effectiveness of the desired transformation. Hence, the excellent activity demonstrated by iridium(I) complexes containing NHC and phosphine ligands in HIE and hydrogenation reactions prompted research in the Kerr group to focus on the development of modular chelating ligands to access novel iridium complexes.[160]

Through a comprehensive experimental and theoretical evaluation of these systems, it was hypothesised that iridium complexes bearing tethered NHC-P ancillary ligands would display improved coordination towards substrates containing sterically demanding coordination groups and substitution patterns (*vide supra*).

Based on the structural similarity of ligands **135a** – **135e** and those reported by Labande and Poli,[157] a route akin to that described therein was pursued. Scheme 1.36 illustrates the proposed synthetic route.
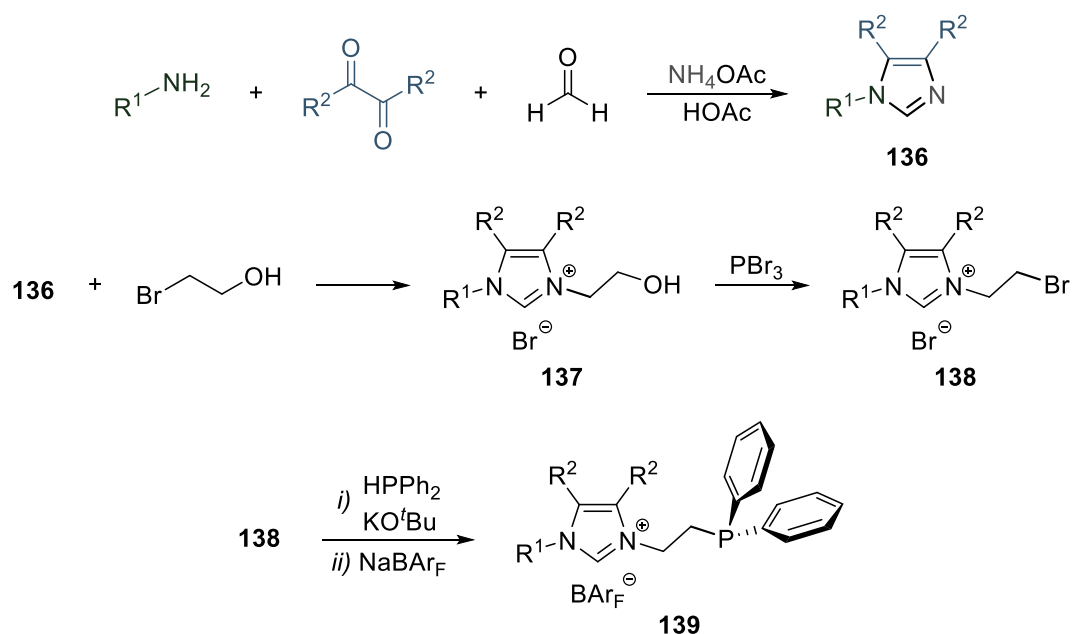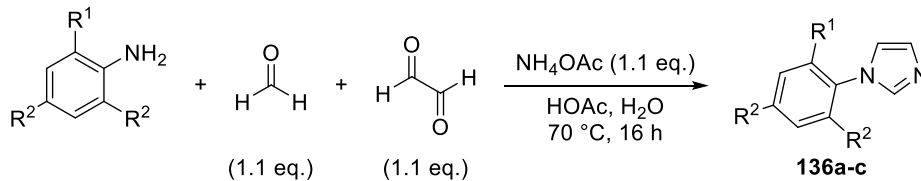
Scheme 1.36: Proposed synthetic route towards imidazolium salts.

Parent imidazoles could be synthesised through a well-established multicomponent reaction involving a suitable parent amine, a diketone or dialdehyde, formaldehyde and an external source of ammonia, to produce thermodynamically favoured product **136**. Subsequent *N*-alkylation with 2-bromoethanol and conversion of the pendant alcohol into an alkyl bromide would deliver 2-(bromoethyl)imidazolium bromides **137**, precursors for the challenging C—P bond forming process. Owing to its lower basicity when compared to dialkyl phosphides,[164] potassium diphenylphosphide could then be employed to displace the bromide in **137** to deliver the desired diphenylphosphino derivative. Finally, a salt exchange process employing NaBAr$_F$ as the source of the non-coordinating counter-anion would deliver the targeted NHC-P precursor **138**. Moreover, previous success in obtaining the parent imidazolium salt of ligand **130**[157,160] makes the strategy shown in Scheme 1.36 more attractive as a means of accessing new chelating ancillary ligands.

Having defined an operative main route for the synthesis of 2-(diphenylphosphino)imidazolium salts **138**, we embarked in this synthetic exploration to access novel precursors.

Based on the motifs presented in Scheme 1.36 and the reported electronic parameters of NHCs,[134,135,149] *N*-aryl-substituted imidazoles bearing phenyl, (2-methyl)phenyl and mesityl substituents were prepared through standard multicomponent reactions[165,167] in moderate yields, as summarised in Table 1.7.

Table 1.7: Synthesis of *N*-aryl-1*H*-imidazoles.

Entry	R^1	R^2	Product	Scale (mol)	Yield (%)
1	H	H	**136a**	0.20	52^a
2	CH$_3$	H	**136b**	0.20	50^a
3	CH$_3$	CH$_3$	**136c**	0.13	49^b

^{a}Isolated yield after distillation under vacuum; ^{b}Isolated yield after extraction and recrystallisation.

With the required imidazoles in hand, we continued the synthetic sequence by performing an *N*-alkylation with 2-bromoethanol, as summarised in Table 1.8.

Table 1.8: Synthesis of 3-(2-hydroxyethyl)-1-aryl-1*H*-imidazolium salts.
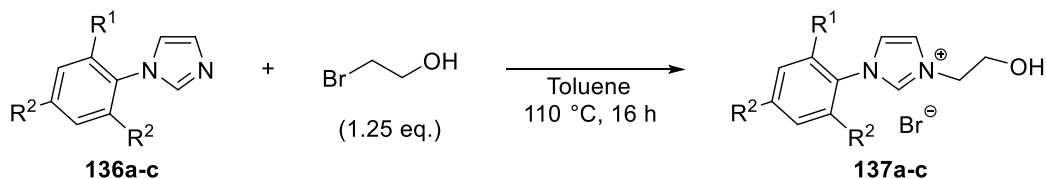
Entry	R^1	R^2	Product	Scale (mmol)	Yield (%)
1	H	H	**137a**	10	98
2	H	CH$_3$	**137b**	10	90
3	CH$_3$	CH$_3$	**137c**	20	88

Thus, the imidazolium products were obtained in good to excellent yields after a simple and convenient purification through trituration of solid products in Et$_2$O. We next converted hydroxy functionalised imidazolium salts **136a-c** to their respective bromides employing PBr$_3$ as a brominating agent, as shown in Table 1.9.

Table 1.9: Synthesis of 3-(2-bromoethyl)-1-aryl-1*H*-imidazolium salts.
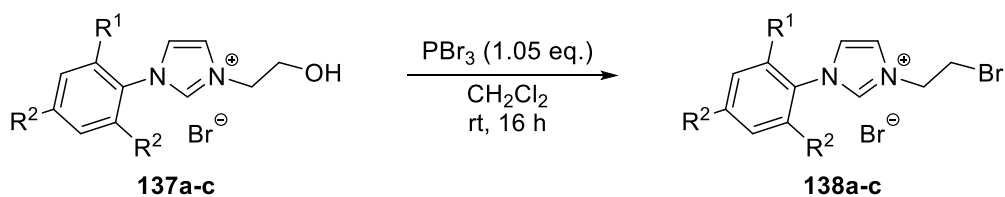
Entry	R^1	R^2	Product	Scale (mmol)	Yield (%)
1	H	H	**138a**	5.0	73
2	H	CH$_3$	**138b**	5.0	87
3	CH$_3$	CH$_3$	**138c**	7.5	71

During our investigations, we observed that isolated yields for products **138a-c** were not sensitive to the exothermic quenching of PBr$_3$ with saturated NaHCO$_3$, however, good yields could only be obtained after multiple extraction steps from the aqueous phase with CH$_2$Cl$_2$. This issue was particularly pronounced for **138a**, which bears a less sterically hindered *N*-phenyl substituent and is appreciably soluble in water.

Once bromoethyl imidazolium bromides were obtained, their conversion to the desired NHC-P precursors commenced. Then, by direct reaction with freshly prepared potassium diphenylphosphide in DMSO, the installation of the desired C—P bond was achieved through S$_N$2 displacements of the parent bromides **138a-c**, followed by salt exchange with NaBAr$_F$ (*cf.* section 3.1.5) to give the corresponding

phosphino-imidazolium salts **139a-c**. Table 1.10 presents the results obtained through this process.

Table 1.10: Synthesis of 3-(2-diphenylphosphinoethyl)-1-aryl-1H-imidazolium salts.
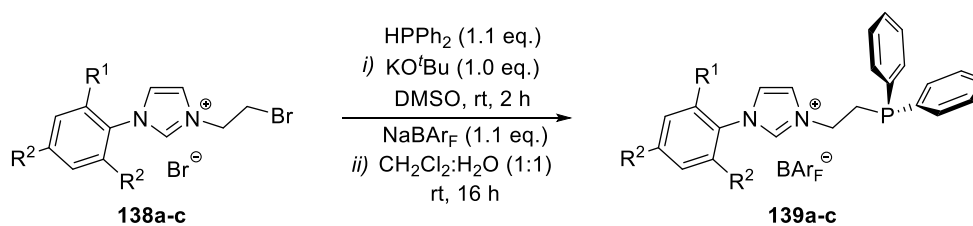
Entry	R^1	R^2	Product	Scale (mmol)	Yield (%)
1	H	H	**139a**	1.0	88
2	H	CH_3	**139b**	2.0	32
3	CH_3	CH_3	**139c**	2.0	58

As depicted in Table 1.10, the desired phosphines were obtained in a two-step process in low to moderate yields. It is important to emphasise that, due to the nature of phosphorus(III) compounds, the synthesis of targeted phosphines was accomplished under oxygen-free conditions to avoid undesired oxidation to corresponding phosphine oxides. Notwithstanding these reaction conditions, the recovery of final products through column chromatography is expected to contribute to lower yields, since oxidation of phosphines is classically accomplished during their purification.[168]

3.1.1 Improved Synthesis of NaBAr$_F$

The ability of non-coordinating anions to enhance the stability, solubility and chemical availability of cationic complexes in reaction media[46,68,81,140] makes the application of these anions very attractive in transition metal catalysis. Therefore, access to a reliable and consistent synthetic method for their synthesis is of paramount importance.

Starting from the original report from Kobayashi *et al.*,[118] attempts within the Kerr group to obtain NaBAr$_F$ suffered from lack of reproducibility, with results fluctuating from low to moderate yields, rarely ever exceeding 50%. Additionally,

the extensive workup, which requires several filtrations of viscous solutions, liquid-liquid extractions and column chromatography, further emphasises the necessity of a reliable and reproducible route to this compound. Hence, in order to analyse possible issues in the synthetic method, a first synthesis was performed following the original report of Kobayashi et al.,[118] as depicted in Scheme 1.37.
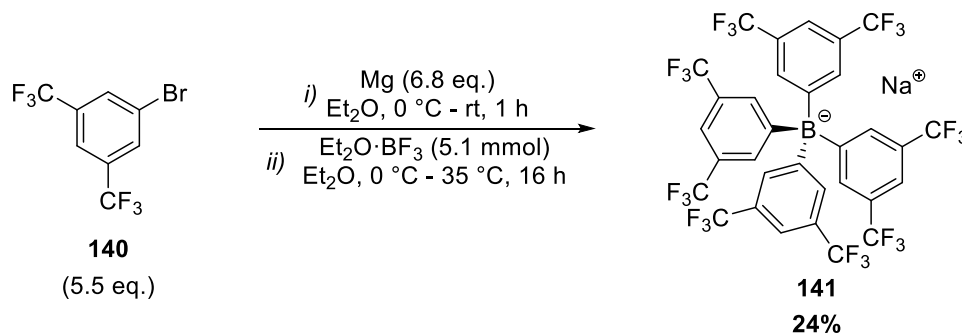
Scheme 1.37: Initial attempt to obtain NaBArF.

The protocol employed consisted in the formation of a Grignard reagent by reacting aryl bromide **140** and Mg in Et_2O, followed by the addition of $Et_2O \cdot BF_3$ in ether to effect the desired arylation at the boron centre. Subsequently, the reaction mixture was quenched with aqueous Na_2CO_3, providing the sodium cation required to form **141**. Further filtration, extraction of the aqueous phase with Et_2O, evaporation of the organic layer and column chromatography afforded **141** in only 24% yield. Moreover, two important features of this protocol became evident, namely:

i.   Only a small excess of magnesium was employed in the reaction with **140**. In the presence of impurities or adventitious water, the amount of active Grignard species would thus be lower than the required to achieve good conversion;

ii.   The reaction is expected to be complete after three B—F substitution processes and a nucleophilic attack on the resulting triarylborane to obtain **141**. Thus, owing to the carbanionic character of organomagnesium compounds[117] and the constant increase in steric hindrance as the substitution progresses, formation of **141** is disfavoured by both electrostatic and steric factors;

Therefore, the following adaptations were hypothesised as beneficial for this reaction: mechanical activation of magnesium turnings in order to increase the effective amount of reactive metal prior to Grignard reagent formation;[169] preparation of an excess of arylating reagent to facilitate equilibrium displacement towards the desired product; washings of combined organic phases with saturated Na_2CO_3 and brine in order to reduce level of impurities, with subsequent improvement in the effectiveness of chromatographic purification. After implementation of these modifications, improved yields were obtained, as demonstrated in Table 1.11.

Table 1.11: Modified protocol for the synthesis of NaBArF.
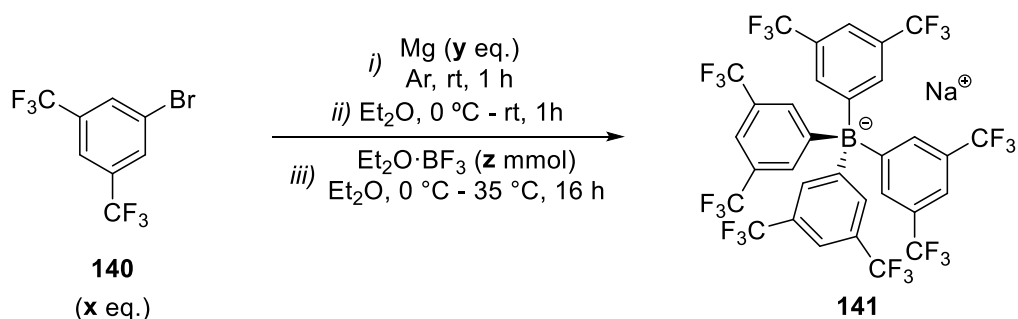
Entry	x (eq.)	y (eq.)	z (mmol)	Yield (%)
1	5.5	6.8	5.1	24^a
2	10	20	7.0	60^b
3	10	20	7.0	79^b

^{a}Orginial procedure employed; ^{b}modified procedure employed.

To our delight, this modified protocol afforded **141** in increased yields and proved reproducible when repeated by other researchers in the group.

3.2 Iridium(I) Complexes Bearing NHC-P Ligands

Synthetic methods for the production of iridium(I) complexes bearing non-tethered NHC and phosphine ligands are well-established in literature, with several of them being explored and improved by the Kerr group.[160] Despite their availability, the nature of NHC-P ligands significantly limits the number of applicable synthetic routes towards the corresponding Ir complexes. Scheme 1.38 illustrates the few

routes already employed to access complexes related to those targeted in this work.[170-172]

Systems depicted in Scheme 1.38 highlight some important aspects of the chelate complex synthesis, namely: a strong base is necessary to generate the free carbene in solution in order to obtain the desired complexes; less encumbered ligands, such as **145**, have higher a propensity to dimerise, thus requiring longer addition times and bases compatible with this requirement;[171] combination of the more reactive iridium precursor **148** with a sterically hindered NHC-P precursor leads to the selective formation of an abnormal carbene;[170] and in the presence of coordinating anions, neutral complexes are obtained instead of targeted ionic pairs.
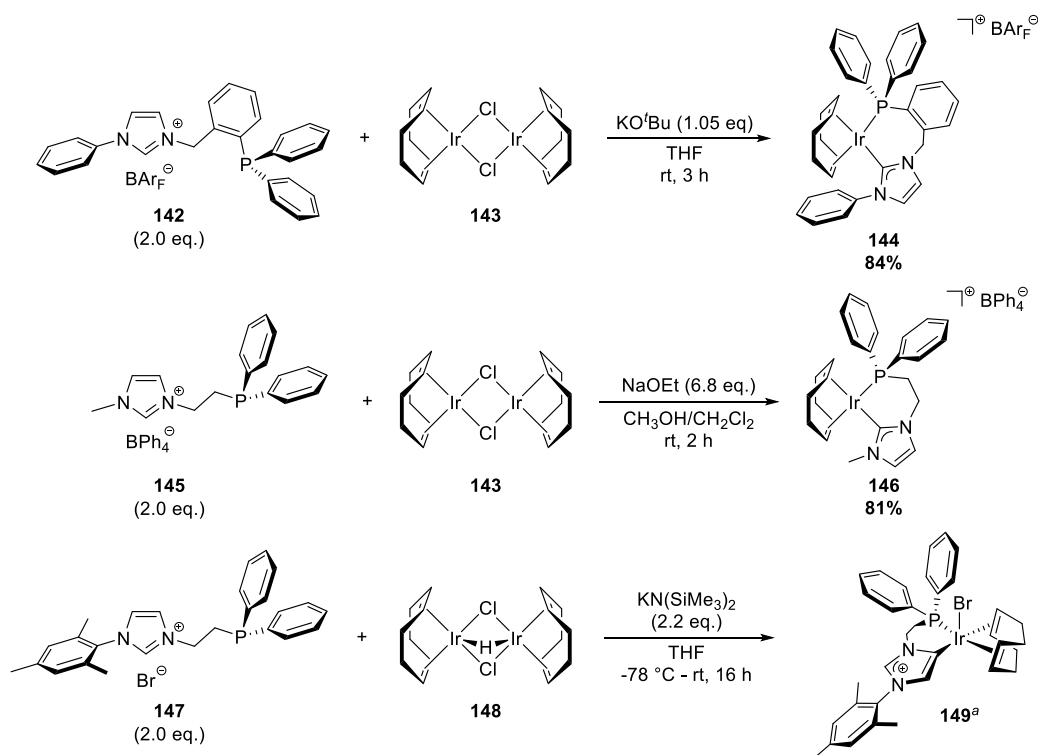
Scheme 1.38: Examples of complexation of NHC-P ligands to Ir.[170-172]

[a]Isolated yield not given.

Owing to their similar steric factors, synthetic methods for complexes **144** and **149** should be more directly applicable to ligands **139a-c**. Moreover, since the approach to **149** led to an abnormal NHC coordination to the metal centre, the route described by Andersson *et al.*[172] was chosen as our initial synthetic method.

Then, precursors **139a-c** were dissolved in THF in the presence of [Ir(COD)Cl]$_2$ and KO^{t}Bu was added to generate the corresponding carbene *in situ*, which would subsequently coordinate to the metal centre. Table 1.12 summarises the results thus obtained.

Table 1.12: Complexation of NHC-P ligands to Ir.
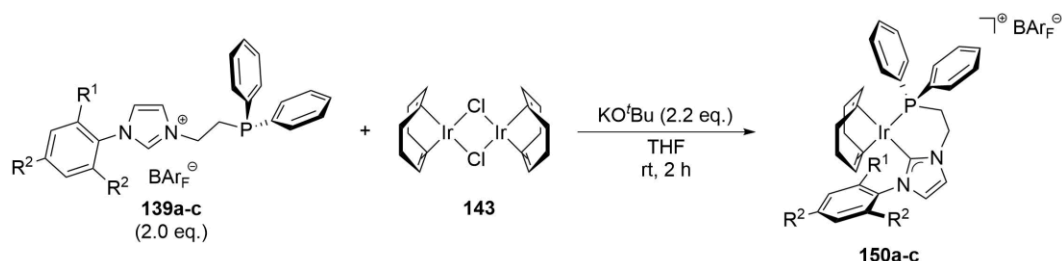
Entry	R^1	R^2	Product	Scale (mmol)	Yield (%)
1	H	H	**150a**	0.16	37
2	CH$_3$	H	**150b**	0.15	50
3	CH$_3$	CH$_3$	**150c**	0.15	31

Despite being successfully synthesised, chelated iridium complexes **150a-c** were obtained in only low to moderate yields. As a cautionary example of related synthetic methods, in their pioneering work involving the synthesis of iridium complexes bearing bulky NHC-P ligands, Danopoulos *et al.* obtained intractable solid mixtures and were able only to isolate **149**, which bears an abnormal NHC unit.[170]

Such observations are in line with the instability of free carbenes which, apart from highly encumbered symmetric species bearing substituents such as mesityl, adamantyl or ^{t}Bu, tend to undergo dimerisation in solution.[132] Another possibility is decomposition of the NHC-P precursors upon interaction of KO^{t}Bu with the acidic protons of the tether, leading to elimination reactions and corresponding lowered yields. Therefore, the reaction conditions employed in this protocol are not fully compatible with the nature of ethylene-tethered imidazolium precursors.

Hence, we considered two possible alternatives: modification of the current method to afford higher yields of the desired iridium complexes; or further investigations into other attractive methodologies.

Owing to the relatively recent emergence of phosphine-functionalised NHCs few investigations have been conducted into the application of the corresponding silver

carbene complexes as transmetallating agents to Ir. Being a reliable method to synthesise iridium complexes bearing non-tethered NHC and phosphine ligands,[160] the use of Ag_2O as an agent to both generate and stabilise carbenes constitutes a desirable alternative to direct deprotonation with strong bases. However, a note of caution should be made: since the NHC-P ligands bear two coordinating sites, different silver aggregates might be expected. On this subject, Hoffman and co-workers reported the formation of unusual silver aggregates upon reaction with imidazolium precursors **151** and **153** (Scheme 1.39), the latter being particularly insoluble in common reaction media, thus being deemed unsuitable for the transmetallation process.[154]
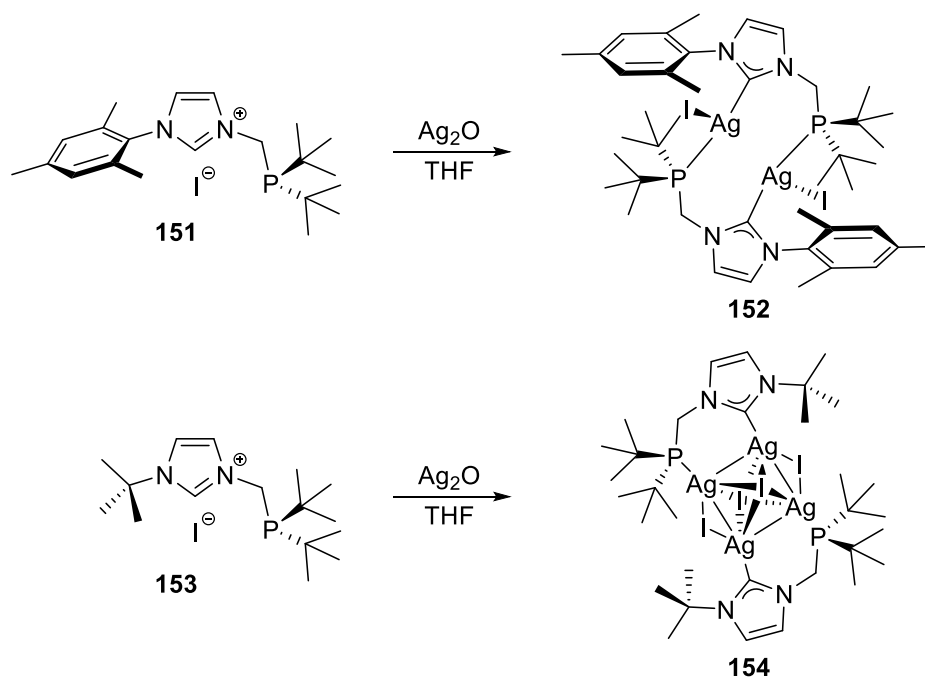
Scheme 1.39: Higher silver aggregates bearing NHC-P ligands.[154]

Moreover, the reduced reactivity of dimers and higher aggregates of silver during carbene transmetallation is well-documented,[173] thus suggesting that direct transference to a suitable iridium precursor without isolation of the silver carbene would be more likely to succeed.

On the other hand, in their attempts to obtain palladium(II) complexes by deprotonation of imidazolium bromide **147**, Danopoulos *et al.* resorted to cooling the reaction medium to low temperatures throughout the complexation event with [(COD)PdBr$_2$].[174] Furthermore, earlier reports from the same research group indicate

free carbene **130**, which bears the more sterically encumbered 2,6-di-*iso*-propylphenyl substituent, crystallises to afford an air sensitive solid, stable up to 0 °C.[175]

This seeming discrepancy in inherent stability of **130** and **147**, the latter being less sterically hindered, thus offering lower steric protection to the carbene formed *in situ* during complexation events, is not totally unexpected. Indeed, dimerisation of 3-substituted-1-mesityl-imidazol-2-ylidenes and their saturated imidazolidine-2-ylidene counterparts is known to occur with asymmetric imidazolium salts featuring low steric congestion at the second nitrogen atom within the azole ring, *e.g.*, with 2-pyridyl-[176] and 2-(4-morpholinyl)phenyl-[177] substituents. In the latter case, Stradiotto *et al.* observed the same divergence in reactivity, namely, a more sterically encumbered morpholine-functionalised NHC bearing the 2,6-di-*iso*-propylphenyl moiety was found to form a stable carbene upon deprotonation under the same reaction conditions which afforded dimers of its mesityl counterpart.[177]

Combining these pieces of evidence, it was reasoned that premature decomposition of carbenes generated upon deprotonation from imidazolium salts **139a-c** with KO*t*Bu accounted for the suboptimal yields of complexes **150a-c**. To that effect, we embarked on a series of experiments to determine whether lower temperatures could prevent decomposition of **139c** during its complexation to Ir. Table 1.13 collates the results obtained.

Table 1.13: Complexation studies with **139c**.
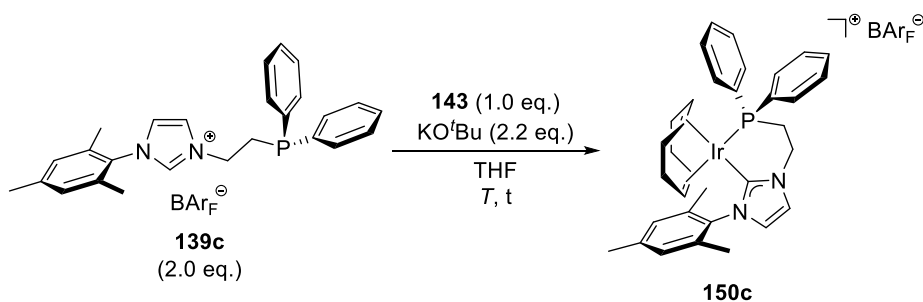
Entry	Scale (mmol)[a]	*T* (°C)	t (h)	Yield (%)
1	0.25	rt	2	20
2[b]	0.25	rt	2	15
3[c]	0.20	-78 °C – rt	3	53
4[c]	0.40	-78 °C – rt	3	62
5[c]	0.80	-78 °C – rt	3	68

[a]based on **139c**; [b]reaction performed at half concentration; [c]deptoronation performed at -78 °C for 1 h, then warmed to rt for 2 h.

Thus, performing the complexation step at half its normal concentration to hinder possible dimerisation of **139c** gave no improvements in the reaction profile (entries 1 – 2). Conversely, when the parent imidazolium salt was dissolved in THF at room temperature and subsequently cooled to -78 °C prior to addition of [Ir(COD)Cl]$_2$ **143** and, then, KO^{t}Bu, a dramatic increase in yield of **150c** from 20 to 53% was observed (entries 1 and 3). Gratifyingly, this approach proved reliable and reproducible upon scaling, securing access to a useful route towards Ir(I) complexes bearing NHC-P ligands.

3.2.1   Analysis of iridium(III) hydrides

In order to gain further insight into the electronic properties of newly synthesised complexes, the analysis of ^{1}H NMR spectrum shifts in the hydridic region of their corresponding iridium(III) dihydrides, generated *in situ* by reaction with H$_2$ in CD$_3$CN, was performed. In these experiments, the coordinating ability of acetonitrile is expected to enhance stability and inhibit fluxional behaviour of iridium(III) hydrides,[128,146] therefore providing a reliable method to analyse electronic parameters through understanding of the *trans-* effects of ancillary ligands.[8] In chelating systems such those under scrutiny, hydrogenation of the coordinated COD ligand produces a mixture of several possible isomers arising from all available permutations of CD$_3$CN and hydride ligands. In this regard, a systematic nomenclature of these species is required to mitigate possible neglection or, conversely, duplication of coordinating compounds rendered equivalent by symmetry operations.[179] Therefore, a variation of the well-established Δ, Λ nomenclature for organometallic complexes[179,180] was adopted, as indicated in Scheme 1.40 for an iridium(III) dihydride bearing an arbitrary NHC-P ligand.
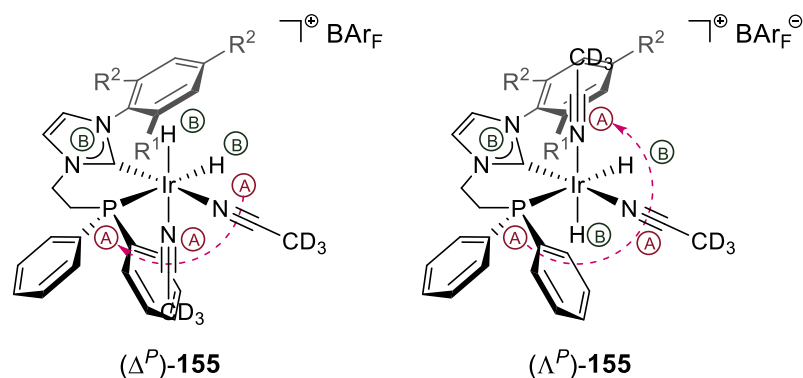
Scheme 1.40: Nomenclature adopted for iridium(III) hydrides.

In this modified version, each pair of d_3-acetonitrile and hydride ligands is taken as a new *cis-* ligated chelating motif which, in fact, establishes a unique stereochemical assignment under the framework of the Δ, Λ stereoisomeric system.[179] Finally, the superscript characters in Scheme 1.40 indicate which of the coordinating atoms of the NHC-P ligand lies *trans-* to a hydride. Employing this systematic classification, Scheme 1.41 illustrates all possible stereoisomeric forms of complexes of type **155** bearing a generic bidentate ligand.
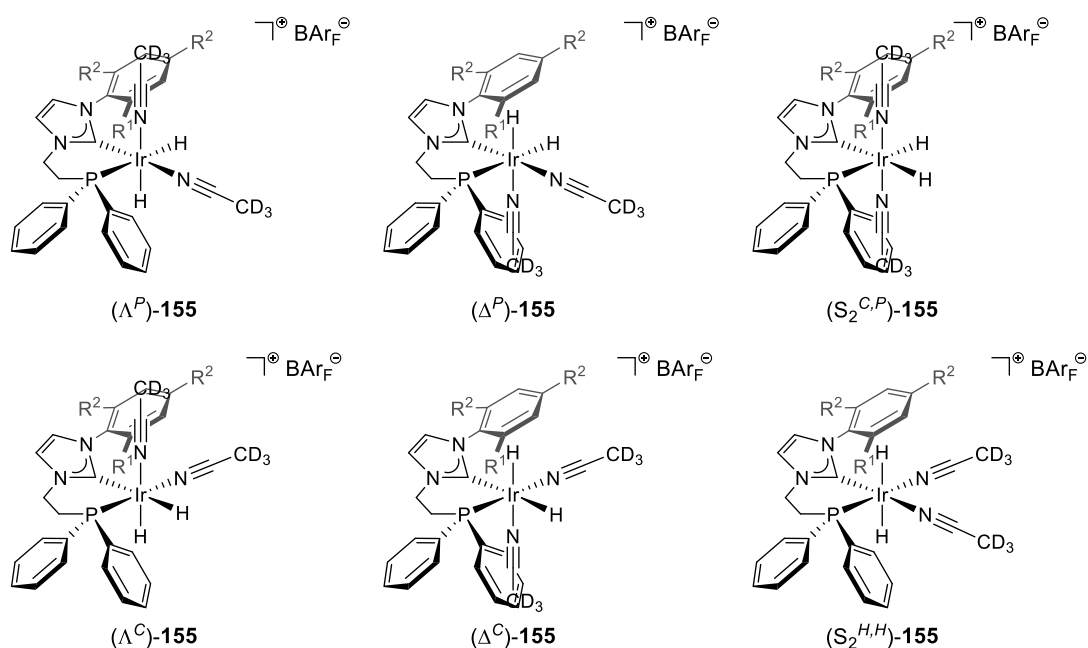
Scheme 1.41: Set of stereoisomeric iridium(III) hydrides.

Four important conclusions which arise upon further inspection of stereoisomers in Scheme 1.41 must be addressed. Firstly, the pairs of structures (Λ^P)-**155** and (Δ^P)-**155**, and (Λ^C)-**155** and (Δ^C)-**155** are enantiomeric complexes of each other. Secondly, complexes ($S_2^{C,P}$)-**155** and ($S_2^{H,H}$)-**155** possess an improper axis of rotation of second order (S_2)[179] across the central plane defined by the NHC-P ligand, therefore, their respective mirror images are equivalent to the parent compounds, thus reducing the total number of stereoisomers by two units. Thirdly, on the grounds of the *trans-* effect of strong σ-donor ligands,[8,179] and the inherent geometry associated with oxidative addition of neutral molecules to organometallic complexes,[8] hydrides of type ($S_2^{H,H}$)-**155** are not expected. Finally, by combining these observations with the documented differences in coupling constants for hydrides at sites *cis-* and *trans-* to phosphines,[10] it is possible to unequivocally assign the composition of a reaction mixture containing all relevant stereoisomeric hydrides of Scheme 1.41.

Thus, from a total of six possible stereoisomeric complexes, a total of four sets of independent signals are expected in the ^{1}H NMR spectrum: one for each of the (Λ^X)-**155**, (Δ^X)-**155** pairs; a third set for ($S_2^{C,P}$)-**155**; and a fourth system corresponding to ($S_2^{H,H}$)-**155** (*N.B.*: its unlikelihood does not justify its neglection). Furthermore, the chemical shifts of the hydridic protons should display an inverse correlation with the electron donating ability of the ligand situated *trans-* to their coordination site. Thus, more σ-donating groups in this position would result in more negative chemical shifts for a given *trans-* hydride. Additionally, the converse applies in terms of π-accepting character, *i.e.*, chemical shifts should decrease with increasing π-acidity of a *trans-* ligand.[8,10] When exposed to an atmosphere of H_2 in d_3-acetonitrile and subsequently analysed by ^{1}H NMR spectroscopy, complexes **150a-c** displayed strikingly distinct behaviours. Table 1.14 summarises the chemical shifts thus observed.

Table 1.14: Observed ^{1}H chemical shifts for metal hydrides.[†]

Entry	Complex	System[a]	H[b]	$\delta_{^1H}$	$^2J_{HH}$	$^2J_{HP}$	I_r
1		H^α,H^β	H^α	-11.8	5.2	20	2.8
2	**150a**	H^α,H^β	H^β	-21.8	5.2	20	2.8
3		H^ι	H^ι	-21.4	—	13	1.0
4		H^α,H^β	H^α	-11.5	5.2	18	1.7
5		H^α,H^β	H^β	-21.8	5.2	21	1.7
6	**150b**	H^γ,H^ε	H^γ	-11.6	5.2	18	1.8
7		H^γ,H^ε	H^ε	-21.7	5.2	20	1.8
8		H^ι	H^ι	-21.2	—	14	1.0
9		H^α,H^β	H^α	-11.6	5.5	18	3.3
10	**150c**	H^α,H^β	H^β	-21.9	5.5	21	3.3
11		H^φ,H^ψ	H^φ	-8.8	4.4	160	1.0
12		H^φ,H^ψ	H^ψ	-20.9	4.4	11	1.0

[†]δ is given in ppm; *J* values are reported in Hz; I_r – relative integration in arbitrary units; [a]relationship determined by integration and intensity of signals in the ^{1}H NMR spectrum; [b]type of hydride *as per* stereochemical environment (*vide infra*).

From the data collated in Table 1.14, it was possible to identify a total of five distinct sets of hydridic signals pertaining to complexes **150a-c**, namely (also, *vide infra*):

i. System H^α,H^β: pair of hydrides featuring $^2J_{HP}$ of approximately 20 Hz, clearly indicating a *cis-* disposition to the phosphorus atom of the NHC-P ligand.[10] This system was assigned to the indistinguishable isomers (Λ^C)-**155** and (Δ^C)-**155** based on the following additional considerations:

    a. H^α signals: feature a downfield shift typical of those observed for hydrides located *trans-* to strong σ-donors,[10] compare well with known *trans-*(C_{NHC},*H*)-[(NHC)IrH$_n$(PR$_3$)$_m$L$_r$] complexes,[181,182] and possess non-negligible $^2J_{HH}$ value, indicating a clear *cis-* disposition with a second, magnetically inequivalent hydride;

    b. H^β signals: posses a strong downfiled shift characteristic of hydrides *trans-* to labile sites coordinated to hard neutral σ-donors such as OR$_2$ and NR$_3$ ligands.[10]

ii. System H^γ,H^ε: displays similar features to those related to hydride pairs within the H^α,H^β system, strongly suggesting chemical equivalence among these iridium complexes. The observed slight discrepancies in chemical shifts for metal hydrides is characteristic of diastereoisomeric systems, indicating the presence of chirality elsewhere in the molecule. Signals within this

system could only be observed with complex **150b**, which features an *o*-Tol *N*-substituent capable of introducing atropoisomerism as a further complicating factor. Hence, this set of signals should correspond to a mixture of four diastereomeric complexes, *i.e.*, (*S*)-(Λ^C)-**155b** and (*S*)-(Δ^C)-**155b** generates a pair of indistinguishable systems, whereas (*R*)-(Λ^C)-**155b** and (*R*)-(Δ^C)-**155b** account for the remaining set.

iii. System H^t: possess chemical shifts that strongly resembles hydrides of type H^β, but lacks any apparent $^2J_{HH}$. These observations do not compare well with known rigid *trans*-(*H,H*)-[(P-N-P)IrH$_2$L],[183] *trans*-(*H,H*)-[(P-C-P)IrH$_2$L],[184] and *trans*-(*H,H*)-*fac*-[(NHC)IrH$_3$(PPh$_3$)$_2$][181] complexes. Moreover, observed chemical shifts, slightly downfield in comparison to those associated with H^β, suggest loss of electron density at the metal centre, which was also observed for cationic iridium(III) complexes that undergo displacement of a hydride ligand by a neutral *N*-donor.[184] Combined, this evidence points to the existence of an iridium complex of type [(NHC-P)IrH(CD$_3$CN)$_n$]$^+$ (*vide infra*).

iv. System H^φ,H^ψ: feature remarkable differences in $^2J_{HP}$ values within the pair, which is typical of complexes containing one dissymetrical hydrides in which one ligand is located *trans*- to a *P*-donor whilst the second ligand occupies a coordinating site *cis*- to the phosphine moiety.[10] These signals also feature the $^2J_{HH}$ value associated with a *cis*-(*H,H*)-dihydride complex, thus being assigned to the enantiomeric pair (Λ^P)-**155** and (Δ^P)-**155**, to which the following considerations also apply:

  a. H^φ signals: depict a characteristic $^2J_{HP}$ value associated to hydrides *trans*- to phosphines,[10] with chemical shifts even more downfield to those associated to H^α. This observation is in line with the presence of a stronger π-acceptor than an NHC, thus corroborating the assignment.

  b. H^ψ signals: possess features which enable its classification in analogy to H^β (*vide supra*).

Collectively, these observations and inferences directly allow the unambiguous assignment of complexes (Λ^C)-**155c**, (Δ^C)-**155c**, (Λ^P)-**155c** and (Δ^P)-**155c** as the

structures arising from reactions of H$_2$ with **150c**. Scheme 1.42 summarises these findings.
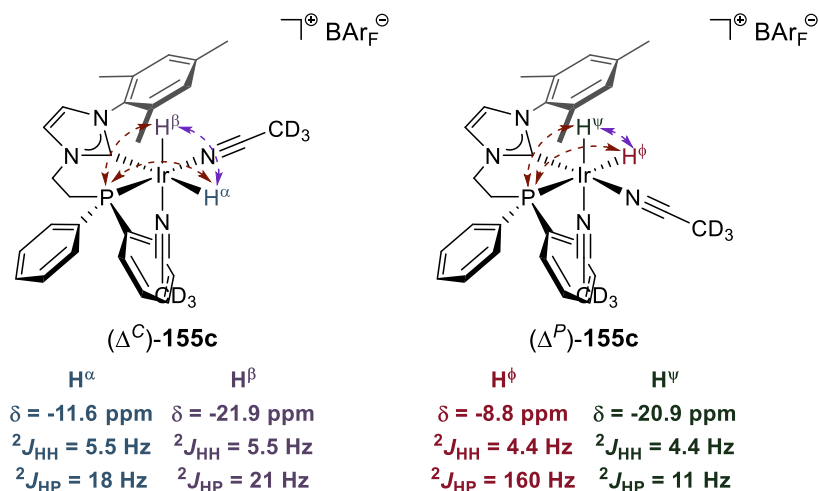
Scheme 1.42: Stereochemical assignment of complexes of type **155c**.†

†Dashed arrows indicate couplings identified in the ^{1}H NMR spectrum; magnetically equivalent complexes of Λ symmetry were omitted for clarity.

The existence of signals type H^t in **155a-b** seemingly creates further complexity to provide a unique identification of stereoisomers derived from parent iridium(I) species **150a-b**. This conundrum can be resolved, however, by recognising the distinct properties of transition metal hydrides.

More specifically, the possibility that H^t signals arise from an octahedral complex of type [(NHC-P)Ir(η^2-H$_2$)L$_n$]$^+$ can be discarded. Iridium complexes bearing loosely bound classical η^2-H$_2$ ligands feature broad signals in the ^{1}H NMR spectrum at all temperatures;[185] readily engage in displacement of molecular hydrogen by acetonitrile;[186] and are usually prone to decomposition through σ-bond metathesis with other ligands within the coordination sphere of the complex.[185] Rigid, non-classical η^2-H$_2$ ligands, on the other hand, commonly resonate in the -4 to -10 ppm range,[186,187] depict high acidity, and often decompose to form their respective monohydrides.[187]

One last possibility, however, is yet to be addressed. Owing to the tendency of η^2-H$_2$ ligands to engage in σ-bond metathesis,[185] and the usual microscopic reversibility of the latter,[87] it is conceivable that upon de-coordination of a CD$_3$CN ligand a

metathetic process indeed takes place to afford a strained transient complex of type *mer*-[(NHC-P)IrH(η^2-H$_2$)(CD$_3$CN)$_{n-1}$]$^+$ (**156**) which then undergoes dissociative ligand exchange with d_3-acetonitrile to afford the required *fac*-[(NHC-P)IrH(CD$_3$CN)$_n$]$^+$ complex **157**, as depicted in Scheme 1.43.
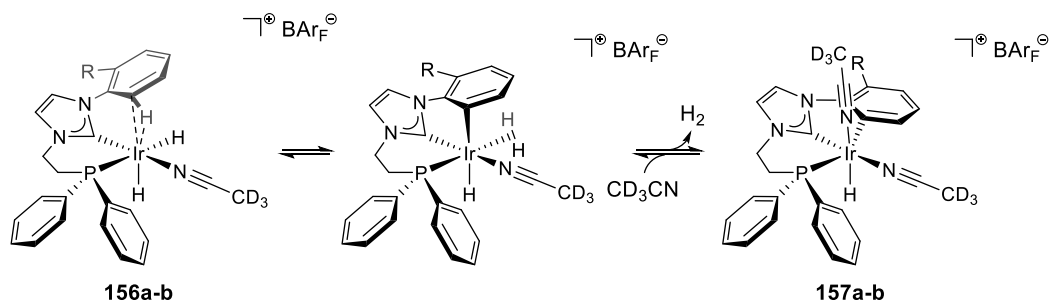
Scheme 1.43: Rationale for assignment of **157a-b**.

The data provided herein, in conjunction with literature data on relevant iridium (poly)hydrides and their reactivity, support formation of **157a-b** in solution during ^{1}H NMR experiments. Finally, we emphasise that no evidence for formation of complexes of type (S$_2$^{H,H})-**155a-c**, nor (S$_2$^{C,P})-**155a-c** was observed.[188] In summary, the stereochemical assignment of complexes **155a-b** can then be completed, as indicated in Scheme 1.44.
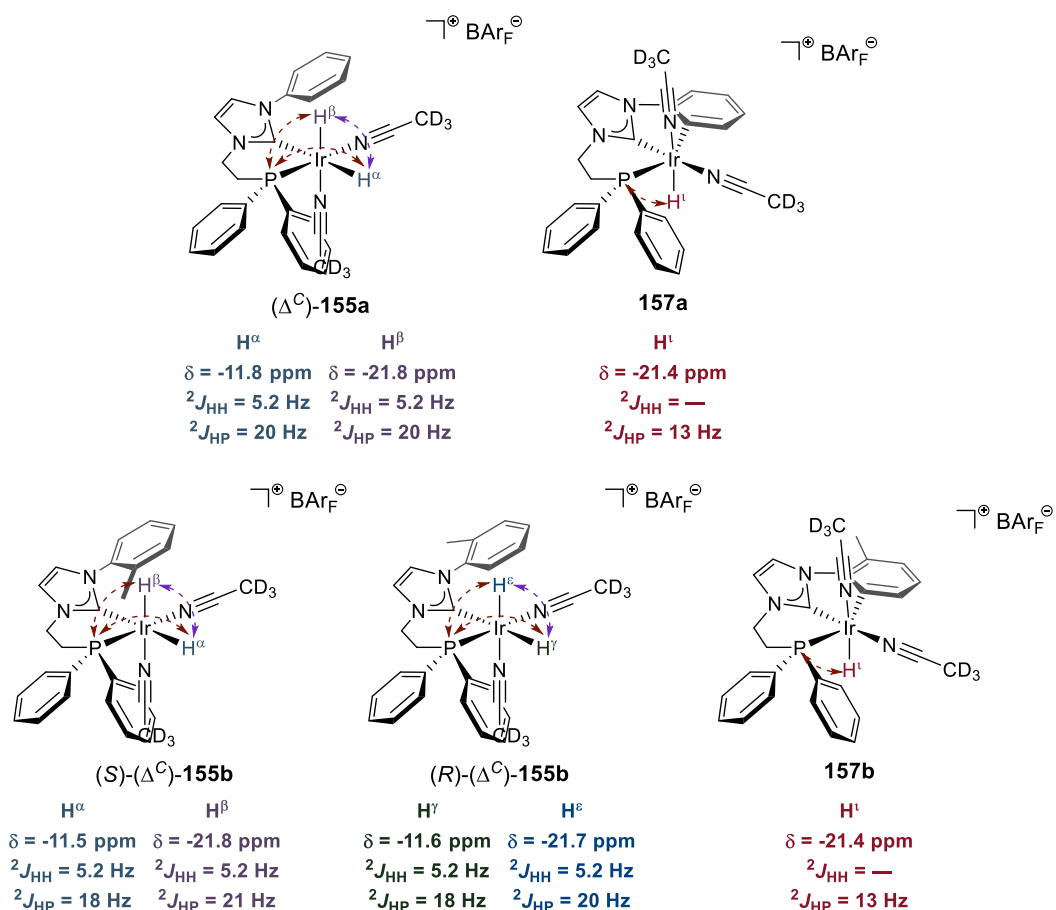
Scheme 1.44: Stereochemical assignment for complexes **155a-b** and **157a-b**.[†]

[†]Dashed arrows indicate couplings identified in the ^{1}H NMR spectrum; systems H^α,H^β and H^γ,H^ϵ were arbitrarily assigned to (*S*)- and (*R*)-(Δ^C)-**155b**, respectively; magnetically equivalent complexes of Λ symmetry were omitted for clarity.

Final support for the assignment of the simpler system comprised by hydrides **155c** was gathered through DFT calculations. Thus, four magnetically inequivalent metal complexes from the set of structures depicted in Scheme 1.45 were optimised at the SMD/M06L/6-31G(d) level of theory with relativistic Sttutgart RSC pseudopotential[189] and associated basis set for Ir employing acetonitrile as solvent (see Computational Details for further information). Notably, the two species observed in the ^{1}H NMR spectrum corresponded to the lowest energy stereoisomers in this set of iridium complexes, whilst ($S_2^{H,H}$)- and ($S_2^{C,P}$)-**155c** are clearly thermodynamically disfavoured, as summarised in Scheme 1.45.
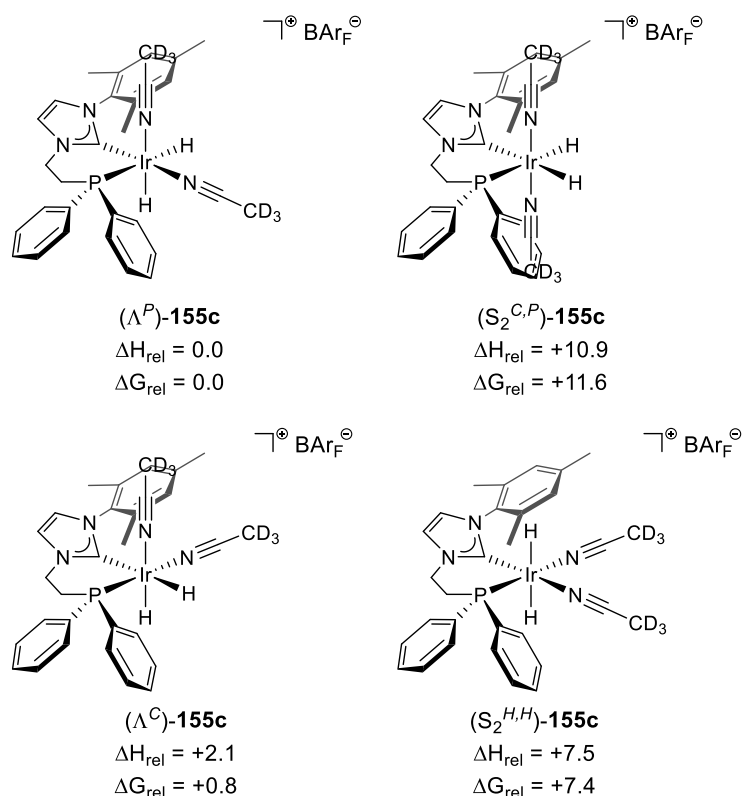
Scheme 1.45: Calculated energies for complexes **155c**.[†]

[†]Energies reported in kcal mol^{-1}; ΔH_{rel} and ΔG_{rel} correspond to relative enthalpies and Gibbs free energies, respectively. See Computational Details for further information.

As a preliminary conclusion, complexes **155a-c** were successfully synthesised and assessed in reactions with molecular hydrogen, which allowed a reasonable stereochemical classification of their respective iridium(III) hydrides. Cognisant of the rich reactivity of these complexes with H_2, and possible routes towards C—H activation through σ-bond metathesis, we commenced the exploration of their activity in HIE.

3.3   Applications in HIE

One of the remaining challenges in isotope exchange reactions catalysed by iridium complexes, which rely on the versatility of directing groups to guide C—H activation and promote isotope delivery, is the expansion of this technology to molecules bearing sterically demanding directing groups. As previously elucidated, few effective catalytic systems that accomplish HIE of this class of compounds have been

reported. A simple survey of marketed drugs indicates there is no shortage of sterically congested fragments which could be exploited through directed HIE. Scheme 1.46 illustrates selected examples in which isotope labelling would be conceivable under the premise that one can access C_{sp^2}—H sites adjacent to these moieties.
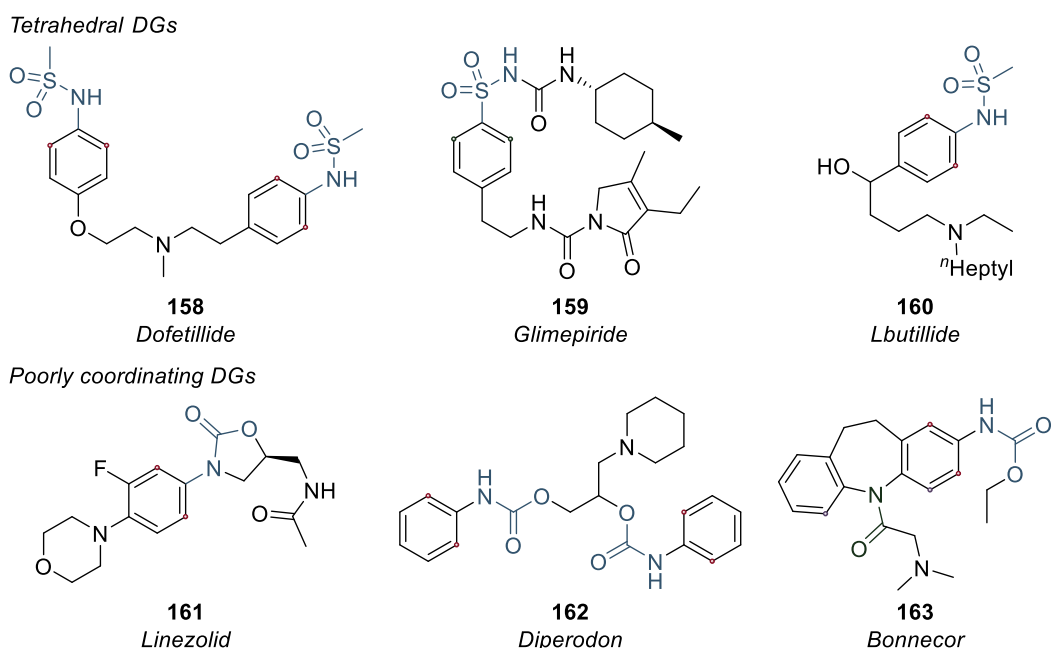
Scheme 1.46: Drug motifs featuring challenging directing functionalities.[†][190-193]

[†]DGs – directing groups.

In the examples featured in Scheme 1.46, Glimepiride **159** is the only drug motif for which activation through a more thermodynamically favourable (*vide supra*) 5-membered metallocyclic intermediate (5-mmi) is possible. The remaining examples possess directing functionalities located at sites for which only a 6-mmi is accessible. Moreover, both the tetrahedral arrangement of sulfur-containing functionalities and the poorly ligating ability of carbamates introduce further difficulties to engage in productive C—H activation and subsequent deuteration at adjacent positions.

Encouraged by previous *in silico* studies which demonstrated an improvement in the binding energy profile of sulfones with iridium complexes bearing chelating ligands which impose lower degree of steric encumbrance around the metal centre,[160] a new question warranted further investigation, *viz.*, is the release in steric pressure a

significant factor in the stabilisation of more strained and congested 6-membered metallacycle intermediates?

Qualitatively, this premise seems promising. Considering the increase in activity towards C—H bond activation processes through 6-mmi mediated by iridium(III) hydrides bearing biphosphine ligands,[127] and the only available report in literature,[121] which was released after the developments presented herein, it is conceivable that a similar effect would be observed when employing catalysts of type **150a-c** in the HIE of substrates to those depicted in Scheme 1.46. Scheme 1.47 provides an illustration of this effect with an arbitrary substrate that undergoes isotope exchange through a 6-mmi.
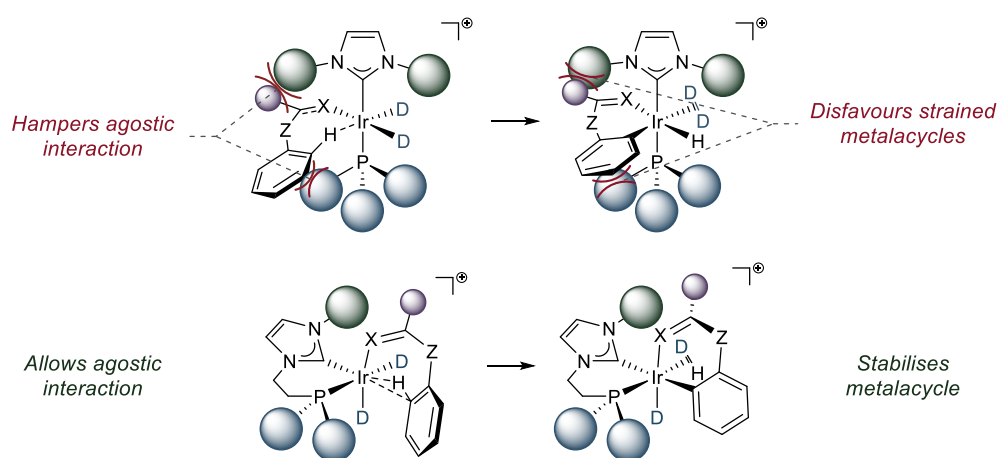
Scheme 1.47: Working hypotheses for productive C—H activation.

Owing to the prevalence of carbamates in pro-drugs and compounds of pharmaceutical relevance, mostly a consequence of their favourable absorption properties and capacity to engage in hydrogen bonding, serving as good isosteres of peptide bonds[191] and phenols;[194] and their ubiquitous presence as protecting groups for nitrogenated molecules, the *N*-(*tert*-butylcarbamoyl)- group (Boc) was selected as a probe for initial tests on catalytic activity.

This choice also stems from a strategic standpoint. In fact, if catalysts of type **150a-c** were able to engage in productive C—H activation events directed by the challenging *N*-Boc functionality, another current dilemma in HIE could be tackled, namely, the labelling of anilines. Analogous to carbamates, anilines are important groups in medicinal chemistry, featuring in several drug motifs[195,196] and being

known contributors to mutagenic effects in mammals,[198,199] thus continuing to be an intensive area of research in the realm of pharmacophores. Scheme 1.48 illustrates the conceived strategy.
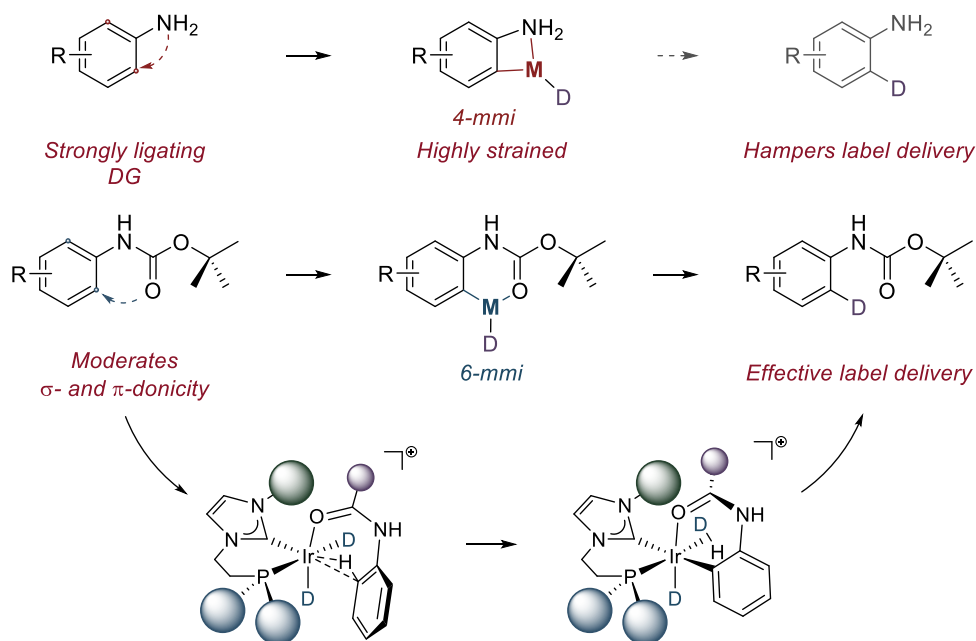
Scheme 1.48: Harnessing the potential of carbamates as directing groups.

Having established a reasonable framework to explore the capabilities of novel iridium(I) complexes, we initiated theoretical and experimental validation of these hypotheses.

3.3.1 Targeting sterically hindered aryl carbamates

One of the fundamental premises of accessing sterically congested directing groups to promote C—H activation is the ability to engage in productive coordination with the catalytically active species. Considering the simpler solution dynamics of **150c** upon exposure to H_2 and insightful previous developments in exploiting DFT to probe HIE reactions,[160] our investigation commenced by calculating the binding energies of relevant *N*-aryl carbamate to iridium(III) deuterides derived from reference catalyst **60** and candidate **150c**, as depicted in Scheme 1.49.
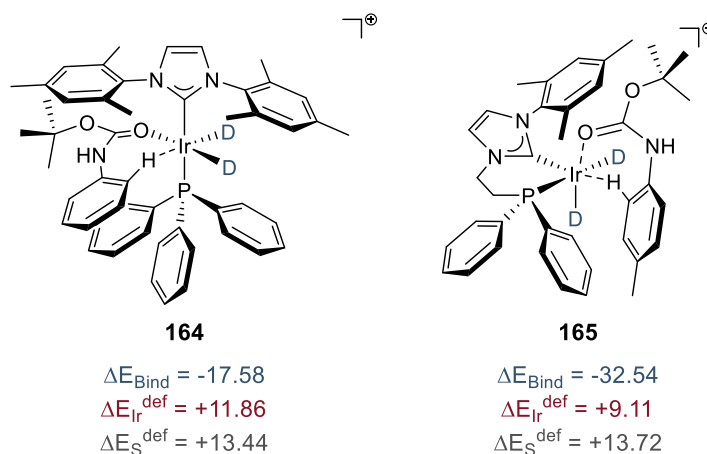
Scheme 1.49: Difference in binding energies.[†]

[†]Energies are given in kcal mol^{-1}; ΔE_{Bind} – binding energy; ΔE_{Ir}^{def} – deformation energy for catalyst fragment; ΔE_S^{def} – deformation energy for substrate fragment.

Notably, interaction energies for **165**, derived from catalyst **150c**, were significantly lower than those arising from **164**, originating from **60**, resulting in an increase in binding capacity of -14.96 kcal mol^{-1}. In addition to providing stronger interaction with the selected molecular probe, **165** displays lower deformation energy than **164**, *i.e.,* the chelating NHC-P framework undergoes fewer distortions and reorientations which create steric interactions during the coordination event than those brought about by **164**. Interestingly, deformation energies associated with the carbamate do not change significantly for this pair, indicating that most of the contributions to the poor binding ability of **164** arise from the requirement to reorient the ancillary ligands.

Another important aspect of an effective catalytic system is the capacity to provide efficient turnover for the desired process. From our detailed previous knowledge on the mechanistic aspects of HIE reactions with catalyst **60**, and the prominent binding ability of **150c**, we anticipated that correct choice of solvent would be paramount to enable efficient labelling of carbamates. The first step in the catalytic cycle is the displacement of two solvent molecules within the coordination sphere of the iridium catalyst by the substrate. Therefore, if we employed a solvent with considerably better ligating properties than those displayed by carbamates, the equilibrium for dissociative ligand exchange would strongly favour the solvent-bound complex. Conversely, if substrate ligation severely dominates the displacement equilibria,

release of labelled material would hamper productive catalysis. Any of these scenarios would result in slow, or even impractical, turnover rates for the reaction and should thus be avoided. We then undertook an *in silico* screening of 12 solvents covering a broad spectrum of physical properties employing catalyst **150a** and *O-tert*-butyl-*N*-phenyl carbamate **166a** as less computationally demanding representatives for assessing displacement equilibria. Table 1.15 collates the results thus obtained.

Table 1.15: Solvent displacement equilibria.[†]
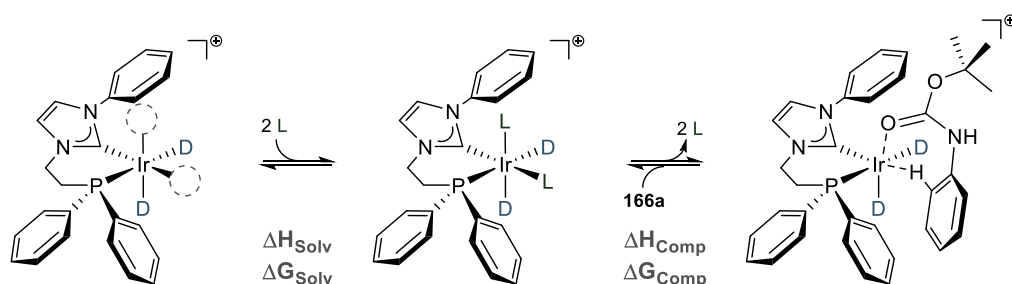
Entry	Solvent	ΔH_{Solv}	ΔG_{Solv}	ΔH_{Comp}	ΔG_{Comp}
1	CH_2Cl_2	-25.85	-0.89	-9.88	-17.55
2	Toluene	-33.03	-6.13	-2.70	-12.30
3	$^{i}Pr_2O$	-38.12	-8.73	2.39	-9.70
4	MTBE	-41.38	-15.51	5.66	-2.92
5	Et_2O	-43.47	-16.55	7.74	-1.88
6	MeOH	-45.28	-23.69	9.55	5.25
7	2-MeTHF	-53.76	-25.99	18.03	7.56
8	H_2O	-48.75	-27.41	13.03	8.98
9	THF	-53.16	-28.57	17.43	10.13
10	$^{i}PrOH$	-55.47	-29.59	19.74	11.16
11	$^{i}PrOC(O)OMe$	-57.18	-31.85	21.46	13.42
12	MeCN	-60.78	-38.39	25.06	19.96

[†]Energies given in kcal mol^{-1}; Solv – solvent coordination event; Comp – substrate complexation.

Inspection of the results in Table 1.15 reveals interesting trends. Firstly, solvation enthalpies are in qualitative agreement with the σ- and π-donor abilities of selected solvents. Secondly, considering the free energies for solvent association – ΔG_{Solv}, poorly ligating ethereal solvents in entries 3 – 5, di-*iso*-propyl ether, methyl *tert*-butyl ether (MTBE) and Et_2O, respectively, appeared as promising candidates for their ability to compete with substrate, slightly favouring coordination of the latter. Finally, the weakly coordinating capacity of carbamates strongly favour solvent

association when the less sterically crowded ether THF and the more ligating ester ^{i}PrOC(O)Me are considered. This screening led us to begin our experimental investigations employing MTBE as solvent: being a bulky ether, this solvent should provide steric protection of reactive intermediates whilst enabling reversible coordination of substrate.

We then synthesised *O-tert*-butyl-(4-methyl)phenyl carbamate **166b** and screened the activity of complexes **150a-c** in HIE reactions. For the sake of comparison, two of our well-established catalysts for labelling of aromatic substrates, **60** and its analogue bearing a tribenzylphosphine ligand – **167**, were also included in our screening, as displayed in Table 1.16.

Table 1.16: Catalyst screening for the HIE of **166b**.
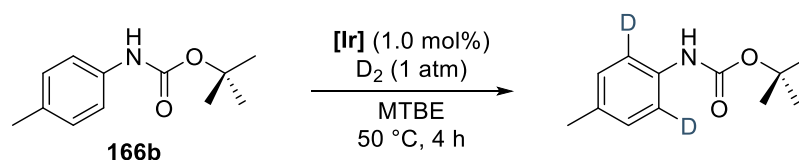
Entry	Catalyst	Incorporation^a	
		%D^b	SD (%)^c
1	**150a**	77	9
2	**150b**	92	2
3	**150c**	94	1
4	**60**	12	3
5	**167**	11	2

^{a}Deuterium incorporation determined by ^{1}H NMR spectroscopy; ^{b}average of three consecutive runs; ^{c}SD – standard deviation.

To our delight, catalysts **150a-c** (entries 1 – 3) were remarkably active in the HIE of carbamate **166b** at a 1.0 mol% loading, with **150b-c** affording excellent levels of incorporation under mild reaction conditions. Conversely, complexes **60** and **167** (entries 4 – 5), bearing a more sterically encumbered combination of monodentate ligands, were ineffective promoters of isotope exchange. These observations are in line with our working hypotheses, thus indicating steric effects are dominant factors in the activation of C—H bonds *ortho-* to sterically hindered directing groups, and that our DFT assisted selection of solvents was efficient at identifying a system capable to provide reaction turnover.

Encouraged by the promising activity of our novel chelating catalysts, we prepared a series of *N*-phenyl carbamates and evaluated these substrates in HIE reactions with the more active catalyst **150c** as illustrated in Scheme 1.50.
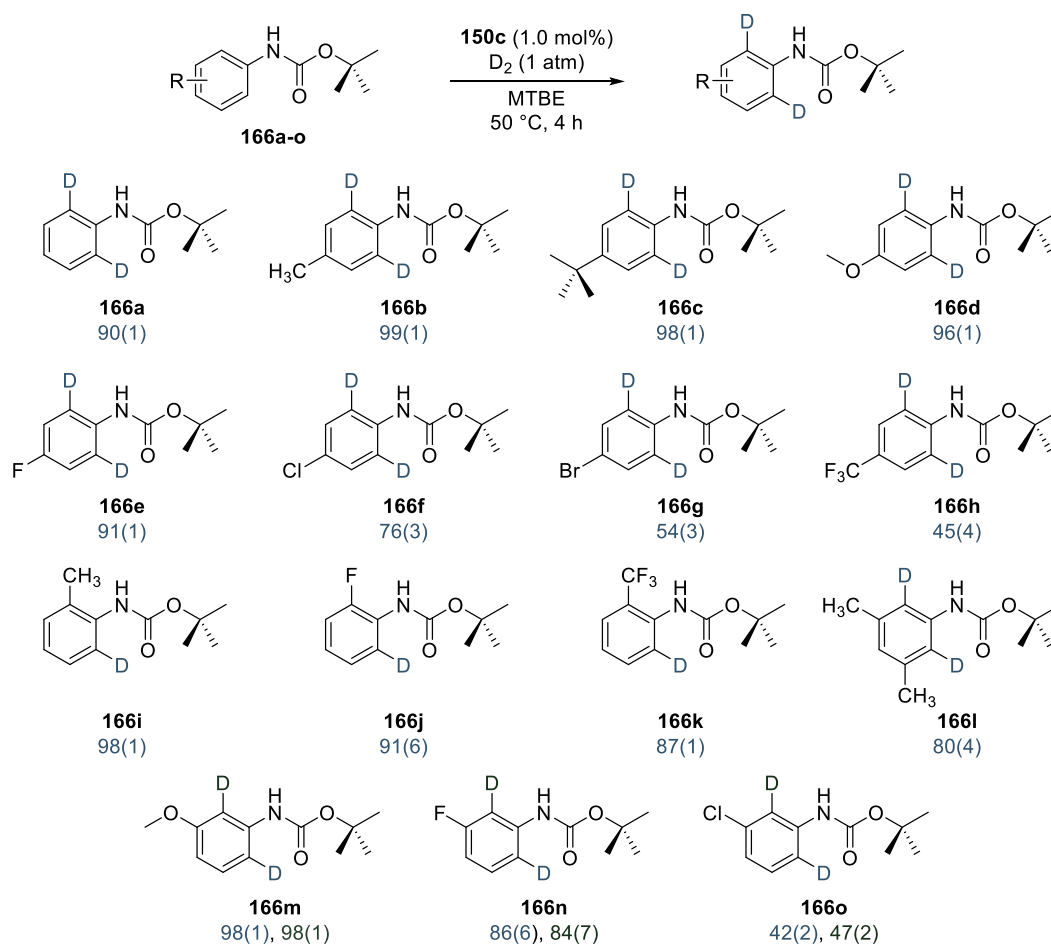
Scheme 1.50: Substrate scope of *N*-aryl carbamates.[†]

[†]Deuterium incorporation determined by ^{1}H NMR spectroscopy. Reported values are average of three runs; standard deviations show in brackets.

Notably, catalyst **150c** was active in the HIE of carbamates bearing substituents with diverse electronic properties in all positions of the aromatic ring, delivering moderate to excellent levels of incorporation at a reduced 1.0 mol% catalyst loading. Inspection of these results reveal some interesting trends. Firstly, levels of deuteration are directly proportional to the electron-donating ability of aromatic substituents at the *para-* position. Thus, substrates **166a-e**, bearing neutral, EDGs and weakly EWGs were deuterated to excellent levels, whereas substrates **166f-h**,

possessing moderate and strong EWGs, were labelled to a lesser extent. This observation suggests the electron density at the carbamate group and, by extension, its coordination to the catalyst, might play a more important role in the reaction mechanism than previously anticipated. Secondly, complex **150c** seems to be incredibly tolerant of steric congestion around the aromatic ring, accommodating well the presence of CH_3 (**166i**) and CF_3 (**166k**) groups at the *ortho-* position, and hindered labelling sites such as those in **166l**. Finally, the apparent disparity in catalytic activity towards substrates **166h** and **166k**, both of which possess the CF_3 substituent, is likely a consequence of the disruption of inductive electron-withdrawing ability of substituents *ortho-* to sterically encumbered groups.[197] In this regard, DFT calculations performed with **166h** and **166k** also revealed a prominent deviation of coplanarity between the aromatic ring and the carbamate for **166k** of 28.4°.

Having scrutinised the activity of **150c** against a range of *N*-aryl carbamates, we pondered whether this catalytic system would be equally active towards the labelling of isoelectronic *O*-phenyl carbamates. To test this premise, we synthesised a small series of substrates bearing *N*-substituents with diverse steric properties and evaluated them in the HIE process employing reaction conditions analogous to those applied for aniline derivatives. Scheme 1.51 presents the results obtained.
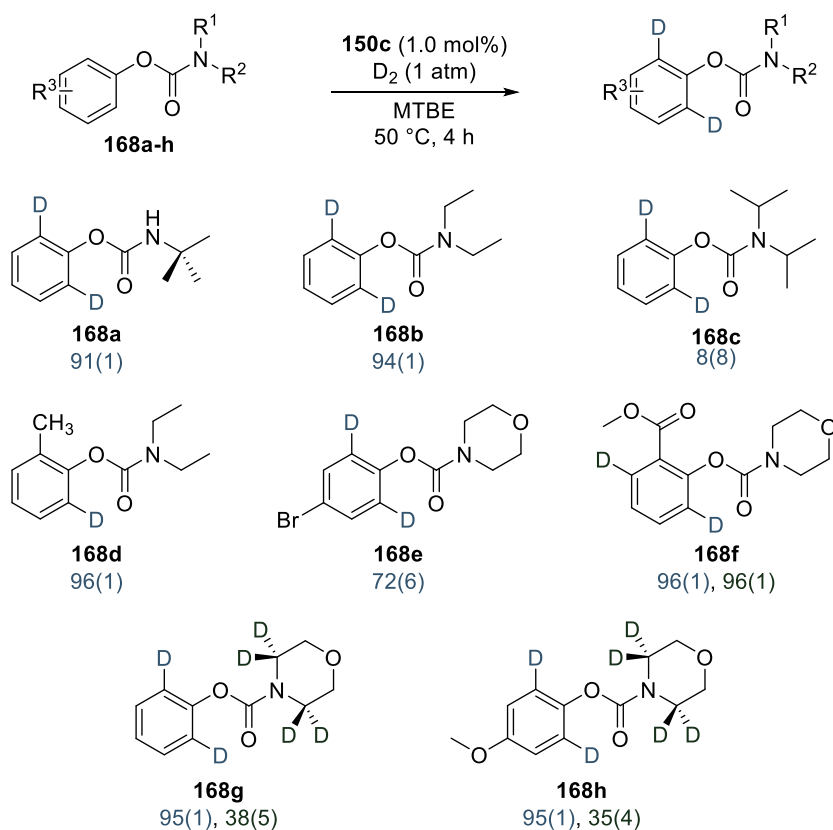
Scheme 1.51: Scope of *O*-aryl carbamates.[†]

[†]Deuterium incorporation determined by ^{1}H NMR spectroscopy. Reported values are average of three runs; standard deviations show in brackets.

Interestingly, **150c** displayed slightly higher catalytic activity in the HIE of *O*-aryl carbamates in comparison to their *N*-aryl counterparts (*cf.* **166g** and **168e**). Moreover, the dependence on steric hindrance around the directing group, but not that imposed by substituents in the aromatic ring, was decisive for effective catalysis, a factor that becomes evident when comparing carbamates **168a-c**. In this series, isomeric carbamates **168a-b** were labelled to similar extents, whilst **168c**, bearing a severely hindered directing group, could not be satisfactorily deuterated. Noteworthily, **150c** was able to label **168f**, a carbamate which also contains an ester functionality, thus indicating the tolerance of the catalyst to intramolecular competition with other weak directing groups. Finally, substrates **168g-h** were also labelled at sites on the morpholine ring, indicating good compatibility of **150c** to activate more challenging C_{sp^3}—H bonds.

Recognising the potential to efficiently deuterate previously neglected labelling sites with our novel chelated complexes, we decided to test **150c** in the HIE of a carbamate derived from a biologically relevant molecule. Hence, we synthesised the respective *O*-phenyl carbamate derived from the amino acid tyrosine and subjected it to standard reaction conditions, as shown in Scheme 1.52.
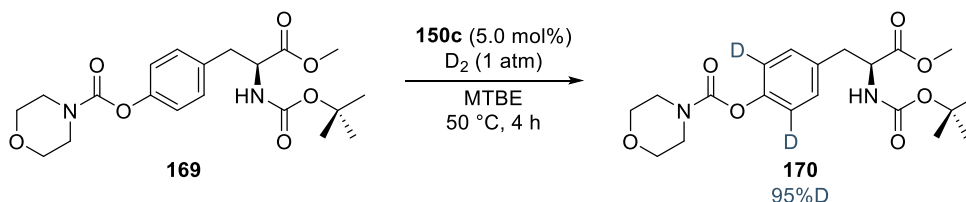
Scheme 1.52: HIE of tyrosine derivative.[†]

[†]Deuterium incorporation determined by ^{1}H NMR spectroscopy. Average of two runs.

To our delight, **150c** effectively labelled the available C_{sp^2}—H sites in the presence of two other interfering ligating groups, *viz.*, the methyl ester and *N*-Boc functionalities. Notably, the position of these two functional groups is appropriate to afford both 5- and 7-membered chelates with iridium(III) hydrides of type **155c**, capable of hampering productive HIE by abstraction of catalytically relevant species from the reaction medium. Notwithstanding this possible setback, the equilibrium seems to favour productive coordination of the desired *O*-aryl carbamate functionality to such extent that C—H activation prevails over undesired chelation by other neighbouring groups.

Finally, we investigated the potential of catalyst **150c** to produce isotopically labelled anilines in a two-step process. Thus, carbamate **166b** was reacted under standard reaction conditions to afford its isotopologue **166b-*d₂*** in 98% yield and 89% incorporation, as illustrated in Scheme 1.53. Subsequent deprotection of the *N*-Boc functionality under acidic conditions produced the desired labelled aniline **171-*d₂*** with complete retention of deuterium.
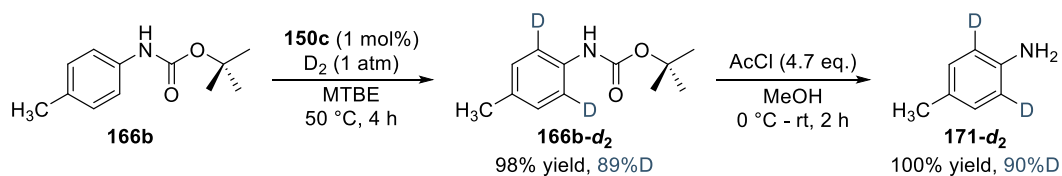
Scheme 1.53: Synthesis of deuterated aniline through a two-step protocol.

Having developed an efficient protocol to perform labelling of substrates bearing challenging sterically hindered directing groups which enabled access to HIE of unprecedented molecular scaffolds, we decided to further investigate the mechanistic aspects of the underlying C—H activation.

3.3.2   Theoretical mechanistic understanding and validation

Guided by the original premise that iridium complexes bearing chelating NHC-P ligands would be more effective at stabilising 6-membered metallacycle intermediates than their heteroleptic monodentate analogues, we began our investigations by calculating the potential energy surface (PES) for C—H activation of probe molecule **166b** with iridium(III) deuterides derived from **60** and **150c** – Scheme 1.54.
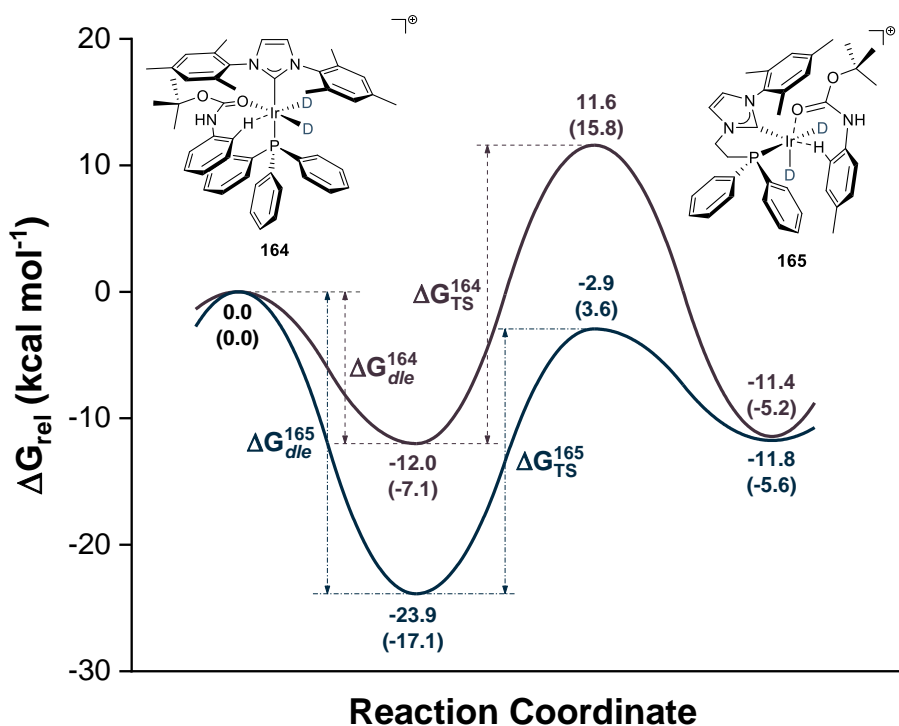
Scheme 1.54: PES for C—H activation of **166b** by catalysts **60** and **150c**.[†]

[†]Reported values are ΔG_{rel}; ΔH_{rel} given in parentheses; reported energies are relative to the respective $[(NHC\text{-}P)IrD_2(CH_2Cl_2)_2]^+$ complexes; ΔG_{dle}^N –energy of dissociative ligand exchange with substrate; ΔG_{TS}^N – activation energy.

Notably, complex **150c**, bearing a chelating NHC-P ligand, engages in a dissociative ligand exchange with substrate **166b** which significantly stabilises the system, with $\Delta G_{dle}^{165} = -23.9$ kcal mol^{-1}. By comparison, complex **60** engages in a similarly favourable equilibrium with **166b**, resulting in ΔG_{dle}^{164} of -12.0 kcal mol^{-1}. The initial doubled exergonicity of substrate engagement by **150c** results in a strong driving force for coordination, thus inhibiting a premature dissociation of carbamate that could hamper C—H activation. Finally, the formation of relevant metallocyclic intermediates requires less disparate activation energies of 23.6 and 21.0 kcal mol^{-1} for intermediates **164** and **165**, respectively. Despite being a seemingly small energetic difference, a $\Delta\Delta G \approx 2.5$ kcal mol^{-1} in favour of C—H activation by complex **150c** would result in a 60-fold increase in reaction rate at 25 °C.

Surprisingly, the energies of 6-membered metallacycles generated by **164** and **165** are essentially equal. Therefore, the high activity of catalysts bearing NHC-P ligands stems from the synergy between their capacity to promote strong binding of weakly

ligating directing groups and their lower activation energies for cleavage of C—H bonds.

These calculations also revealed a previously unexpected feature of intermediate **165**. More specifically, metallacycle formation seemed to proceed *via* a pathway that did not require the typical fluxional process to enable subsequent C—D bond formation. In fact, the direction of the σ-bond metathesis involving **165** implied the production of a HD molecule *cis-* to the newly generated Ir—C bond. Similar processes involving **164** deliver a *trans-*(η^2-D$_2$) ligand for which fluxionality is known to precede the deuteration event. We thus proceeded to evaluate the full PES for HIE of **166b** with catalyst **150c**, as depicted in Scheme 1.55.
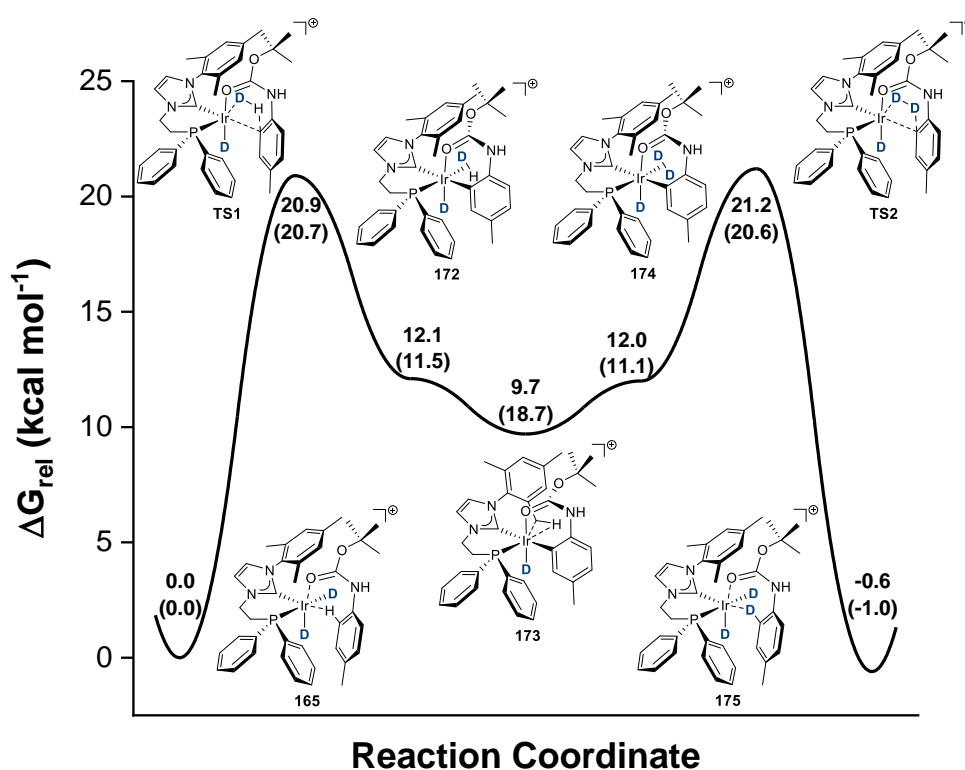
Scheme 1.55: Full PES for the HIE of **166b**.[†]

[†]Reported values are ΔG_{rel}; ΔH_{rel} given in parentheses.

The located pathway consisted of substrate coordination with formation of agostic interaction delivering **165**, followed by a C—H activation through **TS1** which generates the requisite 6-mmi in **172**, proceeding through an overall barrier of 20.9 kcal mol^{-1}. This intermediate then undergoes de-coordination of a HD molecule to

afford coordinatively unsaturated complex **173**, which is stabilised by an agostic interaction with a methyl group from the mesityl substituent within the NHC. Association of D_2 then ensues to deliver **174**, which engages in C—D bond formation *via* **TS2**, thus introducing the label into the coordinated substrate in intermediate **175**. Is must be emphasised that all attempts to locate a transition state for a fluxional process to promote exchange between the coordinated HD molecule and the apical deuteride in **172** were unsuccessful.

Careful inspection of geometrical differences between 6-membered metallocyclic intermediated generated by **164** and **165** helped elucidate the underlying factors dictating a change in direction of the σ-bond metathesis responsible for C—H activation, as illustrated in Scheme 1.56.

172

| $d^*_{Ir}{}^{(\sigma)}$ | $d_{Ir}{}^{(\sigma)}$ | $d^*_{Ir}{}^{(\sigma)}$ | $d_{Ir}{}^{(\sigma)}$ |

| σ^*_{PC} σ_{HD} | σ_P σ^*_{HD} | σ^*_{CC} σ_{HD} | σ_C σ^*_{HD} |

| Ir ← HD donation | Ir → HD back-donation | Ir ← HD donation | Ir → HD back-donation |

176
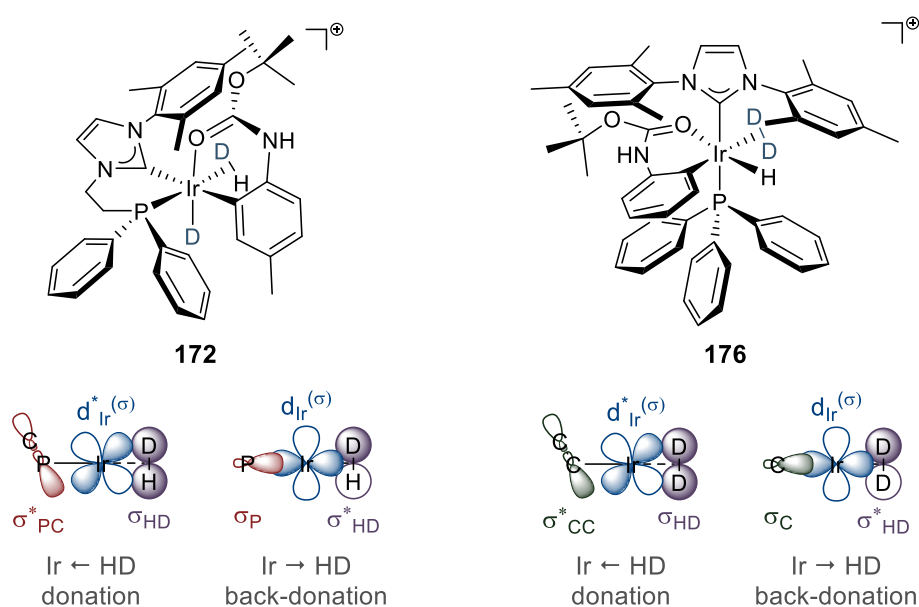
Scheme 1.56: Metallocyclic intermediates with simplified bonding interactions.

Since molecular hydrogen is a very weak σ-donor, its ability to coordinate to organometallic complexes is intrinsically related to the capacity of the metal centre to engage in productive back-donation with the $\sigma^*_{H_2}$ orbital. Therefore, both η^2-HD and η^2-D_2 are expected to bind to the most electron-rich orbitals of iridium in **172** and **176**. In the former case, the mandatory *cis-* geometry of the NHC-P ligand forces the incoming HD ligand to be positioned *trans-* to the PPh$_2$ fragment, a strong σ-donor which also displays good π-accepting character.

Alternatively, if we required **172** to mimic the σ-bond metathesis performed by **176**, the hypothetical D_2 ligand thus produced would occupy a site *trans-* to the oxygen atom from the carbamate, a significantly poorer σ-donor than its phosphorus counterpart. Conversely, if we forced **176** to parallel the C—H activation event observed for **172**, a similar destabilisation would be observed, as we placed a HD molecule *trans-* to the carbamate. Thus, the observed discrepancy in the direction of the σ-bond metathesis performed by these complexes is a consequence of inherently different orbital interactions in these systems. Finally, we completed our investigations by performing an intrinsic reaction coordinate (IRC) to ensure the transition state located unequivocally connected intermediates **165** and **172**, as illustrated in Scheme 1.57.
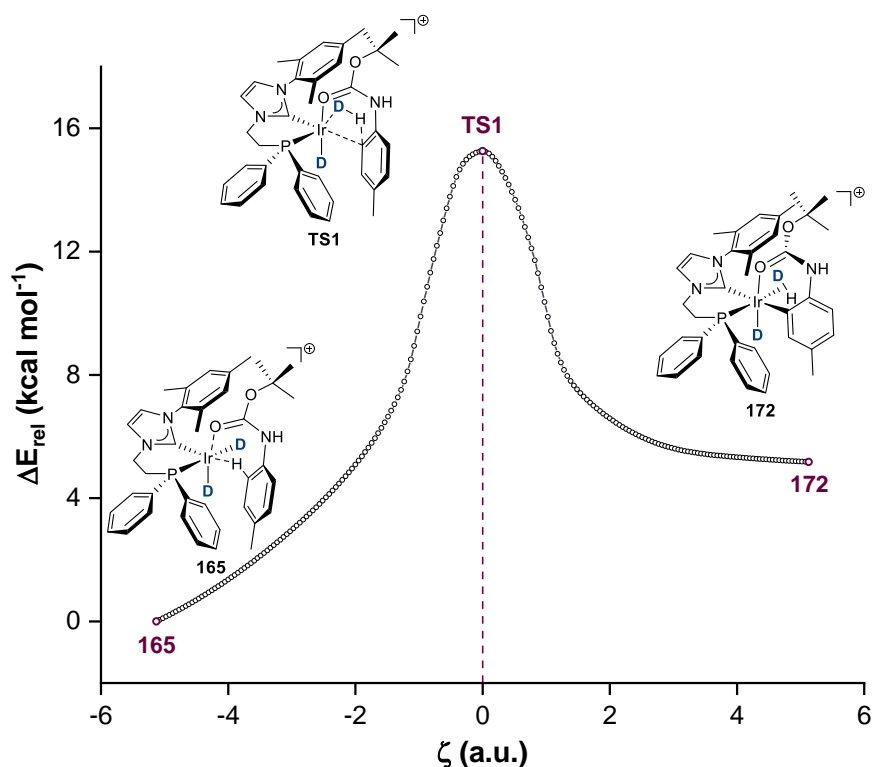
Scheme 1.57: IRC for transition state **TS1**. [†]

[†]ζ – reaction coordinate in atomic units.

Once a reasonable understanding of the reaction mechanism underlying the labelling of carbamates had been established, experimental validation of these premises was warranted. We commenced our investigations by estimating the kinetic isotope effect

(KIE) associated with the proposed C—H activation, which required calculation of a reversed pathway in which **166b-d_2** was converted to **166b-d_1** *via* the corresponding **TS1** isotopomer. These results are outlined in Scheme 1.58.
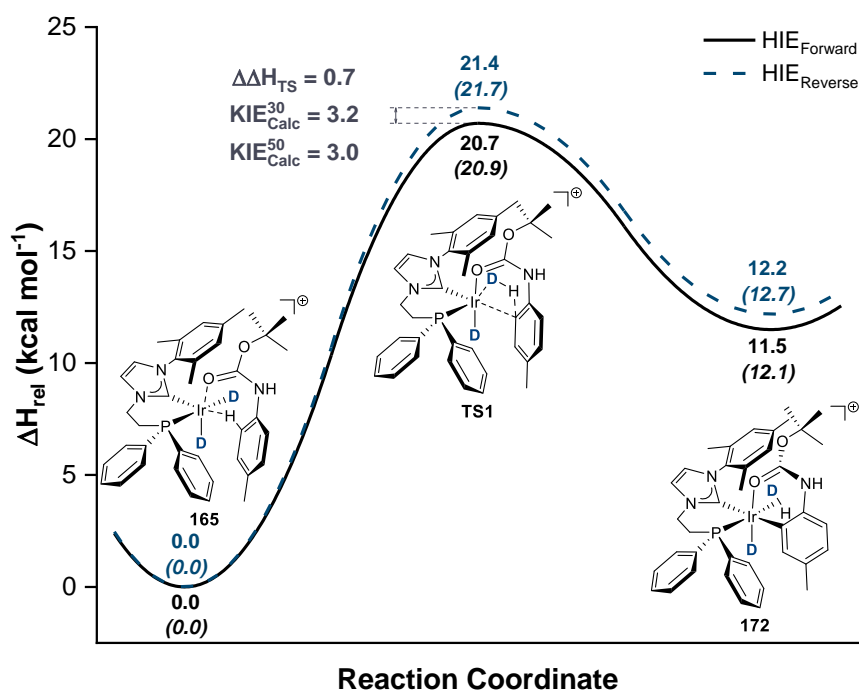
Scheme 1.58: Calculated KIE for C—H activation of **166b**.[†]

[†]Reported values are ΔH_{rel}; ΔG_{rel} given in parentheses.

An important consideration involved in the estimation of KIE values require further discussion. Cognisant of the nearly isentropic nature of σ-bond metathesis involving coordinated H_2 molecules,[87] and the well-documented issues related to accurate entropy calculations by semi-empiric methods,[200] we opted for employing ΔH_{rel} values in our KIE calculations (see Computational Details for further information), which afforded estimates of 3.0 and 3.2 at 50 and 30 °C, respectively.

Having established expected kinetic isotope effect values, we began our experimental investigations by measuring the rate of reaction for both forward and reverse HIE processes with substrate **166b** and catalyst **150c**, as depicted in Scheme 1.59.
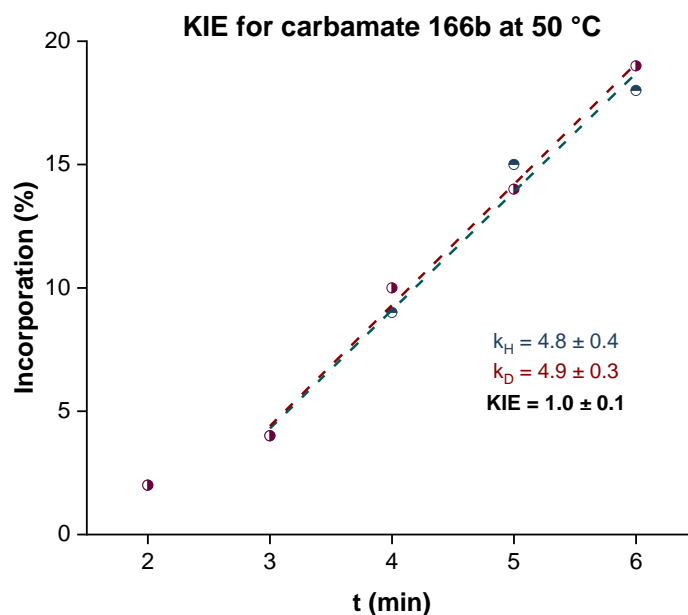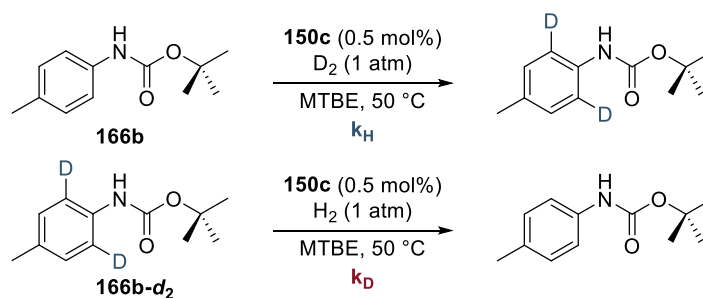
Scheme 1.59: KIE measurement for **166b**.[†]

[†]Rates given in %D min^{-1}.

Surprisingly, the HIE of **166b** was characterised by a KIE of 1.0 ± 0.1, unequivocally determining that C—H activation *was not the rate limiting step in the reaction*. Taking into consideration our earlier calculations, which indicated that **150c** binds **166b** with high exergonicity, we hypothesised substrate coordination and release of labelled material were occurring at rates comparable or, in fact, slower than the rate for productive C—H activation, thus hindering the observation of a direct KIE. Indeed, cases in which association and dissociation of substrate are important confounding factors in KIE measurements are known.[201]

Notwithstanding this minor setback, we postulated that a carbamate bearing a less sterically encumbered *O*-methyl substituent would engage in ligand displacement equilibria at faster rates than those experimentally observed for **166b**, effectively allowing for accurate KIE measurements and providing a valid molecular probe for

our endeavour to validate our mechanistic hypothesis. The validity of this assumption, however, is intrinsically dependent on similar energetic profiles for C—H activation of **166b** and its *O*-methyl counterpart **177**. Consequently, we proceeded to calculate the PES for HIE with **177** and provided an estimate for its KIE value, as depicted in Scheme 1.60.
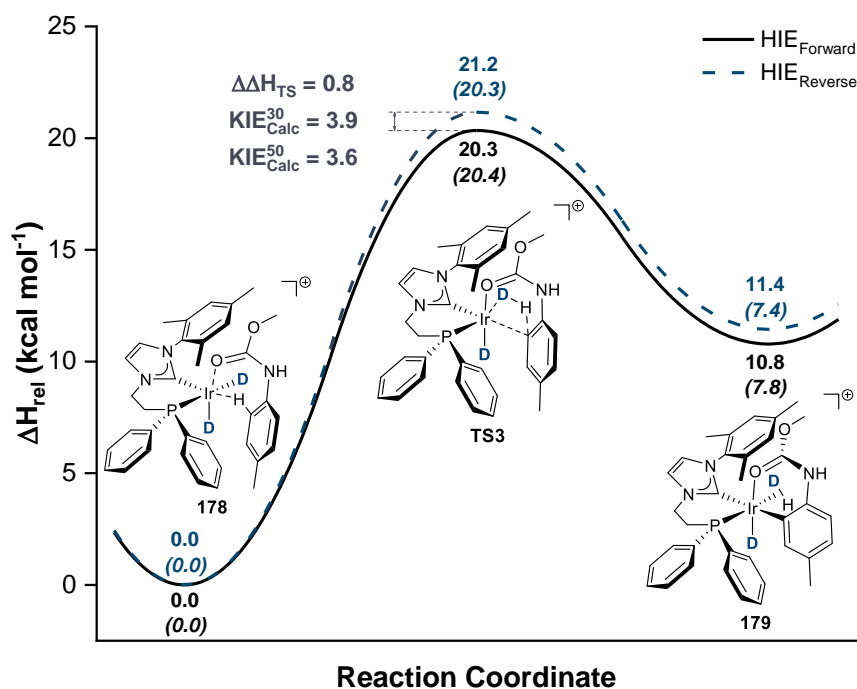
Scheme 1.60: PES for C—H activation of **177** and estimation of KIE values.[†]

[†]Reported values are ΔH_{rel}; ΔG_{rel} given in parentheses.

Gratifyingly, the PES for the HIE of *O*-methyl carbamate **177** was similar to the process calculated for **166b**, affording KIE values of 3.9 and 3.6 at 50 and 30 °C, respectively. Finally, we synthesised **177** and performed the requisite rate measurements to enable experimental validation of our estimates, as shown in Scheme 1.61.
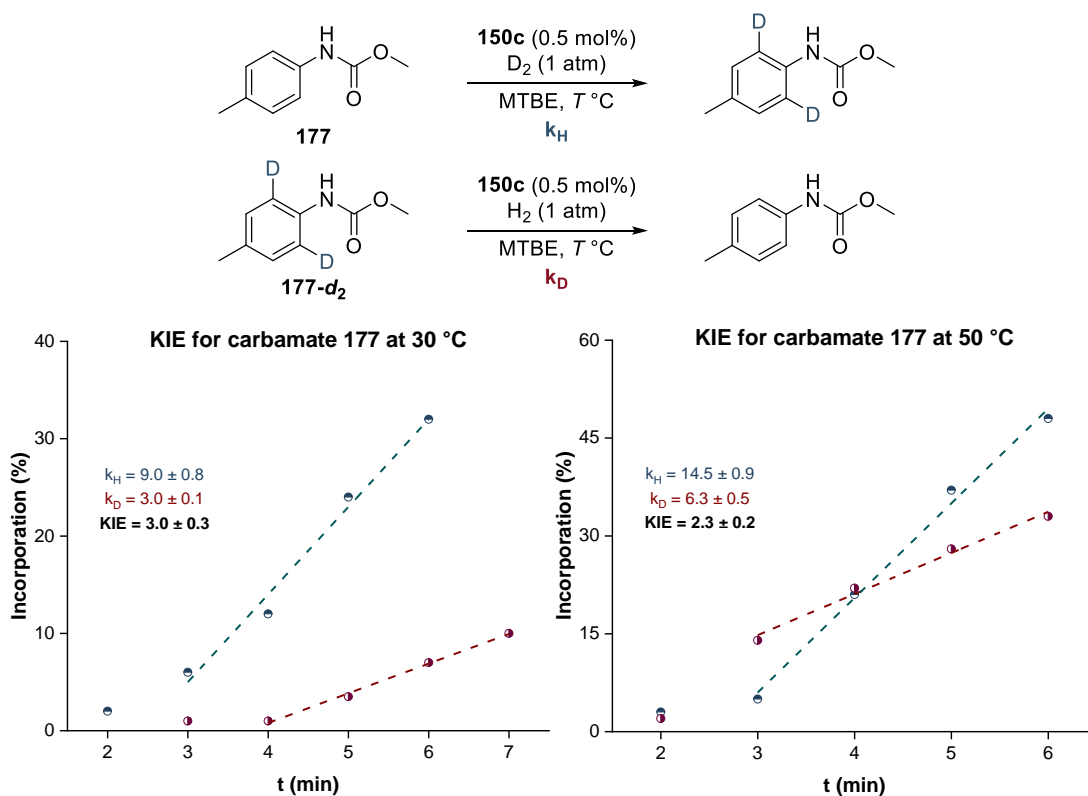
Scheme 1.61: KIE measurements for **177**.[†]

[†]Rates given in %D min^{-1}.

Notably, normal KIE values of 3.0 ± 0.3 and 2.3 ± 0.2 at 30 and 50 °C, respectively, were observed for C—H activation of **177**. From the kinetic data gathered for **166b**, we anticipated participation of substrate coordination in the determination of KIE values in Scheme 1.61. Therefore, observed rate constants are a composite of two well-defined equilibria, as illustrated in Scheme 1.62.
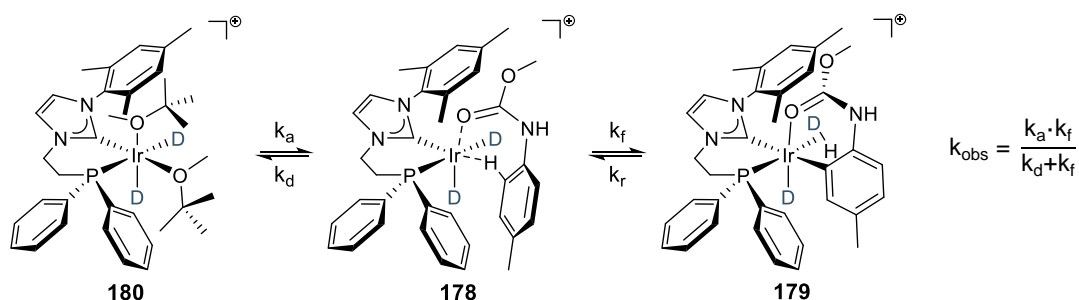
Scheme 1.62: Equilibria and rate law for C—H activation of **177**.[†]

[†]Individual rate constants: k_a – substrate association; k_d – substrate dissociation; k_f and k_r – forward and reverse σ-bond metathesis, respectively.

Assuming the steady-state approximation[202] applies for complex **178**, then the rate law for σ-bond metathesis is a composite of coordination and C—H bond cleavage, as indicated in the equation for k_{obs} in Scheme 1.62. As previously discussed, in the case of **166b**, $k_f \gg k_d$, and $k_{obs} \approx k_a$, given only small differences are expected for association rates of carbamate and its labelled analogue, KIE measurements for *O-tert*-butyl carbamate **166b** would tend to a value of 1. This is clearly not the case for its *O*-methyl counterpart **177**, which displays pronounced isotope effects.

Therefore, by considering a scenario in which $k_d \gg k_f$, we obtain $k_{obs} \approx k_a \cdot k_f/k_d$, which affords the following KIE expression:

$$KIE = \frac{\left[k_a^{(H)} \cdot k_f^{(H)}\right] \cdot k_d^{(D)}}{\left[k_a^{(D)} \cdot k_f^{(D)}\right] \cdot k_d^{(H)}}$$

Importantly, it is possible to recognise the inseparable nature of substrate association equilibrium and KIE measurements for **177**. Moreover, good qualitative agreement between calculated and observed kinetic isotope effect values for **177**, obtained under the assumption that C—H bond breaking dominates the rate expression for KIE, led us to conclude that coordination of substrate has only a minor effect in the reaction rates of less sterically hindered **177**. From the same perspective, the converse applies to bulkier *O-tert*-butyl carbamate **166b**, with rate constants for association and dissociation of isotopologues **166b** and **166b-*d₂*** dominating the overall rate expression, thus preventing direct observation of a KIE value which allows for reasonable comparison with our DFT calculations.

In summary, a combination of *in silico* studies and kinetic data at different temperatures for **177** permitted validation of the mechanistic pathway outlined in Schemes 1.56 and 1.58. As a final remark, we emphasise that similar cases of attenuation of observed KIE values, and even complete overriding of the rate expression, by coordinative events have been reported in detail elsewhere. For instance, Bergman *et al.*, whilst studying C—H activation of benzene by [Cp*(PMe₃)IrH₂], determined a diminished KIE of 1.26 ± 0.06 for this process;[203] and Parkin *et al.* observed predominance of substrate association in the activation of benzene by *ansa*-{[Me₂Si(C₅Me₄)₂]W}, which afforded a unitary kinetic isotope effect value.[204]

At the outset of these studies, we were able to propose the mechanism for the HIE of hindered carbamates illustrated in Scheme 1.63, which employs substrate **177** as a representative example.
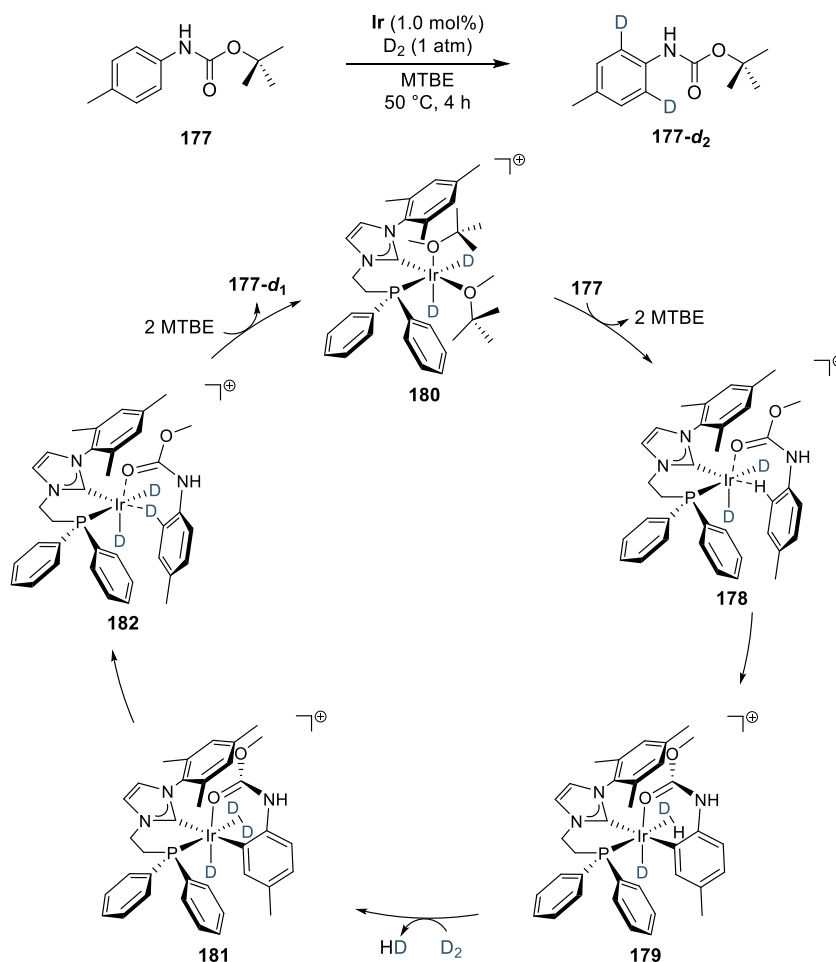
Scheme 1.63: Mechanistic proposal for HIE of carbamates.

Thus, coordination of carbamate to iridium *bis*-solvate **180** affords agostically bound intermediate **178**, which engages in C—H activation yielding metallocyclic intermediate **179**. Subsequent exchange of a DH molecule by molecular deuterium then takes place to afford intermediate **181**, which undergoes C—D bond formation and installs the label at the coordinated substrate in **182**. A final ligand exchange with two molecules of solvent restarts the catalytic cycle and releases **177-d_1**, that can re-enter the cycle to yield fully deuterated product **177-d_2**.

Throughout these investigations, we developed profound interest in exploring the nature of the C—H activation event in more detail, aiming to gather a better understanding of factors controlling this delicate process. We then embarked in a detailed DFT study that would hopefully enable us to create a simpler, deconvoluted view of this process.

3.3 Statistical model for enthalpies of activation enabled by DFT

In previous sections, we developed a mechanistic rationale for the HIE of sterically hindered carbamates. These studies indicated that the coordination of substrate and the C—H activation, which leads to productive formation of a 6-mmi, operated as competing rate limiting processes in the reaction. Since steric components are intrinsically associated with the nature of *O*-substituents, which can be easily tuned during substrate synthesis, we sought to investigate in more details the factors that govern the C—H activation event. More specifically, the barrier of activation for σ-bond metathesis was identified as a key element in the reaction pathway, therefore we aimed at identifying easily computable descriptors that predict the corresponding activation energies, thus resulting in its decomposition into chemically meaningful parameters. Ultimately, this model would allow for facile access to estimates of the activation energy, which typically require computationally demanding techniques for transition state determination, and would enable the identification of useful factors for subsequent catalyst design.

Thus, considering the conclusions derived from our rate measurements, we decided to begin our investigations exploring the activation energies for C—H bond cleavage in *O*-methyl carbamates. Accordingly, we conceived a set of aryl carbamates bearing various substituents with different steric and electronic properties, as shown in Scheme 1.64.
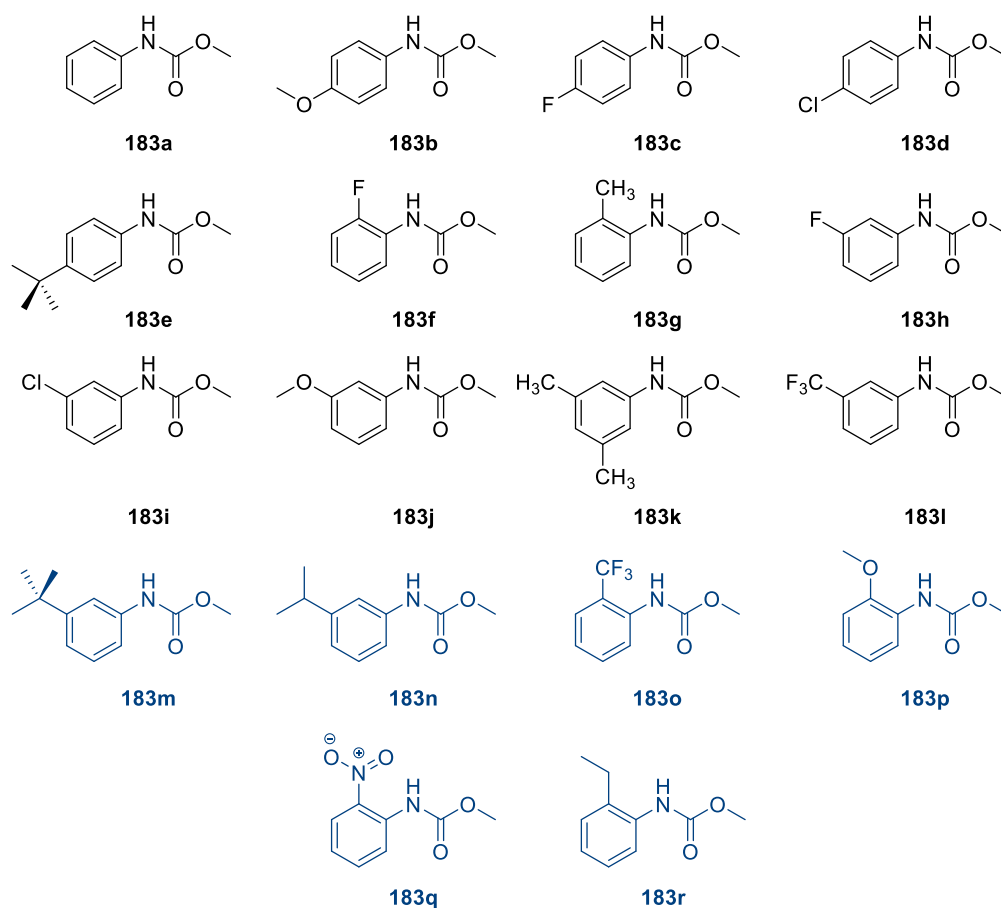
Scheme 1.64: Carbamates selected for DFT modelling.[†]

[†]Colour code for structures: black – calibration set; blue – validation set.

Whilst aiming to arrive at an experimentally testable statistical model, we shortened our selection to include synthetically accessible compounds for which acquisition of rate data would be feasible. Consequently, carbamates **183a-l** were selected as the calibration set required for mathematical correlation of predictors generated by DFT; whereas compounds **183m-r** comprised a small validation set, included to test predictability and identify possible shortcomings of our method.

Having defined a reasonable collection of compounds, we proceeded to conduct single point calculations to gather DFT data on carbamates **183a-r**. More specifically, each substrate was optimised and had its PES for C—H activation evaluated. Scheme 1.65 summarises this workflow.
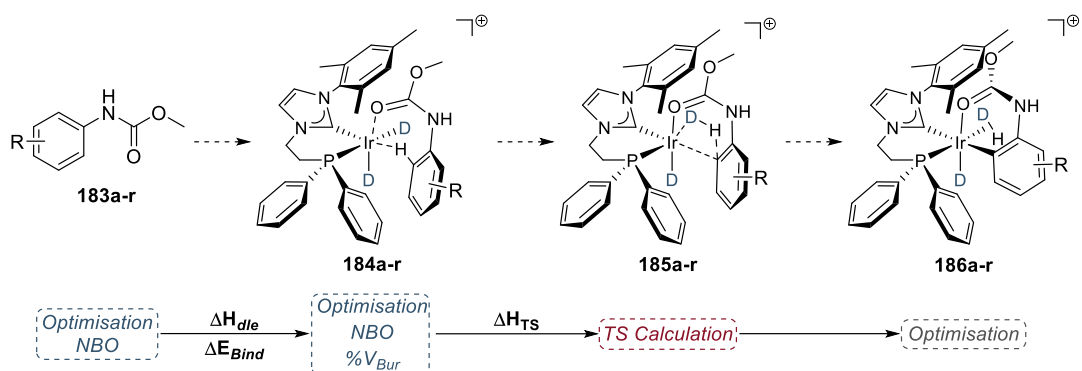
Scheme 1.65: Workflow of DFT calculations.[†]

[†]ΔH_{dle} – enthalpy of ligand exchange; ΔE_{Bind} – binding energy; ΔH_{TS} – enthalpy of activation; NBO – natural bond orbital analysis; $\%V_{Bur}$ – percent buried volume.

Owing to our previous knowledge of the reaction mechanism, we anticipated intermediates of type **184a-r** would play a central role in defining the kinetics of the reaction and, hence, would be crucial to determine enthalpies of activation for C—H bond cleavage. Accordingly, the agostically ligated species were scrutinised in more detail to afford mathematical descriptors suitable for the estimation of ΔH_{TS} values.

It is important to emphasise that the selection of DFT techniques able to extract geometric parameters, orbital interaction data, and three-dimensional volumetric distribution of ancillary ligands in **184a-r** was not arbitrary. Specifically, it was a combination of our experimental evidence for strong dependence on steric parameters and the idiosyncratic features of σ-bond metathesis[87] that led us to predict the existence of a strong correlation between activation energies and the stereo-electronic properties of intermediates **184a-r**.

Therefore, we conducted a total of 126 single point calculations, as follows: 3 sets of 18 optimisations and frequency calculations to collect geometrical and thermodynamic parameters from species **183**, **184** and **186**; 2 sets of 18 NBO[205] coupled to frequency calculations for generation of second-order perturbative analysis data for **183** and **184**; 18 transition state determinations for structures **185**; and 18 Counterpoise calculations[148] to gather binding energy data. As the final step in this procedure, we extracted buried volume parameters from structures **184a-r** to determine important steric factors arising from interactions between ancillary ligands and coordinated carbamates.

After extensive analysis of variance[206] and single variable correlations of more than 35 individual descriptors extracted from our DFT modelling, we identified three important groups of parameters that often featured among good predictors of activation energy. Namely, the sum of second-order perturbative energies originating from the $\sigma_{C—H}$ orbital implicated in the agostic interaction of species **184** – $E^2[\sigma_{C—H\rightarrow Ir}]$; the distance between Ir and the hydrogen centre transferred during the C—H activation – $d_{Ir\cdots H}$; and $\%V_{Bur}$ data generated by applying the quadrant model for asymmetric induction in enantioselective catalysis[207] to intermediates **184** (see Scheme 1.67 for an illustration of this concept).

Gratifyingly, all statistically significant variables identified in this search also carried reasonable physicochemical meaning. More precisely, $E^2[\sigma_{C—H\rightarrow Ir}]$ provides an estimate of σ-donation from the agostic C—H bond at the carbamate, $d_{Ir\cdots H}$ is correlated to the extent with which orbitals from the iridium centre interact with the bond to be activated, and $\%V_{Bur}$ values describe the degree of physical distortion that takes place at the NHC-P ligand framework upon substrate association. Combined, these parameters should approximate both electronic and steric influences associated with the C—H activation under scrutiny.

Encouraged by these findings, we proceeded to employ multivariate analysis to identify useful predictors for ΔH_{TS}. Thus, a two-step protocol consisting of identification of best variable subsets followed by multivariate regression afforded three possible candidates for our final model, as depicted in Scheme 1.66.

MODEL 1: $\Delta H_{Pred} = \alpha_0 + \alpha_1 \cdot V_{Bur}^{NW} + \alpha_2 \cdot V_{Bur}^{SE} + \alpha_3 \cdot E^2[\sigma_{C—H\rightarrow Ir}]$

Descriptor	Value	p_{value}
α_0	-(140 ± 42)	0.011
α_1	0.87 ± 0.32	0.026
α_2	2.17 ± 0.76	0.021
α_3	0.464 ± 0.041	<0.001
r^2_{adj}	0.920	
r^2_{pred}	0.854	
s_D	0.621	

MODEL 2: $\Delta H_{Pred} = \alpha_0 + \alpha_1 \cdot V_{Bur}^{NE} + \alpha_2 \cdot E^2[\sigma_{C—H\rightarrow Ir}] + \alpha_3 \cdot d_{Ir---H}$

Descriptor	Value	p_{value}
α_0	-(118 ± 50)	0.045
α_1	1.08 ± 0.61	0.114
α_2	0.368 ± 0.056	<0.001
α_3	24 ± 14	0.121
r^2_{adj}	0.889	
r^2_{pred}	0.845	
s_D	0.732	

MODEL 3: $\Delta H_{Pred} = \alpha_0 + \alpha_1 \cdot V_{Bur}^{NW} + \alpha_2 \cdot V_{Bur}^{SE} + \alpha_3 \cdot E^2[\sigma_{C—H\rightarrow Ir}] + \alpha_4 \cdot d_{Ir---H}$

Descriptor	Value	p_{value}
α_0	-(159 ± 48)	0.012
α_1	0.81 ± 0.33	0.046
α_2	2.03 ± 0.78	0.036
α_3	0.449 ± 0.44	<0.001
α_4	11 ± 12	0.391
r^2_{adj}	0.919	
r^2_{pred}	0.842	
s_D	0.628	

Scheme 1.66: Multivariate regression models and associated descriptors.[†]

[†]$\%V_{Bur}$ parameters are reported for the relevant quadrant; p_{value} – significance p test value; r^2_{adj} – adjusted regression coefficient; r^2_{pred} – predicted regression coefficient; s_D – standard deviation.

Meticulous inspection of the statistical descriptors associated with each model was particularly insightful. Firstly, all three statistical models obtained displayed high linearity and reasonable predictive power, as evidenced by r^2_{pred} values greater than 0.80. This parameter measures the capacity of the model to predict entries in the data set by systematically excluding each data point, re-fitting a new model for this smaller subset, and estimating the missing value. Secondly, inspection of calculated significance p test values for fitting coefficients, which describe *the probability that the given coefficient does not fit the data*, indicate that only Model 1 contains statistically significant predictors, *i.e.*, $p(\alpha_j) < 0.05$. This observation suggested the desired molecular orbital information was satisfactorily described by $E^2[\sigma_{C-H \to Ir}]$, a variable derived from NBO analysis, hence, inclusion of the geometric parameter d_{Ir---H} introduced risk of overfitting. Finally, confirmation that Model 1 was a suitable candidate for a useful predictive tool was obtained by comparison of buried volume descriptors. Scheme 1.67 depicts the location of the four quadrants in $\%V_{Bur}$ model.
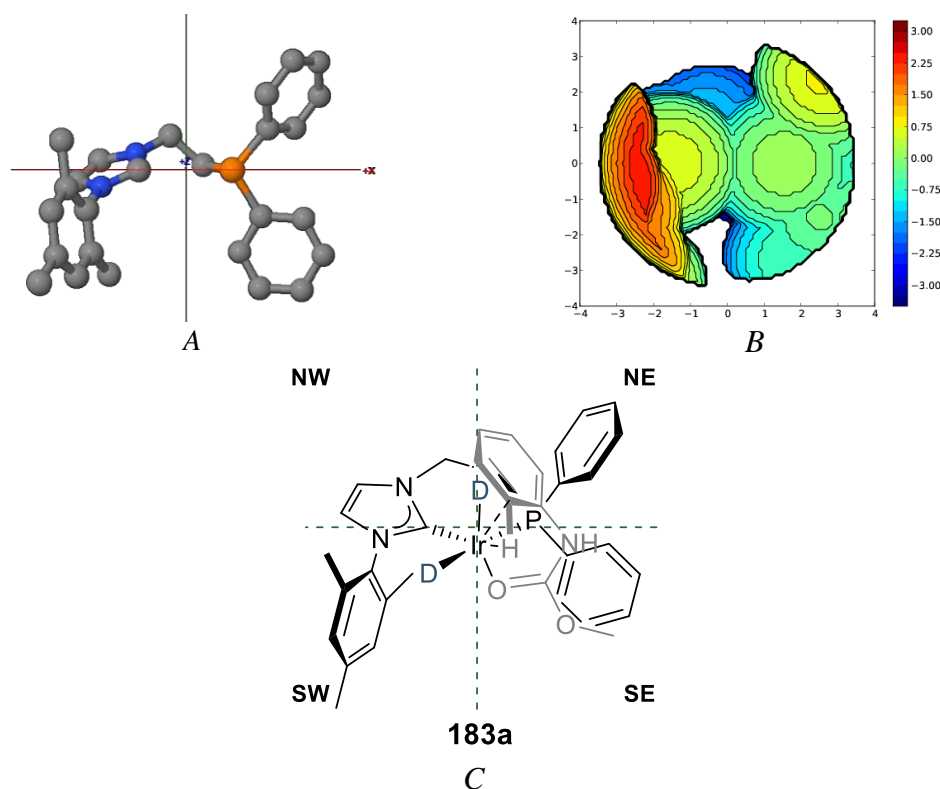
Scheme 1.67: Decomposition of $\%V_{Bur}$ in the quadrant model for **183a**.[†]

[†]*A*: ball-and-stick representation of NHC-P ligand; *B*: steric map for the ancillary ligand; *C*: representation of complex **183a** fitted to the quadrant model with substrate superimposed in grey.

As illustrated in Scheme 1.66*C*, the carbamate tends to orient itself along an axis that crosses quadrants SE and NW. In the specific view employed by %V_{Bur} calculations, the steric information of the directing group is captured by the SE quadrant, whereas remaining steric contributions from the aryl moiety are contained within the NW sector. Therefore, it is reasonable to expect %V_{Bur}^{SE} and %V_{Bur}^{NW} would be better steric descriptors than the remaining two variables in the quadrant analysis. Notably, these are precisely the factors employed by Model 1, which possess the highest predictability among all candidates.

Finally, we concluded our statistical evaluation by calculating the Durbin-Watson statistics for serial correlation (Φ_{D-W}) for all three models.[208] This parameter measures the likelihood of unforeseen auto-correlation among variables employed in the model and serves as a diagnostic tool for inadequate fitting. Calculation of the Durbin-Watson values for regression models yields the figures presented in Table 1.17. Analysis of these parameters require comparison to upper and lower bounds for significance testing. More specifically, if the Φ_{D-W} value obtained for a given model is greater than the threshold Φ_{D-W}^{U}, then, no auto-correlation among variables is expected. Conversely, if the calculated Φ_{D-W} is lower than Φ_{D-W}^{L}, positive serial correlation exists, and the model does not adequately describe the data. Values that lie in between these boundaries are not decisive, hence, risk of auto-correlation cannot be discarded.

Table 1.17: Durbin-Watson statistics for regression models.

Model	Φ_{D-W}	Φ_{D-W}^{U}	Φ_{D-W}^{L}
1	1.6642	1.5793	0.8122
2	0.7812	1.5793	0.8122
3	1.3959	1.8640	0.6576

Notably, whilst Model 1 passed this auto-correlation test, Models 2 and 3 failed to provide values greater than the established upper bound, with the former clearly displaying serial correlation among variables, and the latter providing inconclusive results. These final observations led us to take Model 1 forward and subjected it to validation by fitting enthalpy data for carbamates **183m-r**, as shown in Scheme 1.68.
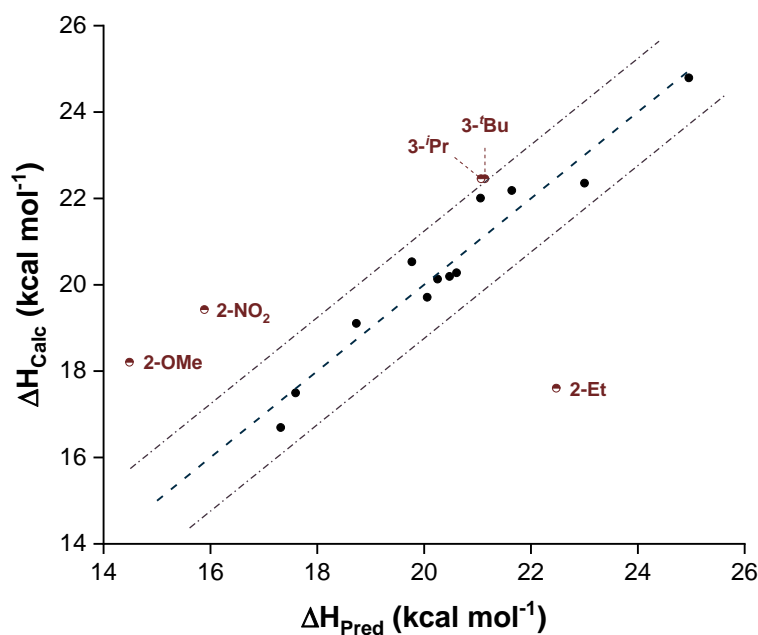
Scheme 1.68: Plot of Model 1 with validation set.[†]

[†]Dashed lines indicate the boundaries of a 95% level of confidence for fitting.

Perhaps unsurprisingly, the model could not fit carbamates bearing substituents at the *ortho*-position bulkier than 2-CH_3 (**183g**, calibration set), as indicated by data points labelled 2-OMe, 2-NO_2 and 2-Et for carbamates in the validation set **183o-r**, respectively. Conversely, sterically encumbered substituents at the *meta*-position were described within the 95% level of confidence.

Two important considerations warrant further discussion. Firstly, we opted to exclude data points in the validation set from our original statistical analysis of variance, a sampling procedure required to avoid unwanted influence of confirmation bias. Secondly, multivariate regression analysis is based on the core assumption that all data points within the model are normally distributed. Consequently, we proceeded to verify whether data points within the validation set were extremes of the normal distribution or, alternatively, outliers within a 95% level of confidence. Scheme 1.69 collates the relevant box plots for each individual predictor in Model 1 including data for both calibration and validation sets.
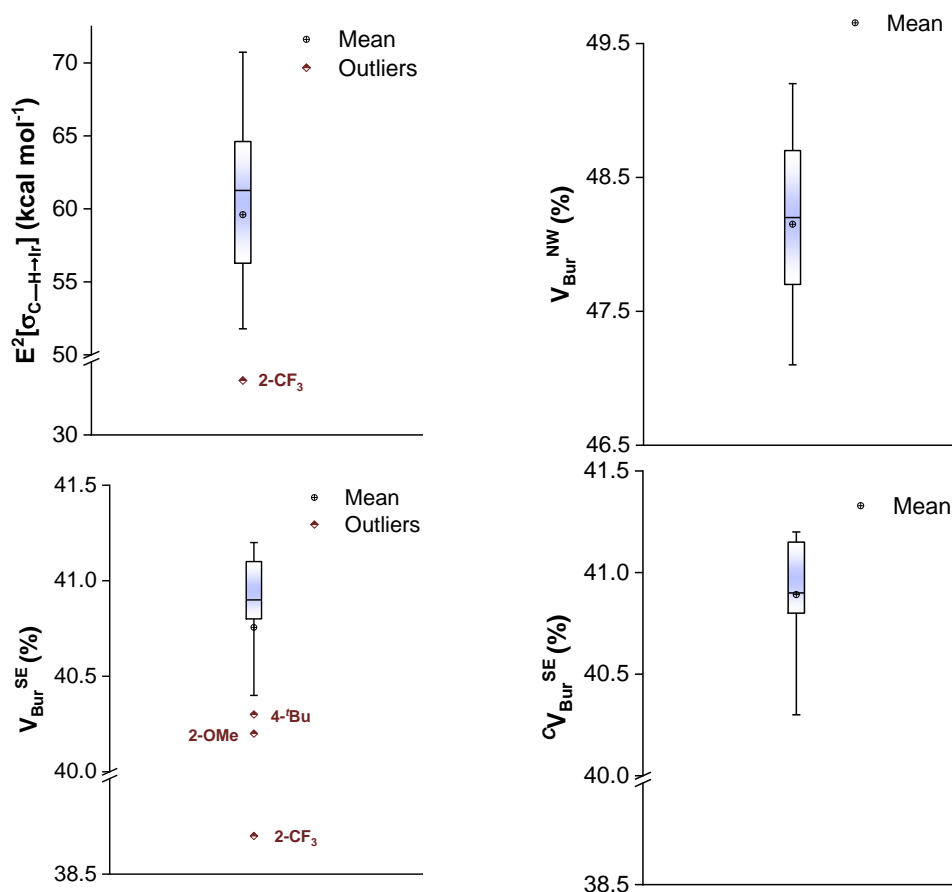
Scheme 1.69: Box plot for predictor in Model 1.[†]

$^{†C}V_{Bur}^{SE}$ – plot of variable $\% V_{Bur}^{SE}$ including only samples in the calibration set.

Inspection of boxplots in Scheme 1.69 was revealing. Carbamate **183o**, bearing a 2-CF$_3$ substituent, was an outlier with respect to two descriptors, thus being unsuitable for direct comparison within this model. Furthermore, its departure from a normal distribution was so extreme that it severely shifted the mean value of the population, causing a lack of fitting for **183e** (4-^{t}Bu, calibration set). For comparison, the last graph in Scheme 1.69 presents a boxplot of $\% V_{Bur}^{SE}$ for the calibration set, which clearly demonstrates **183e** is not an outlier of the normally distributed population.

These last statistically driven enquiries let us to conclude that the devised multivariate model provides useful predictions of ΔH_{TS} whilst employing intuitive physicochemical descriptors, however, it is unfit to offer predictions for carbamates bearing sterically encumbered substituents *ortho-* to the directing group.

To summarise, we were able to employ DFT methods and multivariate statistical analysis to provide a deconvolution of the enthalpy of activation for C—H bond

cleavage into computationally inexpensive descriptors with sound physicochemical relevance. This rather simple regression model provides an estimate of ΔH_{TS} while circumventing the need for a transition state search, a task that normally requires large computational demands and often fails to provide the required structure.

4. Conclusions

At the outset of our investigations, we developed a robust, modular and scalable synthetic route which enabled access to unprecedented iridium complexes bearing chelating NHC-P ligands. Furthermore, by analysing the solution behaviour of iridium(III) hydrides, we gathered fundamental knowledge on their intrinsic stereo-electronic properties, factors that were of paramount importance during our mechanistic investigations.

3 New Complexes
Novel chelating ligands
Modular synthesis

Dynamic Solution
Behaviour
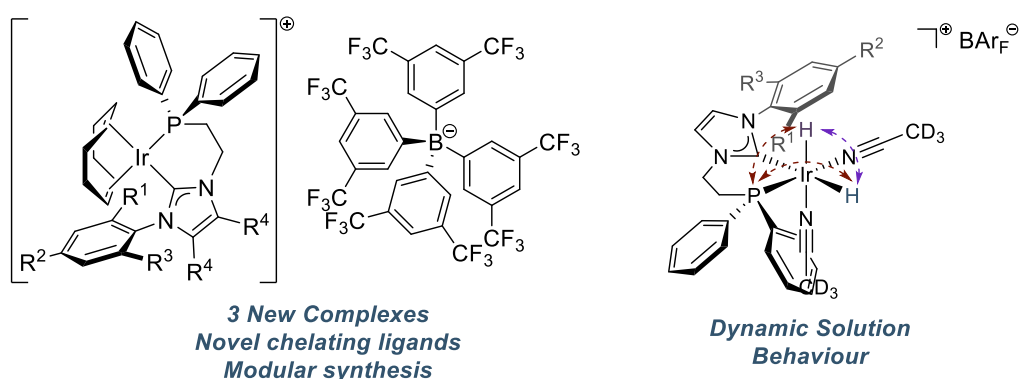
Scheme 1.70: Novel iridium complexes.

From the fundamental understanding thus obtained, and our extensive knowledge on hydrogen isotope exchange, we endeavoured to develop a highly efficient C—H functionalisation protocol targeting challenging sterically hindered carbamates, ultimately delivering good to high levels of incorporation for more than 20 examples. During these investigations, we managed to demonstrate our novel iridium complexes can also be employed to explore C—H activation at sp^3 sites adjacent to poorly coordinating, hindered directing groups, which are ubiquitous in pharmaceutically relevant compounds.
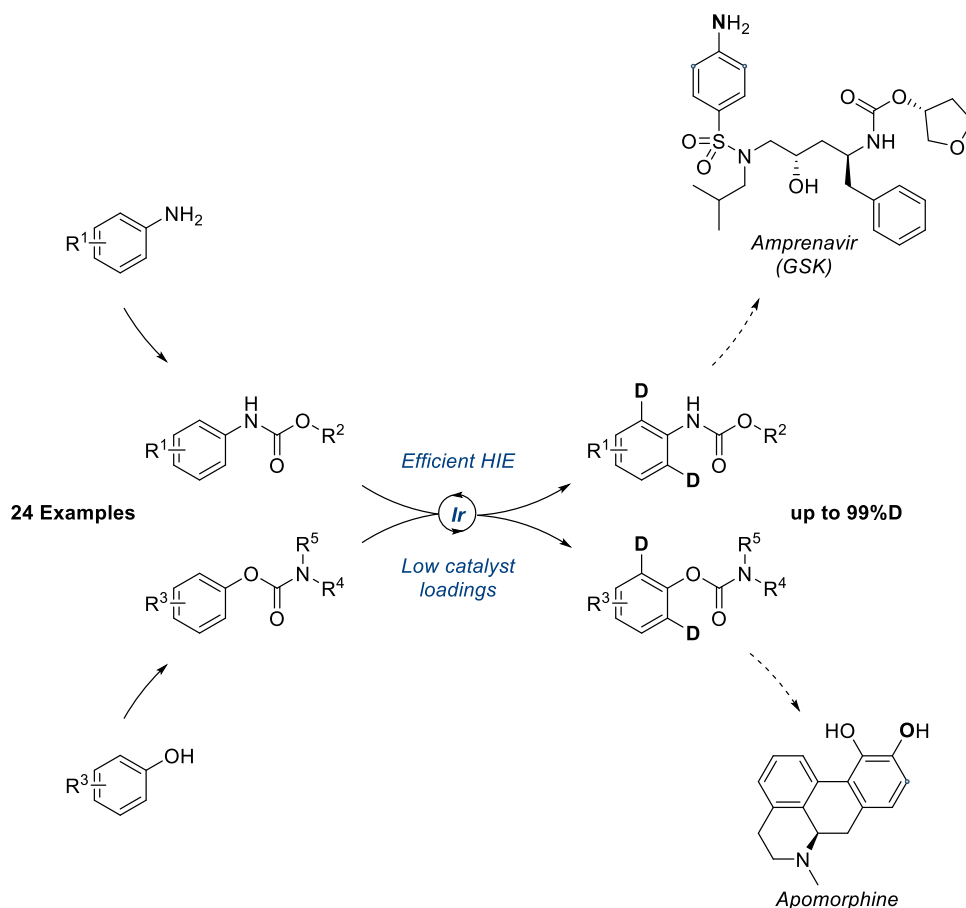
Scheme 1.71: Strategic development of HIE protocol.

A third aspect of this work dealt with the development of a thorough understanding of the reaction mechanism. Through a combination of theoretical and experimental techniques, we explored the mechanistic aspects of this C—H functionalisation protocol. A more detailed kinetic analysis delivered a better understanding of factors that determine the rate limiting step, corroborating our results from DFT and enabling us to arrive at a concise mechanistic rationale.
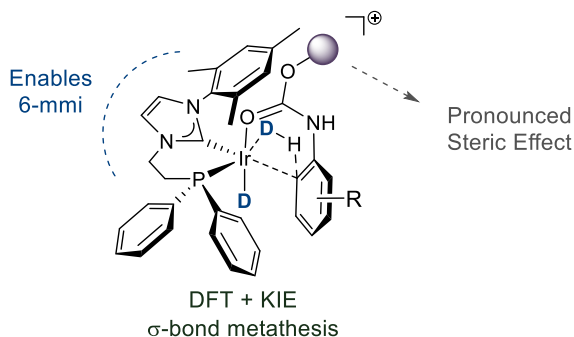
Scheme 1.72: Mechanistic understanding.

Finally, we proceeded to investigate the steric and electronic factors that govern the C—H activation of sterically hindered carbamates. Thus, by employing a thorough DFT and statistical study, we were able to make the first steps towards a model which enables the decomposition of activation energies into simpler descriptors. Notably, this approach unveiled the clear participation of orbital interactions between agostically bonded C—H fragments and iridium, whilst offering an expedient method for its quantification. This finding can now be employed to further our understanding of the elusive agostic interactions to explore other avenues in C—H activation protocols.
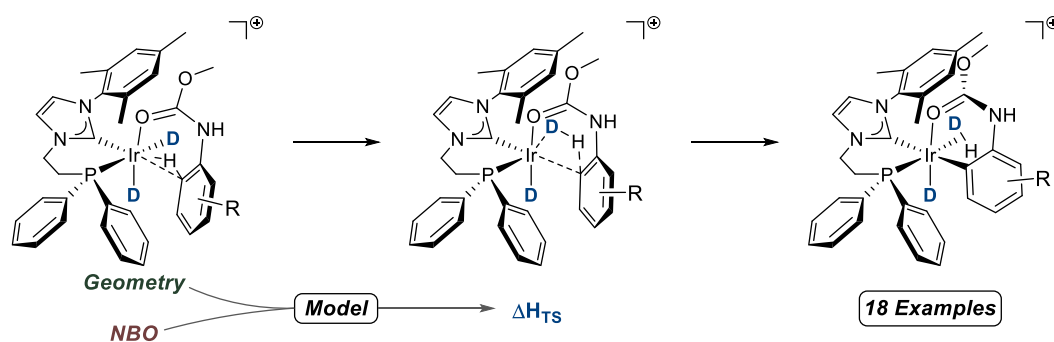
Scheme 1.73: Statistical model for prediction of ΔH_{TS}.

5. Future Work

Throughout this chapter, we explored the concept of C—H functionalisation to perform isotope exchange *ortho-* to sterically encumbered carbamates. Our exploration of *N*-aryl carbamates only included *O-tert*-butyl- substituents, thus, there are opportunities to extent the current scope to other *O*-substituted analogues and, possibly, carbamides. Additionally, the ability to perform HIE of compounds bearing hindered directing groups could also enable applications to benzylamines, as illustrated in Scheme 1.74.
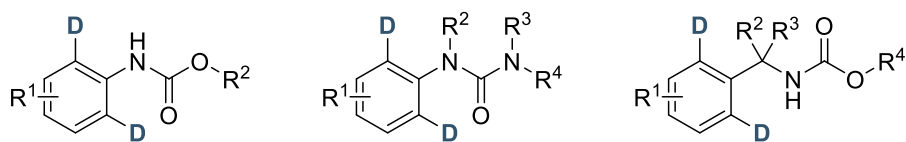
Remaining opportunities in HIE

Celiprolol
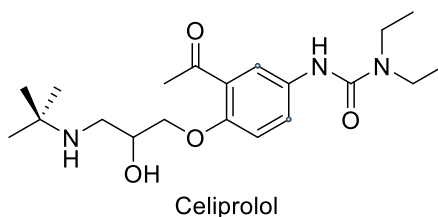
Scheme 1.74: Further explorations in HIE of hindered directing groups.[209]

In a second line of enquiry, carbamates could be directly employed as cross-coupling agents in palladium[210] and nickel[211] catalysis, thus enabling synthesis of deuterated arylated scaffolds in an expedient fashion, as illustrated in Scheme 1.75.
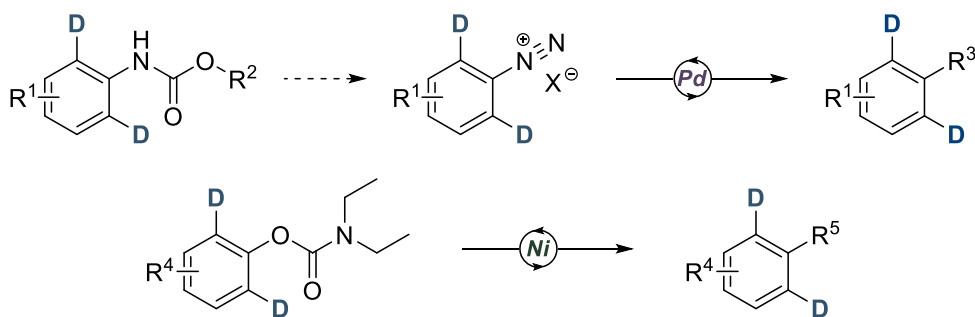
Several applications in sequential HIE/coupling

Scheme 1.75: Synthetic applications of deuterated carbamates

Finally, we previously introduced a model for prediction of enthalpies of activation employing *O*-methyl-*N*-aryl carbamates as probe molecules. Experimental validation and further kinetic studies on these systems could enable us to derive a deeper understanding of intrinsic parameters that govern experimentally elusive[212] agostic interactions.

6. Experimental Section

6.1 General experimental details

All chemical reagents and solvents were purchased from commercial sources (Acros Organics, Alfa Aesar, Sigma Aldrich and Strem Chemicals) and used without further purification, unless otherwise stated.

Dry dichloromethane was obtained by refluxing with CaH_2 and subsequent distillation under a nitrogen atmosphere. Dry tetrahydrofuran (THF) was obtained by refluxing with sodium wire employing sodium ketyl as an indicator, followed by distillation under a nitrogen atmosphere. Dry dimethyl sulfoxide (DMSO) was obtained by refluxing over CaH_2 under an atmosphere of argon followed by fractional distillation under vacuum and stored over 4 Å molecular sieves. Methyl-*tert*-butyl ether (MTBE) was purified by fractional distillation from CaH_2 under an argon atmosphere and stored over 4 Å molecular sieves. Dry Et_2O and toluene were obtained from a PureSolv SPS-400-5 Solvent Purification System immediately prior to use. Phenyl chloroformate was purified by vacuum distillation and stored over 4 Å molecular sieves prior to use.

Thin layer chromatography was performed using Merck silica plates (Silica gel 60 F254) and revealed under ultraviolet irradiation at 254 nm. Whenever required, solutions of potassium permanganate, vanillin and ninhydrin were used as revealing agents.

NMR spectra were acquired on a Bruker DPX 400 spectrometer at the respective frequencies for ^1H, ^{11}B, ^{13}C, ^{19}F and ^{31}P of 400, 128, 101, 376 and 162 MHz. Chemical shifts and coupling constants are reported in ppm and Hertz, respectively.

High resolution mass spectrometry (HRMS) data were obtained at the EPSRC UK National Mass Spectrometry Facility at Swansea University, employing nanoelectrospray ionization (ESI) method coupled to a Thermo Scientific LTQ-Orbitrap XL as mass analyser.

Melting points were measured in a Griffin C110230 Melting Point Apparatus.

Infrared spectra were acquired in a Shimadzu IRAffinity-1 FTIR spectrometer.

6.2 General procedures for the synthesis of imidazolium ligands

6.2.1 Preparation of 1-aryl-1H-imidazoles[165]
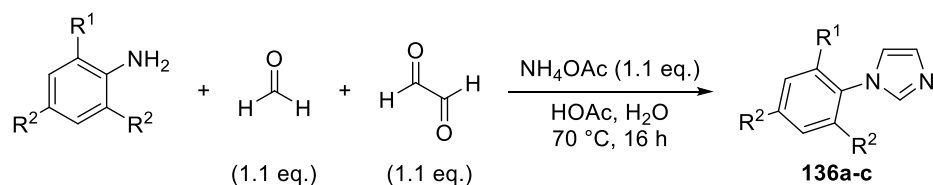
To a three-necked round-bottomed flask equipped with a magnetic stirrer bar, a dropping funnel and a condenser were added acetic acid, formaldehyde solution (37% wt. in water) and glyoxal solution (40% wt. in water). In a conical flask equipped with a magnetic stirrer bar were added acetic acid, ammonium acetate, water and the appropriate aniline. This mixture was stirred at room temperature until a viscous solution was obtained, which was then transferred to the dropping funnel and subsequently added dropwise to the reaction flask at 70 °C in a temperature-controlled silicone oil bath. After completion of the addition, the dropping funnel was replaced by a glass stopper and the reaction mixture was stirred at 70 °C for 16 h. The dark-coloured mixture thus obtained was allowed to cool to room temperature and slowly poured into a saturated aqueous $NaHCO_3$ solution under vigorous stirring to allow the evolved gases to dissipate. After completion of the addition, the mixture was allowed to stir at room temperature for 1 h and subsequently filtered. The filtrate was then extracted three times with ethyl acetate and organic phases were combined, dried over Na_2SO_4 and filtered. The solvent was then evaporated under reduced pressure and the dark brown crude reaction mixture submitted to short-path distillation under vacuum to give the N-aryl imidazole as a viscous liquid.

6.2.2 Preparation of 3-(2-hydroxyethyl)-1-substituted imidazolium salts[213]

137a-c
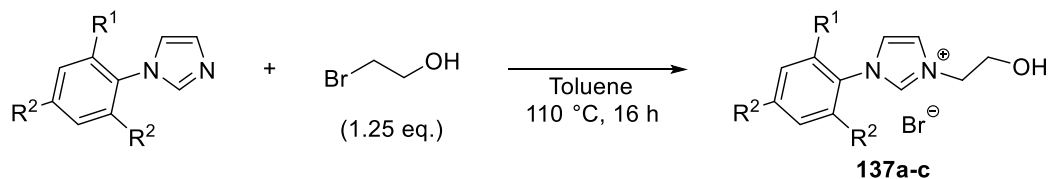
To a flame-dried round-bottomed flask equipped with a magnetic stirrer bar and a condenser were added the appropriate imidazole and toluene. The mixture was stirred at room temperature until complete dissolution of the imidazole. Then, 2-bromoethanol was added via syringe in one portion and the reaction mixture was heated to 110 °C for 16 h. The mixture was then allowed to cool to room temperature and subsequently cooled to 0 °C in an ice-water bath. The supernatant was removed by pipette and the remaining oil washed multiple times with diethyl ether until the formation of a solid was observed. The solid thus obtained was triturated with diethyl ether, decanted and the solvent removed by pipette. The finely divided solids thus obtained were dried under reduced pressure and stored in a vacuum oven for 16 h prior to use.

6.2.3 Preparation of 3-(2-bromoethyl)-1-substituted imidazolium salts[213]

137a-c   **138a-c**
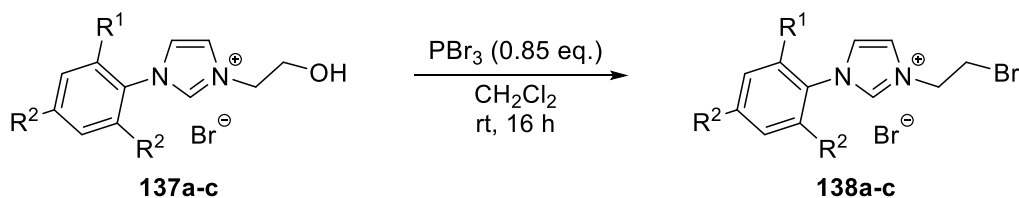
To a flame-dried round-bottomed flask equipped with a magnetic stirrer was added the appropriate 3-(1-hydroxyethyl)-1-substituted imidazolium bromide, the atmosphere was evacuated and replenished with argon, and this process repeated a further two times. Dry CH_2Cl_2 was then added at room temperature and the mixture was vigorously stirred until the solids were suspended. The reaction mixture was cooled to 0 °C in an ice-water bath and phosphorus(III) bromide was added dropwise at 0 °C. The reaction vessel was subsequently allowed to warm to room temperature and stirred for 16 h. The reaction mixture was then slowly poured into a conical flask containing saturated aqueous $NaHCO_3$ solution which was previously cooled to 0 °C in an ice-water bath and was stirred manually then subsequently transferred to a separating funnel. The bottom, organic layer was collected, and the remaining

aqueous phase extracted five times with CH_2Cl_2. The organic phases were combined, dried over Na_2SO_4, filtered and evaporated under reduced pressure to afford the imidazolium bromides.

6.2.4 Preparation of 3-(2-(diphenylphosphinoethyl)-1-substituted-imidazolium salts[213,214]
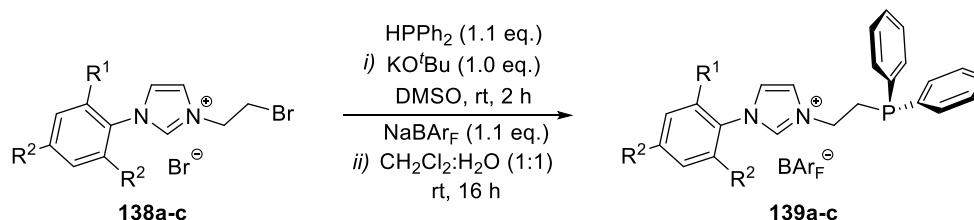
Unless otherwise stated, all manipulations were performed under an argon atmosphere employing standard Schlenk techniques and degassed solvents. To a flame-dried round-bottomed flask equipped with a magnetic stirrer bar was added the appropriate 3-(2-bromoethyl)-1-substituted-imidazolium bromide. The atmosphere was evacuated and replenished with argon, and this process repeated a further two times. Dry dimethylsulfoxide was added via syringe and the mixture was stirred at room temperature until complete dissolution of the solid. In a second flame-dried round-bottomed flask equipped with a magnetic stirrer bar was added potassium tert-butoxide. The atmosphere was evacuated and replenished with argon, and this process repeated a further two times. Dry dimethylsulfoxide was added via syringe, then diphenylphosphine was added dropwise under vigorous and constant stirring, with evolution of a characteristic dark red colour due to the formation of potassium

diphenylphosphide. This mixture was allowed to stir at room temperature for 1 h and then subsequently added dropwise to the reaction mixture (*ca.* 1 drop every 2 seconds), under constant and vigorous stirring at room temperature. During addition, the disappearance of the red colour is indicative of phosphide consumption. After completion of the addition, the reaction mixture was allowed to stir at room temperature for 2 h and was then quenched with degassed water.

The extraction apparatus (*left*) was evacuated and replenished with

Extraction Apparatus argon, and this process repeated a further two times. The reaction

mixture was then transferred to the separating funnel via syringe, and water and CH_2Cl_2 (5:10 volume ratio relative to the reaction mixture) were added. Under a constant stream of argon, the separation funnel was detached from the apparatus and the lower adaptor was obstructed by a glass stopper. The decanting funnel was vigorously shaken and re-positioned onto the collection flask. After phase separation, the bottom, organic layer was collected, and the aqueous layer was extracted two more times in a similar fashion. The combined organic phases were concentrated under reduced pressure to an approximate volume of 20 mL. The atmosphere was replenished with argon and a stirrer bar was introduced. Subsequently, water (20 mL) was added, followed by addition of $NaBAr_F$, and the mixture was allowed to stir vigorously for 16 h under an argon atmosphere. The reaction mixture was then transferred to a similar extraction apparatus, the organic layer was decanted and collected. The remaining aqueous phase was extracted with CH_2Cl_2 (3×50 mL), following the procedure stated above. The combined organic phases were dried over Na_2SO_4, filtered under air and the solvent evaporated under reduced pressure. The resulting residue was purified by column chromatography on silica gel with gradient elution, employing mixtures of petroleum ether and CH_2Cl_2 as eluent ($0 - 50\%$ CH_2Cl_2 in petroleum ether) to afford the target imidazolium salts as off-yellow, air stable solids. (*N.B.: Due to their basicity, fast addition of diphenylphosphide anion must be avoided in order to favour the nucleophilic substitution pathway over competing elimination processes.*)

6.3 General procedure for the synthesis of iridium(I) complexes[214]
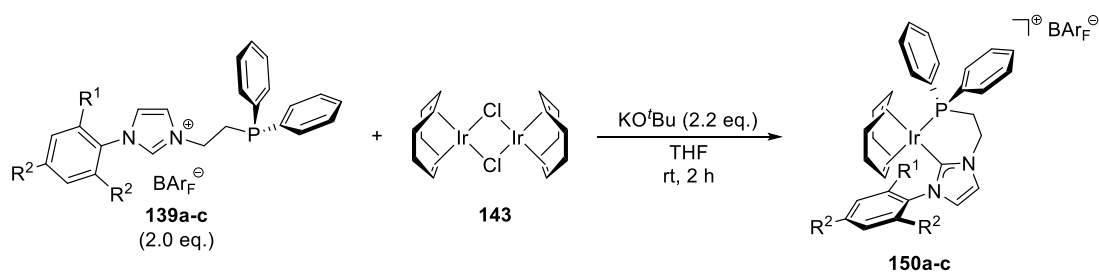
To a flame-dried Schlenk flask equipped with a magnetic stirrer bar was added bis(1,5-cyclooctadiene)diiridium(I) chloride. The atmosphere was evacuated and replenished with argon, and this process repeated a further two times. Dry THF was added via syringe and the mixture stirred until complete dissolution, forming an

orange solution. The appropriate imidazolium salt was added, and the mixture allowed to stir at room temperature for 5 min. Potassium *tert*-butoxide was then added, and an immediate colour change from orange to red was observed. The reaction mixture was then stirred for 2 h at room temperature, with evolution of a dark red colour. The solvent was evaporated, the solid residue re-dissolved in CH_2Cl_2 and purified by column chromatography on silica gel using gradient elution, with mixtures of petroleum ether and CH_2Cl_2 (0 – 50% CH_2Cl_2 in petroleum ether) to afford the desired iridium(I) complexes as red crystalline solids which were dried in vacuum oven for 16 h prior to use.

6.4 General procedure for the preparation of *N*-aryl carbamates[215]
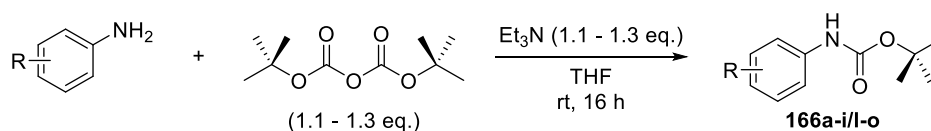
To a flame dried round-bottomed flask equipped with a magnetic stirrer bar were added the appropriate aniline, triethylamine and anhydrous THF, and the mixture was stirred at room temperature until a homogeneous solution was obtained. Then, di-*tert*-butyl dicarbonate was added in one portion and the reaction mixture was vigorously stirred at room temperature for the allocated reaction time under a constant argon atmosphere. After reaction completion (assessed by TLC analysis of the reaction mixture), the solvent was evaporated under reduced pressure, the residue was suspended in Et_2O (15 mL) and filtered through a plug of cotton wool. The remaining solids were washed with Et_2O (2 × 5 mL) and the filtrate was evaporated under reduced pressure. Unless stated otherwise, the resulting residue was purified by column chromatography on silica gel employing gradient elution with mixtures of petroleum ether and Et_2O.

6.5 General procedure for hydrogen isotope exchange (HIE) of carbamates
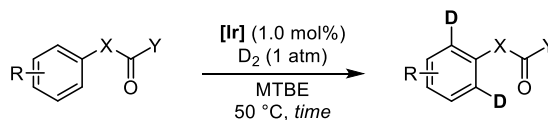
To a flame-dried round-bottom flask fitted with a glass stopper, equipped with two side stopcocks and a stirrer bar, the iridium catalyst and the desired carbamate were added under a constant stream or argon, then, the atmosphere was evacuated and carefully replenished with argon. Methyl-*tert*-butyl ether (MTBE) was then added, the resulting mixture was thoroughly stirred at room temperature and subsequently immersed in a dry ice-acetone bath at -78 °C under an atmosphere of argon. A balloon of D_2 was connected to one of the side stopcocks, the atmosphere was evacuated and replenished with D_2, and this process was repeated a further two times at -78 °C. After the third gas exchange cycle, both stopcocks were firmly closed, the flask was immediately transferred to an oil bath heated to 50 °C and the glass stopper was physically restrained to prevent leakage of gases and solvent due to the increase in pressure inside the vessel. After the allocated reaction time, one of the stopcocks was open to the atmosphere, the solution was filtered through a small pipette containing a plug of silica gel, the filtrate was collected, and the solids were washed with Et_2O (2 × 2.5 mL). The combined filtrates were evaporated under reduced pressure to afford deuterated carbamates of interest. Deuterium incorporation was determined by ^1H NMR spectroscopy of the products thus obtained. The calibration of integrals was performed against a peak corresponding to a position in which deuterium incorporation was not expected, and the percent deuterium incorporation was calculated according to the expression in Eq. S1:

$$\%Deuterium\ incorporation = 100 - \left[\left(\frac{residual\ integral}{number\ of\ labelling\ sites}\right) \cdot 100\right] \quad (Eq.\ S1)$$

6.6 General procedure for HIE of carbamates employing Radley's Carousel

To an oven-dried Radley's Carousel 12 Plus Station glass tube equipped with a magnetic stirrer bar were added the iridium catalyst and the desired carbamate, the tube was sealed at the screwcap with the gas inlet open, and immediately connected to the carousel station which was kept under a constant stream of argon. This process

was repeated for the remaining tubes until all parallel experiments were set up. Then, the atmosphere was evacuated and carefully replenished with argon, MTBE was then introduced whilst thoroughly rinsing the walls of the tube, and this process was repeated for all relevant experiments. The upper part of the Radley's Carousel was then detached and transferred to a dry ice-acetone bath at -78 °C, and the reaction mixtures were stirred at that temperature for approximately 5 minutes under a constant stream of argon. A balloon of D_2 was connected to the system, the atmosphere inside the reaction tubes was evacuated and replenished with D_2, and this process was repeated a further two times. The gas inlet in each screwcap was then closed, the system was returned to the base of the carousel apparatus, which was kept at 50 °C, and the reaction mixtures were allowed to stir at that temperature. After the allocated reaction time, the tubes were open to the atmosphere, the reaction mixture was transferred to a round-bottom flask, the tube was rinsed with Et_2O (2×4 mL), and the combined ethereal phases were evaporated under reduced pressure. The resulting residue was re-dissolved in Et_2O (2 mL), filtered through a small pipette containing a plug of silica gel, the filtrate was collected, and the solids were washed with Et_2O (2×2.5 mL). The combined filtrates were evaporated under reduced pressure to afford deuterated carbamates of interest. Deuterium incorporation was determined by ^{1}H NMR spectroscopy of the products thus obtained. The percent deuterium incorporation was calculated by Eq. S1 in a similar manner to that described in general procedure 1.5.

6.7 General procedure for rate measurement of HIE reactions

To a flame-dried round-bottom flask fitted with a glass stopper, equipped with two side stopcocks and a stirrer bar, the iridium catalyst and the desired carbamate were added under a constant stream or argon, then, the atmosphere was evacuated and carefully replenished with argon. The glass stopper was replaced by a rubber septum and methyl-*tert*-butyl ether (MTBE) was then added, the resulting mixture was thoroughly stirred at room temperature and subsequently immersed in a dry ice-acetone bath at -78 °C under an atmosphere of argon. The reaction mixture was allowed to stir at -78 °C for 10 min to ensure complete temperature equilibration. A

balloon filled with either D_2 (forward process) or H_2 (reverse process) was then connected to one of the side stopcocks, the atmosphere was evacuated and replenished with the gas of choice, and this process was repeated a further two times at -78 °C. After the third gas exchange cycle, the stopcock connected to the argon line was firmly closed while the second stopcock, which provided communication between the system and the balloon, was left open. The flask was then immediately transferred to an oil bath heated to the desired temperature, and the initial time for the rate experiment was recorded. After an allocated sampling time, an aliquot of the reaction mixture was removed via a 1.0 mL syringe equipped with a long disposable needle, which were both previously purged with argon three times to ensure preservation of the inert conditions within the reaction vessel. The solution thus collected was immediately transferred to a vial containing MeCN (2.0 mL) in order to guarantee quenching of the HIE process, and the remaining aliquots were collected in a similar fashion. Upon completion of the sampling process, the solutions obtained during the rate experiment were evaporated under reduced pressure. Each aliquot thus obtained was re-dissolved in Et_2O (1.0 mL), filtered through a small plug of silica gel, and the solids were washed with Et_2O (2 × 2.0 mL). The filtrate was then evaporated under reduced pressure and the resulting solid residue was analysed by ^{1}H NMR spectroscopy in order to determine the level of deuterium incorporation, which was calculated according to the expression in Eq. S1.

6.8 Synthesis of imidazolium ligands

Procedures reported in this section are representative of several individual runs and reflect all aspects of the preparative work undertaken. Different scales were pursued during long term synthesis, however, there were no significant variations from protocols described herein.

6.8.1 Synthesis of 1-aryl-1*H*-imidazoles

1-Phenyl-1*H*-imidazole – **136a** (Table 1.7, Entry 1)
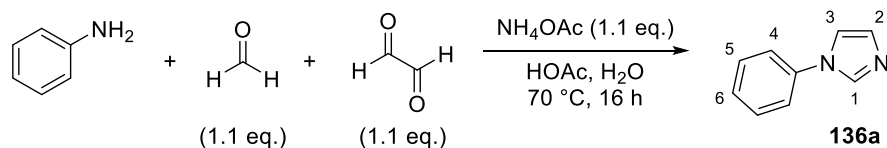
Following general procedure 6.2.1, acetic acid (52.4 mL), formaldehyde (37% wt. in water, 16.4 mL, 0.220 mol) and glyoxal (40% wt. in water, 24.7 mL, 0.215 mol) were added to the reaction vessel. In a conical flask, the mixture containing aniline was prepared by subsequent addition of acetic acid (52.0 mL), ammonium acetate (16.38 g, 0.213 mol), water (4.8 mL, 0.266 mol) and aniline (18.0 mL, 0.198 mol). The title compound was isolated by short-path distillation under vacuum to afford 1-phenyl-1*H*-imidazole (**136a**) as a light yellow viscous liquid (14.83 g, **52% yield**).

Analytical data for **136a** is consistent with previously reported data:[216]

^{1}H NMR (400 MHz, CDCl$_3$): δ 7.83 (s, 1H, H^1), 7.47-7.43 (m, 2H, H^5), 7.37-7.32 (m, 3H, H^4/H^6), 7.25 (d, $^3J_{HH}$ = 1.0 Hz, 1H, H^3), 7.18 (d, $^3J_{HH}$ = 1.0 Hz, 1H, H^2).

^{13}C NMR (101 MHz, CDCl$_3$): δ 137.5, 135.8, 130.6, 130.1, 127.6, 121.6, 118.4.

FTIR (neat, cm^{-1}): 3109, 3048, 1599, 1504, 1481, 1458, 1302, 1246, 1111, 1055, 962, 903, 814, 756, 731, 691, 658, 633, 610.

1-(*o*-Tolyl)-1*H*-imidazole – **136b** (Table 1.7, Entry 2)
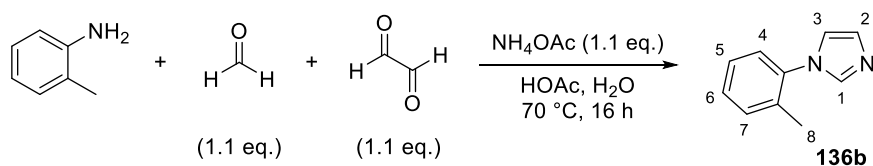
Following general procedure 6.2.1, acetic acid (52.4 mL), formaldehyde (37% wt. in water, 16.4 mL, 0.220 mol) and glyoxal (40% wt. in water, 24.7 mL, 0.215 mol) were added to the reaction vessel. In a conical flask, the mixture containing aniline was prepared by subsequent addition of acetic acid (52.0 mL), ammonium acetate (16.4 g, 0.213 mol), water (4.80 mL, 0.266 mol) and *o*-toluidine (21.0 mL, 0.198 mol). The title compound was isolated by short-path distillation under vacuum to

afford 1-(*o*-tolyl)-1*H*-imidazole (**136b**) as a light brown viscous oil (15.6 g, **50% yield**).

Analytical data for **136b** is consistent with previously reported data:[216]

^{1}H NMR (400 MHz, CDCl$_3$): δ 7.56 (t, ^{1}H, $^4J_{HH}$ = 1.0 Hz, H^1), 7.35-7.25 (m, 3H, H^5/H^6/H^7), 7.20-7.18 (m, 1H, H^4), 7.17 (t, J_{HH} = 1.0 Hz, 1H, H^3), 7.03 (t, J_{HH} = 1.0 Hz, 1H, H^2), 2.15 (s, 3H, H^8).

^{13}C NMR (101 MHz, CDCl$_3$): δ 137.7, 136.8, 134.1, 131.5, 129.5, 129.0, 127.0, 126.7, 120.7, 17.8.

FTIR (neat, cm^{-1}): 3107, 3030, 2955, 1580, 1501, 1479, 1462, 1308, 1238, 1107, 1057, 962, 903, 816, 762, 739, 718, 662.

1-Mesityl-1*H*-imidazole – **136c** (Table 1.7, Entry 3)
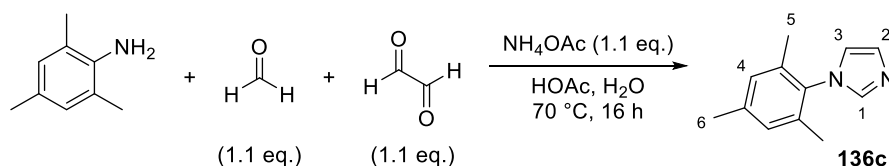
To a three-necked round-bottom flask equipped with a magnetic stirrer bar, a dropping funnel and a condenser were added acetic acid (35.0 mL), formaldehyde (37% wt. in water, 10.8 mL, 0.145 mol) and glyoxal (40% wt. in water, 16.3 mL, 0.142 mol). In a conical flask equipped with a magnetic stirrer bar were added acetic acid (34.2 mL), ammonium acetate (10.8 g, 0.140 mol), water (3.15 mL, 0.175 mol) and 2,4,6-trimethylaniline (18.3 mL, 0.130 mol). This mixture was stirred at room temperature until a viscous solution was obtained, which was then transferred to the dropping funnel and subsequently added dropwise to the reaction flask at 70 °C in a temperature controlled silicone oil bath. After completion of the addition, the dropping funnel was replaced with a glass stopper and the reaction mixture was stirred at 70 °C for 16 h. The dark-coloured mixture thus obtained was allowed to cool to room temperature and slowly poured into saturated aqueous NaHCO$_3$ solution under vigorous stirring to allow the evolved gases to dissipate. After completion of the addition, the mixture was allowed to stir at room temperature for 1 h and subsequently filtered and the solids were washed with water. The brown solid thus obtained was dried in air and treated with petroleum ether at 60 °C, and the

organic layer developed a dark yellow colour. The ethereal solution was then collected, and this extraction procedure repeated three times. The combined organic phases were then evaporated under reduced pressure to afford 1-mesityl-1*H*-imidazole (**136c**) as a pale yellow crystalline solid (11.9 g, **49% yield**).

Analytical data for **136c** is consistent with previously reported data:[165]

^{1}H NMR (400 MHz, CDCl$_3$): δ 7.41 (t, $^4J_{HH}$ = 1.1 Hz, 1H, H^1), 7.21 (t, J_{HH} = 1.1 Hz, 1H, H^3), 6.95 (s, 2H, H^4), 6.87 (t, J_{HH} = 1.1 Hz, 1H, H^2), 2.32 (s, 3H, H^6), 1.97 (s, 6H, H^5).

^{13}C NMR (101 MHz, CDCl$_3$): δ 139.1, 137.7, 135.7, 133.6, 129.8, 129.2, 120.3, 21.2, 17.5.

Melting point: 100-102 °C.

FTIR (neat, cm^{-1}): 3094, 2976, 2955, 2920, 1499, 1458, 1314, 1236, 1097, 1069, 907, 870, 816, 781, 669, 617.

6.8.2 Synthesis of 3-(2-hydroxyethyl)-1-substituted imidazolium salts

3-(2-Hydroxyethyl)-1-phenyl-imidazolium bromide – **137a** (Table 1.8, Entry 1)
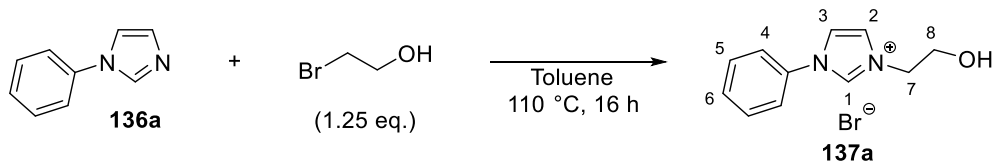
Following general procedure 6.2.2, imidazole **136a** (1.44 g, 10.0 mmol), toluene (30.0 mL) and 2-bromoethanol (0.900 mL, 13.0 mmol) were reacted at 110 °C for 16 h. After purification by trituration with diethyl ether, 3-(2-hydroxyethyl)-1-phenyl-imidazolium bromide (**137a**) was isolated as a light pink solid (2.63 g, **98% yield**).

^{1}H NMR (400 MHz, DMSO-d_6): δ 9.85 (t, $^4J_{HH}$ = 1.6 Hz, 1H, H^1), 8.34 (t, $^4J_{HH}$ = 1.5 Hz, 1H, H^3), 8.02 (t, $^4J_{HH}$ = 1.5 Hz, 1H, H^2), 7.82-7.80 (m, 2H, H^4), 7.69-7.65 (m, 2H, H^5), 7.61-7.58 (m, 1H, H^6), 4.31 (t, $^3J_{HH}$ = 5.0 Hz, 2H, H^8), 3.83 (t, $^3J_{HH}$ = 5.0 Hz, 2H, H^9), (OH not observed).

^{13}C NMR (101 MHz, DMSO-d_6): δ 135.6, 134.7, 130.2, 129.8, 123.7, 121.8, 121.0, 59.2, 52.2.

Melting point: 96-98 °C.

FTIR (neat, cm^{-1}): 3267, 3064, 2999, 2925, 2872, 1598, 1570, 1550, 1497, 1222, 1073, 1057, 870, 753, 687, 640, 627.

HRMS (positive ESI): m/z calculated for [M]$^+$ C$_{11}$H$_{13}$N$_2$O$^+$: 189.1022; found: 189.1018.

3-(2-Hydroxyethyl)-1-(*o*-tolyl)-imidazolium bromide – **137b** (Table 1.8, Entry 2)
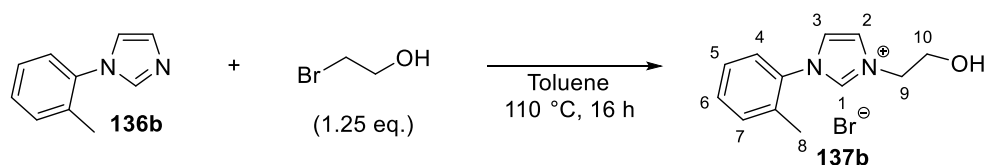
Following general procedure 6.2.2, imidazole **136b** (1.58 g, 10.0 mmol), toluene (30.0 mL) and 2-bromoethanol (0.900 mL, 13.0 mmol) were reacted at 110 °C for 16 h. After purification by trituration with diethyl ether, 3-(2-hydroxyethyl)-1-(*o*-tolyl)-imidazolium bromide (**137b**) was isolated as a light yellow solid (2.56 g, **90% yield**).

^{1}H NMR (400 MHz, DMSO-*d_6*): δ 9.55 (t, $^4J_{HH}$ = 1.6 Hz, 1H, H^1), 8.08 (t, J_{HH} = 1.5 Hz, 1H, H^3), 8.02 (t, J_{HH} = 1.5 Hz, 1H, H^2), 7.56-7.52 (m, 3H, H^4/H^5/H^7), 7.48-7.44 (m, 1H, H^6), 4.32 (t, $^3J_{HH}$ = 5.2 Hz, 2H, H^9), 3.82 (t, $^3J_{HH}$ = 5.2 Hz, 2H, H^{10}), 2.23 (s, 3H, H^8) , (OH not observed).

^{13}C NMR (101 MHz, DMSO-*d_6*): δ 137.3, 134.2, 133.4, 131.6, 130.6, 127.4, 126.5, 123.7, 123.1, 59.2, 52.1, 17.1.

Melting point: 108-110 °C.

FTIR (neat, cm^{-1}): 3258, 3082, 3009, 1569, 1553, 1497, 1223, 1190, 1068, 771, 663 cm^{-1}.

HRMS (positive ESI): m/z calculated for [M]$^+$ C$_{12}$H$_{15}$N$_2$O$^+$: 203.1179; found: 203.1175.

3-(2-Hydroxyethyl)-1-mesityl-imidazolium bromide – **137c** (Table 1.8, Entry 3)
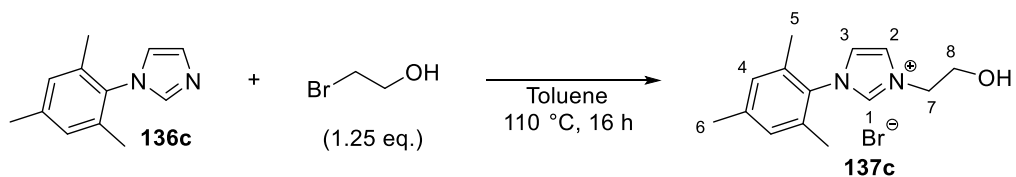
Following general procedure 6.2.2, imidazole **136c** (3.73 g, 20 mmol), toluene (60 mL) and 2-bromoethanol (1.8 mL, 25 mmol) were reacted at 110 °C for 16 h. After purification by trituration with diethyl ether, 3-(2-hydroxyethyl)-1-mesityl-imidazolium bromide (**136d**) was isolated as a white solid (5.48 g, **88% yield**).

Analytical data for **136d** is consistent with previously reported data:[213]

^{1}H NMR (400 MHz, CDCl$_3$): δ 10.14 (t, $^4J_{HH}$ = 1.5 Hz, 1H, H^1), 8.16 (t, J_{HH} = 1.5 Hz, 1H, H^3), 7.15 (t, J_{HH} = 1.5 Hz, 1H, H^2), 6.99 (s, 2H, H^4), 5.24 (t, $^3J_{HH}$ = 5.4 Hz, 2H, H^7), 4.03 (t, $^3J_{HH}$ = 5.4 Hz, 2H, H^8), 2.33 (s, 3H, H^6), 2.07 (s, 6H, H^5) , (OH not observed).

^{13}C NMR (101 MHz, CDCl$_3$): δ 141.6, 138.1, 134.3, 130.5, 129.9, 124.1, 122.7, 51.6, 31.9, 21.1, 17.6.

Melting point: 164-166 °C.

FTIR (neat, cm^{-1}): 3388, 3057, 3032, 1562, 1543, 1485, 1447, 1368, 1202, 1078, 1065, 864, 756, 677, 638.

6.8.3 Synthesis of 3-(2-bromoethyl)-1-substituted imidazolium salts

3-(2-Bromoethyl)-1-phenyl-imidazolium bromide – **138a** (Table 1.9, Entry 1)
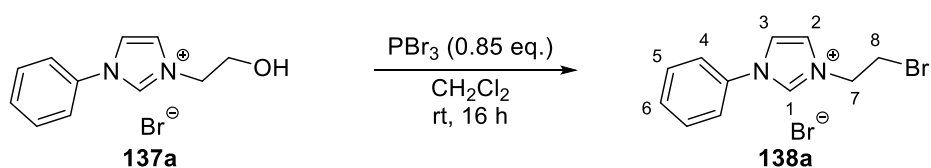
Following general procedure 6.2.3, imidazolium salt **137a** (1.35 g, 5.00 mmol) was reacted with PBr$_3$ (0.400 mL, 4.30 mmol) in dry CH$_2$Cl$_2$ (25 mL) under an argon atmosphere for 16 h to afford 3-(2-bromoethyl)-1-phenyl-imidazolium bromide (**138a**) as a white solid (1.21 g, **73% yield**).

¹H NMR (400 MHz, DMSO-d_6): δ 9.99 (t, $^4J_{HH}$ = 1.8 Hz, 1H, H¹), 8.40 (t, J_{HH} = 1.7 Hz, 1H, H³), 8.12 (t, J_{HH} = 1.7 Hz, 1H, H²), 7.81 (d, $^3J_{HH}$ = 8.0 Hz, 2H, H⁴), 7.67 (dd, $^3J_{HH}$ = 8.0 Hz, $^3J_{HH}$ = 7.3 Hz, 2H, H⁵), 7.61 (t, $^3J_{HH}$ = 7.3 Hz, 1H, H⁶), 4.72 (t, $^3J_{HH}$ = 5.8 Hz, 2H, H⁷), 4.05 (t, $^3J_{HH}$ = 5.8 Hz, 2H, H⁸).

¹³C NMR (101 MHz, DMSO-d_6): δ 135.9, 134.6, 130.3, 129.9, 123.5, 121.8, 121.1, 50.6, 31.0.

Melting point: 166-168 °C.

FTIR (neat, cm⁻¹): 3056, 2973, 2631, 1570, 1551, 1436, 1270, 1226, 1071, 758, 744, 683, 610.

HRMS (positive ESI): m/z calculated for [M]⁺ $C_{11}H_{12}{}^{79}BrN_2{}^+$: 251.0178; found: 251.0180; calculated for $C_{11}H_{12}{}^{81}BrN_2{}^+$: 253.0158; found: 253.0155.

3-(2-Bromoethyl)-1-(o-tolyl)-imidazolium bromide – **138b** (Table 1.9, Entry 2)
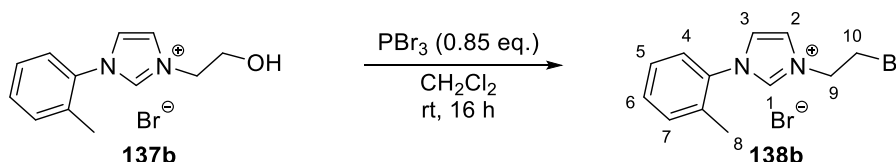
Following general procedure 6.2.3, imidazolium salt **137b** (1.42 g, 5.00 mmol) was reacted with PBr₃ (0.400 mL, 4.30 mmol) in dry CH₂Cl₂ (25 mL) under an argon atmosphere for 16 h to afford 3-(2-bromoethyl)-1-(o-tolyl)-imidazolium bromide (**138b**) as a white solid (1.51 g, **87% yield**).

¹H NMR (400 MHz, DMSO-d_6): δ 9.67 (t, $^4J_{HH}$ = 1.7 Hz, 1H, H¹), 8.13 (t, $^4J_{HH}$ = 1.7 Hz, 1H, H³), 8.12 (t, $^4J_{HH}$ = 1.7 Hz, 1H, H²), 7.56-7.52 (m, 3H, H⁴/H⁵/H⁷), 7.50-7.48 (m, 1H, H⁶), 4.72 (t, $^3J_{HH}$ = 5.8 Hz, 2H, H⁹), 4.05 (t, $^3J_{HH}$ = 5.8 Hz, 2H, H¹⁰), 2.22 (s, 3H, H⁸).

¹³C NMR (101 MHz, DMSO-d_6): δ 137.6, 134.1, 133.4, 131.6, 130.8, 127.5, 126.4, 124.0, 123.8, 50.4, 31.5, 17.0.

Melting point: 132-134 °C.

FTIR (neat, cm⁻¹): 3009, 2982, 1560, 1551, 1497, 1261, 1219, 1190, 1069, 785, 752, 658, 625.

HRMS (positive ESI): m/z calculated for [M]⁺ $C_{12}H_{14}{}^{79}BrN_2{}^+$: 265.0335; found: 265.0337; calculated for $C_{12}H_{14}{}^{81}BrN_2{}^+$: 267.0314; found: 267.0312

3-(2-Bromoethyl)-1-mesityl-imidazolium bromide – **138c** (Table 1.9, Entry 3)
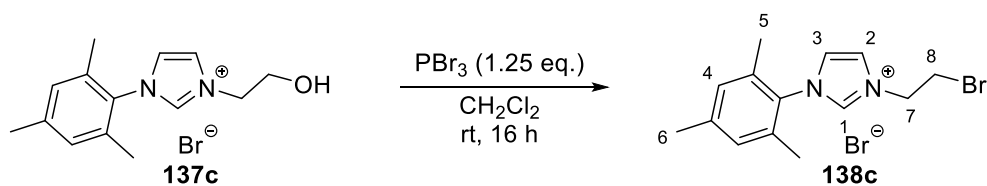
Following general procedure 6.2.3, imidazolium salt **137c** (2.34 g, 7.50 mmol) was reacted with PBr$_3$ (0.900 mL, 9.60 mmol, 1.25 eq.) in dry CH$_2$Cl$_2$ (38 mL) under an argon atmosphere for 16 h to afford 3-(2-bromoethyl)-1-mesityl-imidazolium bromide (**138c**) as a white solid (2.01 g, **71% yield**).

^{1}H NMR (400 MHz, CDCl$_3$): δ 9.76 (t, $^4J_{HH}$ = 1.7 Hz, 1H, H^1), 7.75 (t, $^4J_{HH}$ = 1.7 Hz, 1H, H^3), 7.13 (t, $^4J_{HH}$ = 1.7 Hz, 1H, H^2), 6.99 (s, 2H, H^4), 4.86 (t, $^3J_{HH}$ = 4.9 Hz, 2H, H^7), 4.03 (t, $^3J_{HH}$ = 4.9 Hz, 2H, H^8), 2.33 (s, 3H, H^6), 2.07 (s, 6H, H^5).

^{13}C NMR (101 MHz, CDCl$_3$): δ 141.6, 138.2, 134.5, 130.7, 130.0, 124.4, 123.0, 51.5, 32.0, 21.3, 17.8.

Melting point: 154-156 °C.

FTIR (neat, cm^{-1}): 3065, 2940, 1562, 1547, 1443, 1258, 1204, 1165, 1065, 858, 845, 781, 673, 642.

HRMS (positive ESI): m/z calculated for [M]$^+$ C$_{14}$H$_{18}$BrN$_2$$^+$: 293.0648; found: 293.0650.

6.8.4 Synthesis of 3-(2-(diphenylphosphinoethyl)-1-substituted-imidazolium salts

3-(2-diphenylphosphinoethyl)-1-phenyl-imidazolium tetrakis[3,5-bis(trifluoromethyl)phenyl)]borate – **139a** (Table 1.10, Entry 1)
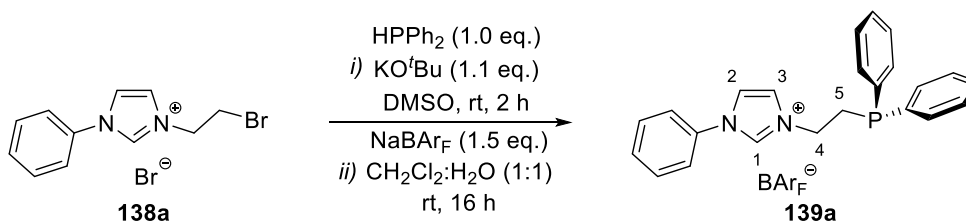
Following general procedure 6.2.4, imidazolium salt **138a** (0.328 g, 0.988 mmol) was dissolved in dry DMSO (1.50 mL) and reacted with a solution of diphenylphosphide, prepared with potassium *tert*-butoxide (0.121 g, 1.08 mmol) in dry DMSO (1.50 mL) and diphenylphosphine (0.180 mL, 1.03 mmol). After extraction and evaporation, the salt exchange was performed with H_2O (20 mL) and sodium tetrakis[3,5-bis(trifluoromethyl)phenyl]borate (NaBAr$_F$, 1.31 g, 1.48 mmol). Purification by column chromatography afforded 3-(2-diphenylphosphinoethyl)-1-phenyl-imidazolium tetrakis[3,5-bis(trifluoromethyl)phenyl]borate (**139a**) as a white solid (1.07 g, **88% yield**).

^{1}H NMR (400 MHz, CDCl$_3$): δ 8.23 (t, $^4J_{HH}$ = 1.7 Hz, 1H, H^1), 7.67 (br s, 8H, Ar-H), 7.60-7.56 (m, 1H, Ar-H), 7.52-746 (m, 7H, Ar-H), 7.36-7.32 (m, 9H, Ar-H), 7.19 (t, J_{HH} = 1.8 Hz, 1H, H^2), 7.15 (t, J_{HH} = 1.8 Hz, 1H, H^3), 7.14-7.12 (m, 2H, Ar-H), 4.31 (dt, $^3J_{HH}$ = 7.0 Hz, $^3J_{HP}$ = 11.6 Hz, 2H, H^4), 2.61 (t, $^3J_{HH}$ = 7.0 Hz, 2H, H^5).

^{13}C NMR (101 MHz, CDCl$_3$): δ 161.7 (q, $^1J_{CB}$ = 49.9 Hz), 139.1, 134.7, 134.6, 133.2, 132.4 (d, $^1J_{CP}$ = 19.8 Hz), 132.1, 131.9, 131.0, 130.1, 129.2 ($^2J_{CP}$ = 7.3 Hz), 128.9 (qq, $^2J_{CB}$ = 33.9 Hz, $^3J_{CF}$ = 2.9 Hz), 124.6 (q, $^1J_{CF}$ = 279.4 Hz), 123.0, 122.4, 117.5 (sept, $^3J_{CF}$ = 4.3 Hz), 49.0 (d, $^2J_{CP}$ = 21.7 Hz), 28.6 ($^1J_{CP}$ = 18.3 Hz).

^{11}B NMR (128 MHz, CDCl$_3$): δ -6.6.

^{19}F NMR (376 MHz, CDCl$_3$): δ -62.4.

^{31}P NMR (162 MHz, CDCl$_3$): δ -22.8.

Melting point: 66-68 °C.

FTIR (neat, cm^{-1}): 3121, 3078, 2965, 1611, 1549, 1495, 1462, 1437, 1352, 1271, 1157, 1117, 885, 839, 762, 743, 716, 691, 681, 667.

HRMS (positive ESI): m/z calculated for [M]$^+$ C$_{23}$H$_{22}$N$_2$P$^+$: 357.1526; found: 357.1521.

3-(2-diphenylphosphinoethyl)-1-(*o*-tolyl)-imidazolium   tetrakis[3,5-bis(trifluoromethyl)phenyl)]borate – **139b** (Table 1.10, Entry 2)
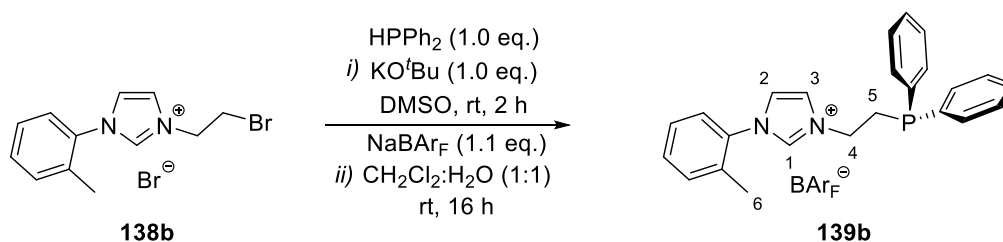
Following general procedure 6.2.4, imidazolium salt **138b** (0.691 g, 2.00 mmol) was dissolved in dry DMSO (3.00 mL) and reacted with a solution of diphenylphosphide, prepared with potassium *tert*-butoxide (0.226 g, 2.01 mmol) in dry DMSO (3.00 mL) and diphenylphosphine (0.360 mL, 2.07 mmol). After extraction and evaporation, the salt exchange was performed with H_2O (20 mL) and sodium tetrakis[3,5-bis(trifluoromethyl)phenyl)]borate (NaBArF, 1.96 g, 2.21 mmol). Purification by column chromatography afforded 3-(2-diphenylphosphinoethyl)-1-(*o*-tolyl)-imidazolium tetrakis[3,5-bis(trifluoromethyl)phenyl)]borate (**139b**) as a white solid (0.806 g, **32% yield**).

^{1}H NMR (400 MHz, CDCl$_3$): δ 8.12 (t, $^4J_{HH}$ = 1.8 Hz, 1H, H^1), 7.66 (br s, 8H, Ar-H), 7.52-7.45 (m, 6H, Ar-H), 7.38-7.34 (m, 10H, Ar-H), 7.32-7.28 (m, 1H, Ar-H), 7.17 (t, J_{HH} = 1.8 Hz, 1H, H^3), 7.13 (t, J_{HH} = 1.8 Hz, 1H, H^2), 7.01-6.99 (m, 1H, Ar-H), 4.31 (dt, $^3J_{HH}$ = 7.1 Hz, $^3J_{HP}$ = 11.2 Hz, 2H, H^4), 2.60 (t, $^3J_{HH}$ = 7.1 Hz, 2H, H^5), 2.05 (s, 3H, H^6).

^{13}C NMR (101 MHz, CDCl$_3$): δ 161.7 (q, $^1J_{CB}$ = 49.8 Hz), 134.8, 134.5 (d, $^2J_{CP}$ = 10.1 Hz), 133.9, 132.9, 132.5, 132.4 (d, $^1J_{CP}$ = 19.8 Hz), 132.3, 130.2, 129.3 (d, $^2J_{CP}$ = 7.3 Hz), 128.9 (qq, $^2J_{CB}$ = 30.7 Hz, $^3J_{CF}$ = 2.9 Hz), 128.2, 125.5, 124.5 (q, $^1J_{CF}$ = 272.6 Hz), 122.5, 117.5 (sept, $^3J_{CF}$ = 4.3 Hz), 48.7 (d, $^2J_{CP}$ = 21.4 Hz), 28.8 (d, $^1J_{CP}$ = 17.6 Hz), 16.9.

^{11}B NMR (128 MHz, CDCl$_3$): δ -6.6.

^{19}F NMR (376 MHz, CDCl$_3$): δ -62.4.

^{31}P NMR (162 MHz, CDCl$_3$): δ -24.1.

Melting point: 78-80 °C.

FTIR (neat, cm^{-1}): 3161, 3123, 3069, 2961, 1611, 1557, 1547, 1493, 1483, 1460, 1437, 1352, 1271, 1155, 1117, 885, 839, 766, 745, 716, 700, 681, 667.

HRMS (positive ESI): m/z calculated for $[M]^+$ $C_{24}H_{24}N_2P^+$: 371.1678; found: 371.1677.

3-(2-diphenylphosphinoethyl)-1-mesityl-imidazolium tetrakis[3,5-bis(trifluoromethyl)phenyl)]borate – **139c** (Table 1.10, Entry 3)
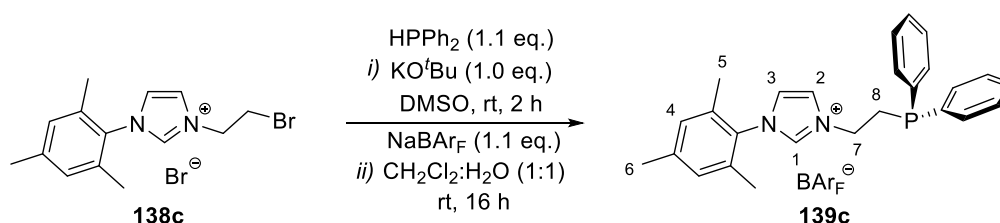
Following general procedure 6.2.4, imidazolium salt **138c** (0.750 g, 2.00 mmol) was dissolved in dry DMSO (3.00 mL) and reacted with a solution of diphenylphosphide, prepared with potassium *tert*-butoxide (0.226 g, 2.01 mmol) in dry DMSO (3.00 mL) and diphenylphosphine (0.360 mL, 2.07 mmol). After extraction and evaporation, the salt exchange was performed with H_2O (20 mL) and sodium tetrakis[3,5-bis(trifluoromethyl)phenyl)]borate (NaBArF, 1.95 g, 2.20 mmol). Purification by column chromatography afforded 3-(2-diphenylphosphinoethyl)-1-mesityl-imidazolium tetrakis[3,5-bis(trifluoromethyl)phenyl)]borate (**139c**) as a white solid (1.46 g, **58% yield**).

^{1}H NMR (400 MHz, CDCl$_3$): δ 8.10 (t, $^4J_{HH}$ = 2.0 Hz, 1H, H^1), 7.67 (br s, 8H, Ar-H), 7.48 (br s, 4H, Ar-H), 7.38-7.34 (m, 10H, Ar-H), 7.15 (t, J_{HH} = 1.7 Hz, 1H, H^3), 7.00 (s, 2H, H^4), 6.99 (t, J_{HH} = 1.7 Hz, 1H, H^2), 4.29 (dt, $^3J_{HH}$ = 7.0 Hz, $^3J_{PH}$ = 11.1 Hz, 2H, H^7), 2.61 (dt, $^3J_{HH}$ = 7.2 Hz, $^2J_{PH}$ = 0.8 Hz, 2H, H^8), 2.31 (s, 3H, H^6), 1.91 (s, 6H, H^5).

^{13}C NMR (101 MHz, CDCl$_3$): δ 161.7 (q, $^1J_{CB}$ = 49.8 Hz), 142.8, 140.1, 136.1, 134.8, 134.6 (d, $^3J_{CP}$ = 3.0 Hz), 134.3 (d, $^2J_{CP}$ = 10.2 Hz), 133.7, 132.5 (d, $^1J_{CP}$ = 19.8 Hz), 130.2 ($^3J_{CP}$ = 4.8 Hz), 129.6, 129.4, 129.3 (d, $^2J_{CP}$ = 7.3 Hz), 128.9 (qq, $^2J_{CB}$ = 33.9 Hz, $^3J_{CF}$ = 2.9 Hz), 126.2, 124.9, 124.5 (q, $^1J_{CF}$ = 272.4 Hz), 122.8, 121.6, 117.5 (sept, $^3J_{CF}$ = 4.1 Hz), 48.4 (d, $^2J_{CP}$ = 19.8 Hz), 28.9 (d, $^1J_{CP}$ = 17.0 Hz), 21.0, 17.1, 16.9.

^{11}B NMR (128 MHz, CDCl$_3$): δ -6.6.

^{19}F NMR (376 MHz, CDCl$_3$): δ -62.4.

³¹P NMR (162 MHz, CDCl₃): δ -25.8.

Melting point: 84-86 °C.

FTIR (neat, cm⁻¹): 3181, 3159, 3127, 3067, 2963, 2924, 1611, 1547, 1483, 1439, 1354, 1273, 1157, 1119, 885, 856, 837, 745, 716, 681, 669.

HRMS (positive ESI): m/z calculated for [M]$^+$ $C_{26}H_{28}N_2P^+$: 399.1995; found: 399.1990.

5.8.4 Preparation of sodium tetrakis[3,5-bis(trifluoromethyl)phenyl)]borate 141

To a flame-dried round-bottomed flask equipped with a magnetic stirrer bar were added magnesium turnings, and the atmosphere was evacuated then replenished with argon, and this process was repeated a further two times. The turnings were vigorously stirred under argon for 1 h and finely divided metal turnings were obtained. Dry diethyl ether was added *via* syringe and the system was cooled to 0 °C in an ice bath. 1,3-bis(trifluoromethyl)-5-bromobenzene was slowly added to the reaction vessel under constant and vigorous stirring at 0 °C. After completion of the addition, the mixture was allowed to warm to room temperature and stirred for 1 h, producing a brown ethereal phase. The flask was cooled to 0 °C in an ice bath and $BF_3 \cdot OEt_2$ was carefully added dropwise and under vigorous stirring. After completion of the addition, the rubber septum was replaced by a cold finger and the reaction was heated to reflux at 35 °C in an electronically controlled oil bath for 18 h. The reaction vessel was allowed to cool to room temperature and the mixture was poured in a saturated solution of sodium carbonate (23.8 g of Na_2CO_3 *per* 100 mL of water) under vigorous stirring. The resulting mixture was filtered multiple times and the solids were washed with diethyl ether. The combined filtrates were collected and transferred to a separating funnel. Once decanted, the bottom, aqueous phase was collected and extracted 5 times with diethyl ether (100 mL *per* 400 mL of aqueous phase). The combined organic phases were dried over Na_2SO_4, filtered and evaporated under reduced pressure to afford a brown mixture with apparent powdered solids. This residue was purified by column chromatography on silica gel, employing gradient elution with mixtures of CH_2Cl_2 and MeOH as eluents (0 – 5% MeOH) to afford the title compound as a white powdered solid.

Results are summarised in Table E1.34.

Table E1.34: Synthesis of NaBAr$_F$ – **141**.[†]

Entry	Index	m$_{Mg}$ (g)	n$_{Mg}$ (mol)	V$_{RBr}$ (mL)	n$_{RBr}$ (mmol)	V$_{Et_2O}$ (mL)
1	T1.11, E1	0.840	0.035	4.85	0.028	26
2	T1.11, E2	3.460	0.14	12.1	0.070	40
3	T1.11, E3	3.420	0.14	12.1	0.070	40

Entry	Index	V$_{BF_3}$ (mL)	n$_{BF_3}$ (mmol)	m$_P$ (g)	Yield (%)
1	T1.11, E1	1.30	5.1	1.086	24
2	T1.11, E2	1.85	7.0	6.920	60
3	T1.11, E3	1.82	7.0	9.090	79

[†]m$_k$, n$_k$ and V$_k$ denotes mass, number of moles and volume of the species indicated; $_{Mg}$ – magnesium turnings; $_{RBr}$ – aryl bromide; $_{BF_3}$ - BF$_3$·Et$_2$O; m$_P$ – mass of product. For index, Tx, Ey reads "Table x, Entry y".

141
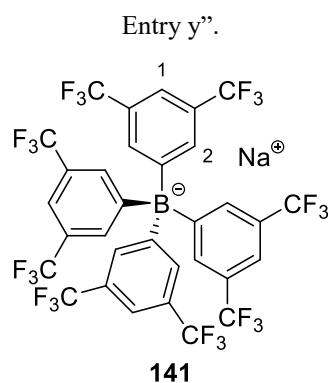
^{1}H NMR (400 MHz, DMSO-d$_6$): δ 7.69 (br s, 4H, H^1), 7.61 (br s, 8H, H^2).

^{11}B NMR (128 MHz, DMSO-d$_6$): δ -6.8.

^{13}C NMR (101 MHz, DMSO-d$_6$): 160.9 (q, $^1J_{CB}$ = 49.8 Hz), 134.0, 128.4 (qq, $^2J_{CB}$ = 33.4 Hz, $^3J_{CF}$ = 3.1 Hz), 124.3 (q, $^1J_{CF}$ = 279.2Hz), 117.4.

^{19}F NMR (376 MHz, DMSO-d$_6$): δ -61.7.

6.8.5 Synthesis of iridium complexes bearing NHC-*P* ligands

η^4-Cycloocta-1,5-diene(3-(2-diphenylphosphinoethyl)-1-phenyl-imidazol-2-ylidene)iridium(I) tetrakis[3,5-bis(trifluoromethyl)phenyl)] borate – **150a** (Table 1.12, Entry 1)
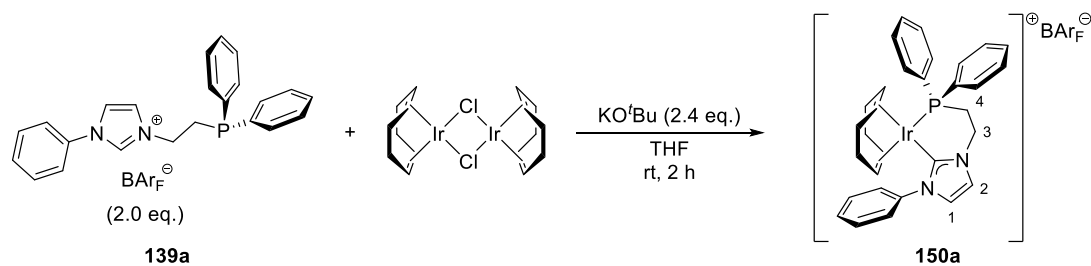
Following general procedure 1.3, bis(1,5-cyclooctadiene)diiridium(I) chloride (0.102 g, 0.152 mmol) was dissolved in dry THF (3.10 mL) and reacted with imidazolium salt **139a** (0.368 g, 0.301 mmol) and *tert*-butoxide (0.040 g, 0.356 mmol). Chromatographic purification afforded η^4-Cycloocta-1,5-diene(3-(2-diphenylphosphinoethyl)-1-phenyl-imidazol-2-ylidene)iridium(I) tetrakis[3,5-bis(trifluoromethyl)phenyl] borate (**150a**) as a red solid (0.170 g, **37% yield**).

^{1}H NMR (400 MHz, CDCl$_3$): δ 7.70 (br s, 9H, Ar-H), 7.51-7.44 (m, 13H, Ar-H), 7.36-7.31 (br m, 5H, Ar-H), 7.01 (d, $^3J_{HH}$ = 2.0 Hz, 1H, H^1), 6.79 (d, $^3J_{HH}$ = 2.0 Hz, 1H, H^2), 4.48 (br d, $^3J_{HP}$ = 24.8 Hz, 2H, H^3), 3.94 (br s, 4H, COD), 2.54 (br s, 2H, H^4), 1.99-1.77 (br m, 8H, COD).

^{13}C NMR (101 MHz, CDCl$_3$): δ 161.7 (q, $^1J_{CB}$ = 50.0 Hz), 134.8, 131.8, 129.8, 129.4 (d, $^1J_{CP}$ = 14.3 Hz), 129.3, (d, $^2J_{CP}$ = 10.3 Hz), 129.1, 129.0, 128.8 (2C), 128.7, 124.6, 124.5 (q, $^1J_{CF}$ = 272.2 Hz), 122.6, 122.0, 117.5 (sept, $^3J_{CF}$ = 3.9 Hz), 81.2, 50.1, 25.6 (d, $^1J_{CP}$ = 38.4 Hz).

^{11}B NMR (128 MHz, CDCl$_3$): δ -6.6.

^{19}F NMR (376 MHz, CDCl$_3$): δ - 62.4.

^{31}P NMR (162 MHz, CDCl$_3$): δ 12.6.

Melting point: 150-152 °C (melted and then decomposed).

FTIR (neat, cm^{-1}): 2361, 2340, 1352, 1273, 1157, 1119, 887, 839, 745, 714, 692, 667.

HRMS (positive ESI): m/z calculated for [M]$^+$ C$_{23}$H$_{21}$IrN$_2$P$^+$: 549.1066; extensive fragmentation observed. However, an ion containing the isotopic pattern of iridium has been identified: m/z calculated for [M]$^+$ C$_{23}$H$_{21}$IrN$_2$OP$^+$: 565.1015; found: 565.1012. The following proposed structure could be obtained through oxidation of the phosphine under ESI conditions:
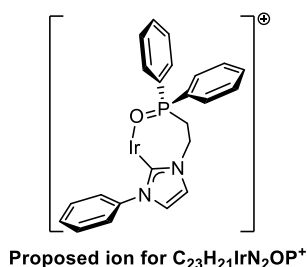
Proposed ion for C$_{23}$H$_{21}$IrN$_2$OP$^+$

η^4-Cycloocta-1,5-diene(3-(2-diphenylphosphinoethyl)-1-(o-tolyl)-imidazol-2-ylidene)iridium(I) tetrakis[3,5-bis(trifluoromethyl)phenyl)] borate – **150b** (Table 1.12, Entry 2)
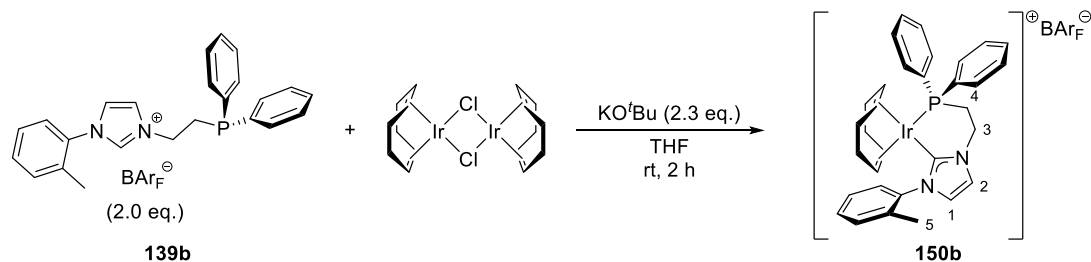
Following general procedure 6.3, bis(1,5-cyclooctadiene)diiridium(I) chloride (0.101 g, 0.150 mmol) was dissolved in dry THF (3.10 mL) and reacted with imidazolium salt **139b** (0.375 g, 0.304 mmol) and potassium *tert*-butoxide (0.039 g, 0.346 mmol). Chromatographic purification afforded η^4-Cycloocta-1,5-diene(3-(2-diphenylphosphinoethyl)-1-(o-tolyl)-imidazol-2-ylidene)iridium(I) tetrakis[3,5-bis(trifluoromethyl)phenyl)] borate (**150b**) as a red solid (0.234 g, **50% yield**).

^{1}H NMR (400 MHz, CDCl$_3$): δ 7.80-7.71 (br s, 9H, Ar-H), 7.68-7.28 (m, 17H, Ar-H), 7.03 (d, $^3J_{HH}$ = 7.8 Hz, 1H, Ar-H), 6.89 (s, 2H, H^1/H^2), 4.56 (br d, $^3J_{HP}$ = 22.2 Hz, 2H, H^3), 4.40-4.10 (br m, 1H, COD), 3.68 (br s, 2H, COD), 2.57 (br s, 2H, H^4), 2.15 (s, 3H, H^5), 2.02-1.49 (br m, 8H, COD).

^{13}C NMR (101 MHz, CDCl$_3$): δ 170.9 (d, $^2J_{CP}$ = 12.5 Hz), 161.7 (q, $^1J_{CB}$ = 49.8), 139.8, 137.8, 134.8, 133.9, 131.8, 131.5, 130.4, 129.2 (d, $^2J_{CP}$ = 10.5 Hz), 128.9 (qq, $^2J_{CB}$ = 31.8 Hz, $^3J_{CF}$ = 3.0 Hz), 127.8, 126.5, 124.5 (q, $^1J_{CF}$ = 272.4 Hz), 121.5, 117.5 (sept, $^3J_{CF}$ = 4.1 Hz), 50.4 (d, $^2J_{CP}$ = 4.4 Hz), 25.5 (d, $^1J_{CP}$ = 38.1 Hz), 17.5.

^{11}B NMR (128 MHz, CDCl$_3$): δ -6.6.

^{19}F NMR (376 MHz, CDCl$_3$): δ - 62.4.

^{31}P NMR (162 MHz, CDCl$_3$): δ 13.1.

Melting point: 164-166 °C (melted and then decomposed).

FTIR (neat, cm^{-1}): 2359, 2336, 1354, 1273, 1157, 1119, 885, 839, 714, 681, 667.

HRMS (positive ESI): m/z calculated for [M]$^+$ C$_{24}$H$_{23}$IrN$_2$P$^+$: 563.1223; extensive fragmentation observed. However, an ion containing the isotopic pattern of iridium has been identified: m/z calculated for [M]$^+$ C$_{24}$H$_{21}$IrN$_2$P$^+$: 561.1066; found: 561.0979. Owing to a larger discrepancy in accurate masses, only a tentative

assignment for the ion under ESI conditions could be proposed. Hence, through sequential C—H activations and loss of H_2, the following ion could be obtained:
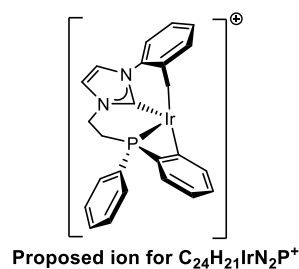
Proposed ion for $C_{24}H_{21}IrN_2P^+$

η^4-Cycloocta-1,5-diene(3-(2-diphenylphosphinoethyl)-1-mesityl-imidazol-2-ylidene)iridium(I) tetrakis[3,5-bis(trifluoromethyl)phenyl)] borate – **150c** (Table 1.12, Entry 3)
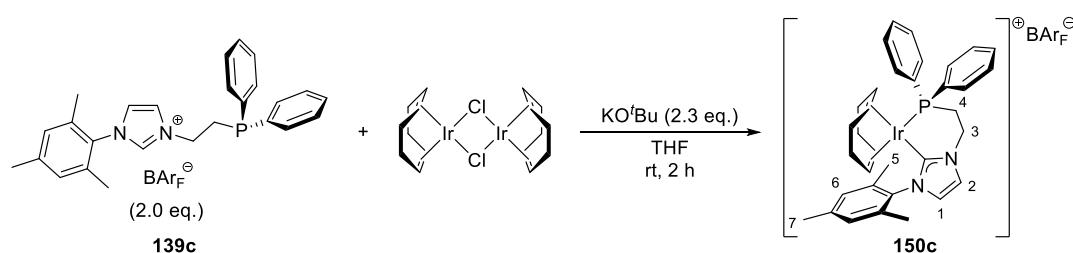
Following general procedure 6.3, bis(1,5-cyclooctadiene)diiridium(I) chloride (0.106 g, 0.158 mmol) was dissolved in dry THF (3.20 mL) and reacted with imidazolium salt **139c** (0.399 g, 0.316 mmol) and potassium *tert*-butoxide (0.038 g, 0.339 mmol). Chromatographic purification afforded η^4-Cycloocta-1,5-diene(3-(2-diphenylphosphinoethyl)-1-mesityl-imidazol-2-ylidene)iridium(I) tetrakis[3,5-bis(trifluoromethyl)phenyl)] borate (**150c**) as a red solid (0.251 g, **31% yield**).

¹H NMR (400 MHz, CDCl₃): δ 7.76-7.72 (br m, 8H, Ar-H), 7.56-7.43 (m, 10H, Ar-H), 7.40-7.33 (m, 4H, Ar-H), 6.99-6.96 (m, 3H, H¹/H⁶), 6.79 (d, $^3J_{HH}$ = 1.9 Hz, 1H, H²), 4.64-4.60 (m, 1H, COD), 4.59-4.53 (m, 1H, COD), 4.44-4.36 (br m, 2H, COD), 3.64-3.57 (br m, 2H, H³), 2.55-2.47 (m, 2H, H⁴), 2.35 (s, 3H, H⁷), 2.01-1.78 (m, 14H, H⁵/COD).

¹³C NMR (101 MHz, CDCl₃): δ 169.3 (d, $^2J_{CP}$ = 11.2 Hz), 161.2 (q, $^1J_{CB}$ = 49.8 Hz), 139.8, 134.4, 134.3, 134.2, 132.0 (d, $^2J_{CP}$ = 10.0 Hz), 131.2, 130.9, 130.4, 128.8, 128.7 (d, $^2J_{CP}$ = 10.0 Hz), 128.4 (qq, $^2J_{CB}$ = 33.4 Hz, $^3J_{CF}$ = 3.1 Hz), 124.1 (q, $^1J_{CF}$ =

279.2 Hz), 124.0, 121.3, 116.9 (m), 88.9 (d, $^2J_{CP}$ = 10.8 Hz), 77.8, 49.9 ($^2J_{CP}$ = 4.6 Hz), 30.8, 30.4, 24.8 (d, $^1J_{CP}$ = 36.7 Hz), 20.4, 17.9.

**^{11}B NMR (128 MHz, CDCl₃):** δ -6.7.

^{19}F NMR (376 MHz, CDCl₃): δ -62.4.

^{31}P NMR (162 MHz, CDCl₃): δ 10.2.

Melting point: 150-152 °C (melted then decomposed).

FTIR (neat, cm⁻¹): 2359, 2336, 1534, 1273, 1155, 1121, 885, 839, 745, 712, 681, 669.

HRMS (positive ESI): m/z calculated for [M]⁺ $C_{26}H_{27}IrN_2P^+$: 591.1536; extensive fragmentation observed. However, an ion containing the isotopic pattern of iridium has been identified: m/z calculated for [M]⁺ $C_{26}H_{25}IrN_2P^+$: 589.1379; found: 589.1381. The following proposed structure could be obtained through sequential C—H activation de-coordination of H₂ under ESI conditions:

Proposed ion for $C_{26}H_{25}IrN_2P^+$
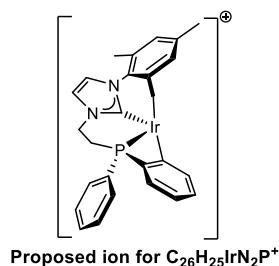
6.8.6 Effect of temperature in the synthesis of iridium(I) catalysts.

Results reported in this section followed two distinct procedures, with the choice of protocol depending on the temperature of the reaction medium. For reactions performed at room temperate, general procedure 5.3 for the synthesis of iridium(I) complexes was employed. Conversely, for synthetic studies performed at -78 °C, a modified version of general procedure 5.3 was adopted. All reactions employed imidazolium salt **139c** as the ligand precursor. Analytical data for products isolated in this series of experiments were identical to those reported for catalyst **150c** and can be found in Section 6.8.5.

*6.8.6.1 Synthesis of catalyst **150c** at reduced temperature.*

To a flame dried Schlenk flask equipped with a stirrer bar was added imidazolium salt **139c**, the atmosphere was evacuated and the solid was stirred under vacuum for 10 min. The atmosphere was then replenished with argon, anhydrous THF was added via syringe and the solid was thoroughly dissolved. The reaction vessel was cooled to -78 °C in a dry ice – acetone bath over the course of 15 min. Then, [Ir(COD)Cl]$_2$ was added under constant vigorous stirring at -78 °C and the mixture was stirred at that temperature for an additional 15 min. KO^{t}Bu was then added in one portion and the reaction mixture was stirred at -78 °C for 1 h. The vessel was allowed to warm to room temperature and the reaction mixture was stirred for an additional 2 h. The resulting dark red solution was evaporated under vacuum and the residue was purified by flash column chromatography employing gradient elution (0 – 50% CH$_2$Cl$_2$/Petroleum ether) to afford η^4-cycloocta-1,5-diene(3-(2-diphenylphosphinoethyl)-1-mesityl-imidazol-2-ylidene)iridium(I) tetrakis[3,5-bis(trifluoromethyl)phenyl] borate (**150c**) as a red solid. The results obtained for this temperature study are reported in Table E1.1.

Table E1.1: Synthesis of catalyst **150c** at reduced temperatures.[†]

Entry	Index[a]	m_{Salt} (mg)	n_{Salt} (mmol)	m_{Ir} (mg)	n_{Ir} (mmol)	m_{KOtBu} (mg)	n_{KOtBu} (mmol)
1[b]	T1.13, E1	317.1	0.251	84.9	0.126	31.9	0.284
2[c]	T1.13, E2	316.1	0.250	84.3	0.126	30.9	0.275
3[d]	T1.13, E3	253.6	0.201	67.4	0.100	26.4	0.235
4[d]	T1.13, E4	507.2	0.402	135.7	0.202	53.6	0.478
5[d]	T1.13, E5	1010.6	0.800	269.7	0.402	103.1	0.919

Entry	Index	V_{THF} (mL)	T (°C)	t (h)	n_P (mg)	Yield (%)
1[b]	T1.13, E1	2.5	rt	2	78.8	20
2[c]	T1.13, E2	5.0	rt	2	60.1	15
3[d]	T1.13, E3	4.0	-78 °C	3	166.9	53
4[d]	T1.13, E4	8.0	-78 °C	3	390	62
5[d]	T1.13, E5	16	-78 °C	3	848	68

[†]m_k – mass of the indicated compound, in mg; n_k – number of mols for the indicated species, in mmol; subscripts denote: $_{Salt}$ – imidazolium salt **139c**; $_{Ir}$ – [Ir(COD)Cl$_2$]; $_P$ – iridium complex **150c**; V_{THF} – volume of THF, in mL; T – temperature; t – time; [a] correspondence to the main text, where Tx, Ey reads "Table x, Entry y"; [b] general procedure 5.3 employed; [c] reaction performed at half concentration; [d] modified procedure employed.

6.8.7 Analysis of iridium(III) hydrides

In these series of experiments, relevant iridium(III) hydrides were generated *in situ* and subsequently analysed by ^{1}H and ^{31}P NMR spectroscopy according to the following procedure.

In an oven-dried NMR tube were added *ca.* 10 mg of the catalyst precursor and 0.6 mL of CD$_3$CN. The solid was thoroughly dissolved and the NMR tube was capped with a Norell® rubber septum cap. The septum was then pierced with a small syringe, which is required to provide a gas outlet for the system. Then, the septum was perforated by a long needle equipped with a control valve directly attached to a balloon filled with hydrogen, and the needle was immersed in the solution until constant, gentle bubbling was observed. Hydrogen bubbling was maintained for 10 minutes, and the long needle was removed from the solution whilst the constant flow of H$_2$ was maintained in the headspace of the NMR tube. Then, the small syringe was removed from the system, swiftly followed by the second needle, the septum was sealed with Parafilm®, and the solution was immediately subjected to ^{1}H NMR spectroscopy employing special acquisition parameters for the ^{1}H nucleus to ensure correct capture of hydridic signals. Thus, an acquisition window of 50 ppm centred at -20 ppm, *i.e.*, each spectrum ranging from +5 to -45 ppm, was employed.

Results obtained employing this method with catalysts **150a-c** are reported in Table 1.14 in the main text.

6.9 Synthesis of substrates

6.9.1 Synthesis of *N*-aryl carbamates

O-tert-butyl-*N*-phenylcarbamate – **166a**
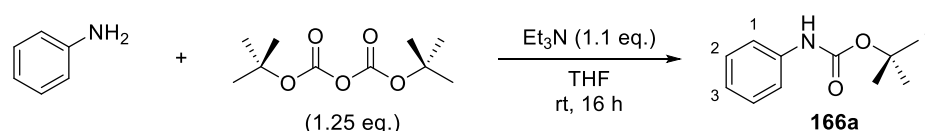
Following general procedure 6.4, aniline (0.910 mL, 10.0 mmol), triethylamine (1.50 mL, 10.8 mmol) and *tert*-butyl dicarbonate (Boc$_2$O, 2.74 g, 12.5 mmol) were reacted in anhydrous THF (30 mL) for 16 h. Chromatographic purification with mixtures of

petroleum ether and Et$_2$O (0 – 10% Et$_2$O) as eluents afforded *O-tert*-butyl-*N*-phenylcarbamate (**166a**) as a white crystalline solid (1.66 g, **86% yield**).

Analytical data for **166a** is consistent with previously reported data:[218,219]

^{1}H NMR (400 MHz, CDCl$_3$): δ 7.38 (d, $^3J_{HH}$ = 8.0 Hz, 2H, H^1), 7.33-7.28 (m, 2H, H^2), 7.05 (tt, $^3J_{HH}$ = 7.3 Hz, $^4J_{HH}$ = 1.2 Hz, 1H, H^3), 6.49 (br s, 1H, NH), 1.55 (s, 9H, H^4).

^{13}C NMR (101 MHz, CDCl$_3$): δ 152.3, 137.8, 128.5, 122.5, 118.0, 80.0, 27.9.

Melting point: 134-136 °C.

IR (neat, cm^{-1}): 3038, 2980, 1686, 1597, 1526, 1501, 1487, 1476, 1439, 1391, 1366, 1312, 1298, 1265, 1238, 1148, 1082, 1053, 1020, 775, 745, 692.

O-tert-butyl-*N*-(4-methylphenyl)carbamate – **166b**
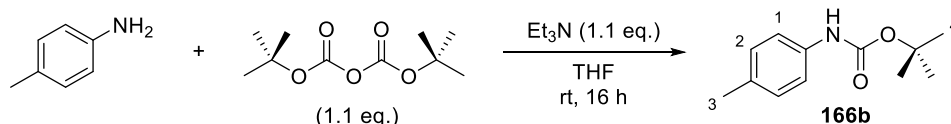
Following general procedure 6.4, *p*-toluidine (0.270 g, 2.52 mmol), triethylamine (0.380 mL, 2.73 mmol) and Boc$_2$O (0.619 g, 2.84 mmol) were reacted in anhydrous THF (7.5 mL) for 16 h. Chromatographic purification was performed with mixtures of petroleum ether and Et$_2$O (0 – 10% Et$_2$O) as eluents. The compound thus obtained was re-crystallized from petroleum ether (60 °C – 0 °C) to afford *O-tert*-butyl-*N*-(4-methyl)phenylcarbamate (**166b**) as a white crystalline solid (0.421 g, **81% yield**).

Analytical data for **166b** is consistent with previously reported data:[219]

^{1}H NMR (400 MHz, CDCl$_3$): δ 7.26 (d, $^3J_{HH}$ = 8.2 Hz, 2H, H^1), 7.11 (d, $^3J_{HH}$ = 8.2 Hz, 2H, H^2), 6.38 (br s, 1H, NH), 2.32 (s, 3H, H^3), 1.54 (s, 9H, H^4).

^{13}C NMR (101 MHz, CDCl$_3$): δ 152.4, 135.2, 132.1, 129.0, 118.2, 79.8, 27.9, 20.2.

Melting point: 88-90 °C.

IR (neat, cm^{-1}): 3350, 3329, 2972, 1694, 1595, 1524, 1449, 1402, 1393, 1364, 1315, 1296, 1233, 1213, 1153, 1123, 1049, 1028, 1018, 839, 814, 772, 762, 723, 658.

O-tert-butyl-*N*-(4-*tert*-butylphenyl)carbamate – **166c**
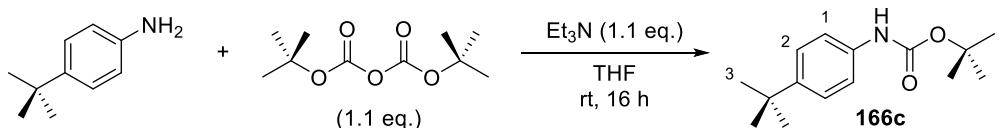
Following general procedure 6.4, 4-(*tert*-butyl)aniline (0.400 mL, 2.51 mmol), triethylamine (0.380 mL, 2.73 mmol) and Boc$_2$O (0.600 g, 2.75 mmol) were reacted in anhydrous THF (7.5 mL) for 16 h. Chromatographic purification was performed with mixtures of petroleum ether and Et$_2$O (0 – 5% Et$_2$O) as eluents. The compound thus obtained was re-crystallized from petroleum ether (60 °C – 0 °C) to afford *O-tert*-butyl-*N*-(4-*tert*-butylphenyl)carbamate (**166c**) as a white crystalline solid (0.472 g, **76% yield**).

Analytical data for **166c** is consistent with previously reported data:[220]

^{1}H NMR (400 MHz, DMSO-*d$_6$*): δ 9.19 (s, 1H, NH), 7.36 (d, $^3J_{HH}$ = 8.6 Hz, 2H, H^1), 7.25 (d, $^3J_{HH}$ = 8.6 Hz, 2H, H^2), 1.47 (s, 9H, H^4), 1.25 (s, 9H, H^3).

^{13}C NMR (101 MHz, DMSO-*d$_6$*): δ 152.8, 144.2, 136.8, 125.1, 117.9, 78.7, 33.8, 31.2, 28.1.

Melting point: 88-90 °C.

IR (neat, cm^{-1}): 3341, 2965, 2953, 1697, 1593, 1522, 1406, 1391, 1368, 1513, 1296, 1267, 1238, 1159, 1117, 1057, 1022, 1015, 833, 773, 754, 679.

HRMS (positive ESI): m/z calculated for [M+Na]$^+$ C$_{15}$H$_{23}$NO$_2$Na$^+$: 272.1621; found: 272.1620.

O-tert-butyl-*N*-(4-methoxyphenyl)carbamate – **166d**
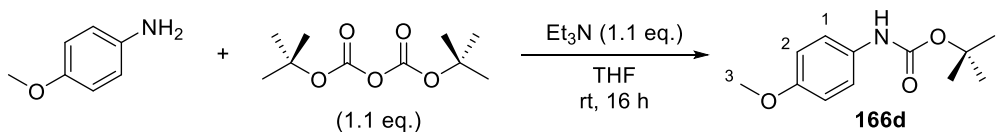
Following general procedure 6.4, 4-(methoxy)aniline (0.309 g, 2.51 mmol), triethylamine (0.380 mL, 2.73 mmol) and Boc$_2$O (0.606 g, 2.78 mmol) were reacted in anhydrous THF (7.5 mL) for 16 h. Chromatographic purification with mixtures of petroleum ether and Et$_2$O (0 – 10% Et$_2$O) as eluents afforded *O-tert*-butyl-*N*-(4-methoxyphenyl)carbamate (**166d**) as a white crystalline solid (0.481 g, **86% yield**).

Analytical data for **166d** is consistent with previously reported data:[220]

^{1}H NMR (400 MHz, DMSO-d_6): δ 9.10 (s, 1H, NH), 7.36 (d, $^3J_{HH}$ = 8.8 Hz, 2H, H^1), 6.83 (d, $^3J_{HH}$ = 8.8 Hz, 2H, H^2), 3.70 (s, 3H, H^3), 1.47 (s, 9H, H^4).

^{13}C NMR (101 MHz, DMSO-d_6): δ 154.4, 152.9, 132.6, 119.6, 113.8, 78.6, 55.1, 28.1.

Melting point: 88-90 °C.

IR (neat, cm^{-1}): 2980, 1749, 1508, 1456, 1445, 1369, 1277, 1248, 1209, 1148, 1117, 1101, 1070, 1051, 1028, 1016, 1007, 957, 934, 891, 868, 829, 818, 781, 750.

O-tert-butyl-*N*-(4-fluorophenyl)carbamate – **166e**
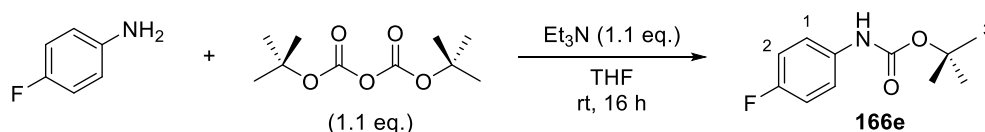
Following general procedure 6.4, 4-fluoroaniline (0.240 mL, 2.53 mmol), triethylamine (0.380 mL, 2.73 mmol) and Boc$_2$O (0.604 g, 2.77 mmol) were reacted in anhydrous THF (7.5 mL) for 16 h. Chromatographic purification was performed with mixtures of petroleum ether and Et$_2$O (0 – 10% Et$_2$O) as eluents. The compound thus obtained was re-crystallized from petroleum ether (60 °C – 0 °C) to afford *O-tert*-butyl-*N*-(4-fluorophenyl)carbamate (**166e**) as a white crystalline solid (0.480 g, **91% yield**).

Analytical data for **166e** is consistent with previously reported data:[223,224]

^{1}H NMR (400 MHz, DMSO-d_6): δ 9.34 (s, 1H, NH), 7.45 (dd, $^3J_{HH}$ = 8.8 Hz, $^4J_{HF}$ = 4.9 Hz, 2H, H^1), 7.07 (dd, $^3J_{HH}$ = $^3J_{HF}$ = 8.9 Hz, 2H, H^2), 1.46 (s, 9H, H^3).

^{13}C NMR (101 MHz, DMSO-d_6): δ 157.4 (d, $^1J_{CF}$ = 238.8 Hz), 152.8, 135.8, 119.7 (d, $^3J_{CF}$ = 5.9 Hz), 115.1 (d, $^2J_{CF}$ = 22.0 Hz), 79.0, 28.1.

^{19}F NMR (376 MHz, DMSO-d_6): δ -121.4.

Melting point: 124-126 °C.

IR (neat, cm^{-1}): 3296, 2978, 1694, 1526, 1512, 1504, 1406, 1393, 1369, 1304, 1269, 1248, 1223, 1215, 1161, 1152, 1096, 1061, 835, 799, 773, 764, 727, 673.

O-tert-butyl-*N*-(4-chlorophenyl)carbamate – **166f**
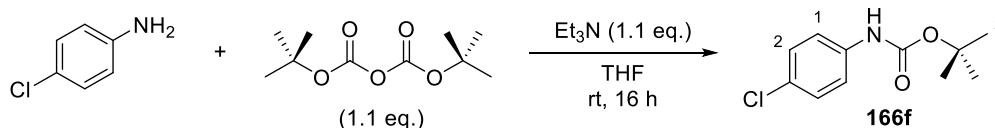
Following general procedure 6.4, 4-chloroaniline (0.320 g, 2.51 mmol), triethylamine (0.380 mL, 2.73 mmol) and Boc$_2$O (0.617 g, 2.83 mmol) were reacted in anhydrous THF (7.5 mL) for 16 h. Chromatographic purification with mixtures of petroleum ether and Et$_2$O (0 – 20% Et$_2$O) as eluents afforded *O-tert*-butyl-*N*-(4-chlorophenyl)carbamate (**166f**) as a white crystalline solid (0.409 g, **72% yield**).

Analytical data for **166f** is consistent with previously reported data:[225,226]

^{1}H NMR (400 MHz, CDCl$_3$): δ 7.35-7.30 (m, 2H, H^1), 7.28-7.24 (m, 2H, H^2), 6.50 (br s, 1H, NH), 1.54 (s, 9H, H^3).

^{13}C NMR (101 MHz, CDCl$_3$): δ 152.1, 136.4, 128.4, 127.5, 119.2, 80.4, 27.8.

Melting point: 100-102 °C.

IR (neat, cm^{-1}): 3300, 2980, 1686, 1591, 1514, 1491, 1476, 1454, 1398, 1368, 1304, 1283, 1269, 1238, 1150, 1092, 1053, 1026, 1013, 903, 831, 822, 766, 660.

O-tert-butyl-*N*-(4-bromophenyl)carbamate – **166g**
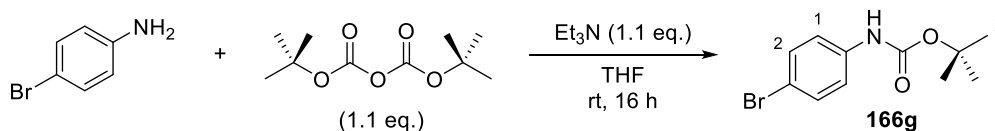
Following general procedure 6.4, 4-bromoaniline (0.571 g, 3.32 mmol), triethylamine (0.510 mL, 3.66 mmol) and Boc$_2$O (0.817 g, 3.74 mmol) were reacted in anhydrous THF (10 mL) for 16 h. Chromatographic purification was performed with mixtures of petroleum ether and Et$_2$O (0 – 10% Et$_2$O) as eluents. The compound thus obtained was re-crystallized from petroleum ether (60 °C – 0 °C) to afford *O-tert*-butyl-*N*-(4-bromophenyl)carbamate (**166g**) as a white solid (0.360 g, **40% yield**).

Analytical data for **166g** is consistent with previously reported data:[227]

¹H NMR (400 MHz, d₆-DMSO): δ 9.48 (s, 1H, NH), 7.42 (app. s, 4H, H¹/H²), 1.48 (s, 9H, H³).

¹³C NMR (101 MHz, d₆-DMSO): δ 152.6, 138.9, 131.3, 119.9, 113.5, 79.3, 28.0.

Melting point: 100-102 °C.

IR (neat, cm⁻¹): 3368, 2980, 1693, 1589, 1508, 1489, 1449, 1389, 1364, 1344, 1304, 1287, 1263, 1231, 1151, 1145, 1069, 1053, 1024, 1007, 953, 930, 905, 876.

O-tert-butyl-*N*-(4-trifluoromethylphenyl)carbamate – **166h**
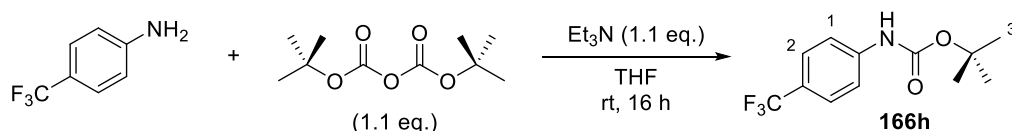
Following general procedure 6.4, 4-(trifluoromethyl)aniline (0.410 mL, 3.26 mmol), triethylamine (0.510 mL, 3.66 mmol) and Boc₂O (0.826 g, 3.78 mmol) were reacted in anhydrous THF (10 mL) for 16 h. Chromatographic purification with mixtures of petroleum ether and Et₂O (0 – 10% Et₂O) as eluents afforded *O-tert*-butyl-*N*-(4-trifluoromethylphenyl)carbamate (**166h**) as a white crystalline solid (0.642 g, **75% yield**).

Analytical data for **166h** is consistent with previously reported data:[223,224]

¹H NMR (400 MHz, DMSO-*d₆*): δ 9.77 (s, 1H, NH), 7.66 (d, $^3J_{HH}$ = 8.7 Hz, 2H, H¹), 7.60 (d, $^3J_{HH}$ = 8.7 Hz, 2H, H²), 1.49 (s, 9H, H³).

¹³C NMR (101 MHz, DMSO-*d₆*): δ 152.6, 143.3, 125.9 (q, $^3J_{CF}$ = 3.5 Hz), 124.5 (q, $^1J_{CF}$ = 271.6 Hz), 122.0 (q, $^2J_{CF}$ = 32.2 Hz), 117.8, 79.7, 28.0.

¹⁹F NMR (376 MHz, DMSO-*d₆*): δ -60.1.

Melting point: 120-122 °C.

IR (neat, cm⁻¹): 3362, 2986, 1701, 1616, 1528, 1506, 1410, 1371, 1331, 1315, 1273, 1234, 1153, 1111, 1069, 1028, 1016, 905, 837, 773, 764, 633, 611.

O-tert-butyl-*N*-(2-methylphenyl)carbamate – **166i**
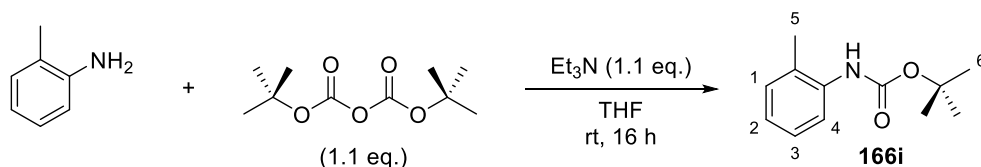
Following general procedure 6.4, *o*-toluidine (0.270 mL, 2.54 mmol), triethylamine (0.380 mL, 2.73 mmol) and Boc$_2$O (0.612 g, 2.80 mmol) were reacted in anhydrous THF (7.5 mL) for 16 h. Chromatographic purification was performed with mixtures of petroleum ether and Et$_2$O (0 – 5% Et$_2$O) as eluents. The compound thus obtained was re-crystallized from petroleum ether (60 °C – 0 °C) to afford *O-tert*-butyl-*N*-(2-methylphenyl)carbamate (**166i**) as a white crystalline solid (0.448 g, **86% yield**).

Analytical data for **166i** is consistent with previously reported data:[228]

^{1}H NMR (400 MHz, CDCl$_3$): δ 7.86 (d, $^3J_{HH}$ = 8.2 Hz, 1H, H^5), 7.21 (t, $^3J_{HH}$ = 7.5 Hz, 1H, H^4), 7.17 (d, $^3J_{HH}$ = 7.6 Hz, 1H, H^2), 7.01 (td, $^3J_{HH}$ = 7.4 Hz, $^4J_{HH}$ = 1.0 Hz, 1H, H^3), 6.28 (br s, 1H, NH), 2.27 (s, 3H, H^1), 1.55 (s, 9H, H^6).

^{13}C NMR (101 MHz, CDCl$_3$): δ 152.6, 135.8, 129.8, 126.7, 126.3, 123.1, 120.4, 79.9, 27.9, 17.2.

Melting point: 78-80 °C.

IR (neat, cm^{-1}): 3269, 2982, 2967, 1701, 1678, 1522, 1487, 1456, 1362, 1292, 1263, 1246, 1153, 1051, 1024, 777, 745, 733, 638, 619, 604.

O-tert-butyl-*N*-(2-fluorophenyl)carbamate – **166j**
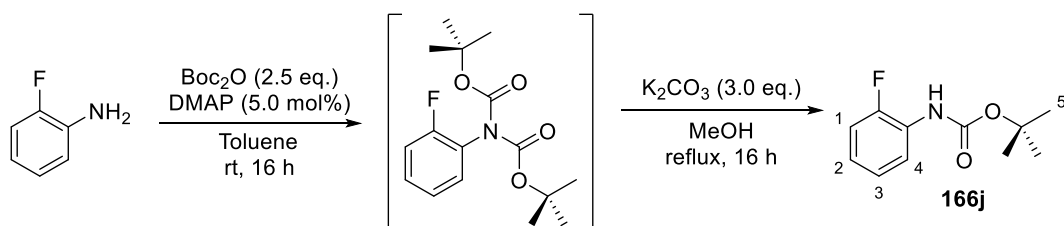
To a flame dried round-bottomed flask containing a magnetic stirrer bar were added DMAP (19.9 mg, 0.163 mmol), Boc$_2$O (1.64 g, 7.52 mmol) and anhydrous toluene (3.00 mL), and the mixture was vigorously stirred at room temperature until a homogeneous solution was obtained. Then, 2-fluoroaniline (0.290 mL, 0.334 g, 3.00 mmol) was added, and the reaction was vigorously stirred under a constant argon

atmosphere at room temperature for 16 h. After reaction completion (assessed by TLC analysis of the reaction mixture), the solvent was evaporated under reduced pressure, the residue was suspended in Et_2O (20 mL) and filtered through plug of cotton wool. The remaining solids were washed with Et_2O (2 × 5 mL) and the filtrate was evaporated under reduced pressure. The resulting residue was re-dissolved in a minimum amount of Et_2O and purified by column chromatography on silica gel employing gradient elution with mixtures of petroleum ether and Et_2O.

The product thus obtained was added to a round-bottomed flask equipped with a magnetic stirrer bar. Then, MeOH (30 mL) and K_2CO_3 (1.26 g, 9.15 mmol) were subsequently added, and the reaction mixture was vigorously stirred and heated to reflux for 16 h. The reaction mixture was then allowed to cool to room temperature, the solvent was evaporated under reduced pressure, the residue was suspended in Et_2O (20 mL) and filtered through a plug of cotton wool. The remaining solids were washed with Et_2O (2 × 5 mL) and the filtrate was evaporated under reduced pressure. The resulting residue was re-dissolved in a minimum amount of Et_2O and purified by column chromatography on silica gel employing gradient elution with mixtures of petroleum ether and Et_2O (0 – 5% Et_2O) as eluent to afford *O-tert*-butyl-*N*-(2-fluorophenyl)carbamate (**166j**) (0.442 g, **70% overall yield**) as a clear viscous oil.

Analytical data for **166j** is consistent with previously reported data:[223,224,229]

^{1}H NMR (400 MHz, CDCl$_3$): δ 8.10 (dd, $^3J_{HH}$ = $^4J_{HF}$ = 8.0 Hz, 1H, H^4), 7.11 (tdd, $^3J_{HH}$ = 7.8 Hz, $^4J_{HH}$ = $^5J_{HF}$ = 0.8 Hz, 1H, H^3), 7.06 (ddd, $^3J_{HF}$ = 11.3 Hz, $^3J_{HH}$ = 8.4 Hz, $^4J_{HH}$ = 1.4 Hz, 1H, H^1), 6.97 (dddd, $^3J_{HH}$ = 8.3 Hz, $^3J_{HH}$ = 7.5 Hz, $^4J_{HF}$ = 5.0 Hz, $^4J_{HH}$ = 1.5 Hz, 1H, H^2), 6.74 (br s, 1H, NH), 1.55 (s, 9H, H^5).

^{13}C NMR (101 MHz, CDCl$_3$): δ 151.9, 151.6 (d, $^1J_{CF}$ = 243.0 Hz), 126.4 (d, $^2J_{CF}$ = 10.0 Hz), 124.0 (d, $^3J_{CF}$ = 3.7 Hz), 122.4 (d, $^3J_{CF}$ = 7.4 Hz), 119.6, 114.2 (d, $^2J_{CF}$ = 19.3 Hz), 80.5, 27.8.

IR (neat, cm^{-1}): 3443, 2978, 1732, 1620, 1520, 1481, 1452, 1368, 1319, 1256, 1233, 1190, 1152, 1105, 1049, 1024, 839, 808, 795, 770, 748.

O-tert-butyl-*N*-(2-(trifluoromethyl)phenyl)carbamate – **166k**
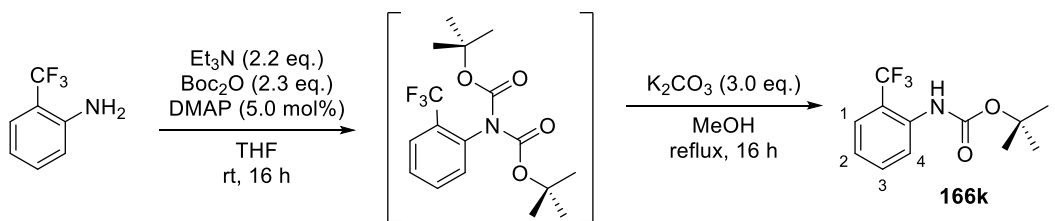
To a flame dried round-bottomed flask containing a magnetic stirrer bar were added DMAP (19.4 mg, 0.159 mmol), Boc$_2$O (1.64 g, 7.50 mmol) and anhydrous THF (3.00 mL), and the mixture was vigorously stirred at room temperature until a homogeneous solution was obtained. Then, triethylamine (1.00 mL, 0.726 g, 7.17 mmol) and 2-(trifluoromethyl)aniline (0.410 mL, 0.526 g, 3.26 mmol) were added, and the reaction was vigorously stirred under a constant argon atmosphere at room temperature for 16 h. After reaction completion (assessed by TLC analysis of the reaction mixture), the solvent was evaporated under reduced pressure, the residue was suspended in Et$_2$O (20 mL) and filtered through a plug of cotton wool. The remaining solids were washed with Et$_2$O (2 × 5 mL) and the filtrate was evaporated under reduced pressure. The resulting residue was re-dissolved in a minimum amount of Et$_2$O and purified by column chromatography on silica gel employing gradient elution with mixtures of petroleum ether and Et$_2$O (0 – 15% Et$_2$O) as eluents to afford *N,N*-bis(*tert*-butoxycarbonyl)-2-(trifluoromethyl)aniline (1.19 g, 98% yield) as a white solid.

A portion of the solid thus obtained (0.520 g, 1.43 mmol) was added to a round-bottomed flask equipped with a magnetic stirrer bar. Then, MeOH (15 mL) and K$_2$CO$_3$ (0.617 g, 4.47 mmol) were subsequently added, and the reaction mixture was vigorously stirred and heated to reflux for 16 h. The reaction mixture was then allowed to cool to room temperature, the solvent was evaporated under reduced pressure, the residue was suspended in Et$_2$O (20 mL) and filtered through a plug of cotton wool. The remaining solids were washed with Et$_2$O (2 × 5 mL) and the filtrate was evaporated under reduced pressure. The resulting residue was re-dissolved in a minimum amount of Et$_2$O and purified by column chromatography on silica gel employing gradient elution with mixtures of petroleum ether and Et$_2$O (0 – 10% Et$_2$O) as eluent to afford *O-tert*-butyl-*N*-(2-(trifluoromethyl)phenyl)carbamate (**166k**) (0.308 g, **82% yield**) as a colourless viscous oil.

Analytical data for **166k** is consistent with previously reported data:[223,224]

^{1}H NMR (400 MHz, DMSO-d_6): δ 8.64 (s, 1H, NH), 7.68 (d, $^3J_{HH}$ = 7.9 Hz, 1H, H^1), 7.64 (t, $^3J_{HH}$ = 7.4 Hz, 1H, H^3), 7.46 (d, $^3J_{HH}$ = 8.0 Hz, 1H, H^4), 7.40 (t, $^3J_{HH}$ = 7.7 Hz, 1H, H^2), 1.42 (s, 9H, H^5).

^{13}C NMR (101 MHz, DMSO-d_6): δ 153.8, 135.8, 132.9, 129.7, 126.3, 126.2, 124.9 (q, $^2J_{CF}$ = 28.8 Hz), 120.9 (q, $^1J_{CF}$ = 273.3 Hz), 79.2, 28.0.

^{19}F NMR (376 MHz, DMSO-d_6): δ -59.2.

IR (neat, cm^{-1}): 3472, 2980, 1740, 1591, 1524, 1454, 1368, 1319, 1285, 1250, 1229, 1153, 1105, 1069, 1047, 1034, 899, 833, 760, 741, 652.

O-tert-butyl-*N*-(3,5-dimethylphenyl)carbamate – **166l**
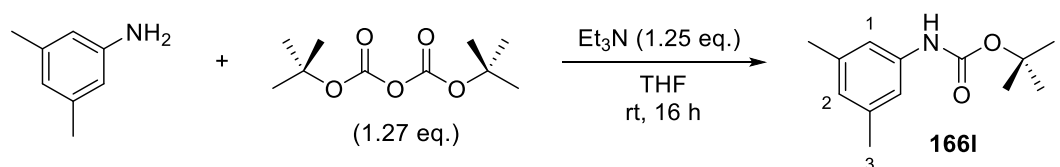
Following general procedure 6.4, 3,5-dimethylaniline (0.410 mL, 3.29 mmol), triethylamine (0.570 mL, 4.10 mmol) and Boc$_2$O (0.908 g, 4.17 mmol) were reacted in anhydrous THF (10 mL) for 16 h. Chromatographic purification was performed with mixtures of petroleum ether and Et$_2$O (0 – 10% Et$_2$O) as eluents. The compound thus obtained was re-crystallized from petroleum ether (60 °C – 0 °C) to afford *O-tert*-butyl-*N*-(3,5-dimethylphenyl)carbamate (**166l**) as a white crystalline solid (0.637 g, **87% yield**).

Analytical data for **166l** is consistent with previously reported data:[230]

^{1}H NMR (400 MHz, DMSO-d_6): δ 9.13 (s, 1H, NH), 7.07 (s, 2H, H^1), 6.58 (s, 1H, H^2), 2.19 (s, 6 H, H^3), 1.45 (s, 9H, H^4).

^{13}C NMR (101 MHz, DMSO-d_6): δ 152.7, 139.3, 137.4, 123.5, 115.9, 78.8, 28.1, 21.1.

Melting point: 88-90 °C.

IR (neat, cm^{-1}): 3356, 2988, 2967, 2164, 1690, 1614, 1601, 1520, 1474, 1431, 1391, 1364, 1275, 1233, 1157, 1076, 1040, 1011, 941, 893, 874, 885.

O-tert-butyl-*N*-(3-methoxyphenyl)carbamate – **166m**
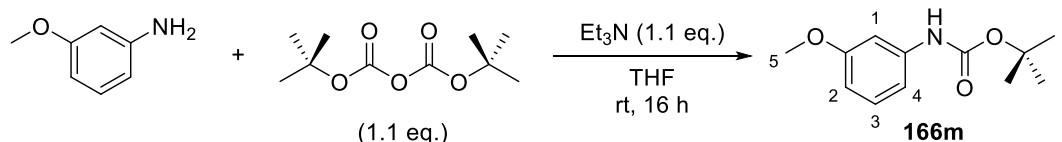
Following general procedure 6.4, 3-methoxyaniline (0.370 mL, 3.30 mmol), triethylamine (0.510 mL, 3.66 mmol) and Boc$_2$O (0.807 g, 3.70 mmol) were reacted in anhydrous THF (10 mL) for 16 h. Chromatographic purification with mixtures of petroleum ether and Et$_2$O (0 – 10% Et$_2$O) as eluents afforded *O-tert*-butyl-*N*-(3-methoxyphenyl)carbamate (**166m**) as a white crystalline solid (0.662 g, **90% yield**).

Analytical data for **166m** is consistent with previously reported data:[231,232]

^{1}H NMR (400 MHz, DMSO-*d$_6$*): δ 9.29 (s, 1H, NH), 7.14 (s, 1H, H^1), 7.13 (t, $^3J_{HH}$ = 8.0 Hz, 1H, H^3), 7.00 (d, $^3J_{HH}$ = 8.0 Hz, 1H, H^4), 6.53 (dd, $^3J_{HH}$ = 8.0 Hz, $^4J_{HH}$ = 2.1 Hz, 1H, H^2), 3.71 (s, 3H, H^5), 1.48 (s, 9H, H^6).

^{13}C NMR (101 MHz, DMSO-*d$_6$*): δ 159.5, 152.6, 140.7, 129.3, 110.4, 107.3, 103.9, 79.0, 54.9, 28.1.

Melting point: 56-58 °C.

IR (neat, cm^{-1}): 3335, 2976, 1694, 1603, 1530, 1450, 1425, 1391, 1366, 1288, 1240, 1206, 1155, 1088, 1051, 1036, 966, 868, 777, 760, 685, 642.

O-tert-butyl-*N*-(3-fluorophenyl)carbamate – **166n**
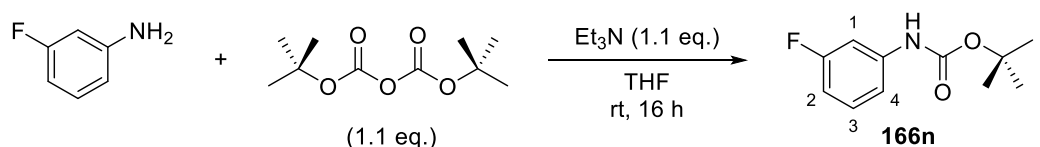
Following general procedure 6.4, 3-fluoroaniline (0.240 mL, 2.49 mmol), triethylamine (0.380 mL, 2.73 mmol) and Boc$_2$O (0.623 g, 2.85 mmol) were reacted in anhydrous THF (7.50 mL) for 16 h. Chromatographic purification was performed with mixtures of petroleum ether and Et$_2$O (0 – 5% Et$_2$O) as eluents. The compound thus obtained was recrystallized from petroleum ether (60 °C – 0 °C) to afford *O-tert*-butyl-*N*-(3-fluorophenyl)carbamate (**166n**) as a white solid (0.350 g, **66% yield**).

Analytical data for **166n** is consistent with previously reported data:[233]

^{1}H NMR (400 MHz, DMSO-d_6): δ 9.56 (br s, 1H, NH), 7.38 (dt, $^3J_{HF}$ = 12.0 Hz, $^4J_{HH}$ = 2.5 Hz, 1H, H^1), 7.31-7.19 (m, 2H, H^3/H^4), 6.77 (ddd, $^3J_{HF}$ = $^3J_{HH}$ = 8.4 Hz, $^4J_{HH}$ = 2.4 Hz, 1H, H^2), 1.48 (s, 9H, H^5).

^{13}C NMR (101 MHz, DMSO-d_6): δ 162.3 (d, $^1J_{CF}$ = 240.6 Hz), 152.6, 141.4 (d, $^3J_{CF}$ = 11.6 Hz), 130.2 (d, $^3J_{CF}$ = 10.0 Hz), 113.8, 108.3 (d, $^2J_{CF}$ = 20.8 Hz), 104.6 ($^2J_{CF}$ = 26.4 Hz), 79.5, 28.0.

^{19}F NMR (376 MHz, DMSO-d_6): δ -112.4.

Melting point: 126-128 °C.

IR (neat, cm^{-1}): 3318, 2984, 1688, 1614, 1603, 1526, 1439, 1393, 1368, 1281, 1260, 1236, 1144, 1086, 1049, 1028, 974, 868, 856, 773, 762, 725, 685.

HRMS (positive ESI): m/z calculated for [M+H]$^+$ $C_{11}H_{14}FNO_2Na^+$: 234.0901; found: 234.0901.

O-tert-butyl-*N*-(3-fluorophenyl)carbamate – **166o**
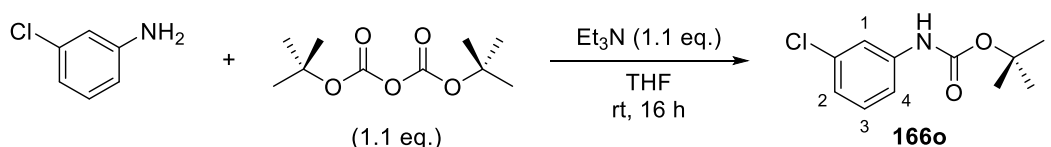
Following general procedure 6.4, 3-chloroaniline (0.260 mL, 2.45 mmol), triethylamine (0.380 mL, 2.73 mmol) and Boc$_2$O (0.609 g, 2.79 mmol) were reacted in anhydrous THF (7.50 mL) for 16 h. Chromatographic purification was performed with mixtures of petroleum ether and Et$_2$O (0 – 10% Et$_2$O) as eluents. The compound thus obtained was re-crystallized from petroleum ether (60 °C – 0 °C) to afford *O-tert*-butyl-*N*-(3-chlorophenyl)carbamate (**166o**) as a white solid (0.341 g, **60% yield**).

Analytical data for **166o** is consistent with previously reported data:[234]

^{1}H NMR (400 MHz, DMSO-d_6): δ 9.56 (s, 1H, NH), 7.62 (t, $^4J_{HH}$ = 1.9 Hz, 1H, H^1), 7.36 (br d, $^3J_{HH}$ = 8.5 Hz, 1H, H^4), 7.27 (t, $^3J_{HH}$ = 8.0 Hz, 1H, H^3), 7.01 (ddd, $^3J_{HH}$ = 7.8 Hz, $^4J_{HH}$ = 1.2 Hz, $^4J_{HH}$ = 1.0 Hz, 1H, H^2), 1.48 (s, 9H, H^5).

^{13}C NMR (101 MHz, DMSO-d_6): δ 152.6, 141.1, 133.1, 130.3, 121.6, 117.3, 116.4, 79.5, 28.0.

Melting point: 78-80 °C.

IR (neat, cm^{-1}): 3329, 1690, 1585, 1512, 1477, 1420, 1393, 1366, 1281, 1237, 1192, 1155, 1096, 1080, 1051, 1024, 997, 935, 868, 845, 775, 762, 681, 654, 617.

6.9.2 Synthesis of *O*-aryl carbamates

N-tert-butyl-*O*-phenylcarbamate – **168a**
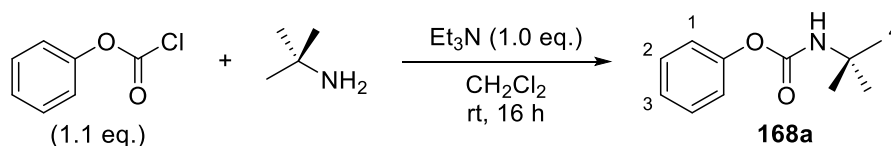
To a flame-dried round-bottom flask equipped with a magnetic stirrer bar were added *tert*-butylamine (0.35 mL, 3.3 mmol), dry CH$_2$Cl$_2$ (3.5 mL) and triethylamine (0.46 mL, 3.3 mmol) and the mixture was thoroughly stirred and cooled to 0 °C in an ice-water bath. Then, phenyl chloroformate (purified by fractional distillation under vacuum, 0.46 mL, 3.7 mmol) was added dropwise at that temperature under constant, vigorous stirring. Upon completion of the addition, the mixture was allowed to warm to room temperature and reacted for 16 h under an argon atmosphere. After reaction completion (assessed by TLC analysis of the reaction mixture), the mixture was quenched by addition of saturated aqueous NaHCO$_3$ (7.5 mL), the aqueous phase was extracted with CH$_2$Cl$_2$ (3 × 20 mL), the combined organic extracts were dried over Na$_2$SO$_4$, filtered and evaporated under reduced pressure. The residue was then purified by column chromatography with gradient elution employing mixtures of petroleum ether and Et$_2$O (0 – 50% Et$_2$O) as eluents to afford *N-tert*-butyl-*O*-phenylcarbamate (**168a**) as a white solid (0.42 g, **66% yield**).

Analytical data for **168a** is consistent with previously reported data:[235]

^{1}H NMR (400 MHz, CDCl$_3$): δ 7.37 (tt, $^3J_{HH}$ = 7.8 Hz, $^4J_{HH}$ = 2.0 Hz, 2H, H^2), 7.20 (tt, $^3J_{HH}$ = 7.4 Hz, $^4J_{HH}$ = 1.5 Hz, 1H, H^3), 7.14 (d, $^3J_{HH}$ = 7.7 Hz, 2H, H^1), 5.01 (br s, 1H, NH), 1.42 (s, 9H, H^4).

^{13}C NMR (101 MHz, CDCl$_3$): δ 152.3, 150.5, 128.7, 124.6, 121.3, 50.3, 28.3.

Melting point: 90-92 °C.

IR (neat, cm^{-1}): 3337, 2974, 1738, 1713, 1682, 1518, 1491, 1477, 1454, 1393, 1364, 1273, 1162, 1155, 1067, 1049, 1022, 993, 955, 932, 903, 837, 826.

HRMS (positive ESI): m/z calculated for [M+H]$^+$ C$_{11}$H$_{16}$NO$_2{}^+$: 194.1176; found: 194.1171.

N,N-diethyl-*O*-phenylcarbamate – **168b**
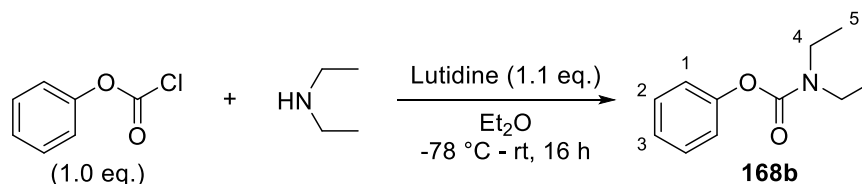
To a flame-dried round-bottom flask equipped with a magnetic stirrer bar were added dry Et$_2$O (30 mL), 2,6-lutidine (0.40 mL, 3.4 mmol) and diethylamine (0.31 mL, 3.0 mmol), and the mixture was thoroughly stirred and cooled to -78 °C in a dry ice-acetone bath. Then, phenyl chloroformate (0.38 mL, 3.0 mmol) was added dropwise at that temperature under constant, vigorous stirring. Upon completion of the addition, the mixture was allowed to stir at -78 °C for 15 min, it was subsequently warmed to room temperature and reacted for 16 h under an argon atmosphere. After reaction completion (assessed by TLC analysis of the reaction mixture), the mixture was transferred to a separating funnel, sequentially washed with 1.0 M NaOH (10 mL), 1.0 M HCl (10 mL), water (10 mL) and brine (10 mL). The organic layer was then dried over Na$_2$SO$_4$, filtered and evaporated under reduced pressure. The resulting residue was purified by column chromatography with gradient elution employing mixtures of petroleum ether and Et$_2$O as eluents (0-10% Et$_2$O). The compound thus obtained was further purified by distillation in vacuum (140 °C at 5 mbar) to afford *N,N*-diethyl-*O*-phenylcarbamate (**168b**) as a colourless viscous oil (0.28 g, **49% yield**).

Analytical data for **168b** is consistent with previously reported data:[236]

^{1}H NMR (400 MHz, CDCl$_3$): δ 7.36 (ddt, $^3J_{HH}$ = 8.6 Hz, $^3J_{HH}$ = 7.5 Hz, $^4J_{HH}$ = 2.2 Hz, 2H, H^2), 7.19 (dt, $^3J_{HH}$ = 7.4 Hz, $^4J_{HH}$ = 1.1 Hz, 1H, H^3), 7.13 (dq, $^3J_{HH}$ = 8.1 Hz, $^4J_{HH}$ = 1.6 Hz, 2H, H^1), 3.50-3.36 (br m, 4H, H^4), 1.33-1.17 (br m, 6H, H^5).

^{13}C NMR (101 MHz, CDCl$_3$): δ 154.3, 151.6, 129.2, 125.0, 121.8, 42.1 (apparent d, $^{rot}\Delta = 34$ Hz),[†] 13.8 (apparent d, $^{rot}\Delta = 84$ Hz).[†]

[†] Signals affected by rotameric effects. $^{rot}\Delta$ indicates the observed separation between peaks.

IR (neat, cm^{-1}): 2978, 1713, 1593, 1497, 1472, 1456, 1414, 1379, 1366, 1350, 1315, 1271, 1225, 1200, 1152, 1096, 1070, 1042, 1024, 959, 937, 907, 818.

N,N-di(*iso*-propyl)-*O*-phenylcarbamate – **168c**
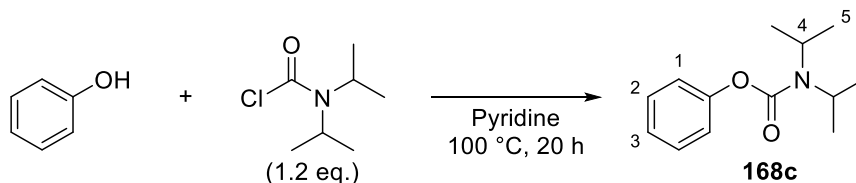
To a round-bottom flask equipped with a magnetic stirrer bar were added phenol (313 mg, 3.33 mmol), *N,N*-di(*iso*-propyl)carbamoyl chloride (675 mg, 4.13 mmol) and pyridine (3.30 mL). The resulting mixture was stirred and heated to 100 °C for 20 h. After reaction completion (assessed by TLC analysis of the reaction mixture), the mixture was treated with Et$_2$O (20 mL), sequentially washed with 1.0 M HCl (2 × 5 mL), 1.0 M NaOH (2 × 5 mL), water (5 mL) and brine (5 mL). The organic layer was then dried over Na$_2$SO$_4$, filtered and evaporated under reduced pressure to afford *N,N*-di(*iso*-propyl)-*O*-phenylcarbamate (**168c**) as a highly viscous oil that solidified upon standing (657 mg, **90% yield**).

Analytical data for **168c** is consistent with previously reported data:[237,238]

^{1}H NMR (400 MHz, CDCl$_3$): δ 7.36 (ddt, $^3J_{HH} = 8.6$ Hz, $^3J_{HH} = 7.5$ Hz, $^4J_{HH} = 2.2$ Hz, 2H, H^2), 7.19 (dt, $^3J_{HH} = 7.5$ Hz, $^4J_{HH} = 1.4$ Hz, 1H, H^3), 7.15-7.10 (m, 2H, H^1), 4.24-3.86 (br m, 2H, H^4), 1.41-1.27 (br m, 12H, H^5).

^{13}C NMR (101 MHz, CDCl$_3$): δ 153.4, 150.9, 128.7, 124.4, 121.3, 46.0 (apparent d, $^{rot}\Delta = 72$ Hz),[†] 20.5 (apparent d, $^{rot}\Delta = 103$ Hz).[†]

[†] Signals affected by rotameric effects. $^{rot}\Delta$ indicates the observed separation between peaks.

Melting point: 40-42 °C.

IR (neat, cm^{-1}): 2968, 2932, 1707, 1668, 1593, 1495, 1456, 1425, 1366, 1317, 1258, 1246, 1198, 1159, 1136, 1097, 1069, 1042, 1020, 982, 964, 914, 893, 874.

N,N-diethyl-*O*-(2-methylphenyl)carbamate – **168d**
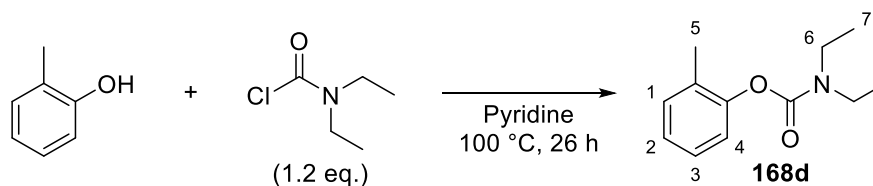
To a round-bottom flask equipped with a magnetic stirrer bar were added 2-methylphenol (369 mg, 3.41 mmol), *N,N*-diethylcarbamoyl chloride (0.520 mL, 4.10 mmol) and pyridine (3.30 mL). The resulting mixture was stirred and heated to 100 °C for 16 h. After reaction completion (assessed by TLC analysis of the reaction mixture), the mixture was treated with Et$_2$O (20 mL), sequentially washed with 1.0 M HCl (2 × 5 mL), 1.0 M NaOH (2 × 5 mL), water (5 mL) and brine (5 mL). The organic layer was then dried over Na$_2$SO$_4$, filtered and evaporated under reduced pressure. The residue thus obtained was purified by column chromatography with gradient elution with mixtures of petroleum ether and Et$_2$O (0-5% Et$_2$O) as eluent to afford *N,N*-diethyl-*O*-(2-methylphenyl)carbamate (**168d**) as a colourless viscous oil (471 mg, **69% yield**).

Analytical data for **168d** is consistent with previously reported data:[239]

^{1}H NMR (400 MHz, CDCl$_3$): δ 7.25-7.18 (m, 2H, H^1/H^3), 7.12 (t, $^3J_{HH}$ = 7.3 Hz, 1H, H^2), 7.09 (d, $^3J_{HH}$ = 7.3 Hz, 1H, H^4), 3.55-3.37 (br m, 4H, H^6), 2.25 (s, 3H, H^5), 1.37-1.20 (br m, 6H, H^7).

^{13}C NMR (101 MHz, CDCl$_3$): δ 153.5, 149.6, 130.4, 130.0, 126.3, 124.8, 121.7, 41.6 (apparent d, $^{rot}\Delta$ = 35 Hz),† 15.8, 13.4 (apparent d, $^{rot}\Delta$ = 85 Hz).†

† Signals affected by rotameric effects. $^{rot}\Delta$ indicates the observed separation between peaks.

IR (neat, cm^{-1}): 2978, 1709, 1491, 1472, 1456, 1412, 1379, 1366, 1350, 1317, 1271, 1219, 1179, 1111, 1096, 1084, 1043, 959, 937, 829.

HRMS (positive ESI): m/z calculated for [M+H]$^+$ C$_{12}$H$_{18}$NO$_2^+$: 208.1332; found: 208.1333.

4-Bromophenyl morpholine-4-carboxylate – **168e**
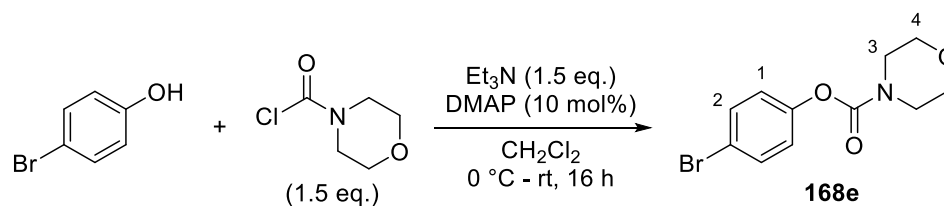
To a flame-dried round-bottom flask equipped with a magnetic stirrer bar were added 4-bromophenol (585 mg, 3.38 mmol), dry CH_2Cl_2 (33.0 mL), and 4-morpholinecarbonyl chloride (0.580 mL, 4.97 mmol). The resulting mixture was stirred and cooled to 0 °C in an ice-water bath. Then, triethylamine (0.690 mL, 4.16 mmol) and DMAP (42.0 mg, 0.344 mmol) were added and the mixture was allowed to react and warm to room temperature for 16 h. After reaction completion (assessed by TLC analysis of the reaction mixture), the mixture transferred to a separating funnel, sequentially washed with 1.0 M HCl (3 × 15 mL), water (25 mL) and brine (25 mL). The organic layer was then dried over Na_2SO_4, filtered and evaporated under reduced pressure. The residue was purified by column chromatography with gradient elution employing mixtures of petroleum ether and Et_2O (0-50% Et_2O) as eluent to afford 4-bromophenyl morpholine-4-carboxylate (**168e**) as a white solid (826 mg, **87% yield**).

^{1}H NMR (400 MHz, DMSO-d_6): δ 7.58 (d, $^3J_{HH}$ = 8.7 Hz, 2H, H^2), 7.14 (d, $^3J_{HH}$ = 8.5 Hz, 2H, H^1), 3.68-3.38 (br m, 8H, H^3/H^4).

^{13}C NMR (101 MHz, DMSO-d_6): δ 152.6, 150.4, 132.1, 124.2, 117.4, 65.7, 44.2 (apparent d, $^{rot}\Delta$ = 73 Hz).[†]

[†] Signals affected by rotameric effects. $^{rot}\Delta$ indicates the observed separation between peaks.

Melting point: 96-98 °C.

IR (neat, cm^{-1}): 2961, 2855, 1717, 1678, 1481, 1412, 1362, 1279, 1240, 1217, 1192, 1163, 1097, 1059, 1022, 1003, 988, 959, 932, 910, 866, 853, 833, 814.

HRMS (positive ESI): m/z calculated for [M+H]$^+$ $C_{11}H_{13}{}^{79}BrNO_3{}^+$: 286.0073; found: 286.0073; calculated for [M+H]$^+$ $C_{11}H_{13}{}^{81}BrNO_3{}^+$: 288.0053; found: 288.0070.

2-(Methoxycarbonyl)phenyl morpholine-4-carboxylate – **168f**
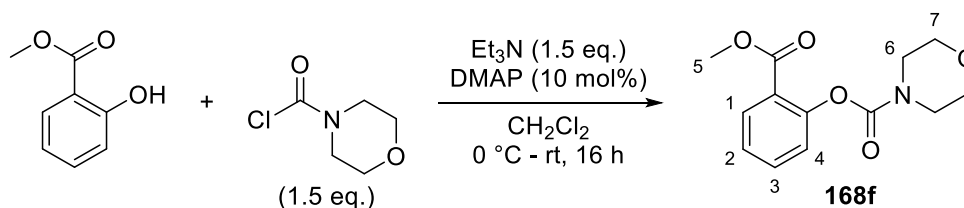
To a flame-dried round-bottom flask equipped with a magnetic stirrer bar were added methyl salicylate (0.400 mL, 3.09 mmol), dry dichloromethane (30 mL), and 4-morpholinecarbonyl chloride (0.540 mL, 4.63 mmol). The resulting mixture was stirred and cooled to 0 °C in an ice-water bath. Then, triethylamine (0.650 mL, 4.66 mmol) and DMAP (40.2 mg, 0.329 mmol) were added and the mixture was allowed to react and warm to room temperature for 16 h. After reaction completion (assessed by TLC analysis of the reaction mixture), the mixture was evaporated under reduced pressure, suspended in Et_2O (30 mL), filtered, the solid were washed with Et_2O (5 mL) and the filtrate was evaporated under reduced pressure. The residue thus obtained was purified by column chromatography with gradient elution employing mixtures of petroleum ether and Et_2O (0-75% Et_2O) as eluent to afford 2-(methoxycarbonyl)phenyl morpholine-4-carboxylate (**168f**) as a white solid (813 mg, **98% yield**).

^{1}H NMR (400 MHz, CDCl$_3$): δ 8.01 (dt, $^3J_{HH}$ = 7.8 Hz, $^4J_{HH}$ = 1.3 Hz, 1H, H^1), 7.56 (dt, $^3J_{HH}$ = 7.8 Hz, $^4J_{HH}$ = 1.4 Hz, 1H, H^3), 7.26 (t, $^3J_{HH}$ = 8.1 Hz, 1H, H^2), 7.19 (dt, $^3J_{HH}$ = 8.0 Hz, $^4J_{HH}$ = 1.1 Hz, 1H, H^4), 3.89 (br s, 3H, H^5), 3.84-3.56 (br m, 8H, H^6/H^7).

^{13}C NMR (101 MHz, CDCl$_3$): δ 164.5, 153.1, 150.6, 133.1, 131.1, 125.1, 123.6, 123.1, 66.1, 51.6, 44.2 (apparent d, $^{rot}\Delta$ = 85 Hz).†

† Signals affected by rotameric effects. $^{rot}\Delta$ indicates the observed separation between peaks.

Melting point: 83-85 °C.

IR (neat, cm^{-1}): 2970, 2862, 1705, 1670, 1645, 1605, 1489, 1542, 1420, 1373, 1362, 1278, 1261, 1242, 1207, 1161, 1126, 1113, 1092, 1063, 1020, 993, 955, 930, 907, 858, 833, 806.

HRMS (positive ESI): m/z calculated for $[M+H]^+$ $C_{13}H_{16}NO_5^+$: 266.1023; found: 266.1021.

Phenyl morpholine-4-carboxylate – **168g**
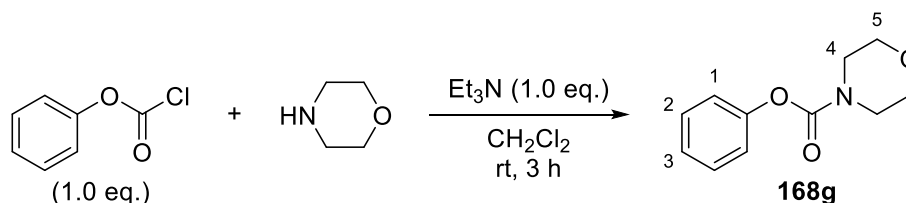
To a flame-dried round-bottom flask equipped with a magnetic stirrer bar were added morpholine (0.260 mL, 2.97 mmol), triethylamine (0.420 mL, 3.01 mmol) and anhydrous dichloromethane (30 mL), and the mixture was stirred and cooled to 0 °C in an ice-water bath. Then, phenyl chloroformate (0.380 mL, 3.03 mmol) was added dropwise at that temperature under constant, vigorous stirring for 3 h. After reaction completion (assessed by TLC analysis of the reaction mixture), the mixture was then transferred to a separating funnel, sequentially washed with 10% HCl (2 × 10 mL), water (20 mL) and brine (10 mL). The organic layer was then dried over Na_2SO_4, filtered and evaporated under reduced pressure to afford a viscous oil that solidified upon standing. The solid thus obtained was washed with petroleum ether and filtered to afford phenyl morpholine-4-carboxylate (**168g**) as a white solid (397 mg, **64% yield**).

Analytical data for **168c** is consistent with previously reported data:[240-242]

^{1}H NMR (400 MHz, CDCl$_3$): δ 7.39 (ddt, $^3J_{HH}$ = 8.5 Hz, $^3J_{HH}$ = 7.6 Hz, $^4J_{HH}$ = 2.0 Hz, 2H, H^2), 7.23 (dt, $^3J_{HH}$ = 7.6 Hz, $^4J_{HH}$ = 1.3 Hz, 1H, H^3), 7.15-7.11 (m, 2H, H^1), 3.80-3.54 (br m, 8H, H^4/H^5).

^{13}C NMR (101 MHz, CDCl$_3$): δ 153.2, 150.8, 128.8, 124.9, 121.2, 66.1, 44.0 (apparent d, $^{rot}\Delta$ = 75 Hz).[†]

[†] Signals affected by rotameric effects. $^{rot}\Delta$ indicates the observed separation between peaks.

Melting point: 46-48 °C.

IR (neat, cm^{-1}): 2978, 1709, 1591, 1491, 1449, 1418, 1368, 1302, 1275, 1240, 1223, 1204, 1163, 1152, 1119, 1067, 1049, 1020, 1001, 982, 955, 910, 845, 812.

4-methoxyphenyl morpholine-4-carboxylate – **168h**
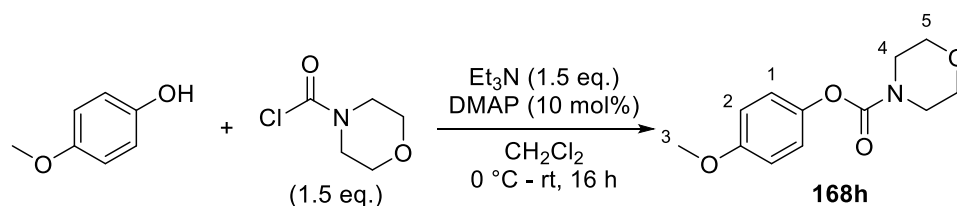
To a round-bottom flask equipped with a magnetic stirrer bar were added 4-methoxyphenol (413 mg, 3.33 mmol), dry dichloromethane (33.0 mL), and 4-morpholinecarbonyl chloride (0.580 mL, 4.97 mmol). The resulting mixture was stirred and cooled to 0 °C in an ice-water bath. Then, triethylamine (0.690 mL, 4.16 mmol) and DMAP (41.3 mg, 0.338 mmol) were added and the mixture was allowed to react and warm to room temperature for 16 h. After reaction completion (assessed by TLC analysis of the reaction mixture), the mixture was transferred to a separating funnel, sequentially washed with 1.0 M HCl (3 × 15 mL), water (25 mL) and brine (25 mL). The organic layer was then dried over Na_2SO_4, filtered and evaporated under reduced pressure. The residue was purified by column chromatography with gradient elution employing mixtures of petroleum ether and Et_2O (0-50% Et_2O) as eluent to afford 4-bromophenyl morpholine-4-carboxylate (**168h**) as a white solid (735 mg, **94% yield**).

^{1}H NMR (400 MHz, DMSO-d_6): δ 7.05 (d, $^3J_{HH}$ = 8.0 Hz, 2H, H^1), 6.93 (d, $^3J_{HH}$ = 8.3 Hz, 2H, H^2), 3.75 (s, 3H, H^3), 3.67-3.37 (br m, 8H, H^4/H^5).

^{13}C NMR (101 MHz, DMSO-d_6): δ 156.5, 153.4, 144.5, 122.7, 114.1, 65.8, 55.3, 44.1 (apparent d, $^{rot}\Delta$ = 69 Hz).[†]

[†] Signals affected by rotameric effects. $^{rot}\Delta$ indicates the observed separation between peaks.

Melting point: 68-70 °C.

IR (neat, cm^{-1}): 2970, 2916, 2891, 2857, 1709, 1672, 1609, 1595, 1504, 1452, 1416, 1634, 1302, 1275, 1236, 1219, 1065, 1022, 989, 858, 847, 831.

HRMS (positive ESI): m/z calculated for [M+H]$^+$ $C_{12}H_{16}NO_4^+$: 238.1074; found: 238.1070.

(*S*)-4-(2-((*tert*-butoxycarbonyl)amino)-3-methoxy-3-oxopropyl)phenyl morpholine-4-carboxylate – **169**
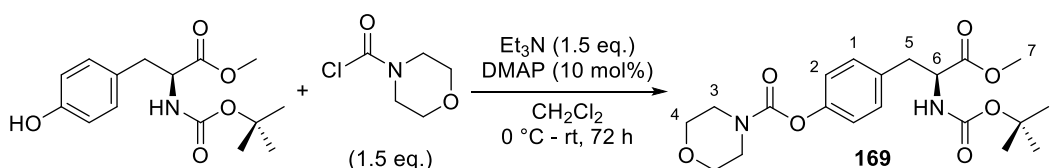
To a flame-dried round-bottom flask equipped with a magnetic stirrer bar were added *N-(tert*-butyloxycarbonyl)-(*L*)-tyrosine methyl ester (589 mg, 1.99 mmol), dry dichloromethane (20 mL) and 4-morpholinecarbonyl chloride (0.350 mL, 3.0 mmol). The resulting mixture was stirred and cooled to 0 °C in an ice-water bath. Then, triethylamine (0.420 mL, 3.01 mmol) and DMAP (25.1 mg, 0.205 mmol) were added and the mixture was allowed to react and warm to room temperature for 72 h. After reaction completion (assessed by TLC analysis of the reaction mixture), the mixture was evaporated under reduced pressure, suspended in Et$_2$O (20 mL), filtered, the solids were washed with Et$_2$O (2 × 5 mL) and the filtrate was evaporated under reduced pressure. The resulting mixture was re-dissolved in chloroform (50 mL), washed with 0.5 M NaOH (3 × 15 mL), the organic layer was dried over Na$_2$SO$_4$, filtered and evaporated under reduced pressure. The solid thus obtained was treated with petroleum ether (60 °C – 0 °C, 100 mL), the supernatant was removed and the remaining solids were purified by column chromatography with gradient elution employing mixtures of petroleum ether and Et$_2$O as eluent (0-75% Et$_2$O) to afford (*S*)-4-(2-((*tert*-butoxycarbonyl)amino)-3-methoxy-3-oxopropyl)phenyl morpholine-4-carboxylate (**169**) as a white solid (473 mg, **58% yield**).

^{1}H NMR (400 MHz, CDCl$_3$): δ 7.14 (d, $^3J_{HH}$ = 8.0 Hz, 2H, H^2), 7.06 (d, $^3J_{HH}$ = 8.0 Hz, 2H, H^1), 5.09-4.86 (m, 1H, NH), 4.66-4.49 (m, 1H, H^6), 3.81-3.54 (m, 11H, H^3/H^4/H^7), 3.18-2.96 (m, 2H, H^5), 1.44 (s, 9H, H^8).

^{13}C NMR (101 MHz, CDCl$_3$): δ 171.7, 154.6, 153.1, 149.8, 132.7, 129.7, 121.2, 79.5, 66.1, 53.9, 51.7, 44.0 (apparent d, $^{rot}\Delta$ = 74 Hz),† 37.1, 27.8.

† Signals affected by rotameric effects. $^{rot}\Delta$ indicates the observed separation between peaks.

Melting point: 121-123 °C.

IR (neat, cm^{-1}): 3350, 2978, 2970, 2947, 1726, 1686, 1520, 1450, 1423, 1391, 1366, 1321, 1296, 1269, 1254, 1236, 1171, 1159, 1111, 1057, 1047, 1020, 993, 951, 897, 854, 833, 808.

HRMS (positive ESI): m/z calculated for [M+NH$_4$]$^+$ C$_{20}$H$_{32}$N$_3$O$_7^+$: 426.2235; found: 426.2227.

6.9.3 Synthesis of *O*-methyl-*N*-aryl carbamate 177[242]
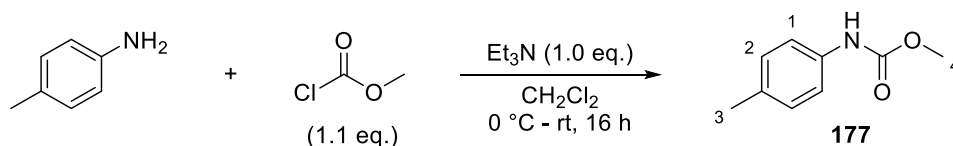
To a flame-dried round-bottom flask equipped with a magnetic stirrer bar were added *p*-toluidine (2.15 g, 20.1 mmol), triethylamine (2.80 mL, 20.1 mmol) and dry dichloromethane (50 mL). The resulting mixture was thoroughly stirred and cooled to 0 °C in an ice-water bath. Then, methyl chloroformate (1.70 mL, 22.0 mmol) was slowly added dropwise under constant, vigorous stirring at 0 °C and under an argon atmosphere. The reaction mixture was allowed to stir at 0 °C for a further 15 min and subsequently allowed to warm to room temperature. After 16 h of reaction, TLC analysis indicated complete consumption of the starting material and the mixture was then diluted with CH$_2$Cl$_2$ (100 mL), washed successively with 5% aqueous HCl (50 mL) and 5% aqueous NaOH (50 mL). The organics were collected, dried over Na$_2$SO$_4$, filtered and evaporated under reduced pressure. The residue thus obtained was suspended in EtOAc (100 mL), silica gel (*ca.* 5 g) was added and the resulting mixture was evaporated under reduced pressure. The resulting solid was loaded into a column and purified by column chromatography with gradient elution employing mixtures of petroleum ether and EtOAc (0 – 50% EtOAc) to afford a solid that was re-crystallised from hot petroleum ether (60 – 0 °C) to afford *O*-methyl-*N*-(4-methyl)phenyl carbamate **177** as a white crystalline solid (1.67 g, **50% yield**).

Analytical data for **177** is consistent with previously reported data:[244]

^{1}H NMR (400 MHz, CDCl$_3$): δ 7.27 (d, $^3J_{HH}$ = 8.2 Hz, 2H, H^1), 7.12 (d, $^3J_{HH}$ = 8.2 Hz, 2H, H^2), 6.57 (br s, 1H, NH), 3.78 (s, 3H, H^4), 2.31 (s, 3H, H^3).

^{13}C NMR (101 MHz, CDCl$_3$): δ 154.2, 135.2, 133.1, 129.6, 118.9, 52.3, 20.7.

Melting point: 96-98 °C.

IR (neat, cm^{-1}): 3323, 3032, 2957, 2916, 2857, 1701, 1638, 1597, 1531, 1512, 1435, 1402, 1350, 1314, 1298, 1229, 1209, 1190, 1165, 1111, 1096, 1067, 1018, 955, 939, 812, 775, 766, 752, 727, 706, 679, 635, 602.

6.9.4 Synthesis of deuterated carbamates for rate studies

d$_2$-O-tert-butyl-*N*-(4-methyl)phenyl carbamate (**166b-d$_2$**)

Following general procedure 1.5 for hydrogen isotope exchange (HIE) of carbamates, catalyst **150c** (15.8 mg, 10.1 μmol, 1.01 mol%) and *O-tert*-butyl-carbamate **166b** (208 mg, 1.00 mmol) were dissolved in MTBE (20.0 mL) and reacted in presence of an atmosphere of D$_2$ for 16 h at 50 °C. After the allocated reaction time, one of the stopcocks was open to the atmosphere to allow release of D$_2$, the mixture was allowed to cool to room temperature and filtered through a small plug of silica gel. The solids were washed with Et$_2$O (2 × 20 mL) and filtrate was evaporated under reduced pressure. The resulting solid was further purified by column chromatography with gradient elution employing mixtures of petroleum ether and Et$_2$O (0 – 10% Et$_2$O) as eluents to afford *d$_2$-O-tert*-butyl-*N*-(4-methyl)phenyl carbamate (**166b-d$_2$**) as a white solid (192 mg, **92% yield**). ^{1}H NMR spectroscopy evidenced a total incorporation of 85%D, and this compound was re-subjected to a deuteration procedure to improve the observed incorporation. Thus, catalyst **150c** (7.2 mg, 4.6 μmol, 0.5 mol%) and carbamate **166b-d$_2$** (188 mg, 0.90 mmol, **85%D**) were dissolved in MTBE (20 mL) and reacted as described above in the presence of an atmosphere of D$_2$ for 4 h at 50 °C. After the allocated reaction time, the system was treated as previously described to afford *d$_2$-O-tert*-butyl-*N*-(4-methyl)phenyl carbamate (**166b-d$_2$**) as a white solid. ^{1}H NMR data indicated a total incorporation of 96%D.

^{1}H NMR (400 MHz, DMSO-d_6): δ 9.19 (br s, 1H, NH), 7.31 (d, $^3J_{HH}$ = 8.8 Hz, 0.08H, residual H^1), 7.04 (s, 2H, H^2), 2.22 (s, 3H, H^3), 1.47 (s, 9H, H^4).

HRMS (positive ESI): m/z calculated for [M+Na]$^+$ C$_{12}$H$_{15}$D$_2$NO$_2$Na$^+$: 232.1277; found: 232.1278.

d$_2$-O-methyl-*N*-(4-methyl)phenyl carbamate (**177-*d$_2$***)

Following general procedure 1.5 for hydrogen isotope exchange (HIE) of carbamates, catalyst **150c** (3.9 mg, 2.5 μmol, 0.5 mol%) and *O*-methyl- carbamate **177** (85.0 mg, 515 μmol) were dissolved in MTBE (10 mL) and reacted in presence of an atmosphere of D$_2$ for 2 h at 50 °C. After the allocated reaction time, one of the stopcocks was open to the atmosphere to allow release of D$_2$, the mixture was allowed to cool to room temperature and filtered through a small plug of silica gel. The solids were washed with Et$_2$O (2 × 20 mL) and filtrate was evaporated under reduced pressure. The resulting solid was further purified by column chromatography with gradient elution employing mixtures of petroleum ether and EtOAc (0 – 50% EtOAc) as eluents to afford *d$_2$-O*-methyl-*N*-(4-methyl)phenyl carbamate (**177-*d$_2$***) as a white solid (81.4 mg, **96% yield**). ^{1}H NMR spectroscopy evidenced a total incorporation of 96%D.

^{1}H NMR (400 MHz, DMSO-*d$_6$*): δ 9.48 (br s, 1H, NH), 7.31 (d, $^3J_{HH}$ = 8.8 Hz, 0.06H, residual H^1), 7.06 (s, 2H, H^2), 3.63 (s, 3H, H^4), 2.22 (s, 3H, H^3).

6.10 HIE of carbamates

Results are reported in full details for each substrate, indicating the percent deuteration obtained for individual runs, and their corresponding average values. Estimation of the standard deviation associated with results reported herein is provided for experiments performed in triplicate. For substrates **167b**, **168f** and **169**, deuterium incorporation was also confirmed by HRMS.

6.10.1 Catalyst screening
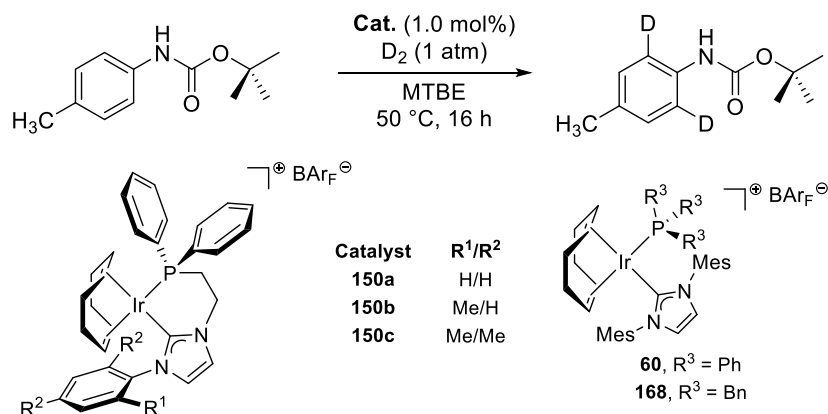
Following general procedure 6.6, the appropriate iridium catalyst and *O-tert*-butyl-*N*-(4-methylphenyl)carbamate (**167b**) were dissolved in MTBE (2.0 mL) and reacted under an atmosphere of D_2 at 50 °C for 16 h. After workup and evaporation of the volatiles, the deuterium incorporation was determined by ^{1}H NMR spectroscopy of isolated compounds. The results obtained along with relevant experimental data related to experiments performed in triplicate are summarized in Table E1.2.

Relevant ^{1}H NMR spectroscopic data for substrate **167b** in **CDCl3**:
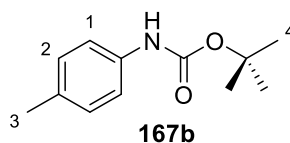
167b

Incorporation expected at: δ 7.26 (H[1]).

Incorporation determined against integral at: δ 7.11 (H[2]).

Table E1.2: Results for the catalyst screen in the HIE of substrate **167b**.[†]

Entry	Catalyst	m_{Ir} (mg)	n_{Ir} (µmol)	m_S (mg)	n_S (µmol)	%D (%)	%D$_{avg}$ (%)	s_D (%)
1		1.6	1.1	21.3	103	80		
2	**150a**	1.4	0.9	20.5	99	84	77	9
3		1.4	0.9	20.8	99	67		
4		1.5	1.0	21.1	102	93		
5	**150b**	1.5	1.0	21.1	102	93	92	2
6		1.4	0.9	21.4	103	90		
7		1.7	1.1	21.2	102	93		
8	**150c**	1.5	1.0	20.8	108	95	94	1
9		1.6	1.0	20.6	99	93		
10		1.7	1.0	20.9	101	15		
11	**60**	1.6	0.9	20.9	101	10	12	3
12		1.7	1.0	21.1	102	11		
13		1.7	1.0	20.6	99	10		
14	**168**	1.7	1.0	20.7	100	10	11	2
15		1.9	1.1	20.8	100	14		

[†]In Table E1.2, symbols represent: m_{Ir} – amount of catalyst, in mg; n_{Ir} – number of moles of catalyst, in µmol; m_S – amount of substrate, in mg; n_S – number of moles of substrate, in µmol; %D – percent deuterium incorporation, determined by ^{1}H NMR spectroscopy, calculated by Eq. 1; %D$_{avg}$ – average of three runs; s_D – estimated standard deviation.

6.10.2 Scope of *N*-aryl carbamates

O-tert-butyl-*N*-phenylcarbamate (**166a**)

Following general procedure 6.6, iridium catalyst **150c** and *O-tert*-butyl-*N*-phenylcarbamate (**166a**) were dissolved in MTBE (2.0 mL) and reacted under an atmosphere of D$_2$ at 50 °C for 4 h. After workup and evaporation of the volatiles, the deuterium incorporation was determined by ^{1}H NMR spectroscopy of isolated compounds. The results obtained along with relevant experimental data related to experiments performed in triplicate are summarized in Table E1.3.

Relevant ^{1}H NMR spectroscopic data for substrate **166a** in **DMSO-d_6:**
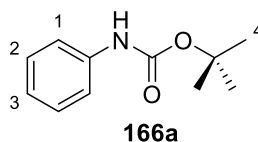
166a

^{1}H NMR data for 166a (400 MHz, DMSO-d_6): δ 9.30 (s, 1H, NH), 7.45 (d, $^3J_{HH}$ = 8.0 Hz, 2H, H^1), 7.24 (t, $^3J_{HH}$ = 8.0 Hz, 2H, H^2), 6.95 (tt, $^3J_{HH}$ = 7.4 Hz, $^4J_{HH}$ = 1.1 Hz, 1H, H^3), 1.48 (s, 9H, H^4).

Incorporation expected at: δ 7.45 (H^1)

Incorporation determined against integral at: δ 6.95 (H^3).

Table E1.3: Results for the HIE of substrate **166a**.[†]

Entry	m_{Ir} (mg)	n_{Ir} (μmol)	m_S (mg)	n_S (μmol)	%D (%)	%D$_{avg}$ (%)	s_D (%)
1	1.5	1.0	19.3	100	89		
2	1.6	1.0	19.2	99	91	90	1
3	1.5	1.0	19.4	100	90		

[†]In Table E1.3, symbols represent: m_{Ir} – amount of catalyst, in mg; n_{Ir} – number of moles of catalyst, in μmol; m_S – amount of substrate, in mg; n_S – number of moles of substrate, in μmol; %D – percent deuterium incorporation, determined by ^{1}H NMR spectroscopy, calculated by Eq. 1; %D$_{avg}$ – average of three runs; s_D – estimated standard deviation.

O-tert-butyl-*N*-(4-methylphenyl)carbamate – **166b**

Following general procedure 6.6, iridium catalyst **150c** and *O-tert*-butyl-*N*-(4-methylphenyl)carbamate (**166b**) were dissolved in MTBE (2.0 mL) and reacted under an atmosphere of D$_2$ at 50 °C for 4 h. After workup and evaporation of the volatiles, the deuterium incorporation was determined by ^{1}H NMR spectroscopy of isolated compounds. The results obtained along with relevant experimental data related to experiments performed in triplicate are summarized in Table E1.4.

Relevant ^{1}H NMR spectroscopic data for substrate **166b** in **DMSO-d_6:**

^{1}H NMR data for 166b (400 MHz, DMSO-d_6): δ 9.18 (s, 1H, NH), 7.34 (d, $^3J_{HH}$ = 8.4 Hz, 2H, H^1), 7.04 (d, $^3J_{HH}$ = 8.2 Hz, 2H, H^2), 2.22 (s, 3H, H^3), 1.47 (s, 9H, H^4).

Incorporation expected at: δ 7.34 (H^1)

Incorporation determined against integral at: δ 7.04 (H^2).

Table E1.4: Results for the HIE of substrate **166b**.[†]

| Entry	m_{Ir} (mg)	n_{Ir} (μmol)	m_S (mg)	n_S (μmol)	%D (%)	%D$_{avg}$ (%)	s_D (%)
1	1.6	1.0	21.2	102	98		
2	1.7	1.1	21	101	99	99	1
3	1.6	1.0	20.9	101	99		

[†]In Table E1.4, symbols represent: m_{Ir} – amount of catalyst, in mg; n_{Ir} – number of moles of catalyst, in μmol; m_S – amount of substrate, in mg; n_S – number of moles of substrate, in μmol; %D – percent deuterium incorporation, determined by ^{1}H NMR spectroscopy, calculated by Eq. 1; %D$_{avg}$ – average of three runs; s_D – estimated standard deviation.

O-tert-butyl-*N*-(4-*tert*-butylphenyl)carbamate (**166c**)

Following general procedure 6.6, iridium catalyst **150c** and *O-tert*-butyl-*N*-(4-*tert*-butylphenyl)carbamate (**166c**) were dissolved in MTBE (2.0 mL) and reacted under an atmosphere of D$_2$ at 50 °C for 4 h. After workup and evaporation of the volatiles, the deuterium incorporation was determined by ^{1}H NMR spectroscopy of isolated compounds. The results obtained along with relevant experimental data related to experiments performed in triplicate are summarized in Table E1.5.

Relevant ^{1}H NMR spectroscopic data for substrate **166c** in **DMSO-*d6*:**

166c

Incorporation expected at: δ 7.36 (H[1])

Incorporation determined against integral at: δ 7.25 (H[2]).

Table E1.5: Results for the HIE of substrate **166c**.[†]

Entry	m_{Ir} (mg)	n_{Ir} (μmol)	m_S (mg)	n_S (μmol)	%D (%)	%D$_{avg}$ (%)	s_D (%)
1	1.6	1.0	24.9	100	98		
2	1.6	1.0	24.9	100	98	98	1
3	1.6	1.0	24.8	99	97		

[†]In Table E1.5, symbols represent: m_{Ir} – amount of catalyst, in mg; n_{Ir} – number of moles of catalyst, in μmol; m_S – amount of substrate, in mg; n_S – number of moles of substrate, in μmol; %D – percent

deuterium incorporation, determined by ^{1}H NMR spectroscopy, calculated by Eq. 1; %D$_{avg}$ – average of three runs; s$_D$ – estimated standard deviation.

O-tert-butyl-*N*-(4-methoxyphenyl)carbamate – **166d**

Following general procedure 6.6, iridium catalyst **150c** and *O-tert*-butyl-*N*-(4-methoxyphenyl)carbamate (**166d**) were dissolved in MTBE (2.0 mL) and reacted under an atmosphere of D$_2$ at 50 °C for 4 h. After workup and evaporation of the volatiles, the deuterium incorporation was determined by ^{1}H NMR spectroscopy of isolated compounds. The results obtained along with relevant experimental data related to experiments performed in triplicate are summarized in Table E1.6.

Relevant ^{1}H NMR spectroscopic data for substrate **166d** in **DMSO-*d$_6$***:

166d

Incorporation expected at: δ 7.36 (H[1])

Incorporation determined against integral at: δ 6.83 (H[2]).

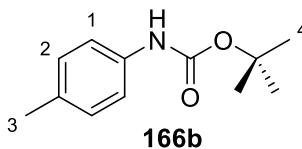**Table E1.6:** Results for the HIE of substrate **166d**.[†]

Entry	m$_{Ir}$ (mg)	n$_{Ir}$ (µmol)	m$_S$ (mg)	n$_S$ (µmol)	%D (%)	%D$_{avg}$ (%)	s$_D$ (%)
1	1.7	1.1	22.9	103	97		
2	1.7	1.1	22.2	99	96	96	1
3	1.6	1.0	22.3	100	96		

[†]In Table E1.6, symbols represent: m$_{Ir}$ – amount of catalyst, in mg; n$_{Ir}$ – number of moles of catalyst, in µmol; m$_S$ – amount of substrate, in mg; n$_S$ – number of moles of substrate, in µmol; %D – percent deuterium incorporation, determined by ^{1}H NMR spectroscopy, calculated by Eq. 1; %D$_{avg}$ – average of three runs; s$_D$ – estimated standard deviation.

O-tert-butyl-*N*-(4-fluorophenyl)carbamate – **166e**

Following general procedure 6.6, iridium catalyst **150c** and *O-tert*-butyl-*N*-(4-fluorophenyl)carbamate (**166e**) were dissolved in MTBE (2.0 mL) and reacted under

an atmosphere of D_2 at 50 °C for 4 h. After workup and evaporation of the volatiles, the deuterium incorporation was determined by ^{1}H NMR spectroscopy of isolated compounds. The results obtained along with relevant experimental data related to experiments performed in triplicate are summarized in Table E1.7.

Relevant ^{1}H NMR spectroscopic data for substrate **166e** in **DMSO-d_6:**

166e

Incorporation expected at: δ 7.45 (H[1])

Incorporation determined against integral at: δ 7.07 (H[2]).

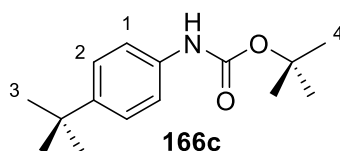**Table E1.7:** Results for the HIE of substrate **166e**.[†]

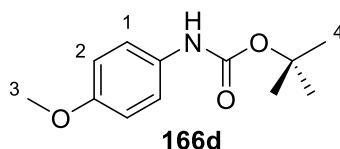| Entry	m_{Ir} (mg)	n_{Ir} (μmol)	m_S (mg)	n_S (μmol)	%D (%)	%D$_{avg}$ (%)	s_D (%)
1	1.6	1.0	21.4	1.6	91		
2	1.6	1.0	21.2	1.6	91	91	1
3	1.7	1.1	21.2	1.7	90		

[†]In Table E1.7, symbols represent: m_{Ir} – amount of catalyst, in mg; n_{Ir} – number of moles of catalyst, in μmol; m_S – amount of substrate, in mg; n_S – number of moles of substrate, in μmol; %D – percent deuterium incorporation, determined by ^{1}H NMR spectroscopy, calculated by Eq. 1; %D$_{avg}$ – average of three runs; s_D – estimated standard deviation.

O-tert-butyl-*N*-(4-chlorophenyl)carbamate – **166f**

Following general procedure 6.6, iridium catalyst **150c** and *O-tert*-butyl-*N*-(4-chlorophenyl)carbamate (**166f**) were dissolved in MTBE (2.0 mL) and reacted under an atmosphere of D_2 at 50 °C for 4 h. After workup and evaporation of the volatiles, the deuterium incorporation was determined by ^{1}H NMR spectroscopy of isolated compounds. The results obtained along with relevant experimental data related to experiments performed in triplicate are summarized in Table E1.8.

Relevant ^{1}H NMR spectroscopic data for substrate **166f** in **DMSO-d_6:**
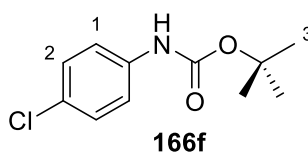
166f

^{1}H NMR data for 166f (400 MHz, DMSO-d_6): δ 9.48 (s, 1H, NH), 7.48 (d, $^3J_{HH}$ = 8.9 Hz, 2H, H^1), 7.29 (d, $^3J_{HH}$ = 9.0 Hz, 2H, H^2), 1.47 (s, 9H, H^3).

Incorporation expected at: δ 7.48 (H^1)

Incorporation determined against integral at: δ 7.29 (H^2).

Table E1.8: Results for the HIE of substrate **166f**.[†]

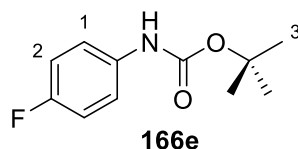| Entry	m_{Ir} (mg)	n_{Ir} (μmol)	m_S (mg)	n_S (μmol)	%D (%)	%D$_{avg}$ (%)	s_D (%)
1	1.6	1.0	22.9	101	80		
2	1.5	1.0	22.6	99	74	76	3
3	1.6	1.0	23.2	102	74		

[†]In Table E1.8, symbols represent: m_{Ir} – amount of catalyst, in mg; n_{Ir} – number of moles of catalyst, in μmol; m_S – amount of substrate, in mg; n_S – number of moles of substrate, in μmol; %D – percent deuterium incorporation, determined by ^{1}H NMR spectroscopy, calculated by Eq. 1; %D$_{avg}$ – average of three runs; s_D – estimated standard deviation.

O-tert-butyl-*N*-(4-bromophenyl)carbamate – **166g**

Following general procedure 6.6, iridium catalyst **150c** and *O-tert*-butyl-*N*-(4-bromophenyl)carbamate (**166g**) were dissolved in MTBE (2.0 mL) and reacted under an atmosphere of D$_2$ at 50 °C for 4 h. After workup and evaporation of the volatiles, the deuterium incorporation was determined by ^{1}H NMR spectroscopy of isolated compounds. The results obtained along with relevant experimental data related to experiments performed in triplicate are summarized in Table E1.9.

Relevant ^{1}H NMR spectroscopic data for substrate **166g** in **DMSO-d_6:**
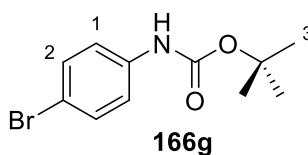
166g

Incorporation expected at: δ 7.42 (H^1)

Incorporation determined against integral at: δ 1.48 (H^3).

Table E1.9: Results for the HIE of substrate **166g**.[†]

Entry	m_{Ir} (mg)	n_{Ir} (µmol)	m_S (mg)	n_S (µmol)	%D (%)	%D$_{avg}$ (%)	s_D (%)
1	1.5	1.0	27.1	100	52		
2	1.6	1.0	27.4	101	58	54	3
3	1.6	1.0	27.1	100	52		

[†]In Table E1.9, symbols represent: m_{Ir} – amount of catalyst, in mg; n_{Ir} – number of moles of catalyst, in µmol; m_S – amount of substrate, in mg; n_S – number of moles of substrate, in µmol; %D – percent deuterium incorporation, determined by ^{1}H NMR spectroscopy, calculated by Eq. 1; %D$_{avg}$ – average of three runs; s_D – estimated standard deviation.

O-tert-butyl-*N*-(4-trifluoromethylphenyl)carbamate – **166h**

Following general procedure 6.6, iridium catalyst **150c** and *O-tert*-butyl-*N*-(4-trifluoromethylphenyl)carbamate (**166h**) were dissolved in MTBE (2.0 mL) and reacted under an atmosphere of D$_2$ at 50 °C for 4 h. After workup and evaporation of the volatiles, the deuterium incorporation was determined by ^{1}H NMR spectroscopy of isolated compounds. The results obtained along with relevant experimental data related to experiments performed in triplicate are summarized in Table E1.10.

Relevant ^{1}H NMR spectroscopic data for substrate **166h** in **DMSO-*d$_6$***:
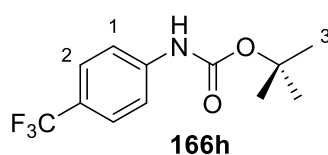
166h

Incorporation expected at: δ 7.66 (H^1)

Incorporation determined against integral at: δ 7.60 (H^2).

Table E1.10: Results for the HIE of substrate **166h**.[†]

Entry	m_{Ir} (mg)	n_{Ir} (µmol)	m_S (mg)	n_S (µmol)	%D (%)	%D$_{avg}$ (%)	s_D (%)
1	1.6	1.0	25.8	99	48		
2	1.7	1.1	26.1	100	41	45	4
3	1.6	1.0	26.6	102	47		

[†]In Table E1.10, symbols represent: m_{Ir} – amount of catalyst, in mg; n_{Ir} – number of moles of catalyst, in µmol; m_S – amount of substrate, in mg; n_S – number of moles of substrate, in µmol; %D – percent deuterium incorporation, determined by ^{1}H NMR spectroscopy, calculated by Eq. 1; %D$_{avg}$ – average of three runs; s_D – estimated standard deviation.

O-tert-butyl-*N*-(2-methylphenyl)carbamate – **166i**

Following general procedure 6.6, iridium catalyst **150c** and *O-tert*-butyl-*N*-(2-methylphenyl)carbamate (**166i**) were dissolved in MTBE (2.0 mL) and reacted under an atmosphere of D$_2$ at 50 °C for 4 h. After workup and evaporation of the volatiles, the deuterium incorporation was determined by ^{1}H NMR spectroscopy of isolated compounds. The results obtained along with relevant experimental data related to experiments performed in triplicate are summarized in Table E1.11.

Relevant ^{1}H NMR spectroscopic data for substrate **166i** in **DMSO-*d6***:
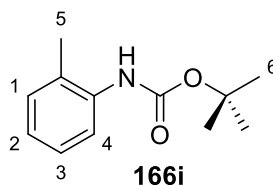
166i

^{1}H NMR data for 166i (400 MHz, DMSO-*d6*): δ 8.48 (s, 1H, NH), 7.32 (d, $^3J_{HH}$ = 7.8 Hz, 1H, H^5), 7.15 (t, $^3J_{HH}$ = 8.2 Hz, 1H, H^4), 7.12 (d, $^3J_{HH}$ = 7.7 Hz, 1H, H^2), 7.03 (t, $^3J_{HH}$ = 7.4 Hz, 1H, H^3), 2.19 (s, 3H, H^3), 1.46 (s, 9H, H^4).

Incorporation expected at: δ 7.32 (H^4)

Incorporation determined against integral at: δ 7.03 (H^3).

Table E1.11: Results for the HIE of substrate **166i**.[†]

Entry	m_{Ir} (mg)	n_{Ir} (µmol)	m_S (mg)	n_S (µmol)	%D (%)	%D$_{avg}$ (%)	s_D (%)
1	1.5	1.0	21.1	102	98		
2	1.5	1.0	21	101	98	98	1
3	1.6	1.0	21.5	104	97		

[†]In Table E1.11, symbols represent: m_{Ir} – amount of catalyst, in mg; n_{Ir} – number of moles of catalyst, in µmol; m_S – amount of substrate, in mg; n_S – number of moles of substrate, in µmol; %D – percent deuterium incorporation, determined by ^{1}H NMR spectroscopy, calculated by Eq. 1; %D$_{avg}$ – average of three runs; s_D – estimated standard deviation.

O-tert-butyl-*N*-(2-fluorophenyl)carbamate – **166j**

Following general procedure 6.6, iridium catalyst **150c** and *O-tert*-butyl-*N*-(2-fluorophenyl)carbamate (**166j**) were dissolved in MTBE (2.0 mL) and reacted under an atmosphere of D$_2$ at 50 °C for 4 h. After workup and evaporation of the volatiles, the deuterium incorporation was determined by ^{1}H NMR spectroscopy of isolated compounds. The results obtained along with relevant experimental data related to experiments performed in triplicate are summarised in Table E1.12.

Relevant ^{1}H NMR spectroscopic data for substrate **166j** in **DMSO-*d₆*:**

166j

^{1}H NMR data for 166j (400 MHz, DMSO-*d₆*): δ 8.90 (s, 1H, NH), 7.60 (dd, $^3J_{HH} = {}^4J_{HF} = 8.5$ Hz, 1H, H^4), 7.23-7.16 (m, 1H, H^3), 7.14-7.05 (m, 2H, H^1/H^2), 1.45 (s, 9H, H^5).

Incorporation expected at: δ 7.60 (H^4)

Incorporation determined against integral at: δ 7.23-7.16 (H^3).

Table E1.12: Results for the HIE of substrate **166j**.[†]

Entry	m_{Ir} (mg)	n_{Ir} (μmol)	m_S (mg)	n_S (μmol)	%D (%)	%D_{avg} (%)	s_D (%)
1	1.7	1.1	21.5	102	94		
2	1.6	1.0	21.7	103	84	91	6
3	1.6	1.0	21.1	100	94		

[†]In Table E1.12, symbols represent: m_{Ir} – amount of catalyst, in mg; n_{Ir} – number of moles of catalyst, in μmol; m_S – amount of substrate, in mg; n_S – number of moles of substrate, in μmol; %D – percent deuterium incorporation, determined by ^{1}H NMR spectroscopy, calculated by Eq. 1; %D_{avg} – average of three runs; s_D – estimated standard deviation.

O-tert-butyl-*N*-(2-(trifluoromethyl)phenyl)carbamate – **166k**

Following general procedure 6.6, iridium catalyst **150c** and *O-tert*-butyl-*N*-(2-(trifluoromethyl)phenyl)carbamate (**166k**) were dissolved in MTBE (2.0 mL) and reacted under an atmosphere of D_2 at 50 °C for 4 h. After workup and evaporation of the volatiles, the deuterium incorporation was determined by ^{1}H NMR spectroscopy of isolated compounds. The results obtained along with relevant experimental data related to experiments performed in triplicate are summarized in Table E1.13.

Relevant ^{1}H NMR spectroscopic data for substrate **166k** in **DMSO-*d₆*:**
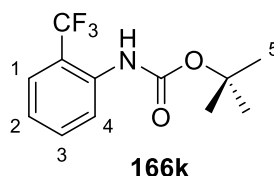
166k

Incorporation expected at: δ 7.46 (H^4)

Incorporation determined against integral at: δ 7.40 (H^2).

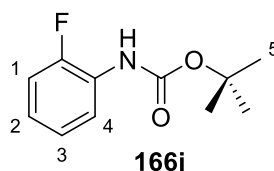**Table E1.13:** Results for the HIE of substrate **166k**.[†]

Entry	m_{Ir} (mg)	n_{Ir} (μmol)	m_S (mg)	n_S (μmol)	%D (%)	%D_{avg} (%)	s_D (%)
1	1.7	1.1	26.6	102	88		
2	1.7	1.1	26.2	100	86	87	1
3	1.6	1.0	26.9	103	86		

[†]In Table E1.13, symbols represent: m_{Ir} – amount of catalyst, in mg; n_{Ir} – number of moles of catalyst, in μmol; m_S – amount of substrate, in mg; n_S – number of moles of substrate, in μmol; %D – percent

O-tert-butyl-*N*-(3,5-dimethylphenyl)carbamate – **166l**

Following general procedure 6.6, iridium catalyst **150c** and *O-tert*-butyl-*N*-(3,5-dimethylphenyl)carbamate (**166l**) were dissolved in MTBE (2.0 mL) and reacted under an atmosphere of D$_2$ at 50 °C for 4 h. After workup and evaporation of the volatiles, the deuterium incorporation was determined by ^{1}H NMR spectroscopy of isolated compounds. The results obtained along with relevant experimental data related to experiments performed in triplicate are summarized in Table E1.14.

Relevant ^{1}H NMR spectroscopic data for substrate **166l** in **DMSO-*d$_6$*:**
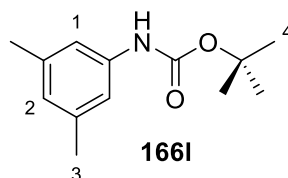
166l

Incorporation expected at: δ 7.07 (H^1)

Incorporation determined against integral at: δ 6.58 (H^2).

Table E1.14: Results for the HIE of substrate **166l**.[†]

Entry	m$_{Ir}$ (mg)	n$_{Ir}$ (μmol)	m$_S$ (mg)	n$_S$ (μmol)	%D (%)	%D$_{avg}$ (%)	s$_D$ (%)
1	1.5	1.0	22.1	100	82		
2	1.6	1.0	21.8	99	76	80	4
3	1.6	1.0	22.1	100	83		

[†]In Table E1.14, symbols represent: m$_{Ir}$ – amount of catalyst, in mg; n$_{Ir}$ – number of moles of catalyst, in μmol; m$_S$ – amount of substrate, in mg; n$_S$ – number of moles of substrate, in μmol; %D – percent deuterium incorporation, determined by ^{1}H NMR spectroscopy, calculated by Eq. 1; %D$_{avg}$ – average of three runs; s$_D$ – estimated standard deviation.

O-tert-butyl-*N*-(3-methoxyphenyl)carbamate – **166m**

Following general procedure 6.6, iridium catalyst **150c** and *O-tert*-butyl-*N*-(3-methoxyphenyl)carbamate (**166m**) were dissolved in MTBE (2.0 mL) and reacted

under an atmosphere of D_2 at 50 °C for 4 h. After workup and evaporation of the volatiles, the deuterium incorporation was determined by ^{1}H NMR spectroscopy of isolated compounds. The results obtained along with relevant experimental data related to experiments performed in triplicate are summarized in Table E1.15.

Relevant ^{1}H NMR spectroscopic data for substrate **166m** in **DMSO-d_6:**
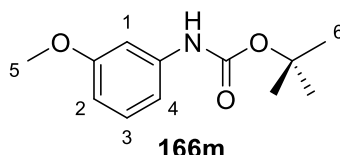
166m

Incorporation expected at: δ 7.14 (H^1) and 7.00 (H^4).

Incorporation determined against integral at: δ 6.53 (H^2).

Table E1.15: Results for the HIE of substrate **166m**.[†]

Entry	m_{Ir} (mg)	n_{Ir} (μmol)	m_S (mg)	n_S (μmol)
1	1.6	1.0	22.6	101
2	1.6	1.0	22.9	103
3	1.5	1.0	22.7	102

| Entry	%D^1 (%)	%D^1_{avg} (%)	s^1_D (%)	%D^4 (%)	%D^4_{avg} (%)	s^4_D (%)
1	99			98		
2	98	98	1	98	98	1
3	98			98		

[†]In Table E1.15, symbols represent: m_{Ir} – amount of catalyst, in mg; n_{Ir} – number of moles of catalyst, in μmol; m_S – amount of substrate, in mg; n_S – number of moles of substrate, in μmol; %D^k – percent deuterium incorporation, determined by ^{1}H NMR spectroscopy, calculated by Eq. 1; %D^k_{avg} – average of three runs; s^k_D – estimated standard deviation; [k] – denotes labelling site.

O-tert-butyl-*N*-(3-fluorophenyl)carbamate – **166n**

Following general procedure 6.6, iridium catalyst **150c** and *O-tert*-butyl-*N*-(3-fluorophenyl)carbamate (**166n**) were dissolved in MTBE (2.0 mL) and reacted under an atmosphere of D_2 at 50 °C for 4 h. After workup and evaporation of the volatiles, the deuterium incorporation was determined by ^{1}H NMR spectroscopy of isolated compounds. The results obtained along with relevant experimental data related to experiments performed in triplicate are summarized in Table E1.16.

Relevant ^{1}H NMR spectroscopic data for substrate **166n** in **DMSO-d_6**:
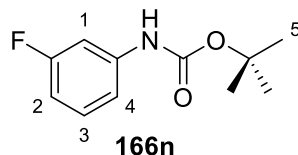
166n

Incorporation expected at: δ 7.38 (H^1) and 7.31-7.19 (H^4).

Incorporation determined against integral at: δ 6.77 (H^2).

Table E1.16: Results for the HIE of substrate **166n**.[†]

Entry	m_{Ir} (mg)	n_{Ir} (μmol)	m_S (mg)	n_S (μmol)
1	1.7	1.1	21.2	100
2	1.6	1.0	21.6	102
3	1.6	1.0	21.3	101

| Entry	%D^1 (%)	%D$^1_{avg}$ (%)	s^1_D (%)	%D^4 (%)	%D$^4_{avg}$ (%)	s^4_D (%)
1	76			79		
2	89	84	7	90	86	6
3	86			88		

[†]In Table E1.16, symbols represent: m_{Ir} – amount of catalyst, in mg; n_{Ir} – number of moles of catalyst, in μmol; m_S – amount of substrate, in mg; n_S – number of moles of substrate, in μmol; %D^k – percent deuterium incorporation, determined by ^{1}H NMR spectroscopy, calculated by Eq. 1; %D$^k_{avg}$ – average of three runs; s^k_D – estimated standard deviation; ^{k} – denotes labelling site.

O-tert-butyl-*N*-(3-fluorophenyl)carbamate – **166o**

Following general procedure 6.6, iridium catalyst **150c** and *O-tert*-butyl-*N*-(3-fluorophenyl)carbamate (**166o**) were dissolved in MTBE (2.0 mL) and reacted under an atmosphere of D$_2$ at 50 °C for 4 h. After workup and evaporation of the volatiles, the deuterium incorporation was determined by ^{1}H NMR spectroscopy of isolated compounds. The results obtained along with relevant experimental data related to experiments performed in triplicate are summarized in Table E1.17.

Relevant ^{1}H NMR spectroscopic data for substrate **166o** in **DMSO-d_6**:

1660
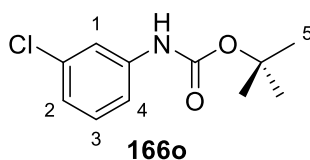
Incorporation expected at: δ 7.62 (H^1) and 7.36 (H^4).

Incorporation determined against integral at: δ 7.01 (H^2).

Table E1.17: Results for the HIE of substrate **1660**.[†]

Entry	m$_{Ir}$ (mg)	n$_{Ir}$ (µmol)	m$_S$ (mg)	n$_S$ (µmol)
1	1.7	1.1	22.6	99
2	1.6	1.0	22.7	100
3	1.7	1.1	22.8	100

Entry	%D^1 (%)	%D$^1_{avg}$ (%)	s^1_D (%)	%D^4 (%)	%D$^4_{avg}$ (%)	s^4_D (%)
1	44			39		
2	48	47	2	43	42	2
3	48			43		

[†]In Table E1.17, symbols represent: m$_{Ir}$ – amount of catalyst, in mg; n$_{Ir}$ – number of moles of catalyst, in µmol; m$_S$ – amount of substrate, in mg; n$_S$ – number of moles of substrate, in µmol; %D^k – percent deuterium incorporation, determined by ^{1}H NMR spectroscopy, calculated by Eq. 1; %D$^k_{avg}$ – average of three runs; s^k_D – estimated standard deviation; [k] – denotes labelling site.

6.10.3 Scope of *O*-aryl carbamates

N-tert-butyl-*O*-phenylcarbamate – **168a**

Following general procedure 6.6, iridium catalyst **150c** and *N-tert*-butyl-*O*-phenylcarbamate (**168a**) were dissolved in MTBE (2.0 mL) and reacted under an atmosphere of D$_2$ at 50 °C for 4 h. After workup and evaporation of the volatiles, the deuterium incorporation was determined by ^{1}H NMR spectroscopy of isolated compounds. The results obtained along with relevant experimental data related to experiments performed in triplicate are summarized in Table E1.18.

Relevant ^{1}H NMR spectroscopic data for substrate **168a** in **CDCl$_3$:**

168a

Incorporation expected at: δ 7.14 (H^1)

Incorporation determined against integral at: δ 7.37 (H^2).

Table E1.18: Results for the HIE of substrate **168a**.[†]

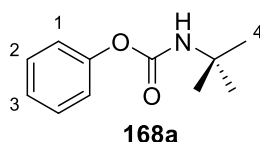| Entry	m_{Ir} (mg)	n_{Ir} (μmol)	m_S (mg)	n_S (μmol)	%D (%)	%D$_{avg}$ (%)	s_D (%)
1	1.6	1.0	19.2	99	92		
2	1.6	1.0	19.7	102	92	91	1
3	1.7	1.1	19.2	99	90		

[†]In Table E1.18, symbols represent: m_{Ir} – amount of catalyst, in mg; n_{Ir} – number of moles of catalyst, in μmol; m_S – amount of substrate, in mg; n_S – number of moles of substrate, in μmol; %D – percent deuterium incorporation, determined by ^{1}H NMR spectroscopy, calculated by Eq. 1; %D$_{avg}$ – average of three runs; s_D – estimated standard deviation.

Compound **168a** from the experiment summarised in entry 1 was recovered as a white solid (19.1 mg, **99%**).

N,N-diethyl-*O*-phenylcarbamate – **168b**

Following general procedure 6.6, iridium catalyst **150c** and *N,N*-diethyl-*O*-phenylcarbamate (**168b**) were dissolved in MTBE (2.0 mL) and reacted under an atmosphere of D$_2$ at 50 °C for 4 h. After workup and evaporation of the volatiles, the deuterium incorporation was determined by ^{1}H NMR spectroscopy of isolated compounds. The results obtained along with relevant experimental data related to experiments performed in triplicate are summarized in Table E1.19.

Relevant ^{1}H NMR spectroscopic data for substrate **168b** in **DMSO-*d6*:**

168b

^{1}H NMR data for 168b (400 MHz, DMSO-d_6): δ 7.37 (tt, $^3J_{HH}$ = 8.1 Hz, $^4J_{HH}$ = 2.1 Hz, 2H, H^2), 7.21 (tt, $^3J_{HH}$ = 7.4 Hz, $^4J_{HH}$ = 1.1 Hz, 1H, H^3), 7.13-7.09 (m, 2H, H^1), 3.35 (br d, $^{rot}\Delta$ = 36 Hz, 4H, H^4), 1.16 (br d, $^{rot}\Delta$ = 34 Hz, 6H, H^5).

Incorporation expected at: δ 7.13-7.09 (H^1)

Incorporation determined against integral at: δ 7.37 (H^2).

Table E1.19: Results for the HIE of substrate **168b**.[†]

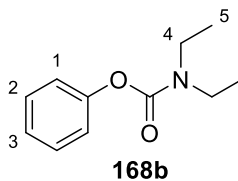| Entry	m$_{Ir}$ (mg)	n$_{Ir}$ (μmol)	m$_S$ (mg)	n$_S$ (μmol)	%D (%)	%D$_{avg}$ (%)	s$_D$ (%)
1	1.7	1.1	19.5	101	94		
2	1.5	1.0	19.6	101	95	94	1
3	1.7	1.1	19.6	101	94		

[†]In Table E1.19, symbols represent: m$_{Ir}$ – amount of catalyst, in mg; n$_{Ir}$ – number of moles of catalyst, in μmol; m$_S$ – amount of substrate, in mg; n$_S$ – number of moles of substrate, in μmol; %D – percent deuterium incorporation, determined by ^{1}H NMR spectroscopy, calculated by Eq. 1; %D$_{avg}$ – average of three runs; s$_D$ – estimated standard deviation.

Compound **168b** from the experiment summarised in entry 2 was recovered as a viscous oil (19.6 mg, **99%**).

N,N-di(*iso*-propyl)-*O*-phenylcarbamate – **168c**

Following general procedure 6.6, iridium catalyst **150c** and *N,N*-di(*iso*-propyl)-*O*-phenylcarbamate (**168c**) were dissolved in MTBE (2.0 mL) and reacted under an atmosphere of D$_2$ at 50 °C for 4 h. After workup and evaporation of the volatiles, the deuterium incorporation was determined by ^{1}H NMR spectroscopy of isolated compounds. The results obtained along with relevant experimental data related to experiments performed in triplicate are summarized in Table E1.20.

Relevant ^{1}H NMR spectroscopic data for substrate **168c** in **CDCl$_3$:**

168c

Incorporation expected at: δ 7.15-7.10 (H^1)

Incorporation determined against integral at: δ 7.36 (H^2).

Table E1.20: Results for the HIE of substrate **168c**.[†]

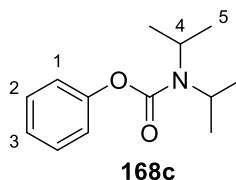| Entry	mIr (mg)	nIr (μmol)	mS (mg)	nS (μmol)	%D (%)	%Davg (%)	sD (%)
1.6	1.0	22.5	102	4	1.6		
1.5	1.0	22.0	99	18	1.5	8	8
1.6	1.0	22.2	100	3	1.6		

[†]In Table E1.20, symbols represent: m_{Ir} – amount of catalyst, in mg; n_{Ir} – number of moles of catalyst, in μmol; m_S – amount of substrate, in mg; n_S – number of moles of substrate, in μmol; %D – percent deuterium incorporation, determined by ^{1}H NMR spectroscopy, calculated by Eq. 1; %D$_{avg}$ – average of three runs; s_D – estimated standard deviation.

Compound **168c** from the experiment summarised in entry 1 was recovered as a white solid (22.3 mg, **99%**).

N,N-diethyl-*O*-(2-methylphenyl)carbamate – **168d**

Following general procedure 6.6, iridium catalyst **150c** and *N,N*-diethyl-*O*-(2-methylphenyl)carbamate (**168d**) were dissolved in MTBE (2.0 mL) and reacted under an atmosphere of D$_2$ at 50 °C for 4 h. After workup and evaporation of the volatiles, the deuterium incorporation was determined by ^{1}H NMR spectroscopy of isolated compounds. The results obtained along with relevant experimental data related to experiments performed in triplicate are summarized in Table E1.21.

Relevant ^{1}H NMR spectroscopic data for substrate **168d** in **CDCl$_3$**:

168d

Incorporation expected at: δ 7.09 (H^4)

Incorporation determined against integral at: δ 7.25-7.18 (H^1/H^3).

Table E1.21: Results for the HIE of substrate **168d**.[†]

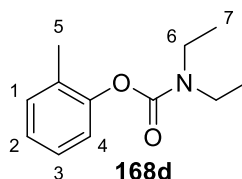| Entry	m_{Ir} (mg)	n_{Ir} (µmol)	m_S (mg)	n_S (µmol)	%D (%)	%D$_{avg}$ (%)	s_D (%)
1	1.6	1.0	21.2	102	96		
2	1.6	1.0	20.5	99	97	96	1
3	1.6	1.0	21.1	102	96		

[†]In Table E1.21, symbols represent: m_{Ir} – amount of catalyst, in mg; n_{Ir} – number of moles of catalyst, in µmol; m_S – amount of substrate, in mg; n_S – number of moles of substrate, in µmol; %D – percent deuterium incorporation, determined by ^{1}H NMR spectroscopy, calculated by Eq. 1; %D$_{avg}$ – average of three runs; s_D – estimated standard deviation.

Compound **168d** from the experiment summarised in entry 1 was recovered as a viscous oil (20.4 mg, **96%**).

4-Bromophenyl morpholine-4-carboxylate – **168e**

Following general procedure 6.6, iridium catalyst **150c** and 4-Bromophenyl morpholine-4-carboxylate (**168e**) were dissolved in MTBE (2.0 mL) and reacted under an atmosphere of D$_2$ at 50 °C for 4 h. After workup and evaporation of the volatiles, the deuterium incorporation was determined by ^{1}H NMR spectroscopy of isolated compounds. The results obtained along with relevant experimental data related to experiments performed in triplicate are summarized in Table E1.22.

Relevant ^{1}H NMR spectroscopic data for substrate **168e** in **DMSO-d_6:**

168e

Incorporation expected at: δ 7.14 (H^1)

Incorporation determined against integral at: δ 7.58 (H^2).

Table E1.22: Results for the HIE of substrate **168e**.[†]

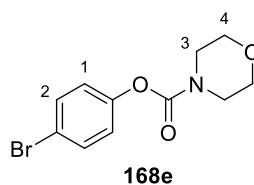| Entry	m_{Ir} (mg)	n_{Ir} (μmol)	m_S (mg)	n_S (μmol)	%D (%)	%D$_{avg}$ (%)	s_D (%)
1	1.6	1.0	29.0	101	79		
2	1.6	1.0	28.8	101	68	72	6
3	1.6	1.0	28.7	100	70		

[†]In Table E1.22, symbols represent: m_{Ir} – amount of catalyst, in mg; n_{Ir} – number of moles of catalyst, in μmol; m_S – amount of substrate, in mg; n_S – number of moles of substrate, in μmol; %D – percent deuterium incorporation, determined by ^{1}H NMR spectroscopy, calculated by Eq. 1; %D$_{avg}$ – average of three runs; s_D – estimated standard deviation.

Compound **168e** from the experiment summarised in entry 3 was recovered as a white solid (28.5 mg, **99%**).

2-(Methoxycarbonyl)phenyl morpholine-4-carboxylate – **168f**

Following general procedure 1.6, iridium catalyst **150c** and 2-(methoxycarbonyl)phenyl morpholine-4-carboxylate (**168f**) were dissolved in MTBE (2.0 mL) and reacted under an atmosphere of D$_2$ at 50 °C for 4 h. After workup and evaporation of the volatiles, the deuterium incorporation was determined by ^{1}H NMR spectroscopy of isolated compounds. The results obtained along with relevant experimental data related to experiments performed in triplicate are summarized in Table E1.23.

Relevant ^{1}H NMR spectroscopic data for substrate **168f** in **CDCl₃:**

Incorporation expected at: δ 8.01 (H^1) and 7.19 (H^4)

Incorporation determined against integral at: δ 7.56 (H^3).

HRMS (positive ESI): m/z calculated for [M+H]$^+$ C$_{13}$H$_{14}$D$_2$NO$_5^+$: 268.1149; found: 268.1147.

Table E1.23: Results for the HIE of substrate **168f**.[†]

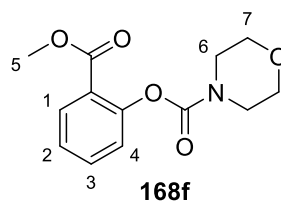| Entry	m_{Ir} (mg)	n_{Ir} (µmol)	m_S (mg)	n_S (µmol)		
1	1.5	1.0	26.5	100		
2	1.6	1.0	26.3	99		
3	1.5	1.0	26.5	100		
Entry	$\%D^1$ (%)	$\%D^1_{avg}$ (%)	s^1_D (%)	$\%D^4$ (%)	$\%D^4_{avg}$ (%)	s^4_D (%)
1	96			96		
2	96	96	1	96	96	1
3	96			96		

[†]In Table E1.23, symbols represent: m_{Ir} – amount of catalyst, in mg; n_{Ir} – number of moles of catalyst, in µmol; m_S – amount of substrate, in mg; n_S – number of moles of substrate, in µmol; $\%D^k$ – percent deuterium incorporation, determined by ^{1}H NMR spectroscopy, calculated by Eq. 1; $\%D^k_{avg}$ – average of three runs; s^k_D – estimated standard deviation; [k] – denotes labelling site.

Compound **168f** from the experiment summarised in entry 1 was recovered as a white solid (26.3 mg, **99%**).

Phenyl morpholine-4-carboxylate – **168g**

Following general procedure 6.6, iridium catalyst **150c** and phenyl morpholine-4-carboxylate (**168g**) were dissolved in MTBE (2.0 mL) and reacted under an atmosphere of D$_2$ at 50 °C for 4 h. After workup and evaporation of the volatiles, the deuterium incorporation was determined by ^{1}H NMR spectroscopy of isolated compounds. The results obtained along with relevant experimental data related to experiments performed in triplicate are summarized in Table E1.24.

Relevant ^{1}H NMR spectroscopic data for substrate **168g** in **DMSO-d_6:**
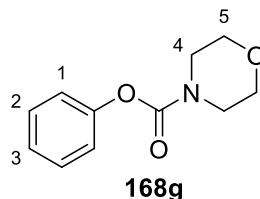
168g

^{1}H NMR data for 168g (400 MHz, DMSO-d_6): δ 7.38 (dt, $^3J_{HH}$ = 8.1 Hz, $^4J_{HH}$ = 2.1 Hz, 2H, H^2), 7.23 (tt, $^3J_{HH}$ = 7.4 Hz, $^4J_{HH}$ = 1.1 Hz, 1H, H^3), 7.16-7.11 (m, 2H, H^1), 3.69-3.62 (br m, 4H, H^4), 3.60-3.38 (br m, 4H, H^5).

Incorporation expected at: δ 7.13 (H[1]) and 3.69-3.62 (H[4]).

Incorporation determined against integral at: δ 7.38 (H[2]).

Table E1.24: Results for the HIE of substrate **168g**.[†]

Entry	m_{Ir} (mg)	n_{Ir} (μmol)	m_S (mg)	n_S (μmol)
1	1.7	1.1	20.7	100
2	1.7	1.1	21.1	102
3	1.6	1.0	20.6	99

| Entry	$\%D^1$ (%)	$\%D^1_{avg}$ (%)	s^1_D (%)	$\%D^4$ (%)	$\%D^4_{avg}$ (%)	s^4_D (%)
1	95			34		
2	95	95	1	38	38	5
3	94			43		

[†]In Table E1.24, symbols represent: m_{Ir} – amount of catalyst, in mg; n_{Ir} – number of moles of catalyst, in μmol; m_S – amount of substrate, in mg; n_S – number of moles of substrate, in μmol; $\%D^k$ – percent deuterium incorporation, determined by ^{1}H NMR spectroscopy, calculated by Eq. 1; $\%D^k_{avg}$ – average of three runs; s^k_D – estimated standard deviation; [k] – denotes labelling site.

Compound **168g** from the experiment summarised in entry 1 was recovered as a white solid (18.8 mg, **91%**).

4-methoxyphenyl morpholine-4-carboxylate – **168h**

Following general procedure 6.6, iridium catalyst **150c** and 4-methoxyphenyl morpholine-4-carboxylate (**168h**) were dissolved in MTBE (2.0 mL) and reacted under an atmosphere of D_2 at 50 °C for 4 h. After workup and evaporation of the volatiles, the deuterium incorporation was determined by ^{1}H NMR spectroscopy of isolated compounds. The results obtained along with relevant experimental data related to experiments performed in triplicate are summarized in Table E1.25.

Relevant ^{1}H NMR spectroscopic data for substrate **168h** in **DMSO-d_6:**

168h

Incorporation expected at: δ 7.05 (H^1) and 3.67-3.37 (H^4)

Incorporation determined against integral at: δ 6.93 (H^2).

Table E1.25: Results for the HIE of substrate **168h**.[†]

Entry	m_{Ir} (mg)	n_{Ir} (µmol)	m_S (mg)	n_S (µmol)		
1	1.7	1.1	23.7	100		
2	1.6	1.0	23.6	99		
3	1.6	1.0	23.7	100		

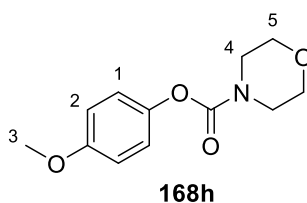| Entry	$\%D^1$ (%)	$\%D^1_{avg}$ (%)	s^1_D (%)	$\%D^4$ (%)	$\%D^4_{avg}$ (%)	s^4_D (%)
1	95			33		
2	95	95	1	38	35	3
3	94			33		

[†]In Table E1.25, symbols represent: m_{Ir} – amount of catalyst, in mg; n_{Ir} – number of moles of catalyst, in µmol; m_S – amount of substrate, in mg; n_S – number of moles of substrate, in µmol; $\%D^k$ – percent deuterium incorporation, determined by ^{1}H NMR spectroscopy, calculated by Eq. 1; $\%D^k_{avg}$ – average of three runs; s^k_D – estimated standard deviation; [k] – denotes labelling site.

Compound **168h** from the experiment summarised in entry 3 was recovered as a white solid (23.3 mg, **98%**).

(*S*)-4-(2-((*tert*-butoxycarbonyl)amino)-3-methoxy-3-oxopropyl)phenyl morpholine-4-carboxylate (**169**)

Following general procedure 6.6, iridium catalyst **150c** and (*S*)-4-(2-((*tert*-butoxycarbonyl)amino)-3-methoxy-3-oxopropyl)phenyl morpholine-4-carboxylate (**169**) were dissolved in MTBE (1.0 mL) and reacted under an atmosphere of D_2 at 50 °C for 4 h. After workup and evaporation of the volatiles, the deuterium incorporation was determined by ^{1}H NMR spectroscopy of isolated compounds. The results obtained along with relevant experimental data related to experiments performed in triplicate are summarized in Table E1.26.

Relevant ^{1}H NMR spectroscopic data for substrate **169** in **CDCl$_3$**:

169

Incorporation expected at: δ 7.06 (H^2)

Incorporation determined against integral at: δ 7.14 (H^1).

HRMS (positive ESI): m/z calculated for [M+NH$_4$]$^+$ C$_{20}$H$_{26}$D$_2$N$_3$O$_7$$^+$: 428.2360; found: 428.2358.

Table E1.26: Results for the HIE of substrate **169**.†

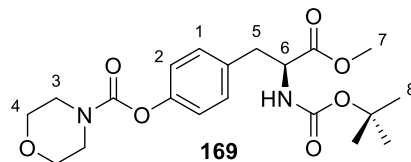| Entry	m$_{Ir}$ (mg)	n$_{Ir}$ (μmol)	m$_S$ (mg)	n$_S$ (μmol)	%D (%)	%D$_{avg}$ (%)	s$_D$ (%)
1	4.0	2.6	20.4	50	97	97	ND
2	3.9	2.5	20.8	51	97		

†In Table E1.26, symbols represent: m$_{Ir}$ – amount of catalyst, in mg; n$_{Ir}$ – number of moles of catalyst, in μmol; m$_S$ – amount of substrate, in mg; n$_S$ – number of moles of substrate, in μmol; %D – percent deuterium incorporation, determined by ^{1}H NMR spectroscopy, calculated by Eq. 1; %D$_{avg}$ – average of three runs; s$_D$ – estimated standard deviation.

Compound **169** from the experiment summarised in entry 2 was recovered as a white solid (19.6 mg, **94%**).

6.10.4 Synthesis of **166b-*d$_2$*** for further hydrolysis

Following general procedure 1.5 for hydrogen isotope exchange (HIE) of carbamates, catalyst **150c** (7.7 mg, 4.9 μmol, 1.0 mol%) and *O-tert*-butyl-carbamate **166b** (103.9 mg, 0.50 mmol) were dissolved in MTBE (10 mL) and reacted in presence of an atmosphere of D$_2$ for 4 h at 50 °C. After the allocated reaction time, one of the stopcocks was open to the atmosphere to allow release of D$_2$, the mixture was allowed to cool to room temperature and the volatiles were evaporated under reduced pressure. The residue thus obtained was purified by column chromatography

with gradient elution, employing mixtures of Et$_2$O and petroleum ether as solvents (0 – 10% Et$_2$O) to afford d_2-O-$tert$-butyl-N-(4-methyl)phenyl carbamate (**166b-d_2**) as a white solid (102.7 mg, **98% yield**). ^{1}H NMR data indicated a total incorporation of 89%D.

^{1}H NMR (400 MHz, CDCl$_3$): δ 7.22 (d, $^3J_{HH}$ = 8.5 Hz, 0.21H, residual H^1), 7.09 (br s, 2H, H^2), 6.38 (br s, 1H, NH), 2.29 (s, 3H, H^3), 1.51 (s, 9H, H^4).

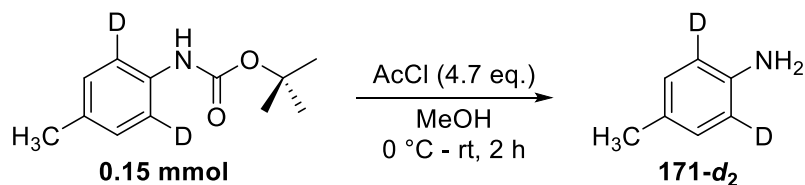**^{13}C NMR (101 MHz, CDCl$_3$):** δ 150.0, 135.7, 132.7, 129.5, 118.6 (t, $^1J_{CD}$ = 27 Hz), 80.5, 28.5, 20.9.

IR (neat, cm^{-1}): 3289, 3109, 3034, 2967, 2926, 2868, 1703, 1684, 1593, 1528, 1472, 1449, 1393, 1366, 1308, 1248, 1223, 1157, 1069, 1049, 1030, 907, 881, 860, 831, 775, 760, 710, 677, 638.

Synthesis of d_2-4-methylaniline **171-d_2** by hydrolysis of **166b-d_2**[245]

To a round-bottomed flask equipped with a magnetic stirrer bar was added methanol (0.5 mL) and the reaction vessel was cooled to 0 °C in an ice-water bath. Then, acetyl chloride (0.05 mL, 0.70 mmol) was slowly added at that temperature, under constant stirring, the reaction vessel was fitted with a glass stopper, and the resulting mixture was stirred for 15 min at 0 °C. Then, carbamate **166b-d_2** (31.0 mg, 0.15 mmol) was added at 0 °C in one portion, the reaction vessel was subsequently warmed to room temperature, and the reaction mixture was stirred at that temperature for 2 h. The mixture was then quenched by careful dropwise addition of saturated NaHCO$_3$ (2.0 mL) under constant, vigorous stirring. The resulting mixture was extracted with Et$_2$O (5 × 5 mL), the combined organic phases were washed with brine (2 mL), dried over Na$_2$SO$_4$, filtered and evaporated under reduced pressure at 0

°C to afford d_2-4-methylaniline (**171-d_2**) as a white solid (16.9 mg, **100% yield**). ^{1}H NMR data indicated a total incorporation of 90%D.

^{1}H NMR (400 MHz, CDCl$_3$): δ 6.98 (br s, 2H, H^2), 6.62 (d, $^3J_{HH}$ = 8.6 Hz, 0.18H, residual H^1), 3.25 (br s, 2H, NH$_2$), 2.25 (s, 3H, H^3).

^{13}C NMR (101 MHz, CDCl$_3$): δ 143.7, 129.8, 128.0, 115.2 (t, $^1J_{CD}$ = 24 Hz), 20.6.

6.11 Rate studies and determination of kinetic isotope effect (KIE)

6.11.1 Experimental results for rate measurement

Throughout sections 6.11.1.1 and 6.11.1.2, results concerning both the forward (C—H deuteration) and the reverse processes (C—D hydrogenation) in the HIE of carbamates of interest are reported. In all cases, the software OriginPro 2017 SR2 was employed to obtain a best linear fit for the rate data. An induction period of approximately 2 min was observed for this particular reaction, which was attributed to the time necessary for the reaction medium to equilibrate its internal temperature to a stage in which the rate limiting step for the process could be surpassed. Hence, the first point in each plot was discarded to ensure reproducibility across runs, and the linear regression for the remaining points was then calculated. The slope of the line thus obtained, and its corresponding error due to fitting, were considered to provide an estimation for the observed reaction rate. The determination of experimental KIE values for substrates **166b** at 50 °C, and **177** at both 30 and 50 °C is described in section 6.11.2.

6.11.1.1 Rate of reactions with *O-tert*-butyl-*N*-aryl carbamate **166b**

Rate measurement at 50 °C – forward process

Following general procedure 6.7 for rate measurement of HIE reactions, catalyst **150c** (4.0 mg, 2.6 µmol, 0.5 mol%) and *O-tert*-butyl-*N*-(4-methyl)phenyl carbamate **166b** (103.2 mg, 498 µmol) were added to the reaction vessel and dissolved in MTBE (20 mL). The resulting mixture was subjected to a rate measurement experiment *as per* the aforementioned general procedure employing D_2 as the reactive gas. Once the reaction vessel was fully immersed in an oil bath previously heated to 50 °C, a timer was started to measure progression of the reaction under study. The first 0.8 mL aliquot was taken after 2 min have elapsed, and the mixture thus collected was immediately transferred to a vial containing MeCN (2.0 mL). Four additional aliquots of 0.8 mL were collected at time intervals of 1 min, *i.e.*, after 3, 4, 5 and then 6 min of reaction, and were treated in an analogous manner to that stated for the first reaction sampling. Each aliquot was then treated as described in general procedure 5.7 and subsequently analysed by ^{1}H NMR spectroscopy employing DMSO-d_6 as solvent. The results thus obtained are summarized in Table E1.27 and plotted in Figure 2.1.

Table E1.27: Rate measurement for the forward HIE reaction of carbamate **166b**.[†]

Entry	Time (min)	%D
1	2	2
2	3	4
3	4	9
4	5	15
5	6	18

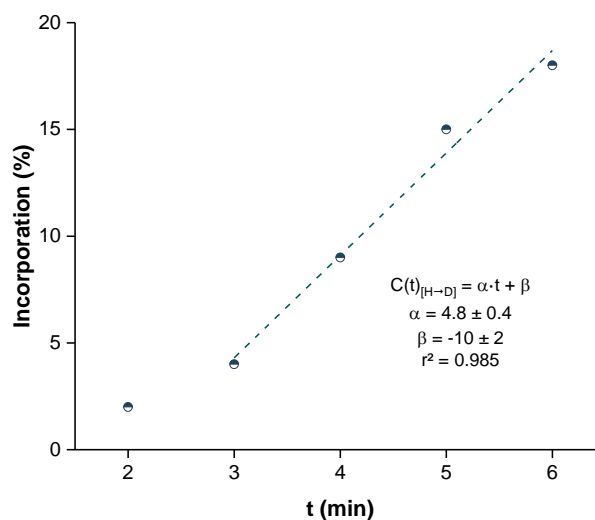[†] Incorporation determined by ^{1}H NMR spectroscopy.

Figure 2.1: Rate measurement for the forward HIE reaction of carbamate **166b**.
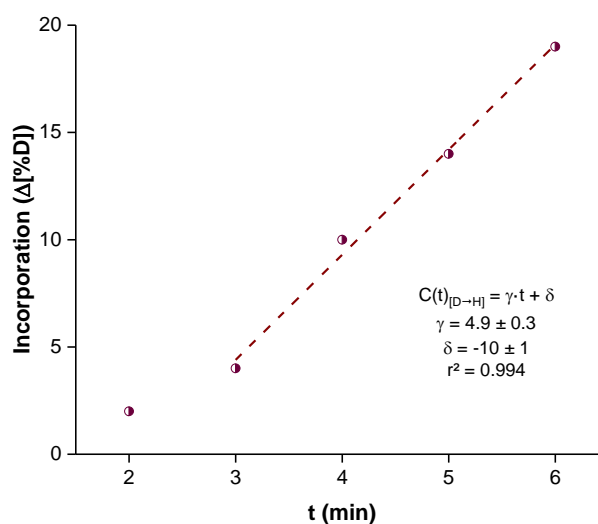
From the data provided in Table E1.27 and the slope of the line obtained in Figure 2.1, it was possible to estimate a reaction rate for the forward process, at 50 °C, equivalent to $k_H = (4.8 \pm 0.4)$ %D min^{-1}.

Rate measurement at 50 °C – reverse process

Following general procedure 6.7 for rate measurement of HIE reactions, catalyst **150c** (4.0 mg, 2.6 μmol, 0.5 mol%) and *d₂-O-tert*-butyl-*N*-(4-methyl)phenyl carbamate **166b-*d₂*** (90%D by ¹H NMR, 104.9 mg, 501 μmol) were added to the reaction vessel and dissolved in MTBE (20 mL). The resulting mixture was subjected to a rate measurement experiment *as per* the aforementioned general procedure employing H₂ as the reactive gas. Once the reaction vessel was fully immersed in an oil bath previously heated to 50 °C, a timer was started to measure progression of the reaction under study. The first 0.8 mL aliquot was taken after 2 min have elapsed, and the mixture thus collected was immediately transferred to a vial containing MeCN (2.0 mL). Four additional aliquots of 0.8 mL were collected at time intervals of 1 min, *i.e.*, after 3, 4, 5 and then 6 min of reaction, and were treated in an analogous manner to that stated for the first reaction sampling. Each aliquot was then treated as described in general procedure 5.7 and subsequently analysed by ¹H NMR spectroscopy employing DMSO-*d₆* as solvent. The results thus obtained are summarized in Table E1.28 and plotted in Figure 2.2.

Table E1.28: Rate measurement for the reverse HIE reaction of carbamate **166b-d_2**.[†]

Entry	Time (min)	%D	Δ[%D]
1	2	88	2
2	3	86	4
3	4	80	10
4	5	76	14
5	6	71	19

[†] Incorporation determined by ^{1}H NMR spectroscopy.

$$C(t)_{[D \to H]} = \gamma \cdot t + \delta$$
$$\gamma = 4.9 \pm 0.3$$
$$\delta = -10 \pm 1$$
$$r^2 = 0.994$$

Figure 2.2: Rate measurement for the reverse HIE reaction of carbamate **166b-d_2**.

From the data provided in Table E1.28 and the slope of the line obtained in Figure 2.2, it was possible to estimate a reaction rate for the reverse process, at 50 °C, equivalent to $k_D = (4.9 \pm 0.3)$ %D min^{-1}.

6.11.1.2 Rate of reactions with *O*-methyl-*N*-aryl carbamate **177**

Rate measurement at 30 °C – forward process

Following general procedure 6.7 for rate measurement of HIE reactions, catalyst **150c** (3.9 mg, 2.5 μmol, 0.5 mol%) and *O*-methyl-*N*-(4-methyl)phenyl carbamate **177** (83.0 mg, 499 μmol) were added to the reaction vessel and dissolved in MTBE (20 mL). The resulting mixture was subjected to a rate measurement experiment *as per* the aforementioned general procedure employing D$_2$ as the reactive gas. Once the reaction vessel was fully immersed in an oil bath previously heated to 30 °C, a timer

was started to measure progression of the reaction under study. The first 0.8 mL aliquot was taken after 2 min have elapsed, and the mixture thus collected was immediately transferred to a vial containing MeCN (2.0 mL). Four additional aliquots of 0.8 mL were collected at time intervals of 1 min, *i.e.*, after 3, 4, 5 and then 6 min of reaction, and were treated in an analogous manner to that stated for the first reaction sampling. Each aliquot was then treated as described in general procedure 5.7 and subsequently analysed by ^{1}H NMR spectroscopy employing DMSO-d_6 as solvent. The results thus obtained are summarized in Table E1.29 and plotted in Figure 2.3.

Table E1.29: Rate measurement for the forward HIE reaction of carbamate **177**.[†]

Entry	Time (min)	%D
1	2	2
2	3	6
3	4	12
4	5	24
5	6	32

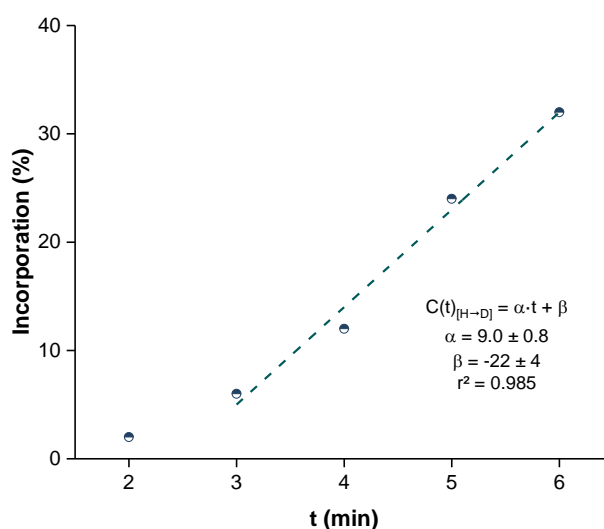[†] Incorporation determined by ^{1}H NMR spectroscopy.

Figure 2.3: Rate measurement for the forward HIE reaction of carbamate **177**.

From the data provided in Table E1.29 and the slope of the line obtained in Figure 2.3, it was possible to estimate a reaction rate for the forward process, at 30 °C, equivalent to $k_H = (9.0 \pm 0.8)$ %D min^{-1}.

Rate measurement at 30 °C – reverse process

Following general procedure 6.7 for rate measurement of HIE reactions, catalyst **150c** (3.9 mg, 2.5 μmol, 0.5 mol%) and d_2-O-methyl-N-(4-methyl)phenyl carbamate **177-d_2** (96%D by ^{1}H NMR, 83.5 mg, 499 μmol) were added to the reaction vessel and dissolved in MTBE (20 mL). The resulting mixture was subjected to a rate measurement experiment *as per* the aforementioned general procedure employing H_2 as the reactive gas. Once the reaction vessel was fully immersed in an oil bath previously heated to 30 °C, a timer was started to measure progression of the reaction under study. The first 0.8 mL aliquot was taken after 3 min have elapsed, and the mixture thus collected was immediately transferred to a vial containing MeCN (2.0 mL). Four additional aliquots of 0.8 mL were collected at time intervals of 1 min, *i.e.*, after 4, 5, 6 and then 7 min of reaction, and were treated in an analogous manner to that stated for the first reaction sampling. Each aliquot was then treated as described in general procedure 5.7 and subsequently analysed by ^{1}H NMR spectroscopy employing DMSO-d_6 as solvent. The results thus obtained are summarized in Table E1.30 and plotted in Figure 2.4.

Table E1.30: Rate measurement for the reverse HIE reaction of carbamate **177-d_2**.[†]

Entry	Time (min)	%D	Δ[%D]
1	3	95	1
2	4	95	1
3	5	92	4
4	6	89	7
5	7	86	10

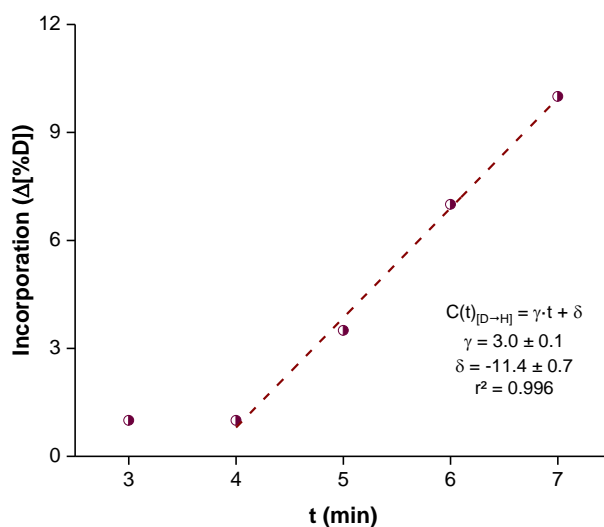[†] Incorporation determined by ^{1}H NMR spectroscopy.

Figure 2.4: Rate measurement for the reverse HIE reaction of carbamate **177-d_2**.

From the data provided in Table E1.30 and the slope of the line obtained in Figure 2.4, it was possible to estimate a reaction rate for the reverse process, at 30 °C, equivalent to $k_D = (3.0 \pm 0.1)$ %D min^{-1}.

Rate measurement at 50 °C – forward process

Following general procedure 6.7 for rate measurement of HIE reactions, catalyst **150c** (3.7 mg, 2.4 μmol, 0.5 mol%) and *O*-methyl-*N*-(4-methyl)phenyl carbamate **177** (82.6 mg, 500 μmol) were added to the reaction vessel and dissolved in MTBE (20 mL). The resulting mixture was subjected to a rate measurement experiment *as per* the aforementioned general procedure employing D_2 as the reactive gas. Once the reaction vessel was fully immersed in an oil bath previously heated to 50 °C, a timer was started to measure progression of the reaction under study. The first 0.8 mL aliquot was taken after 2 min have elapsed, and the mixture thus collected was immediately transferred to a vial containing MeCN (2.0 mL). Four additional aliquots of 0.8 mL were collected at time intervals of 1 min, *i.e.*, after 3, 4, 5 and then 6 min of reaction, and were treated in an analogous manner to that stated for the first reaction sampling. Each aliquot was then treated as described in general procedure 5.7 and subsequently analysed by ^{1}H NMR spectroscopy employing DMSO-*d_6* as

solvent. The results thus obtained are summarized in Table E1.31 and plotted in Figure 2.5.

Table E1.31: Rate measurement for the forward HIE reaction of carbamate **177**.[†]

Entry	Time (min)	%D
1	2	3
2	3	5
3	4	21
4	5	37
5	6	48

[†] Incorporation determined by ^{1}H NMR spectroscopy.

$$C(t)_{[H \to D]} = \alpha \cdot t + \beta$$
$$\alpha = 14.5 \pm 0.9$$
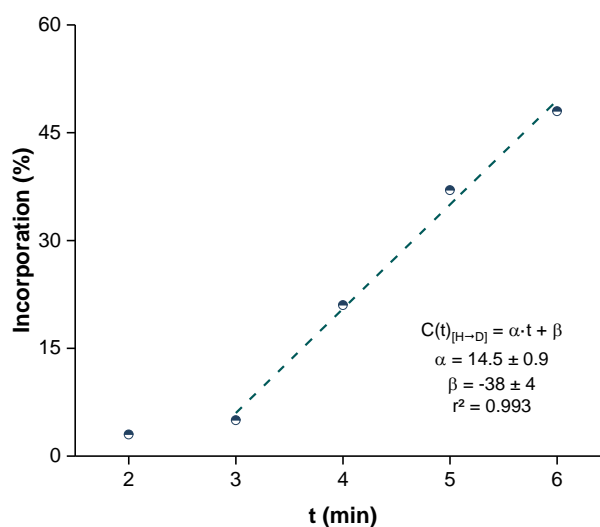$$\beta = -38 \pm 4$$
$$r^2 = 0.993$$

Figure 2.5: Rate measurement for the forward HIE reaction of carbamate **177**.

From the data provided in Table E1.31 and the slope of the line obtained in Figure 2.5, it was possible to estimate a reaction rate for the forward process, at 50 °C, equivalent to $k_H = (14.5 \pm 0.9)$ %D min^{-1}.

Rate measurement at 50 °C – reverse process

Following general procedure 6.7 for rate measurement of HIE reactions, catalyst **150c** (3.8 mg, 2.4 μmol, 0.5 mol%) and d_2-O-methyl-N-(4-methyl)phenyl carbamate **177-d_2** (94%D by ^{1}H NMR, 83.4 mg, 499 μmol) were added to the reaction vessel and dissolved in MTBE (20 mL). The resulting mixture was subjected to a rate measurement experiment *as per* the aforementioned general procedure employing H$_2$

as the reactive gas. Once the reaction vessel was fully immersed in an oil bath previously heated to 50 °C, a timer was started to measure progression of the reaction under study. The first 0.8 mL aliquot was taken after 2 min have elapsed, and the mixture thus collected was immediately transferred to a vial containing MeCN (2.0 mL). Four additional aliquots of 0.8 mL were collected at time intervals of 1 min, *i.e.*, after 3, 4, 5 and then 6 min of reaction, and were treated in an analogous manner to that stated for the first reaction sampling. Each aliquot was then treated as described in general procedure 5.7 and subsequently analysed by ^{1}H NMR spectroscopy employing DMSO-d_6 as solvent. The results thus obtained are summarized in Table E1.32 and plotted in Figure 2.6.

Table E1.32: Rate measurement for the reverse HIE reaction of carbamate **177-d_2**.[†]

Entry	Time (min)	%D	Δ[%D]
1	2	92	2
2	3	80	14
3	4	72	22
4	5	66	28
5	6	61	33

[†] Incorporation determined by ^{1}H NMR spectroscopy.

$$C(t)_{[D \rightarrow H]} = \gamma \cdot t + \delta$$
$$\gamma = 6.3 \pm 0.5$$
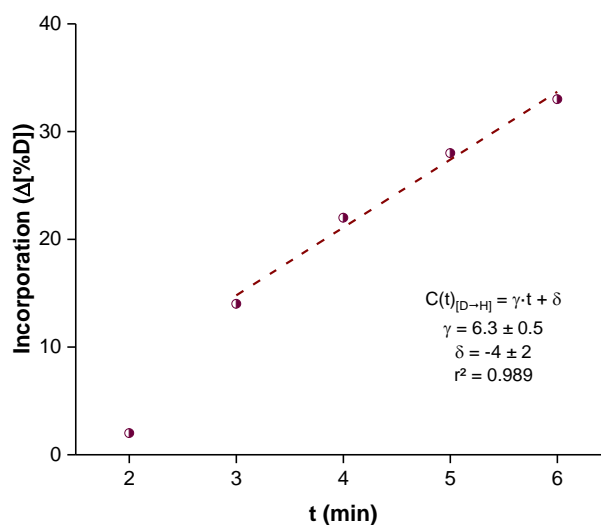$$\delta = -4 \pm 2$$
$$r^2 = 0.989$$

Figure 2.6: Rate measurement for the reverse HIE reaction of carbamate **177-d_2**.

From the data provided in Table E1.32 and the slope of the line obtained in Figure 2.6, it was possible to estimate a reaction rate for the reverse process, at 50 °C, equivalent to $k_D = (6.3 \pm 0.5)$ %D min^{-1}.

6.11.2 Determination of KIE

Considering the data collated in sections 6.11.1.1 and 6.11.1.2, it was possible to determine the KIE values of interest. Thus, by applying the definition of kinetic isotope effect of a given process,[201] it follows:

$$KIE = \frac{k_H}{k_D}$$

Moreover, by considering the error due to fitting associated with each individual linear regression, it is possible to estimate the following uncertainty for the KIE values – σ_{KIE}:[246]

$$\sigma_{KIE} = \sqrt[2]{\sum_{i=1}^{n} \left(\frac{\partial KIE}{\partial k_i}\right)^2} \equiv KIE \cdot \sqrt[2]{\left(\frac{\sigma_{k_H}}{k_H}\right)^2 + \left(\frac{\sigma_{k_D}}{k_D}\right)^2}$$

Where σ_{kH} and σ_{kD} correspond to the error due to fitting the rates for the forward reaction – k_H, and the analogous rate for the reverse process – k_D, respectively. Therefore, from these definitions is possible to calculate KIE values for the HIE reaction of carbamates **166b** and **177**, and the results obtained are summarised in Table E1.33:

Table E1.33: KIE values for the HIE of carbamates **166b** and **177**.

Entry	Carbamate	T (°C)	k_H (%D min^{-1})	k_D (%D min^{-1})	KIE	σ_{KIE}
1	**167b**	50	4.8 ± 0.4	4.9 ± 0.3	1.0	0.1
2	**176**	30	9.0 ± 0.8	3.0 ± 0.1	3.0	0.3
3	**176**	50	14.5 ± 0.9	6.3 ± 0.5	2.3	0.2

Finally, Figure 2.7 aggregates all data plots in section 5.5.1 in order to provide a visual representation of the KIE summarised in Table E1.33.
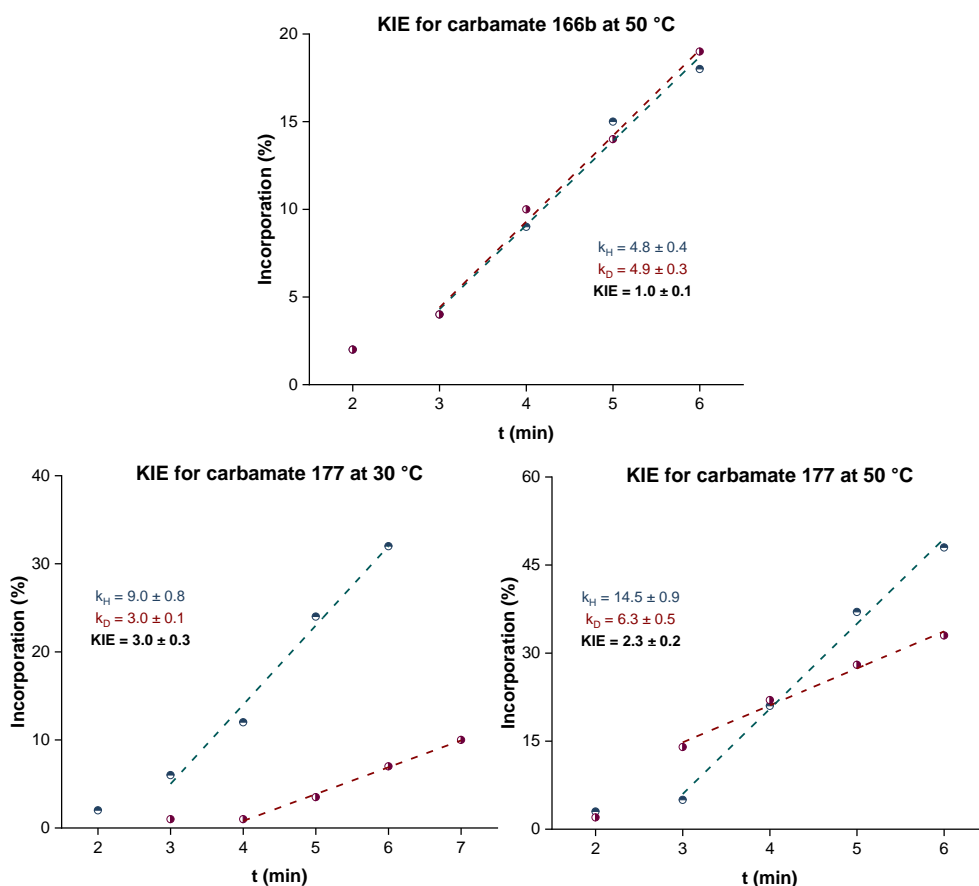
Figure 2.7: Aggregate data for rate experiments with carbamates **166b** (*top*) and **177** (*left* and *right*). Rate values are given in %D min^{-1}.

7. Computational details

A series of DFT techniques were employed to evaluate catalytically relevant iridium(III) deuterides, their corresponding adducts with carbamates, and their solvated counterparts.

7.1 General considerations

All DFT calculations were performed with the Gaussian09 quantum chemistry package[247] employing the meta-GGA functional of Truhlar and Zhao[248] – M06L – with associated 6-31G(d) basis set for light atoms, and Stuttgart RSC effective core potentials and associated basis set for iridium.[189]

Structures corresponding to intermediates in all potential energy surfaces described herein were confirmed to be minima through vibrational frequency calculations and depicted no imaginary frequencies. Transition states were located employing the Synchronous Transit-Guided Quasi-Newton method[249] – QST3 – with inclusion of relevant guesses for transition state geometry and confirmed by vibrational frequency calculation which featured a unique imaginary frequency. Intrinsic reaction coordinate calculations were performed in two separate steps, one for each direction of the potential energy surface (forward and reverse pathways) employing transition states previously obtained *via* the QST3 method. NBO analysis[147] were performed in Gaussian09 with its integrated NBO 3.0 package. Unless otherwise stated, all calculations were performed in the gas phase. All relevant output files are provided in Appendix A.

Analysis of variance for individual descriptors in multivariate regression models in conjunction with all graphical elements presented herein were obtained employing the OriginPro 2017 SR2 software package. Detailed statistical analysis of each of the predictive models reported, estimation of best subsets for multivariate analysis, calculation of regression coefficients and Durbin-Watson statistics were performed with the Minitab® 17 Statistical Software.

7.2 Calculation of buried volume with the SambVca 2.0 web application.

$\%V_{Bur}$ values employed to formulate multivariate regression models were obtained employing the SambVca 2.0 web application.[152] Hence, previously optimised structures were visualised in GaussView 5.0[250] and exported in .PDB format to afford an appropriate input file for extraction of buried volume data.

Each file was then uploaded to the SambVca 2.0 server and the standard orientation procedure recommended for chelating ligands was employed. More precisely, the iridium centre was selected as the centre of the putative sphere; the coordinated carbon atom from NHC and the phosphorus atom from the phosphine moiety were selected for z-axis definition; and only the P atom from the phosphine was selected for x-axis definition. Then, *all atoms that did not constitute the NHC-P ligand framework were deleted*. This step is crucial to ensure that only the steric information

conveyed by the ancillary ligand is captured. Finally, the sphere radius and mesh spacing were kept at 3.5 and 0.05 Å, respectively. Reports generated in the web application were saved in .PDF format and the associated steric maps were exported in .PNG format. All relevant files obtained by this method are included in **Appendix A**, and relevant values are provided in Section 6.3.

7.3 Multivariate analysis for enthalpy prediction

The construction of multivariate regression models included two separate stages, namely, data acquisition and statistical analysis, as detailed in the following sections.

7.3.1 Data acquisition

Three distinct types of variables were compiled and analysed by statistical methods, *viz.*, structural data, steric information and electronic parameters.

Structural data was directly obtained from Gaussian09 output files in the GaussView 5.0 software. The parameter selected for further analysis was the distance from the iridium centre and the hydrogen atom within the C—H bond involved in the agostic interaction with coordinated carbamates – $d_{Ir\cdots H}$. The associated distance to the carbon atom within the same bond was initially considered as a relevant parameter, however, it showed no statistical significance for any feasible predictive model, being ultimately removed from the final data set.

Steric information was obtained directly from $\%V_{Bur}$ data calculated with the SambVca 2.0 application and included: the total buried volume for the ligand set within a given iridium(III) deuteride adduct- $\%V_{Bur}^{Tot}$; each of its four components obtained by decomposition of the steric information in the quadrant model - $\%V_{Bur}^{NW}$, $\%V_{Bur}^{NE}$, $\%V_{Bur}^{SW}$ and $\%V_{Bur}^{SE}$ for north-west, north-east, south-west and south-east quadrants, respectively.

Electronic information was extracted from outputs of the NBO analyses performed. It is important to emphasise that each NBO calculation was performed in conjunction with a frequency determination. This process is crucial to provide an accurate estimation of force constants and enforce computation of second-order perturbative

interactions which, in the NBO decomposition theory,[147] describe the degree with which a chemical bond engages in electronic interactions with the remaining parts of the molecule. This electronic term is often named donor-acceptor interaction.

Once suitable output files were obtained with the Gaussian09 package, the .LOG files were opened in Microsoft Word and each of the donor-acceptor interactions associated with the agostically ligated C—H bond were mapped. As a result, two sets of second-order perturbative energies – E^2 – was obtained: the first set of interactions describe unidirectional terms of type $Ir \rightarrow \sigma^*_{C-H}$ and are associated to backdonation from the organometallic fragment to the coordinated C—H bond; the second group of values describe unidirectional terms in the reverse orientation, *i.e.*, $\sigma_{C-H} \rightarrow Ir$, being primarily associated with the σ-donation arising from the bonding orbital of the C—H fragment. Donor-acceptor interaction values obtained in this treatment were added to provide the final descriptors subjected to further statistical analysis: $E^2[Ir \rightarrow \sigma^*_{C-H}]$ and $E^2[\sigma_{C-H} \rightarrow Ir]$. Finally, a formal definition is provided:

$$E^2[\sigma_{C-H} \rightarrow Ir] = \sum_{i=1}^{n} E^2[\sigma_{C-H} \rightarrow \varphi_i^*(Ir)]$$

$$E^2[Ir \rightarrow \sigma_{C-H}^*] = \sum_{j=1}^{n} E^2[\varphi_j(Ir) \rightarrow \sigma_{C-H}^*]$$

Where:

σ_{C-H} – NBO orbital for the bonding C—H covalent bond;

σ^*_{C-H} – NBO orbital for the anti-bonding C—H covalent bond;

$\varphi(Ir)$ – NBO orbitals from the iridium centre that possess bonding character and participates in second-order interactions with the agostic C—H fragment;

$\varphi^*(Ir)$ – NBO orbitals from the iridium centre that possess anti-bonding character and participates in second-order interactions with the C—H bond;

Collectively, the data acquired is summarised in Table E1.34. It is important to emphasise that only selected parameters were employed in the final fitting model, and the values provided herein comprise the initial input for best subset analysis (*vide infra*).

Table E1.34: Data employed in statistical analysis.[†]

Entry	Carbamate	$d_{Ir\cdots H}$	$\%V_{Bur}^{Tot}$	$\%V_{Bur}^{NW}$	$\%V_{Bur}^{NE}$	$\%V_{Bur}^{SW}$	$\%V_{Bur}^{SE}$
1	**183a**	2.65596	49.4	48.7	47.3	60.7	40.9
2	**183b**	2.65290	49.1	48.9	47.3	59.6	40.4
3	**183c**	2.67735	49.4	47.2	47.1	62.0	41.2
4	**183d**	2.66575	49.4	47.8	47.4	61.6	40.9
5	**183e**	2.65755	49.3	48.3	46.9	61.6	40.3
6	**183f**	2.63367	49.4	49.2	47.5	60.1	40.8
7	**183g**	2.62423	49.5	47.1	46.9	62.8	41.2
8	**183h**	2.65041	49.5	48.1	47.6	61.1	41.2
9	**183i**	2.66858	49.5	48.4	47.9	60.9	41.0
10	**183j**	2.63368	49.4	47.8	48.0	61.1	40.8
11	**183k**	2.66186	49.7	48.1	48.1	61.3	41.1
12	**183l**	2.67466	49.3	49.1	47.1	60.0	40.9
13	**183m**	2.62349	49.5	47.2	47.9	62.0	41.0
14	**183n**	2.64556	49.5	48.3	47.6	61.3	40.8
15	**183o**	2.60484	49.6	48.8	46.5	64.5	38.7
16	**183p**	2.63223	49.7	47.7	47.8	63.0	40.2
17	**183q**	2.63597	49.3	48.5	47.3	60.4	41
18	**183r**	2.63516	49.8	47.5	47.4	63.2	41.2

Table E1.34 continued…

Entry	Carbamate	$E^2[Ir \rightarrow \sigma^*_{C-H}]$	$E^2[\sigma_{C-H} \rightarrow Ir]$	ΔH_{TS}
1	**183a**	2.26	61.16	20.28
2	**183b**	2.08	68.29	22.35
3	**183c**	2.22	61.81	20.13
4	**183d**	2.52	61.67	19.71
5	**183e**	2.3	60.68	19.11
6	**183f**	2.14	53.58	16.69
7	**183g**	2.19	56.27	17.49
8	**183h**	2.31	60.6	20.19
9	**183i**	2.36	59.45	20.53
10	**183j**	2.18	65.55	22.18
11	**183k**	2.72	70.73	24.79
12	**183l**	2.45	61.37	22.01
13	**183m**	2.27	64.61	22.45
14	**183n**	2.34	63.32	22.45
15	**183o**	3.32	33.73	15.49
16	**183p**	2.44	53.07	18.21
17	**183q**	2.3	65.04	17.6
18	**183r**	2.45	51.78	19.42

[†]$d_{Ir\cdots H}$ – distance between the iridium and the agostically bound hydrogen, in Å; %VBur values are given in %; second-order perturbative interactions are given in kcal mol^{-1}; ΔH_{TS} – enthalpy of C—H activation obtained from QST3 calculations.
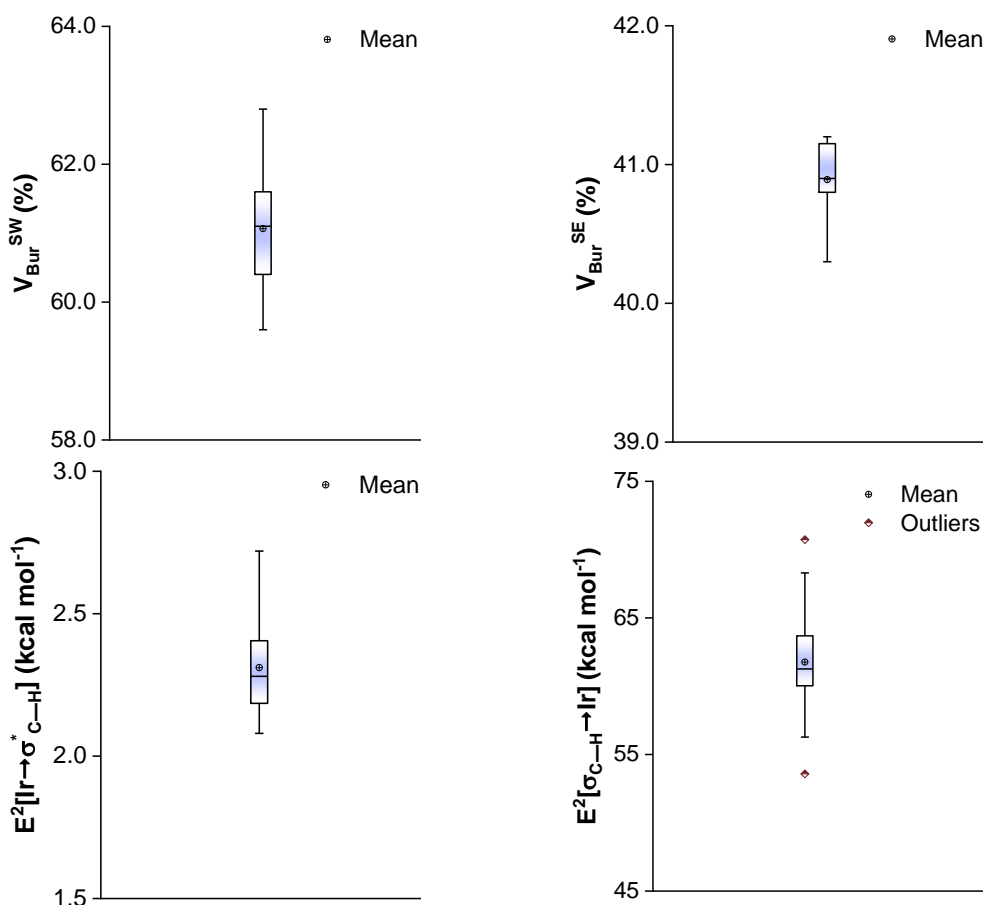
7.3.2 Statistical analysis

Parameters included in Table E1.34 were split into two sets, namely: calibration set, which included data for carbamates **183a-l** and were directly employed in the regression model; and validation set, which included the remaining data points for

183m-r. The calibration set was subjected to analysis of variance and each of the variables was graphically examined as a boxplot, process that ensures expedient identification of data points for carbamates that deviate from a normal distribution across multiple predictors. If a given substrate in the calibration set appeared as a consistent outlier in several boxplots, this structure would be deemed unsuitable for use in the regression model. This process enforces reasonable proximity to a normal distribution, which is required for further multivariate regression. Plots generated by this method are provided in Schemes E1.1 and E1.2. Only 3 outliers were found, namely: **183b** for the variable $\%V_{Bur}^{Tot}$; and **183f** and **183k** for the descriptor $E^2[\sigma^*_{C—H}{\rightarrow}Ir]$. Those deviations were considered inconsequential for the overall model, as these substrates did depict anomalous behaviour in any other aspect.

Scheme E1.1: Boxplot for variables in Table E1.34.

Scheme E1.2: Boxplot for variables in Table E1.34.

The full data set, which comprised a 12×8 matrix of predictors (P) and a 12×1 vector containing the response variable (R), was then subjected to a best subset analysis in Minitab® 17. This statistical treatment performs several multivariate regressions employing the P matrix to predict the response values in R. Then, standard deviations, errors and correlation coefficients are generated for each regression and a selection of best candidates for predicting the desired property, in this case ΔH_{TS}, is reported by the software alongside the relevant statistic parameters. It is important to emphasise that this entire process was performed *without adding a label* for the predictors in the matrix P, and it was deemed necessary to avoid unconscious influences from confirmation bias while selecting the best possible regression model.

Once identified, the name of the variables was then revealed by direct comparison of the data points with values in Table E1.34. The three best candidates for regression

models were then selected, the variables were compiled and fitted to predict ΔH_{TS}. These models can be found in Scheme 1.65 in Section 3.4.

Regression coefficients, correlation coefficients, standard deviations, significance p test values and the Durbin-Watson statistics were directly calculated in Minitab® 17. The regression coefficients were then employed to predict ΔH_{TS} values for both calibration and validation sets. These results are provided in Table E1.35, and the appropriate discussions regarding their significance and implications can be found in Section 3.4.

Table E1.35: Results obtained for multivariate regression models.[†]

Entry	Carbamate	ΔH_{TS}	$\Delta H^{(1)}$	$\Delta H^{(2)}$	$\Delta H^{(3)}$
1	**183a**	20.28	20.63	20.06	20.47
2	**183b**	22.35	23.03	22.61	22.78
3	**183c**	20.13	20.28	20.60	20.39
4	**183d**	19.71	20.08	20.59	20.08
5	**183e**	19.11	18.76	19.49	18.73
6	**183f**	16.69	17.34	16.94	17.02
7	**183g**	17.49	17.62	17.05	17.23
8	**183h**	20.19	20.50	20.04	20.28
9	**183i**	20.53	19.80	20.38	19.80
10	**183j**	22.18	21.67	21.89	21.26
11	**183k**	24.79	24.98	24.59	24.75
12	**183l**	22.01	21.08	20.37	21.09
13	**183m**	15.49	3.22	7.84	3.20
14	**183n**	22.45	21.14	21.18	20.65
15	**183o**	22.45	21.07	20.92	20.80
16	**183p**	18.21	14.49	17.04	14.34
17	**183q**	17.60	22.48	21.00	22.03
18	**183r**	19.42	15.89	16.20	15.66

[†]$\Delta H^{(k)}$ indicates the prediction for each model k; all energies are given in kcal mol^{-1}.

7.4 Prediction of KIE values

Computation of the KIE values was accomplished through analysis of both forward and reverse reactions within the HIE process. Accordingly, the C—H activation of compounds **166b** and **177**, and the analogous C—D activation of **166b-d_2** and **177-d_2**, were computed and the corresponding transition states for σ-bond metathesis were located. Comparison of the relative enthalpies of activation for both processes

thus allowed the estimation of expected KIE values at 30 and 50 °C according to the relationship below:

$$KIE = \frac{k_H}{k_D} = e^{\frac{\Delta\Delta H_{D-H}}{RT}}$$

Where:

k_H is the predicted rate for C—H activation;

k_D is the predicted rate for C—D activation;

$\Delta\Delta H_{D-H}$ is the difference in relative enthalpies of C—D and C—H activation, *i.e.*, $\Delta\Delta H_{D-H} = \Delta H_D - \Delta H_H$, in kcal mol^{-1};

R is the gas constant, in kcal K^{-1} mol^{-1};

T is the temperature in K.

8. References

[1] Greenaway, A. M.; Lancashire, R. J., *J. Chem. Educ.* **1982**, *59*, 419.

[2] Vaska, L., *J. Am. Chem. Soc.* **1961**, *83*, 756.

[3] Vaska, L.; DiLuzio, J. W., *J. Am. Chem. Soc.* **1961**, *83*, 2784.

[4] Vaska, L., *Acc. Chem. Res.* **1968**, *1*, 335.

[5] Seechurn, C. C. C. J.; Kitching, M. O.; Colacot, T. J.; Snieckus, V., *Angew. Chem. Int. Ed.* **2012**, *51*, 5062.

[6] "Web of Science", *Web of Science [v.5.29]*, Clarivate Analytics, 31/07/2018, http://webofknowledge.com.

[7] Negishi, E. I. (ed.) *Handbook of Organopalladium Chemistry for Organic Synthesis*. New York: Wiley Interscience; 2002, 3279p.

[8] Hartwig, J. F. (ed.) *Organotransition Metal Chemistry: From Bonding to Catalysis*. Sausalito: University Science Books; 2010, 1127p.

[9] Greenwood, N. N.; Earnshaw, A. *Chemistry of the Elements*. Oxford: Butterworth Heinemann; 1984, 1542p.

[10] Crabtree, R. H., *The Organometallic Chemistry of Transition Metals*. 4th ed., New Jersey: Wiley-Interscience; 2005, 546p.

[11] Hartwig, J. F., *Acc. Chem. Res.* **1998**, *31*, 852.

[12] Suzuki, A. *Angew. Chem. Int. Ed.* **2011**, *50*, 6723.

[13] Negishi, E. I., *Angew. Chem. Int. Ed.* **2011**, *50*, 6738.

[14] Sonogashira, K., *J. Organomet. Chem.* **2002**, *63*, 46.

[15] Scott, W. J.; Stille, J. K., *J. Am. Chem. Soc.* **1986**, *108*, 3033.

[16] Colby, D. A.; Tsai, A. S.; Bergman, R. G.; Ellman, J. A., *Acc. Chem. Res.* **2012**, *45*, 814.

[17] Crabtree, R. H., *Acc. Chem. Res.* **1990**, *23*, 95.

[18] Oro, L. A. (ed.); Claver, C. (ed.) *Iridium Complexes in Organic Synthesis.* Weinheim: WILEY-VCH; 2009, 417p.

[19] Andersson, P. G. (ed.), *Top. Organomet. Chem.*, **2011**, *34*, 234p.

[20] Crabtree, R. H.; Felkin, H.; Morris, G. E., *J. Organomet. Chem.* **1977**, *141*, 205.

[21] Crabtree, R. H., *Acc. Chem. Res.* **1979**, *12*, 331.

[22] Suggs, J. W.; Cox, S. D.; Crabtree, R. H.; Quirk, J. M., *Tetrahedron Lett.*, **1981**, *22*, 303.

[23] Crabtree, R. H.; Davis, M. K., *Organometallics*, **1983**, *2*, 681.

[24] Crabtree, R. H.; Davis, M. K., *J. Org. Chem.*, **1986**, *51*, 2655.

[25] Janowicz, A. H.; Periana, R. A.; Buchanan, J. M.; Kovac, C. A.; Stryker, J. M.; Wax, M. J.; Bergman, R. G., *Pure Appl. Chem.* **1984**, *56*, 13.

[26] Crabtree, R. H.; Felkin, H.; Morris, G. E., *J. Organomet. Chem.* **1976**, *113*, C7.

[27] Voutchkova, A. M.; Gnanamgari, D.; Jakobsche, C. E.; Butler, C.; Miller, S. J.; Parr, J.; Crabtree, R. H., *J. Organomet. Chem.* **2008**, *693*, 1815.

[28] Balcells, D.; Nova, A.; Clot, E.; Gnanamgari, D.; Crabtree, R. H.; Eisenstein, O., *Organometallics* **2008**, *27*, 2529.

[29] Gnanamgari, D.; Sauer, E. L. O.; Schley, N. D.; Butler, C.; Incarvito, C. D.; Crabtree, R. H., *Organometallics* **2009**, *28*, 321.

[30] Dobereiner, G. E.; Nova, A.; Schley, N. D.; Hazari, N.; Miller, S. J.; Eisenstein, O.; Crabtree, R. H., *J. Am. Chem. Soc.* **2011**, *133*, 7547.

[31] Manas, M. G.; Graeupner, J.; Allen, L. J.; Dobereiner, G. E.; Rippy, K. C.; Hazari, N.; Crabtree, R. H., *Organometallics* **2013**, *32*, 4501.

[32] Hintermair, U.; Campos, J.; Brewster, T. P.; Pratt, L. M.; Schley, N. D.; Crabtree, R. H., *ACS Catal.* **2014**, *4*, 99.

[33] Arndsten, B. A.; Bergman, R. G.; Mobley, T. A.; Peterson, T. H., *Acc. Chem. Res.* **1995**, *28*, 154.

[34] Arndsten, B. A.; Bergman, R. G., *Science* **1995** *270*, 1970.

[35] Golden, J. T.; Andersen, R. A.; Bergman, R. G., *J. Am. Chem. Soc.* **2001**, *123*, 5837.

[36] Klei, S. R.; Tilley, T. D.; Bergman, R. G., *J. Am. Chem. Soc.* **2000**, *122*, 1816.

[37] Klei, S. R.; Golden, J. T.; Tilley, T. D.; Bergman, R. G., *J. Am. Chem. Soc.* **2002**, *124*, 2092.

[38] Choi, J.; Wang, D. Y.; Kundu, S.; Choliy, Y.; Emge, T. J.; Krogh-Jespersen, K.; Goldman, A. S., *Science* **2011**, *332*, 1545.

[39] Biswas, S.; Huang, Z.; Choliy, Y.; Wand, D. Y.; Brookhart, M.; Krogh-Jespersen, K.; Goldman, A. S., *J. Am. Chem. Soc.* **2012**, *134*, 13276.

[40] Nawara-Hultzsch, A. J.; Hackenberg, J. D.; Punji, B.; Supplee, C.; Emge, T. J.; Bailey, B. C.; Schrock, R. R.; Brookhart, M.; Goldman, A. S., *ACS Catal.* **2013** *3*, 2505.

[41] Kundu, S.; Choi, J.; Wang, D. Y.; Choliy, Y.; Emge, T. J.; Krogh-Jespersen, K.; Goldman, A. S., *J. Am. Chem. Soc.* **2013**, *135*, 5127.

[42] Cheng, C.; Kim, B. G.; Guironnet, D.; Brookhart, M.; Guan, C.; Wang, D. Y.; Krogh-Jespersen, K.; Goldman, A. S., *J. Am. Chem. Soc.* **2014**, *136*, 6672.

[43] Hackenberg, J. D.; Kundu, S.; Emge, T. J.; Krogh-Jespersen, K.; Goldman, A. S., *J. Am. Chem. Soc.* **2014**, *136*, 8891.

[44] Müller, D.; Umbricht, G.; Weber, B.; Pfaltz, A., *Helv. Chim. Acta* **1991**, *74*, 232.

[45] Helchem, G.; Pfaltz, A., *Acc. Chem. Res.* **2000**, *33*, 336.

[46] Smidt, S. P.; Zimmermann, N.; Studer, M.; Pfaltz, A., *Chem. Eur. J.* **2004**, *10*, 4685.

[47] Wang, G.; Franke, J.; Ngo, C. Q.; Krische, M. J., *J. Am. Chem. Soc.* **2015**, *137*, 7915

[48] Ganić, A.; Pfalzt, A., *Chem. Eur. J.* **2012**, *18*, 6724.

[49] Schramm, Y.; Barrios-Landeros, F.; Pfaltz, A., *Chem. Sci.* **2013**, *4*, 2760.

[50] Gruber, S.; Neuburger, M.; Pfaltz, A., *Organometallics* **2013**, *32*, 4702.

[51] Schumacher, A.; Bernasconi, M.; Pfaltz, A., *Angew. Chem. Int. Ed.* **2013**, *52*, 7422.

[52] Gruber, S.; Pfaltz, A., *Angew. Chem. Int. Ed.* **2014**, *53*, 1896.

[53] Kim, I. S., Ngai, M. Y.; Krische, M. J., *J. Am. Chem. Soc.* **2008**, *130*, 6340.

[54] Kim, I. S., Ngai, M. Y.; Krische, M. J., *J. Am. Chem. Soc.* **2008**, *130*, 14891.

[55] Kim, I. S.; Han, S. B.; Krische, M. J, *J. Am. Chem. Soc.* **2009**, *131*, 2514.

[56] Lu, Y.; Kim, I. S.; Hassan, A.; Del Valle, D. J., Krische, M. J., *Angew. Chem. Int. Ed.* **2009**, *48*, 5018.

[57] Hassan, A.; Zbieg, J. R.; Krische, M. J., *Angew. Chem. Int. Ed.* **2011**, *50*, 3493.

[58] Gao, X.; Zhang, Y. J.; Krische, M. J., *Angew. Chem. Int. Ed.* **2011**, *50*, 4173.

[59] Moran, J.; Smith, A. G.; Carris, R. M.; Johnson, J. S.; Krische, M. J., *J. Am. Chem. Soc.* **2011**, *133*, 18618.

[60] Montgomery, T. P.; Hassan, A.; Park, B. Y.; Krische, M. J., *J. Am. Chem. Soc.* **2012**, *134*, 11100.

[61] Montgomery, T. P.; Hassan, A.; Park, B. Y.; Krische, M. J., *J. Am. Chem. Soc.* **2012**, *134*, 11100.

[62] Dechert-Schmitt, A. M. R.; D. C. Schmitt, Krische, M. J., *Angew. Chem. Int. Ed.* **2013**, *52*, 3195.

[63] Feng, J.; Garza, V. J.; Krische, M. J., *J. Am. Chem. Soc.* **2014**, *136*, 8911.

[64] Brown, J. A.; Irvine, S.; Kennedy, A. R.; Kerr, W. J., Andersson, S.; Nilsson, G. N., *Chem. Commun.* **2008**, 1115.

[65] Nilson, G. N.; Kerr, W. J., *J. Label Compd. Radiopharm.* **2010**, *53*, 662.

[66] Bennie, L. S.; Fraser, C. J.; Irvine, S.; Kerr, W. J.; Andersson, S.; Nilsson, G. N., *Chem. Commun.* **2011**, *47*, 11653.

[67] Cochrane, A. R.; Irvine, S.; Kerr, W. J.; Reid, M.; Andersson, S.; Nilsson, G. N., *J. Label Compd. Radiopharm.* **2013**, *56*, 451.

[68] Kennedy, A. R.; Kerr, W. J.; Moir, R.; Reid, M., *Org. Biomol. Chem.* **2014**, *12*, 7927.

[69] Kerr, W. J.; Mudd, R. J.; Paterson, L. C.; Brown, J. A., *Chem. Eur. J.* **2014**, *20*, 14604.

[70] Brown, J. A.; Cochrane, A. R.; Irvine, S.; Kerr, W. J.; Mondal, B.; Parkinson, J. A.; Paterson, L. C.; Reid, M.; Tuttle, T.; Andersson, S.; Nilsson, G. N., *Adv. Synth. Catal.* **2014**, *356*, 3551.

[71] Kerr, W. J.; Reid, M.; Tuttle, T., *ACS Catal.* **2015**, *5*, 402.

[72] Atzrodt, J.; Derdau, V.; Kerr, W. J.; Reid, M.; Rojahn, P.; Weck, R., *Tetrahedron* **2015**, *71*, 1924.

[73] Devlin, J.; Kerr, W. J.; Lindsay, D. M.; McCabe, T. J. D.; Reid, M.; Tuttle, T., *Molecules* **2015**, *20*, 11676.

[74] Kerr, W. J.; Reid, M.; Tuttle, T., *ACS Catal.* **2015**, *5*, 402.

[75] Kerr, W. J.; Lindsay, D. M.; Reid, M.; Atzrodt, J.; Derdau, V.; Rojahn, P.; Weck, R., *Chem. Commun.* **2016**, *52*, 6669.

[76] Kerr, W. J.; Lindsay, D. M.; Owens, P. K.; Reid, M.; Tuttle, T.; Campos, S., *ACS Catal.* **2017**, *7*, 7182.

[77] Kerr, W. J.; Reid, M.; Tuttle, T., *Angew. Chem. Int. Ed.* **2017**, *56*, 7808.

[78] Atzrodt, J.; Derdau, V.; Kerr, W. J.; Reid, M., *Angew. Chem. Int. Ed.* **2018**, *57*, 1758.

[79] Atzrodt, J.; Derdau, V.; Kerr, W. J.; Reid, M., *Angew. Chem. Int. Ed.* **2018**, *57*, 3022.

[80] Xue, X. S.; Ji, P.; Zhou, B.; Cheng, J. P., *Chem. Rev.* **2017**, *117*, 8622.

[81] Esteruelas, M. A.; López, A. M.; Oliván, M., *Chem. Rev.* **2016**, *116*, 8770.

[82] Bromberg, S. E.; Yang, H.; Asplund, M. C.; Lian, T.; McNamara, B. K.; Kotz, K. T.; Yeston, J. S.; Wilkens, M.; Frei, H.; Bergman, R. G.; Harris, C. B., *Science* **1997**, *278*, 260.

[83] Shilov, A. E.; Shul'pin, G. B., *Chem. Rev.* **1997**, *97*, 2879.

[84] Davies, D. L.; Macgregor, S. A.; McMullin, C. L., *Chem. Rev.* **2017**, *117*, 8649.

[85] Ziegler, T.; Folga, E.; Berces, A., *J. Am. Chem. Soc.* **1993**, *115*, 636.

[86] Vastine, B. A.; Hall, M. B., *J. Am. Chem. Soc.* **2007**, *129*, 12068.

[87] Perutz, R. N.; Sabo-Etienne, S., *Angew. Chem. Int. Ed.* **2007**, *46*, 2578.

[88] Yi, H.; Zhang, G.; Wang, H.; Huang, Z.; Wang, J.; Singh, A. K.; Lei, A., *Chem. Rev.* **2017**, *117*, 9016.

[89] Prier, C. K.; Rankic, D. A.; MacMillan, D. W. C., *Chem. Rev.* **2013**, *113*,

[90] Hoyano, J. K.; McMaster, A. D.; Graham, W. A. G., *J. Am. Chem. Soc.* **1983**, *105*, 7190.

[91] Bischof, S. M.; Ess, D. H; Meier, S. K.; Oxgaard, J.; Nielsen, R. J.; Bhalia, G.; Goddard III, W. A.; Periana, R. A., *Organometallics* **2010**, *29*, 742.

[92] Phillips, N.; Treasure, L.; Rees, N. H.; Tirfoin, R.; McGrady, J. E.; Aldridge, S., *Eur. J. Inorg. Chem.* **2014**, 4877.

[93] Kohls, P.; Jadhav, D.; Pandey, G.; Reiser, O., *Org. Lett.* **2012**, *14*, 672.

5322.

[94] Chatt, J.; Duncanson, L. A., *J. Chem. Soc.*, **1953**, 2939.

[95] Chatt, J.; Duncanson, L. A.; Venanzi, L. M., *J. Chem. Soc.*, **1955**, 4456.

[96] Appelhans, L. N.; Zuccaccia, D.; Kovacevic, A.; Chianese, A. R.; Miecznikowski, J. R.; Macchioni, A.; Clot, E.; Eisenstein, O.; Crabtree, R. H., *J. Am. Chem. Soc.* **2005**, *127*, 16299.

[97] Ito, J.; Kaneda, T.; Nishiyama, H., *Organometallics* **2012**, *31*, 4442.

[98] Mutlib, A., *Chem. Res. Toxicol.* **2008**, *21*, 1672.

[99] Penner, N.; Xu, L.; Prakash, C., *Chem. Res. Toxicol.* **2012**, *25*, 513.

[100] Hewavitharana, A. K., *J. Chomratogr. A* **2011**, *1218*, 359.

[101] Junk, T.; Catallo, W. J., *Chem. Soc. Rev.* **1997**, *26*, 401.

[102] Atzrodt, J.; Derdau, V.; Fey, T.; Zimmermann, J., *Angew. Chem. Int. Ed.* **2007**, *46*, 7744.

[103] Lockley, W. J. S. (ed.); Heys, J. R. (ed.) *Metal-catalysed Hydrogen Isotope Exchange*, special issue of *J. Label. Compd. Radiopharm.*, Chichester, 2010, Vol. 53, pp. 635-751.

[104] Leppälä, E.; Wähälä, K., *J. Label. Compd. Radiopharm.* **2004**, *47*, 25.

[105] Junk, T.; Catallo, W. J., *Tetrahedron Lett.* **1996**, *37*, 3445.

[106] Derdau, V.; Atzrodt, J., *Synlett* **2006**, 1918.

[107] Chatterjee, B.; Krishnakumar, V.; Gunanathan, C., *Org. Lett.* **2016**, *18*, 5892.

[108] Hodges, R. J.; Garnett, J. L., *J. Catal.*, **1969**, *13*, 83.

[109] Hesk, D.; Das, P. R.; Evans, B., *J. Label Compd. Radiopharm.*, **1995**, *36*, 497.

[110] Lockley, W. J. S., *J. Label Compd. Radiopharm.*, **1983**, *21*, 45.

[111] Regen, S. L., *J. Org. Chem.* **1973**, *39*, 260.

[112] Chodosh, D. F.; Crabtree, R. H., *J. Organomet. Chem.*, **1978**, *161*, C67.

[113] Lee, H. M.; Jiang, T.; Stevens, E. D.; Nolan, S. P., *Organometallics*, **2001**, *20*, 1255.

[114] Vázquez-Serrano, L. D.; Owens, B. T.; Buriak, J. M., *Chem. Commun.*, **2002**, 2518.

[115] Vázquez-Serrano, L. D.; Owens, B. T.; Buriak, J. M., *Inorg. Chim. Acta*, **2006**, *359*, 2786.

[116] Strem Chemicals Inc. Catalogue, available at http://www.strem.com, 01/08/2018.

[117] Huheey, J. E.; Keiter, R. L.; Keiter, E. A., *Inorganic Chemistry: principles of structure and reactivity*. 4th ed., New York: HarperCollins; 1993, 964p.

[118] Nishida, H.; Takada, N.; Yoshimura, M.; Sonoda, T.; Kobayashi, H., *Bull. Chem. Soc. Jpn.*, **1984**, *57*, 2600.

[119] Burhop, A.; Weck, R.; Atzrodt, J.; Derdau, V., *Eur. J. Org. Chem.* **2017**, 1418.

[120] Perry, M. C.; Cui, X.; Powell, M. T.; Hou, D. R.; Reibenspies, J. H.; Burgess, K., *J. Am. Chem. Soc.* **2003**, *125*, 113.

[121] Jess, K.; Derdau, V.; Weck, R.; Atzrodt, J.; Freytag, M.; Jones, P. G.; Tamm, M., *Adv. Synth. Catal.* **2017**, *359*, 629.

[122] Valero, M.; Burhop, A.; Jess, K.; Weck, R.; Tamm, M.; Atzrodt, J.; Derdau, V., *J. Label. Compd. Radiopharm.* **2018**, *61*, 380.

[123] Valero, M.; Weck, R.; Güssregen, S.; Atzrodt, J.; Derdau, V., *Angew. Chem. Int. Ed.* **2018**, *57*, 8159.

[124] Yu, R. P.; Hesk, D.; Rivera, N.; Pelczer, I.; Chirik, P. J., *Nature* **2016**, *529*, 195.

[125] Palmer, W. N.; Chirik, P. J., *ACS Catal.* **2017**, *7*, 5674.

[126] Loh, Y. Y.; Nagao, K.; Hoover, A. J.; Hesk, D.; Rivera, N. R.; Colletti, S. L.; Davies, I. W.; MacMillan, D. W. C., *Science* **2017**, *358*, 1182.

[127] Shu, A. Y. L.; Chen, W.; Heys, J. R., *J. Organomet. Chem.* **1996**, *524*, 87.

[128] Heys, J. R., *J. Label Compd. Radiopharm.* **2007**, *50*, 770.

[129] Gusev, D. G.; Berke, H., *Chem. Ber.* **1996**, *129*, 1143.

[130] Penning, T. D.; Talley, J. J.; Bertenshaw, S. R.; Carter, J. S.; Collins, P. W.; Docter, S.; Graneto, M. J.; Lee, L. F.; Malecha, J. A.; Miyashiro, J. M.; Rogers, R. S.; Rogier, D. J.; Yu, S. S.; Anderson, G. D.; Burton, E. G.; Cogburn, J. N.; Gregory, S. A.; Koboldt, C. M.; Perkins, W. E.; Seibert, K.; Veenhuizen, A. W.; Zhang, Y. Y.; Isakson, P. C., *J. Med. Chem.* **1997**, *40*, 1347.

[131] Arduengo, A. J.; Harlow, R. L., Kline, M., *J. Am. Chem. Soc.* **1991**, *113*, 361.

[132] Glorius, F. (ed.), *Top. Organomet. Chem.* **2007**, 231p.

[133] Fürstner, A.; Alcarazo, M.; César, V.; Lehmann, C. W., *Chem. Commun.* **2006**, 2176.

[134] Herrmann, W. A.; Köcher, C., *Angew. Chem. Int. Ed.* **1997**, *36*, 2162.

[135] Hopkinson, M. N.; Richter, C.; Schedler, M.; Glorius, F., *Nature* **2014**, *510*, 485.

[136] Salvi, N.; Belpassi, L.; Tarantelli, F., *Chem. Eur. J.* **2010**, 16, 7231.

[137] Marchione, D.; Belpassi, L.; Bistoni, G., Macchioni, A.; Tarantelli, F.; Zuccacia, D., *Organometallics* **2014**, *33*, 4200.

[138] Jahnke, M. C.; Hahn, F. E., *Top. Organomet. Chem.* **2010**, *30*, 95.

[139] Imamoto, T.; Tamura, K.; Zhang, Z.; Horiuchi, Y.; Sugiya, M.; Yoshida, K.; Yanagisawa, A.; Gridnev, I. D., *J. Am. Chem. Soc.* **2012**, *134*, 1754.

[140] Surry, D. S.; Buchwald, S. L., *Chem. Sci.* **2011**, *2*, 27.

[141] Tang, W.; Zang, X., *Chem. Rev.* **2003**, *103*, 3029.

[142] Dunne, B. J.; Morris, R. B.; Orpen, A. G., *J. Chem. Soc. Dalton Trans.* **1991**, 653.

[143] Poater, A.; Cosenza, B.; Correa, A.; Giudice, S.; Ragone, F.; Scarano, V.; Cavallo, L., *Eur. J. Inorg. Chem.* **2009**, 1759.

[144] Clavier, H.; Nolan, S. P., *Chem. Commun.* **2010**, *46*, 841.

[145] Tolman, C. A., *Chem. Rev.* **1977**, *77*, 313.

[146] Kelly, R. A.; Clavier, H.; Giudice, S.; Scott, N. M.; Stevens, E. D.; Bordner, J.; Samardjiev, I.; Hoff, C. D.; Cavallo, L.; Nolan, S. P., *Organometallics* **2008**, *27*, 202.

[147] Dorta, R.; Stevens, E. D.; Scott, N. M.; Costabile, C.; Cavallo, L.; Hoff, C. D.; Nolan, S. P., *J. Am. Chem. Soc.* **2005**, *127*, 2485.

[148] Bowen, J. P.; Sorensen, J. B.; Kirschner, K. N., *J. Chem. Educ.* **2007**, *84*, 1225.

[149] Nelson, D. J.; Nolan, S. P., *Chem. Soc. Rev.* **2013**, *42*, 6723.

[150] Krygowski, T. M.; Stępień, B. T., *Chem. Rev.* **2005**, *105*, 3482.

[151] Ananikov, V. P.; Musaev, D. G.; Morokuma, K., *Eur. J. Inorg. Chem.* **2007**, 5390.

[152] Falivene, L.; Credendino, R.; Poater, A.; Petta, A.; Serra, L.; Oliva, R.; Scarano, V.; Cavallo, L., *Organometallics* **2016**, *35*, 2286.

[153] Kühl, O., *Chem. Soc. Rev.* **2007**, *36*, 592.

[154] Brill, M.; Kühnel, E.; Scriban, C.; Rominger, F.; Hofmann, P., *Dalton Trans.* **2013**, *42*, 12861.

[155] Quan, X.; Kerdphon, S.; Andersson, P. G., *Chem. Eur. J.* **2015**, *21*, 3576.

[156] Marchenko, A. P.; Koidan, H. N.; Huryeva, A. N.; Zarudnitskii, E. V.; Yurchenko, A. A.; Kostyuk, A. N., *J. Org. Chem.* **2010**, *75*, 7141.

[157] Wolf, J.; Labande, A.; Natella, M.; Daran, J. C.; Poli, R., *J. Mol. Cat. A- Chem.* **2006**, *259*, 205.

[158] Marchenko, A.; Koidan, G.; Hurieva, A. N.; Vlasenko, Y.; Kostyuk, A.; Biffs, A., *Organometallics* **2016**, *35*, 762.

[159] Wheaton, C. A.; Bow, J. P. J.; Stradiotto, M., *Organometallics* **2013**, *32*, 6148.

[160] Reid, M., *On the Design and Further Applications of Iridium(I) Complexes in Hydrogen Isotope Exchange Processes*, Ph. D Thesis, University of Strathclyde, **2015**, 335p.

[161] Bappert, E.; Helmchen, G., *Synlett* **2004**, 1789.

[162] Passays, J.; Ayad, T.; Ratovelomanana-Vidal, V.; Gaumont, A. C.; Jubault, P.; Leclerc, E.; *Tetrahedron Asymmetr.* **2011**, *22*, 562.

[163] Becht, J. M.; Bappert, E.; Helmchen, G., *Adv. Synth. Catal.* **2005**, *347*, 1495.

[164] McKinstry, L.; Livinghouse, T., *Tetrahedron Lett.*, **1994**, *35*, 9319.

[165] Su, H. L.; Pérez, L. M.; Lee, S. J.; Reibenspies, J. H.; Bazzi, H. S.; Bergbreiter, D. E., *Organometallics* **2012**, *31*, 4063.

[166] Occhipinti, G.; Jensen, V. R.; Törnroos, K. W.; Frøysten, N. A.; Bjørsvik, H. R., *Tetrahedron,* **2009**, *65*, 7186.

[167] Gardiner, M. G.; Herrmann, W. A.; Reisinger, C. P.; Schwarz, J.; Spiegler, M., *J. Organomet. Chem.*, **1999**, *572*, 239.

[168] Allen, D. W., *Organophosphorus Chem.*, **2015**, *44*, 1.

[169] Baker, K. V.; Brown, J. M.; Hughes, N.; Skarnulis, A. J.; Sexton, A., *J. Org. Chem.*, **1991**, *56*, 698.

[170] Stylianides, N.; Danopoulos, A. A.; Tsoureas, N., *J. Organomet. Chem.*, **2005**, *690*, 5948.

[171] Field, L. D.; Messerle, B. A.; Vuong, K. Q.; Turner, P., *Organometallics*, **2005**, *24*, 4241.

[172] Li, J. Q.; Andersson, P. G, *Chem. Commun.* **2013**, *49*, 6131.

[173] Lin, I. J. B.; Vasam, C. S., *Coord. Chem. Rev.*, **2007**, *251*, 642.

[174] Tsoureas, N.; Danopoulos, A. A.; Tulloch, A. A. D.; Light, M. E., *Organometallics* **2003**, *22*, 4750.

[175] Danopoulos, A. A.; Winston, S.; Gelbrich, T.; Hursthouse, M. B.; Tooze, R. P., *Chem. Commun.* **2002**, 482.

[176] Lake, B. R. M.; Ariafard, A.; Willans, C. E., *Chem. Eur. J.* **2014**, *20*, 12729.

[177] Wheaton, C. A.; Stradiotto, M., *Can. J. Chem.* **2013**, *91*, 755.

[178] Torres, O.; Martín, M.; Sola, E., *Organometallics*, **2009**, *28*, 863.

[179] Cotton, F. A.; Wilkinson, G., *Advanced Inorganic Chemistry: A Comprehensive Text*. New York: Wiley-Interscience; 1980, 4th ed., 1396p.

[180] Atkins, P.; Overton, T.; Rourke, J.; Weller, M.; Armstrong, F.; Hagerman, M., *Shriver & Atkins' Inorganic Chemistry*. New York: W. H. Freeman and Company; 2010, 824p.

[181] Dobereiner, G. E.; Nova, A.; Schley, N. D.; Hazari, N.; Miller, S. J.; Eisenstein, O.; Crabtree, R. H., *J. Am. Chem. Soc.* **2011**, *113*, 7547.

[182] Gründemann, S.; Kovacevic, A.; Albrecht, M.; Faller, J. W.; Crabtree, R. H., *Chem. Commun.* **2001**, 2274.

[183] Findlater, M.; Bernskoetter, W. H.; Brookhart, M., *J. Am. Chem. Soc.* **2010**, *132*, 4534.

[184] Goldberg, J. M.; Cherry, S. D. T.; Guard, L. M.; Kaminsky, W.; Goldberg, K. I.; Heinekey, D. M., *Organometallics* **2016**, *35*, 3546.

[185] Crabtree, R. H., *Chem. Rev.* **2016**, *116*, 8750.

[186] Crabtree, R. H.; Lavin, M.; Bonneviot, L., *J. Am. Chem. Soc.* **1986**, *106*, 4032.

[187] Pons, V.; Heinekey, M., *J. Am. Chem. Soc.* **2003**, *125*, 8428.

[188] Schultz, K. M.; Goldberg, K. I.; Gusev, D. G.; Heinekey, D. M., *Organometallics* **2011**, *30*, 1429.

[189] Andrae, R.; Häußermann, U.; Dolg, M.; Stoll, H.; Preuß, H., *Theor. Chim. Acta* **1990**, *77*, 123.

[190] Feng, M.; Tang, B.; Liang, S. H.; Jiang, X., *Curr. Top. Med. Chem.* **2006**, *16*, 1200.

[191] Ghosh, A. K.; Brindisi, M., *J. Med. Chem.* **2015**, *58*, 2895.

[192] Hroboňová, K.; Lehotay, J.; Čižmárik, J.; Armstrong, D. W., *J. Pharm. Biomed. Anal.* **2002**, *30*, 875.

[193] Skoldinov, A. P.; Kaverina, N. V.; Gritsenko, A. N.; Lyskovtsev, V. V.; Wunderlich, H.; Stark, A.; Zenker, A.; Loman, D.; Poppe, H.; Barch, R., *Pharm. Chem. J.* **1996**, *30*, 166.

[194] Meanwell, N. A., *J. Med. Chem.* **2011**, *54,* 2529.

[195] Langlois, M.; Fischmeister, R., *J. Med. Chem.* **2003**, *46*, 319.

[196] Bulic, B.; Pickhardt, M.; Mandelkow, E., *J. Med. Chem.* **2013**, *46*, 4135.

[197] Hansch, C.; Leo, A.; Taft, R. W., *Chem. Rev.* **1991**, *91*, 165.

[198] *Some Aromatic Amines, Organic Dyes, and Related Exposures*; IARC Monographs on the Evaluation of Carcinogenic Risks to Humans, Vol. 99; International Agency for Research on Cancer: Lyon, France, 2010; pp 1−658.

[199] Birch, A. M.; Groombridge, S.; Law, R.; Leach, A. G.; Mee, C. D.; Schramm, C., *J. Med. Chem.* **2012**, *55*, 3923.

[200] Hopmann, K. H., *Organometallics* **2016**, *35*, 3795.

[201] Gómez-Gallego, M.; Sierra, M. A., *Chem. Rev.* **2011**, *111*, 4857.

[202] McNaught A. D.; Wilkinson, A., *IUPAC Compendium of Chemical Terminology*, 2nd ed. Oxford: Blackwell Scientific Publications; 2014, pp.1444-5.

[203] Peterson, T. H.; Golden, J. T.; Bergman, R. G., *J. Am. Chem. Soc.* **2001**, *123*, 455.

[204] Churchill, D. G.; Janak, K. E.; Wittenberg, J. S.; Parkin, G., *J. Am. Chem. Soc.* **2003**, *125*, 1403.

[205] Reed, A. E.; Curtiss, L. A.; Weinhold, F., *Chem. Rev.* **1988**, *88*, 899.

[206] Hirsch, R. F., *Anal. Chem.* **1977**, *49*, 691.

[207] Walsh, P. J.; Kozlowski, M. C., *Fundamentals of Asymmetric Catalysis*. Sausalito: University Science Books; 2009, pp.114-164.

[208] Durbin, J.; Watson, G. S., *Biometrika* **1951**, *38*, 159.

[209] Joshi, R. A.; Gurjar, M. K.; Tripathy, N. K., *Org. Process. Res. Dev.* **2001**, *5*, 176.

[210] Zong, Y.; Hu, J.; Sun, P.; Jiang, X., *Synlett* **2012**, *23*, 2393.

[211] Quasdorf, K. W.; Riener, M.; Petrova, K. V.; Garg, N. K., *J. Am. Chem. Soc.* **2009**, *131*, 17748.

[212] Brookhart, M.; Green, M. L. H.; Parkin, G., *P. Nat. Acad. Sci.* **2007**, *104*, 6908.

[213] Wolf, J.; Labande, A.; Daran, J. C.; Poli, R., *J. Organomet. Chem.* **2006**, *691*, 433.

[214] Quan, X.; Kerdphon, S.; Andrsson, P. G., *Chem. Eur. J.* **2015**, *25*, 3576.

[215] Yip, K. T.; Yang, M.; Law, K. L.; Zhu, N. Y.; Yang, D., *J. Am. Chem. Soc.* **2006**, *128*, 3130.

[216] Li, H. X.; Zhao, W.; Li, H. Y.; Xu, Z. L.; Wang, W. X.; Lang, J. P., *Chem. Commun.* **2013**, *49*, 4259.

[217] Moon, S. Y.; Kim, U. B.; Sung, D. B.; Kim, W. S., *J. Org. Chem.* **2015**, *80*, 1856.

[218] Davis, M. C.; Groshens, T. J., *Tetrahedron Lett* **2012**, *53*, 4154.

[219] Xiong, T.; Li, Y.; Lv, Y.; Zhang, Q., *Chem. Commun.* **2010**, *46*, 6831.

[220] Ma, F.; Xie, X.; Zhang, L.; Peng, Z.; Ding, L.; Fu, L.; Zhang, Z., *J. Org. Chem.* **2012**, *77*, 5279.

[221] Medina-Ramos, W.; Mojica, A.; Cope, E. D.; Hart, R. J.; Pollet, P.; Eckert, C. A.; Liotta, C. L., *Green Chem.* **2014**, *16*, 2147.

[222] Ren, L.; Jiao, N., *Chem. Commun.* **2014**, *50*, 3706.

[223] Wan, Y.; Gray, N. S. (Novartis AG); WO2007/016228 A2, **2007**.

[224] Belleza, F.; Cipiciani, A.; Ruzziconi, R.; Spizzichino, S., *Fluorine Chem.* **2008**, *129*, 97.

[225] Vilaivan, T., *Tetrahedron Lett.* **2006**, *47*, 6739.

[226] Reddy, N. V.; Prasad, K. R.; Reddy, P. S.; Kantam, M. L.; Reddy, K. R., *Org. Biomol. Chem.* **2014**, *122*, 175-2175.

[227] Augustine, J. K.; Bombrun, A.; Mandal, A. B.; Alagarsamy, P.; Atta, R. N.; Selvam, P., *Synthesis* **2011**, *9*, 1477.

[228] Dai, Q.; Li, P.; Ma, N.; Hu, C., *Org. Lett.* **2016**, *18*, 5560.

[229] Jensen, T.; Pedersen, H.; Bang-Andersen, B.; Madsen, R.; Jørgensen, M., *Angew. Chem. Int. Ed.* **2008**, *47*, 888

[230] Lebel, H.; Leogane, O., *Org. Lett.* **2006**, *8*, 5717.

[231] Gould, S. J.; Eisenberg, R. L., *J. Org. Chem.* **1991**, *56*, 6666

[232] Sokolovs, I.; Lubriks, D.; Suna, E., *J. Am. Chem. Soc.* **2014**, *136*, 6920.

[233] Rauf, W.; Thompson, A. L.; Brown, J. M., *Chem. Commun.* **2009**, 3874.

[234] Guilarte, V.; Catroviejo, M. P.; García, P. G.; Rodríguez, M. A. F., Sanz, R., *J. Org. Chem.* **2011**, *76*, 3416.

[235] Ghodsinia, S. S. E.; Akhlaghinia, B., *Phosphorus Sulfur* **2016**, *191*, 104.

[236] Lo, H. J.; Lin, C. Y.; Tseng, M. C.; Chein, R. J., *Angew. Chem. Int. Ed.* **2014**, *53*, 9026.

[237] Clayden, J.; Helliwell, M.; McCarthy, C.; Westlund, N., *J. Chem. Soc., Perkin Trans. 1* **2000**, 3232.

[238] Hutchby, M.; Houlden, C. E.; Ford, J. G.; Tyler, S. N. G.; Gagné, M. G.; Lloyd-Jones, G. C.; Booker-Milburn, K. I., *Angew. Chem. Int. Ed.* **2009**, *48*, 8721.

[239] Yamazaki, K.; Kawamorita, S.; Omiya, H.; Sawamura, M., *Org. Lett.* **2010**, *12*, 3978.

[240] Cerecetto, H.; Di Maio, R.; Ibarruri, G.; Seoane, G.; Denicola, A.; Peluffo, G.; Quijano, C.; Paulino, M., *Il Farmaco* **1998**, *53*, 89.

[241] Xiong, W.; Qi, C.; Guo, T.; Zhang, M.; Chen, K.; Jiang, H., *Green Chem.* **2017**, *19*, 1642.

[242] Milburn, R. R.; Snieckus, V., *Angew. Chem. Int. Ed.* **2004**, *43*, 892.

[243] Hooker, J. M.; Reibel, A. T.; Hill, S. M.; Schueller, M. J., *Angew. Chem. Int. Ed.* **2009**, *48*, 3482.

[244] Yang, Q.; Robertson, A.; Alper, R., *Org. Lett.* **2008**, *10*, 5079.

[245] Zaitsev, V. G.; Daugulis, O., *J. Am. Chem. Soc.* **2005**, *127*, 4156.

[246] Andraos, J., *J. Chem. Educ.* **1996**, *73*, 150.

[247] Gaussian 09, Revision D.01, Frisch, M. J.; Trucks, G. W.; Schlegel, H. B.; Scuseria, G. E.; Robb, M. A.; Cheeseman, J. R.; Scalmani, G.; Barone, V.; Mennucci, B.; Petersson, G. A.; Nakatsuji, H.; Caricato, M.; Li, X.; Hratchian, H. P.; Izmaylov, A. F.; Bloino, J.; Zheng, G.; Sonnenberg, J. L.; Hada, M.; Ehara, M.; Toyota, K.; Fukuda, R.; Hasegawa, J.; Ishida, M.; Nakajima, T.; Honda, Y.; Kitao, O.; Nakai, H.; Vreven, T.; Montgomery, J. A., Jr.; Peralta, J. E.; Ogliaro, F.; Bearpark, M.; Heyd, J. J.; Brothers, E.; Kudin, K. N.; Staroverov, V. N.; Kobayashi, R.; Normand, J.; Raghavachari, K.; Rendell, A.; Burant, J. C.; Iyengar, S. S.; Tomasi, J.; Cossi, M.; Rega, N.; Millam, J. M.; Klene, M.; Knox, J. E.; Cross, J. B.; Bakken, V.; Adamo, C.; Jaramillo, J.; Gomperts, R.; Stratmann, R. E.; Yazyev, O.; Austin, A. J.; Cammi, R.; Pomelli, C.; Ochterski, J. W.; Martin, R. L.; Morokuma, K.;

Zakrzewski, V. G.; Voth, G. A.; Salvador, P.; Dannenberg, J. J.; Dapprich, S.; Daniels, A. D.; Farkas, Ö.; Foresman, J. B.; Ortiz, J. V.; Cioslowski, J.; Fox, D. J. Gaussian, Inc., Wallingford CT, 2009.

[248] Zhao, Y.; Truhlar, D. G., *Theor. Chem. Acc.* **2008**, *120*, 215.

[249] Peng, C.; Schlegel, H. B., *Israel J. Chem.* **1993**, *33*, 449.

[250] GaussView, Version 5.0.9, Dennington, R.; Keith, T.; Millam, J., Semichem Inc., Shawnee Mission, KS, 2009.

CHAPTER 2

Hydroarylation of Olefins: Development and Applications

1. Introduction

Throughout Chapter 1 we explored a rather simple, and yet powerful premise in transition metal catalysis, *i.e.*, by exploiting C—H activation to generate reactive metallocyclic intermediates, we were able to engage a transient Ir—C bond in further reactions. In that instance, our aim was to develop efficient processes for HIE, thus requiring that the key metallacycle participated in a second reaction with molecular D_2. During our investigations, we reviewed in some depth the requirements for productive C—H activation and the nature of 5- and 6-membered metallacycles of iridium.

From the fundamental understanding gathered throughout these studies, we envisioned that our novel iridium complexes could be strategically employed to promote transformations with reactive partners other than molecular deuterium, thus affording a second avenue into synthetically useful protocols. This desire led us to quickly identify sequential C—H activation and C—C bond formation protocols as a synthetically valuable extension of our current research. The development of a viable catalytic system to accomplish this endeavour, and the theoretical investigation of the process thus discovered, are the subjects of the present discussion.

1.1 Transition Metal-Catalysed C—H Functionalisation

Encompassing the own definition of an organic compound, C—H bonds are ubiquitous in both naturally occurring and synthetic molecules.[1] Unsurprisingly, the capacity to selectively exploit C—H bonds to construct C—X bonds (X = B, C, N, O) represents one of the most traditional goals of chemistry and remains a subject of intensive research.

Historically, initial examples of C—H activation by stoichiometric metalation reactions employing Ni,[2] Pd and Pt[3] salts date from the 1960s. These early examples were regarded as serendipitous,[4] and their progression to catalytic systems that could

construct C—X bonds was hampered by a profound lack of mechanistic knowledge at that time.[5] Since these pioneering investigations, which demonstrated transition metal complexes could be employed to directly functionalise otherwise chemically inert C—H bonds, this field gained substantial traction, with more contemporaneous methods being regarded as standard transformations in organic chemistry.[1] Scheme 2.1 presents a few examples, bearing both historical and synthetic relevance, that accomplish C—H activation.

The transformations presented in Scheme 2.1 provide a broad summary of both the synthetic potential of these versatile reactions, and the inherent complexity of the task at hand, *viz.*, selectively engage less reactive C—H bonds in a productive reaction pathway whilst avoiding other chemically active functional groups within the molecular scaffold.
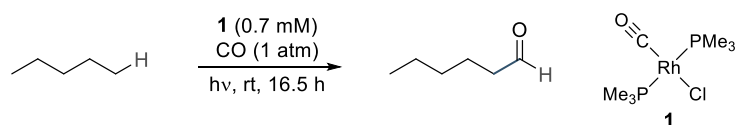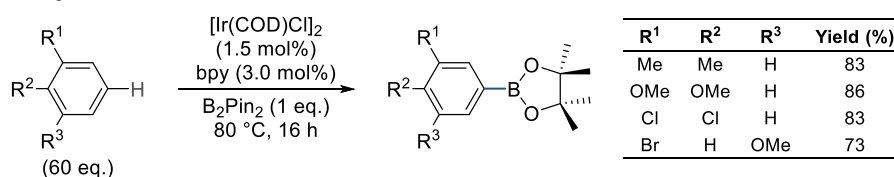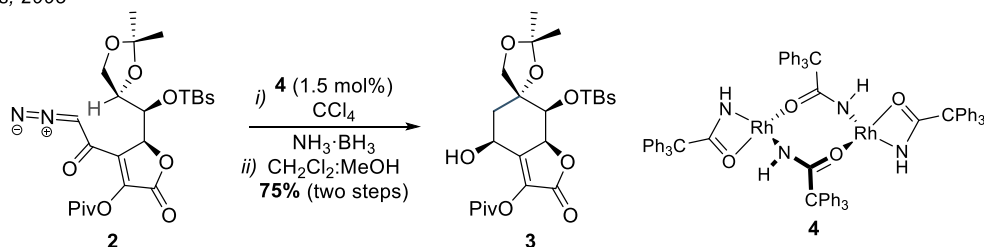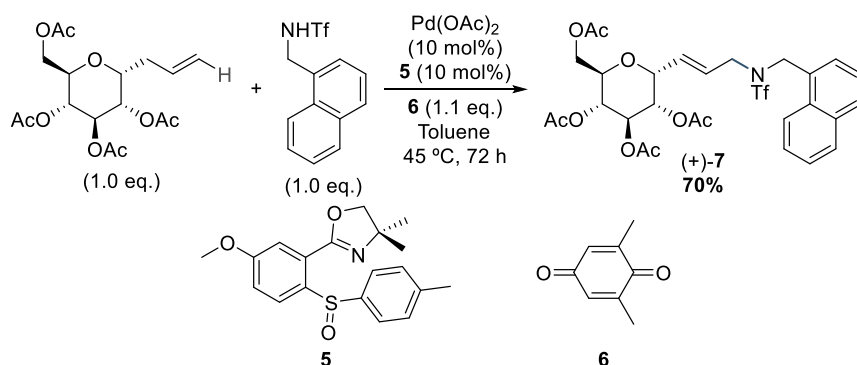
Scheme 2.1: Examples of catalytic C—H functionalisation.[†6-9]

[†]bpy – bipyridine.

In this regard, several strategies emerged throughout the last four decades of intensive research in this subject.[5,10] Amongst these, it is often possible to identify the presence of at least one of the following fundamental aspects:[10-12] i) shielding of the metal centre by sterically congested ligands, typically required to improve stability of reactive intermediates or, conversely, enhance selectivity in undirected C—H activation processes;[12] ii) assistance by ligation to neighbouring groups, effectively directing the reactive metal species towards a desired C—H fragment;[12] iii) exploitation of the inherently higher reactivity of C—H bonds in close proximity to more reactive functionalities to impart selectivity.[11] Once again, Scheme 2.1 exemplifies systems that applied these ideas to solve synthetic challenges and accomplish C—H activation by different means.

Thus, Tanaka *et al.*[6] explored the high reactivity of coordinatively unsaturated Rh^{III} centres, formed upon photoexcitation of **1**, to effect C—H activation through oxidative addition of rather inert terminal bonds in pentane. A subsequent migratory insertion into a CO ligand would then deliver hexanal, in one of the first examples of selective carbonylation of alkanes.

Miyaura, Hartwig and their co-workers,[7] in an earlier disclosure of the now well-developed C—H borylation reactions, were unable to determine whether a σ-bond metathesis at an Ir(III) boryl complex, or a direct oxidative addition to afford an Ir^{V} intermediate, was responsible for the C—H bond cleavage that precedes C—B bond formation.[7,13]

In an elegant instance of application of rhodium carbenoids to promote C—H insertion into the Rh—C bond, Du Bois *et al.* exploited the presence of a neighbouring methyne proton in **2** to perform a challenging cyclisation which, after 1,2-reduction of the resulting enone, afforded **3**, a key intermediate in their total synthesis of (–)-tetrodotoxin.[8] Finally, White *et al.* employed a concerted metalation-deprotonation mediated by acetate ligands in Pd(OAc)$_2$ to form a key (η^3-allyl)palladium complex which, in turn, undergoes nucleophilic substitution with triflamides to generate the sugar derivative (+)-**7** in good yield.[9]

In addition to their synthetic utility, some other features of transition metal-catalysed C—H functionalisation strategies warrant further discussion. Firstly, by avoiding the need to introduce more reactive C—X bonds (X = Cl, Br, I, OTf, and other pseudo-

halides), thus providing access to classical organic methods, these protocols shorten synthetic routes, often improving atom economy throughout the synthesis.[1,10-12] Secondly, the presence of a transition metal mediator introduces the opportunity to perform enantioselective processes by means of strategic selection of chiral ancillary ligands.[14,15] Finally, by exploring reaction manifolds that are inaccessible to conventional transition metal-free processes, C—H functionalisation methods can effect unique transformations based on disconnections that are currently not possible by a combination of classical protocols.[1,11,12,16] These principles are exemplified in Schemes 2.2 and 2.3
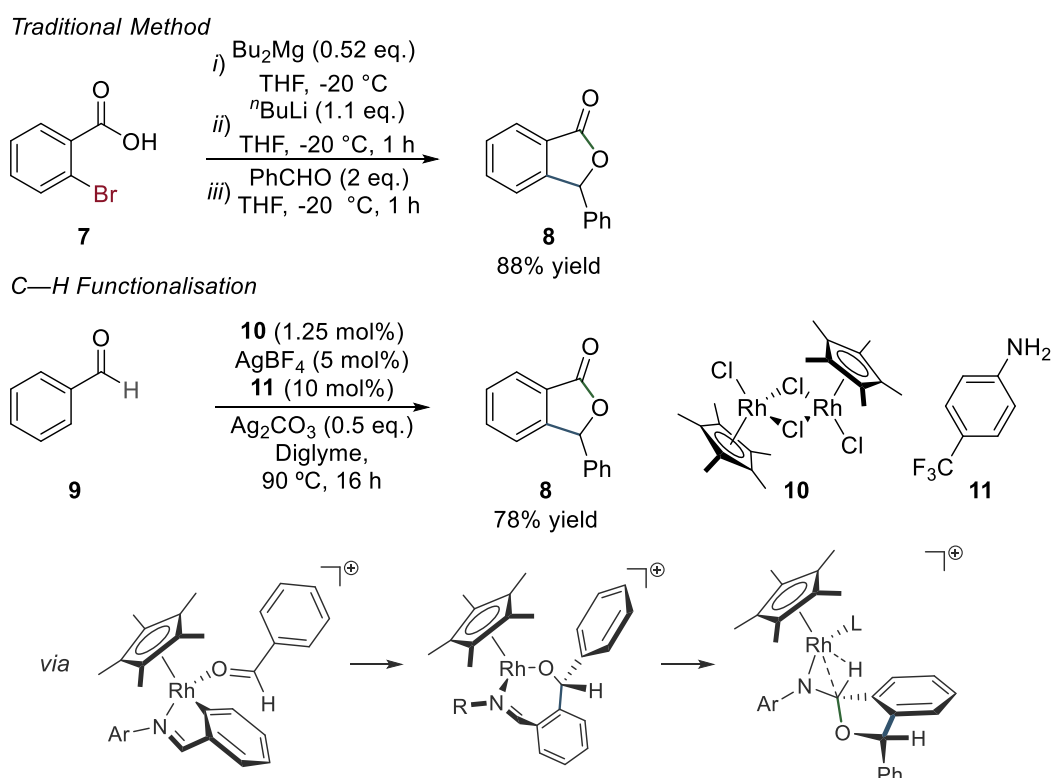
Scheme 2.2: Contrasting a traditional[17] method with a C—H functionalisation[18]

Hence, the examples in Scheme 2.2 demonstrate different approaches to isobenzofuranone **8**. A representative traditional method constructed heterocycle **8** *via* a reaction sequence involving initial formation of a magnesium dicarboxylate, lithium-halogen exchange and quenching with benzaldehyde to afford the lactam ring in **8**.[17] This method requires superstoichiometric quantities of base metals, uses a

halogenated starting material, and employs a 2-fold excess of benzaldehyde to produce **8** in 88% yield.

Conversely, a C—H functionalisation protocol achieved the same transformation *via* enamine-assisted rhodium catalysis, thus building the target bicycle through sequential C—H activation, two migratory insertions into the polarised π bonds to construct the C—C and C—O bonds, β-hydride elimination and aldimine hydrolysis, delivering **8** in 78% yield.[18] In this overall rhodium-catalysed dimerization of benzaldehyde, no halogenated starting material was employed, nor an excess of the electrophilic partner was required, streamlining the synthetic strategy and broadening functional group tolerance.

Asymmetric C—H Actviation

R[1]	Yield (%)	*ee* (%)
4-ClC$_6$H$_4$	80	95
2-MeC$_6$H$_4$	90	97
1-Naphthyl	84	97
Me	75	88
Et	66	95

Cascade C—H Activation / Carbonylation / Lactamisation
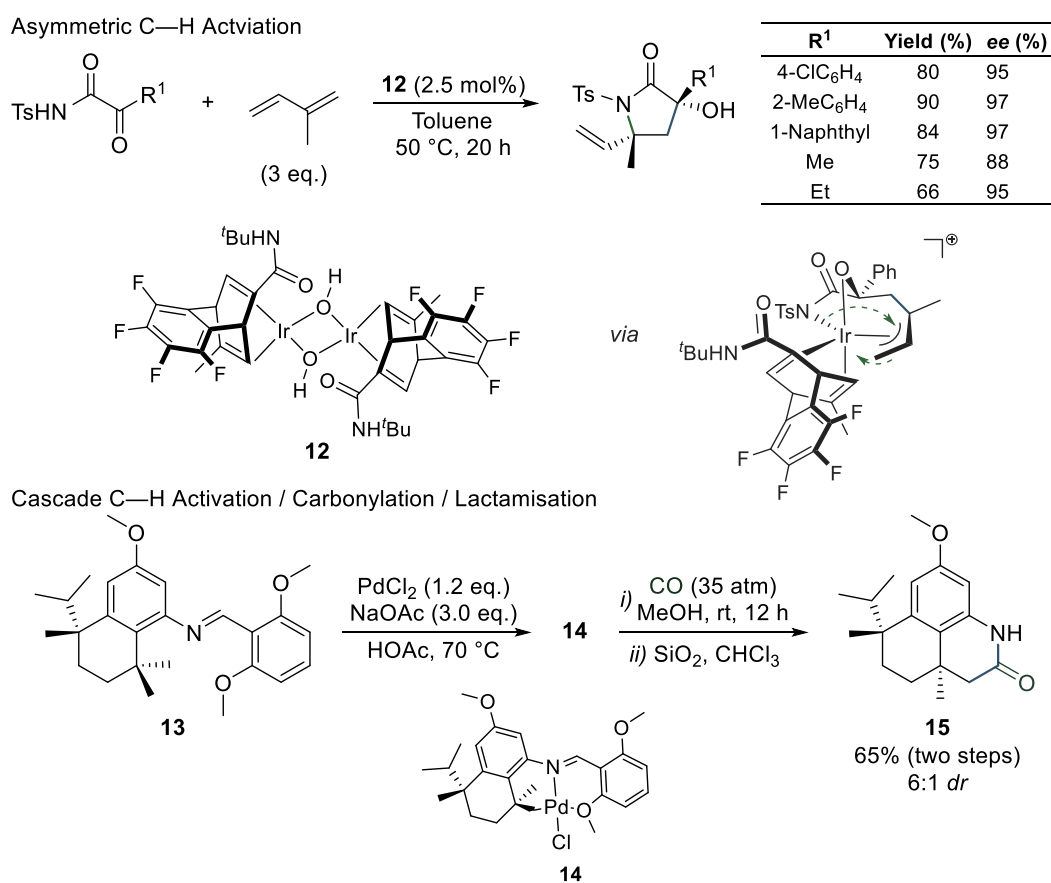
Scheme 2.3: Examples of enantioselective[19] and novel cascade[20] processes.

Yet another significant advantage of C—H functionalisation reactions is exemplified by the asymmetric synthesis of 3-hydroxy-2-pyrrolidinones mediated by iridium catalyst **12**,[19] depicted in Scheme 2.3. This process swiftly introduces molecular

complexity, employing the inexpensive isoprene as a coupling partner, and results in excellent enantiomeric excesses.

The final example illustrates a process which is currently not accessible through means other than C—H activation. In this regard, treatment of enamine **13** with Pd(OAc)$_2$ afforded palladacycle **14** which, upon exposure to carbon monoxide in methanol, and subsequent enamine hydrolysis, delivered tricyclic lactam **15** in 65% yield.[20] It is worth emphasising that the introduction of a (pseudo)halogen at the desired methyl group in **13**, which could provide access to existing carbonylative cyclisation methods,[21] is not viable. More specifically, classical radical-mediated protocols would likely engage in reactions with at least one of the 10 inherently more reactive C—H bonds within **13**, *i.e.*, 5 aromatic positions, 3 methoxide groups, and C—H fragments at the aldimine and isopropyl methyne positions.[22] Moreover, the location of the requisite methyl group, which is adjacent to a quaternary carbon atom, thus lacking nearby polarising functional groups that could render its hydrogen atoms acidic, precludes the application of traditional directed *ortho-* metalation protocols relying on lithium and magnesium bases in conjunction with electrophilic quenching with X$_2$ (X = Cl, Br, I).[23]

The examples presented throughout this section help demonstrate the outstanding versatility of C—H functionalisation, presenting a short account of challenges and strategies related to selective C—H bond activation methods. Detailed mechanistic knowledge of these systems, gathered through intensive research over the last four decades, has resulted in a more mature field of organic chemistry that witnesses no shortage of applications. Of note, are methods that rely on C—H activation to construct new C—X bonds, with X most commonly representing boron,[24-29] nitrogen,[30-34] oxygen,[30,31,34,35] fluorine,[32,35-37] higher halogens[30,35,36] and, of special relevance to the present discussion, carbon.[11,32,35,38-47]

1.2 Harnessing C—H Activation to Construct C—C Bonds

The inherent capacity of C—H bond functionalisation to produce compounds with higher synthetic value in an atom economic fashion led to the development of several novel protocols which effectively replace the original hydrogen atom by a heavier

element, some of which were briefly addressed in Section 1.1. The importance of omnipresent C—C bonds to all fields of chemistry led to the development of a vast number of protocols which build these bonds through C—H activation.[38-47]

One of the core principles of these catalytic systems is the ability metallocyclic intermediates possess to engage in reactions with carbon-based electrophiles and nucleophiles.[48] This versatility has enabled several interesting applications in organic synthesis, some of which are illustrated in Scheme 2.4.
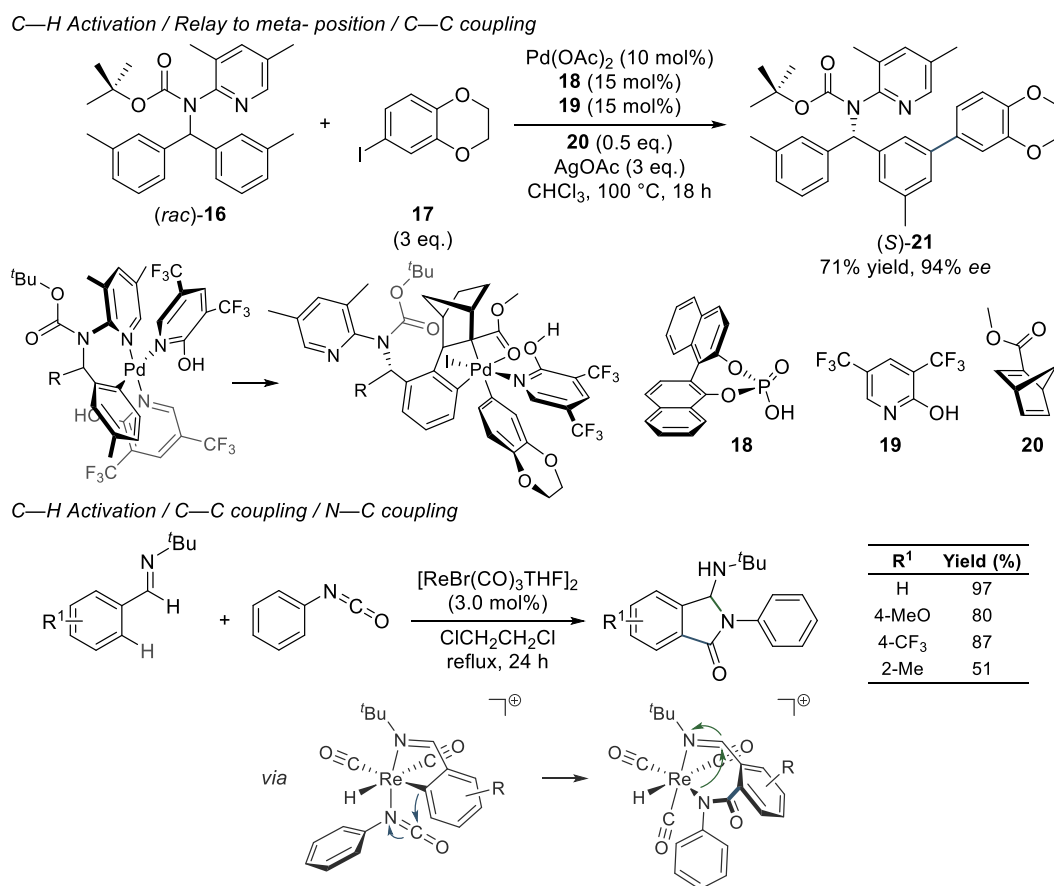
Scheme 2.4: C—H functionalisation protocols that build C—C bonds.[49,50]

Despite their remarkable synthetic utility, catalytic systems which endeavour to promote sequential C—H activation and C—C bond formation events must possess a series of properties, namely:

i)   Judicious choice of ancillary ligands is required to adjust the electronic properties of the metal centre involved in the C—H activation event. Furthermore, the mechanism responsible for the activation process

determines the extent of electron density required by a given metal.[11,12] For instance, C—H cleavage through direct oxidative addition requires electron-rich metal centres, thus being adequately enhanced by strong σ-donor ligands. Conversely, the same ligand set is likely to inhibit activation events that proceed through electrophilic metalation;[11]

ii)   Productive engagement of a coupling partner to effect C—C bond-formation is intrinsically dependent on steric and electronic properties of the metallocyclic intermediate in which the coupling takes place.[48] More specifically, whilst polydentate, sterically hindered ligands are best suited for C—C bond formation events which rely on nucleophilic attack at a coordinated ligand, the opposite is true for processes that employ electrophilic coupling partners, the latter requiring vacant coordination sites in the vicinity of the M—C bond;[11,48]

iii) The sequential nature of C—H functionalisation protocols requires transition metal complexes able to promote several distinct, and often conflicting, individual steps throughout the catalytic cycle. Therefore, it is imperative that an appropriate set of ancillary ligands and additives is employed to promote catalyst turnover and avoid side reactions that result in catalyst decomposition.[11,12]

Therefore, it is the strategic combination of a well-devised mechanistic rationale with a ligand set that adequately modulates the metal centre, accelerating the more cumbersome steps in the catalytic cycle, which enables the development of a successful catalytic system (please, refer to Chapter 1 for a discussion of topics on fundamental aspects of C—H activation and their mechanisms; and general properties of common ligands in catalysis).

A brief illustration of these factors is presented in Scheme 2.4 alongside synthetic applications which effect C—C bond formation employing ketones[51] and sulfinyl imines[52] as coupling partners to deliver high synthetic value.
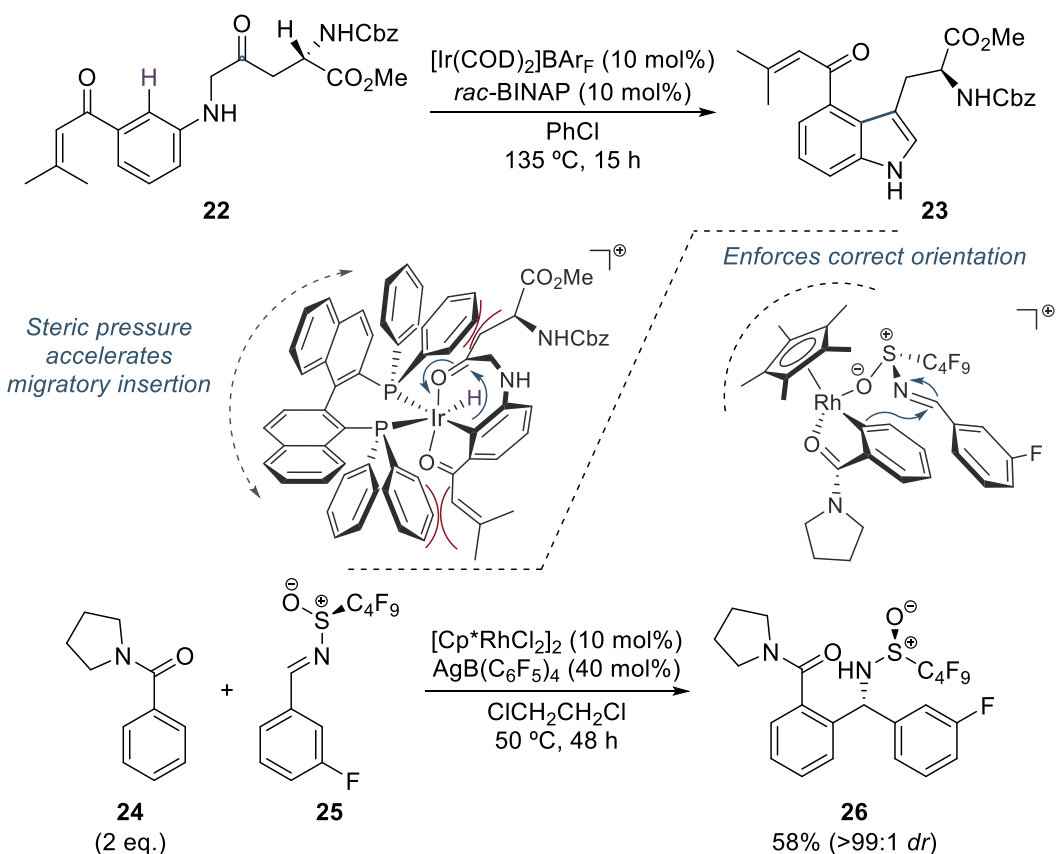
Scheme 2.4: Strategies for the synthesis of indoles[51] and chiral amines.[52]

The guiding principles presented throughout this section fostered successful application of C—H functionalisation in several C—C bond-forming processes exploiting a large array of coupling partners. Among these, polarised π bonds of type C=O and C=N,[44] carbon monoxide,[21,44,53] diazo-compounds,[54] organic halides[55-57] and pseudo-halides,[55,58] tin and boron derivatives,[55-57] as well as alkynes[55,59-68] and alkenes[14,44,55,59,66,68-70] are most commonly employed.

1.2.1 Hydroarylation of Olefins

Owing to the prominence of C—C cross-coupling protocols as efficient synthetic methods towards alkynes and alkenes,[71-75] and recent progress towards reactions that accomplish analogous transformations, whereby a C—H bond replaces one of the coupling partners (*vide supra*), significant efforts have been devoted to translating the broad applicability of the former to the field of C—H activation.[55,59-70]

Consequently, the last four decades of research have culminated in the development of two broad classes of C—H functionalisation protocols, *viz.*: oxidative methods, in which an external oxidant[69] or a sacrificial functional group[76] ensures preservation of the oxidation level of a given coupling partner;[69] and hydrogenative methods, whereby a metal hydride generated during the catalytic cycle returns the hydrogen atom to the substrate and effects an overall reduction of the unsaturated functionality.[70] Methodologies that rely on the latter operational principle are often prefixed with hydro-,[70,77] thus indicating its reductive nature.

Despite the relevance of oxidative protocols to the synthesis of alkynyl-[78-81] and alkenyl-[69] derivatives, a detailed discussion of their application and mechanistic aspects is outside the scope of the present work, with examples being included only when deemed pertinent.

Hydrogenative methods, on the other hand, are inherently endowed with a valuable synthetic opportunity. More specifically, when employed in conjunction with alkynes, these methods can result in stereospecific synthesis of olefins, whereby the geometric configuration depends on the nature of the carbometallation step.[64] Furthermore, when unsymmetrical alkenes are explored as coupling partners, a stereogenic centre can be formed,[70] possibly in a stereoselective fashion.[14,70] This additional factor enables expedient generation of molecular complexity, thus rendering hydrogenative methods valuable synthetic tools. Representative examples of both oxidative and reductive protocols are presented in Scheme 2.5.

Beyond offering aromatic C—H bonds as atom-economical and alternative coupling partners for traditional coupling methods, hydroarylation protocols offer unique synthetic opportunities. By typically requiring soft, electron-rich late transition metal centres to successfully engage in C—H activation,[11] these methods can be employed in complex reaction sequences that rely on well-understood catalytic principles, thus emerging as highly attractive approaches for the synthesis of natural products, pharmaceutical compounds and chemical commodities of industrial relevance.[82]

Oxidative, Sacrificial Group

R[1]	R[2]	Yield (%)
H	Si(Me)$_3$	62
CO$_2$Me	Ph	76
CO$_2$Me	^{n}Bu	64
CO$_2$Me	Si(Me)$_3$	90

Hydrogenative

R[3]	Yield (%)
C$_6$H$_5$	62
2-MeC$_6$H$_4$	76
4-FC$_6$H$_4$	64
1-Naphthyl	90

Synergistic, External Oxidant

R[4]	R[5]	n	Yield (%)
H	Ph	0	45
H	Me	1	73
5-F	Ph	1	60
6-Cl	Ph	1	65
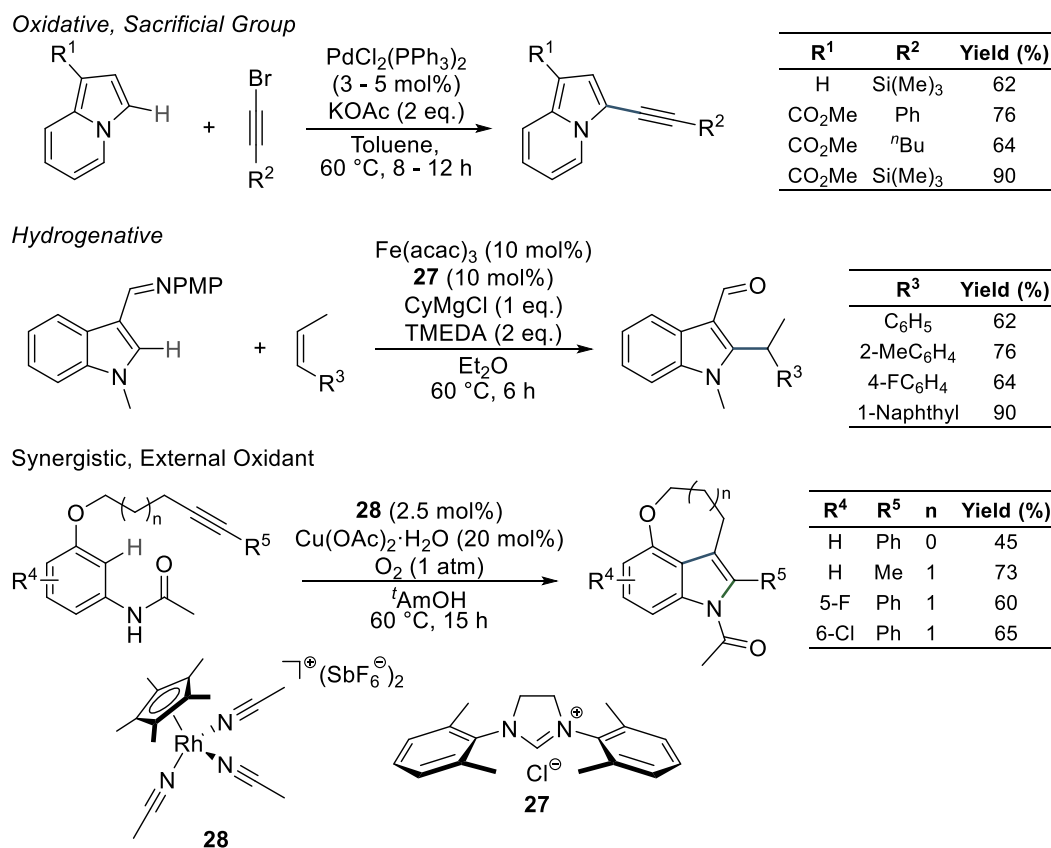
Scheme 2.5: Examples of hydroarylative methods.[†,78,83,84]

[†]For the iron-catalysed reaction (*centre*) the product is obtained after imine hydrolysis.

Unsurprisingly, this field experienced exceptional development since the seminal report by Murai *et al.*, in 1993, on the directed hydroarylation of aromatics employing hindered terminal olefins as coupling partners under ruthenium catalysis.[85] Since then, considerable effort has been devoted to expanding the applicability of these methods, with special focus on broadening substrate scope, modifying the regioselectivity to favour branched products, and introducing efficient asymmetric catalysts to afford enantioenriched compounds. Scheme 2.6 presents selected examples from Murai's system and illustrates two additional milestones witnessed in the last 25 years of intermolecular hydroarylation reactions.

1st Report, Murai 1993

R[1]	R[2]	R[3]	Yield (%)
Me	Me	H	100
Me	Me	CH$_2$TMS	100
Me	Me	^{t}Bu	99
^{t}Bu	H	Si(OEt)$_3$	100

RuH$_2$(CO)(PPh$_3$)$_3$
(2 - 6 mol%)
Toluene
110 °C

(1 - 6 eq.)
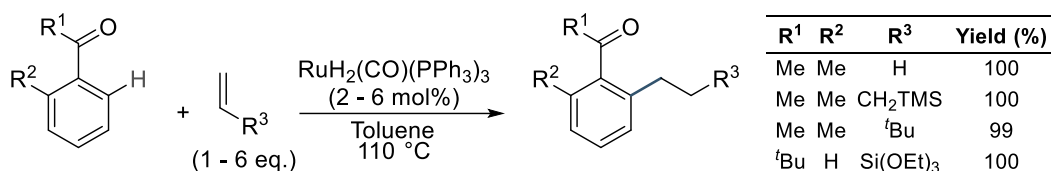
1st Branch-Selective, Yoshikai 2011

R[4]	R[5]	Yield (%)	b:l
3-OMe	H	67	>99:1
4-OMe	H	82	96:4
H	4-Me	93	>99:1
H	4-Ph	80	99:1

CoBr$_2$ (10 mol%)
PCy$_3$ (10 mol%)
TMSCH$_2$MgBr
(0.8 eq.)
THF, 60 °C
12 - 52 h
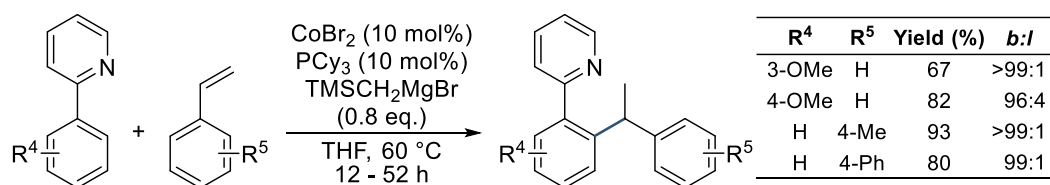
1st Enantioselective, Nishimura 2017

R[6]	R[7]	Yield (%)	ee (%)
Ph	Me	87	94
Ph	Bn	92	87
^{n}Pr	Bn	87	94
CO$_2$Et	Bn	87	78

[Ir(COD)Cl]$_2$ (2.5 mol%)
(R)-binap* (5 mol%)
NaBAr$_F$ (10 mol%)
Toluene, 60 - 80 °C
24 - 48 h

(1.1 eq.)
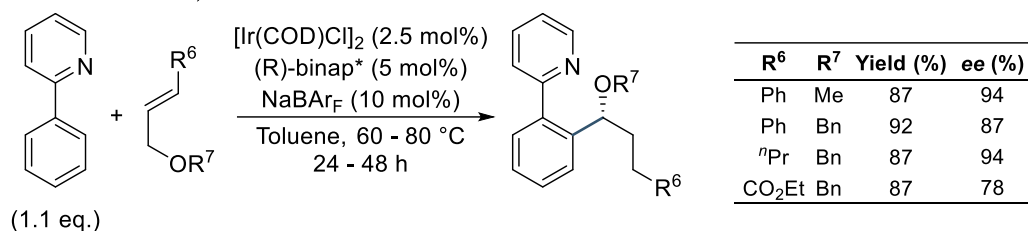
Scheme 2.6: Developments in intermolecular hydroarylation of olefins.[†85-87]

[†]b:l – branch to linear selectivity; (R)-Binap* -variant of (R)-Binap with PR$_2$ moieties where R = 3,5-(CH$_3$)$_2$-4-(CH$_3$O)C$_6$H$_2$; earlier enantioselective processes with < 85% *ee* were not included.[88,89]

Murai's seminal work relied on a directed C—H activation of aromatic ketones to afford stable ruthenacycles that, upon exposure to suitable terminal olefins bearing sterically hindered substituents, effected regioselective C—C bond-formation to afford linear products with remarkable efficiency.[85] Despite its importance as a pioneering method, the high tendency of ruthenium complexes to promote preferential Ru—H migratory insertion into olefins, over the alternative carbometallation process,[70] restricted the applicability of this protocol to the generation of linear products.

Notably, it took almost two decades for the disclosure of a catalytic method that could reverse the regioselective outcome of Murai-type reactions. Thus, Yoshikai *et al.* accomplished this task by careful selection of strong σ-donor ligands that released steric congestion around the cobalt centre.[86] In their contribution, they also disclosed the use of IMes as an alternative ligand which accomplished exquisite linear selectivity.[86] The authors rationalised the observed regiochemical outcome on the ability of the phosphine-ligated cobalt complex to stabilise a putative η^3-benzyl

intermediate, formed upon hydrometallation, that was a necessary species *en route* to branched products.[86] Later, detailed computational studies revealed that this phenomenon, although correct as far as the formation of a stable η^3-benzyl complex is concerned, is not responsible for defining the regioselectivity of the process.[90] Rather, it is steric destabilisation of the transition state associated with the subsequent C—C reductive elimination by the IMes ligand that drives the observed selectivity.[90]

Since Murai's report, other researchers have investigated different organometallic complexes, with special focus devoted to transition metal catalysts displaying higher preference for more synthetically valuable branched products. While pursuing this goal, Nishimura *et al.*[87] discovered the first general enantioselective method for the hydroarylation of styrene derivatives. Their iridium-based system employed a chiral bisphosphine of the BINAP family to impart chirality during the product- and enantio-determining C—C bond-forming step.[87] The authors attributed the high enantioselectivity of their process to a reaction pathway which proceeds through reversible hydrometallation prior to irreversible C—C reductive elimination, thus allowing equilibration of reactive intermediates which favours only one of the enantiomers.[87] Again, subsequent DFT studies contradicted Nishimura's original hypothesis. More specifically, implication of a preferential carbometallation of olefins over the competing Ir—H migratory insertion as the productive reaction pathway has received growing support by theoretical studies of similar reaction processes.[91,92] Indeed, Huang *et al.*[93] reported similar findings for Nishimura's stereoselective process, for which initial hydrometallation led to the formation of a stable metallacycle that does not proceed to energetically feasible C—C bond-formation. Instead, all pathways for sequential carbometallation followed by C—H reductive elimination led to lower energy barriers.[93]

These three seminal examples help illustrate both the complexity and versatility associated with directing group assisted hydroarylative processes. Focusing on the latter, several research groups reported reactions catalysed by different transition metal complexes, mainly based on Co,[86,89,94-99] Ni,[100-104] Ru,[85,105-111] Rh[112-121] and Ir,[87,122-133] although occasional reports of reactions with other metals can also be found.[70,82]

It is worth emphasising some clear distinctions in reactions catalysed by these transition metals. Firstly, hydroarylation of olefins is typically classified in three broad categories according to the reaction outcome,[70,82] *i.e.*, intramolecular processes, which afford cyclic products; and selective intermolecular transformations which generate either linear, or branched products. Importantly, enantioselective processes have been reported for both intra-[82] and branch-selective intermolecular systems.[70,82,87-89]

Secondly, distinct reaction mechanisms have been proposed for complexes based on different transition metals, with two slightly divergent pathways being largely accepted (*vide infra*). Thirdly, systems that rely on first-row transition metals, in particular Cr, Fe and Co, require stoichiometric or super-stoichiometric amounts of alkylmagnesium additives to ensure catalyst turnover,[70,82] thus hindering their functional group compatibility, and applicability to late stage functionalisation of complex molecular scaffolds. Finally, metals other than Ru, Rh, and Ir have only been successfully employed in the hydroarylation of substrates bearing strongly ligating *N*-heterocycles,[82] severely restricting their application to a narrow group of molecules. Scheme 2.7 depicts interesting applications disclosed within the last four decades featuring both inter- and intramolecular systems.

Thus, Ackermann *et al.* reported the first system able to perform hydroarylative reactions of methylenecyclopropanes without ring opening.[108] Even though the substrate scope features only four compounds, the authors demonstrate the remarkable ability of ruthenium complexes to retain strained three-membered rings under hydroarylation conditions. The authors attributed their findings to a regioselective Ru—H insertion, affording a terminal cyclopropenecarbinyl- ligand, followed by fast reductive elimination to retain the three-membered ring.[108]

The second example in Scheme 2.7 highlights another significant development in the field. More specifically, Bower *et al.* demonstrated one of the first generally applicable hydroarylation methods that affords branched products with high selectivity.[126,127] In their two initial contributions, they employed [Ir(COD)$_2$]X (X = BAr$_F$ or OTf) in conjunction with ligand **30,** a perfluorinated analogue of dppb, and collectively explored more than 40 substrates, which proceeded in high yields and good to excellent selectivity for the branched product.[126,127] Based on deuterium

labelling studies,[126] the authors unequivocally demonstrated that H/D scrambling between terminal and internal positions of styrene takes place under the reaction conditions, thus suggesting the observed high selectivity arises from an initial, reversible Ir—H migratory insertion followed by irreversible C—C reductive elimination (*vide infra* for a more detailed discussion on this subject).

Ackermann, 2008 - Linear-Selective

R^1	R^2	R^3	Yield (%)
H	Ph	H	53
OMe	Ph	H	78
H	H	CH$_2$	33
OMe	H	CH$_2$	85
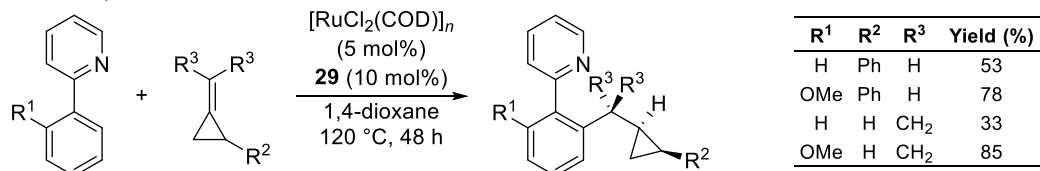
Bower, 2015 - Branch-Selective

R^4	R^5	Yield (%)
2-Me	Ph	73
4-Br	Ph	60
3-Me	Me	92
3-Me	^{i}Bu	99
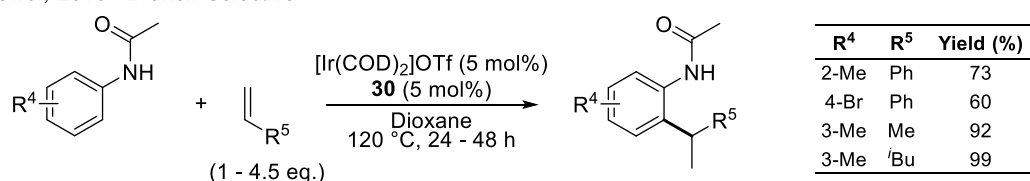
Cramer, 2014 - Enantioselective Intramolecular

R^6	R^7	Yield (%)	ee (%)
H	OBn	86	91
2-Me	OBn	94	93
3-Br	OBn	74	90
4-NO$_2$	OBn	51	82
H	Me	80	92

29

30

31
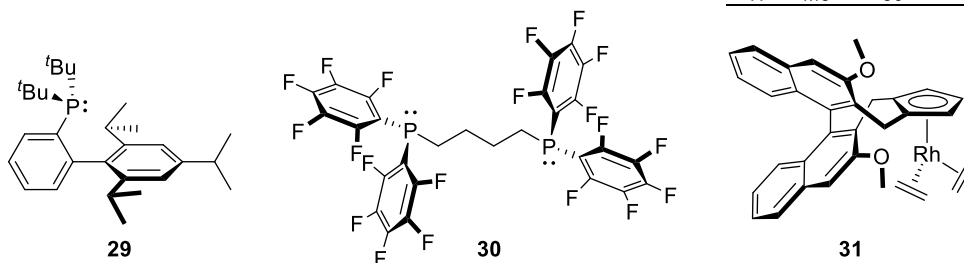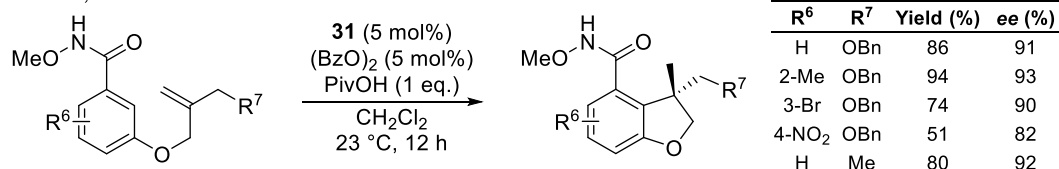
Scheme 2.7: Applications of hydroarylation of olefins.[108,119,127]

Finally, Cramer *et al.* elegantly demonstrated an enantioselective intramolecular hydroarylation of *N*-methoxybenzamides mediated by rhodium catalyst **31** that proceeds with high enantioselectivity.[119] Their remarkably mild reaction conditions likely stem from the use of a tailored *N*-methoxycarbonyl directing group, which is known to form a strong N—Rh bond upon coordination and deprotonation,[134,135] favouring cyclometallation at the *ortho-* position. Notably, the cyclopentadienyl ligand of **31**, previously disclosed by the same group,[136] was the first ligand set able

to promote both intra-[119] and intermolecular[136] reactions to afford enantioenriched cyclic products.

As demonstrated throughout this section, the hydroarylation of olefins remains a subject of intense scrutiny by the scientific community. By avoiding the need for pre-functionalisation of the aromatic partner prior to C—C cross-coupling, this process has large synthetic potential, in many cases offering viable alternatives to traditional palladium-catalysis. Most of its success stems from equally intense efforts to understand and control the various mechanistic aspects involved in these challenging processes.

1.2.2 Mechanistic Aspects

Some of the mechanistic features related to transformations presented in Section 1.2.1 have already been mentioned, but a more detailed exploration is warranted. Before we commence our discussion in this topic, however, it is worth emphasising that the term "hydroarylation" has been employed to describe three independent processes.[82] Namely, reactions that perform C—H activation *via* direct electrophilic metalation of electron-rich aromatics, thus forming a Wheland intermediate characteristic of a Friedel-Crafts mechanism, can engage in further reaction with olefins to afford alkylated compounds;[82] a second analogous system for which the term hydroarylation has been employed involves π-coordination to olefins, typically by cationic complexes of Ag, Au and high-valent Pd species,[82] and subsequent attack by the aryl moiety. These processes also generate an aryl cation intermediate for which deprotonation is required to restore aromaticity. Finally, a third system is the one briefly mentioned during discussion of catalysts based on Ru, Rh and Ir, *i.e.*, C—H activation occurs either *via* direct oxidative addition to a low valent metal species $(Ru^0, Rh^I$ or $Ir^I)$, or through a CMD pathway whenever the catalytically active species features a high valent metal centre $(Ru^{II}, Rh^{III}$ and $Ir^{III})$. In either case, the resulting organometallic complex features an aryl- ligand that is directly implicated in the C—C bond-forming step.[82]

Despite their unmistakable versatility and usefulness to synthetic chemists,[137,138] reactions that proceed through electrophilic, Friedel-Crafts mechanisms are outside

the scope of this chapter, and we will focus our discussion on aspects associated with the third group of processes.

Thus, as previously mentioned, two main pathways have been proposed for hydroarylation reactions catalysed by Ru, Rh and Ir complexes, fundamentally varying in the order of the C—H and C—C insertion steps into the olefinic coupling partner. In this regard, detailed mechanistic studies disclosing theoretical, or experimental data, have been reported for reactions performed with all three metals.

Hence, while mechanistic studies performed by Murai *et al.*,[139] which included ^{2}H and ^{13}C KIE data, are rather uncontroversial, this is not the case for Bower's intermolecular hydroarylation reactions catalysed by Ir complexes.[126] Accordingly, the latter serves as an interesting case study for exploration of both reaction manifolds. Scheme 2.8 illustrates the two possible outcomes for the hydroarylation of benzamide **32** with styrene **33** and represents a system that forms the C—C bond by a migratory insertion which precedes C—H reductive elimination. These pathways, computed by Huang *et al.*,[92] were found to proceed with the lowest energy barriers, and disagree with Bower's original assumption[126] (*cf.* Section 1.2.1 for description; *vide infra* for discussion).

In their detailed theoretical studies,[92] Huang and Liu calculated energies barriers for all geometrically allowed C—H and C—C bond-forming events that could afford the observed linear and branched products **34l** and **34b**, respectively. Their findings were consistent with a reaction that starts with replacement of both COD ligands in [Ir(COD)$_2$]BАr$_F$ by ligand **30**, and substrate **32** to afford intermediate **35**. This catalytically active species would then perform C—H activation by direct oxidative addition with a barrier of 20.3 kcal mol^{-1} to afford, after coordination of styrene **33**, complexes **36l** (linear pathway, top) or its olefinic rotamer **36b** (branched pathway, bottom).[92] Simple rotation of coordinated styrene was found to be facile and would allow for free interconversion between **36b** and **36l**, although the latter was favoured by 4.0 kcal mol^{-1} and would, thus, be largely predominant in this equilibrium.[92]
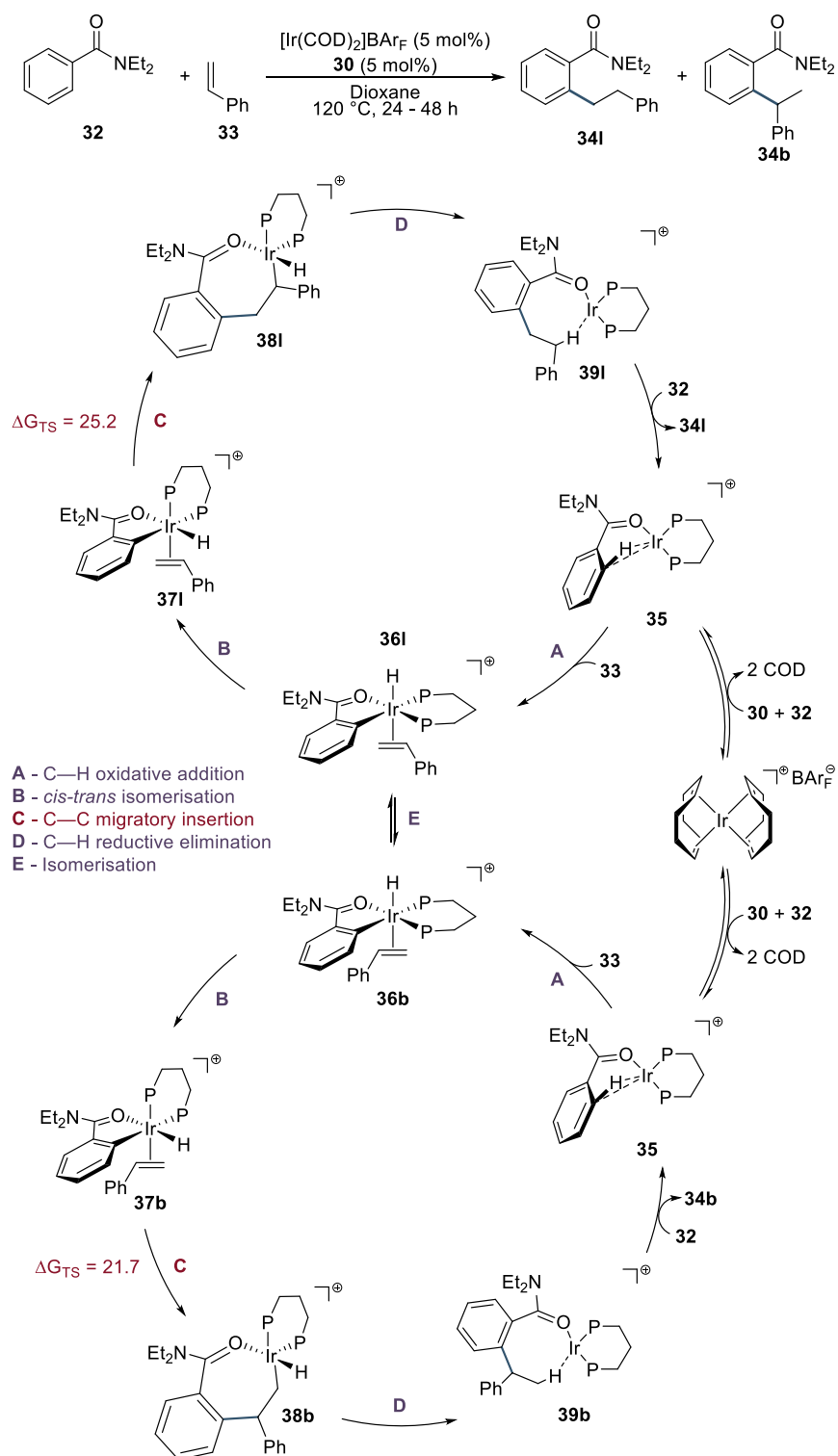
Scheme 2.8: Huang's proposal for Bower's system.[†][92]

[†]Labels b and l indicate branched and linear, respectively; simplified version of ligand **30** shown; energies are given in kcal mol^{-1}.

Both pathways would then require C—C bond-formation through migratory insertion of the coordinated aryl substituent into the olefin of **33**. However, the *trans*-disposition of hydride and olefin ligands in complexes of type **36** strongly inhibit carbometallation,[92] thus requiring isomerisation of the bisphosphine ligand to afford intermediates **37l** and **37b**. The authors attributed the destabilisation of direct migratory insertions at **36l** and **36b** to the stronger σ-donating ability of a *trans*-hydride in the latter, which would enhance Ir→$\pi^{*}_{C=C}$ back-donation into the olefinic system, hence diminishing its electrophilicity and hampering C—C bond formation.[92] Once facile isomerisation to **37l** and **37b** is complete, calculated energy barriers for subsequent productive carbometallation, also shown in Scheme 2.8, suggest branch-selective migratory insertion to afford **38b** is preferred over its linear counterpart, with a $\Delta\Delta G_{TS} = 3.5$ kcal mol^{-1} that favours formation of **38b**.[92] Based on this energy difference, Huang and Liu estimated Bower's hydroarylation should afford a selectivity of **34l**:**34b** of 1:99,[92] *i.e.*, near exclusive formation of branched product **34b**, which is in good agreement with original experimental data. Finally, C—H reductive elimination from intermediates **38b** and **38l** would proceed with barriers of 17.8 and 13.3 kcal mol^{-1},[92] respectively, thus not being implicated in the product determining step, nor being itself rate limiting. In addition to these findings, Huang and Liu also computed energies for a mechanism that would follow Bower's original proposal.

The latter mostly agrees with the pathway shown in Scheme 2.8 but diverges in the fate of intermediates **37b** and **37l**.[92,126] These features are illustrated in Scheme 2.9, alongside ^{2}H labelling data disclosed by Bower *et al.* in their seminal contribution.[126]
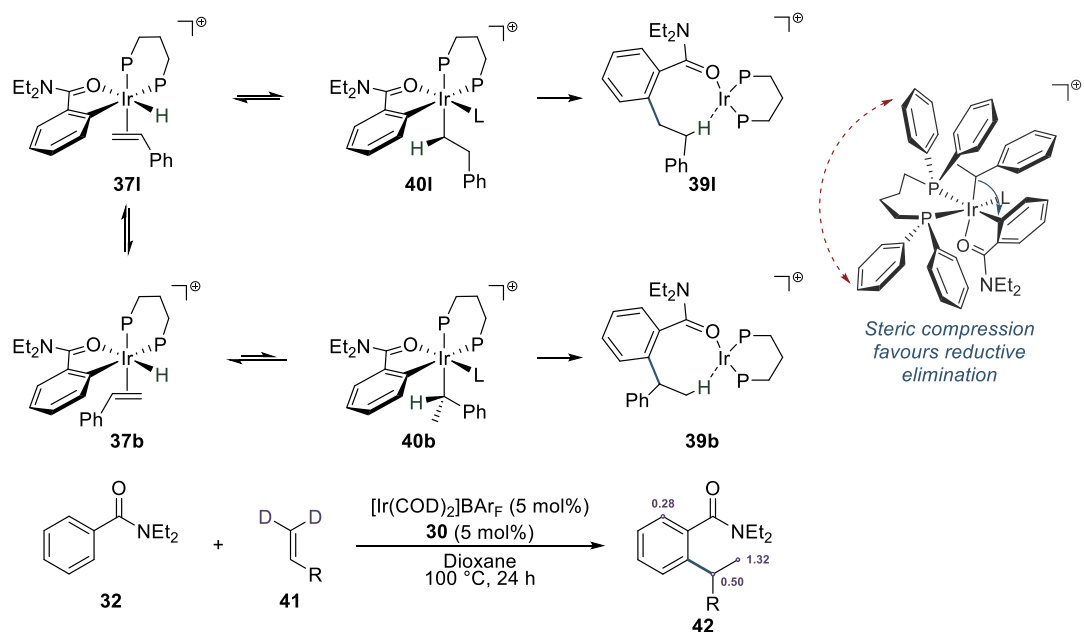
Scheme 2.9: Original mechanistic proposal and supporting ^{2}H labelling data.[†][126]

†R = 4-(CH$_3$)C$_6$H$_4$.

Therefore, in their first publication in this area, the authors explained the observed selectivity by invoking reversible Ir—H migratory insertion into the coordinated olefin of intermediates **37b** and **37l**, respectively generating the secondary alkyl-iridium complex **40b** and its primary counterpart **40l**. A C—C reductive elimination would then ensue to produce complexes **39b** and **39l**,[126] effectively re-entering Huang's mechanism[92] in Scheme 2.8. The observed high selectivity for branched products was attributed to a "cooperative destabilisation"[126] effect, in which the larger bite angle of dbbp-analogue **30** exerts steric pressure over the secondary alkyl-fragment in **38b**, thus lowering its stability;[140] and concomitant acceleration of a subsequent reductive elimination due to similar steric pressure effects.[141,142] This rationale is illustrated for a putative iridium(III) intermediate shown in Scheme 2.9 (*right*).

As evidence towards the pathway in Scheme 2.9, Bower *et al.* conducted deuterium labelling experiments employing d_2-4-methylstyrene **41** as a substrate and observed incorporation at three distinct positions in the resulting product **42**.[126] More specifically, although some deuterium retention was observed, affording 1.32 D at the substituent in **42**, incorporation was also observed at the internal olefinic position (0.50 D) and *ortho-* to the amide directing group (0.28 D).[126] These findings, which

imply reversibility of both Ir—H migratory insertion and oxidative addition steps,[143] let the authors to assume the reaction pathway in Scheme 2.9 is operative.

It is important to emphasise some key aspects implicated in both rationales discussed thus far. Firstly, the mechanistic picture originally brought forward by Bower *et al.*[126] is largely remnant from well-established ruthenium systems studied by Murai and co-workers,[139] for which extensive kinetic data is available. Note, however, that this is not the case for both rhodium- and iridium-catalysed processes. In this regard, the existing literature on the mechanisms of organometallic reactions indicates that one should exercise caution before assuming that two different transition metal centres proceed through the same pathway.[48]

Secondly, reports that unequivocally demonstrate a C—C reductive elimination of alkyliridium(III) intermediates are rare. In this regard, carefully designed studies performed by Goldman *et al.*,[144] which employed P-C-P pincer ligands of type [{$C_6H_3(CH_2P^tBu_2)_2$}Ir(R^1)R^2], provided compelling evidence that aryl-alkyl reductive elimination from iridium(III) intermediates are inherently high in energy, with barriers that surpass those associated with the analogous C_{sp^3}—C_{sp^3} eliminations.[144] Moreover, by conducting parallel kinetic experiments and DFT calculations, the authors pointed to the need for aryl ligands to perform a sterically disfavoured rotation, which places the arene π-system and the Ir—C bond involved in the elimination process in a coplanar arrangement, in order to access the requisite transition state for reductive elimination.[144] However, it is not evident that such a process would be possible in Bower's constrained system.

Finally, in the absence of ^{2}H and ^{13}C KIE measurements to corroborate either Huang's or Bower's proposal, is not possible to define which of these mechanisms is more likely. To that effect, a later, more detailed mechanistic study conducted by Bower and co-workers addressed these issues.[133]

While developing an enantioselective variant of their earlier process,[133] the authors performed kinetic isotope effect experiments with both ^{2}H and ^{13}C isotopologues, aiming for a thorough mechanistic picture of the process. Scheme 2.10 illustrates some of the interesting substrates investigated in this major development, and Scheme 2.11 presents their mechanistic findings.
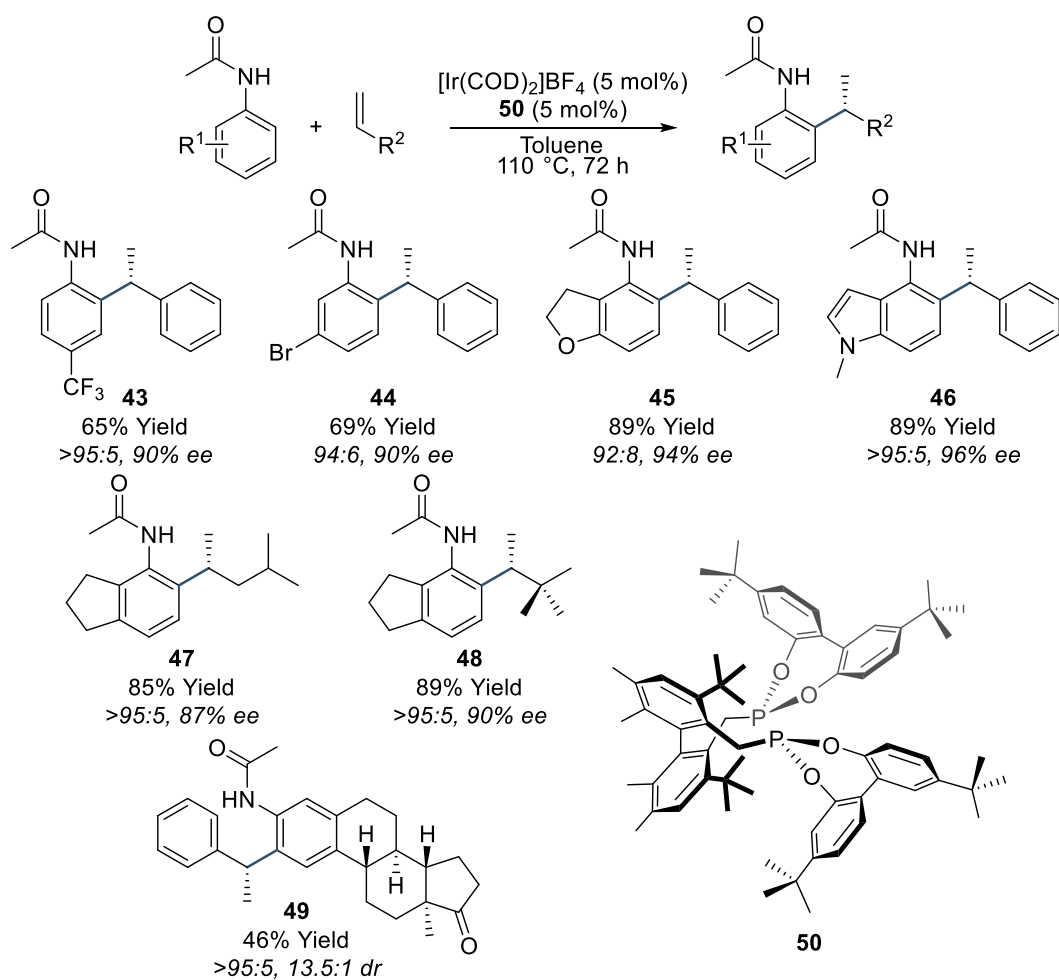
Scheme 2.10: Examples of enantioselective hydroarylation of olefins. [†][133]

[†]Reported ratios indicates branched to linear selectivity.

Notably, a large substrate scope was reported by the authors, with all compounds formed in good yields, with excellent selectivity for the branched product and high *ee* values.[133] The method was applicable to steroidal molecules such as **49**, and thiophenes (not shown), highlighting the applicability and relevance of their development. Interestingly, the authors had to develop a new class of chelating, highly hindered biphosphites to achieve good enantiomeric excesses,[133] with **50** being largely applicable to benzamides.
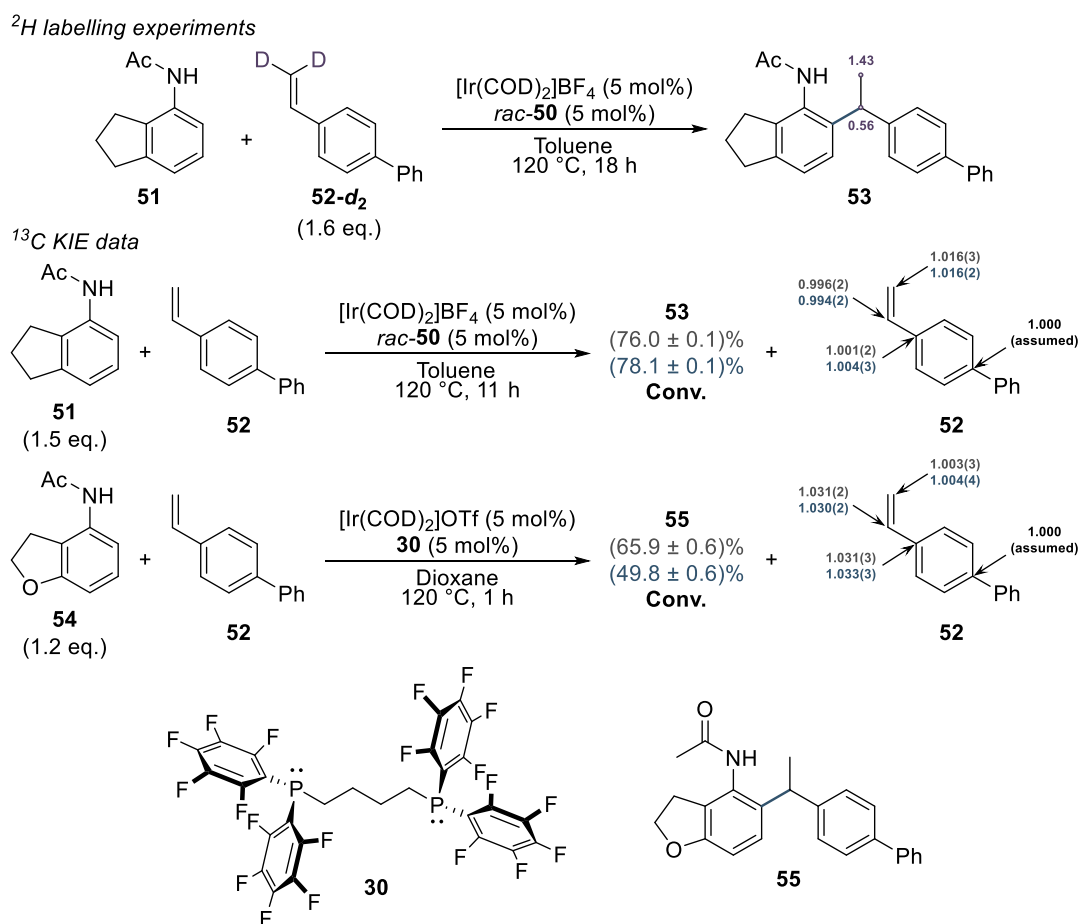
Scheme 2.11: Mechanistic data reported by Bower *et al.* [†][133]

[†]Conv. – conversion; ^{13}C KIE data collected following the method reported by Singleton *et al.*[145]

During their mechanistic studies, the results of which are highlighted in Scheme 2.11, the authors found evidence for reversible hydrometallation through migratory insertion into olefins, as demonstrated by deuterium scrambling at the tertiary alkyl position of product **53**,[133,143] hence, being analogous to their earlier proposal[126] for reactions with ligand **30** (*vide supra*). Surprisingly, their ^{13}C KIE data indicated no primary kinetic isotope effect[133,145] at the carbon atoms within the newly generated C—C bond, instead, an unequivocal KIE was observed for the terminal olefinic carbon, only. This unexpected observation led the authors to conclude that a C—H reductive elimination is rate limiting for this process.[133] Note that the absence of a ^{13}C KIE at both carbons which participate in the C—C bond-forming event effectively discards the possible existence of a rate limiting C—C reductive elimination for reactions performed in presence of ligand **50**.

The contradiction with their earlier proposal prompted the authors to study the mechanism of their original process in more detail. Hence, ^{13}C KIE data revealed primary isotope effects at both carbon atoms involved in the formation of the C—C bond, but negligible effect was observed at the terminal position of the olefin.[133] These findings, indeed, are *suggestive* of a reaction manifold through fast, reversible hydrometallation followed by rate limiting reductive elimination.

In this regard, we already discussed the plausibility of the latter in the context of alkyliridium(III) intermediates (*vide supra*). Unfortunately, reactions for which migratory insertion of M—C bonds into coordinated olefins is rate limiting are known to result in similar ^{13}C KIE data,[146,147] with the magnitude of such an effect at the C=C terminus depending on the geometry around this carbon atom at the transition state.[148-150] An interesting example is provided by the cyclopropanation of styrene catalysed by rhodium(II) complexes of the family $[Rh_2\{OC(O)R\}_4]$. Singleton *et al.*[149] elegantly demonstrated these reactions proceed by a mechanism whereby insertion of the alkene into a rhodium carbenoid intermediate is rate limiting, affording ^{13}C KIE values of 1.024(3) and 1.004(2) for the terminal and internal olefinic carbons, respectively.[149] Although the reaction is concerted, the authors found these processes are characterised by highly asynchronous transition state structures in which more pronounced KIE values are observed at the olefinic carbon closest to the carbenoid at the transition state.[149] Once again, absent of DFT calculations to determine expected KIE values,[148-150] thus providing a more complete data set, precludes full clarification of Bower's original proposal.

Throughout this section we explored two related reaction pathways for which kinetic and theoretical data is available. The discussion developed herein illustrated the mechanistic intricacies of the hydroarylation of olefins, which are especially prominent in reactions catalysed by iridium complexes. Existing data offers strong evidence for facile carbometallation and rate limiting C—H reductive elimination with ligand **50** but is inconclusive for reactions in the presence of **30**. Moreover, it is important to note that, by exploring Bower's original proposal (*cf.* Scheme 2.9 and associated discussion) as a case study, we already disclosed the mechanism proposed by Murai and co-workers[139] for reactions catalysed by ruthenium complexes.

Intramolecular reactions proceed through mechanisms analogous to the ones already covered and will be considered in further details in Section 3.3.

In summary, hydroarylation of olefins represents a highly attractive method for the rapid construction of molecular complexity from simple scaffolds. In its relatively short history, when compared to well-established C—C cross-coupling methods under palladium catalysis,[71-75] the field has experienced exceptional growth, with several milestones illustrated throughout this section. Despite its evident versatility and appeal to the synthetic community, many aspects of the reaction remain largely unsolved.

More specifically, very few catalysts were found to effect intermolecular reactions with good regioselective control in favour of the branched product, with Bower's system representing a likely candidate for a generally applicable method.

Secondly, current efficient catalytic protocols are limited to tailored directing groups and strongly coordinating *N*-heterocycles, a feature which is even more prominent in intramolecular variants which rely on long-lived metallacycles for productive olefin insertion and, consequently, C—C bond formation. In this regard, although *ortho*-directed cyclisation reactions that afford 5- and 6-membered rings are well-documented, this process failed to deliver protocols applicable to exocyclic olefins, an attractive target for the rapid construction of tricyclic motifs with high sp^3-character.

2. Proposed Work

Our initial studies will focus on the catalytic activity of iridium complex **57** in intramolecular arylation reactions. Special attention will be dedicated to the identification of a suitable directing group and additives required to favour the desired process. With a viable system in hand, we will then perform optimisation of the reaction conditions to deliver a more synthetically useful protocol. These concepts are illustrated in Figure 2.1.
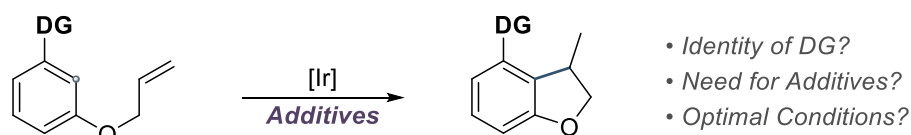
Figure 2.1: Key questions during reaction development.

Once a successful molecular scaffold has been established, we will synthesise a series of compounds strategically designed to answer important questions about the limitations and strengths of our new catalytic system. More specifically, we aim to address three main questions, *viz.*, tolerance to substitution at aromatic positions; identity of the (hetero)atom linker, and tolerance to steric hindrance at the olefinic portion. We will also briefly investigate the possibility of employing our method in the synthesis of tricyclic motifs bearing quaternary benzylic stereocentres, as depicted in Scheme 2.12.
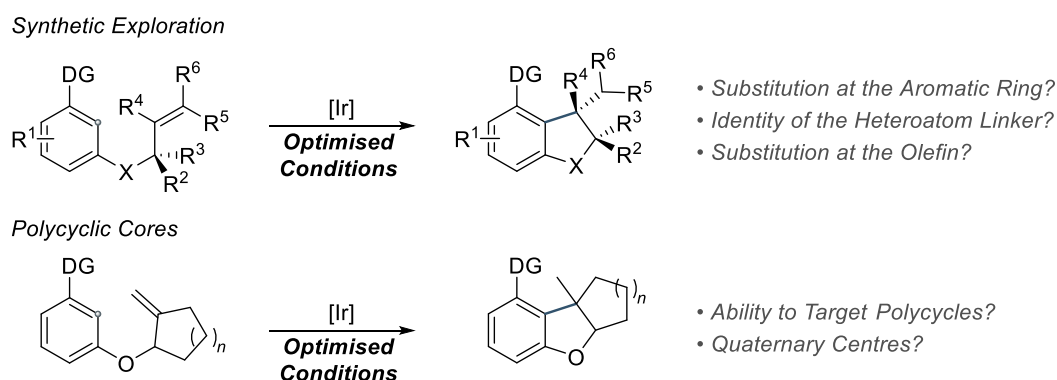
Scheme 2.12: Key questions to be addressed during substrate scope.

Finally, we will employ a suite of DFT techniques to better understand the reaction process, preferably arriving at a plausible mechanistic rationale. The understanding derived from these *in silico* studies should guide later searches for experimentally observable kinetic parameters to validate our proposal, and elucidate the effect caused by the degree of substitution at the olefin.

3. Results and Discussion

3.1 Intramolecular Hydroarylation of Olefins: Reaction Development

In previous sections, we have explored some theoretical aspects of the hydroarylation reaction, noting its robust synthetic versatility. We also demonstrated key examples in which iridium catalysts bearing chelating ligands were effective in performing intermolecular reactions with high selectivity for branched products.[126,133]

Despite these attractive features, and our desire to explore intramolecular hydroarylation reactions, possibly delivering tertiary and congested quaternary stereocentres in a racemic fashion, we needed to identify a suitable system for our synthetic explorations.

Accordingly, we commenced our studies by addressing the first crucial parameter in these reactions, *viz.*, the identity of the directing group. In this regard, in Section 1.1 – 1.2 we illustrated the directing functionalities typically employed in reactions which rely on chelation-assisted C—H activation. More specifically, the existing literature (*vide supra*) indicates that strongly ligating directing groups are often required to sufficiently stabilise metallocyclic intermediates formed throughout the reaction, with most common functionalities including amides, ketones and other carbonyl-containing directing groups. Scheme 2.13 summarises prototypical examples of competent substrates found to engage in intramolecular hydroarylation with Ru, [111,151] Rh[116-119,152,153] and Ir[128] catalysts, and offers a critical assessment of these systems.
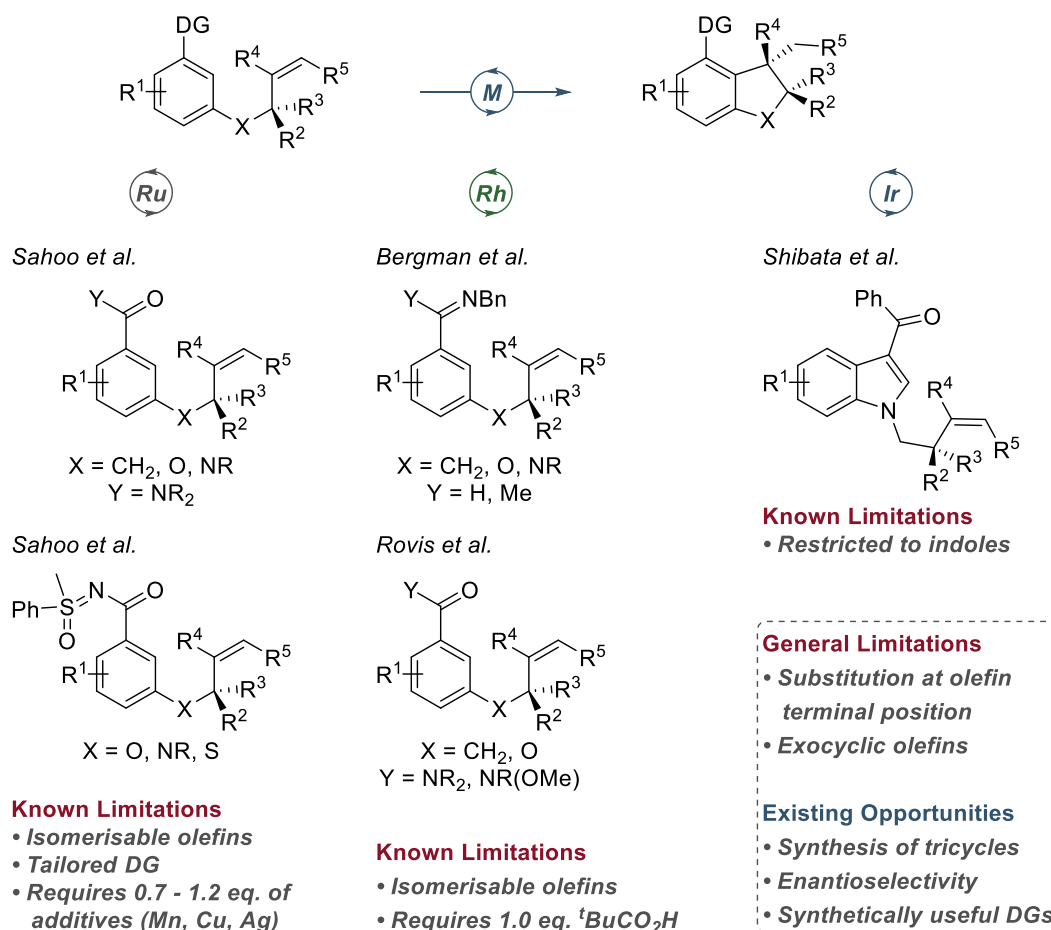
Scheme 2.13: Reported intramolecular systems[111,116-119,128,151-153] and critical assessment.

Therefore, with the notable exception of Shibata's system,[128] which is the only known example of its kind in iridium catalysis, intramolecular processes reported by Sahoo *et al.*[111,151] and Rovis *et al.*[118] require up to 1.2 eq. of additives to promote catalyst turnover, being largely restricted to 1,1-disubstituted alkenyl units. In this regard, Bergman and co-workers reported more detailed mechanistic studies employing Wilkinson's catalyst – [(PPh$_3$)$_3$RhCl] – and demonstrated the strong tendency of Rh(III) hydrides to isomerise olefins bearing a terminal CH=CH$_2$ unit.[116] Presumably, oxidative addition followed by hydrometallation would afford a rhodacycle that readily engages in β-hydride elimination,[116] an assumption that was latter explored by Rovis *et al.* to afford unsaturated products,[118] thus realising a dehydrogenative process that resembles the Heck reaction.[72,118]

It is also important to note that all intramolecular reactions highlighted in Scheme 2.13 failed to deliver products when olefins with two terminal substituents were employed as substrates. This is a known limitation among all systems, and is likely a consequence of significant destabilisation of the metallacycle formed upon the first migratory insertion event. Finally, these reactions have employed strongly ligating directing groups, often containing a combination of *O*- and *N*- donors, to achieve catalytic efficiency, and reactions with simpler, more synthetically useful directing groups are desirable.

Cognisant of these issues and aiming to develop a method that did not rely on decorated directing groups, we commenced our investigations employing a ketone functionality under reaction conditions akin to those reported by Bergman *et al.*[116] for reactions catalysed by the closest possible analogue of our systems, *i.e.*, Rh(I). Thus, we reacted 3-allyloxyacetophenone **56** with our iridium catalyst **57** (*cf.* **150c** in Chapter 1) in diglyme at 120 °C for 16 h and analysed the composition of the reaction mixture by ^{1}H NMR spectroscopy, a technique which proved well suited for this transformation owing to large differences in chemical shifts for the olefin in the starting material and the desired aliphatic product.[116] Scheme 2.14 summarises our observations.
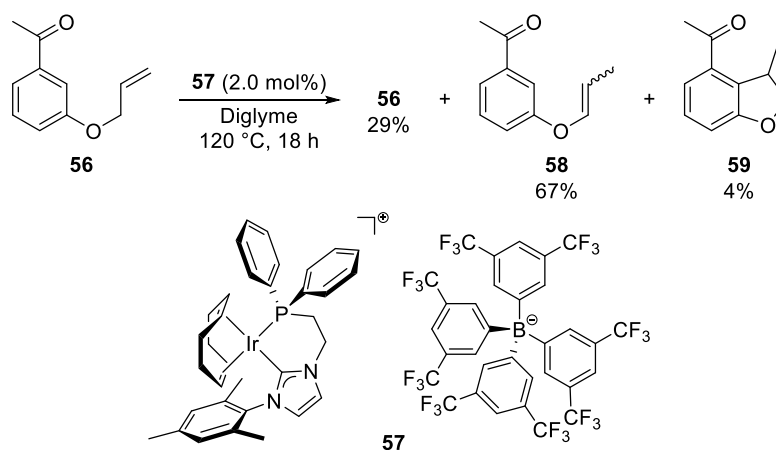
Scheme 2.14: Initial observation of intramolecular hydroarylation.

Encouraged by the identification of the desired product **59**,[116] we decided to embark on a more detailed study to determine whether we could control the reactivity of **57** to improve conversion towards dihydrobenzofuran **59**. Note that the production of both **58**[154] and **59** under the reaction conditions are *suggestive* of an iridium(III)

hydride species in solution, which is highly competent to promote β-hydride elimination to afford vinyl ether **58**, but does not offer sufficient evidence of its existence.

Thus, by assuming that currently known mechanistic pathways for iridium-catalysed hydroarylation reactions (*vide supra*) are also operative in our system, we could infer **57** was effective in promoting chelation-assisted oxidative addition of aromatic C—H bonds in the parent ketone, however, the resulting metal hydride species was rather ineffective at the C—C bond-forming step. Several factors could be responsible for this behaviour, the most likely candidates being the highly strained nature of the necessary *fac*-(O,C,C=C) conformation adopted by the metallacycle intermediate **61**, formed prior to migratory insertion events; and the availability of long-lived species possessing vacant coordination sites at the metal centre immediately after the undesired hydrometallation step – **62a** and **62c**. These phenomena are summarised in Scheme 2.15.
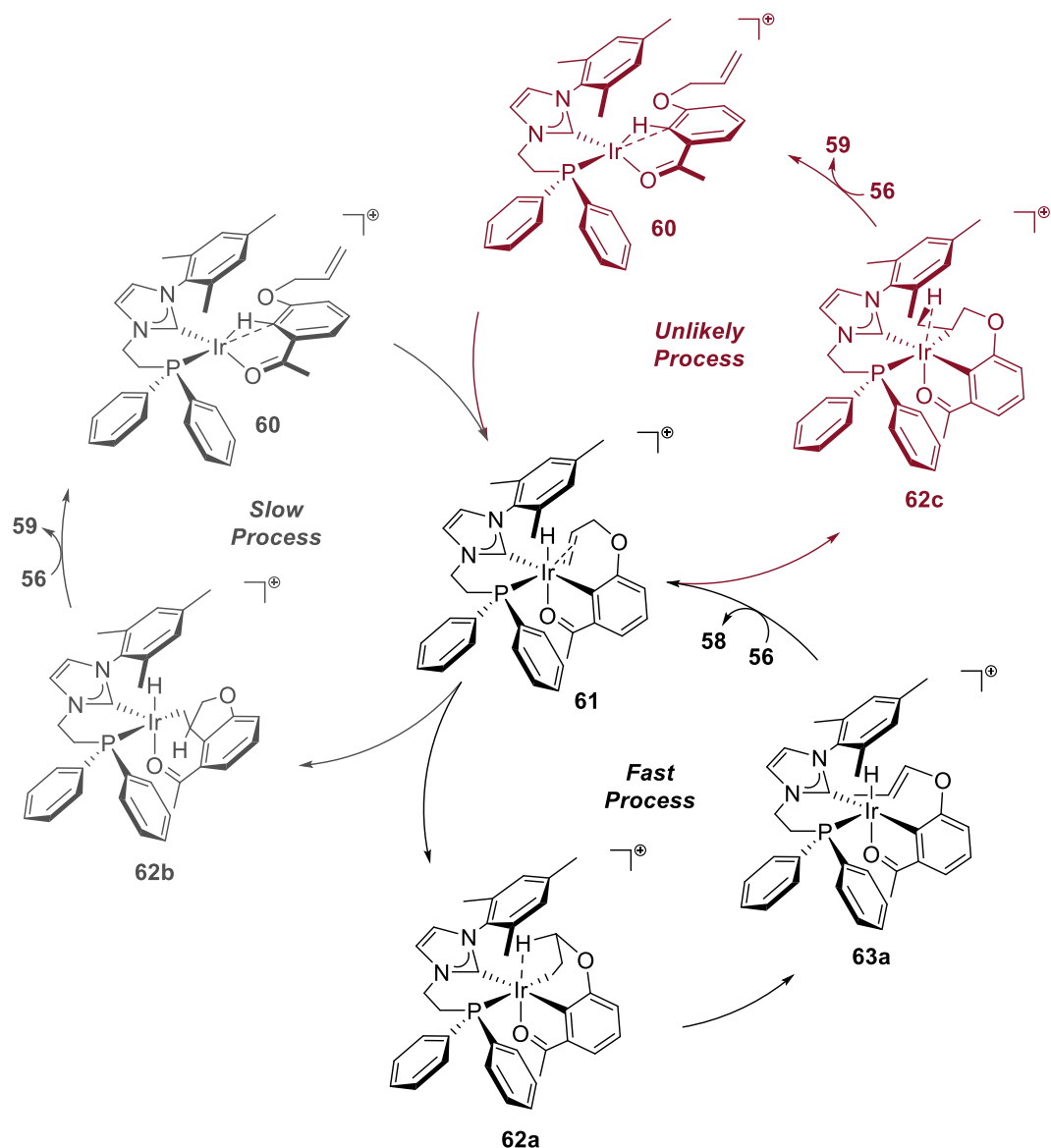
Scheme 2.15: Tentative proposal for preferential formation of **58**.[†]

[†]Simplified mechanism shown; geometries are only representative; three competing pathways are considered: β-hydride elimination to afford **58** (black, bottom left); C—C migratory insertion to afford **59** (grey, top left); C—C reductive elimination to afford **59** (red, top right).

Accordingly, we hypothesised that three main pathways were possible under the reaction conditions. More specifically, dissociative ligand exchange between the coordinated COD in **57** and substrate **56** would afford intermediates **60** in Scheme 2.15 (top right and top left). Subsequent C—H oxidative addition would produce key intermediate **61**, a common species to all competing catalytic processes, the fate of which is responsible for the observed products. Hence, a fast process involving a

reversible Ir—H migratory insertion into the coordinated olefin of **61** would deliver **62a**, which features an agostic interaction with a C—H bond α- to the phenolic oxygen in the parent substrate. This intermediate would then engage in a β-hydride elimination, affording iridium-ligated vinyl ether **63a**. A final ligand displacement with **56** restates the catalytically active species and releases isomerised product **58**.

In a second reaction manifold, metallacycle **61** would engage in productive Ir—C migratory insertion, delivering **62b** which, upon C—H reductive elimination and ligand displacement, generates the desired product **59**. Owing to the very low conversions observed, we assumed this was a rather slow process. Finally, a third pathway could also account for the observation of **59**, *i.e.*, Ir—H migratory insertion in **61** would produce **62c**, from which a subsequent C—C reductive elimination must ensue to afford **59** and restart the catalytic cycle. Note, however, that existing mechanistic data does not favour the participation of **62c** as a necessary intermediate *en route* to **59**.

From these inferences, it was evident that any catalytically competent system for hydroarylation reactions based on **57** would require an experimentally viable solution for the observed complex mechanistic behaviour. In this regard, it is important to reiterate the main factors known to affect β-hydride elimination:

i)   Existence of vacant sites: it has been extensively demonstrated that the occurrence of β-elimination reactions in transition metal complexes[155-158] depend on the availability of vacant coordination sites around the metal centre;

ii) Ligand set: studies on the electronic effects of ligands in organometallic complexes indicate strong σ-donors tend to destabilise transition states associated with β-hydride elimination,[155,156] a factor that is likely a reflection of the reduced electrophilicity of the metal centre, which results in a less effective $\sigma_{C—H} \rightarrow d^{*}_{M}$ interaction responsible for the weakening of the C—H bond.[156-158]

Therefore, by combining these two factors, we arrived at the following conclusions: inclusion of an additive that inhibits the existence of vacant sites around the metal centre during the reaction is likely to diminish production of **58**; lowering the

electrophilicity of iridium(III) intermediates could also have a positive effect in reducing the rate of β-hydride elimination.

Consequently, we decided to modify our strategy in two ways, *viz.*, a more detailed study on the effect of additives was required to test the hypotheses outlined above; and a change of directing group could be necessary in order to afford more stable metallacycles from which C—C bond formation could occur. To that end, we synthesised two analogues of ketone **56** possessing ester and carboxylic acid functionalities, **64** and **65**, respectively, and subjected these substrates to two sets of conditions. The results are summarised in Table 2.1:

Table 2.1: Screen of directing groups and base additive.

56 (X = CH₃)   58 (X = CH₃)   59 (X = CH₃)
64 (X = OCH₃)   66 (X = OCH₃)   68 (X = OCH₃)
65 (X = OH)   67 (X = OH)   69 (X = OH)
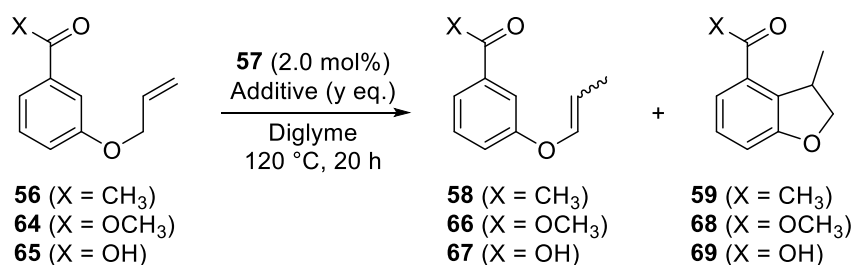
Entry	X	Additive	y (eq.)	Conversion (%)^a		
				S.M	Isomer^b	Product
1^c	CH₃	—	—	29	67	4
2		KOAc	1.0	> 95	—	—
3	OCH₃	—	—	21	79	—
4		KOAc	1.0	> 95	—	—
5	OH	—	—	> 95	—	—
6		K₂CO₃	1.0	72	14	14
7		K₂CO₃	0.1	71	—	29
8^d		K₂CO₃	0.1	60	—	40

^{a}Determined by ^{1}H NMR spectroscopy of the reaction mixture; ^{b}Combined *E*- and *Z*- isomers; cResults also illustrated in Scheme 2.14. ^{d}5.0 mol% **57** was employed.

Thus, our initial assessment of directing groups (entries 1, 3 and 5) was discouraging. More specifically, in the absence of any additives, substrates **56** and **64**, bearing a ketone and an ester functionality, respectively, displayed poor reactivity and preferentially afforded isomerised products **58** and **66**. Compound **65**, on the other hand, remained unreacted under our initial reaction conditions. Moreover, addition of KOAc seemed to strongly inhibit reactivity for substrates **56** and **64** (entries 2 and 4). It is unclear whether catalyst **57** engages in a decomposition pathway in presence of

acetate anions, or whether reaction inhibition was caused by complete displacement of substrates by AcO⁻, thus inhibiting reactivity. We then isolated a mixture of vinyl ether isomers **58** and re-subjected these species to our reaction conditions without KOAc (not shown, see Experimental Details for further information), with no significant changes in mixture composition being observed. These data suggested iridium(III) hydride species formed during the reaction were unable to engage in productive reactions with vinyl ether **58**, which is in line with the reactivity of rhodium and ruthenium complexes highlighted in Scheme 2.13.[111,118,151]

Undeterred by these findings and recognising that other bases could have different effects in the reactivity of the proton donor **65**, we subjected this benzoic acid to reaction conditions employing K_2CO_3 as a base – entry 6. Gratifyingly, strong suppression of isomerisation was observed in this case, albeit this phenomenon was accompanied by equally low reactivity towards the desired product **69**. Lowering the amount of added base to 10 mol% (entry 7) and increasing the catalyst loading to 5 mol% (entry 8) afforded promising results. Note that the choice of K_2CO_3 as an additive in reactions with **65** was not arbitrary. More specifically, we already mentioned the importance of tightly bound metallocyclic intermediates in the stabilisation of iridium complexes capable to engage in productive C—C bond-formation. Accordingly, we envisioned that an inorganic base could engage in an effective acid-base equilibrium with **65**, affording carboxylates able to associate with our cationic iridium complex with strong intermolecular interactions governed by ionic attraction.[159] As the data suggests, this assumption was indeed fruitful (also, see Section 3.3).

It is important to emphasise that, although carboxylic acids have been employed in intermolecular hydroarylation of alkynes catalysed by Ru,[160] no such transformation involving alkenes to afford cyclised products has been reported. Moreover, the functional group under consideration meets the criteria outlined at the beginning of our discussion, *i.e.*, a simple motif with synthetically useful applications.

Accordingly, we decided to pursue a hydroarylation process featuring a carboxylic acid directing group. However, a more detailed optimisation study was required before we could meet our primary goal. Hence, we performed a Design of Experiments employing a fractional factorial central composite design to investigate

the effect of catalyst and additive loadings, temperature and concentration. The results obtained are summarised in Table 2.2 and in the Pareto chart in Figure 2.1 (please, see Experimental Details for further information).

Table 2.2: Results from design of experiment.[†]

HO O   **57** (x mol%)   X O
65   K$_2$CO$_3$ (y mol%)   69
Diglyme
T, 20 h
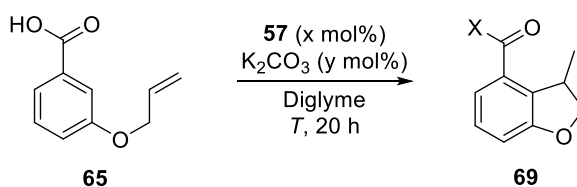
Entry[a]	X (mol%)	y (mol%)	T (°C)	V (mL)	Conversion (%)[b]		
					65	69	Other[c]
1[d]	5.0	25	90	1.5	79.6	10.7	9.7
2	5.0	125	90	1.5	61.5	25.6	12.9
3	5.0	125	90	0.5	80.0	9.5	10.5
4	1.0	25	90	1.5	100	—	—
5	1.0	125	90	1.5	96.3	1.3	2.4
6[d]	5.0	25	90	0.5	87.8	3.4	8.8
7	1.0	25	90	0.5	100	—	—
8	1.0	125	90	0.5	100	—	—
9	1.0	125	150	1.5	77.4	5.8	16.8
10	5.0	125	150	1.5	4.6	81.0	14.4
11	**5.0**	**25**	**150**	**1.5**	**—**	**96.5**	**3.5**
12	5.0	125	150	0.5	10.1	63.6	26.3
13[d]	1.0	25	150	1.5	46.6	30.7	22.7
14	**5.0**	**25**	**150**	**0.5**	**—**	**93.6**	**6.4**
15	1.0	125	150	0.5	71.0	8.8	20.2
16[d]	1.0	25	150	0.5	64.8	5.2	30.0
17	3.5	75	120	1.0	72.3	10.6	17.1
18	3.5	75	120	1.0	25.0	50.0	25.0
19	3.5	75	120	1.0	35.7	35.7	28.6

[†]T – temperature; V – volume of diglyme; [a]entries given in the order required by the DOE; [b]determined by ^{1}H NMR spectroscopy of the reaction mixture; [c]combined value for side products; [d]small amounts of deallylated products observed.
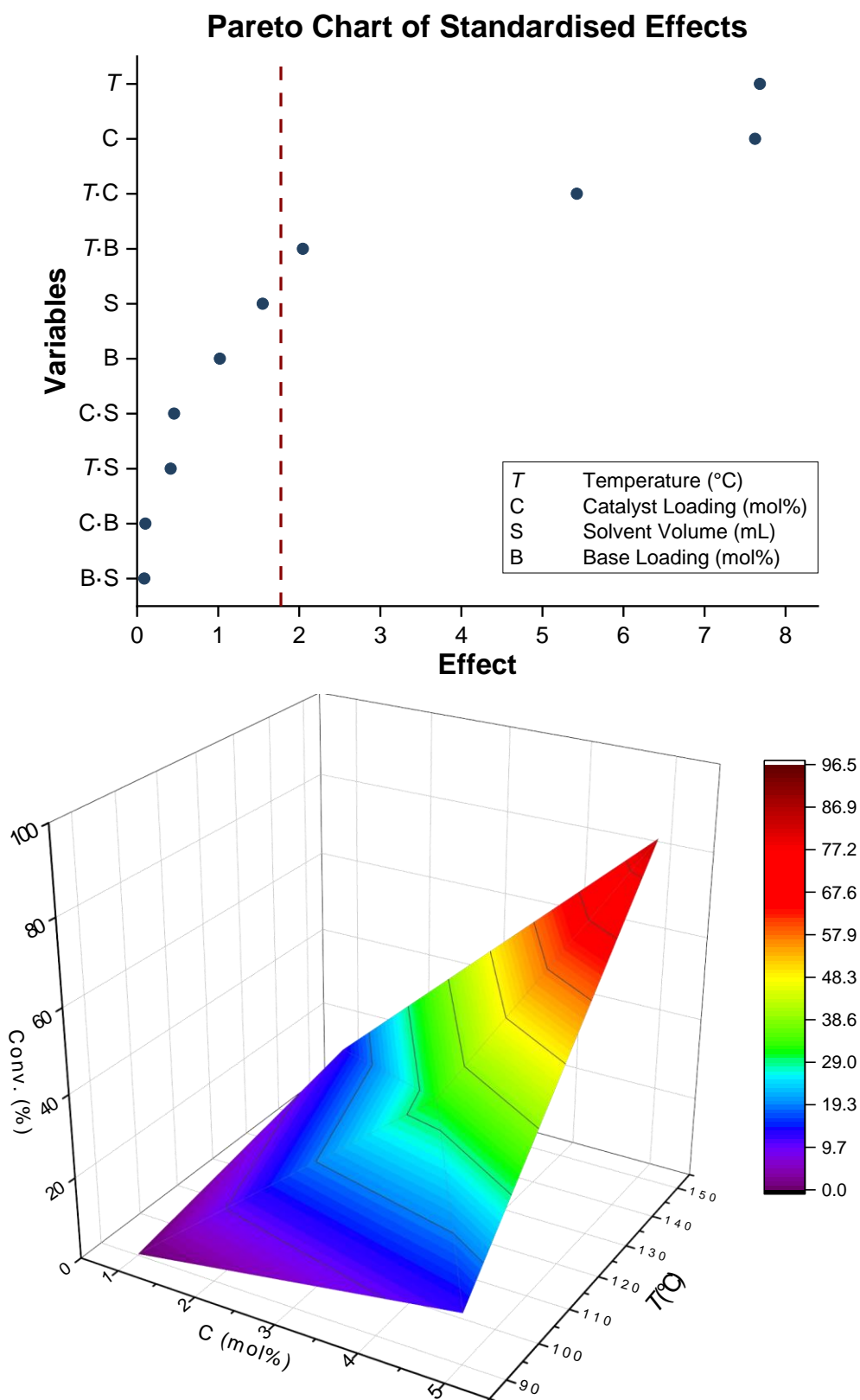
Figure 2.1: Pareto chart of effects from experimental design (*top*) and response surface for most significant variables (*bottom*).[†]

[†]Dashed line indicates the significance threshold for standardised effects; Conv. – converstion.

To our delight, significant improvement in conversions towards the desired product **69** were observed following our short optimisation study. As evidenced by entries 11 and 14 in Table 2.2, and in the chart displayed in Figure 2.1, increasing the temperature of the reaction from 120 to 150 °C, and increasing the catalyst loading to 5.0 mol% proved beneficial for the reaction. In this regard, analysis of the data for normalised effects — a statistical descriptor for the influence of a given variable in the observed conversion to product **69** — indicated that reactions performed at higher catalyst loadings and temperatures were suitable candidates for a synthetically useful protocol.

Having recognised the potential of our novel chelating catalysts to perform intramolecular hydroarylation processes to quickly introduce molecular complexity in simple scaffolds, we embarked on a more comprehensive synthetic exploration.

3.2 Exploiting Carboxylic Acids to Build Molecular Complexity

Our synthetic studies began with the identification of molecular scaffolds that could provide valuable information for future reaction development. More specifically, we aimed to gather a better understanding of the limitations and capabilities of our system and study its suitability to access complex molecular structures. The latter remains to be demonstrated by existing technologies and would represent a valuable tool in drug discovery and in the synthesis of natural products.

Therefore, we focused on the preparation of key molecules that would help us explore three main features, namely, substitution at the aromatic ring and olefin portion of the molecule; tolerance to nitrogen linkers; and ability to form congested tricyclic rings. Once our main lines of enquiry were identified, we selected viable synthetic routes and prepared the substrates illustrated in Scheme 2.16.

An outline of the general aspects associated with the synthetic route displayed in Scheme 2.16 is given in the subsequent discussion, with Experimental Details containing further information on the specific substrates.

Hence, we started our synthesis of substrates **72a-m** from commercially available benzoic acids bearing the appropriate substituents at the aromatic ring. Installation of

a methyl ester was required to avoid undesired reactivity of the carboxylate moiety during subsequent steps in our route and esterification was straightforwardly accomplished under standard conditions employing SOCl$_2$ in MeOH, affording esters **70a-f**.

Once obtained, esters **70** were divided in three subgroups. The first of these comprised compounds **64** and **70a-e**, which were ready for the installation of an allyl side chain, and were thus subjected to alkylation conditions employing the appropriate allylic bromide as an electrophile to deliver *O*-allyl esters **71a-e** and **71i-j**. A second set of substrates was derived from 3-aminobenozic ester **70f** and were prepared by two sequential steps involving introduction of the requisite protecting group followed by alkylation with allyl bromide to afford esters **71f-h**.

Finally, the third group of substrates in our synthetic studies were esters **71k-m**, which required additional elaboration of the side chain prior – **71k** – or after *O*-alkylation – **71m,n**. In this regard, **71k** was obtained through a Mitsunobu reaction with the appropriate *Z*-olefin, whereas esters **71m** and **71n** were obtained in two steps, requiring alkylation with 2-chlorocyclopentanone and 2-chlorocyclohexanone, respectively, and subsequent methylenation by Wittig reaction. From compounds **71a-m**, we conducted simple deprotection of the methyl esters by standard hydrolysis conditions, and obtained carboxylic acids **72a-m.**

Synthetic route

70
(80 - 100%)

71
(62 - 98%)

72
(63 - 99%)

Aromatic ring substitution

65

72a

72b

72c

72d

Nature of the linker

72e

72f

72g

72h

Substitution at the olefin

72i

72j

72k

72l

72m
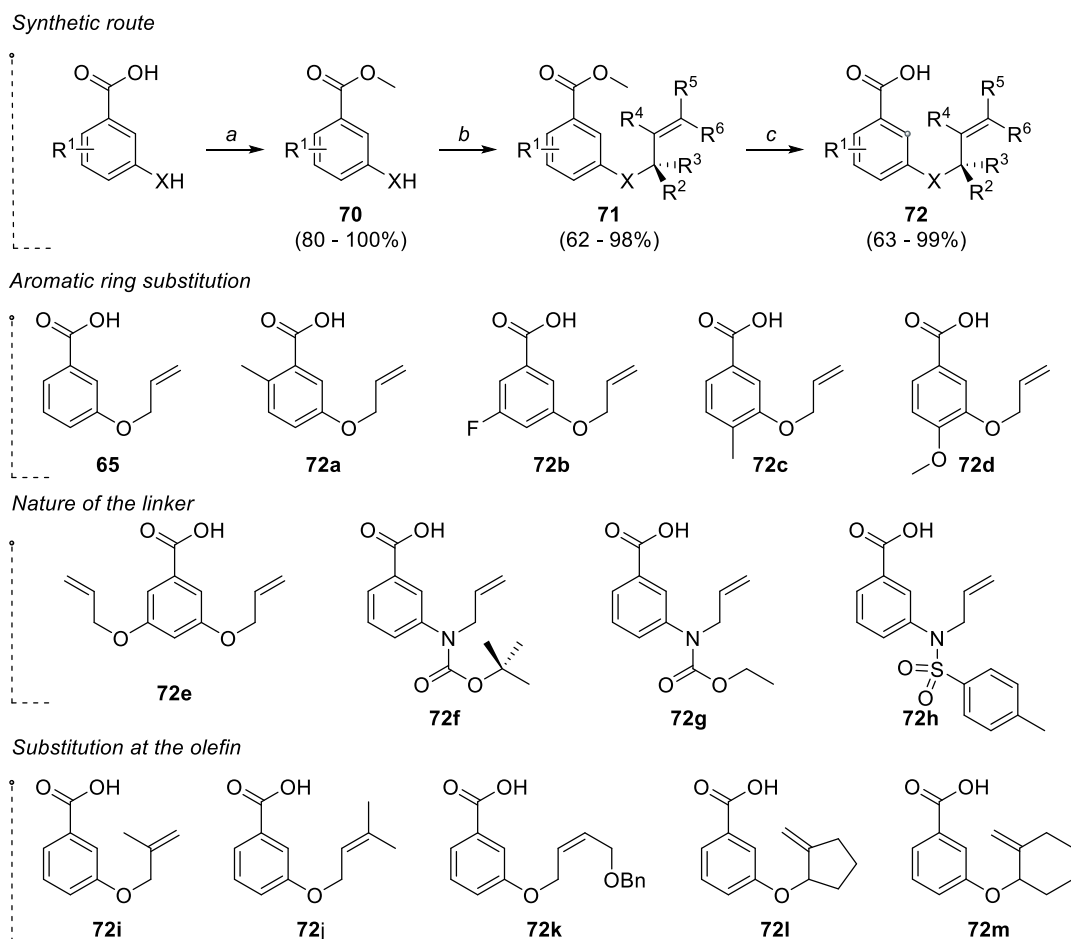
Scheme 2.16: General synthetic strategy and substrates synthesised: *a* –
esterification; *b* – introduction of allyl chain; *c* – saponification.[†]

[†]Yield range shown in brackets. See Experimental Details for further information.

With the desired set of 14 representative carboxylic acids in hand, we conducted a
series of hydroarylation test reactions employing 5 mol% of iridium catalyst **57** in
diglyme at 150 °C and 10 mol% K_2CO_3 as an additive. Our observations are
summarised in Scheme 2.17.
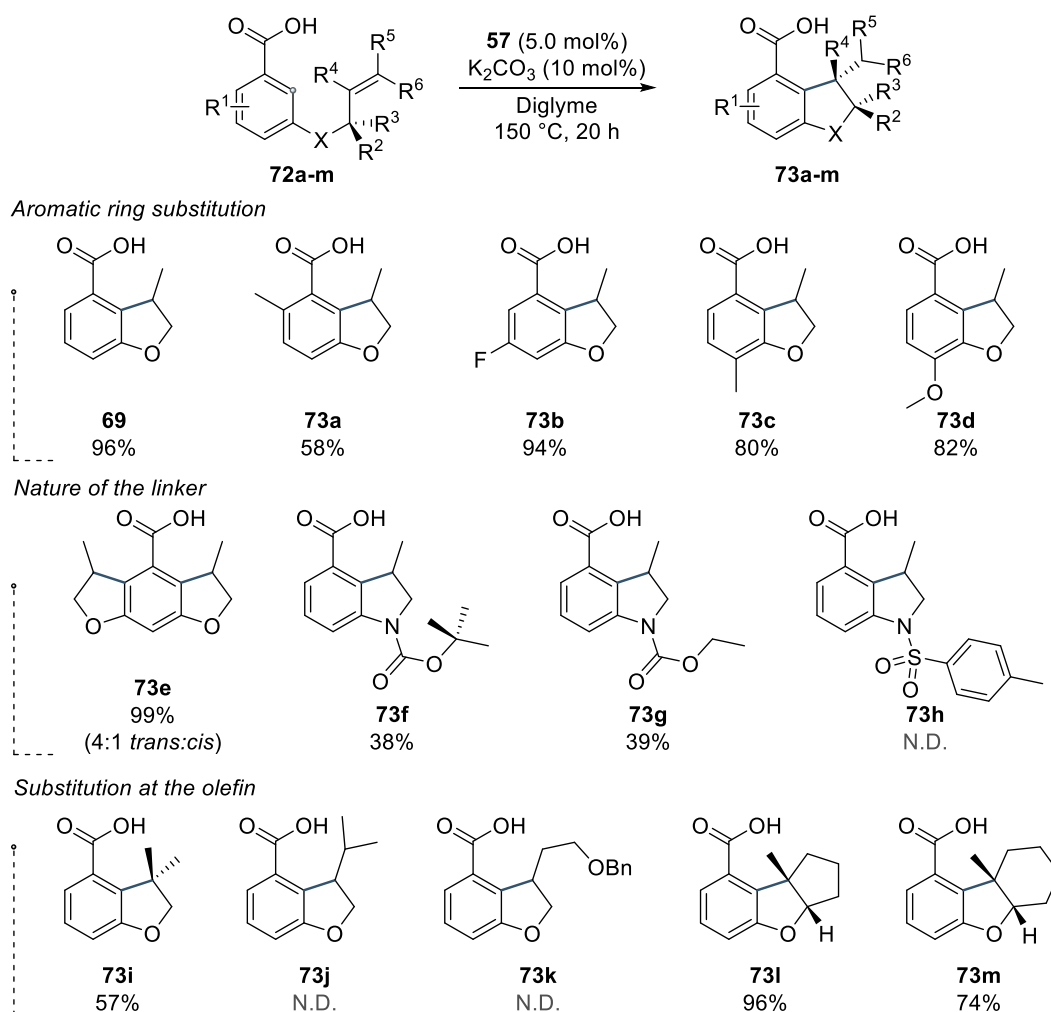
Scheme 2.17: Catalytic tests for hydroarylation of benzoic acids.[†]

[†]Reported values are conversions determined by ^{1}H NMR spectroscopy.

Inspection of the conversions observed in our test reactions provided useful pieces of information regarding the synthetic applicability of our new methodology. Concerning our first line of enquiry, shown in the first row of Scheme 2.17, it was possible to verify a good tolerance to substituents at all positions of the aromatic ring. Perhaps the only exception to this trend was substrate **72a**, bearing a methyl substituent *ortho-* to the carboxylic acid, which was less effective under our reaction conditions, but still afforded a good 58% conversion to **73a**. The latter observation points towards sensitivity to steric interactions at the vicinity of the directing group, which is unsurprising giving the highly congested nature of the metallocyclic intermediates formed during the reaction (*vide infra*). It is important to notice, however, that when the analogous intermolecular hydroarylation method initially

developed by Bower *et al.*[126] was employed in reactions with *N,N*-dimethyl-2-ethylbenzamide, a substrate that necessarily forms 5-mmi featuring a methyl substituent *ortho-* to the directing group, no reaction was observed. Our system, on the other hand, does not seem to share the same limitation.

The second line of enquiry addressed by our experiments concerned the nature of linkers within the allyl portion of the molecule. More specifically, the promising reaction profile for the synthesis of dihydrobenzofurans indicated potential to explore symmetric 5,6,5-tricyclic systems and synthetically relevant indolines. Accordingly, when substrates **72e-h** were subjected to our standard reaction conditions, high conversions to the desired product were observed for tricycle **73e**, but *N*-linked analogues **73f-h** were obtained in moderate yields. In this context, inclusion of nitrogen heteroatoms within the molecule is a known issue shared by similar existing methods. For instance, while investigating the ruthenium-catalysed intramolecular hydroarylation of 1,1-disubstituted olefins, Sahoo *et al.*[111] had to resort to an increased catalyst loading of 10 mol% in the presence of 20 mol% AgSbF$_6$ and 50 mol% Mn(OAc)$_2$, the latter being competent Lewis acids that could engage in coordination to nitrogenated centres and inhibit catalytic suppression. These considerations reveal that catalyst **57** has good potential to deliver synthetically useful transformations without the need for two additional transition metal salts in the reaction medium, albeit optimisation will be required before we can deliver an appealing strategy. A last important observation in this set of experiments is the existence of diastereoselectivity during sequential cyclisation events which afforded **73e**. Upon formation of the first dihydrobenzofuran ring, a tertiary benzylic stereocentre was installed in one of the portions of the molecule, consequently, subsequent coordination and C—H activation events with this chiral molecule will generate a set of diastereomeric iridium complexes that effect C—C bond formation at different rates. This concept is illustrated in Scheme 2.18 for a set of two arbitrary iridium(III) intermediates (*R*)-(Δ)-**74** and (*S*)-(Δ)-**74** (see Section 3.3.1 in Chapter 1 for a brief discussion on the chirality of iridium hydrides).
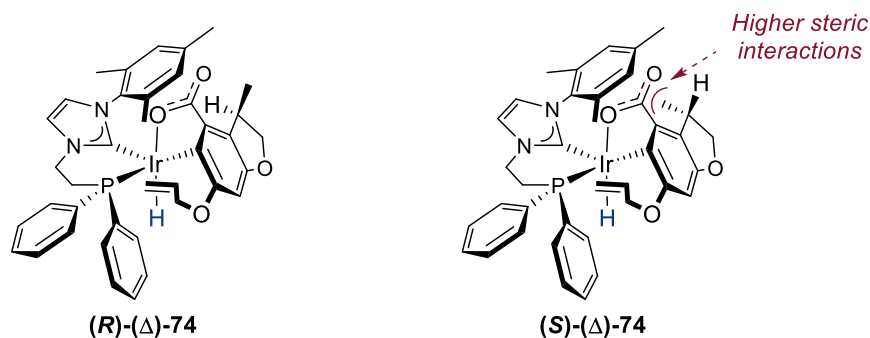
Scheme 2.18: Diastereomeric iridium hydride complexes formed *en route* to **73e**.

Specifically, formation of *cis*-**73e** requires diastereomeric iridium complexes akin to (*S*)-(Δ)-**74** in Scheme 2.18. These species feature unfavourable steric interactions between the benzylic stereocentre and the ancillary ligands and, consequently, should require higher energy barriers during the subsequent migratory insertion event responsible for generating the second 5-membered ring. These features also suggest complex **57** can be employed in the context of diastereomeric cyclisation reactions *via* hydroarylation.

Finally, our third line of investigation concerned the degree of substitution at the olefinic portion in substrates **72i-m**. Hence, although a methyl substituent at the internal position of the alkene was tolerated, as evidenced by moderate conversion towards **73i**, substitution at the olefin terminus resulted in complete suppression of reaction. Notably, both **72j** and **72k**, respectively bearing a terminal *gem*-dimethyl substituent and a stereochemically defined *Z*-olefin, failed to afford desired carboxylic acids **72j-k**. Given the structure of our chelating ligand set, and similar phenomena reported in the existing literature (*vide supra*), these observations indicate the existence of severe steric interactions in the C—C bond-forming step for **72j-k**, thus precluding their conversion to the desired products.

Notwithstanding these setbacks, a more encouraging reaction profile was observed for **72l-m**, substrates which contain exocyclic olefins. In the latter cases, swift conversion to congested bicycles **73l-m**, featuring quaternary benzylic stereocentres, was observed. Moreover, ^{1}H NMR spectroscopy indicated preferential formation of the expected *cis*-junction within these bicyclic motifs. As we previously discussed, similar reactivity is yet to be realised by existing technologies, thus representing a synthetically attractive method for rapid introduction of molecular complexity.

Our efforts to directly isolate products **69** and **73a-m** was frustrated by the inability to separate these molecules from their isomeric carboxylic acids counterpart, substrates **65** and **72a-m**. Despite several attempts at chromatographic purification, the minimal difference in polarity between the allylic side chain and their corresponding dihydrobenzofurans rendered these mixtures inseparable. In fact, Sahoo *et al.* also reported a similar issue when employing their Ru catalysts in reactions with isomerisable allylic substrates.[111]

Therefore, owing to time constraints, we decided to focus on an alternative strategy. Accordingly, we conducted a two-step protocol consisting of hydroarylation and subsequent methylation of the carboxylic acid to afford the corresponding methyl esters. It is important to note that similar challenges in separating the final products resulted in a smaller synthetic exploration. To this effect, the results obtained are depicted in Scheme 2.19.
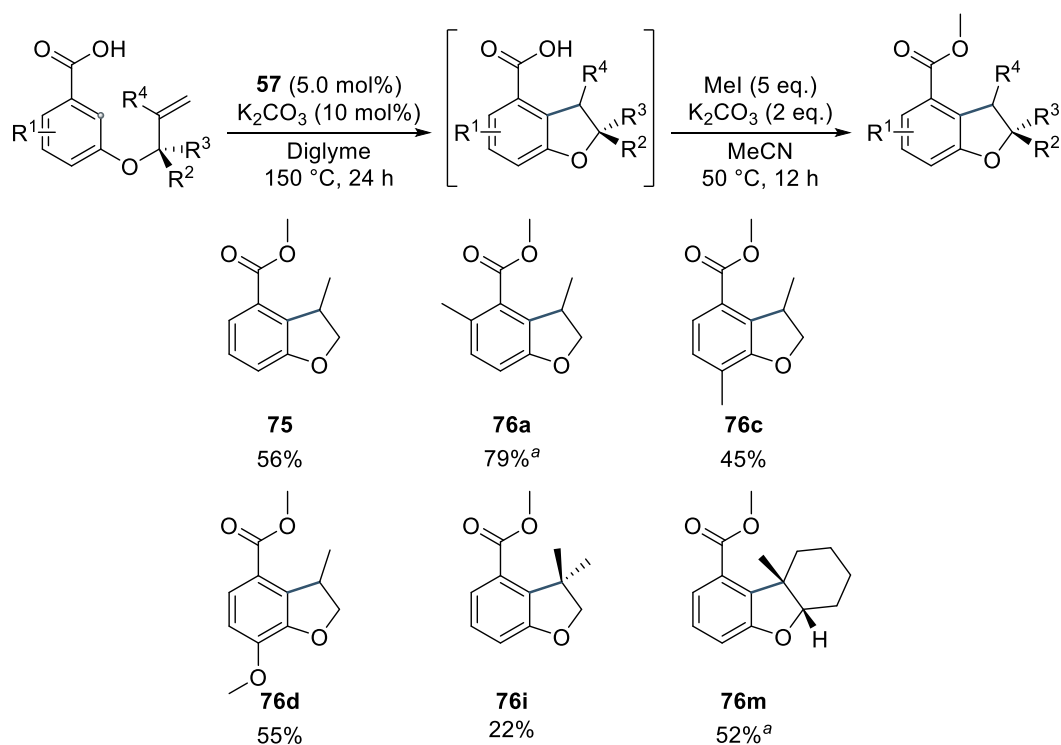
Scheme 2.19: Esters synthesised by sequential hydroarylation and methylation.[†]

[†]Reported values are isolated yields over 2 steps; [a]reactions performed for 48 h.

Gratifyingly, the observed reactivity obtained by our previous catalytic tests was maintained, with ester of types **75** and **76** being isolated in low (**76i**) to good yields

(**76a**). It is important to note, however, that inspection of the data in Scheme 2.18 prompted us to increase the reaction time from 24 to 48 h for substrates **72a** and **72m**, which originally featured lower conversions than other compounds explored. Thus, substrates subjected to extended reaction times delivered improved and more synthetically appealing yields. Comparison to reported experimental conditions by Bower *et al.* also reveals extended reaction times for more substituted substrates, typically varying from 48 – 72 h.[126,133]

In summary, throughout this section, we have applied fundamental mechanistic principles to establish a new reactivity mode for catalysts bearing chelating NHC-P ligands. Once this new transformation was identified, we successfully employed Design of Experiments to streamline the optimisation of reaction conditions.

Finally, we embarked on a synthetic exploration aimed at answering key concepts that should guide further reaction development, namely: tolerance of substituents at the aromatic ring and olefin portions of the molecule; nature of the heteroatom linker within the side chain; and ability to construct bicyclic motifs bearing congested quaternary benzylic stereocentres. These questions were briefly explored by investigating 14 selected compounds, 6 of which were successfully isolated as the respective methyl esters in a convenient two-step protocol.

At the outset of our synthetic studies, we arrived at a synthetically attractive methodology to swiftly introduce molecular complexity in simple scaffolds. Nonetheless, a more complete mechanistic understanding of the present system was warranted, which prompted us to investigate the hydroarylation of olefins from a theoretical perspective.

3.3 Developing a Mechanistic Rationale Through DFT

In previous sections we presented a description of the current mechanistic understanding and potential controversies associated with iridium-catalysed hydroarylation reactions. Available kinetic data reported by Bower *et al.* during their enantioselective studies employing ligand **50**,[133] in conjunction with DFT calculations performed by Wang and Liu,[92] favours a reaction pathway characterised by the following steps: C—H activation through direct oxidative addition into a low

valent iridium(I) species; Ir—C migratory insertion into the coordinated olefin; and C—H reductive elimination to afford the final product of hydroarylation.

Furthermore, owing to the low likelihood of a C—C reductive elimination from an iridium(III) metallocyclic intermediate,[144] we decided to focus our theoretical investigations on the evaluation of the energetic profile for a reaction pathway akin to that proposed by Bower and co-workers for ligand **50**.[133]

Accordingly, we commenced our DFT studies by locating the stationary points for all plausible intermediates in a hydroarylation reaction with substrate **65**. Once identified, these minima of the potential energy surface were connected by their transition states employing the Transit Guided Quasi-Newton Method (see Computational Details for further information). Finally, the validity of all transition states was then confirmed by intrinsic reaction coordinate (IRC) calculations.

Before we explore the results obtained at the outset of our theoretical investigations, it is necessary to reiterate an important difference between iridium complex **57** and the catalyst originally developed by Bower *et al.*, namely, in their seminal contribution, the authors employed ligand **30**, a close analogue of dppb and, therefore, a symmetrical ligand. In our case, however, **57** features an unsymmetrical NHC-P chelating ligand, consequently, the formation of a metallacycle intermediate upon C—H activation may give rise to a chiral iridium(III) hydride. This latter feature introduces further complexity to our analysis.

Notwithstanding, we started by locating all 32 geometrically allowed metallocyclic intermediates presumably formed after oxidative addition of carboxylic acid **65**, *i.e.*, 16 diastereomeric iridium(III) adducts and their corresponding isomers formed upon rotation of the allylic double bond, which gives rise to an additional set of 16 rotamers. Our main goal was to identify isomers possessing prohibitively high relative energies and exclude these from further consideration

In this regard, it is important to note that, in the best possible scenario, in which positional isomerisation of ligands around the metal centre and rotation of the double bond were not necessary, the exploration of all possible 32 potential energy surface trajectories would imply in the calculation of 128 stationary points, 96 transition states and 192 individual IRC determinations. The latter was not feasible under our current computational budget; therefore, our efforts were focused in locating one of

the likely reaction pathways to determine an upper energetic threshold, ultimately characterising the expected rate limiting step required for future experimental validation.

At the outset of our initial exploration, we verified large differences in relative energies amongst the 32 diastereomeric metallocyclic iridium(III) hydrides. Six representative structures located for these complexes and their respective relative energies are illustrated in Scheme 2.20.

(Λ)-**77a**	(Δ)-**77c**	(Λ)-**77e**
$\Delta G_r = 0.0$	$\Delta G_r = 12.9$	$\Delta G_r = 29.8$
$\Delta H_r = 0.0$	$\Delta H_r = 12.9$	$\Delta H_r = 30.0$

(Λ)-**77b**	(Δ)-**77d**	(Λ)-**77f**
$\Delta G_r = 2.8$	$\Delta G_r = 15.0$	$\Delta G_r = 30.8$
$\Delta H_r = 3.1$	$\Delta H_r = 15.5$	$\Delta H_r = 29.6$
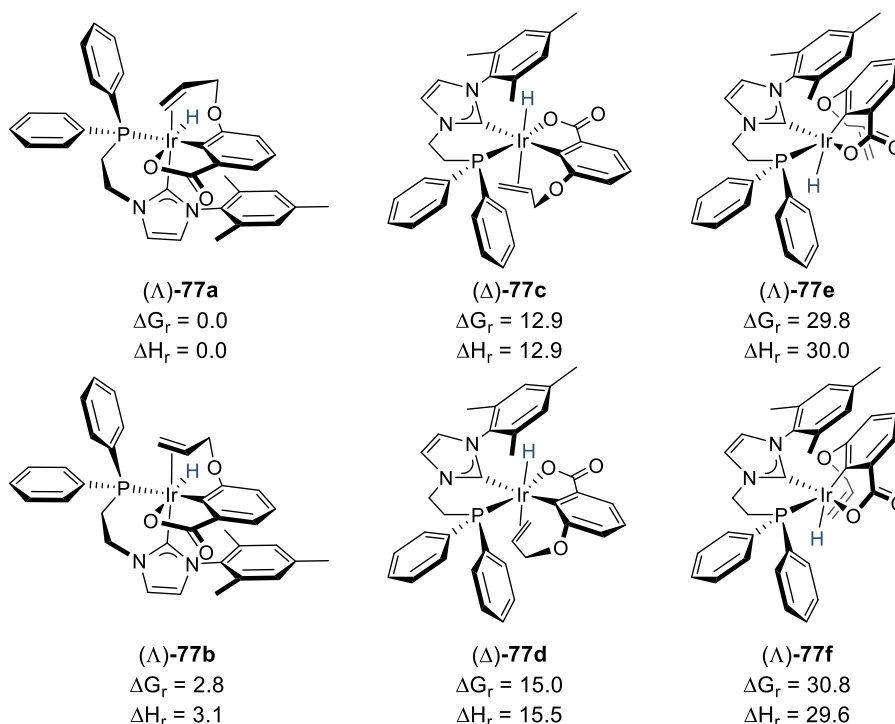
Scheme 2.20: Representative diastereomers and associated energies.[†]

[†]Energies given in kcal mol^{-1}.

Notably, the calculated relative energies differed by values as high as 30 kcal mol^{-1} for diastereomers (Λ)-**77e** and (Λ)-**77f**, which confirmed our original assumption, *i.e.*, some of the geometrical viable isomers could be too high in energy to constitute plausible intermediates in the reaction pathway. Closer analysis of the geometrical features within these structures indicate two main influences for the observed discrepancies in energy, *viz.*, electronic destabilisation and steric repulsion. More specifically, the six complexes shown in Scheme 2.20 cover both extremes in energy, with (Λ)-**77a** being the minimum, and (Λ)-**77f** the maximum in energy; and offers a

complex with energies that approach the average value amongst the 32 calculated isomers, (Δ)-**77c**. The remaining three structures comprise their respective olefin rotamers. Hence, while (Λ)-**77a** minimises electronic interactions by placing all strong σ-donors *trans*- to much weaker donors, this is not the case for (Λ)-**77f**, the latter placing the hydride and the aryl ligand in a *trans*- disposition. Additionally, (Λ)-**77e** and (Λ)-**77f** are further destabilised by steric interactions with both the mesityl *N*-substituent and the phosphine within the ancillary ligand framework.

Once energetically unattainable structures were discarded, we continued our exploration by evaluating the full reaction process. To help guide our exploration towards a more computationally efficient enterprise, we focused our search based on two observations. Firstly, the large energetic distribution found for complexes of type **77** indicated that the most feasible reaction trajectories would afford intermediates in which electronic interactions are minimised. To that end, given the necessity to occupy four coordination sites with fragments from the substrate, namely, carboxylate, aryl, hydride and olefin; a best case for electronic stabilisation would be obtained within an (H,O)-*trans*- geometry, *i.e.*, respectively a very strong and a poor σ-donor.[48]

Secondly, the necessity to perform a migratory insertion into a coordinated alkene helped us identify a suitable candidate for a low energy transition state. More specifically, by requiring a geometrical disposition in which the π-accepting olefin is situated *trans*- to the poorest σ-donor available within the coordination sphere, we expected a less effective $d_{Ir} \rightarrow \pi^*_{C=C}$ back donation and, hence, diminished electron density at this antibonding orbital. In this regard, current models of orbital interactions for migratory insertion events[161-163] suggests depletion of electron density at the $\pi^*_{C=C}$ should lower the activation barrier for the overall process, consequently leading to a transition state with reasonable energetics. Indeed, Huang and Liu in their evaluation of the intermolecular hydroarylation catalysed by iridium complexes suggests the existence of similar effects in their systems.[92]

In our case, the substrate engages in C—H activation to afford metallacycles that will necessarily adopt an (O,C,C=C)-*fac*- conformation prior to migratory insertion. This is a consequence of the requirement for co-planarity between the migrating group and the π-system of the olefin, and the existence of a strong (O,C)-chelate between

the carboxylate moiety and the aryl bonded to iridium. Hence, the only three geometrically allowed options for a ligand *trans-* to the alkene during a productive migratory insertion would be the hydride, the carbene from the NHC, and the phosphine ligand. Amongst these, the PPh$_2$ fragment should be the less competent σ-donor and was a likely candidate for further exploration.

Following these premises, and after some frustrated attempts to arrive at a pathway with reasonable energetics from (Λ)-**77a**, we were able to locate a plausible reaction trajectory for our hydroarylation reaction. These results are summarised in Schemes 2.21 and 2.22.
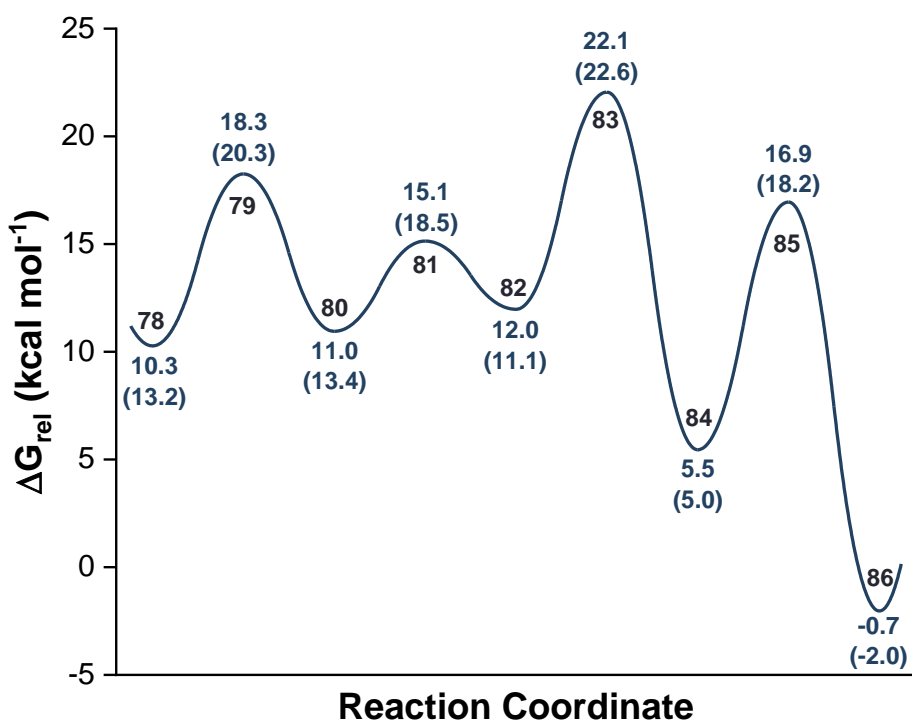
Scheme 2.21: Potential energy surface for the intramolecular hydroarylation.[†]

[†]Reported values are ΔG_{rel} with respect to (Λ)-**77a**; ΔH_{rel} reported in parentheses.
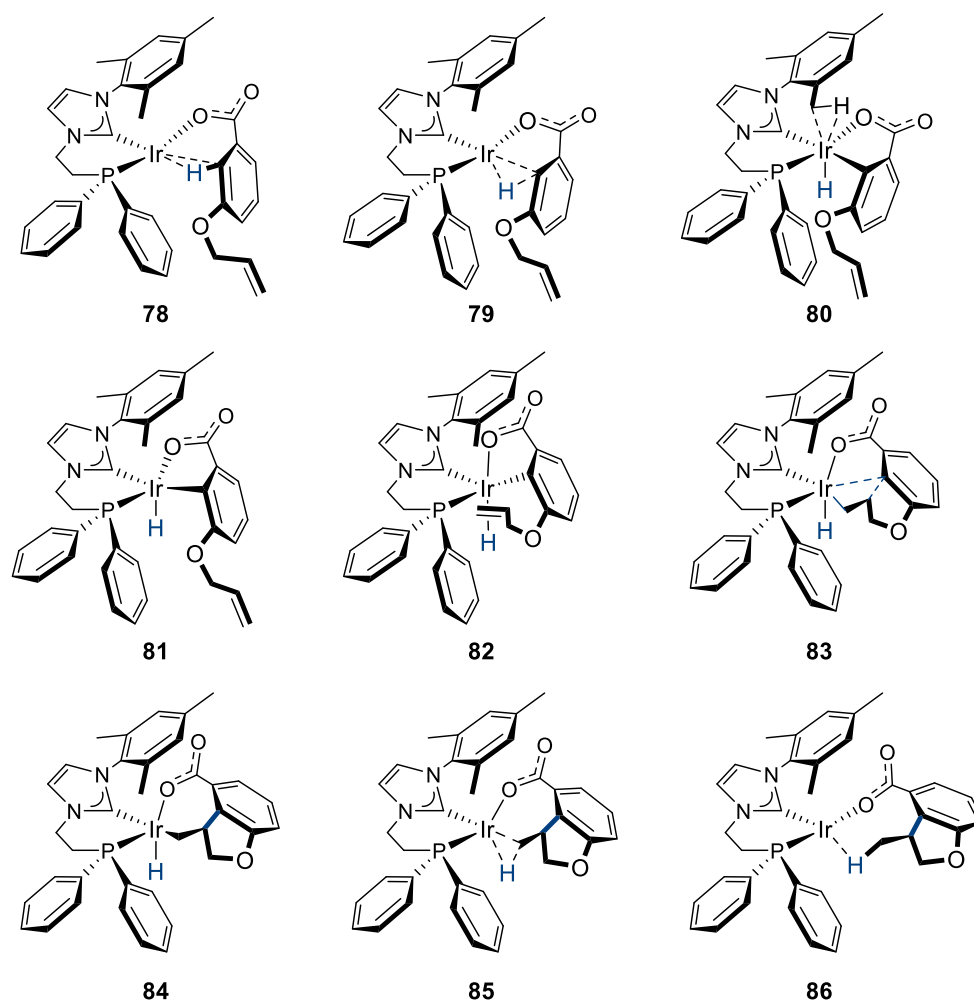
Scheme 2.22: Structure of located iridium complexes in the reaction pathway.

Therefore, the reaction starts with coordination of the carboxylate derived from substrate **65** to the iridium complex to afford intermediate **78**, which features an agostic interaction with the C—H bond to be activated *trans-* to the electron-rich NHC ligand. Oxidative addition then proceeds *via* transition state **79** to afford iridium(III) intermediate **80** with an overall barrier of 18.3 kcal mol^{-1}. Owing to the geometrical constraints imposed by the chelated substrate, during the C—H activation event the olefin is unable to coordinate to the vacant coordination site generated upon oxidative addition, and this site is then stabilised in **80** by an agostic interaction with the mesityl substituent in the NHC-P ligand. An isomerisation event was then required to allow alkene coordination to the metal centre, and this was accomplished through facile rotation of the carboxylate ligand to displace the weakly bound mesityl fragment, affording pentacoordinate intermediate **81**, and subsequent

coordination of the olefin to afford intermediate **82**, which is ready for the key C—C bond-forming event. Accordingly, migratory insertion through transition state **83** generates the 7-membered metallacycle intermediate **84** with an activation barrier of only 22.1 kcal mol^{-1}. Finally, a C—H reductive elimination from **84** occurs *via* transition state **85** and generates the desired product **86** with a 16.9 kcal mol^{-1} barrier. Some interesting features in this PES merit some consideration. Firstly, the calculation predicts the occurrence of a rate limiting migratory insertion, which is also expected to be irreversible. Note that reverting the subsequent reductive elimination should proceed with lower energy than that required to break the newly formed C—C bond. More precisely, the calculated $\Delta\Delta G^{(85.83)} = \Delta G^{(85)} - \Delta G^{(83)}$ is 5.2 kcal mol^{-1} favouring reductive elimination. Once again, assuming the Eyring-Polanyi equation applies to our system, that would result in *c.a.* 2800-fold increase in rate for C—H reductive elimination, thus, the reverse aryl- migration to cleave the C—C bond would be impractical.

Secondly, from our previous discussion on electronic influences on the energetics of metallacycles, it is possible to infer that a synergistic effect accounts for the rather low energy required for reaching key transition state **85**. More specifically, the steric hindrance imposed by the *N*-mesityl substituent of the carbene tends to restrict coordination at the side *trans-* to the phosphorus atom to planar ligands, which can reorient themselves and avoid destabilising steric interactions, or to small ligands. This steric component dictates the geometry of **82**, therefore, necessarily placing the olefin *trans-* to the carbene ligand. Thus, it is possible that the steric compression imposed by the mesityl substituent promotes an orientation of the olefin which is more suitable to C—C bond formation.

Our last line of theoretical enquiry concerned the catalytic competence of complex **57** in hydroarylation reactions with substrates bearing sterically hindered olefins. Thus, we investigated the energetic profile of substrates **72i-j** and **72l-m** in the migratory insertion described by the sequence **82** → **83** → **84**. More specifically, once optimised metallocyclic intermediates of type **82** and **84** were available, we located the respective transition states **83** connecting these species and evaluated their intrinsic reaction coordinate profile, as illustrated in Scheme 2.23.
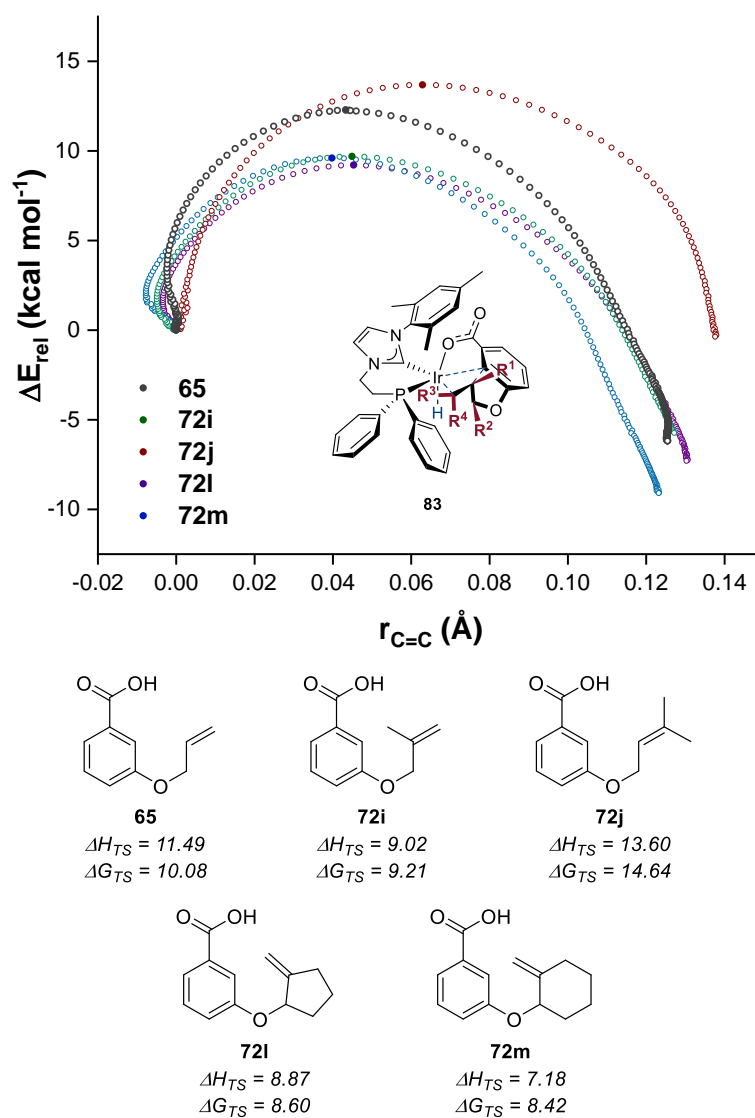
Scheme 2.23: Comparison of molecular reaction coordinates (*top*) and transition state energies for relevant substrates (*bottom*) for the migratoy insertion step.[†]

[†]Solid points indicate the position of transition states for each substrate; energies are given in kcal mol^{-1} and are relative to intermediates of type **82** in Scheme 2.22.

It is relevant to emphasise that comparisons provided in Scheme 2.23 were plotted against the variation of an internal molecular coordinate, *i.e.*, the change in distance between the two carbon atoms within the olefin. This procedure was originally proposed by Houk and Bickehaulpt[164,165] while investigating elementary reactions in organometallic complexes and is recommended as a more accurate descriptor of the reaction progress, since it is not influenced by other molecular motions within the transition metal complex.[165]

Notably, inspection of the IRC profiles for substrates in Scheme 2.23 indicates subtle changes in the position of the transition state in the PES for each substrate. Thus, exocyclic substrate **72m** displays the earliest transition state, suggesting that coordination of the olefin prior to migratory insertion gives rise to a structure in which the π-orbitals of the C=C bond are well-aligned to the C_{Ar}—Ir bond, hence reducing the degree of molecular reorganisation necessary to accomplish cyclisation. In fact, at the beginning of the reaction coordinate, substrate **72m** displays the smallest departure from a coplanar arrangement with the C_{Ar}—Ir bond, featuring a deviation of only 11.1º. On the other hand, substrate **72j** has both the latest transition state and the highest olefin misalignment among all structures, *i.e.*, 21.5º. In conjunction, these parameters indicate that the failure of **72j** to engage in productive reaction is a consequence of synergistic steric and electronic interactions. More specifically, the higher degree of substitution around the C=C bond hinders its approach to the metal centre which, in turn, forces the $\pi_{C=C}$ system farther away from the coplanar arrangement necessary to reach the transition state, ultimately resulting in additional energetic penalty.

Another important feature depicted in Scheme 2.23 is the instability of the metallocyclic intermediate after C—C bond formation with **72j**. Whilst the remaining substrates feature an overall decrease in relative energy after the migratory insertion, this is not the case for **72j**. This lack of energetic stabilisation should result in an easier reversibility of the C—C bond formation process, thus contributing for a poor reaction profile.

In summary, we were able to fully explore a viable reaction pathway for the hydroarylation of olefins catalysed by complex **57** employing substrate **65** as a probe molecule. The located pathway features three key steps: C—H activation *via* direct oxidative addition, a rate limiting migratory insertion that proceeds through an overall barrier of 22.1 kcal mol^{-1}, and a C—H reductive elimination that affords the desired product.

Importantly, these calculations allow us to make two important predictions about the kinetics of the reaction, *i.e.*, since the limiting step does not involve C—H bond breaking, a negligible ^{2}H KIE is expected; and a primary ^{13}C KIE is likely for both carbons involved in the C—C bond forming event. Considering our earlier

discussion on the effect of asynchronous transition state geometries on ^{13}C KIE values, and the observed sensitivity of activation energies to the degree of substitution at the C=C bond, in the absence of more sophisticated tools to quantify the expected isotope effects at the olefin terminus, it is not possible to infer whether a significant KIE can be expected for the corresponding carbon atom.

4. Conclusions

The knowledge gathered during our earlier studies on the nature of the C—H activation led us to investigate the functionalisation of inactivated C—H bonds to promote intramolecular hydroarylation reactions. Based on fundamental mechanistic aspects of our iridium complexes, we were able to identify a suitable directing group for further synthetic exploration. Moreover, we successfully employed Design of Experiments to optimise the reaction conditions, enabling us to develop a regioselective hydroarylative process. These features are illustrated in Scheme 2.23.
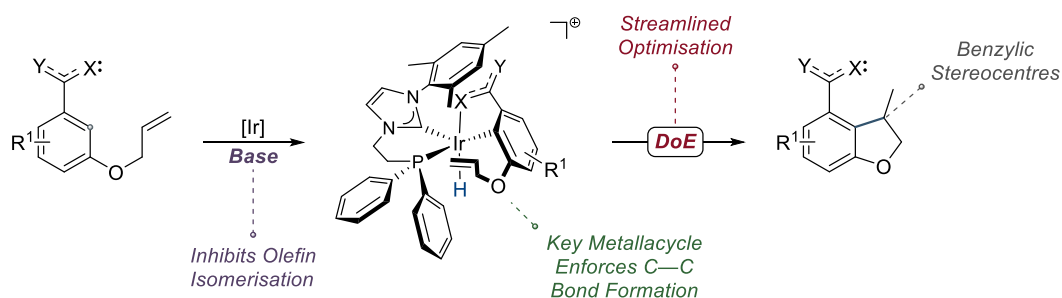
Scheme 2.23: Fundamentals of the intramolecular hydroarylation process.

Through strategic exploration of carboxylic acids, which generate a transient strongly coordinating directing group upon deprotonation, we conceived a substrate scope to enable a rapid assessment of the limitations and capabilities of this novel protocol. In particular, we were able to demonstrate our iridium catalysts are well-suited for the construction of tertiary and quaternary benzylic stereocentres through C—H functionalisation of synthetically versatile benzoic acids. Importantly, this catalytic protocol successfully promoted the hydroarylation of substrates bearing olefinic systems which are exocyclic to 5- and 6-membered carbocycles, affording quaternary carbon-carbon bonds in an expedient fashion.
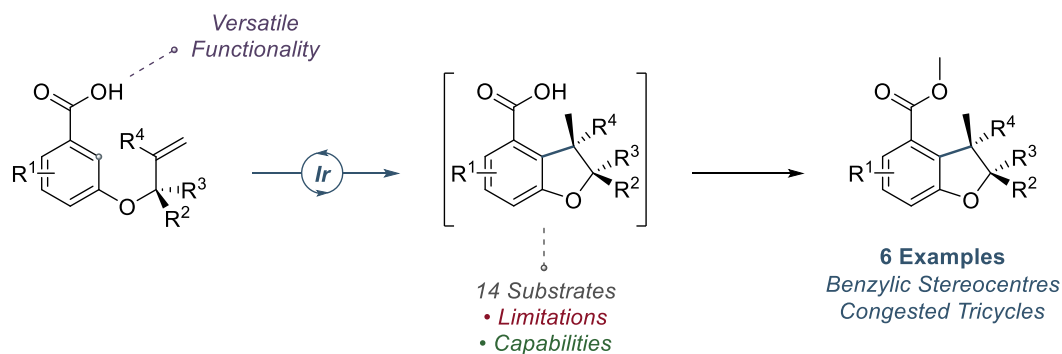
Scheme 2.24: Evaluation of key features within the substrate scope.

In a last line of enquiry, we employed DFT techniques to study the full mechanistic pathway involved in our hydroarylation reaction. These studies helped us establish a mechanistic proposal featuring C—H activation through direct oxidative addition to afford strongly ligated 5-membered metallocyclic intermediates, which then undergo C—C bond formation *via* rate limiting migratory insertion into the olefin, and a final C—H reductive elimination affords the desired products. Finally, we briefly investigated the effect of substituted olefins in the activation energy for the C—C bond formation. Our findings indicated a delicate balance between the steric hindrance at the alkene terminus and electronic properties of its iridium adduct dictate the height of activation barriers.

5. Future Work

Throughout this chapter, we devoted considerable attention to reaction development and evaluation of limitations to the substrate scope. Consequently, our synthetic exploration was focused in addressing main limitations within the field, *viz.*, reliance on strongly ligating, tailored directing groups; and synthesis of tricyclic motifs featuring a quaternary benzylic stereocentre. Thus, by demonstrating our catalytic system can readily overcome these issues, we secured the possibility to directly target the synthesis of congested 6-5-5 and 6-5-6 tricycles *via* hydroarylation processes, as depicted in Scheme 2.25.
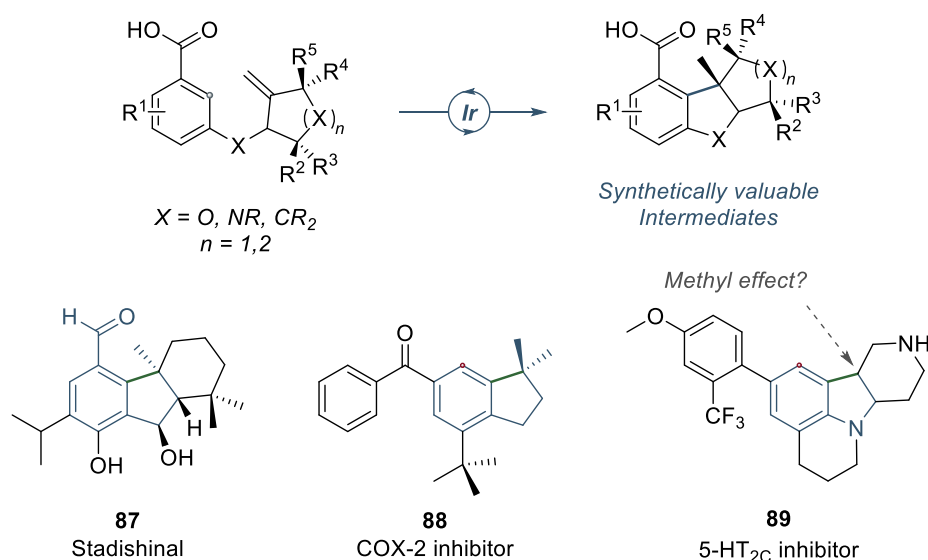
Scheme 2.25: Expansion of current scope and possible applications.[166-168]

As illustrated in Scheme 2.25, bi- and tricyclic systems are ubiquitous in natural products and pharmaceuticals. Simple examples highlighted include the natural product stadishinal (**87**),[166] and COX-2 inhibitor **88**,[167] which bear quaternary benzylic carbon centres; and the 5-HT$_{2C}$ inhibitor **89**[168] illustrates another possible area of investigation, namely, the application of our technology in the introduction of methyl groups to modulate pharmacological properties and inhibitory selectivity.[169] Other interesting expansions concern the synthesis of polycyclic furans and pyrroles, and spirocyclic molecules. Scheme 2.26 illustrates these concepts.
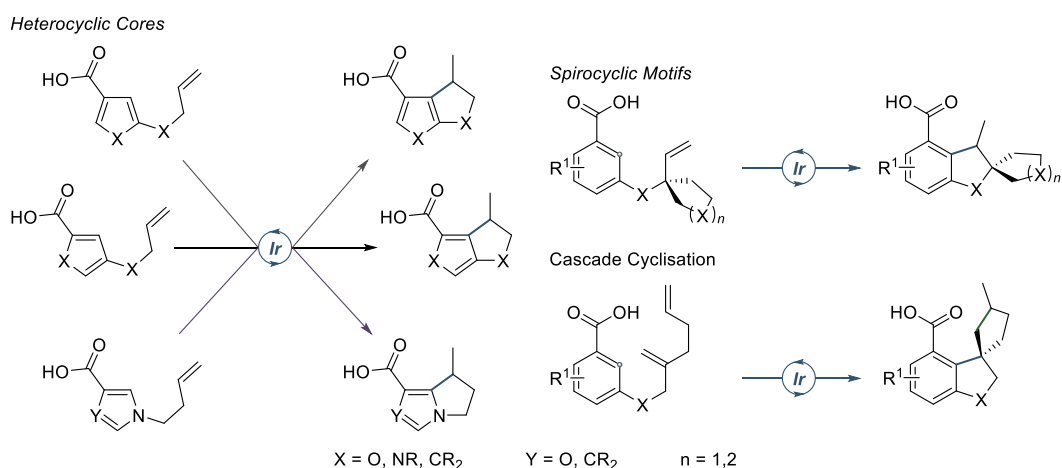
Scheme 2.26: Strategies targeting heterocycles and spirocyclic molecules.

Finally, by recognising the possibility to introduce benzylic stereocentres in a stereoselective fashion, it is possible to improve the current ligand set to enable enantioselective transformations. One such chelating NHC-P ligand is illustrated in Scheme 2.27.
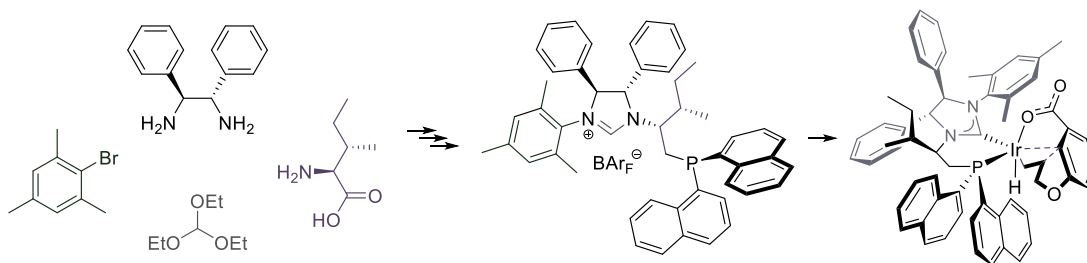
Scheme 2.27: Towards enantioselective hydroarylation.

6. Experimental Section

6.1 General

All chemical reagents and solvents were purchased from commercial sources (Acros Organics, Alfa Aesar, Sigma Aldrich and Strem Chemicals) and used without further purification, unless otherwise stated.

Dry dichloromethane was obtained by refluxing with CaH_2 and subsequent distillation under a nitrogen atmosphere. Dry tetrahydrofuran (THF) was obtained by refluxing with sodium wire employing sodium ketyl as an indicator, followed by distillation under a nitrogen atmosphere. Diglyme was purified by fractional distillation from CaH_2 under vacuum and stored over 4Å molecular sieves. Dry toluene was obtained from a PureSolv SPS-400-5 Solvent Purification System immediately prior to use.

Thin layer chromatography was performed using Merck silica plates (Silica gel 60 F254) and revealed under ultraviolet irradiation at 254 nm. Whenever required, solutions of potassium permanganate, vanillin and ninhydrin were used as revealing agents.

NMR spectra were acquired on a Bruker DPX 400 spectrometer at the respective frequencies for ^{1}H, ^{13}C and ^{19}F of 400, 101 and 376 MHz. Chemical shifts and coupling constants are reported in ppm and Hertz, respectively.

High resolution mass spectrometry (HRMS) data were obtained at the EPSRC UK National Mass Spectrometry Facility at Swansea University, employing nanoelectrospray ionization (ESI) method coupled to a Thermo Scientific LTQ-Orbitrap XL as mass analyser.

Melting points were measured in a Griffin C110230 Melting Point Apparatus.

Infrared spectra were acquired in a Shimadzu IRAffinity-1 FTIR spectrometer.

6.1.1 General procedure for the synthesis of methyl esters

To a round-bottomed flask equipped with a magnetic stirrer bar were added the carboxylic acid and methanol. The mixture was thoroughly stirred and cooled to 0 °C in an ice-water bath. The reaction vessel was fitted with a rubber septum and subjected to a constant stream of argon. Then, $SOCl_2$ was added dropwise at an approximate dropping rate of 0.1 mL min^{-1} and under vigorous, constant stirring. The mixture was allowed to stir at 0 °C for an additional 15 min, subsequently allowed to warm to room temperature and the reaction progress was monitored by TLC. When complete consumption of the starting material was observed, the mixture was evaporated under reduced pressure and subjected to the workup procedure described in full details for each substrate. The desired methyl esters were used in the next step without further purification.

6.1.2 General procedure for allylation of phenols

To a round-bottomed flask equipped with a magnetic stirrer bar were added NaI, K_2CO_3, the desired phenol and acetone. The mixture was thoroughly stirred at room temperature and allyl bromide was added dropwise under constant, vigorous stirring.

The vessel was fitted with a condenser and heated to the appropriate temperature in an oil bath for the allocated reaction time. After complete consumption of the starting material, as determined by TLC analysis of the reaction mixture, the vessel was allowed to cool to room temperature. The volatiles were evaporated under reduced pressure and the residue thus obtained was subjected to the workup procedure described in detail for each substrate.

6.1.3 General procedure for hydrolysis of methyl esters with 1M NaOH

To a round-bottomed flask equipped with a magnetic stirrer bar were added the appropriate methyl esters and MeOH. The reaction mixture was thoroughly stirred at room temperature and 1 M NaOH was added under constant vigorous stirring. The mixture was then heated to 50 °C in an oil bath for the allocated reaction time. After complete consumption of the starting material, assessed by TLC analysis of the reaction mixture, the reaction vessel was allowed to cool to room temperature and the volatiles were evaporated under reduced pressure. Unless otherwise stated, the resulting mixture was suspended in H_2O (10 mL mmol^{-1} of substrate), extracted twice with Et_2O (1:1 V_{Et_2O}/V_{H_2O}) and the organic phases were discarded. The aqueous phase was acidified to pH ~ 1 by careful addition of 12 M HCl, extracted three times with Et_2O (2:1 V_{Et_2O}/V_{H_2O}). The combined organic phases were dried over Na_2SO_4, filtered and evaporated under reduced pressure to afford the desired carboxylic acids.

6.1.3 General procedure for hydroarylation test reactions

To a flame-dried 5 mL microwave vial equipped with a magnetic stirrer bar were added K_2CO_3, the appropriate carboxylic acid and iridium catalyst **57**. The atmosphere was evacuated and carefully replenished with argon, and this process was repeated a further two times. Then, anhydrous diglyme was introduced via syringe, the vial was sealed and immersed in an oil bath pre-heated to 150 °C for 20 h. After the allocated reaction time, the reaction mixture was allowed to cool to room temperature, transferred to a separating funnel and diluted with Et_2O (25 mL). The

resulting mixture was washed with 0.5 M HCl (5 × 10 mL), brine (10 mL), dried over Na_2SO_4, filtered and evaporated under reduced pressure. The residue thus obtained was analysed by ^1H NMR spectroscopy and conversions were recorded based on diagnostic peaks for each substrate.

6.1.4 General procedure for hydroarylation and methylation sequence

To a flame-dried 10 mL round bottomed flask equipped with a magnetic stirrer bar were added K_2CO_3, the appropriate carboxylic acid and iridium catalyst **57**. The atmosphere was evacuated and carefully replenished with argon, and this process was repeated a further two times. Then, anhydrous diglyme was introduced *via* syringe and the rubber septum was replaced by a greased glass stopper. The flask was then immersed in an oil bath pre-heated to 150 °C, the stopper was physically restrained with a metal clamp and the reaction mixture was allowed to stir at that temperature for the allocated reaction time. The vessel was then allowed to cool to room temperature, the reaction mixture was transferred to a separating funnel, diluted with Et_2O (50 mL), washed with 0.5 M HCl (5 × 20 mL), brine (10 mL), dried over Na_2SO_4, filtered and evaporated under reduced pressure. The resulting residue was re-dissolved in acetonitrile and transferred to a round-bottomed flask equipped with a magnetic stirrer bar. Then, K_2CO_3 and MeI were added and the resulting mixture was heated to 50 °C in an oil bath for the allocated reaction time. The vessel was then allowed to cool to room temperature, the reaction mixture was transferred to a separating funnel, diluted with Et_2O (40 mL) and washed with H_2O (40 mL). The organic phases were collected, and the aqueous layer was extracted with Et_2O (2 × 40 mL). The combined organic phases were washed with brine (10 mL), dried over Na_2SO_4, filtered and evaporated under reduced pressure. The residue thus obtained was purified by column chromatography employing isocratic elution with mixtures of Et_2O and petroleum ether (1% Et_2O) to afford the desired products.

6.2   Synthesis of substrates

Experimental details reported in this section describe the full synthetic route for each substrate. Thus, the ordering of experiments parallels the preparative steps required for each compound. Intermediates *en route* to the final compounds are identified by suffixing their number with a new letter. The sequence for compound **72h** is depicted below as an example.
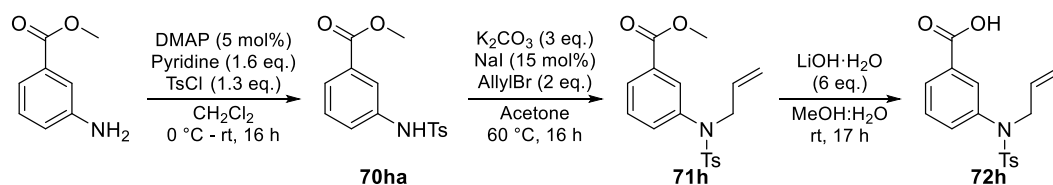
1-(3-(allyloxy)phenyl)ethan-1-one – **56**
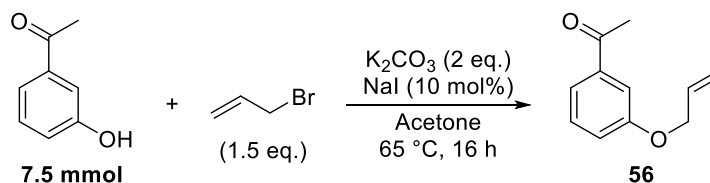
Following general procedure 6.1.2, NaI (116 mg, 0.77 mmol), K$_2$CO$_3$ (2.065 g, 14.9 mmol) and 3-hydroxyacetophenone (1.027 g, 7.54 mmol) were dissolved in acetone (40 mL) and reacted with allyl bromide (1.0 mL, 11.5 mmol) at 65 °C for 16 h. The residue obtained after evaporation was suspended in H$_2$O (50 mL) and partitioned with Et$_2$O (100 mL). The organic phases were collected, and the aqueous phase was extracted with Et$_2$O (3 × 75 mL). The combined organic phases were dried over Na$_2$SO$_4$, filtered and evaporated under reduced pressure. The crude mixture was subsequently purified by column chromatography employing gradient elution with mixtures of EtOAc and petroleum ether as eluents (0 – 20% Et$_2$O) to afford 1-(3-(allyloxy)phenyl)ethan-1-one (**56**) as a clear light yellow oil (1.246 g, **93% yield**). Analytical data for **56** is consistent with previously reported data:[170]
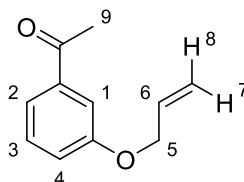
¹H NMR (400 MHz, CDCl₃): δ 7.54 (d, $^3J_{HH}$ = 7.6 Hz, 1H, H²), 7.51-7.48 (m, 1H, H¹), 7.36 (t, $^3J_{HH}$ = 7.9 Hz, 1H, H³), 7.12 (d, $^3J_{HH}$ = 8.3 Hz, 1H, H⁴), 6.06 (ddt, $^3J_{HH}$ = 17.2 Hz, $^3J_{HH}$ = 10.6 Hz, $^3J_{HH}$ = 5.3 Hz, 1H, H⁶), 5.43 (ddt, $^3J_{HH}$ = 17.3 Hz, $^4J_{HH}$ = $^2J_{HH}$ = 1.5 Hz, 1H, H⁷), 5.31 (ddt, $^3J_{HH}$ = 10.4 Hz, $^4J_{HH}$ = $^2J_{HH}$ = 1.5 Hz, 1H, H⁸), 4.59 (d, $^3J_{HH}$ = 5.2 Hz, 2H, H⁵), 2.59 (s, 3H, H⁹).

¹³C NMR (101 MHz, CDCl₃): δ 198.0, 158.9, 138.6, 133.0, 129.7, 121.3, 120.3, 118.1, 113.5, 69.1, 26.8.

IR (neat, cm⁻¹): 3078, 2922, 2864, 1680, 1593, 1580, 1483, 1437, 1423, 1356, 1329, 1269, 1206, 1163, 1092, 1074, 1022, 1009, 991, 970, 957, 928, 872, 856, 787, 758, 718, 687, 608.

*Sequence for 3-(allyloxy)benzoic acid – **65***

64a   **64**   **65**
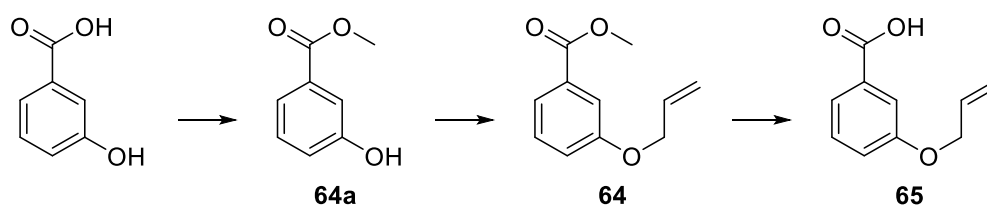
Methyl 3-hydroxybenzoate – **64a**
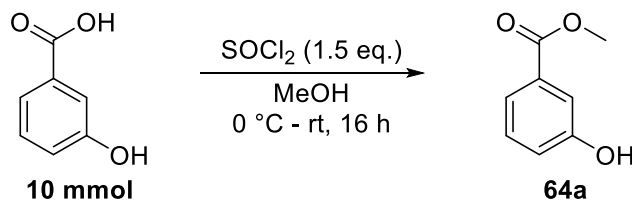
Following general procedure 6.1.1, 3-hydroxybenzoic acid (1.385 g, 10.0 mmol) was dissolved in methanol (15 mL) and reacted with SOCl₂ (1.1 mL, 15.1 mmol) for 16 h. The residue obtained after evaporation was suspended in H₂O (50 mL) and extracted with EtOAc (3 × 50 mL). The combined organic phases were washed with saturated aqueous NaHCO₃ (2 × 50 mL), dried over Na₂SO₄, filtered and evaporated under reduced pressure to afford methyl 3-hydroxybenzoate (**64a**) as a white solid (1.462 g, **96% yield**).

Analytical data for **64a** is consistent with previously reported data:[171]
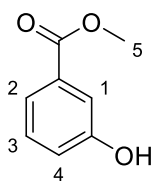
¹H NMR (400 MHz, CDCl₃): δ 7.61 (dt, $^3J_{HH}$ = 7.8 Hz, $^4J_{HH}$ = 1.3 Hz, 1H, H²), 7.58 (dd, $^4J_{HH}$ = 2.5 Hz, $^4J_{HH}$ = 1.5 Hz, 1H, H¹), 7.31 (dt, $^3J_{HH}$ = 7.9 Hz, 1H, H³) 7.07 (ddd, $^3J_{HH}$ = 8.2 Hz, $^4J_{HH}$ = 2.6 Hz, $^4J_{HH}$ = 1.0 Hz, 1H, H⁴), 5.74 (br s, 1H, OH), 3.92 (s, 3H, H⁵).

¹³C NMR (101 MHz, CDCl₃): δ 167.4, 156.0, 131.5, 129.9, 122.1, 120.4, 116.5, 52.5.

Melting point: 66-68 °C.

IR (neat, cm⁻¹): 3080, 3021, 2982, 2951, 2868, 1719, 1651, 1593, 3366, 2961, 1690, 1597, 1503, 1435, 1354, 1306, 1238, 1223, 1186, 1157, 1105, 1072, 995, 968, 910, 883, 795, 758, 721, 685, 677.

Methyl 3-(allyloxy)benzoate – **64**
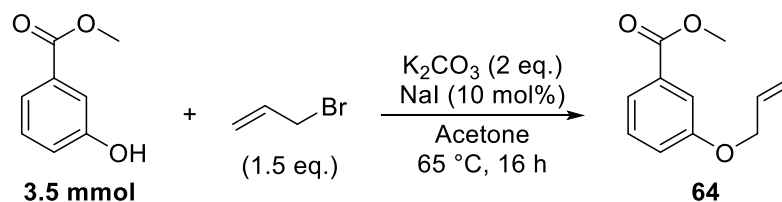
Following general procedure 6.1.2, NaI (76 mg, 0.51 mmol), K₂CO₃ (1.385 g, 10.0 mmol) and methyl 3-hydroxybenozoate (0.761 g, 5.00 mmol) were dissolved in acetone (27 mL) and reacted with allyl bromide (0.7 mL, 8.09 mmol) at 65 °C for 16 h. TLC analyses employed 10% EtOAc in petroleum ether. The residue obtained after evaporation was suspended in Et₂O (75 mL) and the organic layer was washed with H₂O (50 mL). The aqueous phase was extracted with Et₂O (3 × 50 mL), the combined organic phases were dried over Na₂SO₄, filtered and evaporated under reduced pressure. The crude mixture was subsequently purified by column chromatography, employing gradient elution with mixtures of Et₂O and petroleum ether as eluents (0 – 20% Et₂O) to afford methyl 3-(allyloxy)benzoate (**64**) as a colourless oil (0.911 g, **95% yield**).

Analytical data for **64** is consistent with previously reported data:[173]
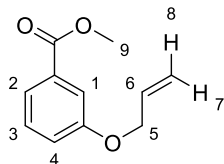
^{1}H NMR (400 MHz, CDCl$_3$): δ 7.63 (dt, $^3J_{HH}$ = 8.0 Hz, $^4J_{HH}$ = 1.4 Hz, 1H, H^2), 7.57 (dd, $^4J_{HH}$ = 2.9 Hz, $^4J_{HH}$ = 1.5 Hz, 1H, H^1), 7.33 (t, $^3J_{HH}$ = 7.9 Hz, 1H, H^3), 7.11 (ddd, $^3J_{HH}$ = 8.3 Hz, $^4J_{HH}$ = 2.5 Hz, $^4J_{HH}$ = 1.3 Hz, 1H, H^4), 6.05 (ddt, $^3J_{HH}$ = 17.3 Hz, $^3J_{HH}$ =10.5 Hz, $^3J_{HH}$ = 5.3 Hz, 1H, H^6), 5.42 (dq, $^3J_{HH}$ = 17.2 Hz, J_{HH} = 1.6 Hz, 1H, H^7), 5.30 (dq, $^3J_{HH}$ = 10.5 Hz, J_{HH} = 1.4 Hz, 1H, H^8), 4.58 (dt, $^3J_{HH}$ = 5.3 Hz, $^4J_{HH}$ = 1.5 Hz, 2H, H^5), 3.90 (s, 3H, H^9).

^{13}C NMR (101 MHz, CDCl$_3$): δ 167.0, 158.7, 133.0, 131.6, 129.5, 122.3, 120.3, 118.0, 115.1, 69.0, 52.3.

IR (neat, cm^{-1}): 3078, 2990, 2949, 2864, 2365, 2345, 2324, 1719, 1585, 1487, 1445, 1423, 1408, 1317, 1275, 1215, 1190, 1157, 1099, 1074, 1024, 993, 926, 889, 878, 799, 785, 754, 683.

3-(allyloxy)benzoic acid – **65**
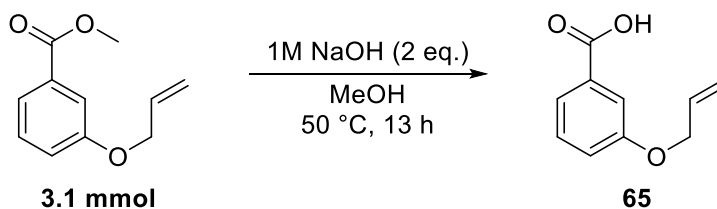
Following general procedure 6.1.3, methyl 3-(allyloxy)benzoate (591.5 mg, 3.08 mmol) was dissolved in MeOH (40 mL) and reacted with 1 M NaOH (6.2 mL, 6.2 mmol) for 13 h. TLC analysis was performed with 10% MeOH in CH$_2$Cl$_2$. After workup, 3-(allyloxy)benzoic acid (**69**) was isolated as a white solid (490.1 mg, **89% yield**).
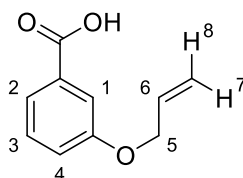
^{1}H NMR (400 MHz, DMSO-d_6): δ 13.0 (s, 1H, OH), 7.54 (dt, $^3J_{HH}$ = 7.6 Hz, $^4J_{HH}$ = 1.2 Hz, 1H, H^2), 7.46 (dd, $^4J_{HH}$ = 2.5 Hz, $^4J_{HH}$ = 1.4 Hz, 1H, H^1), 7.41 (t, $^3J_{HH}$ = 7.9 Hz, 1H, H^3), 7.21 (ddd, $^3J_{HH}$ = 8.4 Hz, $^4J_{HH}$ = 2.9 Hz, $^4J_{HH}$ = 1.0 Hz, 1H, H^4), 6.05 (ddt, $^3J_{HH}$ = 17.3 Hz, $^3J_{HH}$ = 10.4 Hz, $^3J_{HH}$ = 5.2 Hz, 1H, H^6), 5.41 (dq, $^3J_{HH}$ = 17.3 Hz, J_{HH} = 1.7 Hz, 1H, H^7), 5.30 (dq, $^3J_{HH}$ = 10.5 Hz, J_{HH} = 1.5 Hz, 1H, H^8), 4.63 (dt, $^3J_{HH}$ = 5.1 Hz, $^4J_{HH}$ = 1.5 Hz, 2H, H^5).

^{13}C NMR (101 MHz, CDCl$_3$): δ 167.1, 158.1, 133.4, 132.2, 129.7, 121.7, 119.5, 117.5, 114.8, 68.3.

Melting point: 68-70 °C.

IR (neat, cm^{-1}): 3075, 2907, 2862, 2822, 2635, 2563, 1682, 1585, 1487, 1449, 1422, 1296, 1285, 1236, 1115, 1078, 1018, 991, 934, 918, 874, 808, 773, 752, 679, 642.

*Sequence for 5-(allyloxy)-2-methylbenzoic acid – **72a***
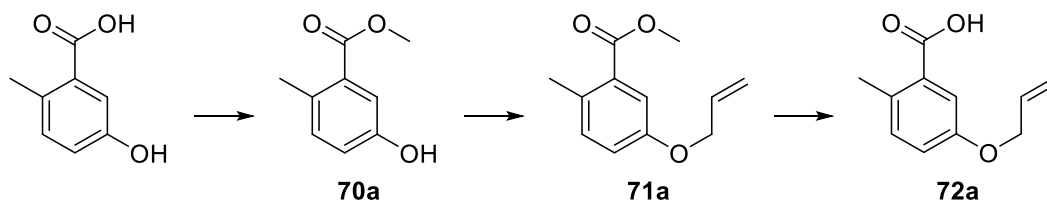
Methyl 2-methyl-5-hydroxybenzoate (**70a**)
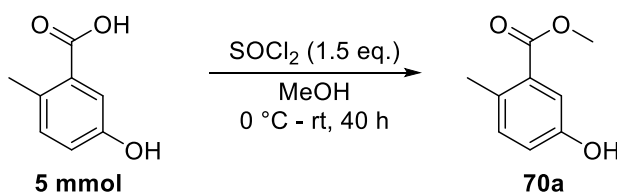
Following general procedure 6.1.2, 2-methyl-5-hydroxybenzoic acid (0.760 g, 5.00 mmol) was dissolved in methanol (7.5 mL) and reacted with SOCl$_2$ (0.55 mL, 7.5 mmol) for 40 h. TLC analysis employed 25% EtOAc in petroleum ether. The residue obtained after evaporation was suspended in H$_2$O (10 mL) and treated with saturated aqueous NaHCO$_3$ (1 mL). The resulting mixture was extracted with EtOAc (3 × 25 mL), the combined organic phases were washed with brine (30 mL), dried over Na$_2$SO$_4$, filtered and evaporated under reduced pressure to afford methyl 2-methyl-5-hydroxybenzoate (**70a**) as a white solid (0.837 g, **100% yield**).

Analytical data for **70a** is consistent with previously reported data:[174,175]
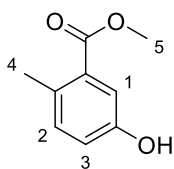
¹H NMR (400 MHz, CDCl₃): δ 7.42 (d, $^4J_{HH}$ = 2.8 Hz, 1H, H¹), 7.11 (d, $^3J_{HH}$ = 8.2 Hz, 1H, H²), 6.91 (dd, $^3J_{HH}$ = 8.2 Hz, $^4J_{HH}$ = 2.7 Hz, 1H, H³), 5.23 (br s, 1H, OH), 3.89 (s, 3H, H⁵), 2.50 (s, 3H, H⁴).

¹³C NMR (101 MHz, CDCl₃): δ 168.2, 153.6, 133.0, 132.4, 130.4, 119.5, 117.3, 52.1, 20.9.

Melting point: 68-70 °C.

IR (neat, cm⁻¹): 3318, 3076, 2953, 2928, 2847, 1692, 1605, 1504, 1454, 1437, 1342, 1312, 1273, 1223, 1192, 1076, 1036, 1007, 976, 881, 829, 800, 783, 758, 654.

Methyl 5-(allyloxy)-2-methylbenzoate – **71a**
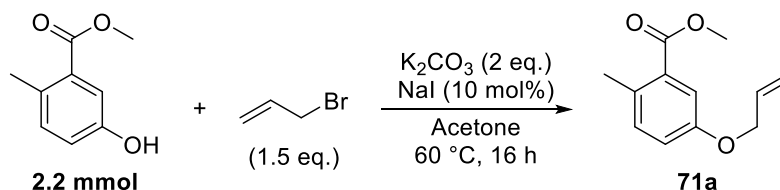
Following general procedure 6.1.2, NaI (46 mg, 0.31 mmol), K₂CO₃ (0.566 g, 4.09 mmol) and methyl 3-hydroxybenozoate (0.332 g, 2.18 mmol) were dissolved in acetone (10 mL) and reacted with allyl bromide (0.26 mL, 3.0 mmol) at 60 °C for 16 h. TLC analysis employed 10% EtOAc in petroleum ether. The residue obtained after evaporation was suspended in H₂O (10 mL) and partitioned with Et₂O (20 mL). The aqueous layer was extracted with Et₂O (2 × 20 mL), and the combined organic phases were washed with brine (10 mL), dried over Na₂SO₄, filtered and evaporated under reduced pressure. The residue was purified by column chromatography employing gradient elution with mixtures of EtOAc and petroleum ether as eluents (0 – 10% EtOAc) to afford methyl 5-(allyloxy)-2-methylbenzoate (**71a**) as a colourless oil (0.372 g, **90% yield**).
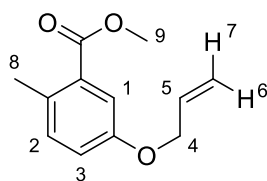
¹H NMR (400 MHz, CDCl₃): δ 7.48 (d, $^4J_{HH}$ = 2.8 Hz, 1H, H¹), 7.16 (d, $^3J_{HH}$ = 8.5 Hz, 1H, H²), 6.99 (dd, $^3J_{HH}$ = 8.4 Hz, $^4J_{HH}$ = 2.8 Hz, 1H, H³), 6.07 (ddt, $^3J_{HH}$ = 17.1 Hz, $^3J_{HH}$ = 10.6 Hz, $^3J_{HH}$ = 5.3 Hz, 1H, H⁵), 5.43 (dq, $^3J_{HH}$ = 17.3 Hz, J_{HH} = 1.4 Hz, 1H, H⁶), 5.31 (dq, $^3J_{HH}$ = 10.9 Hz, J_{HH} = 1.4 Hz, 1H, H⁷), 4.56 (dt, $^3J_{HH}$ = 5.3 Hz, $^4J_{HH}$ = 1.3 Hz, 2H, H⁴), 3.90 (s, 3H, H⁹), 2.54 (s, 3H, H⁸).

¹³C NMR (101 MHz, CDCl₃): δ 167.3, 155.9, 132.6, 132.1, 131.9, 129.7, 118.6, 117.2, 115.6, 68.5, 51.3, 20.3.

IR (neat, cm⁻¹): 3088, 3024, 2951, 2928, 2862, 1719, 1647, 1609, 1570, 1499, 1435, 1410, 1383, 1364, 1315, 1281, 1271, 1252, 1211, 1155, 1142, 1101, 1072, 1026, 997, 924, 889, 872, 820, 810, 799, 785, 764, 745, 687, 627.

HRMS (positive ESI): m/z calculated for [M+H]⁺ $C_{12}H_{15}O_3$: 207.1016; found: 207.1014.

5-(allyloxy)-2-methylbenzoic acid – **72a**
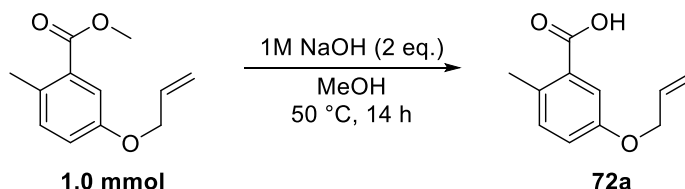
Following general procedure 6.1.3, methyl 5-(allyloxy)-2-methylbenzoate (206.5 mg, 1.00 mmol) was dissolved in and MeOH (13 mL) and reacted with 1 M NaOH (2.0 mL, 2.0 mmol) for 14 h. TLC analysis was performed with 10% EtOAc in petroleum ether. After workup, 5-(allyloxy)-2-methylbenzoic acid (**72a**) was isolated as a white solid (167.5 mg, **87% yield**).
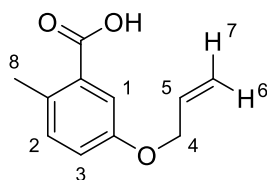
¹H NMR (400 MHz, DMSO-d_6): δ 12.8 (br s, 1H, OH), 7.35 (d, $^4J_{HH}$ = 2.8 Hz, 1H, H¹), 7.20 (d, $^3J_{HH}$ = 8.5 Hz, 1H, H²), 7.05 (dd, $^3J_{HH}$ = 8.3 Hz, $^4J_{HH}$ = 2.8 Hz, 1H, H³), 6.03 (ddt, $^3J_{HH}$ = 17.2 Hz, $^3J_{HH}$ = 10.4 Hz, $^3J_{HH}$ = 5.2 Hz, 1H, H⁵), 5.39 (dq, $^3J_{HH}$ = 17.2 Hz, J_{HH} = 1.6 Hz, 1H, H⁶), 5.26 (dq, $^3J_{HH}$ =10.6 Hz, J_{HH} = 1.3 Hz, 1H, H⁷), 4.58 (dt, $^3J_{HH}$ = 5.1 Hz, $^4J_{HH}$ =1.4 Hz, 2H, H⁴), 2.45 (s, 3H, H⁸).

¹³C NMR (101 MHz, DMSO-d_6): δ 168.4, 155.9, 133.6, 132.5, 131.2, 130.9, 118.3, 117.3, 115.8, 68.2, 20.3.

Melting point: 91-92 °C

IR (neat, cm⁻¹): 2967, 2928, 2882, 2853, 2818, 2627, 2571, 1690, 1676, 1645, 1605, 1578, 1499, 1450, 1416, 1379, 1315, 1285, 1265, 1236, 1204, 1150, 1105, 1076, 1026, 1011, 988, 930, 868, 831, 777, 683.

HRMS (positive ESI): m/z calculated for [M+H]⁺ $C_{11}H_{13}O_3$: 193.0865; found: 193.0870.

*Sequence for 3-(allyloxy)-5-fluorobenzoic acid – **72b***
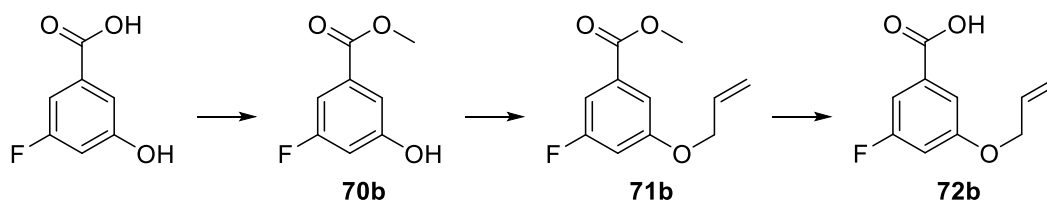
Methyl 3-fluoro-5-hydroxybenzoate – **70b**
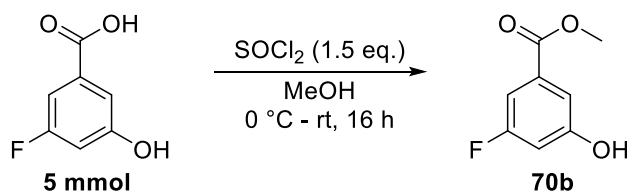
Following general procedure 6.1.1, 3-fluoro-5-hydroxybenzoic acid (0.783 g, 5.02 mmol) was dissolved in methanol (7.5 mL) and reacted with SOCl₂ (0.55 mL, 7.5 mmol) for 16 h. TLC analysis employed 25% EtOAc in petroleum ether. The residue obtained after evaporation was suspended in H₂O (10 mL) and partitioned with EtOAc (30 mL). This mixture was treated with saturated aqueous NaHCO₃ (1 mL) and the organic phase was collected. The aqueous layer was then extracted with EtOAc (3 × 30 mL), and the combined organic phases were washed with brine (20

mL), dried over Na_2SO_4, filtered and evaporated under reduced pressure to afford methyl 3-fluoro-5-hydroxybenzoate (**70b**) as a white solid (0.809 g, **95% yield**).
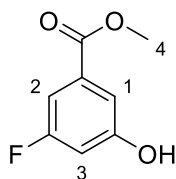

1H NMR (400 MHz, DMSO-d_6): δ 10.4 (s, 1H, OH), 7.22 (t, $^4J_{HH}$ = 1.6 Hz, 1H, H^1), 7.11 (dt, $^3J_{HF}$ = 9.0 Hz, $^4J_{HH}$ = 1.5 Hz, 1H, H^2), 6.85 (dt, $^3J_{HF}$ = 10.6 Hz, $^4J_{HH}$ = 2.3 Hz, 1H, H^3), 3.84 (s, 3H, H^4).

13C NMR (101 MHz, DMSO-d_6): δ 165.2 (d, $^4J_{CF}$ = 4.0 Hz), 162.7 (d, $^1J_{CF}$ = 243 Hz), 159.2 (d, $^3J_{CF}$ = 12.3 Hz), 132.1 (d, $^3J_{CF}$ = 10.0 Hz) 112.3, 107.3 (d, $^2J_{CF}$ = 23.1 Hz), 106.2 (d, $^2J_{CF}$ = 23.6 Hz), 52.4.

19F NMR (376 MHz, DMSO-d_6): δ -111.3.

Melting point: 134-136 °C.

IR (neat, cm^{-1}): 3337, 3078, 3015, 2961, 2853, 1694, 1607, 1547, 1508, 1456, 1437, 1339, 1300, 1254, 1190, 1138, 1096, 991, 903, 868, 851, 826, 762, 665, 638.

HRMS (negative ESI): m/z calculated for [M-H]$^-$ $C_8H_6O_3F$: 169.0306; found: 169.0310.

Methyl 3-(allyloxy)-5-fluorobenzoate – **71b**
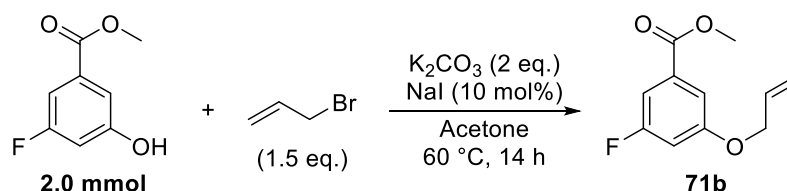
Following general procedure 6.1.2, NaI (35 mg, 0.23 mmol), K_2CO_3 (0.556 g, 4.02 mmol) and methyl 3-fluoro-5-hydroxybenzoate (0.332 g, 2.00 mmol) were dissolved in acetone (10 mL) and reacted with allyl bromide (0.26 mL, 3.0 mmol) at 60 °C for 14 h. TLC analysis employed 25% EtOAc in petroleum ether. The residue obtained after evaporation was suspended in H_2O (10 mL) and partitioned with Et_2O (20 mL). The aqueous layer was extracted with Et_2O (2 × 20 mL), and the combined organic phases were washed with brine (10 mL), dried over Na_2SO_4, filtered and evaporated under reduced pressure. The residue was purified by column chromatography

employing gradient elution with mixtures of Et$_2$O and petroleum ether as eluents (0 –
20% Et$_2$O) to afford methyl 3-(allyloxy)-5-fluorobenzoate (**71b**) as a colourless oil
(0.389 g, **93% yield**).
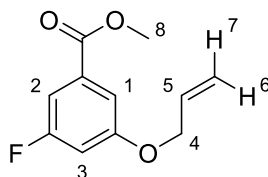
^{1}H NMR (400 MHz, CDCl$_3$): δ 7.41-7.38 (m, 1H, H^1), 7.34 (d, $^3J_{HF}$ = 8.7 Hz, 1H,
H^2), 6.84 (dt, $^3J_{HF}$ = 10.2 Hz, $^4J_{HH}$ = 2.4 Hz, 1H, H^3), 6.05 (ddt, $^3J_{HH}$ = 17.1 Hz, $^3J_{HH}$
= 10.5 Hz, $^3J_{HH}$ = 5.3 Hz, 1H, H^5), 5.44 (dt, $^3J_{HH}$ = 17.3 Hz, J_{HH} = 1.5 Hz, 1H, H^6),
5.33 (ddd, $^3J_{HH}$ = 10.3 Hz, J_{HH} = 1.3 Hz, 1H, H^7), 4.59 (dt, $^3J_{HH}$ = 5.3 Hz, $^4J_{HH}$ = 1.4
Hz, 2H, H^4), 3.93 (s, 3H, H^8).

^{13}C NMR (101 MHz, CDCl$_3$): δ 165.4 (d, $^4J_{CF}$ = 4.3 Hz), 162.7 (d, $^1J_{CF}$ = 246 Hz),
159.3 (d, $^3J_{CF}$ = 10.8 Hz), 132.1 (d, $^3J_{CF}$ = 10.0 Hz), 131.8, 117.7, 110.8 (d, $^4J_{CF}$ = 3.1
Hz), 108.5 (d, $^2J_{CF}$ = 23.9 Hz), 106.9 (d, $^2J_{CF}$ = 24.7 Hz), 68.8, 51.9.

^{19}F NMR (376 MHz, CDCl$_3$): δ -110.9.

IR (neat, cm^{-1}): 3090, 2953, 2363, 2326, 1722, 1649, 1607, 1591, 1435, 1425, 1366,
1335, 1306, 1269, 1238, 1227, 1190, 1140, 1094, 1040, 1001, 930, 889, 862, 841,
766, 669.

HRMS (positive ESI): m/z calculated for [M+H]$^+$ C$_{11}$H$_{12}$O$_3$F$^+$: 211.0770; found:
211.0775.

3-(allyloxy)-5-fluorobenzoic acid – **72b**
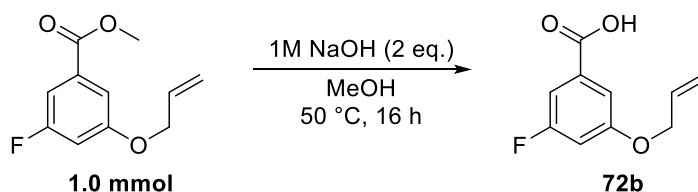
Following general procedure 6.1.3, 3-(allyloxy)-5-fluorobenzoate (210.7 mg, 1.00
mmol) was dissolved in MeOH (13 mL) and reacted with 1 M NaOH (2.0 mL, 2.0
mmol) for 16 h. TLC analysis was performed with 25% EtOAc in petroleum ether.

After workup, 3-(allyloxy)-5-fluorobenzoic acid (**72b**) was isolated as a white solid (187.4 mg, **95% yield**).
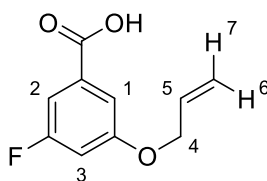
^{1}H NMR (400 MHz, DMSO-d_6): δ 13.3 (br s, 1H, OH), 7.31 (br s, 1H, H^1), 7.25 (br d, $^3J_{HF}$ = 8.0 Hz, 1H, H^2), 7.13 (dt, $^3J_{HF}$ = 10.7 Hz, $^4J_{HH}$ = 2.1 Hz, 1H, H^3), 6.04 (ddt, $^3J_{HH}$ = 17.2 Hz, $^3J_{HH}$ = 10.6 Hz, $^3J_{HH}$ = 5.3 Hz, 1H, H^5), 5.41 (dt, $^3J_{HH}$ = 17.4 Hz, $^4J_{HH}$ = 1.5 Hz, 1H, H^6), 5.29 (dt, $^3J_{HH}$ = 10.5 Hz, $^4J_{HH}$ = 1.3 Hz, 1H, H^7), 4.66 (dt, $^3J_{HH}$ = 4.9 Hz, $^4J_{HH}$ = 1.3 Hz, 2H, H^4).

^{13}C NMR (101 MHz, DMSO-d_6): δ 166.0 (d, $^4J_{CF}$ = 3.0 Hz), 162.6 (d, $^1J_{CF}$ = 243 Hz), 159.5 (d, $^3J_{CF}$ = 11.6 Hz), 133.6 (d, $^3J_{CF}$ = 9.2 Hz), 133.0, 117.9, 111.7, 108.0 (d, $^2J_{CF}$ = 23.1 Hz), 106.7 (d, $^2J_{CF}$ = 25.2 Hz), 68.8.

^{19}F NMR (376 MHz, DMSO-d_6): δ -110.9.

Melting point: 74-76 °C.

IR (neat, cm^{-1}): 3073, 2924, 2870, 2824, 2639, 2519, 1690, 1649, 1595, 1477, 1460, 1445, 1422, 1369, 1329, 1310, 1267, 1231, 1140, 1101, 1040, 991, 935, 868, 768, 735, 665, 621.

HRMS (negative ESI): m/z calculated for [M-H]$^-$ C$_{10}$H$_8$O$_3$F: 195.0463; found: 195.0467.

Sequence for 3-(allyloxy)-4-methylbenzoic acid – **72c**
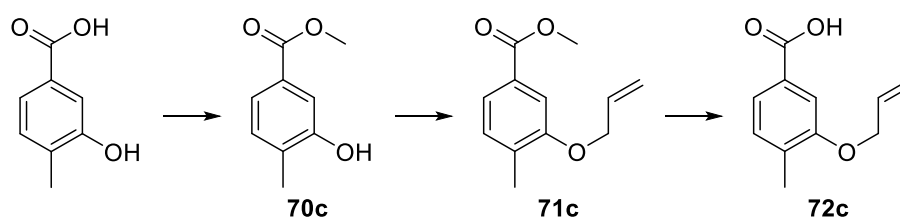
Methyl 3-hydroxy-4-methylbenzoate – **70c**
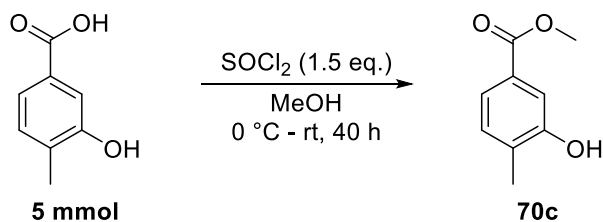
Following general procedure 6.1.1 for the synthesis of methyl esters, 3-hydroxy-4-methylbenzoic acid (0.762 g, 5.01 mmol) was dissolved in methanol (7.5 mL), then $SOCl_2$ (0.55 mL, 7.5 mmol) was added at 0 °C, and the mixture was allowed to react for 40 h. The volatiles were then evaporated under reduced pressure, the residue thus obtained was suspended in H_2O (10 mL) and partitioned with EtOAc (25 mL). This mixture was treated with saturated aqueous $NaHCO_3$ (1 mL) and the organic phase was collected. The aqueous layer was then extracted with EtOAc (2 × 25 mL), and the combined organic phases were washed with saturated aqueous $NaHCO_3$ (20 mL), H_2O (20 mL), brine (30 mL), dried over Na_2SO_4, filtered and evaporated under reduced pressure to afford methyl 3-hydroxy-4-methylbenzoate (**70c**) as a white solid (0.777 g, **93% yield**).
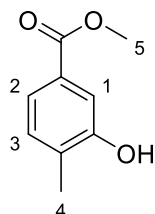
¹H NMR (400 MHz, CDCl₃): δ 7.58 (d, $^4J_{HH}$ = 1.6 Hz, 1H, H^1), 7.54 (dd, $^3J_{HH}$ = 7.8 Hz, $^4J_{HH}$ = 1.6 Hz, 1H, H^2), 7.20 (d, $^3J_{HH}$ = 7.8 Hz, 1H, H^3), 5.65 (br s, 1H, OH), 3.93 (s, 3H, H^5), 2.33 (s, 3H, H^4).

¹³C NMR (101 MHz, CDCl₃): δ 166.9, 153.5, 130.5, 129.7, 128.4, 121.4, 115.3, 51.7, 15.6.

Melting point: 116-118 °C.

IR (neat, cm⁻¹): 3285, 3277, 3028, 2953, 2156, 1694, 1611, 1591, 1435, 1414, 1379, 1371, 1294, 1234, 1184, 1136, 1099, 1034, 999, 910, 887, 826, 808, 762, 719, 691, 685.

Methyl 3-(allyloxy)-4-methylbenzoate – **71c**
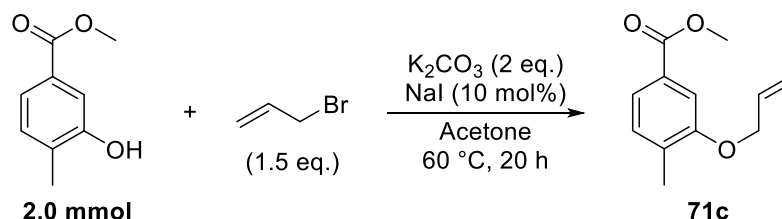
Following general procedure 6.1.2 for the allylation of phenols, NaI (33 mg, 0.22 mmol), K_2CO_3 (0.554 g, 4.01 mmol) and methyl 3-hydroxy-4-methylbenozoate (0.332 g, 2.00 mmol) were dissolved in acetone (10 mL) and reacted with allyl bromide (0.26 mL, 3.0 mmol) at 60 °C for 20 h. After complete consumption of the starting material, determined by TLC analysis of the reaction mixture (10% EtOAc in petroleum ether), the mixture was allowed to cool to room temperature and the volatiles were evaporated under reduced pressure. The residue thus obtained was suspended in H_2O (10 mL) and partitioned with Et_2O (20 mL). The aqueous layer was extracted with Et_2O (2 × 20 mL), and the combined organic phases were washed with brine (20 mL), dried over Na_2SO_4, filtered and evaporated under reduced pressure. The residue was purified by column chromatography, employing gradient elution with mixtures of Et_2O and petroleum ether as eluents (0 – 7.5% Et_2O) to afford methyl 3-(allyloxy)-4-methylbenzoate (**71c**) as a colourless oil (0.315 g, **76% yield**).

Analytical data for **71c** is consistent with previously reported data:[176]
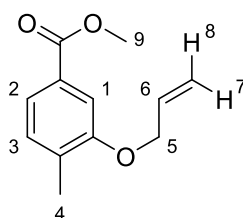
^{1}H NMR (400 MHz, CDCl₃): δ 7.58 (dd, $^3J_{HH}$ = 7.7 Hz, $^4J_{HH}$ = 1.5 Hz, 1H, H^2), 7.49 (d, $^4J_{HH}$ = 1.4 Hz, 1H, H^1), 7.21 (d, $^3J_{HH}$ = 7.8 Hz, 1H, H^3), 6.10 (ddt, $^3J_{HH}$ = 17.2 Hz, $^3J_{HH}$ = 10.3 Hz, $^3J_{HH}$ = 5.2 Hz, 1H, H^6), 5.47 (dq, $^3J_{HH}$ = 17.4 Hz, J_{HH} = 1.7 Hz, 1H, H^7), 5.31 (dq, $^3J_{HH}$ = 10.6 Hz, J_{HH} = 1.4 Hz, 1H, H^8), 4.62 (dt, $^3J_{HH}$ = 5.0 Hz, $^4J_{HH}$ = 1.5 Hz, 2H, H^5), 3.92 (s, 3H, H^9), 2.32 (s, 3H, H^4).

^{13}C NMR (101 MHz, CDCl$_3$): δ 166.7, 156.0, 132.6, 132.3, 130.0, 128.3, 121.5, 116.7, 111.2, 68.2, 51.5, 16.1.

IR (neat, cm^{-1}): 3084, 3019, 2988, 2949, 2924, 1717, 1647, 1609, 1582, 1504, 1433, 1410, 1377, 1317, 1288, 1263, 1231, 1186, 1155, 1126, 1101, 1016, 999, 922, 899, 876, 833, 795, 758, 708, 694, 656, 637, 623.

HRMS (positive ESI): m/z calculated for [M+H]$^+$ C$_{12}$H$_{15}$O$_3$: 207.1016; found: 207.1015.

3-(allyloxy)-4-methylbenzoic acid – **72c**
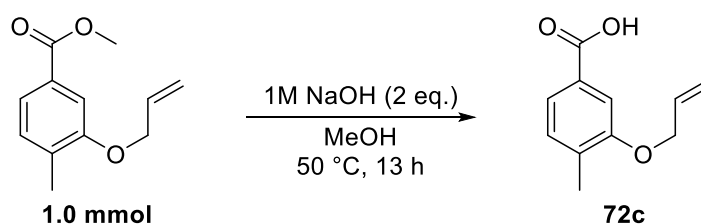
Following general procedure 6.1.3, 3-(allyloxy)-4-methylbenzoate (204.1 mg, 0.99 mmol) was dissolved in MeOH (13 mL) and reacted with 1 M NaOH (2.0 mL, 2.0 mmol) for 16 h. TLC analysis was performed with 25% Et$_2$O in petroleum ether. After workup, 3-(allyloxy)-4-methylbenzoic acid (**72c**) was isolated as a white solid (175.7 mg, **92% yield**).
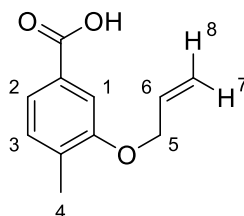
^{1}H NMR (400 MHz, CDCl$_3$): δ 7.68 (dd, $^3J_{HH}$ = 7.7 Hz, $^4J_{HH}$ = 1.3 Hz, 1H, H^2), 7.56 (d, $^4J_{HH}$ = 1.0 Hz, 1H, H^1), 7.26 (dd, $^3J_{HH}$ = 7.7 Hz, $^4J_{HH}$ = 1.0 Hz, 1H, H^3), 6.12 (ddt, $^3J_{HH}$ = 17.2 Hz, $^3J_{HH}$ = 10.3 Hz, $^3J_{HH}$ = 5.2 Hz, 1H, H^6), 5.49 (dq, $^3J_{HH}$ = 17.2 Hz, J_{HH} = 1.6 Hz, 1H, H^7), 5.33 (dq, $^3J_{HH}$ = 10.6 Hz, J_{HH} = 1.5 Hz, 1H, H^8), 4.65 (dt, $^3J_{HH}$ = 5.1 Hz, $^4J_{HH}$ = 1.6 Hz, 2H, H^5), 2.35 (s, 3H, H^4).

^{13}C NMR (101 MHz, CDCl$_3$): δ 171.6, 156.1, 133.5, 132.5, 130.1, 127.4, 122.3, 116.9, 111.6, 68.3, 16.2.

Melting point: 138-139 °C.

IR (neat, cm^{-1}): 2959, 2907, 2835, 1680, 1651, 1605, 1574, 1557, 1504, 1454, 1420, 1358, 1323, 1300, 1269, 1246, 1196, 1155, 1132, 1107, 1026, 1007, 995, 989, 961, 943, 928, 870, 837, 808, 799, 781, 764, 727, 660, 635.

HRMS (positive ESI): m/z calculated for [M+H]$^+$ C$_{11}$H$_{13}$O$_3$: 193.0865; found: 193.0867.

Sequence for 3-(allyloxy)-4-methoxybenzoic acid – **72d**
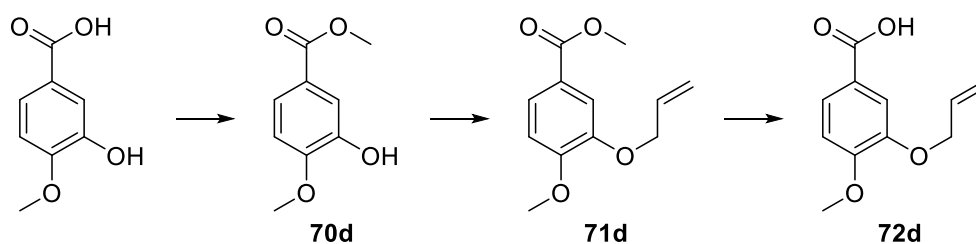
Methyl 3-hydroxy-4-methoxybenzoate – **70d**
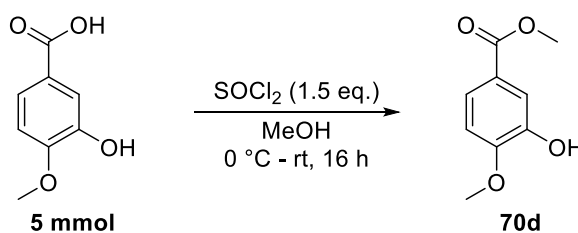
Following general procedure 6.1.1 for the synthesis of methyl esters, 3-hydroxy-4-methoxybenzoic acid (0.844 g, 5.02 mmol) was dissolved in methanol (7.5 mL), then SOCl$_2$ (0.55 mL, 7.5 mmol) was added at 0 °C, and the mixture was warmed to room temperature and reacted for 16 h. TLC analysis of the reaction mixture (25% EtOAc in petroleum ether) indicated consumption of the starting material and the volatiles were then evaporated under reduced pressure. The residue thus obtained was suspended in H$_2$O (10 mL) and partitioned with EtOAc (30 mL). This mixture was treated with saturated aqueous NaHCO$_3$ (1 mL) and the organic phase was collected. The aqueous layer was then extracted with EtOAc (2 × 30 mL), and the combined organic phases were washed with saturated aqueous NaHCO$_3$ (10 mL), brine (10 mL), dried over Na$_2$SO$_4$, filtered and evaporated under reduced pressure to afford methyl 3-hydroxy-4-methoxybenzoate (**70d**) as a highly viscous, light brown oil (0.728 g, **80% yield**).

Analytical data for **70d** is consistent with previously reported data:[177]
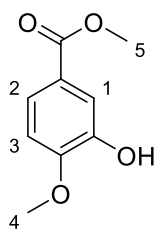
^{1}H NMR (400 MHz, CDCl$_3$): δ 7.64-7.60 (m, 2H, H^1/H^2), 6.87 (d, $^3J_{HH}$ = 8.2 Hz, 1H, H^3), 5.86 (br s, 1H, OH), 3.94 (s, 3H, H^5), 3.89 (s, 3H, H^4).

^{13}C NMR (101 MHz, CDCl$_3$): δ 166.4, 150.0, 144.8, 122.8, 122.3, 115.1, 109.4, 55.5, 51.5.

IR (neat, cm^{-1}): 3406, 3013, 2953, 2843, 1697, 1611, 1587, 1508, 1466, 1439, 1352, 1306, 1275, 1219, 1206, 1192, 1167, 1123, 1101, 1020, 984, 930, 883, 816, 795, 758, 723, 700, 689, 629.

Methyl 3-(allyloxy)-4-methoxybenzoate – **71d**
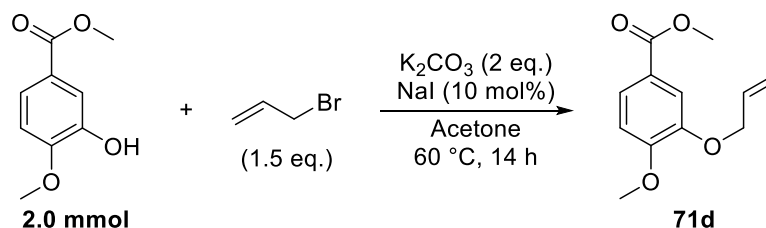
Following general procedure 6.1.2 for the allylation of phenols, NaI (37 mg, 0.25 mmol), K$_2$CO$_3$ (0.558 g, 4.04 mmol) and methyl 3-hydroxy-4-methoxybenzoate (0.363 g, 1.99 mmol) were dissolved in acetone (10 mL) and reacted with allyl bromide (0.26 mL, 3.0 mmol) at 60 °C for 14 h. After complete consumption of the starting material, determined by TLC analysis of the reaction mixture (25% EtOAc in petroleum ether), the mixture was allowed to cool to room temperature and the volatiles were evaporated under reduced pressure. The residue thus obtained was suspended in H$_2$O (10 mL) and partitioned with Et$_2$O (20 mL). The aqueous layer was extracted with Et$_2$O (2 × 20 mL), and the combined organic phases were washed with brine (10 mL), dried over Na$_2$SO$_4$, filtered and evaporated under reduced pressure. The residue was purified by column chromatography employing gradient elution with mixtures of Et$_2$O and petroleum ether as eluents (0 – 40% Et$_2$O) to

afford methyl 3-(allyloxy)-4-methoxybenzoate (**71d**) as a white solid (0.342 g, **77% yield**).
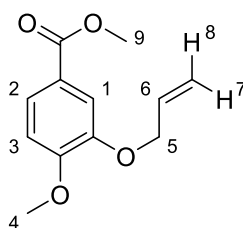
^{1}H NMR (400 MHz, CDCl$_3$): δ 7.70 (dd, $^3J_{HH}$ = 8.4 Hz, $^4J_{HH}$ = 1.9 Hz, 1H, H^2), 7.58 (d, $^4J_{HH}$ = 1.9 Hz, 1H, H^1), 6.91 (d, $^3J_{HH}$ = 8.3 Hz, 1H, H^3), 6.12 (ddt, $^3J_{HH}$ = 17.1 Hz, $^3J_{HH}$ = 10.6 Hz, $^3J_{HH}$ = 5.4 Hz, 1H, H^6), 5.46 (dt, $^3J_{HH}$ = 17.2 Hz, $^4J_{HH}$ = 1.5 Hz, 1H, H^7), 5.33 (dt, $^3J_{HH}$ = 10.3 Hz, $^4J_{HH}$ = 1.4 Hz, 1H, H^8), 4.68 (dt, $^3J_{HH}$ = 5.3 Hz, $^4J_{HH}$ = 1.4 Hz, 2H, H^5), 3.95 (s, 3H, H^9), 3.91 (s, 3H, H^4).

^{13}C NMR (101 MHz, CDCl$_3$): δ 166.3, 152.9, 147.0, 132.3, 123.3, 122.1, 117.9, 113.4, 110.1, 69.3, 55.5, 51.5.

Melting point: 58-60 °C.

IR (neat, cm^{-1}): 3084, 2949, 2907, 2843, 2615, 1705, 1667, 1649, 1587, 1512, 1464, 1443, 1423, 1366, 1342, 1294, 1267, 1217, 1190, 1157, 1130, 1099, 1015, 999, 978, 930, 870, 839, 791, 779, 762, 729, 662, 631.

HRMS (positive ESI): m/z calculated for [M+H]$^+$ C$_{12}$H$_{15}$O$_4$$^+$: 223.0965, found: 223.0965.

3-(allyloxy)-4-methoxybenzoic acid – **72d**
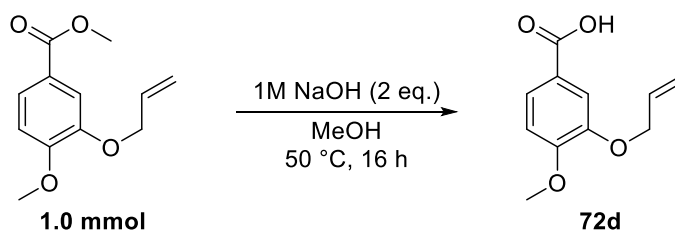
Following general procedure 6.1.3, 3-(allyloxy)-4-methoxybenzoate (222.4 mg, 1.00 mmol) was dissolved in MeOH (13 mL) and reacted with 1 M NaOH (2.0 mL, 2.0 mmol) for 16 h. TLC analysis was performed with 25% EtOAc in petroleum ether. After workup, 3-(allyloxy)-4-methoxybenzoic acid (**72d**) was isolated as a white solid (132.3 mg, **63% yield**).
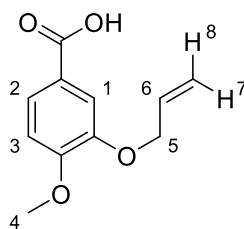
^{1}H NMR (400 MHz, DMSO-d_6): δ 12.64 (br s, 1H, OH), 7.58 (d, $^3J_{HH}$ = 8.1 Hz, 1H, H^2), 7.46 (s, 1H, H^1), 7.06 (d, $^3J_{HH}$ = 8.3 Hz, 1H, H^3), 6.05 (ddt, $^3J_{HH}$ = 16.4 Hz, $^3J_{HH}$ = 10.6 Hz, $^3J_{HH}$ = 5.0 Hz, 1H, H^6), 5.40 (br d, $^3J_{HH}$ = 17.3 Hz, 1H, H^7), 5.27 (br d, $^3J_{HH}$ = 10.4 Hz, 1H, H^8), 4.61 (br d, $^3J_{HH}$ = 4.2 Hz, 2H, H^5), 3.84 (s, 3H, H^4).

^{13}C NMR (101 MHz, DMSO-d_6): δ 167.0, 152.9, 147.1, 133.6, 123.4, 122.9, 117.6, 113.6, 111.2, 68.9, 55.7.

Melting point: 140-142 °C.

IR (neat, cm^{-1}): 2957, 2914, 2841, 1678, 1585, 1518, 1427, 1412, 1368, 1344, 1300, 1265, 1221, 1188, 1134, 1109, 1016, 1003, 949, 941, 922, 866, 839, 822, 781, 760, 725, 654, 629.

HRMS (negative ESI): m/z calculated for [M-H]$^-$ C$_{11}$H$_{11}$O$_4^-$: 207.0663; found: 207.0667.

Sequence for 3,5-bis(allyloxy)benzoic acid – **72e**
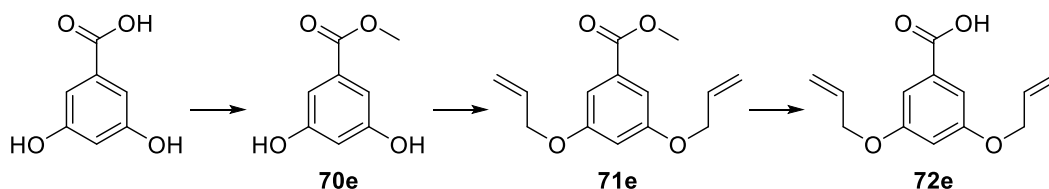
Methyl 3,5-dihydroxybenzoate (**70e**)
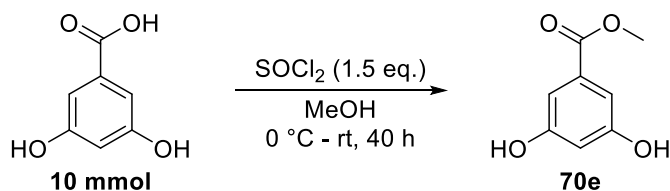
Following general procedure 6.1.2 for the synthesis of methyl esters, 3,5-dihydroxybenzoic acid (1.558 g, 10.1 mmol) was dissolved in methanol (15 mL), then SOCl$_2$ (1.1 mL, 15.1 mmol) and the mixture was allowed to react for 40 h. The

volatiles were then evaporated under reduced pressure, and the residue thus obtained was dissolved in H_2O (20 mL) and treated with saturated aqueous $NaHCO_3$ (2 mL). The resulting mixture was extracted with EtOAc (3 × 50 mL), and the combined organic phases were washed with brine (40 mL), dried over Na_2SO_4, filtered and evaporated under reduced pressure to afford methyl 3,5-dihydroxybenzoate (**70e**) as a light cream solid (1.574 g, **93% yield**).

Analytical data for **70e** is consistent with previously reported data:[178]
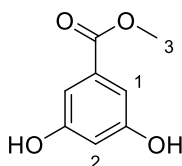
^{1}H NMR (400 MHz, DMSO-d_6): δ 9.62 (s, 2H, OH), 6.82 (d, $^4J_{HH}$ = 2.2 Hz, 2H, H^1), 6.45 (t, $^4J_{HH}$ = 2.3 Hz, 1H, H^2), 3.79 (s, 3H, H^3).

^{13}C NMR (101 MHz, DMSO-d_6): δ 166.3, 158.6, 131.3, 107.2, 107.1, 52.0.

Melting point: 159-161 °C.

IR (neat, cm^{-1}): 3372, 3235, 3088, 2997, 2951, 1688, 1634, 1599, 1485, 1441, 1325, 1304, 1261, 1206, 1161, 1101, 1016, 995, 907, 870, 854, 833, 766, 667.

Methyl 3,5-bis(allyloxy)benzoate (**71e**)
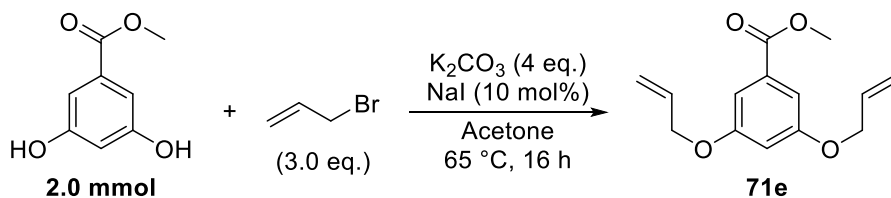
Following general procedure 6.1.2 for the allylation of phenols, NaI (29 mg, 0.19 mmol), K_2CO_3 (1.110 g, 8.03 mmol) and methyl 3,5-dihydroxybenozoate (0.336 g, 2.00 mmol) were dissolved in acetone (20 mL) and reacted with allyl bromide (0.52 mL, 6.0 mmol) at 65 °C for 16 h. After complete consumption of the starting material, determined by TLC analysis of the reaction mixture (10% EtOAc in petroleum ether), the mixture was allowed to cool to room temperature and the solvent was evaporated under reduced pressure. The residue thus obtained was suspended in Et_2O (30 mL) and the organic phase was washed with water (15 mL). The aqueous layer was extracted with Et_2O (2 × 30 mL), and the combined organic

phases were washed with brine (20 mL), dried over Na$_2$SO$_4$, filtered and evaporated under reduced pressure. The crude mixture was purified by column chromatography, employing gradient elution with mixtures of EtOAc and petroleum ether as eluents (0 – 10% EtOAc) to afford methyl 3,5-bis(allyloxy)benzoate (**71e**) as a colourless viscous oil which solidified upon standing (0.431 g, **87% yield**).

Analytical data for **71e** is consistent with previously reported data:[179]
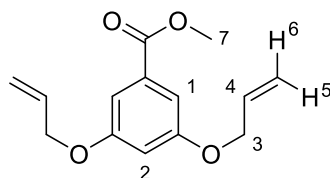
^{1}H NMR (400 MHz, CDCl$_3$): δ 7.19 (d, $^4J_{HH}$ = 2.5 Hz, 2H, H^1), 6.68 (t, $^4J_{HH}$ = 2.3 Hz, 1H, H^2), 6.04 (ddt, $^3J_{HH}$ = 17.2 Hz, $^3J_{HH}$ = 10.4 Hz, $^3J_{HH}$ = 5.2 Hz, 2H, H^4), 5.41 (dq, $^3J_{HH}$ = 17.0 Hz, J_{HH} = 1.6 Hz, 2H, H^5), 5.29 (dq, $^3J_{HH}$ = 10.7 Hz, J_{HH} = 1.4 Hz, 2H, H^6), 4.55 (dt, $^3J_{HH}$ = 5.3 Hz, $^4J_{HH}$ = 1.6 Hz, 4H, H^3), 3.89 (s, 3H, H^7).

^{13}C NMR (101 MHz, CDCl$_3$): δ 166.9, 159.7, 132.9, 132.1, 118.0, 108.3, 107.2, 69.2, 52.3.

Melting point: 27-29 °C.

IR (neat, cm^{-1}): 3080, 3021, 2982, 2951, 2868, 1719, 1651, 1593, 1445, 1435, 1423, 1346, 1321, 1298, 1258, 1227, 1165, 1150, 1103, 1053, 1032, 991, 932, 893, 872, 860, 847, 762, 675, 658, 631.

3,5-bis(allyloxy)benzoic acid – **72e**
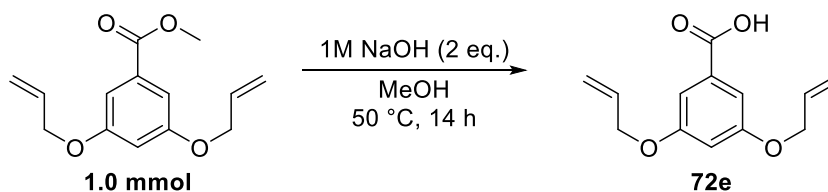
Following general procedure 6.1.3, 3,5-bis(allyloxy)benzoate (248.2 mg, 1.00 mmol) was dissolved in MeOH (13 mL) and reacted with 1 M NaOH (2.0 mL, 2.0 mmol) for 14 h. TLC analysis was performed with 10% EtOAc in petroleum ether. After workup, 3,5-bis(allyloxy)benzoic acid (**72e**) was isolated as a white solid (218.8 mg, **93% yield**).

Analytical data for **72e** is consistent with previously reported data:[180,181]
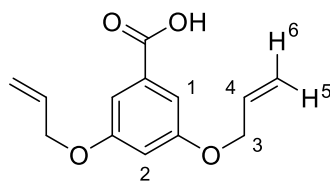
^{1}H NMR (400 MHz, DMSO-d_6): δ 13.0 (br s, 1H, OH), 7.07 (d, $^4J_{HH}$ = 2.2 Hz, 2H, H^1), 6.79 (t, $^4J_{HH}$ = 2.1 Hz, 1H, H^2), 6.04 (ddt, $^3J_{HH}$ = 17.3 Hz, $^3J_{HH}$ =10.5 Hz, $^3J_{HH}$ = 5.2 Hz, 2H, H^4), 5.40 (dq, $^3J_{HH}$ = 17.3 Hz, J_{HH} = 1.5 Hz, 2H, H^5), 5.27 (dq, $^3J_{HH}$ = 10.5 Hz, J_{HH} = 1.2 Hz, 2H, H^6), 4.61 (br d, $^3J_{HH}$ = 5.1 Hz, 4H, H^3).

^{13}C NMR (101 MHz, DMSO-d_6): δ 166.9, 159.2, 133.4, 132.8, 117.5, 107.8, 106.2, 68.4.

Melting point: 64-65 °C.

IR (neat, cm^{-1}): 3021, 2961, 2924, 2864, 2641, 2531, 1690, 1647, 1593, 1472, 1445, 1420, 1410, 1364, 1344, 1300, 1273, 1175, 1157, 1101, 1045, 1026, 991, 941, 930, 880, 851, 802, 766, 746, 675, 654, 615.

Sequence for 3-(allyl(tert-butoxycarbonyl)amino)benzoic acid – **72f**
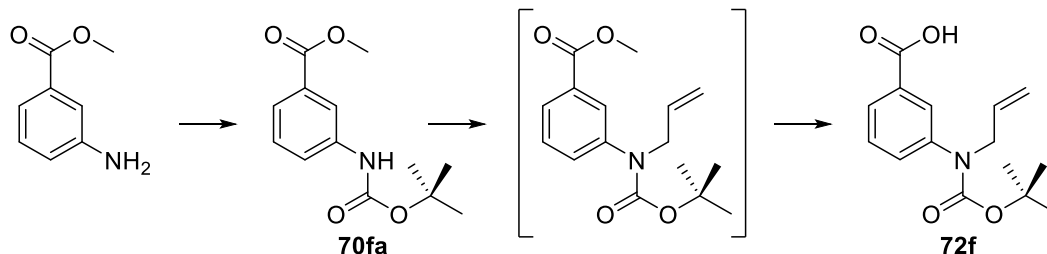

Methyl 3-aminobenzoate (**70f**)
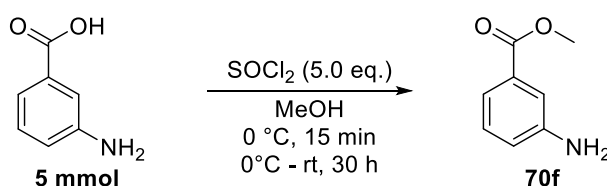
To a round-bottomed flask equipped with a magnetic stirrer bar were added 3-aminobenzoic acid (0.688 g, 5.02 mmol) and methanol (25 mL). A rubber septum was fitted to the reaction vessel and the mixture was subjected to a constant stream of argon. The mixture was then cooled to 0 °C in an ice-water bath and SOCl$_2$ (1.85 mL, 25 mmol) was added dropwise at that temperature under constant, vigorous

stirring. The reaction mixture was allowed to stir at 0 °C for an additional 15 min and subsequently warmed to room temperature and stirred at that temperature for a further 30 h. After complete consumption of the starting material, determined by TLC analysis of the reaction mixture (50% EtOAc in petroleum ether), the solvent was evaporated under reduced pressure and the residue thus obtained was dissolved in H_2O (50 mL). This solution was transferred to a separating funnel, EtOAc (100 mL) was then added and the biphasic system was treated with saturated aqueous $NaHCO_3$ (10 mL). Then, the pH of the aqueous phase was adjusted to ~7 by careful addition of 12 M HCl, the organic phases were collected, and the aqueous layer was extracted with EtOAc (2 × 75 mL). The combined organic phases were washed with brine (60 mL), dried over Na_2SO_4, filtered and evaporated under reduced pressure to afford methyl 3-aminobenzoate (**70f**) as a viscous brown oil (0.720 g, **95% yield**). Analytical data for **70f** is consistent with previously reported data:[182]
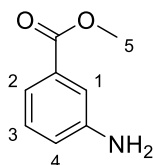
^{1}H NMR (400 MHz, CDCl₃): δ 7.42 (dt, $^3J_{HH}$ = 7.8 Hz, $^4J_{HH}$ = 1.3 Hz, 1H, H[2]), 7.35 (dd, $^4J_{HH}$ = 2.0 Hz, 1H, H[1]), 7.20 (t, $^3J_{HH}$ = 7.9 Hz, 1H, H[3]), 6.85 (dd, $^3J_{HH}$ = 8.0 Hz, $^4J_{HH}$ = 2.5 Hz, 1H, H[4]), 3.88 (s, 3H, H[5]), 3.74 (br s, 2H ,NH₂).

^{13}C NMR (101 MHz, CDCl₃): δ 167.4, 146.6, 131.2, 129.4, 119.8, 119.5, 115.9, 52.1.

Methyl 3-((*tert*-butoxycarbonyl)amino)benzoate (**70fa**)
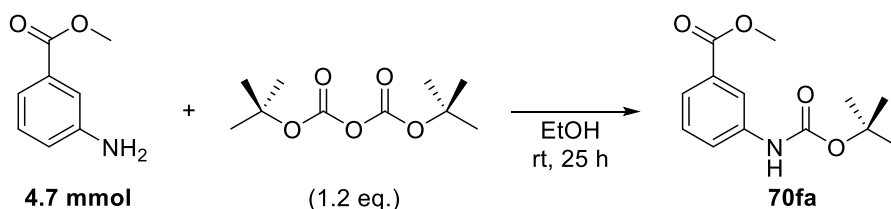
To a round-bottomed flask equipped with a magnetic stirrer bar were added methyl 3-aminobenzoate (0.711 g, 4.70 mmol), ethanol (9.5 mL) and Boc₂O (1.241 g, 5.69 mmol), and the reaction mixture was stirred at room temperature for 25 h. The mixture was then evaporated under reduced pressure, and the residue was purified by

column chromatography with gradient elution, employing mixtures of Et$_2$O and petroleum ether as eluents (0 – 40% Et$_2$O) to afford methyl 3-((tert-butoxycarbonyl)amino)benzoate (**70fa**) as a white solid (1.059 g, **90% yield**). Analytical data for **70fa** is consistent with previously reported data:[183]
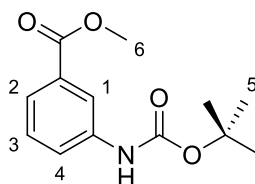
^{1}H NMR (400 MHz, CDCl$_3$): δ 7.96 (t, $^4J_{HH}$ = 1.9 Hz, 1H, H^1), 7.71 (dt, $^3J_{HH}$ = 7.8 Hz, $^4J_{HH}$ = 1.3 Hz, 1H, H^2), 7.66 (br d, $^3J_{HH}$ = 7.8 Hz, 1H, H^4), 7.36 (dd, $^3J_{HH}$ = 7.9 Hz, 1H, H^3), 6.60 (br s, 1H, NH), 3.90 (s, 3H, H^6), 1.52 (s, 9H, H^5).

^{13}C NMR (101 MHz, CDCl$_3$): δ 167.0, 152.7, 138.8, 131.1, 129.2, 124.3, 123.0, 119.5, 81.1, 52.3, 28.5.

Melting point: 102-104 °C.

IR (neat, cm^{-1}): 3348, 2974, 2926, 1726, 1701, 1609, 1533, 1489, 1450, 1437, 1418, 1387, 1364, 1317, 1306, 1287, 1229, 1153, 1115, 1086, 1057, 982, 907, 866, 770, 752, 681, 656, 646, 635, 621.

3-(allyl(*tert*-butoxycarbonyl)amino)benzoic acid – **72f**
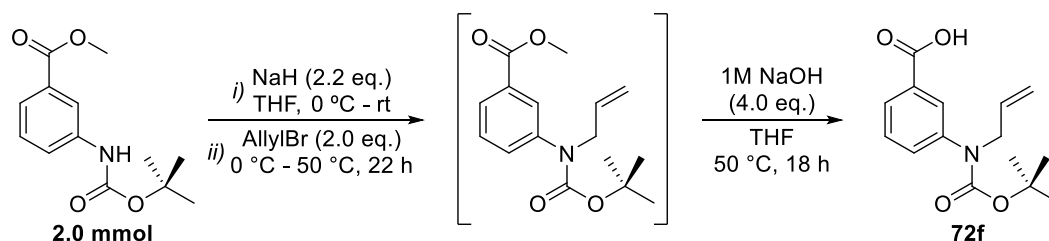
To a flame-dried round-bottomed flask equipped with a magnetic stirrer bar were added methyl 3-((*tert*-butoxycarbonyl)amino)benzoate (0.502 g, 2.00 mmol) and anhydrous THF (20 mL). The reaction mixture was cooled to 0 °C in an ice-water bath, then, NaH (60% in mineral oil, 0.178g, 4.45 mmol) was added under constant vigorous stirring at that temperature. The mixture was stirred at 0 °C for 15 min, subsequently allowed to warm to room temperature and stirred at that temperature for a further 30 min. The vessel was then cooled to 0 °C in an ice-water bath, allyl bromide (0.35 mL, 4.0 mmol) was added dropwise under constant vigorous stirring,

and the mixture was allowed to stir at 0 °C for a further 15 min. The reaction vessel was then transferred to an oil-bath pre-heated to 50 °C and kept at that temperature under constant stirring for a further 22 h. TLC analysis (25% Et₂O in petroleum ether) indicated complete consumption of the starting material and the reaction vessel was allowed to cool to room temperature. Then, 1M NaOH (8.0 mL, 8.0 mmol) was added under constant, vigorous stirring, the reaction mixture was returned to the oil-bath and stirred for a further 18 h at 50 °C. TLC analysis (25% Et₂O in petroleum ether) indicated complete consumption of the methyl ester, the reaction mixture was allowed to cool to room temperature and the volatiles were evaporated under reduced pressure. The residue was then dissolved in H₂O (20 mL), extracted with Et₂O (2 × 40 mL) and the combined organic phases were discarded. The aqueous phase was acidified to pH ~ 2 by careful addition of 12 M HCl, extracted with Et₂O (3 × 40 mL), and the combined organic phases were washed with brine (40 mL), dried over Na₂SO₄, filtered and evaporated under reduced pressure. The residue thus obtained was purified by column chromatography employing gradient elution employing mixtures of Et₂O and petroleum ether as eluents (0 – 50% Et₂O, then 50% Et₂O + 0.1% AcOH) to afford 3-(allyl(*tert*-butoxycarbonyl)amino)benzoic acid (**72f**) as a highly viscous colourless oil that solidified upon standing. (0.522 g, **94% yield** over two steps).
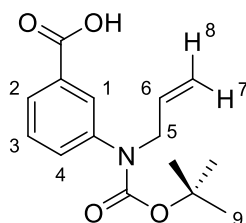
¹H NMR (400 MHz, CDCl₃): δ 7.98 (t, $^4J_{HH}$ = 1.9 Hz, 1H, H¹), 7.92 (dt, $^3J_{HH}$ = 7.8 Hz, $^4J_{HH}$ = 1.4 Hz, 1H, H²), 7.50 (br d, $^3J_{HH}$ = 8.2 Hz, 1H, H⁴), 7.42 (t, $^3J_{HH}$ = 7.8 Hz, 1H, H³), 5.92, (ddt, $^3J_{HH}$ = 17.3 Hz, $^3J_{HH}$ = 10.0 Hz, $^3J_{HH}$ = 5.5 Hz, 1H, H⁶), 5.17 (ddt, $^3J_{HH}$ = 17.4 Hz, $^4J_{HH}$ = 1.7 Hz, $^2J_{HH}$ = 1.5 Hz, 1H, H⁷), 5.16 (dq, $^3J_{HH}$ = 10.0 Hz, J_{HH} = 1.4 Hz, 1H, H⁸), 4.27 (dt, $^3J_{HH}$ = 5.6 Hz, $^4J_{HH}$ = 1.5 Hz, 2H, H⁵), 1.46 (s, 9H).

¹³C NMR (101 MHz, CDCl₃): δ 171.4, 154.4, 143.2, 134.0, 131.8, 130.1, 128.8, 127.9, 127.5, 117.0, 81.1, 66.0, 28.4.

Melting point: 56-58 °C.

IR (neat, cm^{-1}): 2978, 2932, 1692, 1605, 1587, 1476, 1456, 1441, 1385, 1354, 1314, 1294, 1265, 1250, 1231, 1161, 1119, 1084, 1069, 1036, 999, 934, 908, 880, 851, 818, 764, 750, 710, 683, 667.

HRMS (positive ESI): m/z calculated for [M+NH$_4$]$^+$ C$_{15}$H$_{23}$N$_2$O$_4$: 295.1652; found: 295.1656.

Sequence for 3-(allyl(ethoxycarbonyl)amino)benzoic acid – **72g**
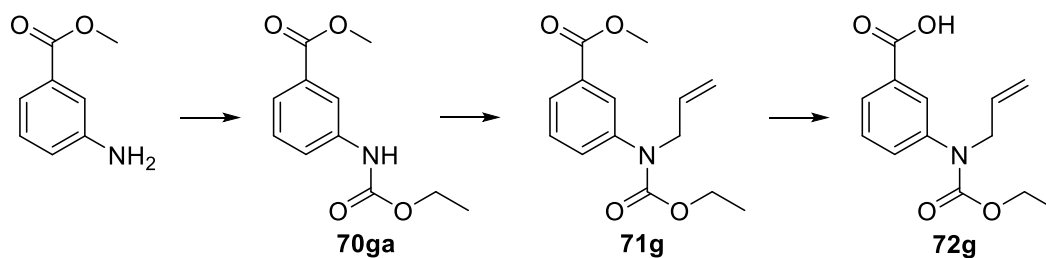
Methyl 3-((ethoxycarbonyl)amino)benzoate – **70ga**
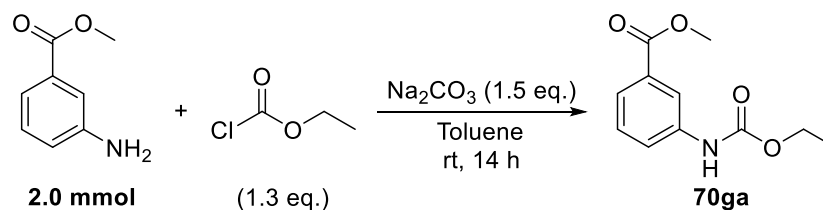
To a flame-dried round-bottomed flask equipped with a magnetic stirrer bar was added Na$_2$CO$_3$ (0.859 g, 8.10 mmol), and the atmosphere was evacuated and replenished with Ar. Then, a solution of methyl 3-aminobenzoate (811 mg, 5.36 mmol) in dry toluene (5 mL) was added *via* syringe, and a second portion of dry toluene (19 mL) was subsequently added. The resulting mixture was thoroughly stirred at room temperature, ethyl chloroformate (0.65 mL, 6.8 mmol) was added dropwise at that temperature, and the mixture was stirred for 14 h. TLC analysis of the reaction mixture (30% EtOAc in petroleum ether) indicated consumption of the parent aniline, and the mixture was then partitioned between H$_2$O (50 mL) and EtOAc (125 mL). The organic layer was collected, and the aqueous phase was extracted with EtOAc (2 × 75 mL). The combined organic phases were washed with 1 M HCl (50 mL), brine (50 mL), dried over Na$_2$SO$_4$, filtered and evaporated under reduced pressure. The residue thus obtained was suspended in EtOAc (20 mL), free-flowing silica gel (~ 1 g) was added and the volatiles were evaporated under reduced

pressure. The resulting solid was loaded into a pre-packed column and purified by chromatography with gradient elution employing mixtures of EtOAc and petroleum ether as eluents (0 – 30% EtOAc) to afford methyl 3-((ethoxycarbonyl)amino)benzoate (**70ga**) as a white solid (1.022 g, **85% yield**).
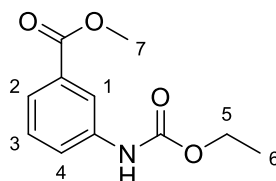
^{1}H NMR (400 MHz, CDCl$_3$): δ 7.98 (t, $^4J_{HH}$ = 2.0 Hz, 1H, H^1), 7.76 (dt, $^3J_{HH}$ = 8.0 Hz, $^4J_{HH}$ = 1.4 Hz, 1H, H^2), 7.74 (br d, $^3J_{HH}$ = 7.6 Hz, 1H, H^4), 7.41 (t, $^3J_{HH}$ = 7.9 Hz, 1H, H^3), 6.73 (br s, 1H, NH), 4.27 (q, $^3J_{HH}$ = 7.1 Hz, 2H, H^5), 3.94 (s, 3H, H^7), 1.34 (t, $^3J_{HH}$ = 7.1 Hz, 3H, H^6).

^{13}C NMR (101 MHz, CDCl$_3$): δ 166.2, 153.0, 137.8, 130.5, 128.7, 124.0, 122.5, 119.0, 60.9, 51.7, 14.0.

Melting point: 112-113 °C.

**IR (neat, cm^{-1}):** 3345, 2986, 2955, 2909, 1734, 1699, 1611, 1597, 1547, 1491, 1445, 1422, 1391, 1323, 1308, 1283, 1217, 1171, 1115, 1070, 1016, 978, 914, 903, 878, 806, 766, 752, 683, 671, 617.

HRMS (positive ESI): m/z calculated for [M+Na]$^+$ C$_{11}$H$_{13}$NO$_4$Na$^+$: 246.0737; found: 246.0737.

Methyl 3-(allyl(ethoxycarbonyl)amino)benzoate – **71g**
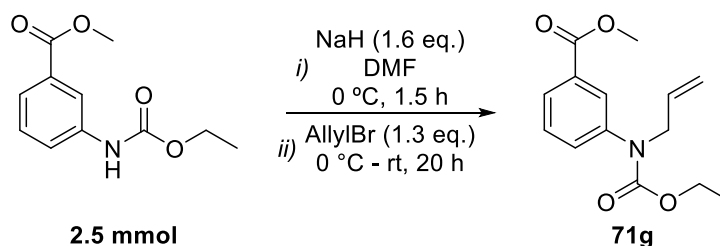
To a flame-dried round-bottomed flask equipped with a magnetic stirrer bar were added NaH (60% in mineral oil, 155.6 mg, 3.89 mmol) and DMF (3.0 mL), and the mixture was cooled to 0 °C in an ice-water bath. Then, a solution of methyl 3-((ethoxycarbonyl)amino)benzoate **70ga** (559.1 mg, 2.50 mmol) in DMF (3.0 mL) was added dropwise under constant vigorous stirring at 0 °C, and the resulting

mixture was stirred at that temperature for a further 1.5 h. Allyl bromide (0.28 mL, 3.2 mmol) was then added dropwise at 0 °C, the resulting mixture was allowed to warm to room temperature and stirred for a further 20 h. The reaction mixture was quenched by careful addition of H_2O (15 mL), transferred to a separating funnel and extracted with EtOAc (3 × 30 mL). The combined organic phases were washed with H_2O (2 × 30 mL), brine (30 mL), dried over Na_2SO_4, filtered and evaporated under reduced pressure. The residue thus obtained was purified by column chromatography with gradient elution employing mixtures of EtOAc and petroleum ether as solvents (0 – 25% EtOAc) to afford methyl 3-(allyl(ethoxycarbonyl)amino)benzoate (**71g**) as a colourless viscous liquid (410.3 mg, **62% yield**).
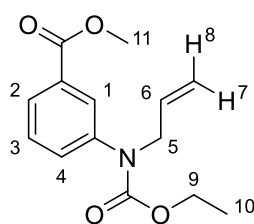
^{1}H NMR (400 MHz, CDCl₃): δ 7.95-7.89 (m, 2H, H^1/H^2), 7.45 (br d, $^3J_{HH}$ = 8.3 Hz, 1H, H^4), 7.42 (t, $^3J_{HH}$ = 7.6 Hz, 1H, H^3), 5.92 (ddt, $^3J_{HH}$ = 16.9 Hz, $^3J_{HH}$ = 10.5 Hz, $^3J_{HH}$ = 5.7 Hz, 1H, H^6), 5.19-5.13 (m, 2H, H^7/H^8), 4.30 (br d, $^3J_{HH}$ = 5.8 Hz, 2H, H^5), 4.19 (q, $^3J_{HH}$ = 7.1 Hz, 2H, H^9), 3.93 (s, 3H, H^{11}), 1.24 (t, $^3J_{HH}$ = 7.1 Hz, 3H, H^{10}).

^{13}C NMR (101 MHz, CDCl₃): δ 166.0, 154.7, 141.9, 133.0, 130.7, 130.5, 128.3, 127.1, 126.8, 116.8, 61.4, 52.4, 51.7, 14.0.

IR (neat, cm^{-1}): 3345, 2986, 2955, 2909, 1734, 1699, 1611, 1597, 1547, 1491, 1445, 1422, 1391, 1323, 1308, 1283, 1217, 1171, 1115, 1070, 1016, 978, 914, 903, 878, 806, 766, 752, 683, 671, 617.

HRMS (positive ESI): m/z calculated for [M+H]$^+$ $C_{14}H_{18}NO_4^+$: 264.1236; found: 264.1239.

3-(allyl(ethoxycarbonyl)amino)benzoic acid – **72g**
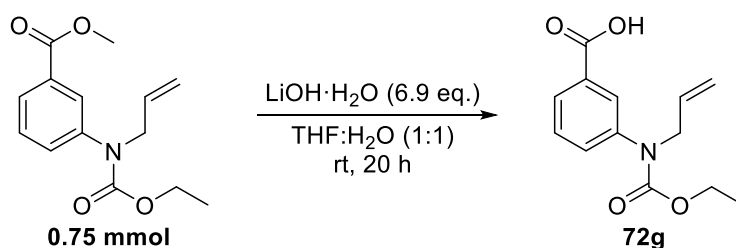
To a round-bottomed flask equipped with a magnetic stirrer bar were added methyl 3-(allyl(ethoxycarbonyl)amino)benzoate (198.5 mg, 0.75 mmol), THF (4.5 mL) and H_2O (4.5 mL), and the mixture was thoroughly stirred at room temperature. Then, LiOH·H_2O (216.4 mg, 5.16 mmol) was added in one portion under constant stirring, and the reaction mixture was stirred for 20 h at room temperature. TLC analysis (50% EtOAc in petroleum ether) indicated consumption of the parent methyl ester, and the reaction mixture was transferred to a separating funnel, partitioned between 0.1 M NaOH (10 mL) and Et_2O (30 mL). The aqueous layer was extracted with Et_2O (2 × 30 mL), the combined organic phases were discarded, and the pH of the remaining mixture was adjusted to ~2 by careful addition of 12 M HCl. The resulting mixture was extracted with Et_2O (3 × 30 mL), the combined organic phases were washed with brine (20 mL), dried over Na_2SO_4, filtered and evaporated under reduced pressure to afford 3-(allyl(ethoxycarbonyl)amino)benzoic acid (**72g**) as a viscous oil (165.8 mg, **88% yield**).
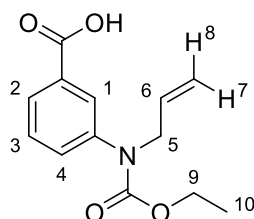
¹H NMR (400 MHz, DMSO-d_6): δ 13.1 (br s, 1H, OH), 7.82 (br t, $^4J_{HH}$ = 1.6 Hz, 1H, H¹), 7.79 (dt, $^3J_{HH}$ = 7.3 Hz, $^4J_{HH}$ = 1.4 Hz, 1H, H²), 7.53 (br dt, $^3J_{HH}$ = 8.2 Hz, $^4J_{HH}$ = 1.8 Hz, 1H, H⁴), 7.49 (t, $^3J_{HH}$ = 7.7 Hz, 1H, H³), 5.88 (ddt, $^3J_{HH}$ = 17.6 Hz, $^3J_{HH}$ = 10.2 Hz, $^3J_{HH}$ = 5.3 Hz, 1H, H⁶), 5.15-5.09 (m, 2H, H⁷/H⁸), 4.28 (dt, $^3J_{HH}$ = 5.5 Hz, $^4J_{HH}$ = 1.4 Hz, 2H, H⁵), 4.10 (q, $^3J_{HH}$ = 7.0 Hz, 2H, H⁹), 1.16 (t, $^3J_{HH}$ = 7.0 Hz, 3H, H¹⁰).

¹³C NMR (101 MHz, DMSO-d_6): δ 166.8, 154.4, 142.1, 134.0, 131.4, 130.7, 129.0, 127.0, 126.7, 116.7, 64.9, 61.3, 14.3.

IR (neat, cm^{-1}): 3073, 2980, 2662, 1694, 1603, 1587, 1485, 1450, 1402, 1379, 1356, 1304, 1236, 1173, 1152, 1111, 1080, 1055, 1034, 1016, 926.

HRMS (negative ESI): m/z calculated for [M-H]$^-$ C$_{13}$H$_{14}$NO$_4^-$: 248.0928; found:248.0932.

Sequence for 3-((N-allyl-4-methylphenyl)sulfonamido)benzoic acid – **72h**

70ha   **71h**   **72h**
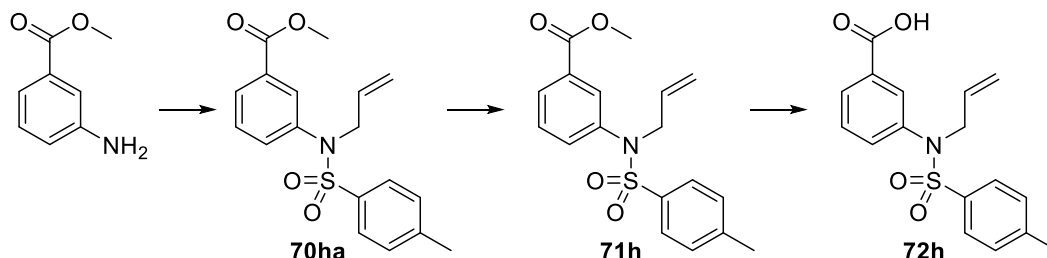
Methyl 3-((4-methylphenyl)sulfonamido)benzoate – **70ha**

8.0 mmol   **70ha**
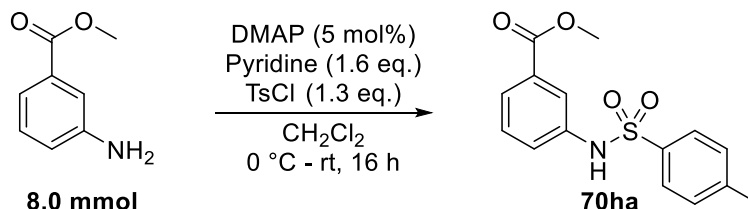
To a flame-dried round-bottomed flask equipped with a stirrer bar were added methyl 3-aminobenzoate (1.207 g, 7.98 mmol), DMAP (49.6 mg, 0.41 mmol), anhydrous CH$_2$Cl$_2$ (40 mL), and pyridine (1.0 mL, 12.4 mmol). The mixture was thoroughly stirred, and the reaction vessel was cooled to 0 °C in an ice-water bath. A solution of tosyl chloride (1.930 g, 10.1 mmol) in anhydrous CH$_2$Cl$_2$ (25 mL) was then slowly added to the reaction vessel at 0 °C under constant and vigorous stirring. The reaction mixture was then allowed to warm to room temperature stirred for a further 16 h. TLC analysis (50% EtOAc in petroleum ether) indicated consumption of the parent aniline, the reaction mixture was then diluted with CH$_2$Cl$_2$ (100 mL) and quenched by addition of 1 M HCl (75 mL). The organic layer was collected, and the aqueous phase was extracted with CH$_2$Cl$_2$ (2 × 125 mL). The combined organic phases were washed with brine (50 mL), dried over Na$_2$SO$_4$, filtered and evaporated under reduced pressure. The residue thus obtained was suspended in EtOAc (90 mL), free-flowing silica gel (~ 3 g) was added and the volatiles were evaporated under reduced pressure. The resulting solid was dry loaded onto a previously packed

column and purified by chromatography with gradient elution employing mixtures of EtOAc and petroleum ether as eluents (0 – 50% EtOAc) to afford methyl 3-((4-methylphenyl)sulfonamido)benzoate (**70ha**) as a white solid (2.269 g, **93% yield**). Analytical data for **70ha** is consistent with previously reported data:[184,185]
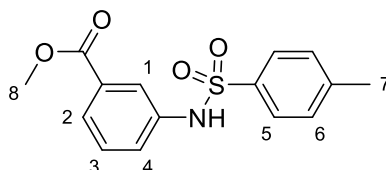

^{1}H NMR (400 MHz, CDCl$_3$): δ 7.79 (dt, $^3J_{HH}$ = 7.7 Hz, $^4J_{HH}$ = 1.3 Hz, 1H, H^2), 7.73 (t, $^4J_{HH}$ = 1.8 Hz, 1H, H^1), 7.70 (d, $^3J_{HH}$ = 8.3 Hz, 2H, H^5), 7.43 (ddd, $^3J_{HH}$ = 8.0 Hz, $^4J_{HH}$ = 2.3 Hz, $^4J_{HH}$ = 1.3 Hz, 1H, H^4), 7.35 (t, $^3J_{HH}$ = 7.9 Hz, 1H, H^3), 7.24 (d, $^3J_{HH}$ = 8.0 Hz, 2H, H^6), 7.10 (br s, 1H, NH), 3.92 (s, 3H, H^8), 2.39 (s, 3H, H^7).

^{13}C NMR (101 MHz, CDCl$_3$): δ 165.9, 143.6, 136.6, 135.4, 130.8, 129.3, 129.0, 126.8, 125.7, 124.9, 121.6, 51.9, 21.0.

Melting point: 145-146 °C.

IR (neat, cm^{-1}): 3225, 3065, 2959, 1701, 1605, 1593, 1476, 1439, 1404, 1335, 1296, 1219, 1180, 1155, 1111, 1090, 1016, 1001, 986, 945, 895, 853, 812, 752, 704, 681, 660, 637, 608.

Methyl 3-((*N*-allyl-4-methylphenyl)sulfonamido)benzoate – **71h**
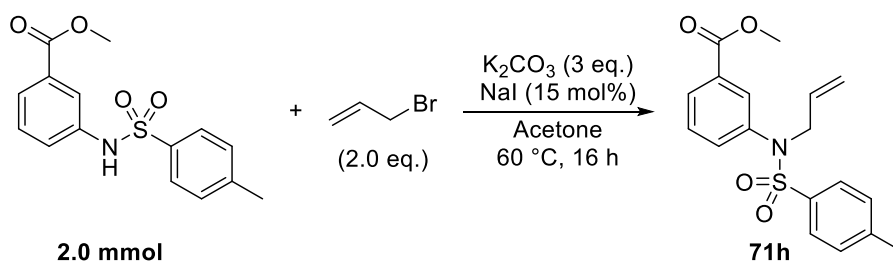
Following general procedure 1.2 for the allylation of phenols, NaI (48 mg, 0.32 mmol), K$_2$CO$_3$ (0.830 g, 6.01 mmol) and methyl 3-((*N*-allyl-4-methylphenyl)sulfonamido)benzoate (0.611 g, 2.00 mmol) were dissolved in acetone (25 mL) and reacted with allyl bromide (0.35 mL, 4.0 mmol) at 60 °C for 16 h. After complete consumption of the starting material, determined by TLC analysis of the reaction mixture (40% EtOAc in petroleum ether), the mixture was allowed to cool

to room temperature and the volatiles were evaporated under reduced pressure. The residue thus obtained was suspended in H_2O (20 mL) and extracted with EtOAc (3 × 40 mL). The combined organic phases were washed with brine (20 mL), dried over Na_2SO_4, filtered and evaporated under reduced pressure. The residue was purified by column chromatography, employing gradient elution with mixtures of EtOAc and petroleum ether as eluents (0 – 30% EtOAc) to afford methyl 3-((*N*-allyl-4-methylphenyl)sulfonamido)benzoate (**71h**) as a light yellow viscous oil (0.663 g, **96% yield**).
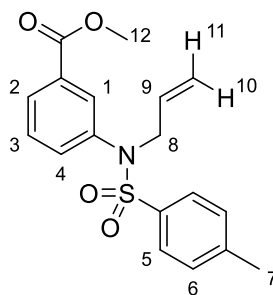
^{1}H NMR (400 MHz, CDCl₃): δ 7.96 (dt, $^3J_{HH}$ = 7.6 Hz, $^4J_{HH}$ = 1.5 Hz, 1H, H^2), 7.70, (t, $^4J_{HH}$ = 1.9 Hz, 1H, H^1), 7.50 (d, $^3J_{HH}$ = 8.3 Hz, 2H, H^5), 7.40 (t, $^3J_{HH}$ = 7.9 Hz, 1H, H^3), 7.32 (ddd, $^3J_{HH}$ = 8.0 Hz, $^4J_{HH}$ = 2.2 Hz, $^4J_{HH}$ = 1.1 Hz, 1H, H^4), 7.28 (d, $^3J_{HH}$ = 7.3 Hz, 2H, H^6), 5.73 (ddt, $^3J_{HH}$ = 17.0 Hz, $^3J_{HH}$ = 10.4 Hz, $^3J_{HH}$ = 6.6 Hz, 1H, H^9), 5.09 (dt, $^3J_{HH}$ = 16.7 Hz, $^4J_{HH}$ = 1.5 Hz, 1H, H^{10}), 5.06 (dt, $^3J_{HH}$ = 9.8 Hz, $^4J_{HH}$ = 1.3 Hz, 1H, H^{11}), 4.20 (dt, $^3J_{HH}$ = 6.3 Hz, $^4J_{HH}$ = 1.3 Hz, 2H, H^8), 3.91 (s, 3H, H^{11}), 2.44 (s, 3H, H^7).

^{13}C NMR (101 MHz, CDCl₃): δ 165.7, 143.3, 139.0, 134.6, 133.1, 132.0, 130.6, 129.1, 128.9, 128.4, 128.3, 127.2, 118.7, 52.8, 51.8, 21.0.

IR (neat, cm^{-1}): 3082, 2951, 1721, 1643, 1585, 1485, 1443, 1346, 1283, 1267, 1215, 1184, 1165, 1107, 1090, 1070, 1015, 988, 974, 926, 881, 829, 814, 766, 748, 706.

HRMS (positive ESI): m/z calculated for [M+H]$^+$ $C_{18}H_{20}SNO_4^+$: 346.1108, found: 346.1111.

3-((N-allyl-4-methylphenyl)sulfonamido)benzoic acid – **72h**
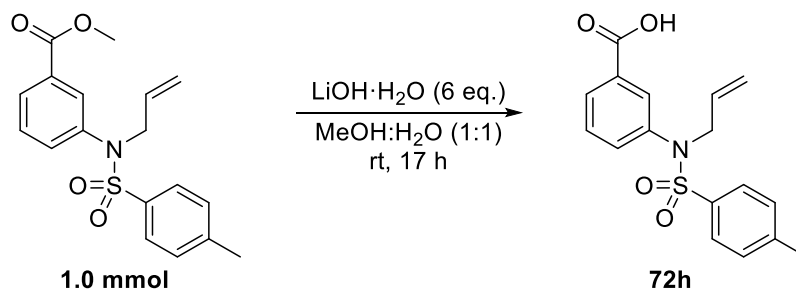
To a round-bottomed flask equipped with a magnetic stirrer bar were added methyl 3-((N-allyl-4-methylphenyl)sulfonamido)benzoate (344.2 mg, 1.00 mmol), MeOH (7.0 mL) and H_2O (3.5 mL), and the mixture was thoroughly stirred at room temperature. Then, LiOH·H_2O (252.2 mg, 6.02 mmol) was added in one portion under constant stirring, and the reaction mixture was stirred for 17 h at room temperature. TLC analysis (50% EtOAc in petroleum ether) indicated consumption of the parent methyl ester, and the reaction mixture was evaporated under reduced pressure. The residue was diluted with H_2O (10 mL), extracted with EtOAc (3 × 20 mL), the combined organic phases were washed with 0.1 M NaOH (2 × 20 mL) and the organic layer was discarded. The aqueous portions were combined, acidified to pH ~ 1 by careful addition of 12 M HCl and extracted with EtOAc (3 × 50 mL). The combined organic phases were washed with brine (20 mL), dried over Na_2SO_4, filtered and evaporated under reduced pressure to afford 3-((N-allyl-4-methylphenyl)sulfonamido)benzoic acid (**72h**) as a yellow solid (286.9 mg, **87% yield**).
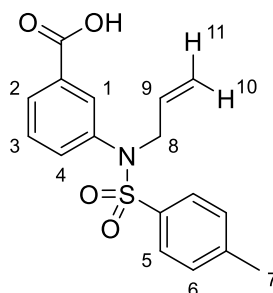
^{1}H NMR (400 MHz, DMSO-d_6): δ 13.0 (br s, 1H, OH), 7.85 (d, $^3J_{HH}$ = 7.8 Hz, 1H, H^2), 7.62 (br s, 1H, H^1), 7.49-7.37 (m, 5H, H^3/H^5/H^6), 7.29 (d, $^3J_{HH}$ = 7.3 Hz, 1H, H^4), 5.69 (ddt, $^3J_{HH}$ = 16.7 Hz, $^3J_{HH}$ = 10.7 Hz, $^3J_{HH}$ = 6.3 Hz, 1H, H^9), 5.13 (dd, $^3J_{HH}$

= 17.1 Hz, $^4J_{HH}$ = 1.1 Hz, 1H, H^{10}), 5.05 (d, $^3J_{HH}$ = 10.1 Hz, 1H, H^{11}), 4.23 (d, $^3J_{HH}$ = 6.0 Hz, 2H, H^8), 2.40 (s, 3H, H^7).

^{13}C NMR (101 MHz, DMSO-d_6): δ 166.5, 143.7, 139.0, 134.6, 132.8, 132.4, 131.5, 129.8, 129.2, 129.1, 128.3, 127.3, 119.0, 52.4, 21.0.

Melting point: 148-150 °C.

IR (neat, cm^{-1}): 2916, 2855, 2656, 2563, 1694, 1599, 1584, 1487, 1445, 1418, 1354, 1342, 1306, 1271, 1213, 1188, 1167, 1119, 1090, 1055, 1013, 1001, 937, 924, 891, 824, 806, 795, 760, 737, 706, 691, 664, 638.

HRMS (negative ESI): m/z calculated for [M-H]$^-$ C$_{17}$H$_{16}$SNO$_4^-$: 330.0806; found: 330.0805.

Sequence for 3-((2-methylallyl)oxy)benzoic acid – **72i**

64a   **71i**   **72i**
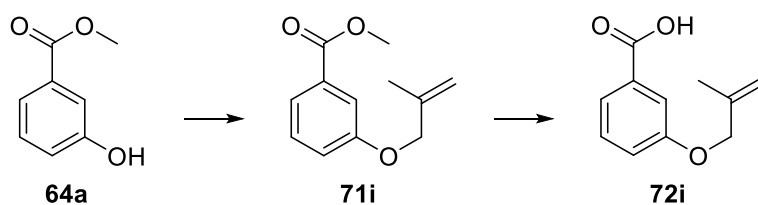
Methyl 3-((2-methylallyl)oxy)benzoate (**71i**)

2.0 mmol   (1.25 eq.)   **71i**
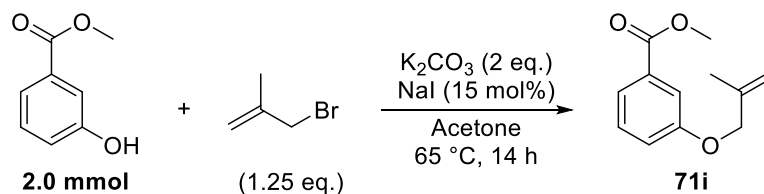
Following general procedure 6.1.2 for the allylation of phenols, NaI (43 mg, 0.29 mmol), K$_2$CO$_3$ (0.560 g, 4.05 mmol) and methyl 3-hydroxybenozoate (0.303 g, 1.99 mmol) were dissolved in acetone (10 mL) and reacted with 3-bromo-2-methylpropene (0.25 mL, 2.5 mmol) at 65 °C for 14 h. After complete consumption of the starting material, determined by TLC analysis of the reaction mixture (10% EtOAc in petroleum ether), the mixture was allowed to cool to room temperature and the solvent was evaporated under reduced pressure. The residue thus obtained was suspended in Et$_2$O (50 mL) and the organic layer was washed with water (20 mL). The aqueous phase was extracted with Et$_2$O (3 × 20 mL), and the combined organic phases were washed with brine (30 mL), dried over Na$_2$SO$_4$, filtered and evaporated

under reduced pressure. The crude mixture was subsequently purified by column chromatography employing gradient elution with mixtures of EtOAc and petroleum ether as eluents (0 – 10% Et_2O) to afford methyl 3-((2-methylallyl)oxy)benzoate (**71i**) as a colourless oil (0.369 g, **90% yield**).
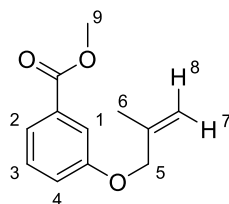

^{1}H NMR (400 MHz, CDCl₃): δ 7.63 (dt, $^3J_{HH}$ = 7.7 Hz, $^4J_{HH}$ = 1.3 Hz, 1H, H²), 7.57 (dd, $^4J_{HH}$ = 2.6 Hz, $^4J_{HH}$ = 1.5 Hz, 1H, H¹), 7.33 (t, $^3J_{HH}$ = 7.9 Hz, 1H, H³), 7.12 (ddd, $^3J_{HH}$ = 8.3 Hz, $^4J_{HH}$ = 2.8 Hz, $^4J_{HH}$ = 1.0 Hz, 1H, H⁴), 5.12-5.09 (m, 1H, H⁷), 5.02-4.98 (m, 1H, H⁸), 4.47 (br s, 2H, H⁵), 3.91 (s, 3H, H⁹), 1.84-1.83 (m, 3H, H⁶).

^{13}C NMR (101 MHz, CDCl₃): δ 167.1, 158.9, 140.6, 131.6, 129.5, 122.2, 120.2, 115.2, 113.1, 72.0, 52.3, 19.5.

IR (neat, cm^{-1}): 2951, 1721, 1585, 1487, 1443, 1277, 1215, 1190, 1099, 1076, 1057, 1022, 993, 897, 795, 754, 681.

HRMS (positive ESI): m/z calculated for [M+H]$^+$ $C_{12}H_{15}O_3$: 207.1021; found: 207.1025.

3-((2-methylallyl)oxy)benzoic acid – **72i**
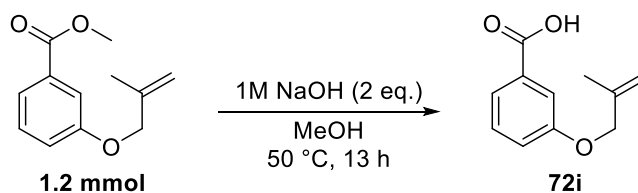
Following general procedure 6.1.3, 3-((2-methylallyl)oxy)benzoate (248.2 mg, 1.20 mmol) was dissolved in MeOH (16 mL) and reacted with 1 M NaOH (2.0 mL, 2.0 mmol) for 13 h. TLC analysis was performed with 10% MeOH in CH_2Cl_2. After workup, 3-((2-methylallyl)oxy)benzoic acid (**72i**) was isolated as a white solid (213.4 mg, **92% yield**).

Analytical data for **72i** is consistent with previously reported data:[186,118]
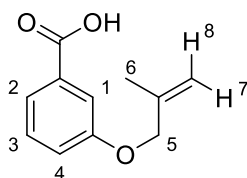
¹H NMR (400 MHz, DMSO-d_6): δ 13.0 (br s, 1H, OH), 7.53 (dt, $^3J_{HH}$ = 7.6 Hz, $^4J_{HH}$ = 1.2 Hz, 1H, H²), 7.46 (dd, $^4J_{HH}$ = 2.8 Hz, $^4J_{HH}$ = 1.5 Hz, 1H, H¹), 7.41 (t, $^3J_{HH}$ = 8.0 Hz, 1H, H³), 7.21 (ddd, $^3J_{HH}$ = 8.3 Hz, $^4J_{HH}$ = 2.8 Hz, $^4J_{HH}$ = 1.0 Hz, 1H, H⁴), 5.07 (s, 1H, H⁷), 4.98 (s, 1H, H⁸), 4.53 (s, 2H, H⁵), 1.78 (s, 3H, H⁶).

¹³C NMR (101 MHz, DMSO-d_6): δ 167.1, 158.2, 140.6, 132.1, 129.7, 121.7, 119.5, 114.9, 112.3, 70.9, 19.1.

Melting point: 74-76 °C.

IR (neat, cm⁻¹): 2968, 2876, 2851, 2820, 2646, 2558, 2523, 1680, 1655, 1601, 1585, 1487, 1447, 1410, 1389, 1321, 1290, 1240, 1155, 1117, 1078, 1051, 1016, 995, 984, 926, 901, 872, 810, 772, 756, 698, 665, 621.

*Sequence for 3-((3-methylbut-2-en-1-yl)oxy)benzoic acid – **72j***
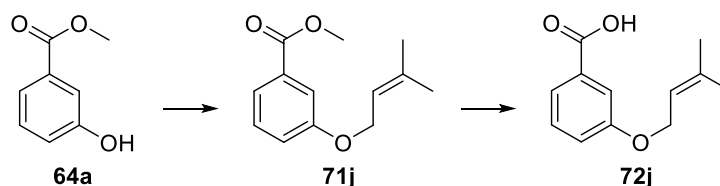
Methyl 3-((3-methylbut-2-en-1-yl)oxy)benzoate – **71j**
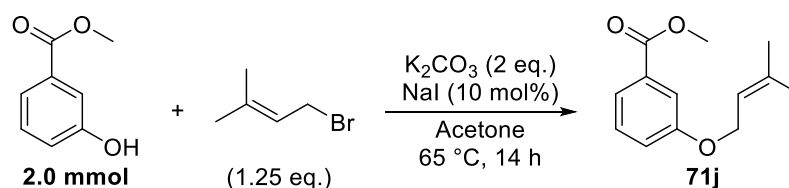
Following general procedure 1.2 for the allylation of phenols, NaI (32.2 mg, 0.21 mmol), K₂CO₃ (0.555 g, 4.02 mmol) and methyl 3-hydroxybenozoate (0.305 g, 2.00 mmol) were dissolved in acetone (10 mL) and reacted with 3-bromo-1,1-dimethylpropene (0.29 mL, 2.5 mmol) at 65 °C for 14 h. After complete consumption of the starting material, determined by TLC analysis of the reaction mixture (10% EtOAc in petroleum ether), the mixture was allowed to cool to room

temperature and the solvent was evaporated under reduced pressure. The residue thus obtained was suspended in Et$_2$O (50 mL) and the organic layer was washed with H$_2$O (20 mL). The aqueous phase was extracted with Et$_2$O (3 × 20 mL), and the combined organic phases were washed with brine (30 mL), dried over Na$_2$SO$_4$, filtered and evaporated under reduced pressure. The residue thus obtained was purified by column chromatography employing gradient elution with mixtures of EtOAc and petroleum ether as eluents (0 – 10% EtOAc) to afford methyl 3-((3-methylbut-2-en-1-yl)oxy)benzoate (**71j**) as a colourless oil (0.431 g, **98% yield**).
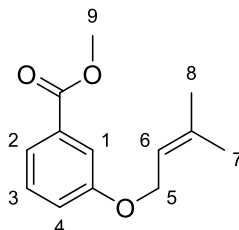
^{1}H NMR (400 MHz, CDCl$_3$): δ 7.62 (dt, $^3J_{HH}$ = 7.6 Hz, $^4J_{HH}$ = 1.4 Hz, 1H, H^2), 7.58 (dd, $^4J_{HH}$ = 2.6 Hz, $^4J_{HH}$ = 1.5 Hz, 1H, H^1), 7.32 (dd, $^3J_{HH}^1$ = $^3J_{HH}^2$ = 8.0 Hz, 1H, H^3), 7.11 (ddd, $^3J_{HH}$ = 8.3 Hz, $^4J_{HH}$ = 2.5 Hz, $^4J_{HH}$ = 1.0 Hz, 1H, H^4), 5.54-5.49 (m, 1H, H^6), 4.55 (d, $^3J_{HH}$ = 6.8 Hz, 2H, H^5), 3.93 (s, 3H, H^9), 1.80 (br s, 3H, H^8), 1.76 (br s, 3H, H^7).

^{13}C NMR (101 MHz, CDCl$_3$): δ 167.2, 159.0, 138.7, 131.5, 129.5, 122.0, 120.4, 119.4, 114.9, 65.1, 52.2, 26.0, 18.4.

IR (neat, cm^{-1}): 3402, 2976, 2951, 1721, 1701, 1655, 1587, 1487, 1445, 1379, 1287, 1277, 1219, 1190, 1157, 1142, 1099, 1076, 1038, 1015, 991, 889, 793, 754, 681.

HRMS (positive ESI): m/z calculated for [M+H]+ C$_{13}$H$_{17}$O$_3$: 221.1172; found: 221.1172.

3-((3-methylbut-2-en-1-yl)oxy)benzoic acid – **72j**
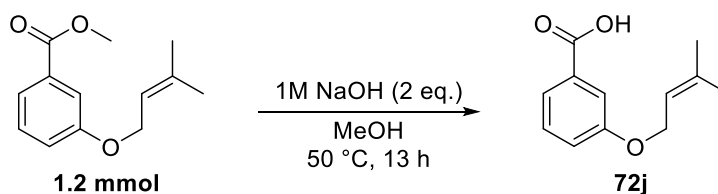
Following general procedure 6.1.3, 3-((2-methylallyl)oxy)benzoate (270.0 mg, 1.23 mmol) was dissolved in MeOH (16 mL) and reacted with 1 M NaOH (2.0 mL, 2.0

mmol) for 13 h. TLC analysis was performed with 10% MeOH in CH$_2$Cl$_2$. After workup, 3-((3-methylbut-2-en-1-yl)oxy)benzoic acid (**72j**) was isolated as a white solid (226.3 mg, **89% yield**).
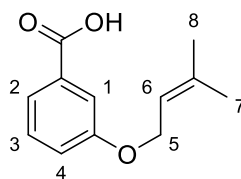
^{1}H NMR (400 MHz, DMSO-d_6): δ 12.9 (br s, 1H, OH), 7.52 (dt, $^3J_{HH}$ = 7.6 Hz, $^4J_{HH}$ = 1.2 Hz, 1H, H^2), 7.44 (dd, $^4J_{HH}$ = 2.9 Hz, $^4J_{HH}$ = 1.5 Hz, 1H, H^1), 7.40 (t, $^3J_{HH}$ = 7.9 Hz, 1H, H^3), 7.18 (ddd, $^3J_{HH}$ = 8.2 Hz, $^4J_{HH}$ = 2.6 Hz, $^4J_{HH}$ = 1.0 Hz, 1H, H^4), 5.46-5.40 (m, 1H, H^6), 4.58 (d, $^3J_{HH}$ = 6.7 Hz, 2H, H^5), 1.75 (s, 3H, H^8), 1.72 (s, 3H, H^7).

^{13}C NMR (101 MHz, DMSO-d_6): δ 167.1, 158.4, 137.3, 132.1, 129.6, 121.4, 119.7, 119.6, 114.6, 64.5, 25.4, 18.0.

Melting point: 83-84 °C.

IR (neat, cm^{-1}): 2965, 2920, 2878, 1682, 1587, 1487, 1450, 1416, 1383, 1371, 1323, 1287, 1275, 1231, 1202, 1159, 1128, 1113, 1076, 1045, 1009, 982, 930, 868, 837, 808, 785, 754, 716, 677, 665, 642, 627.

HRMS (positive ESI): m/z calculated for [M+H]$^+$ C$_{12}$H$_{15}$O$_3$: 207.1016; found: 207.1016.

*Sequence for (Z)-3-((4-(benzyloxy)but-2-en-1-yl)oxy)benzoic acid –* **72k**
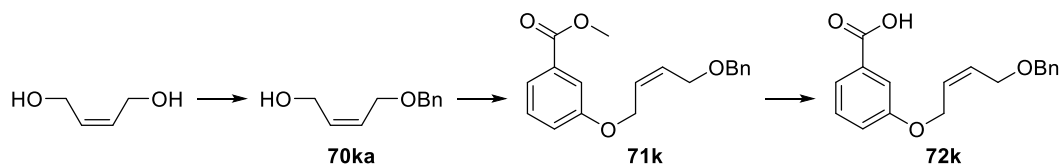
(*Z*)-4-(benzyloxy)but-2-en-1-ol – **70ka**
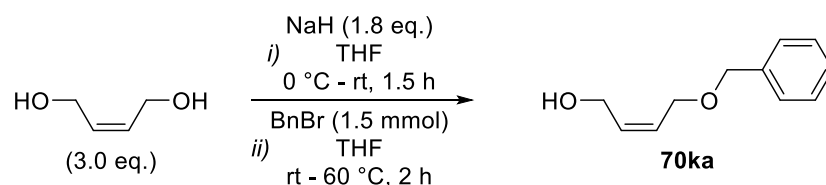
To a flame-dried round-bottomed flask equipped with a magnetic stirrer bar were added (*Z*)-but-2-ene-1,4-diol (0.37 mL, 4.5 mmol) and anhydrous THF (2.0 mL), and

the reaction vessel was cooled to 0 °C in an ice-water bath. Then, NaH (60% in mineral oil, 64 mg, 2.67 mmol) was added in one portion to the reaction flask at 0 °C and under constant, vigorous stirring. The mixture was then allowed to warm to room temperature and stirred for 1.5 h. Then, benzyl bromide (0.18 mL, 1.5 mmol) was added dropwise to the reaction mixture, at room temperature, the reaction vessel was subsequently heated to 60 °C in an oil bath and the mixture was stirred at that temperature for a further 2 h. The reaction vessel was allowed to cool to room temperature, and the reaction medium was quenched by careful addition of 1 M HCl (2 mL). The resulting mixture was then partitioned between 1 M HCl (3 mL) and CH_2Cl_2 (10 mL) and the organic layer was collected. The aqueous phase was extracted with CH_2Cl_2 (2 × 10 mL), and the combined organic phases were washed with brine (10 mL), dried over Na_2SO_4, filtered and evaporated under reduced pressure. The residue was purified by column chromatography with gradient elution, employing mixtures of EtOAc and petroleum ether as eluents (0 – 25% EtOAc, then 40% EtOAc) to afford (Z)-4-(benzyloxy)but-2-en-1-ol (**70ka**) as a colourless oil (225.6 mg, **84% yield**).

Analytical data for **70ka** is consistent with previously reported data:[187]
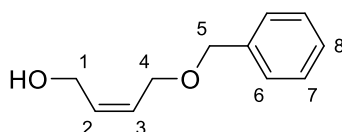
^{1}H NMR (400 MHz, CDCl$_3$): δ 7.40-7.29 (m, 5H, H^6/H^7/H^8), 5.84 (dtq, $^3J_{HH}$ = 11.1 Hz, $^3J_{HH}$ = 6.3 Hz, $^4J_{HH}$ = 1.1 Hz, 1H, H^2), 5.76 (dtq, $^3J_{HH}$ = 11.2 Hz, $^3J_{HH}$ = 6.1 Hz, $^4J_{HH}$ = 1.1 Hz, 1H, H^3), 4.55 (s, 2H, H^5), 4.19 (d, $^3J_{HH}$ = 6.2 Hz, 2H, H^1), 4.12 (d, $^3J_{HH}$ = 6.1 Hz, H^4), 2.13 (br s, 1H, OH).

^{13}C NMR (101 MHz, CDCl$_3$): δ 137.4, 131.9, 128.0, 127.8, 127.4, 127.3, 72.0, 65.2, 58.2.

IR (neat, cm^{-1}): 3424, 3030, 2924, 2864, 1719, 1701, 1497, 1452, 1364, 1314, 1271, 1204, 1173, 1092, 1070, 1026, 914, 827, 739, 714, 698, 652, 610.

Methyl (*Z*)-3-((4-(benzyloxy)but-2-en-1-yl)oxy)benzoate – **71k**
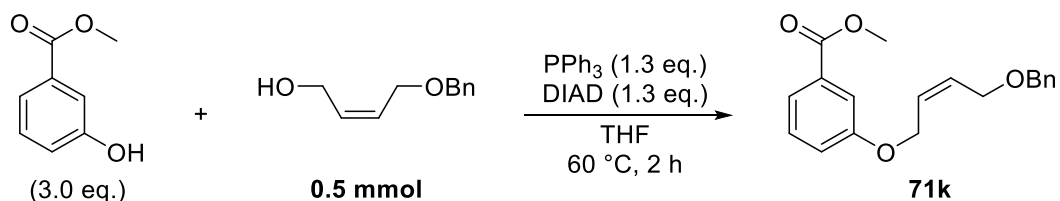
To a flame-dried 20 mL microwave vial equipped with a magnetic stirrer bar were added methyl 3-hydroxybenzoate (229.1 mg, 1.51 mmol) and PPh₃ (170.3 mg, 0.65 mmol), the atmosphere was evacuated and replenished with Ar. Then, a solution of (*Z*)-4-(benzyloxy)but-2-en-1-ol (88.8 mg, 0.50 mmol) in anhydrous THF (1.0 mL) was introduced *via* syringe, followed by a second portion of anhydrous THF (4.0 mL). The resulting mixture was thoroughly stirred at room temperature, and DIAD (0.13 mL, 0.66 mmol) was carefully added dropwise at that temperature. The reaction mixture was then heated to 60 °C in an oil bath and subsequently stirred at that temperature for 2 h. TLC analysis of the reaction mixture (10% EtOAc in petroleum ether) indicated consumption of the parent alcohol, the reaction mixture was then allowed to cool to room temperature, and the volatiles were evaporated under reduced pressure. The residue thus obtained was purified by column chromatography with gradient elution employing mixtures of EtOAc and petroleum ether as eluents (0 – 10% EtOAc) to afford methyl (*Z*)-3-((4-(benzyloxy)but-2-en-1-yl)oxy)benzoate (**71k**) as viscous oil (142.3 mg, **91% yield**).
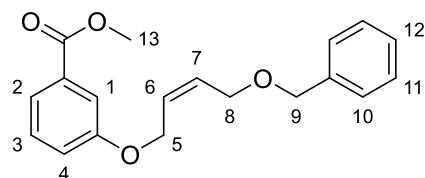

¹H NMR (400 MHz, CDCl₃): δ 7.65 (dt, $^3J_{HH}$ = 7.8 Hz, $^4J_{HH}$ = 1.3 Hz, 1H, H²), 7.55 (dd, $^4J_{HH}$ = 2.6 Hz, $^4J_{HH}$ = 1.5 Hz, 1H, H¹), 7.36-7.27 (m, 6H, H³/H¹⁰/H¹¹/H¹²), 7.08 (ddd, $^3J_{HH}$ = 8.3 Hz, $^4J_{HH}$ = 2.7 Hz, $^4J_{HH}$ = 1.0 Hz, 1H, H⁴), 5.89-5.86 (m, 2H, H⁶/H⁷), 4.08 (br d, $^3J_{HH}$ = 4.1 Hz, 2H, H⁵), 4.55 (s, 2H, H⁹), 4.17 (br d, $^3J_{HH}$ = 4.3 Hz, 2H, H⁸), 3.91 (s, 3H, H¹³).

¹³C NMR (101 MHz, CDCl₃): δ 167.0, 158.6, 138.1, 131.6, 130.3, 129.6, 128.6, 128.0, 127.9, 122.3, 120.2, 114.9, 72.6, 66.0, 64.4, 52.3.

IR (neat, cm^{-1}): 3028, 2949, 2855, 2345, 2322, 1719, 1584, 1487, 1445, 1414, 1389, 1362, 1317, 1275, 1215, 1190, 1157, 1098, 1074, 1028, 993, 945, 901, 887, 880, 843, 799, 785, 754, 737, 698, 683, 650, 610.

HRMS (positive ESI): m/z calculated for [M+H]$^+$ C$_{19}$H$_{21}$O$_4$: 313.1440; found: 313.1442.

(*Z*)-3-((4-(benzyloxy)but-2-en-1-yl)oxy)benzoic acid – **72k**
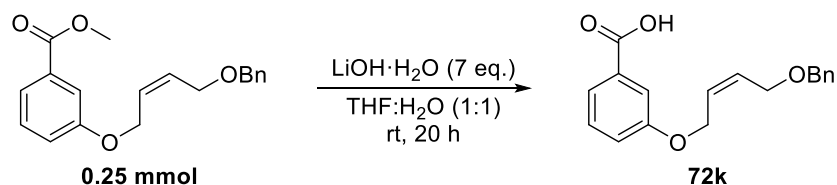
To a round-bottomed flask equipped with a magnetic stirrer bar were added methyl (*Z*)-3-((4-(benzyloxy)but-2-en-1-yl)oxy)benzoate (76.8 mg, 0.25 mmol), THF (1.5 mL) and H$_2$O (1.5 mL), and the mixture was thoroughly stirred at room temperature. Then, LiOH·H$_2$O (74.6 mg, 1.78 mmol) was added in one portion under constant stirring, and the reaction mixture was stirred for 20 h at room temperature. TLC analysis (50% EtOAc in petroleum ether) indicated consumption of the parent methyl ester, and the reaction mixture was then diluted with 0.1 M NaOH (5 mL). The resulting mixture was extracted with Et$_2$O (3 × 15 mL), and the combined organic layers were discarded. The aqueous phase was acidified to pH ~ 2 by careful addition of 12 M HCl, then extracted with Et$_2$O (3 × 20 mL), and the combined organic phases were washed with brine (20 mL), dried over Na$_2$SO$_4$, filtered and evaporated under reduced pressure to afford to afford (*Z*)-3-((4-(benzyloxy)but-2-en-1-yl)oxy)benzoic acid (**72k**) as a white solid (72.9 mg, **99% yield**).
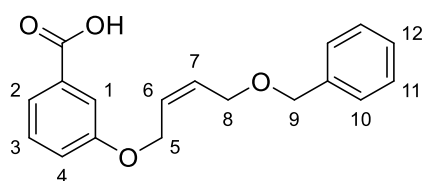
^{1}H NMR (400 MHz, CDCl$_3$): δ 11.4 (br s, 1H, OH), 7.76 (dt, $^3J_{HH}$ = 7.5 Hz, $^4J_{HH}$ = 1.3 Hz, 1H, H^2), 7.64 (dd, $^4J_{HH}$ = 2.4 Hz, $^4J_{HH}$ = 1.4 Hz, 1H, H^1), 7.43-7.29 (m, 6H, H^3/H^{10}/H^{11}/H^{12}), 7.17 (ddd, $^3J_{HH}$ = 8.2 Hz, $^4J_{HH}$ = 2.7 Hz, $^4J_{HH}$ = 1.0 Hz, 1H, H^4),

5.92 (t, $^3J_{HH}$ = 3.7 Hz, 2H, H^6/H^7), 4.68 (d, $^3J_{HH}$ = 3.8 Hz, 2H, H^5), 4.59 (s, 2H, H^9), 4.21 (d, $^3J_{HH}$ = 3.8 Hz, 2H, H^8).

^{13}C NMR (101 MHz, CDCl$_3$): δ 171.3, 158.0, 137.4, 130.1, 129.7, 129.1, 128.0, 127.4, 127.3, 127.2, 122.4, 120.7, 114.7, 72.0, 65.4, 63.8.
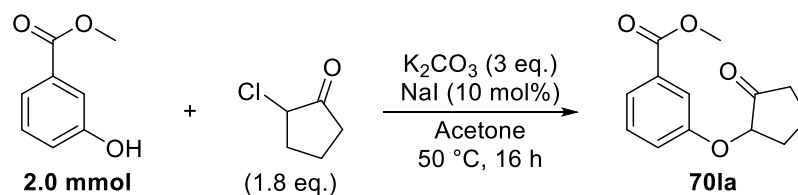
Melting point: 60-62 °C.

IR (neat, cm^{-1}): 3026, 2959, 2916, 2862, 2565, 1682, 1599, 1585, 1489, 1450, 1416, 1385, 1371, 1319, 1292, 1240, 1206, 1117, 1080, 1020, 1009, 988, 976, 962, 928, 912, 876, 808, 777, 748, 716, 698, 679, 662, 615.

HRMS (negative ESI): m/z calculated for [M-H]$^-$ C$_{18}$H$_{17}$O$_4{}^-$: 297.1132; found: 197.1130.

Sequence for 3-((2-methylenecyclopentyl)oxy)benzoic acid – **72l**
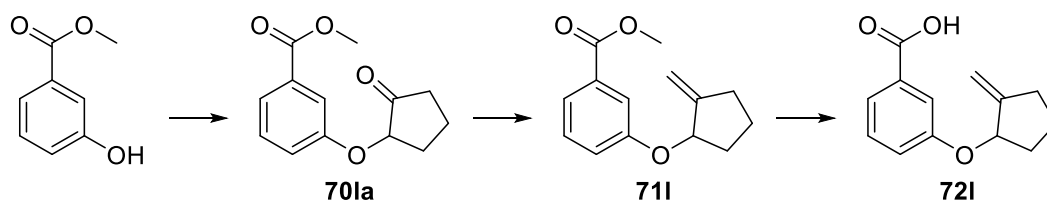

Methyl 3-((2-oxocyclopentyl)oxy)benzoate (**70la**)

To a round-bottomed flask equipped with a magnetic stirrer bar were added NaI (50 mg, 0.33 mmol), K$_2$CO$_3$ (1.252 g, 9.06 mmol), methyl 3-hydroxybenzoate (0.458 g, 3.01 mmol) and acetone (15 mL). The mixture was thoroughly stirred at room temperature and 2-chlorocyclopentanone (0.630 g, 5.32 mmol) was then added in one portion under constant, vigorous stirring (*N.B.: 2-chlorocyclopentanone is thermally unstable, thus, it should be preferably weighed immediately after removal from storage at -20 °C, in its solid form, and used without delay*). The reaction vessel was then heated to 50 °C in an oil bath for 16 h. The mixture was then allowed to cool to room temperature and the volatiles were evaporated under reduced pressure. The residue thus obtained was suspended in water (20 mL), partitioned with EtOAc (40 mL) and the organic layer was collected. The aqueous phase was extracted with

EtOAc (2 × 40 mL), the combined organic phases were washed with 0.1 M NaOH (2 × 20 mL), brine (20 mL), dried over Na$_2$SO$_4$, filtered and evaporated under reduced pressure. The residue was purified by column chromatography with gradient elution employing mixtures of EtOAc and petroleum ether as eluents (0 – 20% EtOAc) to afford methyl 3-((2-oxocyclopentyl)oxy)benzoate (**70la**) as a light yellow oil (0.549 g, **78% yield**).
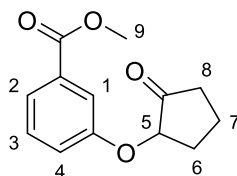

^{1}H NMR (400 MHz, CDCl$_3$): δ 7.68 (dt, $^3J_{HH}$ = 7.7 Hz, $^4J_{HH}$ = 1.3 Hz, 1H, H^2), 7.63 (dd, $^4J_{HH}$ = 2.6 Hz, $^4J_{HH}$ = 1.5 Hz, 1H, H^1), 7.36 (t, $^3J_{HH}$ = 8.0 Hz, 1H, H^3), 7.20 (ddd, $^3J_{HH}$ = 8.3 Hz, $^4J_{HH}$ = 2.7 Hz, $^4J_{HH}$ = 1.0 Hz, 1H, H^4), 4.69 (t, $^3J_{HH}$ = 8.5 Hz, 1H, H^5), 3.92 (s, 3H, H^9), 2.59-2.29 (m, 3H, H^8/H$^{8'}$/H^7), 2.21-2.12 (m, 1H, H$^{7'}$), 2.04-1.91 (m, 2H, H^6/H$^{6'}$).

^{13}C NMR (101 MHz, CDCl$_3$): δ 213.0, 166.2, 157.5, 131.0, 129.0, 122.4, 120.5, 115.4, 79.1, 51.7, 34.7, 28.9, 16.7.

IR (neat, cm^{-1}): 2951, 2882, 2841, 1751, 1715, 1678, 1641, 1584, 1547, 1485, 1445, 1402, 1350, 1275, 1223, 1190, 1171, 1155, 1142, 1103, 1082, 1026, 1001, 947, 883, 810, 797, 756, 727, 683, 621.

HRMS (positive ESI): m/z calculated for [M+H]$^+$ C$_{13}$H$_{15}$O$_4^+$: 235.0970; found: 235.0971.

Methyl 3-((2-methylenecyclopentyl)oxy)benzoate – **71l**
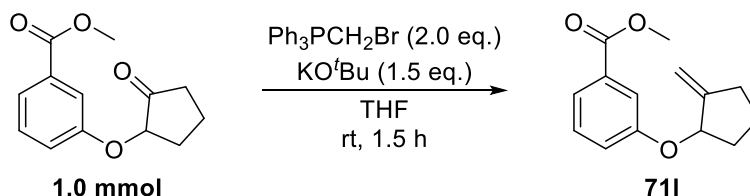
To a flame-dried round-bottomed flask were added Ph$_3$PCH$_2$Br (736.0 mg, 2.06 mmol) and anhydrous THF (90 mL), and the mixture was thoroughly stirred at room temperature. KO^{t}Bu (223.7 mg, 1.47 mmol) was then added to the reaction vessel in one portion and under constant vigorous stirring, and this mixture was stirred for a

further 15 min at room temperature. The reaction mixture was kept under vigorous stirring and a solution of methyl 3-((2-oxocyclopentyl)oxy)benzoate (235.6 mg, 1.01 mmol) in anhydrous THF (10 mL) was then added to the reaction vessel *via* syringe at a fast rate (*ca.* 8 mL min^{-1}). The resulting mixture was stirred for a further 1.5 h at room temperature. TLC analysis (25% EtOAc in petroleum ether) indicated consumption of the parent ketone, and the reaction mixture was then quenched by addition of H_2O (10 mL) at room temperature and the volatiles were evaporated under reduced pressure. The residue was diluted with H_2O (10 mL), extracted with Et_2O (5 × 30 mL), washed with brine (30 mL), dried over Na_2SO_4, filtered and evaporated under reduced pressure. The residue thus obtained was purified by column chromatography with gradient elution, employing mixtures of Et_2O and petroleum ether as eluents (0 – 5% Et_2O, then 10% Et_2O) to afford methyl 3-((2-methylenecyclopentyl)oxy)benzoate (**71l**) as a colourless oil (166.7 mg, **71% yield**).
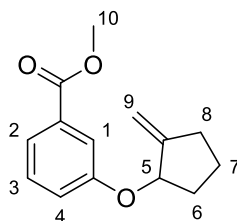

^{1}H NMR (400 MHz, CDCl$_3$): δ 7.65-7.60 (m, 2H, H^1/H^2), 7.33 (t, $^3J_{HH}$ = 8.1 Hz, 1H, H^3), 7.14 (ddd, $^3J_{HH}$ = 8.2 Hz, $^4J_{HH}^1$ = 2.7 Hz, $^4J_{HH}^1$ = 1.3 Hz, 1H, H^4), 5.20-5.18 (m, 1H, H^9), 5.14-5.12 (m, 1H, H$^{9'}$), 5.02-4.97 (m, 1H, H^5), 3.91 (s, 3H, H^{10}), 2.60-2.48 (m, 1H, H^8), 2.41-2.30 (m, 1H, H$^{8'}$), 2.13-2.04 (m, 1H, H^6), 1.95-1.81 (m, 2H, H$^{6'}$/H^7), 1.77-1.68 (m, 1H, H$^{7'}$).

^{13}C NMR (101 MHz, CDCl$_3$): δ 167.1, 158.4, 150.7, 131.5, 129.5, 122.2, 121.4, 116.5, 110.4, 80.5, 52.3, 32.7, 30.7, 22.3.

IR (neat, cm^{-1}): 3076, 2951, 2872, 2845, 1721, 1663, 1584, 1485, 1443, 1346, 1275, 1215, 1188, 1157, 1140, 1099, 1078, 1051, 1028, 1003, 991, 959, 889, 833, 797, 754.

HRMS (positive ESI): m/z calculated for [M+H]$^+$ C$_{14}$H$_{17}$O$_3^+$: 233.1178; found: 233.1177.

3-((2-methylenecyclopentyl)oxy)benzoic acid – **72l**
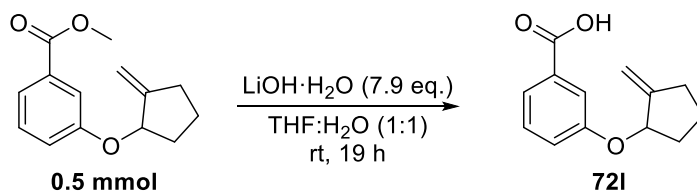
To a round-bottomed flask equipped with a magnetic stirrer bar were added methyl 3-((2-methylenecyclopentyl)oxy)benzoate (114.8 mg, 0.49 mmol), THF (3.3 mL) and H_2O (3.3 mL), and the mixture was thoroughly stirred at room temperature. Then, LiOH·H_2O (162.3 mg, 3.87 mmol) was added in one portion under constant stirring, and the reaction mixture was stirred for 19 h at room temperature. TLC analysis (50% EtOAc in petroleum ether) indicated consumption of the parent methyl ester, and the reaction mixture was then diluted with 0.1 M NaOH. The resulting mixture was extracted with Et_2O (3 × 20 mL), and the combined organic layers were discarded. The aqueous phase was acidified to pH ~2 by careful addition of 12 M HCl, extracted with Et_2O (3 × 30 mL), and the combined organic phases were washed with brine (10 mL), dried over Na_2SO_4, filtered and evaporated under reduced pressure to afford 3-((2-methylenecyclopentyl)oxy)benzoic acid (**72l**) as a white solid (98.2 mg, **91% yield**).
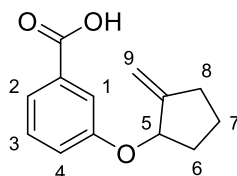

^{1}H NMR (400 MHz, CDCl$_3$): δ 7.74 (dt, $^3J_{HH}$ = 7.6 Hz, $^4J_{HH}$ = 1.2 Hz, 1H, H^2), 7.72 (dd, $^4J_{HH}$ = 2.5 Hz, $^4J_{HH}$ = 1.8 Hz, 1H, H^1), 7.40 (t, $^4J_{HH}$ = 7.9 Hz, 1H, H^3), 7.23 (ddd, $^3J_{HH}$ = 8.2 Hz, $^4J_{HH}$ = 2.6 Hz, $^4J_{HH}$ = 1.0 Hz, 1H, H^4), 5.24-5.22 (m, 1H, H^9), 5.19-5.16 (m, 1H, H$^{9'}$), 5.06-5.02 (m, 1H, H^5), 2.64-2.52 (m, 1H, H^8), 2.45-2.35 (m, 1H, H$^{8'}$), 2.19-2.08 (m, 1H, H^6), 1.99-1.86 (m, 2H, H$^{6'}$/H^7), 1.82-1.72 (m, 1H, H$^{7'}$), (OH not observed).

^{13}C NMR (101 MHz, CDCl$_3$): δ 171.4, 157.8, 150.0, 130.0, 129.0, 122.2, 121.8, 116.2, 109.8, 79.9, 32.0, 30.0, 21.7.
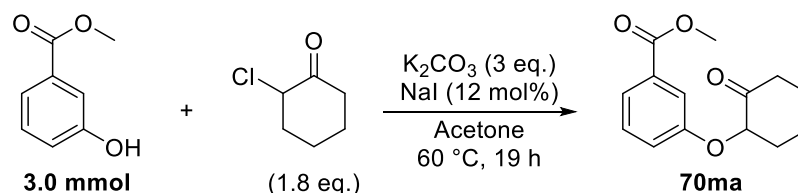
Melting point: 56-58 °C.

IR (neat, cm^{-1}): 3076, 2951, 2872, 2845, 1721, 1663, 1584, 1485, 1443, 1346, 1275, 1215, 1188, 1157, 1140, 1099, 1078, 1051, 1028, 1003, 991, 959, 889, 833, 797, 754.

HRMS (negative ESI): m/z calculated for [M-H]$^-$ C$_{13}$H$_{13}$O$_3$: 217.0870; found: 217.0873.

Sequence for 3-((2-methylenecyclohexyl)oxy)benzoic acid – **72m**
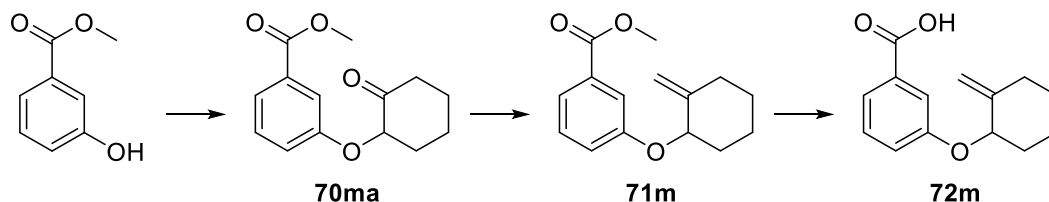
Methyl 3-((2-oxocyclohexyl)oxy)benzoate – **70ma**

To a round-bottomed flask equipped with a magnetic stirrer bar were added NaI (53 mg, 0.35 mmol), K$_2$CO$_3$ (1.256 g, 9.09 mmol), methyl 3-hydroxybenzoate (0.460 g, 3.02 mmol) and acetone (15 mL). The mixture was thoroughly stirred at room temperature and 2-chlorocyclohexanone (0.707 g, 5.33 mmol) was then added in one portion under constant, vigorous stirring. The reaction vessel was then heated to 60 °C in an oil bath for 19 h. The mixture was then allowed to cool to room temperature and the solvent was evaporated under reduced pressure. The residue thus obtained was partitioned between water (20 mL) and EtOAc (40 mL), and the organic phase was collected, then the aqueous layer was extracted with EtOAc (2 × 40 mL). The combined organic phases were washed with 0.1 M NaOH (2 × 20 mL), brine (40 mL), dried over Na$_2$SO$_4$ and evaporated under reduced pressure. The residue was then purified by column chromatography with gradient elution employing mixtures of EtOAc and petroleum ether as eluents (0 – 25% EtOAc) to afford methyl 3-((2-oxocyclohexyl)oxy)benzoate (**70ma**) as a highly viscous, light yellow oil (0.563 g, **75% yield**).
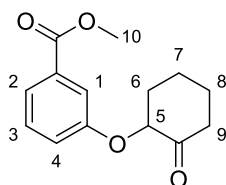
¹H NMR (400 MHz, CDCl₃): δ 7.63 (dt, $^3J_{HH}$ = 7.7 Hz, $^4J_{HH}$ = 1.2 Hz, 1H, H²), 7.47 (dd, $^4J_{HH}$ = 2.6 Hz, $^4J_{HH}$ = 1.5 Hz, 1H, H¹), 7.31 (t, $^3J_{HH}$ = 8.0 Hz, 1H, H³), 7.08 (ddd, $^3J_{HH}$ = 8.3 Hz, $^4J_{HH}$ = 2.6 Hz, $^4J_{HH}$ = 1.0 Hz, 1H, H⁴), 4.72 (ddd, $^3J_{HH}$ = 9.7 Hz, $^3J_{HH}$ = 5.6 Hz, $^4J_{HH}$ = 1.1 Hz, 1H, H⁵), 3.89 (s, 3H, H¹⁰), 2.66-2.57 (m, 1H, H⁹), 2.47-2.32 (m, 2H, H⁹'/H⁶), 2.09-1.98 (m, 3H, H⁶'/H⁸/H⁸'), 1.83-1.74 (m, 2H, H⁷/H⁷').

¹³C NMR (101 MHz, CDCl₃): δ 207.5, 166.9, 157.7, 131.5, 129.6, 122.8, 120.8, 115.9, 80.8, 52.3, 40.8, 34.5, 27.8, 23.1.

IR (neat, cm⁻¹): 3069, 2943, 2926, 2872, 1721, 1713, 1599, 1585, 1489, 1468, 1443, 1321, 1277, 1244, 1236, 1213, 1192, 1165, 1107, 1088, 1067, 1036, 1001, 955, 924, 893, 880, 837, 812, 797, 756, 685, 667, 610.

HRMS (positive ESI): m/z calculated for [M+NH₄]⁺ $C_{14}H_{20}NO_4^+$: 266.1387; found: 266.1383.

Methyl 3-((2-methylenecyclohexyl)oxy)benzoate – **71m**
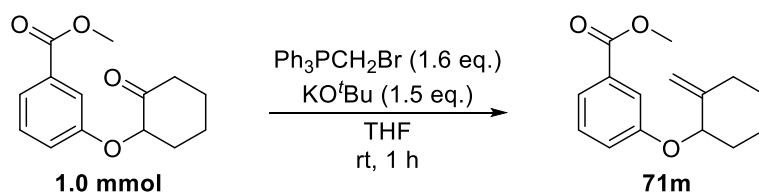
To a flame-dried round-bottomed flask were added Ph₃PCH₂Br (572.9 mg, 1.60 mmol) and anhydrous THF (90 mL), and the mixture was thoroughly stirred at room temperature. KO^{t}Bu (165.1 mg, 1.47 mmol) was then added to the reaction vessel in one portion and under constant vigorous stirring, and this mixture was stirred for a further 15 min at room temperature. The reaction mixture was kept under vigorous stirring and a solution of methyl 3-((2-oxocyclohexyl)oxy)benzoate (247.3 mg, 1.00 mmol) in anhydrous THF (10 mL) was then added to the reaction vessel via syringe at a fast rate (*ca.* 8 mL min⁻¹). The resulting mixture was stirred for a further 1 h at room temperature. TLC analysis (10% Et₂O in petroleum ether) indicated consumption of the parent ketone, and the reaction mixture was then quenched by

addition of H_2O (10 mL) at room temperature and the volatiles were evaporated under reduced pressure. The residue was purified by column chromatography with gradient elution employing mixtures of Et_2O and petroleum ether as eluents (0 – 5% Et_2O, then 10% Et_2O) to afford methyl 3-((2-methylenecyclohexyl)oxy)benzoate (**71m**) as a clear viscous oil (192.6 mg, **78% yield**).
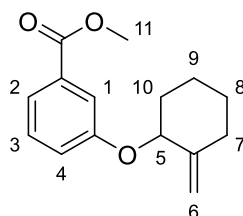

^{1}H NMR (400 MHz, CDCl$_3$): δ 7.62 (dt, $^3J_{HH}$ = 7.7Hz, $^4J_{HH}$ = 1.2 Hz, 1H, H^2), 7.61-7.59 (m, 1H, H^1), 7.33 (t, $^3J_{HH}$ = 7.9 Hz, 1H, H^3), 7.13 (ddd, $^3J_{HH}$ = 8.2 Hz, $^4J_{HH}$ = 2.6 Hz, $^4J_{HH}$ = 1.0 Hz, 1H, H^4), 4.90 (br s, 1H, H^6), 4.87 (br s, 1H, H$^{6'}$), 4.68 (dd, $^3J_{HH}$ = 8.0 Hz, $^3J_{HH}$ = 3.8 Hz, 1H, H^5), 3.92 (s, 3H, H^{11}), 2.47-2.39 (m, 1H, H^7), 2.19-2.09 (m, 1H, H$^{7'}$), 2.05-1.78 (m, 3H, H^{10}/H$^{10'}$/H^8), 1.74-1.51 (m, 3H, H$^{8'}$/H^9/H$^{9'}$).

^{13}C NMR (101 MHz, CDCl$_3$): δ 166.5, 157.6, 146.6, 130.8, 128.7, 121.4, 120.6, 116.1, 108.1, 78.1, 51.6, 33.5, 32.7, 27.4, 22.7.

IR (neat, cm^{-1}): 3069, 2943, 2926, 2872, 1721, 1713, 1599, 1585, 1489, 1468, 1443, 1321, 1277, 1244, 1236, 1213, 1192, 1165, 1107, 1088, 1067, 1036, 1001, 955, 924, 893, 880, 837, 812, 797, 756, 685, 667, 610.

HRMS (positive ESI): m/z calculated for [M+H]$^+$ C$_{15}$H$_{19}$O$_3^+$: 247.1329; found: 247.1330.

3-((2-methylenecyclohexyl)oxy)benzoic acid – **72m**
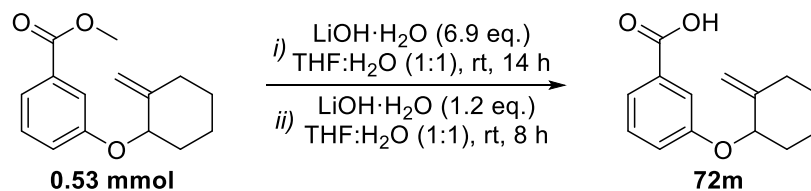
To a round-bottomed flask equipped with a magnetic stirrer bar were added methyl 3-((2-methylenecyclohexyl)oxy)benzoate (131.5 mg, 0.53 mmol), THF (3.6 mL) and H_2O (3.6 mL), and the mixture was thoroughly stirred at room temperature. Then, LiOH·H_2O (152.6 mg, 3.64 mmol) was added in one portion under constant stirring,

and the reaction mixture was stirred for 14 h at room temperature. TLC analysis (25% EtOAc in petroleum ether) indicated incomplete consumption of the parent methyl ester, and another portion of LiOH·H$_2$O (25.7 mg, 0.61 mmol) was added to the reaction mixture, which was stirred for a further 8 h. Upon reassessment by TLC analysis (25% EtOAc in petroleum ether), no residual methyl ester was observed, and the reaction mixture was diluted with H$_2$O (10 mL), extracted with Et$_2$O (3 × 25 mL), and the combined organic layers were discarded. The aqueous phase was acidified to pH ~ 1 by careful addition of 12 M HCl, extracted with Et$_2$O (3 × 30 mL), and the combined organic phases were washed with brine (20 mL), dried over Na$_2$SO$_4$, filtered and evaporated under reduced pressure to afford 3-((2-methylenecyclohexyl)oxy)benzoic acid (**72m**) as a white solid (105.7 mg, **85% yield**).
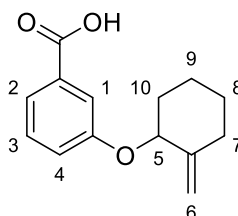
^{1}H NMR (400 MHz, DMSO-d_6): δ 12.9 (br s, 1H, OH), 7.50 (dt, $^3J_{HH}$ = 7.5 Hz, $^4J_{HH}$ = 1.1 Hz, 1H, H^2), 7.44 (dd, $^4J_{HH}$ = 2.4 Hz, $^4J_{HH}$ = 1.4 Hz, 1H, H^1), 7.38 (t, $^3J_{HH}$ = 7.9 Hz, 1H, H^3), 7.20 (ddd, $^3J_{HH}$ = 8.3 Hz, $^4J_{HH}$ = 2.8 Hz, $^4J_{HH}$ = 1.0 Hz, 1H, H^4), 4.84-4.79 (m, 3H, H^5/H^6/H$^{6'}$), 2.36-2.27 (m, 1H, H^{10}), 2.17-2.08 (m, 1H, H$^{10'}$), 1.99-1.90 (m, 1H, H^7), 1.87-1.77 (m, 1H, H$^{7'}$), 1.74-1.52 (m, 3H, H^8/H$^{8'}$/H^9), 1.51-1.40 (m, 1H, H$^{9'}$).

^{13}C NMR (101 MHz, DMSO-d_6): δ 167.1, 157.5, 147.0, 132.0, 129.6, 121.5, 120.5, 116.1, 108.1, 77.4, 33.5, 32.6, 27.4, 22.6.

Melting point: 86-87 °C.

IR (neat, cm^{-1}): 2936, 2859, 1721, 1655, 1584, 1485, 1443, 1275, 1215, 1190, 1152, 1098, 1072, 1061, 1040, 1003, 993, 961, 899, 864, 827, 793, 754, 683, 633.

HRMS (negative ESI): m/z calculated for [M-H]$^-$ C$_{14}$H$_{15}$O$_3^-$: 231.1027; found: 231.1028.

6.3   Hydroarylation Reactions

6.3.1 Test Reactions for Reaction Development

All test reactions reported herein were conducted according to the general procedure 6.1.3 for hydroarylation test reactions. ^{1}H NMR spectroscopy analysis was employed to assess overall conversion ($C_\%$) by comparing the integration of diagnostic peaks from to the starting material (I_{SM}) to those arising from isomerised structures (I_{ISO}) and the product (I_P), according to Equation (6.1):

$$C_\% = 100\,\frac{I_P}{I_{SM} + I_{ISO} + I_P} \quad (6.1)$$

Experimental data is presented for each substrate with the relevant ^{1}H NMR data. Recorded conversions are reported in Schemes and Tables specified for each substrate.

1-(3-(allyloxy)phenyl)ethan-1-one – **56** (Scheme 2.14 and Table 2.1)

Following general procedure 6.1.3, iridium catalyst **57** and 1-(3-(allyloxy)phenyl)ethan-1-one (**56**) were reacted in diglyme at 120 °C for 20 h. After workup and evaporation of the volatiles, the conversion was determined by ^{1}H NMR spectroscopy of recovered compounds. The relevant experimental data is summarised in Table E2.1

Relevant ^{1}H NMR spectroscopic data for substrate **56** in **CDCl₃**:
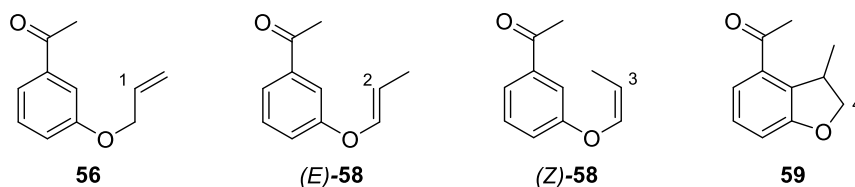
56   *(E)*-**58**   *(Z)*-**58**   **59**

Reference peak expected at: δ 6.06 (ddt, $^3J_{HH}$ = 17.2 Hz, $^3J_{HH}$ = 10.6 Hz, $^3J_{HH}$ = 5.3 Hz, H^1).

Conversions determined by comparison with peaks at: δ 5.45 (dq, $^3J_{HH}$ = 12.2 Hz, $^3J_{HH}$ = 6.8 Hz, H^2), 4.98 (dq, $^3J_{HH}$ = 6.6 Hz, $^3J_{HH}$ = 6.5 Hz, H^3), 4.56 (t, J_{HH} = 8.3 Hz, H^4).

Table E2.1: Hydroarylation test reaction with **56**.[†]

Index	m_S (mg)	n_S (μmol)	m_{Ir} (mg)	n_{Ir} (μmol)	V_{Sol} (mL)	m_{KOAc} (mg)	n_{KOAc} (μmol)
T2.1, E1	18.2	103	2.8	1.8	1.0	—	—
T2.1, E2	18.0	102	3.0	1.9	1.0	9.8	101

Index	Conversion (%)			
	56	**(E)-58**	**(Z)-58**	**59**
T2.1, E1	29	28	39	4
T2.1, E2	>95	—	—	—

[†]In Table E2.1, symbols represent: m$_j$ –amount of compound, in mg; n$_j$ – number of moles of compound, in μmol; subscripts represent: S – substrate; Ir – catalyst; V$_{Sol}$ – volume of diglyme, in mL. For index, Tx, Ey reads "Table x, Entry y".

Test reaction with a mixture of vinyl ethers (E)-58 and (Z)-58.

Vinyl ether (E)-**58** and (Z)-**58** were obtained from combined reaction mixtures of catalytic tests performed under identical conditions.

Thus, following general procedure 6.1.3, iridium catalyst **57** and 1-(3-(allyloxy)phenyl)ethan-1-one (**56**) were reacted in diglyme at 120 °C for 20 h. After workup and evaporation of the volatiles, the conversion was determined by ^{1}H NMR spectroscopy of recovered compounds. The relevant experimental data is summarised in Table E2.2

Relevant ^{1}H NMR spectroscopic data for substrate **56** in **CDCl₃:**
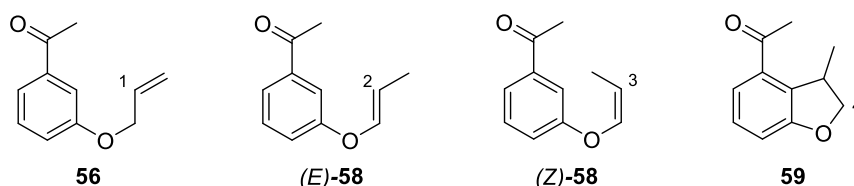
**Reference peak expected at:** δ 6.06 (ddt, $^3J_{HH}$ = 17.2 Hz, $^3J_{HH}$ = 10.6 Hz, $^3J_{HH}$ = 5.3 Hz, H^1).

Conversions determined by comparison with peaks at: δ 5.45 (dq, $^3J_{HH}$ = 12.2 Hz, $^3J_{HH}$ = 6.8 Hz, H^2), 4.98 (dq, $^3J_{HH}$ = 6.6 Hz, $^3J_{HH}$ = 6.5 Hz, H^3), 4.56 (dd, $^2J_{HH}$ = $^3J_{HH}$ = 8.3 Hz, H^4).

Table E2.2: Hydroarylation test reaction with **56**.[†]

Entry	m_S (mg)	n_S (µmol)	m_{Ir} (mg)	n_{Ir} (µmol)	V_{Sol} (mL)	Conversion (%)			
						56	(E)-58	(Z)-58	59
1	18.1	103	2.9	1.9	1.0	21	42	32	5
2	17.8	101	2.9	1.9	1.0	7	41	46	6

[†]In Table E2.2, symbols represent: m_j –amount of compound, in mg; n_j – number of moles of compound, in µmol; subscripts represent: S – substrate; Ir – catalyst; V_{Sol} – volume of diglyme, in mL.

These reaction mixtures were then combined and purified by column chromatography with gradient elution employing mixtures of EtOAc in petroleum ether as eluents (0 – 20% EtOAc) to afford a mixture of (E)-**58**, (Z)-**58** and **59** (37:55:7) as a colourless liquid (19.1 mg).

(E)-**58** (Z)-**58** **59**
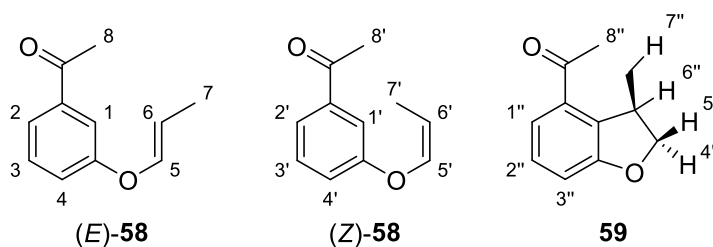
^{1}H NMR (400 MHz, CDCl$_3$): δ 7.64 (d, $^3J_{HH}$ = 7.6 Hz, 2H, H^2/H$^{2'}$), 7.53-7.49 (m, 1H, H$^{2''}$), 7.42 (t, $^3J_{HH}$ = 8.0 Hz, 1H, H$^{3'}$), 7.41 (t, $^3J_{HH}$ = 7.9 Hz, 1H, H^3), 7.22 (dd, $^3J_{HH}$ = 8.0 Hz, $^4J_{HH}$ = 2.5 Hz, 1H, H$^{4'}$), 7.19 (dd, $^3J_{HH}$ = 7.8 Hz, $^4J_{HH}$ = 2.5 Hz, 1H, H^4), 7.00 (d, $^3J_{HH}$ = 8.1 Hz, 1H, H$^{3''}$), 6.46 (dq, $^3J_{HH}$ = 12.3 Hz, $^4J_{HH}$ = 1.6 Hz, 1H, H^5), 6.43 (dq, $^3J_{HH}$ = 6.4 Hz, $^4J_{HH}$ = 1.9 Hz, 1H, H$^{5'}$), 5.45 (dq, $^3J_{HH}$ = 12.2 Hz, $^3J_{HH}$ = 6.9 Hz, 1H, H^6), 4.98 (dq, $^3J_{HH}$ = 6.6 Hz, $^3J_{HH}$ = 6.7 Hz, 1H, H$^{6'}$), 4.56 (t, J_{HH} = 8.3 Hz, 1H, H$^{5''}$), 4.30 (dd, $^2J_{HH}$ = 8.5 Hz, $^3J_{HH}$ =2.8 Hz, 1H, H$^{4''}$), 4.06-3.99 (m, 1H, H$^{6''}$), 2.62 (s, 9H, H^8/H$^{8'}$/H$^{8''}$), 1.74 (dd, $^3J_{HH}$ = 7.0 Hz, $^4J_{HH}$ = 1.8 Hz, 3H, H^7), 1.71 (dd, $^3J_{HH}$ = 7.0 Hz, $^4J_{HH}$ = 1.6 Hz, 3H, H$^{7'}$), 1.26 (d, $^3J_{HH}$ = 6.9 Hz, 3H, H$^{7''}$).

(N.B.: The peak for $H^{2''}$ is obscured by peaks at δ 7.42 ($H^{3'}$) and 7.41 (H^3), and were not reported above)

This mixture of isomeric compounds (Mixture A) was then employed in a second catalytic test. Hence, following general procedure 6.1.3, iridium catalyst **57** (3.1 mg, 2.0 μmol) and Mixture A (17.9 mg, 102 μmol) were reacted in diglyme at 120 °C for 20 h. After workup and evaporation of the volatiles, the relative composition was determined by ^{1}H NMR spectroscopy of recovered compounds. The following equation illustrates the observed changes in composition.
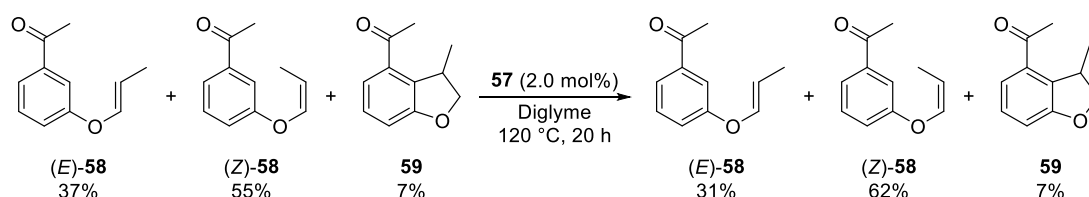

No significant changes in relative composition were observed.

Methyl 3-(allyloxy)benzoate – **64** (Table 2.1)

Following general procedure 6.1.3, iridium catalyst **57** and methyl 3-(allyloxy)benzoate (**64**) were reacted in diglyme at 120 °C for 20 h. After workup and evaporation of the volatiles, the conversion was determined by ^{1}H NMR spectroscopy of recovered compounds. The relevant experimental data is summarised in Table E2.3

Relevant ^{1}H NMR spectroscopic data for substrate **64** in **CDCl₃**:
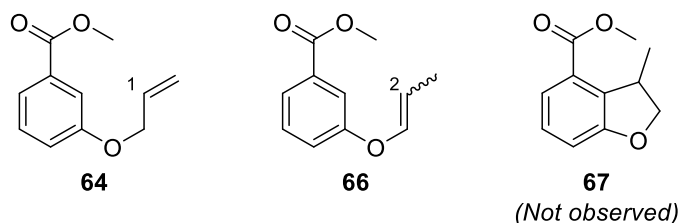
Reference peak expected at: δ 6.05 (ddt, $^3J_{HH}$ = 17.3 Hz, $^3J_{HH}$ =10.5 Hz, $^3J_{HH}$ = 5.3 Hz, 1H, H^1).

Conversions determined by comparison with peaks at: δ 4.98 (dq, $^3J_{HH}$ = 6.9 Hz, $^3J_{HH}$ = 6.1 Hz, H^2).

Table E2.3: Hydroarylation test reaction with **64**.[†]

Index	m_S (mg)	n_S (μmol)	m_{Ir} (mg)	n_{Ir} (μmol)	V_{Sol} (mL)	m_{KOAc} (mg)	n_{KOAc} (μmol)
T2.1, E3	19.0	99	2.9	1.9	1.0	—	—
T2.1, E4	19.5	101	2.8	1.8	1.0	14.0	113

Index	Conversion (%)		
	64	66	67
T2.1, E3	21	79	—
T2.1, E4	>95	—	—

[†]In Table E2.3, symbols represent: m_j –amount of compound, in mg; n_j – number of moles of compound, in μmol; subscripts represent: S – substrate; Ir – catalyst; V_{Sol} – volume of diglyme, in mL. For index, Tx, Ey reads "Table x, Entry y".

3-(allyloxy)benzoic acid – **65** (Table 2.1)

Following general procedure 6.1.3, iridium catalyst **57** and 3-(allyloxy)benzoate (**65**) were reacted in diglyme at 120 °C for 20 h. After workup and evaporation of the volatiles, the conversion was determined by ^{1}H NMR spectroscopy of recovered compounds. The relevant experimental data is summarised in Table E2.4

Relevant ^{1}H NMR spectroscopic data for substrate **65** in **DMSO-d_6:**
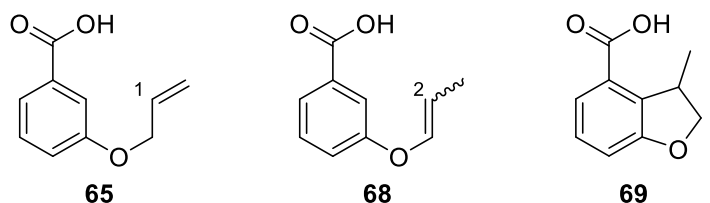
65 **68** **69**

Reference peak expected at: δ 6.05 (ddt, $^3J_{HH}$ = 17.3 Hz, $^3J_{HH}$ =10.5 Hz, $^3J_{HH}$ = 5.3 Hz, 1H, H^1).

Conversions determined by comparison with peaks at: δ 4.98 (dq, $^3J_{HH}$ = 4.98 Hz, $^3J_{HH}$ = 6.6 Hz, H^2), 4.51 (t, J_{HH} = 8.4 Hz, H^3).

Table E2.4: Hydroarylation test reaction with **65**.[†]

Index	m_S (mg)	n_S (μmol)	m_{Ir} (mg)	n_{Ir} (μmol)	V_{Sol} (mL)	$m_{K_2CO_3}$ (mg)	$n_{K_2CO_3}$ (μmol)
T2.1, E5	17.9	100	3.1	2.0	1.0	—	—
T2.1, E6	17.7	99	2.9	1.9	1.0	14.7	106
T2.1, E7	17.2	97	3.0	1.9	1.0	1.5	11
T2.1, E8	17.0	95	7.5	4.8	1.0	1.4	10

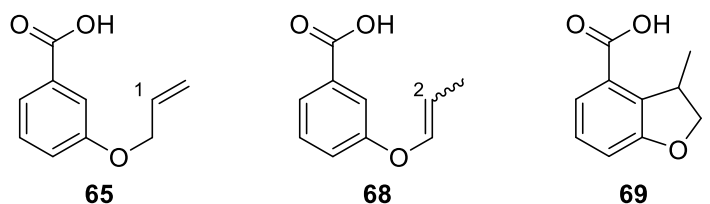| Index	Conversion (%)		
	65	68	69
T2.1, E5	>95	—	—
T2.1, E6	72	14	14
T2.1, E7	71	—	29
T2.1, E8	60	—	40

[†]In Table E2.4, symbols represent: m_j – amount of compound, in mg; n_j – number of moles of compound, in μmol; subscripts represent: S – substrate; Ir – catalyst; V_{Sol} – volume of diglyme, in mL. For index, Tx, Ey reads "Table x, Entry y".

3-(allyloxy)benzoic acid – **65** (Table 2.2)

Following general procedure 6.1.3, iridium catalyst **57** and 3-(allyloxy)benzoic acid (**65**) were reacted in diglyme at the appropriate temperature for 20 h. After workup and evaporation of the volatiles, the conversion was determined by ^{1}H NMR spectroscopy of recovered compounds. The relevant experimental data is summarised in Table E2.5

Relevant ^{1}H NMR spectroscopic data for substrate **65** in **DMSO-d_6:**

65   **68**   **69**

Reference peak expected at: δ 6.05 (ddt, $^3J_{HH}$ = 17.3 Hz, $^3J_{HH}$ = 10.5 Hz, $^3J_{HH}$ = 5.3 Hz, 1H, H[1]).

Conversions determined by comparison with peaks at: δ 4.98 (dq, $^3J_{HH}$ = 4.98 Hz, $^3J_{HH}$ = 6.6 Hz, H[2]), 4.51 (dd, $^2J_{HH}$ = $^3J_{HH}$ = 8.4 Hz, H[4]).

Table E2.5: Hydroarylation test reaction with **65**.[†]

Index	m_S (mg)	n_S (μmol)	m_{Ir} (mg)	n_{Ir} (μmol)	V_{Sol} (mL)	m_{KOAc} (mg)	n_{KOAc} (μmol)	θ (ºC)
T2.2, E1	13.4	75.2	5.8	3.7	1.5	2.5	18	
T2.2, E2	13.4	75.2	5.8	3.7	1.5	13.0	94	
T2.2, E3	13.3	74.6	5.8	3.7	0.5	13.1	95	
T2.2, E4	13.3	74.6	1.2	0.8	1.5	3.2	23	
T2.2, E5	13.4	75.2	1.2	0.8	1.5	12.8	93	90
T2.2, E6	13.4	75.2	5.7	3.6	0.5	2.5	18	
T2.2, E7	13.3	74.6	1.3	0.8	0.5	2.8	20	
T2.2, E8	13.5	75.8	1.3	0.8	0.5	12.8	93	
T2.2, E9	13.6	76.3	1.2	0.8	1.5	12.9	93	
T2.2, E10	13.5	75.8	5.7	3.6	1.5	13.2	96	
T2.2, E11	13.5	75.8	5.8	3.7	1.5	2.5	18	
T2.2, E12	13.3	74.6	5.8	3.7	0.5	13.1	95	150
T2.2, E13	13.3	74.6	1.2	0.8	1.5	2.7	20	
T2.2, E14	13.5	75.8	5.7	3.6	0.5	2.6	19	
T2.2, E15	13.7	76.9	1.2	0.8	0.5	13.2	96	
T2.2, E16	13.6	76.3	1.2	0.8	0.5	2.5	18	
T2.2, E17	13.5	75.8	3.5	2.2	1.0	7.7	56	
T2.2, E18	13.5	75.8	3.5	2.2	1.0	8.0	58	120
T2.2, E19	13.4	75.2	3.4	2.2	1.0	7.9	57	

Index	Conversion (%)			
	65	68	69	Other
T2.2, E1	79.6	3.2	10.7	6.4
T2.2, E2	61.5	12.8	25.6	—
T2.2, E3	80.0	10.5	9.5	—
T2.2, E4	100	—	—	—
T2.2, E5	96.3	2.4	1.3	—
T2.2, E6	87.8	—	3.4	8.8
T2.2, E7	100	—	—	—
T2.2, E8	100	—	—	—
T2.2, E9	77.4	16.8	5.8	—
T2.2, E10	4.6	14.4	81.0	—
T2.2, E11	—	3.5	96.5	—
T2.2, E12	10.1	26.3	63.6	—
T2.2, E13	46.6	3.8	30.7	18.8
T2.2, E14	—	6.4	93.6	—
T2.2, E15	71.0	20.2	8.8	—
T2.2, E16	64.8	5.3	5.2	24.6
T2.2, E17	72.3	17.0	10.6	—
T2.2, E18	25.0	25.0	50.0	—
T2.2, E19	35.7	28.6	35.7	—

[†]In Table E2.5, symbols represent: m_j –amount of compound, in mg; n_j – number of moles of compound, in μmol; subscripts represent: S – substrate; Ir – catalyst; V_{Sol} – volume of diglyme, in mL; θ – temperature, in ºC. For index, Tx, Ey reads "Table x, Entry y".

## 6.3.2 Test Reactions for Exploration of Substrate Scope

In the following section, the experimental details for results presented in Scheme 2.17 are reported. Experimental data is presented for each substrate with the relevant ^{1}H NMR data. Recorded conversions are reported in Schemes and Tables specified for each substrate and were calculated according to equation 6.1.

Whenever presented, *additional diagnostic peaks for ^{1}H NMR spectroscopy were not employed for determination of conversion.* These signals were only employed to confirm the proposed molecular structure.

3-(allyloxy)benzoic acid – **65** (Scheme 2.17)

Following general procedure 6.1.3, K_2CO_3 (1.4 mg, 10.1 μmol), iridium catalyst **57** (5.8 mg, 3.7 μmol), and carboxylic acid **65** (13.4 mg, 75.2 μmol) were reacted in diglyme (1.5 mL) at 150 °C for 20 h. After workup and evaporation of the volatiles, the conversion was determined by ^{1}H NMR spectroscopy of recovered compounds.

Relevant ^{1}H NMR spectroscopic data for substrate **65** in **DMSO-d_6:**
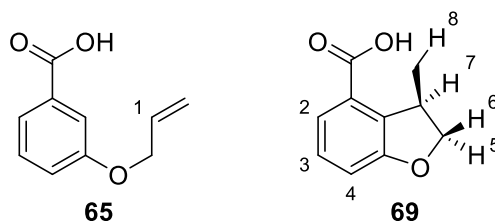
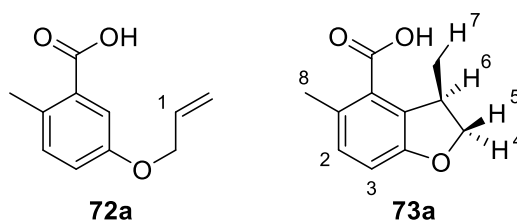**Reference peak expected at:** δ 6.05 (ddt, $^3J_{HH}$ = 17.3 Hz, $^3J_{HH}$ =10.5 Hz, $^3J_{HH}$ = 5.3 Hz, 1H, H^1).

Conversions determined by comparison with peaks at: 4.51 (dd, $^2J_{HH}$ = $^3J_{HH}$ = 8.4 Hz, H^6), 4.25 (dd, $^2J_{HH}$ = 8.5 Hz, $^3J_{HH}$ = 2.8 Hz, H^5).

Additional diagnostic peaks also found at: δ 7.40 (dd, $^3J_{HH}$ = 7.8 Hz, $^4J_{HH}$ = 1.1 Hz, H^2), 7.22 (dd, $^3J_{HH}^1$ = $^3J_{HH}^2$ = 7.9 Hz, H^3), 7.00 (d, $^3J_{HH}$ = 7.9 Hz, H^4), 3.90-3.80 (m, H^7), 1.21 (d, $^3J_{HH}$ = 6.8 Hz, H^5).

3-(allyloxy)benzoic acid – **72a** (Scheme 2.17)

Following general procedure 6.1.3, K$_2$CO$_3$ (1.0 mg, 7.2 μmol), iridium catalyst **57** (4.6 mg, 2.9 μmol), and carboxylic acid **72a** (11.5 mg, 59.8 μmol) were reacted in diglyme (1.2 mL) at 150 °C for 20 h. After workup and evaporation of the volatiles, the conversion was determined by ^{1}H NMR spectroscopy of recovered compounds.

Relevant ^{1}H NMR spectroscopic data for substrate **72a** in **DMSO-d_6:**

72a   **73a**

Reference peak expected at: δ 6.03 (ddt, $^3J_{HH}$ = 17.2 Hz, $^3J_{HH}$ = 10.4 Hz, $^3J_{HH}$ = 5.2 Hz, 1H, H^1).

Conversions determined by comparison with peaks at: 4.13 (dd, $^2J_{HH}$ = 8.4 Hz, $^3J_{HH}$ = 4.4 Hz, H^4).

Additional diagnostic peaks also found at: δ 7.00 (d, $^3J_{HH}$ = 8.2 Hz, H^2), 6.77 (d, $^3J_{HH}$ = 8.1 Hz, H^3), 4.54 (dd, $^2J_{HH}$ = $^3J_{HH}$ = 8.5 Hz, H^5), 3.74-3.62 (m, 1H, H^6), 1.18 (d, $^3J_{HH}$ = 6.9 Hz, H^7).

3-(allyloxy)-5-fluorobenzoic acid – **72b** (Scheme 2.17)

Following general procedure 6.1.3, K$_2$CO$_3$ (1.0 mg, 7.2 μmol), iridium catalyst **57** (4.7 mg, 3.0 μmol), and carboxylic acid **72b** (11.8 mg, 60.1 μmol) were reacted in diglyme (1.2 mL) at 150 °C for 20 h. After workup and evaporation of the volatiles, the conversion was determined by ^{1}H NMR spectroscopy of recovered compounds.

Relevant ^{1}H NMR spectroscopic data for substrate **72b** in **DMSO-d_6:**

72b   **73b**
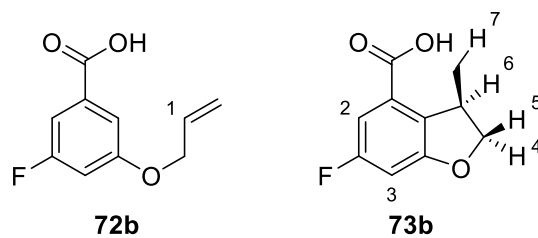
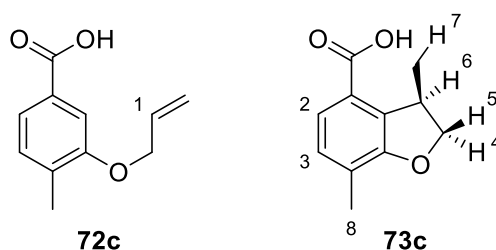**Reference peak expected at:** δ 6.04 (ddt, $^3J_{HH}$ = 17.2 Hz, $^3J_{HH}$ = 10.6 Hz, $^3J_{HH}$ =5.3 Hz, 1H, H^1).

Conversions determined by comparison with peaks at: δ 4.58 (dd, $^2J_{HH}$ = $^3J_{HH}$ = 8.4 Hz, H^5), 4.31 (dd, $^2J_{HH}$ = 8.5 Hz, $^3J_{HH}$ = 2.3 Hz, H^4).

Additional diagnostic peak also found at δ 7.10 (dd, $^3J_{HF}$ = 9.8 Hz, $^4J_{HH}$ = 2.1 Hz, H^2), 6.94 (dd, $^3J_{HF}$ = 9.2 Hz, $^4J_{HH}$ = 1.8 Hz, H^3), 3.89-3.77 (m, H^6), 1.20 (d, $^3J_{HH}$ = 7.1 Hz, H^7).

3-(allyloxy)-4-methylbenzoic acid – **72c** (Scheme 2.17)

Following general procedure 6.1.3, K$_2$CO$_3$ (0.9 mg, 6.5 μmol), iridium catalyst **57** (4.8 mg, 3.1 μmol), and carboxylic acid **72c** (11.6 mg, 60.3 μmol) were reacted in diglyme (1.2 mL) at 150 °C for 20 h. After workup and evaporation of the volatiles, the conversion was determined by ^{1}H NMR spectroscopy of recovered compounds.

Relevant ^{1}H NMR spectroscopic data for substrate **72c** in **CDCl₃:**

72c   **73c**

Reference peak expected at: δ 6.12 (ddt, $^3J_{HH}$ = 17.2 Hz, $^3J_{HH}$ = 10.3 Hz, $^3J_{HH}$ = 5.2 Hz, 1H, H^1).
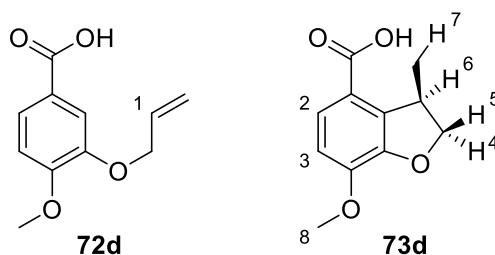
Conversions determined by comparison with peaks at: δ 4.34 (dd, $^2J_{HH}$ = 8.6 Hz, $^3J_{HH}$ = 2.4 Hz, H^5), 4.04-3.94 (m, H^6).

Additional diagnostic peak also found at δ 7.57 (d, $^3J_{HH}$ = 8.0 Hz, H^2), 7.07 (d, $^3J_{HH}$ = 8.0 Hz, H^3), 4.58 (dd, $^2J_{HH}$ = $^3J_{HH}$ = 8.3 Hz, H^4), 2.30 (s, H^8), 1.35 (d, $^3J_{HH}$ = 6.9 Hz, H^7).

3-(allyloxy)-4-methoxylbenzoic acid – **72d** (Scheme 2.17)

Following general procedure 6.1.3, K$_2$CO$_3$ (0.9 mg, 6.5 µmol), iridium catalyst **57** (4.6 mg, 2.9 µmol), and carboxylic acid **72d** (12.6 mg, 60.5 µmol) were reacted in diglyme (1.2 mL) at 150 °C for 20 h. After workup and evaporation of the volatiles, the conversion was determined by ^{1}H NMR spectroscopy of recovered compounds.

Relevant ^{1}H NMR spectroscopic data for substrate **72d** in **DMSO-d_6:**

72d   **73d**

Reference peak expected at: δ 6.12 (ddt, $^3J_{HH}$ = 17.2 Hz, $^3J_{HH}$ = 10.3 Hz, $^3J_{HH}$ = 5.2 Hz, 1H, H^1).

Conversions determined by comparison with peaks at: δ 4.49 (dd, $^2J_{HH}$ = $^3J_{HH}$ = 8.4 Hz, H^5), 4.27 (dd, $^2J_{HH}$ = 8.8 Hz, $^3J_{HH}$ = 2.6 Hz, H^4).
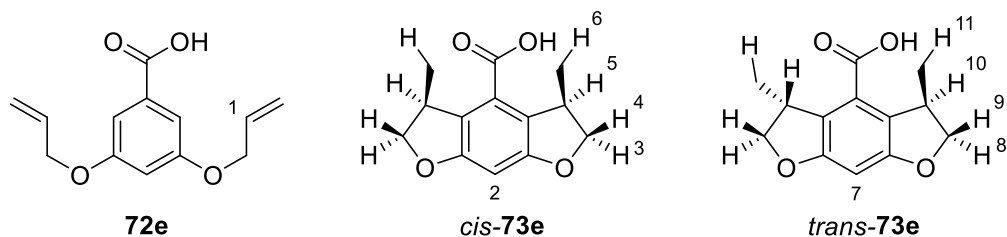
Additional diagnostic peak also found at: δ 7.45 (d, $^3J_{HH}$ = 8.6 Hz, H^2), 6.93 (d, $^3J_{HH}$ = 8.6 Hz, H^3), 1.20 (d, $^3J_{HH}$ = 7.0 Hz, H^7).

3,5-bis(allyloxy)benzoic acid – **72e** (Scheme 2.17)

Following general procedure 6.1.3, K$_2$CO$_3$ (1.1 mg, 8.0 µmol), iridium catalyst **57** (4.8 mg, 3.1 µmol), and carboxylic acid **72e** (14.1 mg, 60.2 µmol) were reacted in

diglyme (1.2 mL) at 150 °C for 20 h. After workup and evaporation of the volatiles, the conversion was determined by ^{1}H NMR spectroscopy of recovered compounds.

Relevant ^{1}H NMR spectroscopic data for substrate **72e** in **DMSO-*d*₆:**

72e   *cis*-**73e**   *trans*-**73e**

Reference peak expected at: δ 6.04 (ddt, $^3J_{HH}$ = 17.3 Hz, $^3J_{HH}$ =10.5 Hz, $^3J_{HH}$ = 5.2 Hz, 2H, H[1]).

Conversions determined by comparison with peaks at: δ 4.63 (dd, $^2J_{HH}$ = $^3J_{HH}$ = 8.5 Hz, H[4]), 4.53 (dd, $^2J_{HH}$ = $^3J_{HH}$ = 8.5 Hz, H[9]), 4.47 (dd, $^2J_{HH}$ = $^3J_{HH}$ = 8.2 Hz, H[9']). Additional diagnostic peak also found at: δ 4.27-4.14 (m, H[5]/H[10]/H[10']), 1.23 (d, $^3J_{HH}$ = 7.0 Hz, H[11]), 1.21 (d, $^3J_{HH}$ = 7.0 Hz, H[11']) 1.12 (d, $^3J_{HH}$ = 7.3 Hz, H[6]).

3-(allyl(*tert*-butoxycarbonyl)amino)benzoic acid – **72f** (Scheme 2.17)

Following general procedure 6.1.3, K₂CO₃ (1.7 mg, 12.3 μmol), iridium catalyst **57** (3.9 mg, 2.5 μmol), and carboxylic acid **72f** (14.3 mg, 51.6 μmol) were reacted in diglyme (1.0 mL) at 150 °C for 20 h. After workup and evaporation of the volatiles, the conversion was determined by ^{1}H NMR spectroscopy of recovered compounds.

Relevant ^{1}H NMR spectroscopic data for substrate **72f** in **CDCl₃:**

72f   **73f**
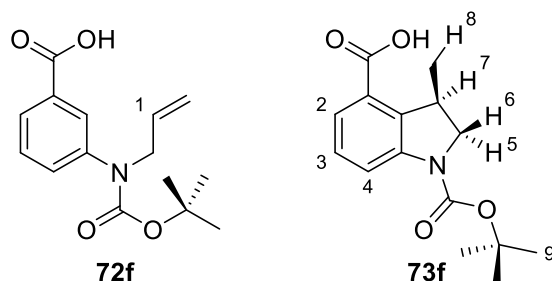
Reference peak expected at: δ 5.92, (ddt, $^3J_{HH}$ = 17.3 Hz, $^3J_{HH}$ = 10.0 Hz, $^3J_{HH}$ = 5.5 Hz, 1H, H^1).
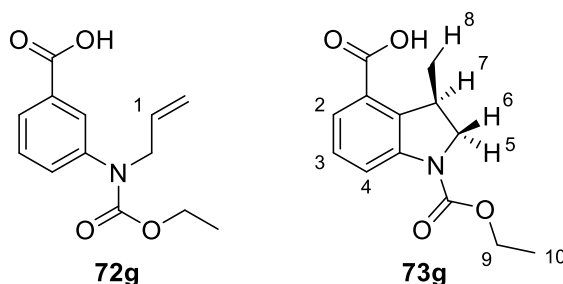
Conversions determined by comparison with peaks at: δ 3.85-3.71 (m, H^7).

Additional diagnostic peak also found at: δ 3.96-3.91 (m, H^5), 1.31 (d, $^3J_{HH}$ = 6.5 Hz, H^8).

3-(allyl(ethoxycarbonyl)amino)benzoic acid – **72g** (Scheme 2.17)

Following general procedure 6.1.3, K$_2$CO$_3$ (0.9 mg, 6.5 μmol), iridium catalyst **57** (4.8 mg, 3.1 μmol), and carboxylic acid **72g** (15.1 mg, 60.6 μmol) were reacted in diglyme (1.2 mL) at 150 °C for 20 h. After workup and evaporation of the volatiles, the conversion was determined by ^{1}H NMR spectroscopy of recovered compounds.

Relevant ^{1}H NMR spectroscopic data for substrate **72g** in **DMSO-d_6:**

72g   **73g**

Reference peak expected at: δ 5.88 (ddt, $^3J_{HH}$ = 17.6 Hz, $^3J_{HH}$ = 10.2 Hz, $^3J_{HH}$ = 5.3 Hz, 1H, H^1).

Conversions determined by comparison with peaks at: δ 3.72-3.68 (m, H^5).

Additional diagnostic peak also found at: δ 4.01-3.97 (m, H^6),

3-((*N*-allyl-4-methylphenyl)sulfonamido)benzoic acid – **72h** (Scheme 2.17)

Following general procedure 6.1.3, K$_2$CO$_3$ (1.2 mg, 8.7 μmol), iridium catalyst **57** (4.9 mg, 3.1 μmol), and carboxylic acid **72h** (20.4 mg, 61.6 μmol) were reacted in diglyme (1.2 mL) at 150 °C for 20 h. After workup and evaporation of the volatiles, the conversion was determined by ^{1}H NMR spectroscopy of recovered compounds.

Relevant ^{1}H NMR spectroscopic data for substrate **72h** in **DMSO-d_6:**

72h

73h
Not observed
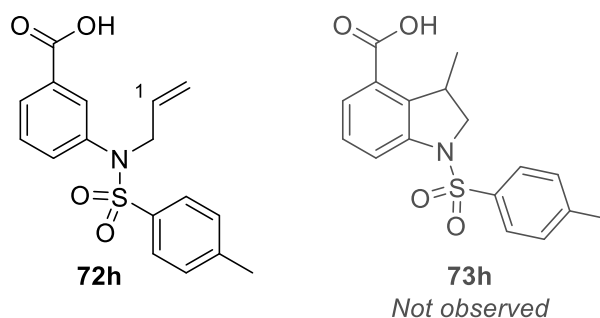
Reference peak expected at: δ 5.69 (ddt, $^3J_{HH}$ = 16.7 Hz, $^3J_{HH}$ = 10.7 Hz, $^3J_{HH}$ = 6.3 Hz, H^1).

No peaks for **73h** were observed. ^{1}H NMR spectroscopy only indicated the presence unreacted carboxylic acid **72h**.

3-((2-methylallyl)oxy)benzoic acid – **72i** (Scheme 2.17)

Following general procedure 6.1.3, K$_2$CO$_3$ (1.2 mg, 8.7 μmol), iridium catalyst **57** (5.7 mg, 3.6 μmol), and carboxylic acid **72i** (14.4 mg, 74.9 μmol) were reacted in diglyme (1.5 mL) at 150 °C for 20 h. After workup and evaporation of the volatiles, the conversion was determined by ^{1}H NMR spectroscopy of recovered compounds.

Relevant ^{1}H NMR spectroscopic data for substrate **72i** in **DMSO-d_6:**

72i

**73i**
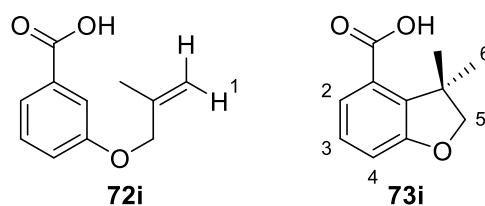
Reference peak expected at: δ 5.07 (s, H^1).

Conversions determined by comparison with peaks at: δ 4.18 (s, H^5).

Additional diagnostic peak also found at: δ 7.30 (d, $^3J_{HH}$ = 7.7 Hz, $^4J_{HH}$ = 1.0 Hz, H^2), 7.21 (dd, $^3J_{HH}{}^1$ = $^3J_{HH}{}^2$ = 7.8 Hz, H^3), 6.98 (dd, $^3J_{HH}$ = 79 Hz, $^4J_{HH}$ = 1.1 Hz, H^4), 1.42 (s, H^6).

3-((3-methylbut-2-en-1-yl)oxy)benzoic acid – **72j** (Scheme 2.17)

Following general procedure 6.1.3, K$_2$CO$_3$ (1.3 mg, 9.4 μmol), iridium catalyst **57** (5.6 mg, 3.6 μmol), and carboxylic acid **72j** (15.6 mg, 75.6 μmol) were reacted in diglyme (1.5 mL) at 150 °C for 20 h. After workup and evaporation of the volatiles, the conversion was determined by ^{1}H NMR spectroscopy of recovered compounds.

Relevant ^{1}H NMR spectroscopic data for substrate **72j** in **DMSO-d_6:**
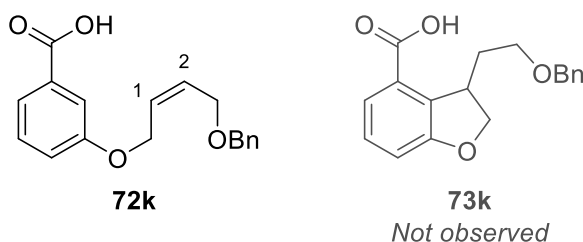

72j

73j
Not observed
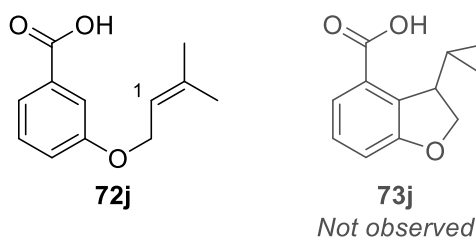
Reference peak expected at: δ 5.46-5.40 (m, H^1).

No peaks for **73j** were observed. ^{1}H NMR spectroscopy only indicated the presence unreacted carboxylic acid **72j**.

(*Z*)-3-((4-(benzyloxy)but-2-en-1-yl)oxy)benzoic acid – **72k** (Scheme 2.17)

Following general procedure 6.1.3, K$_2$CO$_3$ (1.0 mg, 7.2 μmol), iridium catalyst **57** (4.7 mg, 3.0 μmol), and carboxylic acid **72k** (18.0 mg, 60.3 μmol) were reacted in diglyme (1.2 mL) at 150 °C for 20 h. After workup and evaporation of the volatiles, the conversion was determined by ^{1}H NMR spectroscopy of recovered compounds.

Relevant ^{1}H NMR spectroscopic data for substrate **72k** in **CDCl$_3$:**

72k

73k
Not observed

Reference peak expected at: δ 5.92 (dd, $^3J_{HH}^1 = {}^3J_{HH}^2 = 3.7$ Hz, H^1/H^2).

No peaks for **73k** were observed. ^{1}H NMR spectroscopy only indicated the presence unreacted carboxylic acid **72k**.

3-((2-methylenecyclopentyl)oxy)benzoic acid – **72l** (Scheme 2.17)

Following general procedure 6.1.3, K$_2$CO$_3$ (1.2 mg, 8.7 μmol), iridium catalyst **57** (4.6 mg, 2.9 μmol), and carboxylic acid **72l** (10.1 mg, 46.3 μmol) were reacted in diglyme (1.2 mL) at 150 °C for 20 h. After workup and evaporation of the volatiles, the conversion was determined by ^{1}H NMR spectroscopy of recovered compounds.

Relevant ^{1}H NMR spectroscopic data for substrate **72l** in **CDCl$_3$:**

72l   **73l**
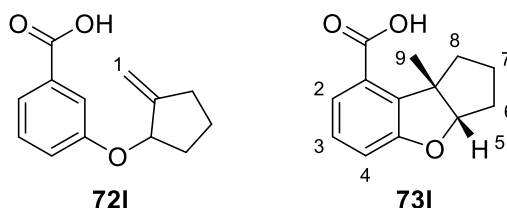
Reference peak expected at: δ 5.24-5.22 (m, H^1), 5.19-5.16 (m, H$^{1'}$).

Conversions determined by comparison with peaks at: δ 4.77 (dd, $^3J_{HH}$ = 5.4 Hz, $^3J_{HH}$ = 3.4 Hz, H^5).
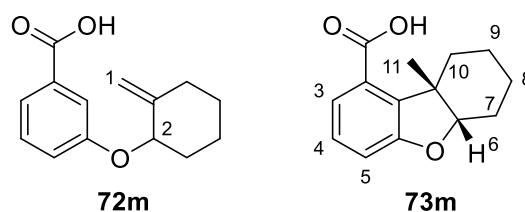
Additional diagnostic peak also found at: δ 7.63 (d, $^3J_{HH}$ = 7.6 Hz, H^2), 7.22 (t, $^3J_{HH}$ = 7.8 Hz, H^3), 6.99 (dd, $^3J_{HH}$ = 8.3 Hz, $^4J_{HH}$ = 1.0 Hz, H^4), 1.80-1.54 (m, H^6/H^7/H^8), 1.28 (s, H^9).

3-((2-methylenecyclopentyl)oxy)benzoic acid – **72m** (Scheme 2.17)

Following general procedure 6.1.3, K$_2$CO$_3$ (1.2 mg, 8.7 μmol), iridium catalyst **57** (4.8 mg, 3.1 μmol), and carboxylic acid **72m** (14.1 mg, 60.7 μmol) were reacted in

diglyme (1.1 mL) at 150 °C for 20 h. After workup and evaporation of the volatiles, the conversion was determined by ^{1}H NMR spectroscopy of recovered compounds.

Relevant ^{1}H NMR spectroscopic data for substrate **72m** in **DMSO-d_6**:

72m   **73m**

Reference peak expected at: δ 4.84-4.79 (m, H^1/H$^{1'}$/H^2).

Conversions determined by comparison with peaks at: δ 4.14 (t, $^3J_{HH}$ = 3.3 Hz, H^6).

Additional diagnostic peaks also found at: δ 7.18 (t, $^3J_{HH}$ = 7.6 Hz, H^4), 6.98 (d, $^3J_{HH}$ = 7.6 Hz, H^5).

6.3.3 Synthesis of Esters *via* Hydroarylation and Methylation Sequence (Scheme 2.19)

Methyl 3-methyl-2,3-dihydrobenzofuran-4-carboxylate - **75**
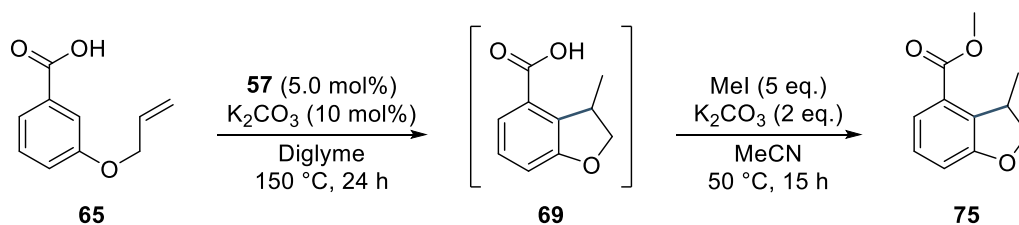
Following general procedure 6.1.4, K$_2$CO$_3$ (1.5 mg, 10.9 μmol), iridium catalyst **57** (7.8 mg, 5.0 μmol), and carboxylic acid **65** (17.8 mg, 99 μmol) were reacted in diglyme (2.0 mL) at 150 °C for 24 h. The residue obtained after workup was re-dissolved in acetonitrile (2.0 mL) and reacted with K$_2$CO$_3$ (32.2 mg, 0.23 mmol) and MeI (0.04 mL, 0.6 mmol) at 50 °C for 15 h. Chromatographic purification afforded methyl 3-methyl-2,3-dihydrobenzofuran-4-carboxylate (**75**) as a colourless oil (10.8 mg, **56% yield** over two steps).
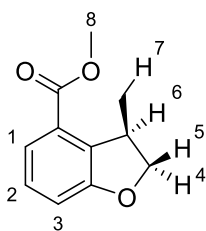
¹H NMR (400 MHz, CDCl₃): δ 7.51 (dd, $^3J_{HH}$ = 7.8 Hz, $^4J_{HH}$ = 1.4 Hz, 1H, H¹), 7.19 (t, $^3J_{HH}$ = 8.0 Hz, 1H, H²), 6.97 (d, $^3J_{HH}$ = 7.6 Hz, 1H, H³), 4.56 (app. t, J_{HH} = 8.2 Hz, 1H, H⁵), 4.29 (dd, $^2J_{HH}$ = 8.6 Hz, $^3J_{HH}$ = 3.0 Hz, 1H, H⁴), 3.98-3.88 (m, 4H, H⁶/H⁸), 1.30 (d, $^3J_{HH}$ =7.2 Hz, 3H, H⁷).

**¹³C NMR (101 MHz, CDCl₃):** δ 166.8, 160.4, 136.2, 128.3, 126.8, 122.5, 114.0, 79.0, 52.0, 37.5, 20.6.

IR (neat, cm⁻¹): 2955, 2924, 2853, 2359, 2332, 1721, 1589, 1445, 1435, 1375, 1331, 1271, 1260, 1236, 1194, 1136, 1096, 1078, 1059, 1022, 962, 941, 903, 808, 752, 735.

HRMS (positive ESI): m/z calculated for [M+H]⁺ $C_{11}H_{13}O_3^+$: 193.0865; found: 193.0868.

Methyl 3,5-dimethyl-2,3-dihydrobenzofuran-4-carboxylate – **76a**
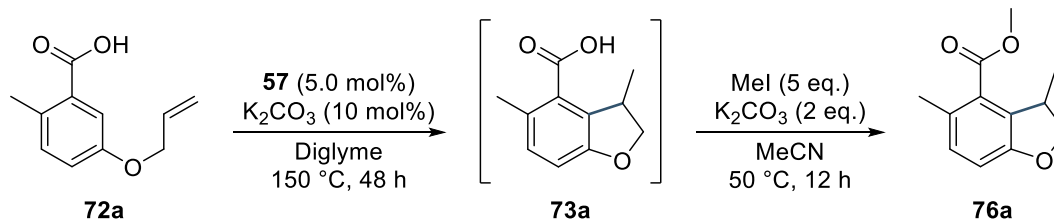
Following general procedure 6.1.4, K₂CO₃ (3.5 mg, 25.3 μmol), iridium catalyst **57** (19.5 mg, 12.5 μmol), and carboxylic acid **72a** (48.4 mg, 252 μmol) were reacted in diglyme (5.0 mL) at 150 °C for 48 h. The residue obtained after workup was re-dissolved in acetonitrile (5.0 mL) and reacted with K₂CO₃ (74.0 mg, 0.54 mmol) and MeI (0.20 mL, 3.2 mmol) at 50 °C for 12 h. Chromatographic purification afforded methyl 3,5-dimethyl-2,3-dihydrobenzofuran-4-carboxylate (**76a**) as a colourless oil (41.0 mg, **79% yield** over two steps).
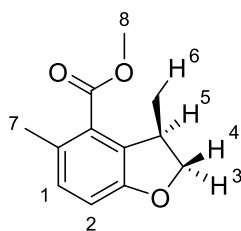
¹H NMR (400 MHz, CDCl₃): δ 6.98 (d, $^3J_{HH}$ = 8.0 Hz, 1H, H¹), 6.78 (d, $^3J_{HH}$ = 8.3 Hz, 1H, H²), 4.59 (app. t, J_{HH} = 8.5 Hz, 1H, H⁴), 4.18 (dd, $^2J_{HH}$ = 8.5 Hz, $^3J_{HH}$ = 4.3 Hz, 1H, H³), 3.90 (s, 3H, H⁸), 3.80-3.71 (m, 1H, H⁵), 2.38 (s, 3H, H⁷), 1.22 (d, $^3J_{HH}$ = 7.0 Hz, 3H, H⁶).

¹³C NMR (101 MHz, CDCl₃): δ 168.6, 158.0, 130.9, 129.6, 128.2, 118.5, 115.2, 112.0, 78.8, 51.9, 37.2, 20.4.

IR (neat, cm⁻¹): 2951, 2926, 1721, 1595, 1477, 1452, 1437, 1377, 1269, 1242, 1227, 1190, 1132, 1076, 1042, 1005, 993, 964, 945, 816, 799, 777, 723.

HRMS (positive ESI): m/z calculated for [M+H]⁺ $C_{12}H_{15}O_3$: 207.1021; found: 207.1021.

Methyl 3,7-dimethyl-2,3-dihydrobenzofuran-4-carboxylate – **76c**
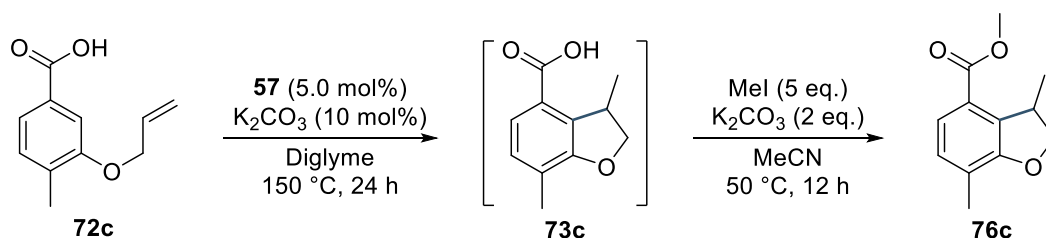
Following general procedure 6.1.4, K₂CO₃ (3.5 mg, 25.3 μmol), iridium catalyst **57** (19.5 mg, 12.5 μmol), and carboxylic acid **72c** (48.1 mg, 250 μmol) were reacted in diglyme (5.0 mL) at 150 °C for 24 h. The residue obtained after workup was re-dissolved in acetonitrile (5.0 mL) and reacted with K₂CO₃ (69.7 mg, 0.50 mmol) and MeI (0.20 mL, 3.2 mmol) at 50 °C for 12 h. Chromatographic purification afforded methyl 3,7-dimethyl-2,3-dihydrobenzofuran-4-carboxylate (**76c**) as a colourless oil (23.4 mg, **45% yield** over two steps).
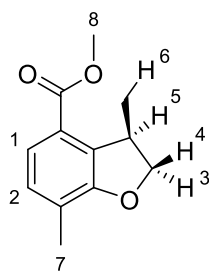
^{1}H NMR (400 MHz, CDCl$_3$): δ 7.44 (d, $^3J_{HH}$ = 7.9 Hz, 1H, H^1), 7.01 (d, $^3J_{HH}$ = 8.0 Hz, 1H, H^2), 4.54 (app. t, J_{HH} = 8.5 Hz, 1H, H^4), 4.29 (dd, $^2J_{HH}$ = 8.5 Hz, $^3J_{HH}$ = 2.5 Hz, 1H, H^3), 3.97-3.87 (m, 4H, H^5/H^8), 2.25 (s, 3H, H^7), 1.29 (d, $^3J_{HH}$ = 6.9 Hz, 3H, H^6).

^{13}C NMR (101 MHz, CDCl$_3$): δ 166.9, 158.5, 134.3, 129.5, 125.2, 124.3, 122.5, 78.8, 51.8, 37.9, 20.6, 15.7.
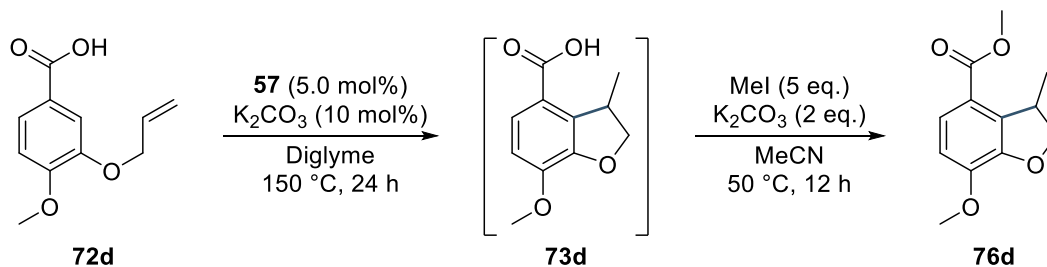
IR (neat, cm^{-1}): 2951, 2924, 1717, 1620, 1585, 1433, 1414, 1373, 1331, 1275, 1261, 1252, 1221, 1190, 1140, 1128, 1070, 1022, 962, 943, 893, 829, 795, 775, 748, 725.

HRMS (positive ESI): m/z calculated for [M+H]$^+$ C$_{12}$H$_{15}$O$_3$: 207.1021; found: 207.1024.

Methyl 7-methoxy-3-methyl-2,3-dihydrobenzofuran-4-carboxylate – **76d**

Following general procedure 6.1.4, K$_2$CO$_3$ (3.4 mg, 24.6 µmol), iridium catalyst **57** (19.5 mg, 12.5 µmol), and carboxylic acid **72a** (51.8 mg, 249 µmol) were reacted in diglyme (5.0 mL) at 150 °C for 24 h. The residue obtained after workup was re-dissolved in acetonitrile (5.0 mL) and reacted with K$_2$CO$_3$ (69.8 mg, 0.51 mmol) and MeI (0.20 mL, 3.2 mmol) at 50 °C for 12 h. Chromatographic purification afforded methyl 7-methoxy-3-methyl-2,3-dihydrobenzofuran-4-carboxylate (**76d**) as a colourless oil (30.5 mg, **55% yield** over two steps).
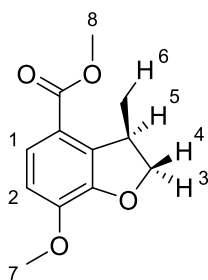
1H NMR (400 MHz, CDCl₃): δ 7.55 (d, $^3J_{HH}$ = 8.5 Hz, 1H, H¹), 6.76 (d, $^3J_{HH}$ = 8.5 Hz, 1H, H²), 4.59 (t, J_{HH} = 8.4 Hz, 1H, H⁴), 4.35 (dd, $^2J_{HH}$ = 8.8 Hz, $^3J_{HH}$ = 2.5 Hz, 1H, H³), 3.97-3.90 (m, 4H, H⁵/H⁸), 3.86 (s, 3H, H⁷), 1.28 (d, $^3J_{HH}$ = 6.9 Hz, 3H, H⁶).

13C NMR (101 MHz, CDCl₃): δ 166.4, 148.4, 148.0, 136.1, 124.5, 119.0, 110.5, 79.6, 56.0, 51.7, 38.3, 20.5.

IR (neat, cm⁻¹): 2953, 2843, 1711, 1614, 1582, 1506, 1435, 1267, 1221, 1202, 1186, 1130, 1092, 1078, 1018, 961, 939, 891, 820, 793, 779, 745, 725, 671, 648.

HRMS (positive ESI): m/z calculated for [M+H]⁺ $C_{12}H_{15}O_4$: 223.0970; found: 223.0968.

Methyl 3,3-dimethyl-2,3-dihydrobenzofuran-4-carboxylate – **76i**
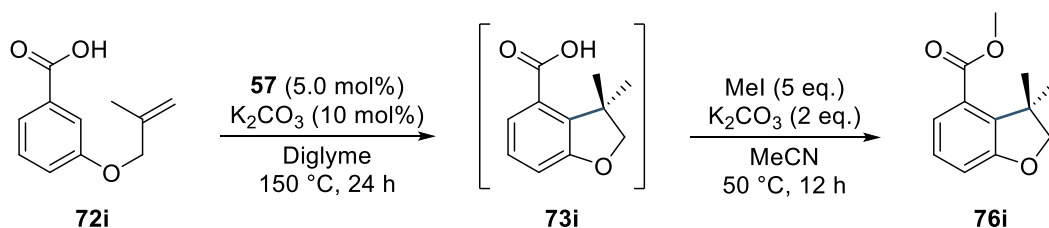
Following general procedure 6.1.4, K₂CO₃ (3.2 mg, 23.2 μmol), iridium catalyst **57** (19.4 mg, 12.4 μmol), and carboxylic acid **72a** (48.2 mg, 251 μmol) were reacted in diglyme (5.0 mL) at 150 °C for 24 h. The residue obtained after workup was re-dissolved in acetonitrile (5.0 mL) and reacted with K₂CO₃ (70.3 mg, 0.51 mmol) and MeI (0.20 mL, 3.2 mmol) at 50 °C for 12 h. Chromatographic purification afforded methyl 3,3-dimethyl-2,3-dihydrobenzofuran-4-carboxylate (**76i**) as a colourless oil (11.4 mg, **22% yield** over two steps).
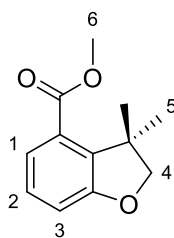
^{1}H NMR (400 MHz, CDCl$_3$): δ 7.40 (dd, $^3J_{HH}$ = 7.8 Hz, $^4J_{HH}$ = 1.1 Hz, 1H, H^1), 7.17 (t, $^3J_{HH}$ = 7.9 Hz, 1H, H^2), 6.96 (dd, $^3J_{HH}$ = 8.0 Hz, $^4J_{HH}$ = 1.0 Hz, 1H, H^3), 4.20 (s, 2H, H^4), 3.90 (s, 3H, H^6), 1.48 (s, 6H, H^5).

^{13}C NMR (101 MHz, CDCl$_3$): δ 167.2, 160.8, 136.6, 128.2, 127.9, 122.9, 114.1, 85.6, 52.0, 43.6, 25.6.

IR (neat, cm^{-1}): 2957, 2924, 2855, 1730, 1585, 1441, 1260, 1192, 1088, 1055, 1013, 864, 793, 754, 704, 685.

HRMS (positive ESI): m/z calculated for [M+H]$^+$ C$_{12}$H$_{15}$O$_3$: 207.1021; found: 207.1023.

Methyl 9a-methyl-5a,6,7,8,9,9a-hexahydrodibenzo[*b,d*]furan-1-carboxylate – **76m**
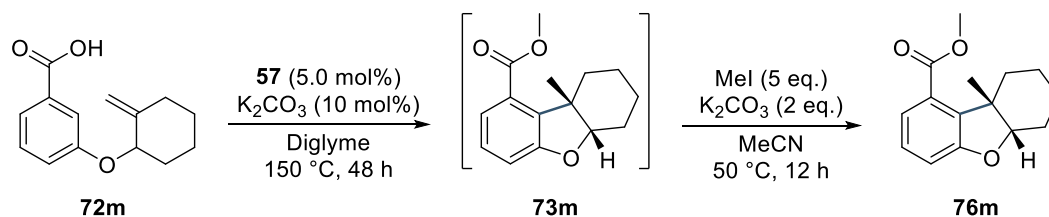
Following general procedure 6.1.4, K$_2$CO$_3$ (3.3 mg, 23.9 μmol), iridium catalyst **57** (19.3 mg, 12.4 μmol), and carboxylic acid **72a** (57.8 mg, 249 μmol) were reacted in diglyme (5.0 mL) at 150 °C for 48 h. The residue obtained after workup was re-dissolved in acetonitrile (5.0 mL) and reacted with K$_2$CO$_3$ (69.4 mg, 0.50 mmol) and MeI (0.20 mL, 3.2 mmol) at 50 °C for 12 h. Chromatographic purification afforded 9a-methyl-5a,6,7,8,9,9a-hexahydrodibenzo[*b,d*]furan-1-carboxylate (**76m**) as a colourless oil (31.9 mg, **52% yield** over two steps).
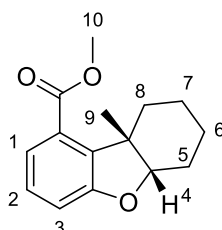
^{1}H NMR (400 MHz, CDCl$_3$): δ 7.33 (dd, $^3J_{HH}$ = 7.8 Hz, $^4J_{HH}$ = 1.4 Hz, 1H, H^1), 7.15 (t, $^3J_{HH}$ = 7.9 Hz, 1H, H^2), 6.97 (dd, $^3J_{HH}$ = 8.0 Hz, $^4J_{HH}$ = 1.3 Hz, 1H, H^3), 4.16 (t, $^3J_{HH}$ = 3.5 Hz, 1H, H^4), 3.89 (s, 3H, H^{10}), 2.18-2.06 (m, 2H, H^5/H^8), 1.78 (dddd, $^2J_{HH}$ = 15.1 Hz, $^3J_{HH}$ = 11.2 Hz, $^3J_{HH}$ = 5.6 Hz, $^3J_{HH}$ = 3.9 Hz, 1H, H$^{5'}$), 1.58-1.40 (m, 8H, H^6/H$^{6'}$/H^7/H$^{7'}$/H$^{8'}$/H^9).

^{13}C NMR (101 MHz, CDCl$_3$): δ 167.6, 159.8, 139.1, 127.9, 127.6, 122.4, 114.1, 88.6, 52.0, 44.6, 33.9, 25.5, 20.9, 20.6, 20.5.

IR (neat, cm^{-1}): 2930, 2859, 1724, 1584, 1439, 1371, 1314, 1260, 1246, 1194, 1146, 1123, 1092, 1018, 989, 957, 914, 872, 814, 799, 752.

HRMS (positive ESI): m/z calculated for [M+H]$^+$ C$_{15}$H$_{19}$O$_3$: 247.1334; found: 127.1341.

7. Computational Details

All calculations were performed according to the general guidelines listed in Chapter 1, Section 6. Please, refer to that section for a list of techniques and associated references. Output files are available in electronic format in **Appendix A**.

The energy for all 32 diastereomeric iridium complexes discussed in Section 3.3 are listed in Table E2.6.

Table E2.6: Energy of diastereomeric iridium complexes of type **77**.

Entry	H (Hartrees)	G (Hartrees)	ΔH_{rel} (kcal mol^{-1})	ΔG_{rel} (kcal mol^{-1})
1	-2173.61612	-2173.72615	0.00000	0.00000
2	-2173.61330	-2173.72334	1.76707	1.76268
3	-2173.61256	-2173.71992	2.23143	3.90813
4	-2173.61161	-2173.71900	2.82882	4.48607
5	-2173.61114	-2173.72161	3.12437	2.84827
6	-2173.61011	-2173.72033	3.77322	3.65023
7	-2173.60936	-2173.71759	4.24322	5.36898
8	-2173.60799	-2173.71603	5.10417	6.35040
9	-2173.60729	-2173.71775	5.54280	5.27171
10	-2173.60698	-2173.71795	5.73858	5.14182
11	-2173.60562	-2173.71780	6.58760	5.23845
12	-2173.60320	-2173.71048	8.10555	9.83057
13	-2173.60145	-2173.71080	9.20557	9.62789
14	-2173.60139	-2173.70972	9.24322	10.30999
15	-2173.60139	-2173.70971	9.24510	10.31626
16	-2173.60095	-2173.71116	9.52246	9.40575
17	-2173.60094	-2173.71121	9.52623	9.37312
18	-2173.59957	-2173.70859	10.38529	11.01657
19	-2173.59778	-2173.70887	11.50853	10.84275
20	-2173.59548	-2173.70556	12.95306	12.91792
21	-2173.59303	-2173.70273	14.48732	14.69189
22	-2173.59146	-2173.70220	15.47753	15.02886
23	-2173.59026	-2173.70206	16.23055	15.11546
24	-2173.58955	-2173.69660	16.67420	18.54229
25	-2173.58314	-2173.69277	20.69402	20.94691
26	-2173.58222	-2173.68780	21.27259	24.06501
27	-2173.58156	-2173.68874	21.68863	23.47452
28	-2173.58066	-2173.69005	22.25213	22.64872
29	-2173.58020	-2173.68967	22.53828	22.88968
30	-2173.57963	-2173.69069	22.89721	22.25088
31	-2173.56892	-2173.67699	29.61784	30.84965
32	-2173.56782	-2173.67871	30.30936	29.76907

The structures of six entries in Table E2.5 have been presented in Section 3.3, and the following correspondence exists: (Λ)-**77a** – entry 1; (Λ)-**77b** – entry 5; (Δ)-**77c** – entry 20; (Δ)-**77d** – entry 22; (Λ)-**77e** – entry 32; (Λ)-**77f** – entry 31.

8. References

[1] Godula, K.; Sames, D., *Science* **2016**, *312*, 67.

[2] Kleiman, J. P.; Dubeck, M., *J. Am. Chem. Soc.* **1963**, *85*, 1544.

[3] Cope, A. C.; Siekman, R. W., *J. Am. Chem. Soc.* **1965**, *87*, 3272.

[4] Bergman, R. G., *Nature* **2007**, *446*, 391.

[5] Ackermann, L., *Chem. Rev.* **2011**, *111*, 1315.

[6] Sakahura, T.; Sodeyama, T.; Sasaki, K.; Wada, K.; Tanaka, M., *J. Am. Chem. Soc.* **1990**, *112*, 7221.

[7] Ishiyama, T.; Takagi, J.; Miyaura, N.; Anastasi, N. R.; Hartwig, J. F., *J. Am. Chem. Soc.* **2002**, *124*, 390.

[8] Hinman, A.; Du Bois, J., *J. Am. Chem. Soc.* **2003**, *125*, 11510.

[9] Ma, R.; White, M. C., *J. Am. Chem. Soc.* **2018**, *140*, 3202.

[10] Arndtsen, B. A.; Bergman, R. G.; Mobley, T. A.; Peterson, T. H., *Acc. Chem. Res.* **1995**, *28*, 154.

[11] Gensch, T.; Hopkinson, M. N.; Glorius, F.; Wencel-Delord, J., *Chem. Soc. Rev.* **2016**, *45*, 2900.

[12] Hartwig, J. F.; Larsen, M. A., *ACS Centr. Sci.* **2016**, *2*, 281.

[13] Boller, T. M.; Murphy, J. M.; Hapke, M.; Ishiyama, T.; Miyaura, N.; Hartwig, J. F., *J. Am. Chem. Soc.* **2005**, *127*, 14263.

[14] Nagamoto, M.; Nishimura, T., *ACS Catal.* **2017**, *7*, 833.

[15] Giri, R.; Shi, B. F.; Engle, K. M.; Maugel, N.; Yu, J. Q., *Chem. Soc. Rev.* **2009**, *38*, 3242.

[16] Wencel-Delord, J.; Glorius, F., *Nature Chem.* **2013**, *5*, 369.

[17] Kato, S.; Nonoyama, N.; Tomimoto, K.; Mase, T., *Tetrahedron Lett.* **2002**, *43*, 7315.

[18] Tan, P. W.; Juwaini, N. A. B.; Seayad, J., *Org. Lett.* **2013**, *15*, 5166.

[19] Hatano, M.; Nishimura, T., *Angew. Chem. Int. Ed.* **2015**, *54*, 10949.

[20] Dangel, B. D.; Godula, K.; Youn, S. W.; Sezen, B.; Sames, D., *J. Am. Chem. Soc.* **2002**, *124*, 11856.

[21] Wu, X. F.; Neumann, H.; Beller, M., *Chem. Rev.* **2013**, *113*, 1.

[22] Fokin, A. A.; Schreiner, P. R., *Chem. Rev.* **2002**, *102*, 1551.

[23] Snieckus, V., *Chem. Rev.* **1990**, *90*, 879.

[24] Ishiyama, T.; Miyaura, *J. Organomet. Chem.* **2003**, *680*, 3.

[25] Mkhalid, I. A. I.; Barnard, J. H.; Marder, T. B.; Murphy, J. M.; Hartwig, J. F., *Chem. Rev.* **2010**, *110*, 890.

[26] Hartwig, J. F., *Chem. Soc. Rev.* **2011**, *40*, 1992.

[27] Ros, A.; Fernández, R.; Lassaletta, J. M., *Chem Soc. Rev.* **2014**, *43*, 3229.

[28] Neeve, E. C.; Geier, S. J.; Mkhalid, I. A. I.; Westcott, S. A.; Marder, T. B., *Chem. Rev.* **2016**, *116*, 9091.

[29] Xu, L.; Wang, G.; Zhang, S.; Wang, H.; Wang, L.; Liu, L.; Jiao, J.; Li, P., *Tetrahedron* **2017**, *73*, 7123.

[30] Kim, J. G.; Shin, K.; Chang, S., *Top. Organomet. Chem.* **2016**, *55*, 29.

[31] Dana, S.; Yadav, M. R.; Sahoo, A. K., *Top. Organomet. Chem.* **2016**, *55*, 189.

[32] Zhou, T.; Shi, Z. J., *Top. Organomet. Chem.* **2016**, *56*, 115.

[33] Louillat, M. L.; Patureau, F. W., *Chem. Soc. Rev.* **2014**, *43*, 901.

[34] Song, G.; Wang, F.; Li, X., *Chem. Soc. Rev.* **2012**, *41*, 3651.

[35] Neufeldt, S. R.; Sanford, M. S., *Acc. Chem. Rev.* **2012**, *45*, 936.

[36] Petrone, D. A.; Ye, J.; Lautens, M., *Chem. Rev.* **2016**, *116*, 8003.

[37] Liang, T.; Neumann, C.N.; Ritter, T., *Angew. Chem. Int. Ed.* **2013**, *52*, 8214.

[38] Wencel-Delord, J.; Patureau, F. W.; Glorius, F., *Top. Organomet. Chem.* **2016**, *55*, 1.

[39] Bellina, F., *Top. Organomet. Chem.* **2016**, *55*, 77.

[40] Soulé, J. F.; Doucet, H., *Top. Organomet. Chem.* **2016**, *55*, 103.

[41] Bruneau, C.; Dixneuf, P. H., *Top. Organomet. Chem.* **2016**, *55*, 137.

[42] Zheng, Q. Z.; *Chem. Soc. Rev.* **2016**, *45*, 4590.

[43] Seregin, I. V.; Gevorgyan, V., *Chem. Soc. Rev.* **2007**, *36*, 1173.

[44] Hummel, J. R.; Boerth, J. A.; Ellman, J. A., *Chem. Rev.* **2017**, *117*, 9163.

[45] Ilies, L.; Nakamura, E., *Top. Organomet. Chem.* **2016**, *56*, 1.

[46] Chatani, N., *Top. Organomet. Chem.* **2016**, *56*, 19.

[47] Hirano, K.; Miura, M., *Top. Organomet. Chem.* **2016**, *56*, 47.

[48] Hartwig, J. F. (ed.) *Organotransition Metal Chemistry: From Bonding to Catalysis*. Sausalito: University Science Books; 2010, 1127p.

[49] Shi, H.; Herron, A. N.; Shao, Y.; Shao, Q.; Yu, J. Q., *Nature* **2018**, *558*, 581.

[50] Kuninobu, Y.; Tokunaga, Y.; Kawata, A.; Takai, K., *J. Am. Chem. Soc.* **2006**, *128*, 2002.

[51] Tahara, Y. K.; Ito, M.; Kanyiva, K. S.; Shibata, T., *Chem. Eur. J.* **2015**, *21*, 11340.

[52] Wangweerawong, A.; Bergman, R. G.; Ellman, J. A., *J. Am. Chem. Soc.* **2014**, *136*, 8520.

[53] Dyker, G., *Angew. Chem. Int. Ed.* **1999**, *38*, 1698.

[54] Xia, Y.; Qiu, D.; Wang, J., *Chem. Rev.* **2017**, *117*, 13810.

[55] Colby, D. A.; Bergman, R. G.; Ellman, J. A., *Chem. Rev.* **2010**, *110*, 624.

[56] Alberico, D.; Scott, M. E.; Lautens, M., *Chem. Rev.* **2007**, *107*, 171.

[57] Baudoin, O., *Chem. Soc. Rev.* **2011**, *40*, 4902.

[58] So, C. M.; Kwong, F. Y., *Chem. Soc. Rev.* **2011**, *40*, 4963.

[59] Huang, Z.; Lim, H. N.; Mo. F.; Young, M. C.; Dong, G., *Chem. Soc. Rev.* **2015**, *44*, 7764.

[60] Nevado, C.; Echavarren, A. M., *Synthesis* **2005**, 167.

[61] Kitamura, T., *Eur. J. Org. Chem.* **2009**, 1111.

[62] Barbour, P. M.; Marholz, L. J.; Chang, L.; Xu, W.; Wang, X., *Chem. Lett.* **2014**, *43*, 572.

[63] Yamamoto, Y., *Chem. Soc. Rev.* **2014**, *43*, 1575.

[64] Dorel, R.; Echavarren, A. M., *Chem. Rev.* **2015**, *115*, 9028.

[65] Manikandan, R.; Jeganmohan, M., *Org. Biomol. Chem.* **2015**, *13*, 10420.

[66] Drapeau, M. P.; Gooßen, L. K., *Chem. Eur. J.* **2016**, *22*, 18654.

[67] Vessally, E.; Edjlali, L.; Hosseinian, A.; Bekhradnia, A.; Esrafili, M. D., *RSC Adv.* **2016**, *6*, 49730.

[68] Neuhaus, J. D.; Willis, M. C., *Org. Biomol. Chem.* **2016**, *14*, 4986.

[69] Le Bras, J.; Muzart, J., *Chem. Rev.* **2011**, *111*, 1170.

[70] Crisenza, G. E. M.; Bower, J. F., *Chem. Lett.* **2016**, *45*, 2.

[71] Suzuki, A., *Angew. Chem. Int. Ed.* **2011**, *50*, 6723.

[72] Negishi, E. I., *Angew. Chem. Int. Ed.* **2011**, *50*, 6738.

[73] Sonogashira, K., *J. Organomet. Chem.* **2002**, *63*, 46.

[74] Scott, W. J.; Stille, J. K., *J. Am. Chem. Soc.* **1986**, *108*, 3033.

[75] Beletskaya, I. P.; Cheprakov, A. V., *Chem. Rev.* **2000**, *100*, 3009.

[76] Song, G.; Li, X., *Acc. Chem. Res.* **2015**, *48*, 1007.

[77] Zhang, J.; Shrestha, R.; Hartwig, J. F.; Zhao, P., *Nature Chem.* **2016**, *8*, 1144.

[78] Seregin, I. V.; Ryabova, V.; Gevorgyan, V., *J. Am. Chem. Soc.* **2007**, *129*, 7742.

[79] He, J.; Wasa, M.; Chan, K. S. L.; Yu, J. Q., *J. Am. Chem. Soc.* **2013**, *135*, 3387.

[80] Zhou, Y.; Zhang, Y.; Wang, J., *Org. Biomol. Chem.* **2016**, *14*, 6638.

[81] Yada, A.; Nishi, S.; Sato, Y.; Ichinoseki, S.; Murakami, M., *J. Chin. Chem. Soc.* **2018**, *65*, 117.

[82] Dong, Z.; Ren, Z.; Thompson, S. J.; Xu, Y.; Dong, G., *Chem. Rev.* **2017**, *117*, 9333.

[83] Wong, M. Y.; Yamakawa, T.; Yoshikai, N., *Org. Lett.* **2015**, *17*, 442.

[84] Zhou, B.; Yang, Y.; Tang, H.; Du, J.; Feng, H.; Li, Y., *Org. Lett.* **2014**, *16*, 3900.

[85] Murai, S.; Kakiuchi, F.; Sekine, S.; Tanaka, Y.; Kamatani, A.; Sonoda, M.; Chatani, N., *Nature* **1993**, *366*, 529.

[86] Gao, K.; Yoshikai, N., *J. Am. Chem. Soc.* **2011**, *133*, 400.

[87] Ebe, Y.; Onoda, M.; Nishimura, T.; Yorimitsu, H., *Angew. Chem. Int. Ed* **2017**, *56*, 5607.

[88] Pan, S.; Ryu, N.; Shibata, T., *J. Am. Chem. Soc.* **2012**, *134*, 17474.

[89] Lee, P. S.; Yoshikai, N., *Org. Lett.* **2015**, *17*, 22.

[90] Yang, Z.; Yu, H.; Fu, Y., *Chem. Eur. J.* **2013**, *19*, 12093.

[91] Zhang, M.; Huang, G., *Dalton Trans.* **2016**, *45*, 3552.

[92] Huang, G.; Liu, P., *ACS Catal.* **2016**, *6*, 809.

[93] Zhang, M.; Hu, L.; Lang, Y.; Cao, Y.; Huang, G., *J. Org. Chem.* **2018**, *83*, 2937.

[94] Gao, K.; Yoshikai, N., *Angew. Chem. Int. Ed.* **2011**, *50*, 6888.

[95] Ilies, L.; Chen, Q.; Zeng, X.; Nakamura, E., *J. Am. Chem. Soc.* **2011**, *133*, 5221.

[96] Ding, Z.; Yoshikai, N., *Angew. Chem. Int. Ed.* **2013**, *52*, 8574.

[97] Lee, P. S.; Yoshikai, N., *Angew. Chem. Int. Ed.* **2013**, *52*, 1240.

[98] Xu, W.; Yoshikai, N., *Angew. Chem. Int. Ed.* **2014**, *53*, 14166.

[99] Andou, T.; Saga, Y.; Komai, H.; Matsunaga, S.; Kanai, M., *Angew. Chem. Int. Ed.* **2013**, *52*, 3213.

[100] Clement, N. D.; Cavell, K. J., *Angew. Chem. Int. Ed.* **2004**, *43*, 3845.

[101] Normand, A. T.; Hawkes, K. J.; Clement, N. D.; Cavell, K. J.; Nakao, Y.; Kashihara, N.; Kanyiva, K. S.; Hiyama, T., *J. Am. Chem. Soc.* **2008**, *130*, 16170.

[102] Nakao, Y.; Idei, H.; Kanyiva, K. S.; Hiyama, T., *J. Am. Chem. Soc.* **2009**, *131*, 15996.

[103] Tamura, R.; Yamada, Y.; Nakao, Y.; Hiyama, T., *Angew. Chem. Int. Ed.* **2012**, *51*, 5679.

[104] Donets, P. A.; Cramer, N., *Angew. Chem. Int. Ed.* **2015**, *54*, 633.

[105] Kakiuchi, F.; Yamauchi, M.; Chatani, N.; Murai, S., *Chem. Lett.* **1996**, *25*, 111.

[106] Jazzar, R. F. R.; Mahon, M. F.; Whittlesey, M. K., *Organometallics* **2001**, *20*, 3745.

[107] Kakiuchi, F.; Kochi, T.; Mizushima, E.; Murai, S., *J. Am. Chem. Soc.* **2010**, *132*, 17741.

[108] Kozhushkov, S. I.; Yufit, D. S.; Ackermann, L., *Org. Lett.* **2008**, *10*, 3409.

[109] Schinkel, M.; Marek, I.; Ackermann, L., *Angew. Chem. Int. Ed.* **2013**, *52*, 3977.

[110] Bartoszewicz, A.; Martín-Matute, B., *Org. Lett.* **2009**, *11*, 1749.

[111] Rit, R. K.; Ghosh, K.; Mandal, R.; Sahoo, A. K., *J. Org. Chem.* **2016**, *81*, 8552.

[112] Carrion, M. C.; Cole-Hamilton, D. J., *Chem. Commun.* **2006**, 4527.

[113] Lenges, C. P.; Brookhart, M., *J. Am. Chem. Soc.* **1999**, *121*, 6616.

[114] Jun, C. H.; Hong, J. B.; Kim, Y. H.; Chung, K. Y., *Angew. Chem. Int. Ed.* **2000**, *39*, 3440.

[115] Tsuchikama, K.; Kuwata, Y.; Tahara, Y. K.; Yoshinami, Y.; Shibata, T., *Org. Lett.* **2007**, *9*, 3097.

[116] Thalji, R. K.; Ahrendt, K. A.; Bergman, R. G.; Ellman, J. A., *J. Am. Chem. Soc.* **2001**, *123*, 9692.

[117] Thalji, R. K.; Ellman, J. A.; Bergman, R. G., *J. Am. Chem. Soc.* **2004**, *126*, 7192.

[118] Davis, T. A.; Hyster, T. K.; Rovis, T., *Angew. Chem. Int. Ed.* **2013**, *52*, 14181.

[119] Ye, B.; Donets, P. A.; Cramer, N., *Angew. Chem. Int. Ed.* **2014**, *53*, 507.

[120] Tan, K. L.; Bergman, R. G.; Ellman, J. A., *J. Am. Chem. Soc.* **2001**, *123*, 2685.

[121] Tsai, A. S.; Wilson, R. M.; Harada, H.; Bergman, R. G.; Ellman, J. *A., Chem. Commun.* **2009**, 3910.

[122] Tsuchikama, K.; Kasagawa, M.; Hashimoto, Y.-K.; Endo, K.; Shibata, T., *J. Organomet. Chem.* **2008**, *693*, 3939.

[123] Bhalla, G.; Oxgaard, J.; Goddard, W. A.; Periana, R. A., *Organometallics* **2005**, *24*, 3229.

[124] Prades, A.; Corberán, R.; Poyatos, M.; Peris, E., *Chem. Eur. J.* **2009**, *15*, 4610.

[125] Pan, S.; Ryu, N.; Shibata, T., *Adv. Synth. Catal.* **2014**, *356*, 929.

[126] Crisenza, G. E. M.; McCreanor, N. G.; Bower, J. F., *J. Am. Chem. Soc.* **2014**, *136*, 10258.

[127] Crisenza, G. E. M.; Sokolova, O. O.; Bower, J. F., *Angew. Chem. Int. Ed.* **2015**, *54*, 14866.

[128] Shibata, T.; Ryu, N.; Takano, H., *Adv. Synth. Catal.* **2015**, *357*, 1131.

[129] Ebe, Y.; Nishimura, T., *J. Am. Chem. Soc.* **2015**, *137*, 5899.

[130] Shirai, T.; Yamamoto, Y., *Angew. Chem. Int. Ed.* **2015**, *54*, 9894.

[131] Hatano, M.; Ebe, Y.; Nishimura, T.; Yorimitsu, H., *J. Am. Chem. Soc.* **2016**, *138*, 4010.

[132] Zhou, X.; Xia, J.; Zheng, G.; Kong, L.; Li, X., *Angew. Chem. Int. Ed.* **2018**, *57*, 6681.

[133] Grélaud, S.; Cooper, P.; Feron, L. J.; Bower, J. F., *J. Am. Chem. Soc.* **2018**, *140*, 9351.

[134] Rakshit, S.; Grohmann, C.; Besset, T.; Glorius, F., *J. Am. Chem. Soc.* **2011**, *133*, 2350.

[135] Guimond, N.; Gorelsky, S. I.; Fagnou, K., *J. Am. Chem. Soc.* **2011**, *133*, 6449.

[136] Ye, B.; Cramer, N., *Science* **2012**, *338*, 504.

[137] Qin, Y.; Zhu, L.; Luo, S., *Chem. Rev.* **2017**, *117*, 9433.

[138] Cho, S. W.; Kin, J. Y.; Kwak, J.; Chang, S., *Chem. Soc. Rev.* **2011**, *40*, 5068.

[139] Kakiuchi, F.; Ohtaki, H.; Sonoda, M.; Chatani, N.; Murai, S., *Chem. Lett.* **2001**, 918.

[140] Harvey, J. N., *Organometallics* **2001**, *20*, 4887.

[141] Marcone, J. E.; Moloy, K. G., *J. Am. Chem. Soc.* **1998**, *120*, 8527.

[142] Culkin, D. A.; Hartwig, J. F., *Organometallics* **2004**, *23*, 3398.

[143] Gómez-Gallego, M.; Sierra, M. A., *Chem. Rev.* **2011**, *111*, 4857.

[144] Ghosh, R.; Emge, T. J.; Krogh-Jespersen, K.; Goldman, A. S., *J. Am. Chem. Soc.* **2008**, *130*, 11317.

[145] Singleton, D. A.; Thomas, A. A., *J. Am. Chem. Soc.* **1995**, *115*, 9357.

[146] Colletto, C.; Islam, S.; Juliá-Hernández, F.; Larrosa, I., *J. Am. Chem. Soc.* **2016**, *138*, 1677.

[147] Yi, C. S.; Lee. D. W., *Organometallics* **2009**, *28*, 4266.

[148] Hirschi, J. S.; Takeya, T.; Hang, C.; Singleton, D. A., *J. Am. Chem. Soc.* **2009**, *131*, 2397.

[149] Nowlan III, D. T; Gregg, T. M.; Davies, H. M. L.; Singleton, D. A., *J. Am. Chem. Soc.* **2003**, *125*, 15902.

[150] Nowlan III, D. T.; Singleton, D. A., *J. Am. Chem. Soc.* **2005**, *127*, 6190.

[151] Ghosh, K.; Rit, R. K.; Ramesh, E.; Sahoo, A. K., *Angew. Chem. Int. Ed.* **2016**, *55*, 7821.

[152] Ahrendt, K. A.; Bergman, R. G.; Ellman, J. A., *Org. Lett.* **2003**, *5*, 1301.

[153] Thalji, R. K.; Ellman, J. A.; Bergman, R. G., *J. Am. Chem. Soc.* **2004**, *126*, 7192.

[154] Harada, H.; Thalji, R. K.; Bergman, R. G.; Ellman, J. A., *J. Org. Chem.* **2008**, *73*, 6772.

[155] Cavell, K. J., *Coord. Chem. Rev.* **1996**, *155*, 209.

[156] Xu, R.; Bittner, M.; Klatt, G.; Köppel, H., *J. Phys. Chem. A* **2008**, *112*, 13139.

[157] Brookhart, M.; Green, M. L. H.; Parkin, G., *P. Natl. Acad. Sci.* **2007**, *104*, 6908.

[158] Scherer, W.; McGrady, G. S., *Angew. Chem. Int. Ed.* **2004**, *43*, 1782.

[159] Salanne, M.; Rotenberg, B.; Jahn, S.; Vuilleumier, R.; Simon, C.; Madden, P. A., *Theor. Chem. Acc.* **2012**, *131*, 1143.

[160] Zhang, J.; Shrestha, R.; Hartwig, J. F.; Zhao, P., *Nature Chem.* **2016**, *8*, 1144.

[161] Ananikov, V. P.; Beletskaya, I. P., *Top. Organomet. Chem.* **2016**, *43*, 1.

[162] Xue, L.; Lin, Z., *Chem. Soc. Rev.* **2010**, *39*, 1692.

[163] Deeth, R. J.; Smith, A.; Brown, J. A., *J. Am. Chem. Soc.* **2004**, *126*, 7144.

[164] Bickelhaupt, M.; Houk, K. N., *Angew. Chem. Int. Ed.* **2017**, *56*, 10070.

[165] de Jong, G. T.; Bickelhaupt, M., *J. Chem. Theor. Comput.* **2007**, *3*, 514.

[166] Majetich, G.; Shimkus, J. M., *J. Nat. Prod.* **2010**, *73*, 284.

[167] Zheng, M.; Zhang, Z.; Zhu, W.; Liu, H.; Luo, X.; Chen, K.; Jiang, H., *Bioorg. Med. Chem.* **2006**, *14*, 3428.

[168] Fevig, J. M.; Feng, J.; Rossi, K. A.; Miller, K. J.; Wu, G.; Hung, C. P.; Ung, T.; Malmstrom, S. E.; Zhang, Ge.; Keim, W. J.; Cullen, M. J.; Rohrbach, K. W.; Qu, Q.; Gan, J.; Pelleymounter, M. A.; Robl, J. A., *Bioorg. Med. Chem. Lett.* **2013**, *23*, 330.

[169] Schönherr, H.; Cernak, T., *Angew. Chem. Int. Ed.* **2013**, *52*, 12256.

[170] Tsai, T. W.; Wang, E. C.; Li, S. R.; Chen, Y. H.; Lin, Y. L.; Wang, Y. F.; Huang, K. S., *J. Chin. Chem. Soc.* **2004**, *51*, 1307.

[171] Yang, L.; Huang, Z.; Li, G.; Zhang, W.; Cao, R.; Wang, C.; Xiao, J.; Xue, D., *Angew. Chem. Int. Ed.* **2018**, *130*, 1986.

[173] Koura, M.; Matsuda, T.; Okuda, A.; Watanabe, Y.; Yamaguchi, Y.; Kurobuchi, S.; Matsumoto, Y.; Shibuya, K., *Bioorg. Med. Chem. Lett.* **2015**, *25*, 2668.

[174] Shinji, C.; Maeda, S.; Imai, K.; Yoshida, M.; Hashimoto, Y.; Miyachi, H., *Bioorg. Med. Chem.* **2006**, *14*, 7625.

[175] Sperry, J.; Gibson, J. S.; Sejberg, J. J. P.; Brimble, M. A., *Org. Biomol. Chem.* **2008**, *6*, 4261.

[176] Tokunaga, T.; Hume, W. E.; Kitoh, M.; Nagata, R.; Kishino, M.; Nagakawa, T.; Nagamine, J.; Taiji, M. (Sumimoto Pharmaceuticals Company); EP1479384 A1, **2003**.

[177] Companys, S.; Pouységu, L.; Peixoto, P. A.; Chassaing, S., *J. Org. Chem.* **2017**, *82*, 3990.

[178] Avlonitis, N.; Debunne, M.; Aslam, T.; McDonald, N.; Haslett, C.; Dhaliwal, K.; Bradley, M., *Org. Biomol. Chem.* **2013**, *11*, 4414.

[179] Elmer, S. L.; Zimmerman, S. C., *J. Org. Chem.* **2004**, *69*, 7363.

[180] van Nunen, J. L. M.; Folmer, B. F. B.; Nolte, R. J. M., *J. Am. Chem. Soc.* **1997**, *119*, 283.

[181] Harnoy, A. J.; Slor, G.; Tirosh, E.; Amir, R. J., *Org. Biomol. Chem.* **2016**, *14*, 5813.

[182] Burkhart, C.; Haberhauer, G., *Eur. J. Org. Chem.* **2017**, 1308.

[183] Brambilla, M.; Tredwell, M., *Angew. Chem. Int. Ed.* **2017**, *56*, 11981.

[184] Rahaim Jr., R. J.; Maleczka Jr., R. E., *Synthesis* **2006**, 3316.

[185] Zhang, W.; Xie, J.; Rao, B.; Luo, M., *J. Org. Chem* **2015**, *80*, 3504.

[186] Song, J. (Emisphere Technologies); WO2018/116141 A1, **2008**.

[187] Könning, D.; Hiller, W.; Christmann, M., *Org. Lett.* **2012**, *14*, 5258.